DOE/ER/40627--2

DE93 005113

*"ELEMENTARY PARTICLE INTERACTIONS"*

# PROGRESS REPORT TO DEPARTMENT OF ENERGY

**DOE DE-FG05-91ER40627**

*(October 1, 1991 - September 30, 1992)*

**W. M. Bugg, G. T. Condo, T. Handler, E. L. Hart, K. Read, and B. F. L. Ward**

**October 1992**

## DISCLAIMER

This report was prepared as an account of work sponsored by an agency of the United States Government. Neither the United States Government nor any agency thereof, nor any of their employees, makes any warranty, express or implied, or assumes any legal liability or responsibility for the accuracy, completeness, or usefulness of any information, apparatus, product, or process disclosed, or represents that its use would not infringe privately owned rights. Reference herein to any specific commercial product, process, or service by trade name, trademark, manufacturer, or otherwise does not necessarily constitute or imply its endorsement, recommendation, or favoring by the United States Government or any agency thereof. The views and opinions of authors expressed herein do not necessarily state or reflect those of the United States Government or any agency thereof.

MASTER

DISTRIBUTION OF THIS DOCUMENT IS UNLIMITED

DOE/ER/40627-2

# *"ELEMENTARY PARTICLE INTERACTIONS"*

## Progress Report

## October 1, 1991 - September 30, 1992

W. M. Bugg, G. T. Condo, T. Handler, E. L. Hart,
K. Read, and B. F. L. Ward

Department of Physics & Astronomy
University of Tennessee
Knoxville, Tennessee 37996-1200

October 1992

PREPARED FOR THE U.S. DEPARTMENT OF ENERGY
UNDER GRANT NUMBER DE-FG05-91ER40627

*"Elementary Particle Interactions"*

# PROGRESS REPORT TO DEPARTMENT OF ENERGY

## DOE DE-FG05-91ER40627

## TASK A

**W. M. Bugg, G. T. Condo, T. Handler,**
**E. L. Hart, and K. Read**

# TASK A

## TABLE OF CONTENTS


*Page*

I. Data Analysis - Fermilab E-745 - E-782 . . . . . 1

II. Photoproduction Experiments at the University of Tennessee

A. BC-72/73/75 . . . . . 3
B. E-687 . . . . . 4
C. Solenoidal Detector Collaboration Efforts . . . . . 7
D. Computer Facilities for the High Energy Physics Group . . . . . 10
E. P-831 . . . . . 12
F. Future Work on SDC . . . . . 14

III. L3

A. L3 Activities . . . . . 16
B. GEM . . . . . 26

IV. SLD . . . . . 30

V. SSC Detector Research and Development

A. Other GEM Activities . . . . . 31
B. Radiation Hardness of Silicon Detector . . . . . 31

VI. List of Publications . . . . . 32

VII. Appendix A, B, C, and D . . . . . 34

# I. DATA ANALYSIS - FERMILAB E-745 - E-782

Work continues on the completed data summary tape from the E-745 high energy neutrino exposure in the Tohoku freon bubble chamber at Fermilab. In particular, Tohoku continues to study hadron formation in neutrino-nucleus interactions, while Brown and Tennessee are working on strange particle production in weak interactions. In a November 1992 SESAPS talk, E. Hart will present our negative conclusions regarding the Fermilab CCFR group's suggestion at Neutrino '92 that they had seen some evidence for the production and decay of a heavy neutral lepton.

Scanning and measuring of the 300,000 picture exposure of 200 GeV/c muons (E-782) is continuing at Tohoku and UT. The status of this effort as of the end of August, 1992 is as follows:

| | | | |
|---|---|---|---|
| Frames scanned | 151,500 | 10,560 useful events located | |
| Events measured | 4,020 | Events cut | 3,200 |

In January of this year, more stringent cuts were initiated to restrict events measured to mostly those with $\nu > 1$ GeV/c. This effort has allowed the rejection of about 75% of the so-called useful events before they are measured, and a factor of two increase in the scanning rate. However, we will still not be able, as things stand, to complete processing all the good film in a reasonable time. It has therefore been agreed to add a new collaborating group to the E-782 experiment. The University of Calcutta,

under an agreement between the NSF and the Indian Government, NSF INT9100666, will use its plentiful scanning personnel to supply Tohoku with pre-scanned film, relieving a bottleneck there due to the very large (frame/high $\nu$ event = $\frac{40}{1}$) ratio of this experiment. Three members of the Calcutta group, under Professor Lali Chatterjee, spent more than a month this summer at Tennessee, being trained in scanning, measuring, and data processing procedures, supported by the joint U.S.-India grant.

Finally the Russian agency, ITEP, decided this spring not to go ahead with project GINES at Protvino, ending considerations of working with them.

# II. PHOTOPRODUCTION EXPERIMENTS AT THE UNIVERSITY OF TENNESSEE

Several of us (George T. Condo and Thomas Handler) have expended considerable effort over the past several years in the study of mesonic states. These mesonic states have been produced in both hadronic production reactions and photoproduction reactions.

## A. BC 72/73/75

In recent years our study of these mesonic states has been done primarily through the photoproduction reactions:

$$\gamma p \rightarrow n\pi^+\pi^+\pi^- \tag{1}$$

$$\gamma p \rightarrow \Delta^{++}\pi^+\pi^-\pi^- \tag{2}$$

The data for these reactions came from an exposure of the SLAC hybrid facility to photons of energy 20 GeV. Our principal results have been the observation of the $a_2^{\pm}(1320)$ vector meson in both reactions. The $a_2^-$ signal in reaction (2) was probably the largest (more than 10s) signal ever obtained in a photoproduction experiment except for the photoproduction of vector mesons. This also proved, contrary to the standard liturgy, that charge exchange photoproduction processes are significant even at photon

energies of 20 GeV. We also found, in both channels, evidence for the photoproduction of a state which has been listed in the Particle Data Tables as $\pi(1775)$ with $I^G(J^{PC}) = 1^-(?^{-+})$. An interesting sidelight of this result is that unless $J^{PC} = 2^{-+}$ for this state, so long as $J < 4$, the state is $q\bar{q}$ exotic ($J^{PC} = 1^{-+}$ or $3^{-+}$). Even if $J^{PC} = 2^{-+}$, this state would appear far too near the $\pi_2(1665)$ to be a candidate for a radial excitation of the $\pi_2(1665)$. Thus it would be strong candidate for a hybrid state.

During this past year we have submitted to Physical Review D the consequences of these results as regards to the $a_1(1260)$. One conclusion, which agrees with those of many other authors, is that the pg radiative width of the $a_1(1260)$ is considerably less than that of the $a_2$; and this result suggests that the mass of the $a_1$ is somewhat less than the average given in the PDT. We also present evidence, from both charge exchange interactions above, that a further higher mass odd-G parity state exists in these spectra. The existence of this state is reinforced by the observation of the $f_2(1270)$ as a decay product of the state. Because the $f_2(1270)$ has $J^{PC} = 2^{++}$, it cannot be directly produced by either one-pion exchange or pomeron exchange. It has appeared in photoproduction experiments only as the decay product of intermediate states.

Work is continuing on analysis of the Data Summary Tape from BC 72/73 where we have isolated the following reactions:

$$\gamma p \rightarrow (n\pi^+)\rho^0 \qquad (3)$$

$$\gamma p \rightarrow (n\pi^+\pi^+\pi^+)\rho^0 \qquad (4)$$

The theory of reaction (3) was described by G. Wolf nearly twenty years ago. Our data are in excellent agreement with his predictions, which have not previously been verified. In both reactions (3) and (4) the $\rho^0$ that is produced has all of the characteristics displayed by elastic $\rho^0$ photoproduction ($\gamma p \rightarrow p\rho^0$). In particular, the $\rho^0$ spectrum is quite skewed about its maximum intensity and a fit of the spectrum to an ordinary Breit-Wigner yields a mass less than 750 MeV. This work is being pursued by Kathy Danyo, a graduate student in our group.

## B. E-687

During the summer of 1991 The University of Tennessee joined experiment E-687 at FNAL. Our initial efforts in this experiment have been devoted to studying light quark meson photoproduction at photon energies of ~300 GeV. The experiment is primarily concerned with studying the decay and production properties of charmed mesons and baryons using photons incident on a beryllium target. In August of 1991, two graduate students, Gavin Blackett and Murali Pisharody, moved to FNAL to participate in the data taking which lasted until January 1992. After an initial period of familiarization, our group was accepted fully into the collaboration. During their stay at FNAL the graduate students became familiar with all aspects of the experiment--from software through hardware. After their stay at FNAL, both graduate students moved

back to Tennessee where they were part of the team that managed the processing of the raw data tapes through the reconstruction programs on the various computer farms at FNAL. The data processing was completed May, 1992. Even though we joined the experiment late in the data taking phase, we have been given access to all the data . The total available data sample is in excess of 350 million events.

We expect that the study of the production of states decaying into $\pi^+\pi^-$, $\pi^+\pi^-\pi^0$, and $\pi^+\pi^+\pi^-\pi^-$ will be the bases for the graduate students' theses. Although the analyses are not complete, a strong diffractively produced r dominates the data as it does at lower energies. In addition, a signal corresponding to a $\rho'(1600)$ is also present in the 4-prong channel. The $\pi^+\pi^-\pi^0$ spectrum shows evidence for the w(785), as well as a small signal in the h(550) mass region. Although the h has been observed in low energy photoproduction experiments (from the excitation of various $N^*$ baryons and their subsequent decays to nucleon-h states), at higher energies, in the forward direction, one does not expect significant direct h production.

The status of the $\rho'(1600)$ has been controversial in the past. Neither the mass value nor the width of the 2p and 4p decay modes are in agreement. The PDT, along with most of the rest of the world, believes that the photoproduced state(s) that decay to 4p is the result of interference between two r' states of masses 1450 and 1700 MeV. We are examining our 4p spectrum to tests its consistency with this hypothesis and also to

ascertain whether there is any evidence for the photoproduction of $\rho_3(1690)$, which could further complicate the analysis.

We expect to continue these analyses and to expand into the study of the charmed mesons and baryons. We are also planning to continue with the collaboration in the next stage of the experiment, P-831.

## C. Solenoidal Detector Collaboration Efforts

The past year has seen a continuation of our involvement in the Superconducting Supercollider research and development effort. We (Thomas Handler and George T. Condo) became a full institutional member of the Solenoidal Detector Collaboration (SDC) at the beginning of 1992. Our efforts are focused on the calorimeter section of the SDC detector.

Prior to the submission of the SDC Technical Design Report on April 1, 1992, extensive calculations were done, in conjunction with P.K. Job of ANL and Tony Gabriel of ORNL, with regards to the various configurations being contemplated for the calorimeter as far as thicknesses and composition of the absorber materials to be used in the hadron section of the calorimeter. The results of some of these calculations have been published[1] in the past year. The configuration that was finally selected uses

---

[1]P. K. Job et al., Nuclr. Instr. and Meth. **A309** (1991) 60.
P. K. Job et al., Nuclr. Instr. and Meth. **A316** (1992) 174.

1" iron in the first section of the hadron calorimeter and 2" iron in the second section. The decision was partly based on the performance characteristics of such a calorimeter and partly on its cost. The electromagnetic section of the calorimeter will use a lead absorber. All sections of the barrel and endcap regions of the calorimeter will use 4mm scintillating tiles with fiber readout as the active medium. Full details of the SDC calorimeter can be found in the SDC Technical Design Report.[2]

In addition to the simulations concerning the proposed SDC calorimeter configuration, additional calculations, using the CALOR89 Monte Carlo code system, were carried out to compare with the FNAL test beam results (T-841). It was found that not only did the predicted resolutions agree with the hanging file test data but that also longitudinal shower profiles matched as well. Further calculations will be carried out and a more detailed comparison will be made with the hanging file test data.

One of the problems facing the SDC collaboration is the high event rate that is expected at the SSC. The interaction rate will be about $10^8$ events/sec at the design luminosity of $10^{33}$. The majority of these events will be of no interest. The question then becomes how to recognize and write to storage the events that might be of interest? One method is to exploit the physical characteristics of the interesting events.

---

[2]Solenoidal Detector Collaboration, SDC-92-201, April 1, 1992.

Certain of the decays of the expected Higgs particles will eventually be manifested in jet production. These jets will appear as large depositions of energy in compact regions of the calorimeter, with the remainder of the calorimeter being quiet. The calorimeter that is being designed for use by the SDC collaboration will be segmented in both h and f. If the calorimeter readout is unfolded along h and f, it would resemble a large grayscale pixel image. Pattern recognition techniques should, therefore, be usable to determine the presence of jet structure in a pp collision.

Artificial Neural Networks (ANNs) have shown themselves to be useful in such pattern recognition problems[3]. One aspect of the usefulness of ANNs is that they are extremely fault tolerant. This means that even if part of the information is missing, i.e. missing pixels, ANNs can still give the correct answers.

ANNs have been successfully applied to off-line problems in high energy physics[4]. It is only recently that the first use of ANNs for triggering has occurred[5]. Working in conjunction with Charles Glover of ORNL, we have attempted to test whether or not ANNs could be used to identify jet events. If ANNs could be shown to work on such a problem, then the ANNs could be used, through the use of VLSI

---

[3]P. K. Simpson, Artificial Neural Systems, Pergamon Press, New York, 1990.

[4]Bruce Denby, FERMILAB-Pub-92/215-E, 1992.

[5]Bruce Denby, FERMILAB-Pub-92/215-E, 1992.

hardware implementation, in either the Level 1 or Level 2 trigger for SDC. The difference between this problem and other applications of ANNs in high energy physics is the large number of inputs to the ANN. Whereas other problems may have had at most two dozen inputs to the ANN, the calorimeter readout that we would need has 960 pixels.

To test the feasibility of the use of ANNs we did a Monte Carlo simulation of the process. We used ISAJET to generate both 2 jet and minimum bias events which when then traced to the calorimeter. Some of the events were used for training the ANN. The remainder of the events were used to test the ANN. Preliminary results gave an 88% probability of correctly identifying 2-jet events. The results of this work were presented at the Computing in High Energy Physics Conference held in Annecy France in September of 1992. Members of the SDC Trigger group, who were at the conference, were very interested in these results and they have suggested that we do a full scale study of the use of ANNs for triggering.

## D. Computer Facilities for the High Energy Physics Group

During March of 1992, the high energy physics group at The University of Tennessee was able to acquire a Silicon Graphics 4D/240GTX computer system (SGI). The computer system initially was configured with 4 processors, a 780 Megabyte hard disk, and 16 Megabytes of memory. The system was initially devoted to SDC calorime-

ter simulation studies using the CALOR89 Monte Carlo code system. When the group joined E-687, the E-687 code system was ported to the workstation, though initially very little analysis was done on the machine.

After the return of the graduate students from FNAL in January 1992, the workstation began to slowly be used for analysis of the E687 data. Data was first skimmed out at FNAL then brought to Tennessee via the electronic networks. It became clear that the SGI would have to upgraded by the addition of exabyte tape drives. Also as the machine became more heavily used for analysis, the amount of user disk space would also have to be increased. At the end of August 1992 two exabyte tape drives and 2 Gigabytes of hard disk space were added to the SGI.

During the summer of 1992, two Science Alliance summer students worked on projects, one for E-687 and the other for SDC. We had effectively five researchers using the SGI. At this time a memory/swapping problem bottleneck was encountered causing at times a long delay in response to commands from the various terminals that interacted with the SGI. The only way to alleviate this problem was by the available random access memory. In September of 1992, an additional 48 Megabytes of memory was installed. With the addition of this main memory, the response of the SGI was considerably improved.

Because of the increased usage of newer languages, such as C, and the increased usage of object oriented programming techniques the SGI system has recently been

enhanced by the addition of the C++ programming language to its repertoire of languages.

The SGI has been of immense value to the University of Tennessee's high energy physics group. Without it, the contributions to the SDC effort would have not been as large.

## E. P-831

The E-687 collaboration has proposed P-831, a continuation of the current experiment, to FNAL. This new experiment would be conducted with an upgraded spectrometer and would take place during the 1994 Fixed target Program at FNAL. The purpose of the continuation would be to accumulate sufficient events for a high precision study of the D semileptonic decay modes, QCD studies of Double D events, a measurement of the absolute branching fraction of the $D^0$, searches for $D^0$ mixing, CP violation, rare and forbidden decays, fully leptonic decays of the $D^+$ and a systematic investigation of charm baryons and their lifetimes. We estimate that the collaboration currently has ~110,000 fully reconstructed charm particles decaying into all charged final states. The new run would allow us to increase this number by a factor of 10 to ~$10^6$ events.

In order to obtain such a large data sample in a reasonable time, the collaboration will ask FNAL to increase the photon flux that is available to the experiment. We

feel that this increased flux can be achieved by utilizing a slightly lower momentum for the extracted main ring beam, thereby yielding more incoming electrons to the radiator and by also utilizing the positrons that are in the secondary particle beam. The E-687 spectrometer, as currently configured, will not be able to handle this increased photon flux. This necessitates an upgrade to the spectrometer. Modifications will have to be made to almost all of the spectrometer elements.

As part of this upgrade effort, The University of Tennessee would, in conjunction with the group from Pavia, Italy, rebuild the current hadron calorimeter. The new hadron calorimeter would have enhanced triggering characteristics and would also be better able to measure neutral particle showers. The basic part of the upgrade of the hadron calorimeter would entail replacing the current gas/proportional tube counters with scintillating tiles using fiber readout. The details of the hadron calorimeter upgrade are detailed in Appendix A. It is expected that the rebuilding of the hadron calorimeter would occur during the summer 1993.

The University of Tennessee has agreed to supply the new phototubes, their bases and shields, and various miscellaneous pieces of hardware such as the boxes to hold the tile system. The total equipment cost, including contingency is $148,000. We also plan on having two students full time at FNAL for two months during the conversion of the hadron calorimeter. This cost would amount to ~$3000 yielding a total cost of ~$151,000.

In addition to the above requests for hardware and support for students, we are asking for sufficient funds to support a post-doctoral fellow, for at least two years, whose time would be devoted to work on P-831/E-831. Besides working on the hardware upgrade on the hadron calorimeter, this person would also work on the physics topics that E-831 will address. Estimated cost for this post-doctoral fellow is ~$55,000 for the first year.

## F. Future Work On SDC

During the coming year, we plan on continuing our work in simulation studies, using the CALOR89 Monte Carlo code system, of the SDC calorimeter. Specifically we plan on carrying out a full set of simulations to compare with the Hanging File Test Run (T-841) that was performed at FNAL during the previous year. This simulation work will be in collaboration with P. K. Job of ANL and Tony Gabriel of ORNL. This comparison will be a straightforward comparison since all the experimental conditions will be known from close communication with the hanging file experimenters at FNAL. This will allow us to take into account, in the simulation analysis programs, all of the experimental variations and manipulations that have been done. If any discrepancies are found, and none have been so far, appropriate modifications to the CALOR89 code system will be made and the simulation process repeated. This work should result in another NIM publication.

The importance of these comparisons with the hanging file test data cannot be underestimated. Eventually the complete SDC detector will have to be simulated so that detector's biases to physics events can be understood. In order to properly use and uderstand these simulations, the Monte Carlo program must be above reproach.

We also plan on doing a full study of the feasibility of using Artificial Neural Networks in the triggering process, either at Level 2 or Level 1, for the SDC detector. As has been shown previously, ANNs seem to be a reliable way of triggering on jets in the barrel and endcap regions of the calorimeter. A systematic study of the ANN configuration needed will be carried out. So that this study can be carried out in an efficient manner, funds are requested to purchase a commercial neural network program that is currently being used by Charles Glover of ORNL. The program is NeuralWorks by NeuralWare, Inc. with an educational institution cost of ~$3500.

# III. L3

## A. L3 Activities

Prof. Read spent 6 weeks working exclusively at the L3 experiment at CERN during July and August 1992. During the rest of the year, his involvement included providing advice on various electronic interlock issues and keeping abreast of developments concerning wide-angle Bhabha scattering.

### Interlock Enhancement

The L3 electromagnetic calorimeter, hereafter referred to as the BGO, has a hierarchical readout system. The level-1 readout which consists of preamps and ADC boards is powered by 106 low-voltage power supplies. These supplies are controlled and monitored by an interlock system whose software was previously written mostly by Prof. Read. The system consists of two "server" IBMPC/AT compatible computers which directly supervise power, a "temperature" PC which monitors the temperature of the electronics, and a "master" PC which supervises the other PC's and makes decisions. These PC's all communicate in real-time many times per second. They constitute a dedicated slow-control stand-alone local area DECNET network. The master PC transfers its information to the online VAX-6310 where it is summarized, logged,

displayed to shift operators, and distributed to other interested parties (L3 slow control, BGO online monitoring).

As of July 1991, when Prof. Read was last at CERN, this system had full functionality but suffered from a fatal communication error which would cause a network link between the master and one or both of the two server PC's to spontaneously drop. It should be noted that due to the fail-safe nature of the system this presents no danger or risk to the electronics; however, such a failure cuts power and has the very undesirable effect of stopping any data collection run in progress. This communication error happened once per week if the master PC was connected via DECNET to the VAX and much less frequently if not. It was inferred that this problem was due to an excess of outside DECNET traffic hampering operation of the ethernet drivers of the PC's. Since the control software for the ethernet drivers was propietary software from a company that did not provide satisfactory support and has since gone out of business, this problem was considered almost impossible to cure directly.

In order to cure this problem Prof. Read had suggested installing a DECNET bridge to filter out unwanted traffic. His colleagues were not able to successfully implement this suggestion, primarily due to difficulty in eliminating unwanted outside broadcast messages. Instead, a student from Lausanne University, A. Kasser, developed software for a new "gateway" PC to simulate the effect of a DECNET bridge. All

DECNET traffic from the PC's goes to the gateway. The gateway is connected to the VAX via TCP/IP.

During his recent trip Read, had a chance to inspect operation of the gateway for the first time. Using a PC for this purpose may seem complicated, but it is actually much cheaper than a CERN-approved programmable bridge and completely adapted to this application. The gateway link to the VAX does die occasionally but this is completely innocuous since it has no effect on the safe operation of the 4 other PC's. The presence of the gateway allows the other PC's to communicate in a "quieter" environment, which appears to improve the robustness of the communication links. The interlock system network currently only drops a link at the rate of once every 6 weeks.

During this trip, Prof. Read provided guidance to a graduate student from Lausanne and a post-doc from Princeton University concerning possible modifications to the interlock system software. As L3 matures, the increasingly smooth operation inexhorably leads to ever more stringent demands on reliability and robustness of software. There is some indication that the likelihood of unexpected communication link failures is reduced if all PC's connected to the network are rebooted after the failure of any one communication link. Given that rebooting all PC's as a matter of course in the event of any network link failure proves desirable, the first issue is how to preserve power in the event of rebooting one of the server PC's which controls power. Possible

software changes include allowing the level-1 power to remain on even during and after a PC reboot providing certain conditions exist.

Read suggested that no changes be implemented until the time of the technical stop for LEP scheduled from mid- to late-September. At that time, it is to be clarified whether global reboot of all the PC's really does increase network reliability. If so, then the changes should be implemented. Read provided detailed descriptions of the actual modifications to the software that would be required, without actually providing any new code. Preserving the power is very straight-forward from both the hardware and software viewpoints. Most of the software modifications concern remembering the previous on/off status and managing the interplay of various time-out conditions. In general, it is better for the actual code to be written by the resident expert (no longer Prof. Read) since he must debug it.

This possible modification then opens the door for a further modification. Prof. Read is considering the feasibility and desirability of having the master PC ordering a hardware reboot of all other PC's and then itself in the event of a link failure. This is a "work-around" that handles virtually all possible rare network glitches (but not broken cables or sick PC's) without cutting power while preserving safety. It relies on satisfactory completion of the less ambitious project to preserve power across PC reboots. It also requires a simple hardware circuit of relays controlled by the master PC that can reboot any PC. It is consistent with a recent online philosophy that the ultimate

solution for rare glitches that cannot be properly diagnosed and corrected is to institute automatic restarting without stopping the run.

Prof. Read also had an opportunity to observe and test a new part of the regular BGO shift display which presents existing interlock status information (using color graphics and pop-up alarm windows) in a very user-friendly fashion that is integrated with the rest of the online command menus and displays.

## Analysis Projects

Prof. Read assisted a colleague and a student in performing data analysis investigating the process $b \rightarrow \chi_c X$ where $\chi_c \rightarrow J/\psi + \gamma$ and $J/\psi \rightarrow \mu^+\mu^-$. This is a reaction that L3 should be especially able to observe due to its excellent muon momentum and photon energy resolution.

When Read arrived, a graduate student, M. Wadhwa, from the University of Annecy had observed a peak of 6 events with a background of 2 in the $J/\psi + \gamma$ invariant mass distribution. The peak was not observed if the photons were paired with false hypothesis $J/\psi$ candidates formed using $\mu^+\mu^-$ pairs with the wrong invariant mass ("sidebands"). However, there were several concerns about the analysis. The peak was observed 80 MeV below the known $\chi_c(3510)$ mass. Also, the peak was sensitive to the version of the reconstruction code that was used. Moreover, an independent analysis by V. Innocente of the University of Naples had failed to observe the same effect.

Read engaged in extensive discussions with M. Wadhwa and V. Innocente, performed data analysis, and scanned candidate event displays in order to help clarify the situation. There was some time pressure since early August was the last possible moment for any new results to be approved to be shown at the upcoming "Rochester" conference in Dallas at which many L3 results were shown. The conference lasted from August 5 through 12.

The analysis begins by selecting $J/\psi \rightarrow \mu^+\mu^-$ candidates. The selection criteria are discussed in a recently submitted paper.[1] A sample of 43 candidates with very little background is obtained. Many of these events also contain low energy photons. By forming $J/\psi + \gamma$ invariant mass combinations one can search for $\chi_c$ candidates. Both the J = 1 and J = 2 states of the $\chi_c$ have appreciable, known branching ratios to $J/\psi + \gamma$. It remains to be determined whether L3 can resolve the two states and how large the J = 2 contribution is. Both CLEO and ARGUS have measured the $B \rightarrow \chi_c X$ branching ratio. L3 can measure the $b \rightarrow \chi_c X$ cross section times branching ratio. CDF has recently reported a measurement. It is unlikely that L3's measurement will be as accurate as CLEO's.

Prof. Read expects to be able to continue to contribute to this analysis from Tennessee since he has access to the data and remains in communication with his

---

[1]"Inclusive J Production in Z° Decays," L3 Collaboration, submitted to Phys. Lett.B.

colleagues. It appears possible that the observed mass shift can largely be eliminated by using the space point of the muon crossing point as the photon origin in the reconstruction of the $\chi_c$ candidate.

Other recent analysis efforts within L3 have led to papers concerning improved Higgs mass limits, QED studies, QCD studies, measurement of inclusive $\eta$ production, improved measurements of the $B^0$—$\bar{B}^0$ mixing parameter, measurements and upper limits on multi-photon final states, measurement of the $Z \to b\bar{b}$ and $Z \to c\bar{c}$ forward-backward asymmetries, and $\tau$ lepton polarization.

## Meetings and Shifts

Prof. Read attended L3 Z-lineshape meetings, B-physics meetings, and private meetings with other physicists. He attended the August L3 general meeting. He attended meetings and engaged in discussions concerning planned upgrades to L3. The following systems will be added: a new silicon strip luminosity monitor, a silicon microstrip vertex detector, and forward-backward muon chambers.

A proposed upgrade to L3 known as L3+1 is to convert L3 from a LEP detector to an LHC detector. This would involve raising the L3 magnet and muon chambers by 1 m in order to be concentric about the new LHC beam pipe. More recently, S. Ting and his colleagues appear to be leaning towards a more ambitious proposal for an essentially new major detector. Read heard conflicting reports concerning whether a

marriage between a successor to L3 and the proposed Compact Muon Solenoid (CMS) was still under consideration. He engaged in unofficial discussions and read recent CMS collaboration metting minutes to try to stay abreast of CMS developments.

Read took 14 BGO data-taking shifts. He explained shift duties and BGO online operations to his colleague H. Cohn who arrived at CERN on July 31. H. Cohn took 14 shifts. Thus, Read and H. Cohn fulfilled their group's annual shift quota during their trips this summer.

In the past year, the L3 data aquisition system has become noticeably more reliable and robust. Whenever beam was delivered during Read's shifts, L3 was fully operational. On the other hand, LEP machine operations are plagued with various unrelated problems. Although significant advances have been made and the prognosis is good, lumisosity and background levels have only recently equaled the performance obtained at the end of last year. Water leaks, RF problems, the difficulty of tracking down some experts on weekends, detector magnet problems, beam-beam interactions, and other problems result in a rather fragile situation. In particular, problems requiring any access to the machine often lead to further difficulties in returning back to standard conditions. There are more sporadic "bad" fills than in late 1991. The net effect is that LEP provides colliding beams during 67% of the time scheduled for physics.

The L3 data rate onto tape is now less than 2 Hz, which is 35% better than last year. This reduction in background is due to the new level-3 trigger for the tracking

chamber (TEC). The 1992 DAQ efficiency is 84%. The most siginificant sources of down time are VAX crashes and cooling problems. Recent 8 x 8-bunch running (discussed below) results in a crossing time of only 11.1 μsec, a factor of two shorter than previously. This increases the L3 dead-time from 5% to 9%. Efforts are underway, particularly by the BGO group, to reduce the dead-time to a more acceptable level.

## LEP Developments

Considerable effort has been made to enhance LEP luminosity. A key part of this plan is to switch from colliding 4 on 4 bunches to colliding 8 on 8 in a pretzel scheme. Alternate SPS cycles are used to interleave two groups of four bunches for each beam. LEP delivered the first collisions with 8 bunches in both LEP beams during Read's trip on July 29. The total beam current for both beams was 4 mA. The instantaneous luminosity was approximately $4 \times 10^{30}$ $cm^{-2}sec^{-1}$ which is no more than during usual 4 x 4 mode. Sparking in the pretzel separators was not a serious problem. The next milestone is to eliminate mis-crossings at each of the 4 interaction points. A significant increase in luminosity is expected.

The same beam optics are used for both the 4 and 8 bunch running in order to optimize efficiency. Recent introduction of polarization wigglers has increased the longitudinal bunch length. This should reduce instabilities in the RF cavities. The maximum peak luminosity achieved is $9 \times 10^{30}$ $cm^{-2}sec^{-1}$.

The LEP developments have led to a much longer luminosity lifetime, resulting in a higher integrated luminosity per "fill." The best LEP fill ever occured during Read's trip (250 $nb^{-1}$).

Advances have been made concerning improving the absolute energy calibration of LEP using a polarized beam. Unlike SLAC, LEP does not provide collisions for physics data collection with polarized beams. (Detector magnets kill the polarization.) With detector magnets off, only the electron beam, and running at 94 GeV, a polarized electron beam was obtained. Prof. Read discussed the current status with an L3 colleague who has accepted a fellowship to work in the LEP polarimeter group for one year.

Rather than injecting polarized $e^-$ like SLAC, LEP obtains a transversely polarized beam spontaneously via the Sokolov-Ternov effect. Wiggler magnets significantly decrease the time needed for the polarization to build up. In 1991, 20% polarization was obtained within 30 minutes. A laser polarimeter is used to measure the degree of polarization. Circularly polarized light is directed at very small angles towards the beam. The amount of deflection of the Compton-backscattered photons depends on the beam polarization. Data gathered during resonant depolarization of the beam will allow an absolute energy calibration of the machine with an uncertainty of significantly less than the present 20 MeV.

During Prof. Read's trip one machine development period was devoted to polarization. It was very frustrating that no polarization was observed. It is difficult to know where to move in the parameter space available to LEP unless at least some amount of polarization is observed.

It appears that the LEP lattice is effected by lunar tidal forces. A clear demonstration of this remarkable effect should be possible in early September when the excursion should be maximal. Software corrections for this effect are being investigated.

## B. GEM

### Overview

Prof. Read has been a member of the GEM Collaboration since its inception. He has been actively involved with their efforts to design a major detector for the SSC. During this past year, GEM submitted and successfully defended their Letter of Intent (LOI). The PAC recommended that GEM proceed to prepare the Technical Design Report (TDR). Recently, GEM has decided against using barium fluoride ($BaF_2$) crystals to perform electromagnetic calorimetry. During the course of the past year Prof. Read's GEM activities increasingly focused more on the proposed central tracker developments. These efforts are discussed below after first describing his activities with the $BaF_2$ subdetector group.

## Barium Fluoride Calorimeter

Read was a member of the $BaF_2$ subdetector group (partly due to his parallel involvement with the L3 BGO subdetector group). Read spent time at Fermilab on three separate occasions to participate in beam tests of a 7 x 7 $BaF_2$ prototype matrix. The test was known as Experiment T-849. The tests were designed to study uniformity, energy and position resolution of the crystals.

Prof. Read attended meetings at Caltech and U.C. San Diego to discuss analysis of test beam data from the Fermilab beam tests of a $BaF_2$ prototype matrix for the proposed GEM detector at the SSC. He contributed to the analysis effort using a local IBM RISC/6000 workstation. He concentrated his analysis efforts on tracking incident particles through the beam spectrometer to make the momentum determination. Also, he investigated and assessed some light reflection programs in order to better understand the light collection efficiency of the crystals. He presented some of his findings at U.C. San Diego.

Read acted as a liaison between the $BaF_2$ subdetector group and the ORNL Instrumentation and Controls Division (I&C) to facilitate development of an active, linear photomultiplier preamp/shaper. After thorough checking of its performance, a satisfactory design was implemented for use during readout of crystals on a cosmic ray stand (after the Fermilab run was over).

## Central Tracker

Prof. Read has attended meetings and run Monte Carlo simulations to participate in development of the proposed silicon central tracker and the surrounding Interpolating Pad Chamber. He has migrated his software activities from an IBM RISC/6000 machine to a powerful local Silicon Graphics workstation. This workstation (unlike the IBM 6000) is one of the types of workstations supported by the SSC Laboratory's computing division.(i.e., analysis code is intended to continue to run on this type of workstation).

## Interpolating Pad Chamber Readout

Prof. Read is currently active in the central tracker group of GEM. His hardware activities include working with the I&C Division of ORNL in order to develop radiation hard readout electronics for the Interpolating Pad Chambers (IPC) which surround the silicon microstrip tracker.

The front-end IPC readout electronics consist of a preamp followed by an analog memory unit (AMU) followed by a flash ADC. The AMU is a switched capacitor array. Due to its close proximity to the interaction point, it must be fabricated using a process resistant to 1 MRad accumulated dose. The 16-channel AMU is 128 cells deep. Efforts this year have concentrated on selecting a foundry for the first radiation hard prototype fabrication run. This year ORNL signed non-disclosure agreements with

Harris and UTMC for their radiation hard processes. They obtained process models to simulate the effects of radiation damage on the circuits. An AMU prototype design was developed this summer using the Harris AVLSI-RA process. The plan calls for several devices on each silicon wafer. Thus, the prototype run should yield variant designs of the AMU: one with a voltage-write, voltage-read topology and another with a voltage-write, charge-read topology. The relative merits of these two topologies are being assessed.

## IV. SLD

SLD completed its very successful 1992 run with 10,700 $Z^0$ with average polarization of 22%. Tennessee completed a study of integrated luminosity for the run, established energy and angular resolution of the Luminosity Monitor through the study of approximately 20,000 Bhabha events, and has begun a detailed comparison of observed radiative events with prediction of theory as incorporated in the BHLUMI Monte Carlo of Jadach and Ward.

A series of presentations at the DPF meeting at Fermilab is presented in Appendix B with preliminary physics results and data on the unique capabilities of the detector.

# V. SSC DETECTOR RESEARCH AND DEVELOPMENT

## A. Other GEM Activities

Other GEM activities include preparation of resistive plate chambers for muon trigger. Tennessee has refurbished a set of drift chambers provided by us for a Fermilab experiment to be used by a muon group at MIT in test stand for RPC. Studies will be carried out on gases and chamber materials to make chambers insensitive to neutrons.

Also extensive studies of calorimeters for GEM have been carried out by a team of Russian visitors under the direction of Y. Kamychkov. These reports are too extensive for inclusion in this progress report but efforts of one member of the team are included as an example in the Appendix C.

## B. Radiation Hardness of Silicon Detector

In addition to construction of large silicon EM calorimeter capable of SSC operation, Tennessee has provided in conjunction with John Walter and IntraSpec, Inc. a systematic program for improvement in radiation hardness properties of silicon detectors in very high neutrino fluxes. This work is not yet complete, but progress to date is included in the renewal proposal and in the Appendix D which is our recent paper on basic mechanisms.

# TASK A

## Publication List

1. "First Measurement of the Left-Right Cross Section Asymmetry in Z Boson Production at $E_{cm}$ = 91.5 GeV," (the SLD Collaboration), XXVI International Conference on High Energy Physics, August 6-12, 1992, Dallas, Texas.

2. "Measurements of Hadronic Decays of $Z^0$ Bosons," (the SLD Collaboration), XXVI International Conference on High Energy Physics, August 6-12, 1992, Dallas, Texas.

3. "A Study of Jet Rates and Measurements of $\alpha_s$ at the $Z^0$ Resonance," (the SLD Collaboration), XXVI International Conference on High Energy Physics, August 6-12, 1992, Dallas, Texas.

4. "A Study of Energy-Energy Correlations and Measurement of $\alpha_s$ at the $Z^0$ Resonance," (the SLD Collaboration), XXVI International Conference on High Energy Physics, August 6-12, 1992, Dallas, Texas.

5. "QCD Studies of Hadronic Decays of $Z^0$ Bosons by SLD," (the SLD Collaboration), XXVI International Conference on High Energy Physics, August 6-12, 1992, Dallas, Texas.

6. "Neutral-Strange-Particle Production in 200 GeV/c $p/\pi^+/K^+$ Interations on Au, Ag, and Mg," (with D. H. Brick, et al.), Phys. Rev. D45, 734 (1992).

7. "Fast Neutron-Induced Charges in Net Impurity Concentrantions of High-Resistivity Silicon," (I. Tsveybak, W. M. Bugg, J. A. Harvey, and J. Walter), to be published in IEEE Transitions of Nuclear Science, 1992.

8. "Decay Properties of Tau Leptons Measured at the $Z^0$ Resonance," (L3 Collaboration), Phys. Lett. B265, 451 (1991).

9. "Measurement of the Lifetime of B-hadrons and a Determination of $|V_{cb}|$," (L3 Collaboration), Phys. Lett. B270, 111 (1991).

10. "Search for Lepton Flavour Violation in $Z^0$ Decays," (L3 Collaboration), Phys. Lett. B271, 453 (1991).

11. "Measurement of the Strong Coupling Constant $\alpha_s$, for Bottom Quarks at the $Z^0$ Resonance," (L3 Collaboration), Phys. Lett. B271, 461 (1991).

12. "A Direct Determination of the Number of Light Neutrino Families from $e^+e^- \rightarrow \nu\bar{\nu}\gamma$ at LEP," (L3 Collaboration), Phys. Lett. B275, 209 (1992).

13. "Electroweak parameters of the $Z^0$ Resonance and the Standard Model," (The LEP Collaborations: ALEPH, DELPHI, L3, and OPAL), Phys. Lett. B276, 247 (1992).

14. "Search for the Neutral Higgs Boson at LEP," (The LEP Collaborations: ALEPH, DELPHI, L3, and OPAL), Phys. Lett. B283, 454 (1992).

15. "Feasibility of Using Neural Networks as a Level 2 Calorimeter Trigger for Jet Tagging," (T. Handler, et al.), to be published in the Proceedings of the Computing in High Energy Physics Conference, Annecy, France, September 21-25, 1992.

16. "Comparison of CALOR89 Model Predictions with Scintillator Plate Calorimeter Data," (P. K. Job, et al.), Nucl. Instr. and Meth. A309, 60 (1991).

17. "Design Considerations for a Scintillating Plate Calorimeter," (P. K. Job, et al.), Nucl. Instr. and Meth. A316, 174 (1992).

18. "Further Results from Charge Exchange Photoproduction," (G. T. Condo, et al.), submitted to Phys. Rev. D1.

# APPENDIX A

**Proposal to Fermilab**
**for E-831**

E 831

# A High Statistics Study of States Containing Heavy Quarks Using the Wideband Photon Beam and the E687 Multiparticle Spectrometer

Submitted by the Wideband Beam Photon Collaboration


S. Bianco, P. Frabetti, A. Zallo, Dip. di Fisica dell'Universita' and INFN - Bologna, I-40126 Bologna, Italy

V. Paolone, P.M. Yager, University of California-Davis, Davis, CA 95616, USA

H. Cheung, J. Ginkel, V.S. Greene, J. Cumalat, University of Colorado, Boulder, CO 80309, USA

J. Butler, L. Gaines, P.H. Garbincius, L. Garren, S. Gourlay, D.J. Harding, P. Kasper, A. Kreymer, P. Lebrun, S. Shukla, Fermilab, Batavia, IL 60510, USA

S. Bianco, F. Fabbri, A. Zallo, Laboratori Nazionali di Frascati, I-00044 Frascati, Italy

R.W. Gardner, J. Wiss, University of Illinois at Urbana-Champaign, Urbana, IL 61801

J.S. Kang, Korea University, Seoul 136-701, Korea

G. Alimonti, G. Bellini, M. Di Corato, G. Giammarchi, F. Levarato, D. Menasce, E. Meroni, L. Moroni, D. Pedrini, L. Perasso, S. Sala, Dip. di Fisica dell'Universita' and INFN - Milano, I-20133 Milan, Italy

F. Davenport, University of North Carolina-Asheville, Ashville, NC 28804, USA

J.F. Filasetta, Northern Kentucky University, Highland Heights, KY 41076, USA

W. Shephard, University of Notre Dame, Notre Dame, IN 46556, USA

V. Arena, G. Boca, C. Castoldi, S. Ratti, P. Vitulo, Dip. di Fisica dell'Universita' and INFN - Pavia, I-27100 Pavia, Italy

A. Lopez, University of Puerto Rico at Mayaguez, Puerto Rico

J. Wilson, University of South Carolina

W. M. Bugg, G.T. Condo, T. Handler, University of Tennessee, Knoxville, TN 37996, USA

P. Sheldon, Vanderbilt University, Nashville, TN 37235, USA


September 1, 1992

# A High Statistics Study of States Containing Heavy Quarks Using the Wideband Photon Beam and the E687 Multiparticle Spectrometer

Submitted by the Wideband Beam Photon Collaboration

September 1, 1992

Summary

The spectrometer used in Fermilab Experiment 687 to study the photoproduction and decay of charmed particles will be upgraded to enable it to accumulate $10^6$ fully reconstructed charm particles. The physics will involve high precision studies of the D semileptonic decays, QCD studies of Double D events, a measurement of the absolute branching fraction for the $D^0$, searches for $D^0$ mixing, CP violation, rare and forbidden decays, fully leptonic decays of the $D^+$ and a systematic investigation of charm baryons and their lifetimes. The estimates of charm yields are based on reasonable extrapolations from channels we have already studied in E687.

The increased yield of charm will be obtained by 1) running at over 5 times the average luminosity of E-687 and 2) increasing the efficiency of the detector by a factor of 2. The increased luminosity will be achieved by lowering the beam energy to 250 GeV, using the positron arm of the beam, running at higher average proton intensity, and (hopefully) employing 900 GeV incident protons. Additional gains can come from using a thicker radiator and/or a thicker target.

The detector must be upgraded to handle the increased luminosity. Major changes are:

1. Speeding up the Hadron Calorimeter and using it in the First Level Trigger to reduce deadtime,
2. Improving the time response of the vertex Microstrip Detector,
3. Deadening the PWCs in the beam region and adding straw tube planes to cover the deadened regions. The straw tubes will, in fact, cover the whole aperture, thereby improving tracking over the entire spectrometer,
4. Speeding up the Front End Electronics by a factor of 10,
5. Speeding up the Data Acquisition System, and
6. Improving the Second Level Trigger.

Additional changes will be made to the Muon system, the Cerenkov system, and the Electromagnetic Calorimeters. The Photon Energy Tagging represents a very difficult problem, which is discussed at length. The energy tagging is necessary for the study of production dynamics.

## Abstract

The spectrometer used in Fermilab Experiment 687 to study the photoproduction and decay of charmed particles will be upgraded to enable it to accumulate $10^6$ fully reconstructed charm particles. The physics will involve high precision studies of the D semileptonic decays, QCD studies of Double D events, a measurement of the absolute branching fraction for the $D^0$, searches for $D^0$ mixing, CP violation, rare and forbidden decays, fully leptonic decays of the $D^+$ and a systematic investigation of charm baryons and their lifetimes.

The purpose of Fermilab Experiment 687 is to study the production and decay of charm and beauty particles using a high intensity, high energy photon beam, the Fermilab Wideband Photon Beam. The E687 spectrometer is shown in Figure 1. E687 finished datataking in January 1992. By the middle of August, 1992 all our data was reconstructed. Results from half the data sample are now being discussed and have been presented at conferences. One result on the observation of a charm-doubly strange baryon, $\Omega_c^0$, is being readied for publication.

Some of the highlights of our results thus far are a large sample of semileptonic decays which lead to the best value for the CKM matrix element $|V_{cs}|$, observation of new charm baryon decay channels, measurement of the lifetimes for four charm baryons, observation of a large sample of $D - \overline{D}$ events, demonstration of our ability to measure absolute branching ratios for the $D^0$, Dalitz plot analysis for several modes, and setting the best limits for $D^0 - \overline{D^0}$ mixing and direct CP violation in the charm sector.

The history of E687 is as follows. We have had three distinct running periods. In each period we have made changes and improved the quality of the data. In the first running period, from June 1987 to February 1988, a sample of about 10,000 fully reconstructed charm particles was obtained. In the second running period, from February to August 1990, about 5 times more data was collected. In the third running period from June 1991 to January 1992 an equal sample to the second running period was obtained. The second and third running periods form a dataset containing 100,000 fully reconstructed charm particles decaying into all charged final states (including those with neutral vees) and a large sample of states with $\pi^0$'s. These charm particles allow us to explore charm spectroscopy at a level never before achieved.

As we look towards the future we believe that we are able to increase our yield of charm particles yet another order of magnitude. The increased statistics will allow us to improve many programmatic measurements and push limits or hopefully observe signals on topics which would indicate new physics. We believe our principal competition will be from CLEO and possibly from other fixed target experiments. The cleanliness of our signals and the ability to accurately measure particles' lifetimes make this experiment unique. We believe that we understand the dynamics of photoproduction and the large samples already in hand allow us to predict with confidence what we can achieve. Our goal has been set to obtain a sample of about one million fully reconstructed charm particles, which is one order of magnitude higher than that obtained in the current run of E687.

This document is organized as follows: Section 1 presents the physics motivation for obtaining a very large sample of charm particles; Section 2 presents method for achieving the higher photon fluxes; Section 3 describes the modifications and upgrades to the spectrometer that are needed to handle the higher intensity (this includes a discussion of changes to the detector, data-acquistion system, and trigger); Section 4 describes additional possible upgrades that will

improve the overall efficiency for reconstructing charm decays; Section 5 presents estimates of the computer resources required for offline analysis of this large dataset; Section 6 explains the beam request and running conditions for the experiment. In some cases, in this document, we list several options or possible approaches to a technical problem. It should be noted that each technical problem whose solution is essential for the success of the experiment has at least one solution that will definitely work and that can be implemented at reasonable cost.

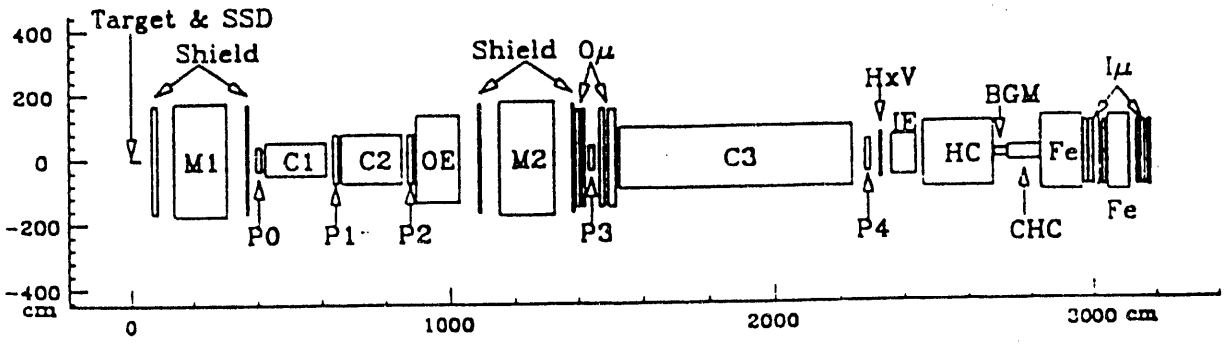


Top View

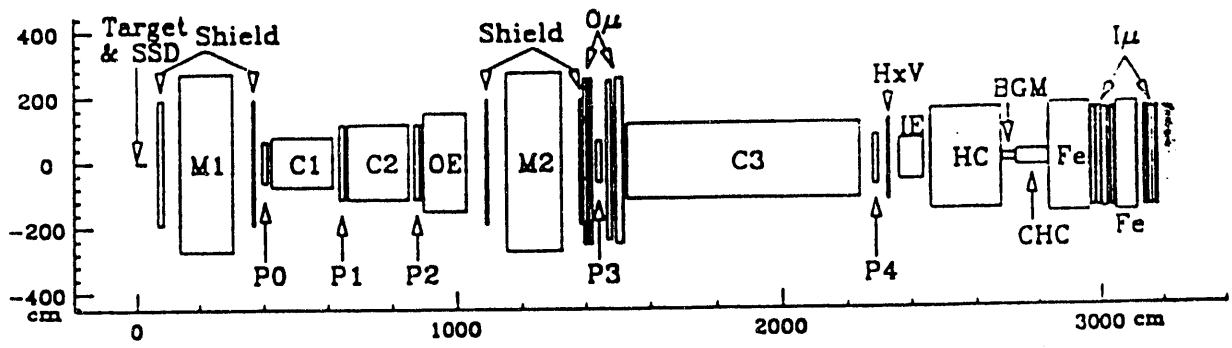


Side View

Figure 1: Schematic representation of E687 spectrometer

# 1 Motivation for a High Luminosity Investigation of Heavy Flavors

The subject of charm spectroscopy is now 15 years old. However, there are still many areas in which our knowledge is rather limited. Information has been accumulated slowly because of the complexity of the final states, the smallness of the cross sections, the small size of the branching fractions, and the large backgrounds. A major goal of the experiment proposed here is to investigate the open issues in the standard model of charm spectroscopy. For example, this experiment is unique in its ability to study charmed baryons, and should be a major contributor to the study of $D^0$-$\bar{D}^0$ mixing and semileptonic decays. These and other "programmatic" studies are discussed below. We also list areas where it is possible to search for new physics, beyond the standard model. These searches will emerge as a by-product of the programmatic investigations and will be referred to, following I. Bigi[1], as High Impact Physics studies.

## 1.1 Programmatic Investigations of Charm

### 1.1.1 $D^0$-$\bar{D}^0$ Mixing and Doubly-Suppressed Cabibbo Decays

In the Standard Model, the classic mechanism for mixing is the box-diagram. Predictions for $D^0$-$\bar{D}^0$ mixing are tiny[2], of order $10^{-6}$, and would be unobservable by any existing or projected experiment. However, it has been observed that, for the charm quark, the box-diagram that contributes most involves light quarks — s and d. As a result, long distance effects could be important, and final state interactions may have to be taken into account[3]. A recent calculation, which maintains a relatively close contact with existing measurements, predicts a mixing parameter r of $5 \times 10^{-3}$[4]. Mixing at this level will be measureable in the proposed experiment.

$D^0$-$\bar{D}^0$ Mixing is studied in the experiment by examining the ratio

$$r = \frac{(D^{*+} \rightarrow D^0\pi^+ \rightarrow (K^+\pi^-)\pi^+}{(D^{*+} \rightarrow D^0\pi^+ \rightarrow (K^-\pi^+)\pi^+} = \frac{WS}{RS} \tag{1}$$

in absence of all backgrounds we can parameterize the right sign,(RS), and the wrong sign, (WS), signals as

$$RS(t) = n\ f(t)\ \frac{e^{-t/\tau_D}}{\tau_D} \tag{2}$$

and

$$WS(t) \approx r\ n\ f(t)\frac{t^2 e^{-t/\tau_D}}{2\tau_D^3} + DCSD\ f(t)\frac{e^{-t/\tau_D}}{\tau_D} \tag{3}$$

where $f(t)$ is a Monte Carlo efficiency correction as a function of t, n is the number of right sign events, and $\tau_D$ is the lifetime of the $D^0$ meson.

Using data from the 1988 run and a portion of the 1990 run E687 has obtained a limit of $r < 0.0034$ at 90% CL. This is slightly better than the previous limit of E691. Presuming that we are able to understand the backgrounds the limit could be lowered to at least $r < 0.001$ at 90% CL using the existing E687 data. With this experiment we would certainly improve the World Limit another factor of $\sqrt{10}$ and it might be possible to achieve a factor of 10 or even observe mixing. Our sensitivity should be below the theoretical limit mentioned above[4] of 0.0005.

The associated topic of doubly-suppressed Cabibbo decays will also be addressed. These decays have branching fractions relative to the allowed decays of $tan^4(\theta_c)$ and should occur at roughly the $0.25 \times 10^{-3}$ level. E691 recently published a possible observation of the doubly-suppressed decay $D^+ \rightarrow \phi K^+$. If this is a real signal, then E687 should have possibly 50 such decays and this experiment should have several hundred decays. In E687 we have also searched for a doubly-supressed decay of $D^+ \rightarrow K^+\pi^-\pi^+$ obtained a limit of $\frac{\Gamma(D^+ \rightarrow K^+\pi^-\pi^+)}{\Gamma(D^+ \rightarrow K^-\pi^+\pi^+)} < 0.01$ at the 90%CL. The best previous limit is from Mark I and is 5 times larger. This experiment should observe several doubly-suppressed Cabbibo decay channels.

### 1.1.2 Semileptonic Decays

Semileptonic decays are interesting because they are easier to interpret theoretically than hadronic decays. There are several important measurements to be made. From measurements of semileptonic branching ratios, the proposed experiment could determine the CKM matrix element $|V_{cs}|$ to 2% and the ratio of elements $|V_{cs}|/|V_{cd}|$ to 4%. In fact, the measurements of this experiment are likely to be limited by theoretical and systematic errors. The form factors for the $D^0$, $D^+$, and the $D_s^+$ mesons will be determined. An interesting theoretical advance by Isgur and Wise[5] shows that measurements of charm form factors can be used to predict beauty form factors. The polarization of the W in $D^0$, $D^+$, and $D_s^+$ decays will be measured, and interference effects, such as those between the $K^*(890)$ and $K^*(1440)$, will also be investigated. Finally, it will be possible to study the semileptonic decays of charm baryons.

The accuracy to which such determinations of the weak mixing parameters can be made depends on the correctness of the theoretical models used to calculate weak current mixing elements. These models will be improved as better data becomes available. In a recent review article[6] of charm mesons the largest deviation from the Standard Model was claimed to be the ratio of $D \rightarrow K^*e^+\nu$ to $D \rightarrow Ke^+\nu$. The accuracy of course also depends on the experimental statistical and systematic errors.

First we address the issue of how well the CKM, $|V_{cs}|$ and $|V_{cd}|$ can be determined through the decays of charm particles. Historically, $|V_{cd}|$, has been obtained from neutrino and anti-neutrino measurements off valence $d$ quarks. The best measurement[7] determines $|V_{cd}| = 0.21 \pm 0.03$. This measurement is

Table 1: Selected Semileptonic Decays

| Mode | Branch Ratio (%) | Exp. |
|---|---|---|
| $D^0 \to e^+X$ | 7.5±1.1±0.4 | MkIII[9] |
| $D^+ \to e^+X$ | 17.0±1.9±0.7 | MkIII[9] |
| $D^0 \to K^-e^+\nu_e$ | 3.8±0.5±0.6 | E691[13] |
| | 3.4±0.5±0.4 | MkIII[10] |
| | 3.8±0.3±0.6 | CLEO[12] |
| | 3.9±0.2±0.7 | ARGUS[6] |
| $D^0 \to K^-\mu^+\nu_\mu$ | 2.5±0.4±0.5 | E653[11] |
| $D^0 \to \pi^-e^+\nu_e$ | $0.39^{+0.23}_{-0.11}\pm0.04$ | MkIII[9] |

Table 2: Number of $D^0$ Reconstructed Decays

| Decay Channel | Br | Events | CKM Element |
|---|---|---|---|
| $K^-l^+\nu$ | 0.034 | 10,000 | $\|V_{cs}\|$ |
| $\pi^-l^+\nu$ | 0.004 | 1200 | $\|V_{cd}\|$ |
| $K^{*-}l^+\nu$ | 0.06 | 1000 | $\|V_{cs}\|$ |
| $\rho^-l^+\nu$ | 0.004 | 600 | $\|V_{cd}\|$ |

dependent on the production cross section for $D^0$ and $D^+$ charm mesons. The measurement is further dependent on the semileptonic branching ratios and the fragmentation function of each charm particle.

Table 1 lists some of the semileptonic decay channels which have been detected. The inclusive D measurements are determined by Mark III[9]. The result from E653[11] uses an inclusive branching fraction of $D^0 \to e^+X = 7.7\pm1.1\%$ and a $D^0$ lifetime measurement of $(4.28\pm0.11)\times10^{-13}$sec. As can be seen there is much work to be done.

In table 2 we present the estimated number of events we will accumulate in this experiment.

In figure 2 we present a signal for $D^0 \to K^-\mu\nu$ from a partial sample of E687 data. It is clear that a remarkably clean signal is observed. E687 measures the ratio $\Gamma(D^0 \to K^-e^+\nu_e)/\Gamma(D^0 \to K^-\pi^+)$ and could use the Mark III branching fraction[9] of $B(D^0 \to K^-\pi^+) = (4.2\pm0.4\pm0.4)\%$ to obtain their measurement of the absolute branching fraction. In addition, the $D^0$ lifetime is used to determine the semileptonic partial rate $\Gamma(D^0 \to K^-e^+\nu_e)$. Finally, the partial width is related to the matrix element and form factor as follows: $\Gamma(D^0 \to K^-e^+\nu_e) = |V_{cs}|^2|f_+(0)|^2 1.82\times\ 10^{10}s^{-1}$. where $|f_+(0)|$ is the form factor evaluated at the four-momentum transfer t equal to zero.

Thus we see that in order to measure matrix element $|V_{cs}|$ to the 2% level, four values need to be determined to better than 2%. First, sufficient number of events must be obtained in the channel $D^0 \to K^-e^+\nu_e$. This factor is accom-

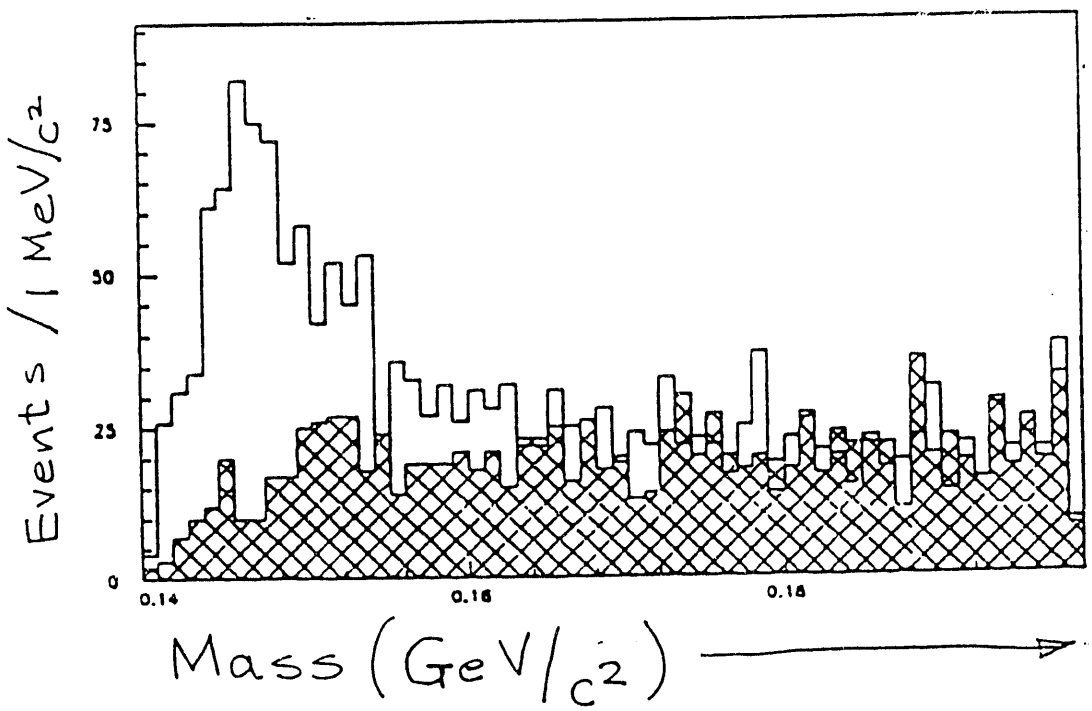


Figure 2 Mass Difference of $D^{*+}$ - $D^0$ with $D^0 \to K^- \mu \nu$. The hatched section of the plot is for wrong sign soft pion events.

plished with 10,000 events. Second, the $D^0$ lifetime needs to be determined to to about the 1% level. This requirement also poses no difficulty as the lifetime is presently measured to 2.5% and E687 will measure it better than 1% by the time this experiment is run. Third, theory is imposed to calculate the form factor. More data can be used to show that the form factor follows a single pole description, but more input from theory is needed here. Fourth, the absolute branching fraction has to be determined to better than 2%. Presently, it is only measured to 10%. A better value is required. E687 will measure the absolute branching fraction to better than 7%. This experiment will attempt to measure the absolute branching fraction to 2%. (See section 1.2.1)

A measurement which is independent of a precise determination of absolute branching fraction is the relative measurement of $RAT$, where $RAT = \Gamma(D^0 \rightarrow \pi^- e^+ \nu_e)/\Gamma(D^0 \rightarrow K^- e^+ \nu_e)$. Hence we can extract

$$|V_{cd}/V_{cs}|^2 = RAT \times (f_+^K(0)/(f_+^\pi(0))^2 \tag{4}$$

The statistical uncertainty is such that the value of RAT will be known to about 4%. The major uncertainty will be how well the form factors can be determined. A significant systematic uncertainty may also be how well the $D^0 \rightarrow \pi^- e^+ \nu_e$ decay can be identified. There is background from $D^0 \rightarrow K^{*-} e^+ \nu_e$ when the $K^0$ is missing and also from $D^0 \rightarrow \rho^- e^+ \nu_e$ when the $\pi^0$ is missing from the $\rho^-$ decay; however both states will be independently measured so that an accurate subtraction is made.

### 1.1.3 $f_D$ – the Pseudoscalar Decay Constant

The simplest of all weak decays are the pure leptonic decays of charmed mesons. The decay probability is in principle well described by the standard model of weak interaction as

$$\Gamma(D^+ \rightarrow l^+ \nu_l) = \frac{G_F^2}{8\pi} f_D^2 \; m_D \; m_l^2 |v_{cd}|^2 (1 - \frac{m_l^2}{m_D^2})^2 \tag{5}$$

If the fully leptonic decay of the $D_s^+$ is calculated, then the $|V_{cs}|$ is substituted for $|V_{cd}|$ and the $D_s^+$ mass is substituted for the $D^+$ mass. In the formula, $G_F$ is the well known fermi coupling constant, $m_D$ is the mass of either the $D^+$ or the $D_s^+$, $m_l$ is the mass of the lepton, and $|V_{cd}|$ & $|V_{cs}|$ are CKM matrix elements. The value $f_D$ describes the effect of the strong interaction on the charm meson-W coupling.

The weak decay constant has been calculated by several theorists with results that $f_D$ is about 200 MeV and and $f_{D_s}$ is slightly larger around 230 MeV. By measuring the leptonic branching fraction and by knowledge of the D meson lifetime and the CKM matrix elements $|V_{cs}|$ and $|V_{cd}|$, the weak decay constants of the D mesons can be determined experimentally. At this time no experimental measurement of the weak decay constants exists; however, MARK III has set an upper limit for $f_D$ of 290 MeV.

Table 3: Calculated Leptonic Branching Fractions

| Decay | Rate ($sec^{-1}$) | Branching Ratio |
|---|---|---|
| $D^+ \rightarrow \tau^+\nu_\tau$ | $8.5\times 10^8$ | $8.8 \times 10^{-4}$ |
| $D^+ \rightarrow \mu^+\nu_\mu$ | $3.3\times 10^8$ | $3.5 \times 10^{-4}$ |
| $D^+ \rightarrow e^+\nu_e$ | $7.6\times 10^3$ | $7.9 \times 10^{-9}$ |
| $D_s^+ \rightarrow \tau^+\nu_\tau$ | $8.6\times 10^{10}$ | $3.8 \times 10^{-2}$ |
| $D_s^+ \rightarrow \mu^+\nu_\mu$ | $9.0\times 10^9$ | $4.0 \times 10^{-3}$ |
| $D_s^+ \rightarrow e^+\nu_e$ | $2.0\times 10^5$ | $9.0 \times 10^{-8}$ |

The table below displays the calculated leptonic decay rate and the expected branching fractions assuming $f_D = 200\ MeV$ and $f_{D_s} = 230\ MeV$, and with $|V_{cd}| = 0.22$ and $|V_{cs}| = 0.97$. The April 1990 Particle Data Book lifetime values for the $D^+$ and $D_s^+$ are used to compute the branching ratio values.

Due to the V-A structure of the weak interaction, the electron decay of the D mesons is very small. The muon decay channel is also helicity suppressed relative to the $\tau$ decay, but due to the limited available phase space it is not suppressed by as much as one might have guessed. It is also worth noting that the $D_s^+ \rightarrow \tau\nu_\tau$ branching ratio is 40 times larger the same mode for the $D^+$, *but* the $D_s^+ \rightarrow \mu\nu_\mu$ branching ratio is only 10 times larger than that decay channel of the $D^+$. When the relative production of the $D^+$ to the $D_s^+$ is considered, then the fully leptonic decay rate to muons is found to be roughly equal in our experiment for both the $D^+$ and the $D_s^+$. The fully leptonic decay to $\tau$ leptons is still dominated by the $D_s^+$ decays.

From the above discussion it is obvious that in order to measure fully leptonic branching fractions, one has to be able to separate $D^+$ from $D_s^+$ decays.

Since the branching fractions are so small, the background channels have to be carefully examined. Clearly, the largest background contamination to the fully leptonic decays will be from semileptonic decays. In fact, the semileptonic branching fractions are much larger than the fully leptonic branching fractions.

With enough statistics it should be possible to obtain a signal of $D \rightarrow \mu^+\nu_\mu$ inclusively. This would be accomplished by taking all muons and electrons which miss the primary vertex. By subtracting the "missed" electron yield from the "missed" muon yield, there should leave an excess of desired muons. However, because the semileptonic decay rate is 20-200 times larger than the fully leptonic decay rate this is impractical. A much better technique is required.

We have investigated in Monte Carlo the use of the well known $D^{+*} - D^+$ mass difference. Specifically, we use $D^{*+} \rightarrow \pi^0 D^+$ and begin by reconstructing the $\pi^0$ and by identifying a muon which is detached from the primary vertex. By requiring a pizero from the $D* - D$ decay, the $D_s^+$ decays are eliminated. We are presently still studying this channel in the E687 data. We have been investigating 5 variables which aid in isolating $D^+ \rightarrow \mu\nu_\mu$ decay channel. These variables are the energy of the muon, the transverse momentum of the muon

Table 4: $D^{**}$ Status

| State | Channel | Mass | Width | Exp. |
|---|---|---|---|---|
| $D_1(2420)^0$ | $D^{*+}\pi^-$ | 2428±3±2 | 20 | CLEO[18] |
| | | 2414±2±5 | 23 | ARGUS[19] |
| | | 2428±8±5 | 13 | E691[17] |
| $D_J(2440)^+$ | $D^{*0}\pi^+$ | 2443±7±5 | 41 | E691[17] |
| $D_2(2460)^0$ | $D^{*+}\pi^-$ | 2461±3±1 | 20 | CLEO[18] |
| | | 2455±3±5 | 15 | ARGUS[20] |
| | | 2459±3±2 | 20 | E691[17] |
| $D_J(2470)^+$ | $D^0\pi^+$ | 2469±4±6 | 23 | ARGUS[21] |
| $D_{s1}(2536)^+$ | $D^{*+}K^0$ | 2536.6±0.7±0.4 | <5.44 | CLEO[18] |
| | | 2435.9±0.9±5 | < 4.6 | ARGUS[22] |

with respect to the beam direction, the transverse momentum of the muon with respect to the $\pi^0$ direction, the impact parameter of the muon at the primary vertex, and finally the reconstructed energy of the D divided by the pion energy.

It would be premature to make a prediction of how many events we might observe, but it is likely that we will produce on order 10,000 $D^+ \rightarrow \mu\nu_\mu$ decays.

### 1.1.4 $D^{**}$ Spectroscopy

Here the effort would be to study and identify all $D^{**}$ (P wave )states and to categorize the states. As the total spin can be 0 or 1, this leads to the possible states $^3P_2$,$^3P_1$,$^1P_1$, and $^3P_0$. The parities of the states are all positive oweing to the odd angular momentum. The decays one studies are $D^*\pi$ and $D\pi$.

The $D_s^{**}$ states will also be interesting and will be investigated. At the present time the $D^{**}$ spectroscopy needs new data. The World data is presented in Table 4.

The Particle Data Group(PDG) reports that the spin and parity of all these states need confirmation. The states at a mass of 2440 MeV/$c^2$ and 2470 MeV/$c^2$ have been omitted from the PDG summary table as too weak. Much more work is needed in pinning down the L=1 charm states. With one order of magnitude more data, this experiment should significant contributions.

### 1.1.5 Baryon Spectroscopy and Lifetimes

The observation of charmed baryons requires large statistics and good particle identification. In addition the experiment must have excellent ability to reconstruct hyperons. The proposed experiment will be unique in its abilites to study charmed baryon spectroscopy and decay.

At present, E687 has reconstructed many different decay channels of the $\Lambda_c^+$. Some of these channels are displayed in figures 3-5. Charmed meson decays

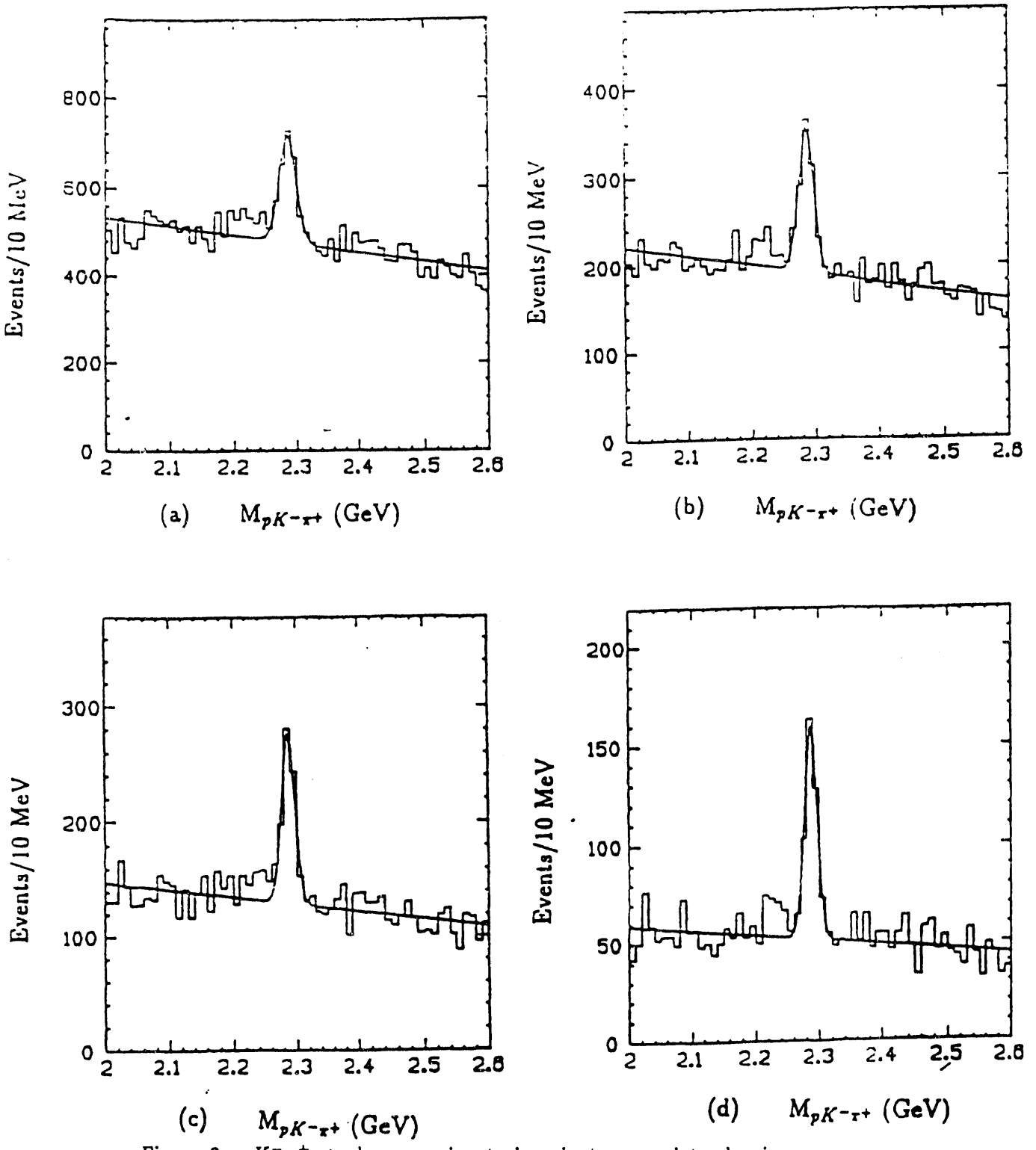


Figure 3: $pK^-\pi^+$ + charge conjugate invariant mass plots showing reconstructed $\Lambda_c^+$'s for different vertexing cuts. (a) $L/\sigma_L$ >4 (no other vertexing cuts), 927±72 fitted events (b) $L/\sigma_L$ >6 (no other vertexing cuts), 665±53 fitted events (c) $L/\sigma_L$ >4 and isolation cuts, 424±36 fitted events (d) $L/\sigma_L$ >6 and isolation cuts, 344±28 fitted events.

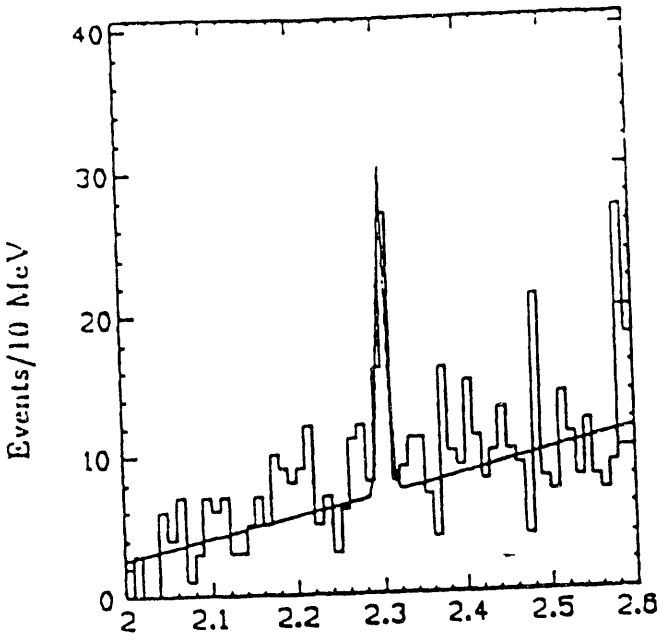


(a) $M(pK^-\pi^+\pi^0)$ (GeV)

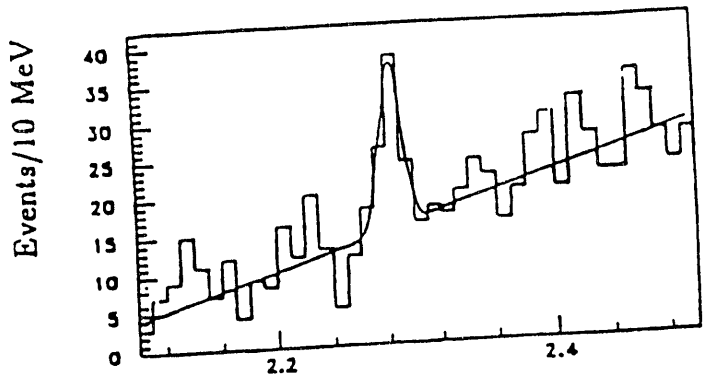


(b) $M(p\pi^+\pi^-\pi^+\pi^-)$ (GeV)

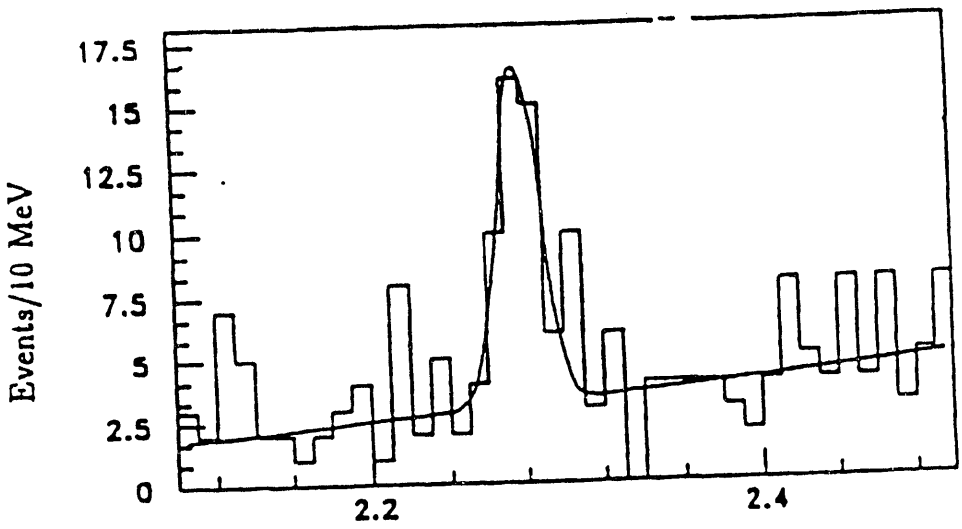


(c) $M(pK^-K^+)$ (GeV)

Figure 4: (a) $pK^-\pi^+\pi^0$ + c.c. invariant mass showing reconstructed $\Lambda_c^+$'s, the $\pi^0$'s were reconstructed in the Inner Electromagnetic Calorimeter and the two photon invariant mass was requirede to be within ±35 MeV of the $\pi^0$ mass. (b) $p\pi^+\pi^+\pi^-\pi^-$ + c.c. invariant mass showing reconstructed $\Lambda_c^+$'s (c) $pK^-K^+$ + c.c. invariant mass.

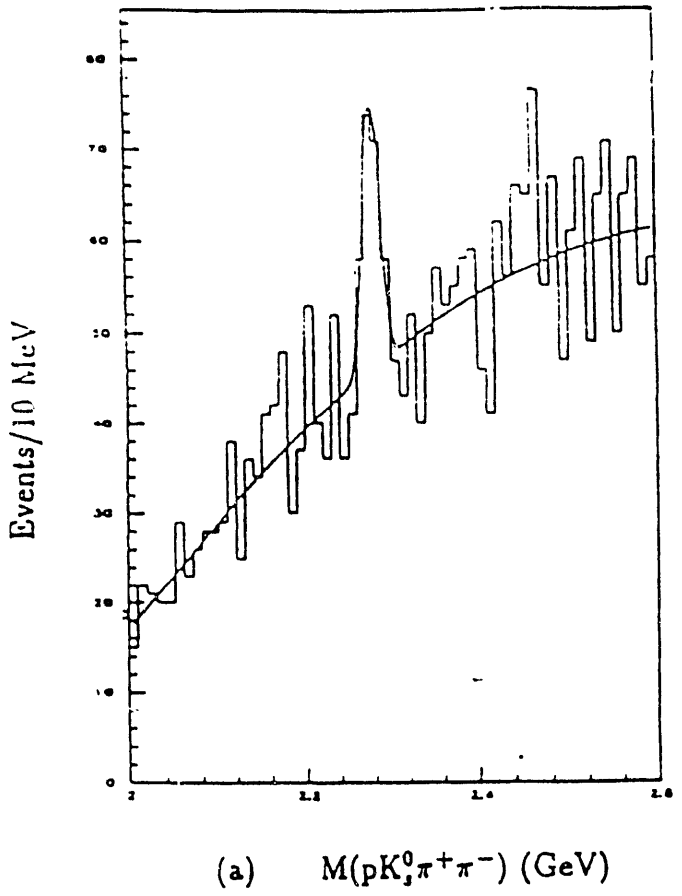


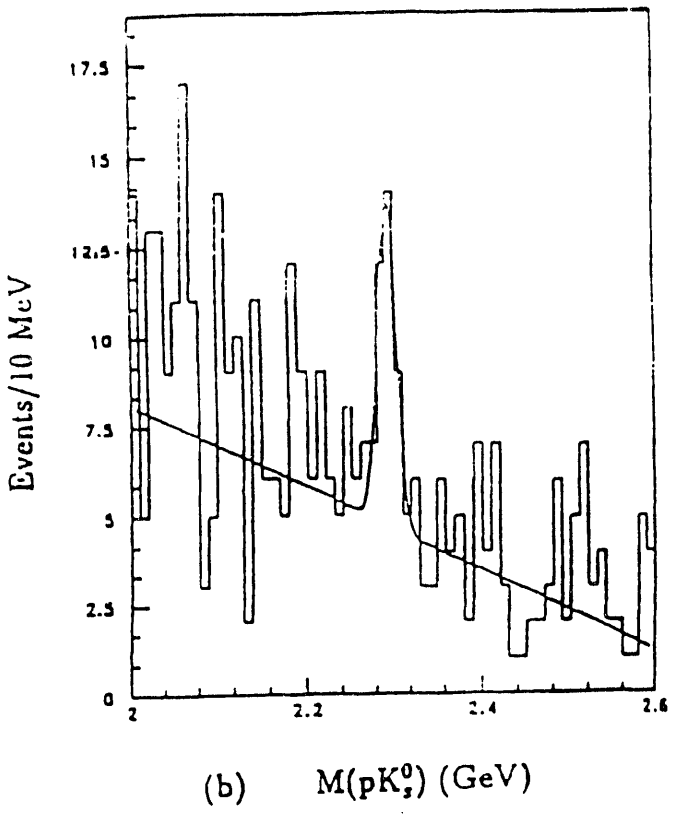


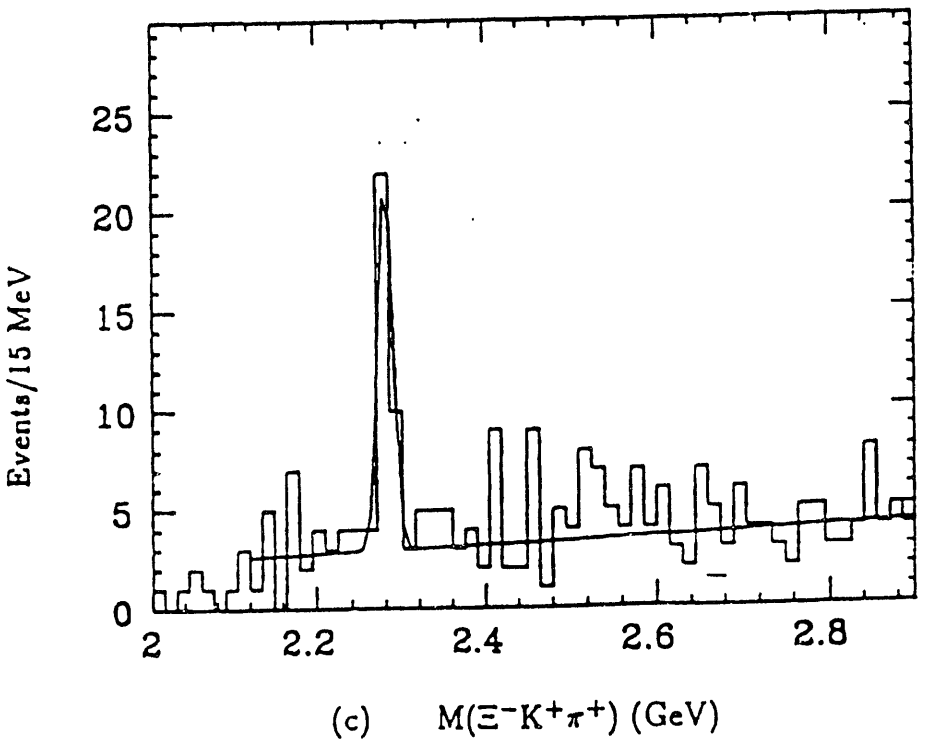


Figure 5: (a) pK$^0_s\pi^+\pi^-$ + c.c invariant mass showing reconstructed $\Lambda_c^+$'s. (b) pK$^0_s$ + c.c. invariant mass (c) $\Xi^-K^+\pi^+$ + c.c. invariant mass.

Table 5: Predicted yields of charmed baryons

| State | Decay | Estimated Events |
|---|---|---|
| $\Lambda_c$(cud) | p-k-$\pi$ | 10,000 |
| $\Sigma_c$(cuu) | add $\pi^+$ | 150 |
| $\Sigma_c$(cdd) | add $\pi^-$ | 300 |
| $\Xi_c$(csu) | $\Xi^-\pi^+\pi^+$ | 1,000 |
| $\Xi_c$(csd) | $\Xi^-\pi^+$ | 400 |
| $\Omega_c$(css) | $\Omega^-\pi^+$ | 200 |

appear to proceed mostly via two-body decays. From the limited information on charm baryon decays this does not appear to be the case. Scaling from last run where we have reconstructed more than 1000 pK$\pi$ $\Lambda_c^+$ decays, it is expected that 10,000 $\Lambda_c^+$ decays can be obtained from this proposed run and maybe a few hundred p-$\pi$ – $\pi$ and p-K-K events. The experiment should also start to examine the semileptonic decays of the $\Lambda_c^+$.

Another issue is the relative lifetimes of charmed baryons. The lifetime of the $\Lambda_c^+$ is much shorter than the lifetime of charmed mesons. This is presumably due to the fact that the decays proceed principally via the $W^+$ exchange diagram, since for baryons this diagram is neither helicity nor color suppressed. There are two lifetime predictions[23] that differ on whether the $\Lambda_c^+$ lifetime is less than or greater than the $\Xi_c$ and the $\Omega_c$. Reliable estimates for the number of reconstructed events we would obtain for these states are possible because we are already observing the states in E687. Figure 6 shows the $\Xi_c^0$ mass plot of the invariant mass of $\Xi^-\pi^+$ while Figure 7 displays 3 decay channels of the $\Xi_c^+$. Lastly Figure 8 presents a mass plot of $\Omega^-\pi^+$ which is consistent with the expected mass of the $\Omega_c^0$. It is surprising that E687 has observed the $\Omega_c^0$, however due to excellent hyperon reconstruction the state is seen without requiring a separation from the primary vertex.

It seems likely that the lifetimes for many of these states will be short enough that our resolution will not be able to accurately ($\pm$ 10%) determine the states lifetime. An order of magnitude more data will allow a much more accurate measurement which will put important constraints on models.

In addition to just measuring lifetimes and masses of these charm baryons the experiment will search for excited baryons which decay hadronically to these ground state baryons. We expect to observe excited charm baryons as well as possible decays of doubly charmed baryons. In table 5 we estimate the predicted yields of charm baryons to be observed in this experiment.

From the table it seems that the experiment will make a major contribution in addressing baryon lifetime questions and in determining the baryon mass spectra.

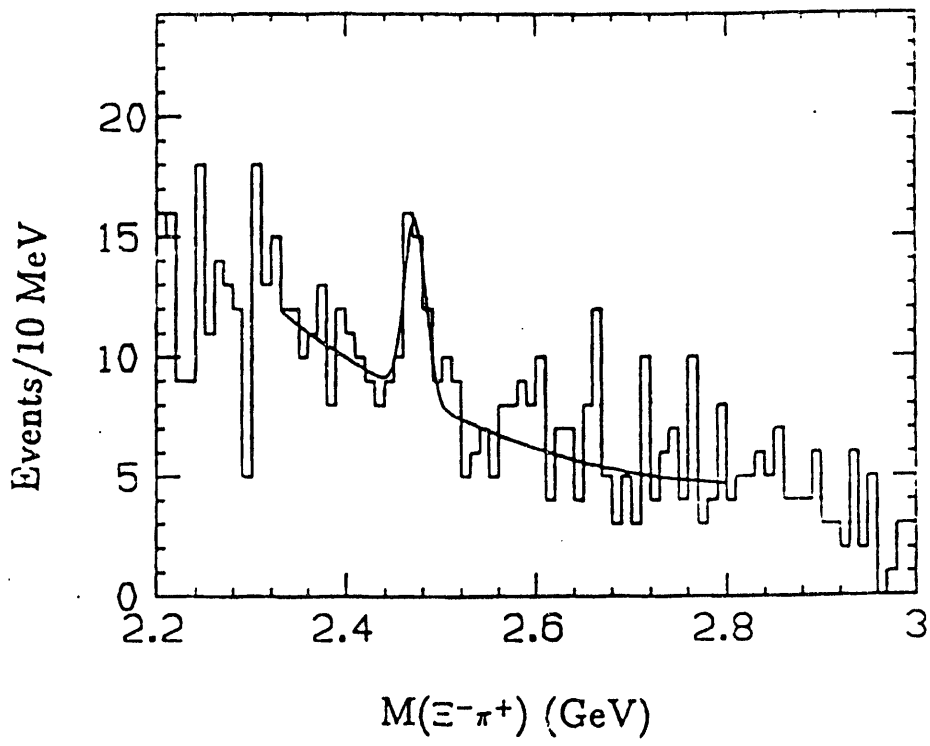


Figure 6: $\Xi^-\pi^+$ + c.c. invariant mass showing reconstructed $\Xi_c^0$'s.

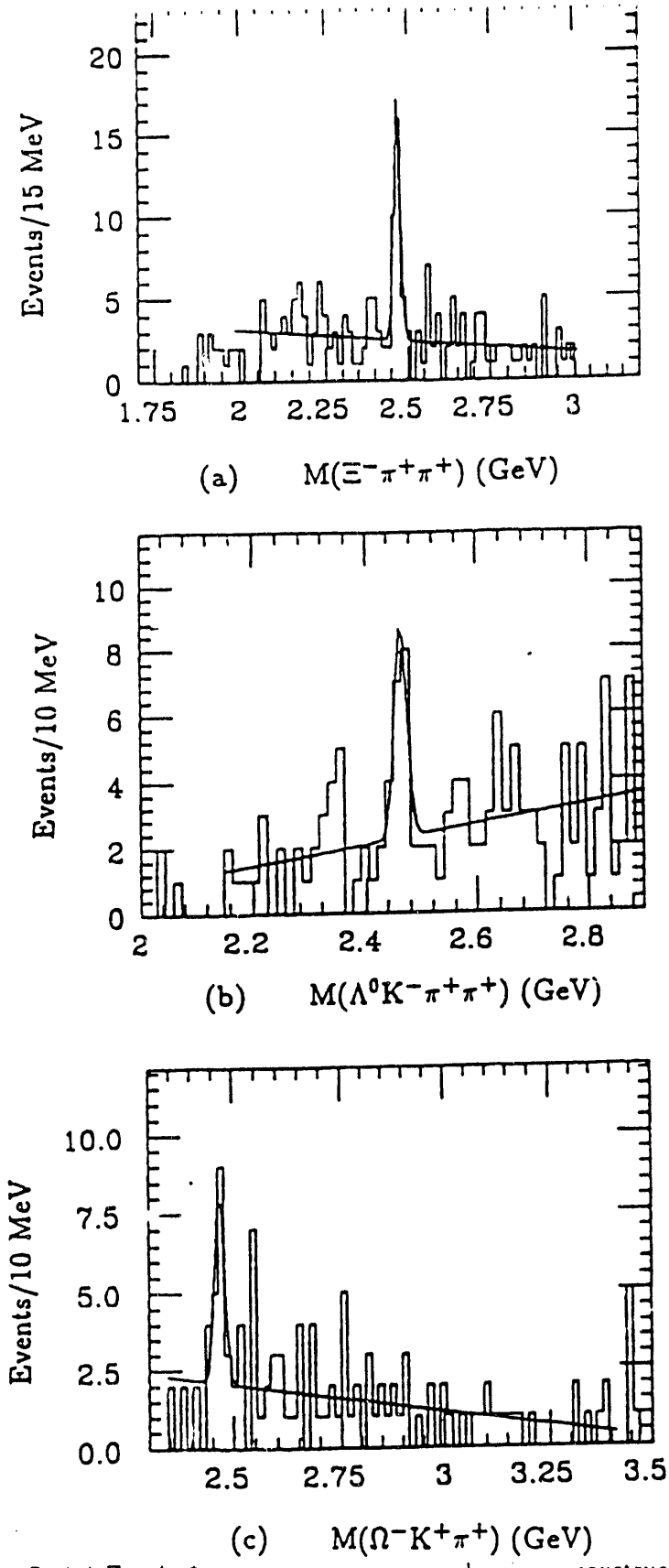


Figure 7. (a) $\Xi^-\pi^+\pi^+$ + c.c. invariant mass showing reconstructed $\Xi_c^+$'s. (b) $\Lambda^0K^-\pi^+\pi^+$ + c.c. invariant mass showing reconstructed $\Xi_c^+$'s. (c) $\Omega^-K^+\pi^+$ + c.c. invariant mass showing reconstructed $\Xi_c^+$'s.

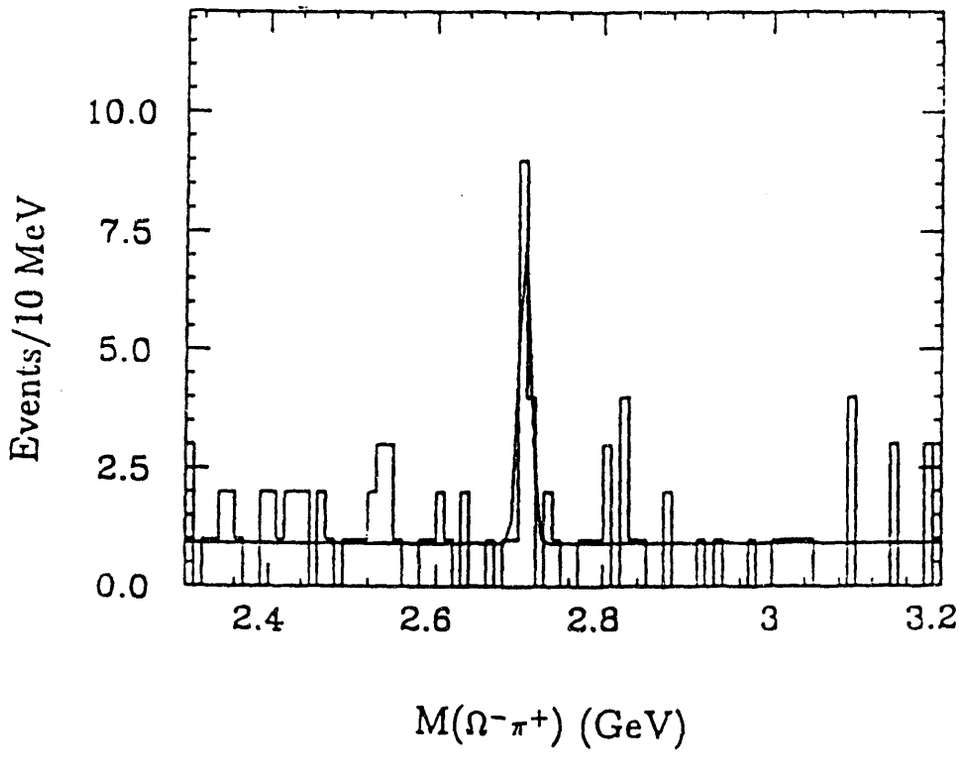


Figure 8: $\Omega^-\pi^+$ + c.c invariant mass showing reconstructed $\Omega_c^0$'s.

### 1.1.6 Charm Photoproduction Dynamics

Although this experiment emphasizes the study of charm decay processes, there is a great deal of interesting charm photoproduction physics which we can address with our anticipated yield of 1 million fully reconstructed charm events. We are particularly excited about the possibilities of making detailed studies of charm photoproduction using events with 2 fully reconstructed charm particles. The physics emphasis of such studies would include:

- Tests of charm particle species correlations. For example, how often are baryon-antibaryon pairs produced? Are $D_s^+$ mesons made with associated $D^0$ mesons and kaons or are they usually made as $D_s$ - $\bar{D}_s$ pairs? What additional particles are created at the charm primary vertex?

- Tests of Charm dressing and gluon radiation phenomena. In the absence of dressing and/or gluon radiation effects photoproduced charm mesons will carry essentially all of the photon lab energy and will be fully acoplanar (back to back transversely) with the incident photon. Measurements of the charm-$\overline{\text{charm}}$ acoplanarity and fraction of the incident photon energy carried by charm-$\overline{\text{charm}}$ pair serves as a direct measurement of dressing and gluon radiation effects which can be compared to theory and standard Monte Carlo simulations such as LUND. The theoretical acoplanarity distribution due to multigluon radiation has been computed[26] for the case of charm hadroproduction.

- Tests of the validity of the photon gluon fusion model. A powerful test of this model involves measurement of the angular distribution between the charm particle and the photon in the charm-$\overline{\text{charm}}$ center of mass. This distribution is expected to become more forward-backward peaked with increasing charm-$\overline{\text{charm}}$ mass as $t$ and $u$ channel poles of the underlying partonic matrix element approach realization.

- Measurement of the gluon structure function of the nucleon. In the photon-gluon fusion model, the cross section for charm photoproduction is directly proportional to the gluon structure function $g(x)$ rather than a convolution over two structure functions as is the case in hadroproduction. The gluon structure of the nucleon controls $x$ distribution of charm event where $x$ is square of charm-$\overline{\text{charm}}$ mass divided by the overall center-of-mass energy. We anticipate making direct measurements of $g(x)$ over the range $0.03 < x < 0.25$.

Using about 1/2 of the E687 data set, we have recently[27] obtained a very clean sample of 200 events with two fully reconstructed $D$'s decaying into the final states $D^o \rightarrow K^-\pi^+$ , $K^-\pi^+\pi^+\pi^-$ and $D^+ \rightarrow K^-\pi^+\pi^+$ final states. This sample is about an order of magnitude larger than previous published of fully reconstructed, photoproduced $D\overline{D}$ events[28] In the next experiment we

anticipate a 5000 event sample. The $D\overline{D}$ signal and some of its properties which bear on charm production dynamics are illustrated in Figure 9. This signal has been augmented with a 2000 event sample obtained from 1/2 of the E687 data set where a fully reconstructed $D$ was found recoiling against a kinematically isolated $\pi$ from the process $D^o \rightarrow \pi D$. This sample allows one to perform many of the same production dynamics studies as the fully reconstructed $D\overline{D}$ sample since the kinematically isolated $\pi$'s momentum can be suitably scaled up to provide an accurate estimate of its parent $D^{*+}$ momenta.

## 1.2 High Impact Physics

### 1.2.1 Absolute Branching Ratios

We believe that it will be possible to obtain competitive measurements of absolute charm branching ratios in this experiment using the decay $D^{*+} \rightarrow \tilde{\pi}^+ D^o$ where presence of a photoproduced $D^o$ can be inferred by kinematically tagging the decay pion (which we will call the $\tilde{\pi}$). The fraction of times that a $\tilde{\pi}$ tagged $D^o$ is observed to decay into a given final state serves to measure its absolute branching ratio.

The $D^{*+} \rightarrow \pi^+ D^o$ tagging technique exploits a $P_t$ and charge-charm correlation between the $D^{*+}$ decay pion and the recoiling, anti-charmed particle. Because of the low Q value for the process $D^{*+} \rightarrow \pi^+ D^o$, the decay pion will have a lab momentum nearly collinear with the parent $D^{*+}$ but diminished by roughly the ratio of the pion mass over the mass of the $D^{*+}$ or a factor of about 1/13.8[24]. Because the $P_t$'s of photoproduced charmed and anticharmed particles are expected and observed[25] to balance to within few GeV, one expects that true $\tilde{\pi}$'s should cluster at small values of

$$\Delta_x = 13.8 P_x^{(\tilde{\pi})} + P_x^{(r)} \quad \text{and} \quad \Delta_y = 13.8 P_y^{(\tilde{\pi})} + P_y^{(r)}$$

relative to the $\vec{P}^{(r)}$ momentum carried by the observed, recoil anti-charmed particle.

We have searched for the expected $\tilde{\pi}$ correlation in our 1990 data where we have use a large, clean sample of reconstructed recoil charm candidates (See Fig. 10) decaying via: $D^o \rightarrow K^-\pi^+$ & $K^-\pi^+\pi^-\pi^+$ and $D^+ \rightarrow K^-\pi^+\pi^+$. Because of their ease of reconstruction, low background contamination, and relatively large branching ratio's, we will call these *golden* mode charm decays.

We look for $\tilde{\pi}$ events among those tracks which are in the primary vertex[29] for the events with a reconstructed charm particle. The recoil charm particle must lie within $2\sigma$ of its nominal mass. Equal width (normalized) mass sidebands are used to subtract recoil charm background. Figure 10 is shows $\Delta_x$ distribution for those primary vertex tracks subjected to the cut $\Delta_y < 1$ GeV. The points joined by the upper solid curve correspond to "right sign" tracks which have an electrical charge equal and opposite to the charm of the recoil charm particle. The point joined by the dashed curve correspond to "wrong

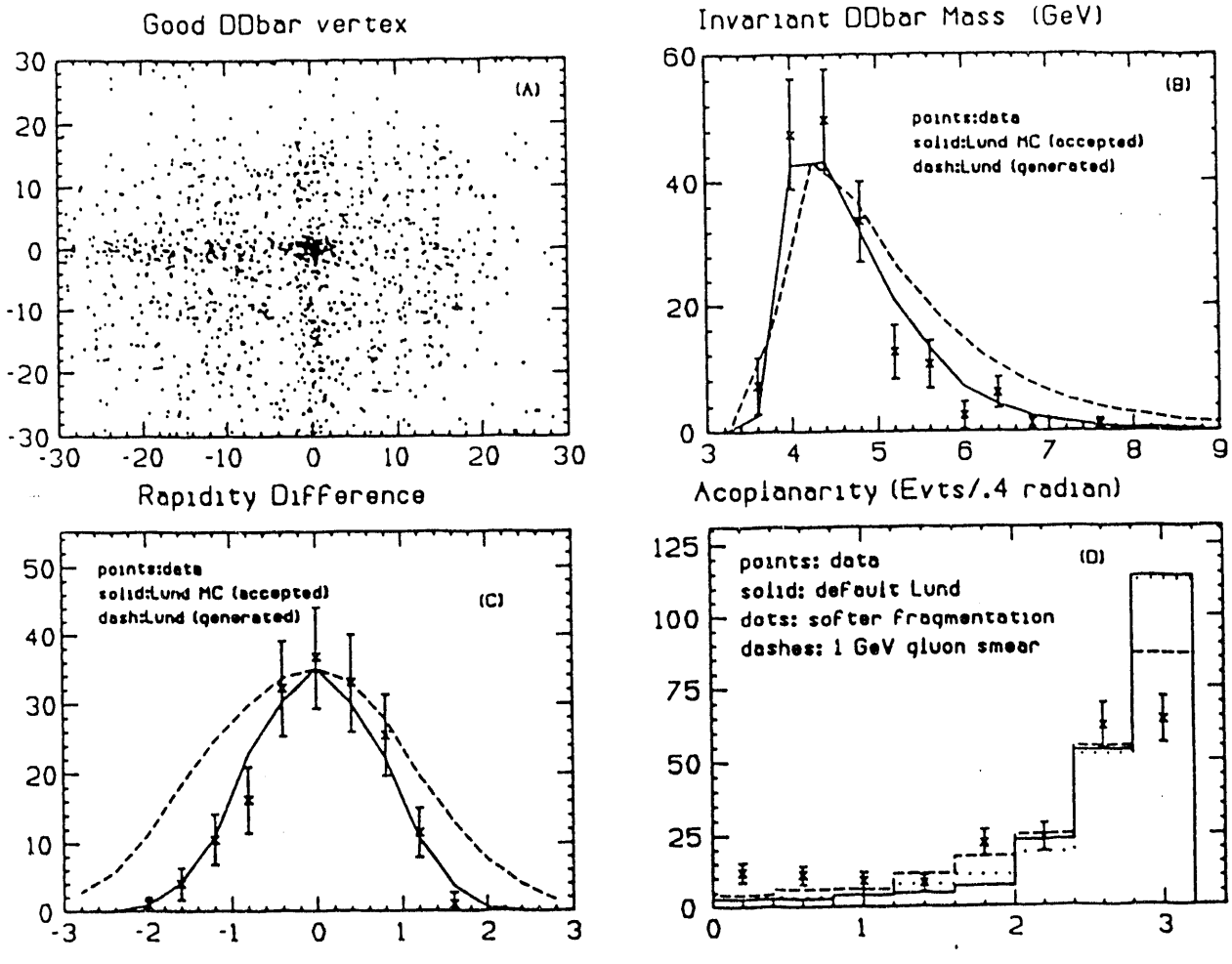


Figure 9: (a) Scatter plot of the normalized mass of detached $D$ candidate versus the normalized mass of the detached, recoil $\overline{D}$ candidate where the recoil D is required to intersect the plotted $D$ with an acceptable vertex confidence level. (b) The background subtracted invariant mass of the $D\overline{D}$ pair compared to the Monte Carlo (solid curve). (c) Rapidity difference ($Y_D - Y_{\overline{D}}$) distribution between the reconstructed $D$ and $\overline{D}$. The distribution is background subtracted and compared to the solid curve computed using the Monte Carlo. (The dashed curves in figures (b-c) represent generated distributions without acceptance effects.) (d) Background subtracted acoplanarity distribution compared to the Monte Carlo (solid curve). The acoplanarity (in radians) is the angle between the plane containing the $D$ momentum and the incident photon and the plane containing the $\overline{D}$ momentum and the incident photon. Several different choices of Monte Carlo parameters are compared.

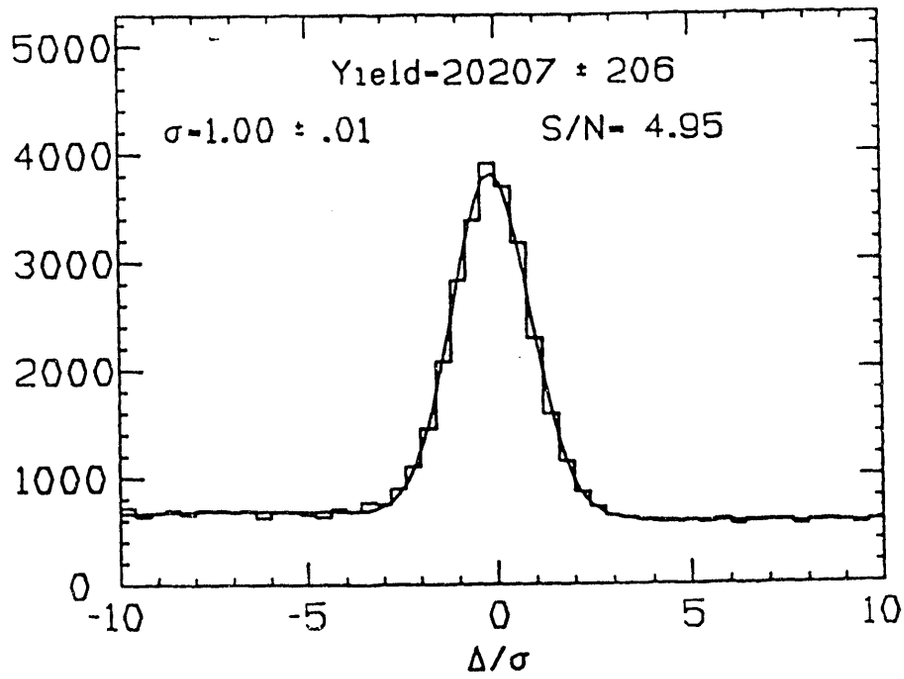


Figure 10: Normalized mass distributions(in measurement standard deviations away from nominal value, $\Delta M/\sigma$) for $D^+ \to K^-\pi^+\pi^+$, $D^0 \to K^-\pi^+$, $D^0 \to K^-\pi^+\pi^+\pi^-$, candidates obtained in the 1990 run of E687 subject to topology dependent vertex detachment cuts ranging from 1 to 10 standard deviations as well as vertex isolation cuts. A signal of 20000 events is observed with a signal to noise of about 5 to 1 and a Gaussian RMS normalized width consistent with unity.

sign" tracks. A clear excess of right sign over wrong sign tracks is observed at $\Delta_z \approx 0$.

Figure 11 compares subtracted distributions of the variable $\Delta_t^2 \equiv \Delta_x^2 + \Delta_y^2$ for tracks in the primary vertex against a recoil charm particle. The upper points are right sign tracks, the lower points are wrong sign tracks. The two curves (right sign solid, wrong sign dashed) are simulated LUND - Pythia - Jetset Monte Carlo[27] $\Delta_t^2$ distributions normalized to the same number number of inclusive $D$'s shown in Figure 10. There is reasonable agreement between the absolutely normalized Monte Carlo and data in both the anticipated level and shape of the wrong sign $\tilde{\pi}$ background. The $\Delta_t^2$ distribution for right sign $\tilde{\pi}$ tracks is somewhat broader in data than in Monte Carlo. This effect is also observed in Figure 12 for the $|\vec{P}_t|$ distribution in fully reconstructed $D$- $\overline{D}$ events. Presumably the real world has somewhat more severe dressing effects than those simulated in Monte Carlo.

The general agreement between data and Monte Carlo helps bolster the case that the $\tilde{\pi}$ events are indeed tags for $D^{*+}$ and can be used to provide absolute neutral $D$ branching ratios.

Since the $\tilde{\pi}$ sample is observed to be 10 % of the inclusive $D$ sample, P831 should produce a huge ($\approx$ 50000 event) $\tilde{\pi}$ sample which can be used to study tagging systematics and backgrounds. The primary source of error on absolute branching ratio measurement using the soft pion technique will be statistical. The soft pion technique requires that both the charm and anti-charm particle in a given event are fully reconstructed. The reduced acceptance from requiring 2 $D$'s and additional branching ratios will result in a considerably smaller expected $D$ - $\overline{D}$ sample than that for either the $\tilde{\pi}$ or inclusive golden mode $D$ sample. Because, the relative branching ratio of the different $D^o$ golden modes will be measured to high statistical precision from the very copious inclusive sample, the fractional error common to each absolute branching ratio will be the fractional error on the total number of golden mode $D$ $\overline{D}$ events of events of the form: $\overline{D}D^{*+} \rightarrow \overline{D}(\pi^+ D^o)$. We can estimate this number using our experience with E687.

In the 1990 data of E687, we observed a yield of 200 reconstructed $D - \overline{D}$ events into the three golden decay modes $K^-\pi^+\pi^+$ , $K^-\pi^+$ and $K^-\pi^+\pi^+\pi^-$. Scaling up by the anticipated luminosity for P831 we expect a 5000 event sample with both a reconstructed golden mode $D$ and $\overline{D}$. About 62 % of these events will have a clean golden mode $D^o$ recoiling against a golden mode $D^o$ or $D^+$. About 20 % of the events with a golden mode $D^o$ will actually originate from $D^{*+} \rightarrow \pi^+ D^o$ decay[30] with an accepted, reconstructible $\pi^+$. Hence about 620 events or 13 % of the 5000 event total $D$ - $\overline{D}$ golden mode sample is usable for purposes of measuring absolute neutral $D$ branching ratios which implies a 4 % fractional error on absolute $D$ branching ratios where only the three golden modes are considered.

The inclusion of additional decay modes will of course further reduce the fractional error below the projected 4 % estimate from P831 using just the golden

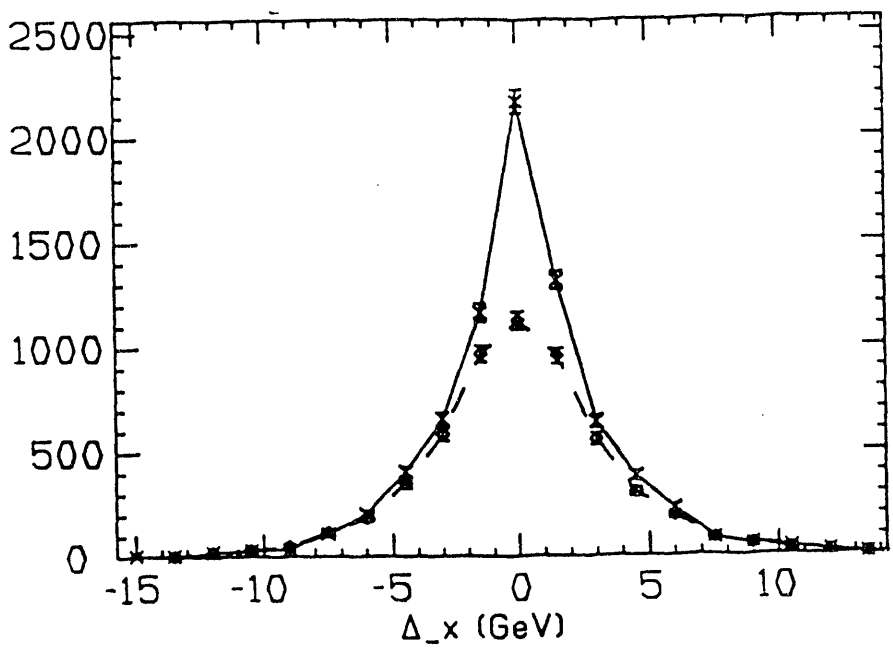


Figure 11: Background subtracted $\Delta_x$ distribution for primary vertex tracks satisfying the cut $\Delta_r < 1$ GeV. The upper solid curve is for (right sign) tracks with a charge not equal to the recoil charm; the lower dashed curve is for (wrong sign) tracks. A clear excess of right sign over wrong sign tracks is observed at $\Delta_x$ , $\Delta_y \approx 0$ indicating a strong signal for the $\bar{\pi}$.

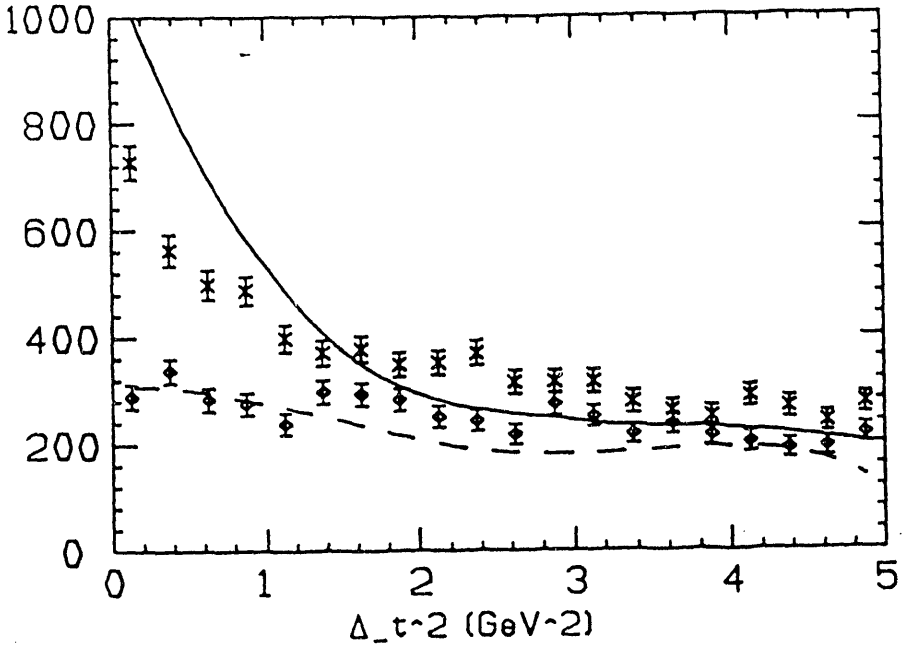


Figure 12: Background subtracted $\Delta_t^2$ distribution for primary vertex tracks. The upper curve (x's) are for right sign tracks. The lower curve (diamonds) are for wrong sign tracks. The upper solid curve is from an absolutely normalized Monte Carlo for right sign tracks; the lower curve is an absolutely normalized Monte Carlo for wrong sign tracks. The Monte Carlo predicts a softer $P_t^2$ distribution than the data for $\bar{\pi}$ events but the level of signal and background and background shape is well predicted.

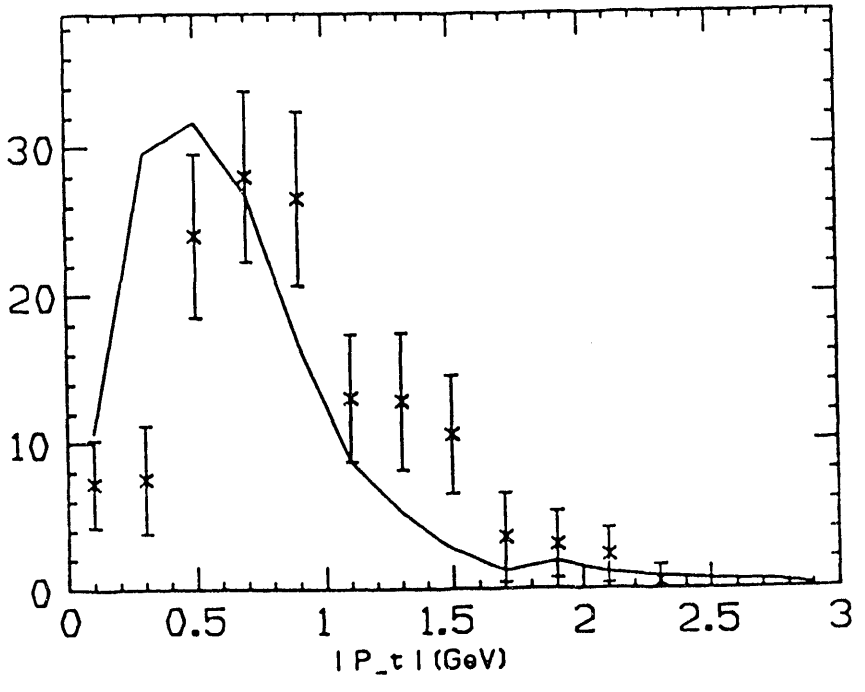


Figure 13 Distribution for $|\vec{P}_t|$ where $\vec{P}_t$ is vector sum of the transverse momenta carried by the $D$ and $\overline{D}$ events in events where both $D$ and $\overline{D}$ are reconstructed into the final states $K\pi$, $K2\pi$ , or $K3\pi$. The data is background subtracted using $D$ and $\overline{D}$ mass sidebands. The solid curve is a LUND Monte Carlo simulation.

modes. We estimate that as much as a factor of two reduction in this fractional error will be possible through the use of additional charm decay modes. Baryon and $D_s^+$ decays can be used along with golden and non-golden $D$ decays to increase the number of $\tilde{\pi}$ tags. The absolute branching for additional, non-golden $D^o$ decays can be included in a global fit (using well measured branching ratios relative to the golden modes) to improve the absolute branching ratio measurement for all neutral $D$ modes. Since the $\tilde{\pi}$ tagging method requires the presence of a $D^*$, a particularly useful class of additional neutral $D$'s are decays into final states with a single missing neutral particle which can be reconstructed exploiting the favorable kinematics of $D^* \rightarrow D^o\pi^+$ decay. Examples include $D^o \rightarrow K^-\pi^+\pi^o$ (with roughly 3× the $K^-\pi^+$ branching ratio) and $D^o \rightarrow K^-\ell^+\nu$ (with a branching roughly equal to that of $K^-\pi^+$ for both the $\mu^+$ and $e^+$ decay). Very clean $D^* - D$ mass difference peak signals can be obtained[31] for these decay modes by using the $D$ flight direction (measured by the line between the primary and secondary vertex) and the $D$ mass constraint to correct for the momentum of the missing neutral.

Using the 1990 data sample of E687, we have demonstrated that it is possible to tag neutral $D$'s by tagging the pion from $D^{*+} \rightarrow D^o\pi^+$ decays. We have also obtained a sample of about 200 fully reconstructed $D$, $\overline{D}$ decays into the three golden modes: $K^-\pi^+$ & $K^-\pi^+\pi^-\pi^+ \& K^-\pi^+\pi^+$. Scaling up our previous results by the anticipated luminosity of P831, we should obtain a fractional error on absolute charm branching ratios of 4 %. We believe that it will be possible to improve this fractional error as much as an additional factor of 2 by considering additional charm species and charm decay modes. We expect to produce a new measurement with complementary systematics which is highly competitive with the existing measurements of charm absolute branching ratios. The present numbers are dominated by recent measurements from ALEPH and older measurements from MarkIII which each have fractional errors on absolute charm branching ratios in the range 12-15%.

### 1.2.2 CP Violation

It has been shown [33] that CP violations in the decay of charm mesons may be significantly enhanced over naive expectactions, without requiring new physics in addition to the standard model. The enhancement is due to strong interactions. The signature for CP violation would be an asymmetry in the decay rate of a Cabibbo suppressed mode and its CP conjugate:

$$\Gamma(D \rightarrow f_{CS}) \neq \Gamma(\overline{D} \rightarrow \bar{f}_{CS}) \tag{6}$$

Cabibbo suppressed modes are required because, in order to exhibit a CP asymmetry, there must be two independent amplitudes that contribute to the same final state. In addition, final state interactions must induce a strong phase shift between the two amplitudes [32] Charm decays are therefore ideal, since they exhibit significant final state interactions. CP violating asymmetries of a few

percent are possible in the standard model [33]. If new physics is introduced into the standard model (extra Higgs multiplets, for example), then asymmetries as large as 10% are possible [32]. This experiment will be sensitive to asymmetries of a few percent in at least two decay modes, and will be sensitive to a 10% asymmetry in at least three modes. In this section, we will first discuss in detail a search for such a decay rate asymmetry, then briefly mention two additional CP violation search strategies.

We will use the following three "high statistics" Cabibbo suppressed decay modes (and their charge conjugates) to search for a CP induced decay rate asymmetry:

$$\begin{aligned} D^+ \to \quad & K^+K^-\pi^+ \text{ (i)} \\ D^{*\mp} \to \pi^+ D^0; \quad & D^0 \to K^+K^- \text{ (ii)} \\ D^{*+} \to \pi^+ D^0; \quad & D^0 \to \pi^+\pi^- \text{ (iii)} \end{aligned} \tag{7}$$

In reactions (ii) and (iii), the sign of the bachelor pion in the $D^*$ decay tags the neutral $D$ as either a $D^0$ or a $\overline{D}^0$. We will refer to these as "$D^*$-tagged" $D^0$ decays.

Consider for the moment reaction (i). If equal numbers of $D^+$ and $D^-$ mesons are produced, then the CP decay rate asymmetry is:

$$\begin{aligned} A_{CP}(KK\pi) &\equiv \frac{\Gamma(D^+\to K^+K^-\pi^+)-\Gamma(D^-\to K^+K^-\pi^-)}{\Gamma(D^+\to K^+K^-\pi^+)+\Gamma(D^-\to K^+K^-\pi^-)} \\ &= \frac{N(D^+\to K^+K^-\pi^+)-N(D^-\to K^+K^-\pi^-)}{N(D^+\to K^+K^-\pi^+)+N(D^-\to K^+K^-\pi^-)} \end{aligned} \tag{8}$$

where $N(D^+ \to K^+K^-\pi^+)$ is the number of reconstructed decays, measured by fitting the mass plot of appropriately selected $K^+K^-\pi^+$ combinations. Similar asymmetry parameters, $A_{CP}(KK)$ and $A_{CP}(\pi\pi)$, can be defined for reactions (ii) and (iii).

It is not necessary to assume equal production, however. The relative $D^+/D^-$ and $D^{*+}/D^{*-}$ production rates can be determined using the Cabibbo favored decay modes:

$$\begin{aligned} D^+ \quad & \to K^-\pi^+\pi^+ \text{ (iv)} \\ D^{*+} \to \pi^+ D^0; \quad & D^0 \to K^-\pi^+ \text{ (v)} \\ D^{*+} \to \pi^+ D^0; \quad & D^0 \to K^-\pi^+\pi^-\pi^+ \text{ (vi)} \end{aligned} \tag{9}$$

and their charge conjugates. These decay modes will not exhibit a CP induced rate asymmetry in the standard model. Since these decays are each roughly an order of magnitude more plentiful than the Cabibbo suppressed modes above, their contribution to the uncertainty in $A_{CP}$ will be small. Using reaction (iv) to correct (i) for the measured $D^+/D^-$ production rates, one obtains:

$$A_{CP}(KK\pi) = \frac{\eta(D^+ \to K^+K^-\pi^+) - \eta(D^- \to K^+K^-\pi^-)}{\eta(D^+ \to K^+K^-\pi^+) + \eta(D^- \to K^+K^-\pi^-)} \tag{10}$$

Table 6: Projected Asymmetry Measurement

| Decay Mode | # Reconstructed | $\sigma(A_{CP})$ | 90% CL Upper Limit |
|---|---|---|---|
| $KK\pi$ | 15000 | 1.7% | 2.8% |
| $KK$ | 5000 | 2.9% | 4.8% |
| $\pi\pi$ | 1500 | 5.2% | 8.6% |

where

$$\eta(D^+ \to K^+K^-\pi^+) = \frac{N(D^+ \to K^+K^-\pi^+)}{N(D^+ \to K^-\pi^+\pi^+)}$$

A similar change for the $D^*$-tagged modes is necessary, where

$$\eta(D^0 \to P^+P^-) = \frac{N(D^0 \to P^+P^-)}{N(D^0 \to K^-\pi^+) + N(D^0 \to K^-\pi^+\pi^-\pi^+)}$$

and $P^+P^- = K^+K^-, \pi^+\pi^-$.

Assuming we achieve our goal of $10^6$ reconstructed charm decays, we will observe approximately 100,000 $D^*$-tagged $D^0/\overline{D}^0 \to K^\mp\pi^\pm, K^\mp\pi^\pm\pi^-\pi^+$ decays, and 250,000 $D^\pm \to K^\mp\pi^\pm\pi^\pm$ decays. Table 6 shows the number of reconstructed $KK\pi$ and $D^*$-tagged $KK$, $\pi\pi$ events we would expect. The table also shows the resulting error in the asymmetry measurement, and the 90% confidence level upper limit we would set on $|A_{CP}|$ for each mode if we saw no effect. We have included in our error calculation the assumption that the mass plots used to fit for the number of events in each decay have a signal to noise of about 1:1. Our estimates for the number of events we will reconstruct are all scaled from signals already observed by E687, with the exception of the $\pi\pi$ decay mode. Note that the strong phase shift due to final state interactions will most likely be different for the three modes, so that each mode is not necessarily expected to exhibit the same asymmetry.

The systematic errors in this measurement should be negligible. For the $D^*$-tagged modes, systematics would have to be due to a charge dependent efficiency for finding the bachelor pion. A similar systematic error would also be necessary for the $D^+$ decay modes. Such a systematic error should be very small, and in any case it would have to be present for the Cabibbo suppressed modes, but not for the Cabibbo favored modes, which seems unlikely.

There are two additional methods [32] we will use to search for evidence of CP violation in charm decay. The first is to look for a time dependent asymmetry in decay modes (ii) and (iii), induced by $D^0 - \overline{D}^0$ mixing. A search for such an asymmetry is very similar to a search for mixing. An observable asymmetry requires the existence of both mixing and a CP violating difference in the decay amplitudes. The second method involves looking for CP asymmetries in final state correlations of the decays of charm mesons to two vector particles, such

Table 7: Limits on Rare D Decays

| Decay Mode | Type of Test | Limit on 90% CL | Experiment |
|---|---|---|---|
| $D^+ \to \pi^+ e^+ e^-$ | FC | $< 2.5\times 10^{-3}$ | Mark2 |
| $D^+ \to \pi^+ \mu^+ \mu^-$ | FC | $< 2.9\times 10^{-3}$ | CLEO |
| $D^+ \to \pi^+ e^\pm e^\mp$ | LF | $< 3.8\times 10^{-3}$ | CLEO |
| $D^+ \to K^+ e^+ e^-$ | | $< 4.8\times 10^{-3}$ | Mark2 |
| $D^+ \to K^+ \mu^+ \mu^-$ | | $< 9.2\times 10^{-3}$ | Mark2 |
| $D^+ \to \pi^- e^+ e^+$ | L | $< 4.8\times 10^{-3}$ | Mark2 |
| $D^+ \to \pi^- \mu^+ \mu^+$ | L | $< 6.8\times 10^{-3}$ | Mark2 |
| $D^+ \to \pi^- e^+ \mu^+$ | L | $< 3.7\times 10^{-3}$ | Mark2 |
| $D^+ \to K^- e^+ e^\mp$ | L | $< 9.1\times 10^{-3}$ | Mark2 |
| $D^0 \to e^+ e^-$ | FC | $< 1.3\times 10^{-4}$ | MKIII |
| $D^0 \to \mu^+ \mu^-$ | FC | $< 1.1\times 10^{-5}$ | E615 |
| $D^0 \to \mu^\pm e^\mp$ | LF | $< 4.1\times 10^{-6}$ | E691 |
| $D^0 \to K^0 e^+ e^-$ | FC | $< 1.7\times 10^{-3}$ | MKIII |
| $D^0 \to \rho e^+ e^-$ | FC | $< 4.5\times 10^{-4}$ | CLEO |
| $D^0 \to \rho \mu^+ \mu^-$ | FC | $< 8.1\times 10^{-4}$ | CLEO |

as $D^+ \to \overline{K}^{*0} K^{*+}$. For example, one could investigate the triple correlation:

$$C_+ = \left\langle \vec{p_0} \cdot \left( \vec{\epsilon_0} \times \vec{\epsilon_+} \right) \right\rangle .$$

CP violation would manifest itself as a non-zero sum of $C_+$ and $C_-$ ($C_-$ is the triple correlation for the CP conjugate decay).

### 1.2.3 Rare and Forbidden Leptonic Decays

These decays have sensitivity to new kinds of physics. While it is very difficult to compete with the severe upper limits which have been set by Kaon decays, there are superstring[34], lepto-quarks[35], and technicolor[36] models in which large flavor-changing neutral current effects would be present in charm decays, but not in kaon decays.

The searches in this experiment should significantly lower the limits of charm decays to leptons in two and three body decays.

In table 7 a list of limits are tabulated. A more complete listing of limits and references can be be found the the latest PDG particle summary book. Following the PDG group we refer to flavor changing neutral current as (FC), lepton number violation as (L), and lepton family number violating as (LF).

# 2 Options for Obtaining Higher Flux

We can increase the number of reconstructed charm events by improving the efficiency and acceptance of the spectrometer and by speeding up the data acquisition system (to decrease deadtime). However, the spectrometer already has a rather large acceptance and good efficiency. One can imagine upgrades that will yield a factor of two gain. At least a factor of 5 gain must, therefore, come from increased luminosity. There are several approaches to achieving higher photon intensity. After a brief summary of the beam performance to date, we discuss some of the options.

## 2.1 Performance of the Wideband Beam

The Wideband beam underwent two upgrades for the 1990-1991 run. The first, the replacement of the beryllium production target by a liquid deuterium target, resulted in an increase in flux by a factor of 1.5, close to the 1.65 that was expected; the second, the use of the positron flux to create photons, resulted in an increase in flux of about 1.5. However, the positron beam had much more "hadronic background" than we expected and was never fully utilized. We investigated this hadronic background from two directions. One effort involved developing a trigger that rejected the hadronic background on the positive side. By the end of the run, the effort had almost produced a successful trigger and offline work has now produced a trigger strategy that will work. The second effort tried to identify and eliminate the hadronic background. It is now rather convincingly established that the background is from $\Lambda$ decays between the downstream end of the target box sweeping magnets and the first bend in the beam. In the 1991 run roughly one-half of the hadronic background was eliminated by adding a dipole magnet between the downstream end of the target box and the first quadrupole. We believe that with our present understanding we can use the positron beam for real data-taking in the future. The yield in the electron beam at 350 GeV/c is $4.8 \times 10^{-5}$ electrons per incident 800 Gev/c proton. If the positron beam is used this becomes $7.0 \times 10^{-5}$ electrons per incident 800 GeV/c proton.

## 2.2 Options for Increasing the Flux

### 2.2.1 Change in Incident Beam Energy

If Fermilab is able to upgrade the proton beam energy, the electron beam flux will increase accordingly. A primary proton energy increase from 800 to 900 GeV/c will result in an improvement of about 1.86 in the secondary electron flux at the nominal momentum setting of 350 GeV/c. The electron flux increase will be a factor of 1.68 if the secondary momentum is set for a mean value of 250 GeV/c.

### 2.2.2 Change in Secondary Beam Momentum

By emphasizing charm physics, it is possible to improve the charm yield by dropping the secondary beam momentum. If the mean momentum is lowered to 250 GeV/c from our standard setting of 350 GeV/c, then the flux should increase by a factor of three (and the relative background in the positron beam will drop quite a bit).

During the 1991 fixed target run a test was performed to measure the electron and positron yield at the 250 GeV setting as well as the hadron contamination. The results can be summarized as follows: In normal running at the 350 GeV negative setting, the beam has 8% pion contamination. If the beam is run with a 350 positive setting, then the positron yield is 50% of the electron yield, but the positive hadron contamination is 60% of the beam. At the 250 GeV setting the electron yield is measured to be 2.64 times larger than the 350 GeV setting. The hadron contamination is now only 6%. At a positive 250 GeV setting the hadron contamination is only 26% while the positron yield is again 50% of the electron yield, but 2.60 times larger than the 350 GeV setting.

If the positive and negative beams are run at the same time, then the hadron contamination is 14% and yield is 1.4 times larger. Hence the beam behaves as expected. The hadron contamination is lower at the 250 GeV setting and the electron and positron flux is 2.6 times higher than at the 350 GeV setting.

### 2.2.3 Fixing the Occlusion in the Positron Arm

The positron arm of the beam should have the same yield as the electron side of the beam. Unfortunately there is an occlusion in the vacuum pipe caused by an offset pipe. The positive arm yield could be doubled by fixing this occlusion. If the a simple solution can be found, then we would like to have it repaired. However, we are not dependent on this repair.

### 2.2.4 Change in Choice of Experiment Parameters

The experimental target can be increased to 15% (from our existing 10%) of an interaction length. In doing this, we lose resolution and acceptance for the interactions in the upstream segments of the target, as the interactions occur further from the microstrip, but do gain in events. We may not gain the entire 50%, but we expect an increase of at least 30%.

It is also possible to increase the radiator. This will increase the number of high energy photons but will also produce dramatically more low energy photons. The ability to do this will depend on how successfully we upgrade the rate capability of the detectors and improve the trigger. It is hard to imagine gaining more than 20-30% by doing this.

Table 8: Summary of luminosity improvements for a charm experiment

| | 350 GeV | 250 GeV | 400 GeV |
|---|---|---|---|
| Positrons | 1.50 | 1.50 | 1.50 |
| Helium in Target Box | 1.1 | 1.1 | 1.1 |
| Accelerator Upgrade to 900 | 1.86 | 1.68 | 2.6 |
| Change Energy from 350 | 1.0 | 2.6 | 0.7 |
| More Intensity | 1.5 | 1.5 | 1.5 |
| Total Gains | 4.6 | 10.8 | 4.5 |

### 2.2.5 Increase in the Number of Incident Protons

We could go from $4 \times 10^{12}$ to $6 \times 10^{12}$ protons on target per pulse. This gives us another factor of 1.5. The places where we could have trouble transporting this much beam are in the cryogenic bends and in the LD2 target. The LD2 target is rated at $10^{13}$ and should be ok. The principal problem is the cryo bends. The bends are supposed to be able to take this rate. The bends have taken rates of over $5 \times 10^{12}$ for short periods of time so there is no reason to believe that this will be a problem. A major question is whether the laboratory would be able to deliver this many protons to us for the duration of the experiment.

### 2.2.6 Changes in the Production Target

A minor improvement would be to put helium into the target box and extend it up to the quadrupoles. Adding helium would decrease the probability for photons to convert to pairs in the target box and after the converter reduce the bremsstrahlung of electrons and positrons. Thus increases the flux by 10%. The addition of helium also reduces the hadronic contamination.

### 2.2.7 Summary of 'Beam Options

Table 8 gives a summary of what should be viewed as "conservative" approaches to increasing the luminosity. Note that in this table we have not included changes to the experiment's operating conditions, such as more target or more radiator, which were also discussed above and can result in additional increases in the luminosity. Note we have also not included any change due to a repaired occlusion in the positive arm.

# 3 Modifications to the apparatus to handle high rates

The main challenge for the apparatus is to be able to handle the increased rate at all levels. Each element will have to operate at at least five times the instantaneous and average rate which it now sees. Because the intensity in the $e^+e^-$ pair region is 500 times that in the rest of the detector, almost all of the difficulties are in the center of the spectrometer. In this section, we discuss how each detector and its associated front-end electronics needs to be modified to handle the increased rates. The required upgrade of the trigger and data acquisition system is also discussed in this section.

## 3.1 Trigger Counters

To handle an instantaneous rate increase of a factor of 5, our trigger counters will need to be changed. We presently trigger on $TR1 \cdot TR2 \cdot (H \times V)_{2\ body}$, where TR1 is a single scintillation counter situated between the target and the silicon microstrip, TR2 is a single scintillation counter located immediately downstream of the microstrip, and $H \times V$ is an array of vertical and horizontal counters placed downstream of the last proportional wire chamber, P4. The symbol 2 *body* refers to the fact that we typically require 2 hits in the $H \times V$ array. Counters TR1 and TR2 presently operate at $1MHz$. At a rate 5 times higher they would barely work.

We have considered two options for replacements of TR1 and TR2. The first option involves replacing these counters with several smaller counters thereby distributing the rate over several phototubes. This choice would obviously work, but since TR1 sets the timing for the entire experiment, then special care would have to be taken when setting up these counters.

The second option would be to replace the scintillators with Cerenkov detectors which are not sensitive to 0 degree pairs. This could , in principle, reduce the trigger rate by a factor of over 100.

The $H \times V$ counters would be replaced by triggers from the Hadron Calorimetry. By changing the Hadron Calorimeter from a gas detector to a scintillator readout (see hadron calorimeter section) it will become easy to generate a fast energy sum. Again this would drastically reduce the Master Gate rate. We intend to partially test this idea in the 1991 run by moving part of the $H \times V$ array behind the Inner Electromagnetic Calorimeter.

## 3.2 Microstrip Detector

The microstrip vertex detector is the E687 spectrometer's most important device for disentangling charm events from the very large backgrounds. It is installed in the region between the target and the first analysis magnet (M1) and consists of twelve microstrip planes, grouped in four stations of three detectors

each, measuring three coordinates at 135, 45 and 90 degrees with respect to the horizontal axis of the spectrometer.

The innermost central region of the system, covering the very forward production cone, has a resolution two times better than the outer region. The first station,which is the most crucial in determining the extrapolated error to the production point in the target, has twice the position accuracy of the other stations.

Each strip is read out by means of a front-end preamplifier, a remote-end amplifier and a charge integrating FLASH ADC. The analog signal at the amplifier output has a semigaussian shape with a base width of 100-120 ns. In the 1990 run the integration time in the ADC was fixed at 130 ns, giving a signal to noise ratio of about 17 for a single minimum ionizing particle. With a flux of about $10^7$ electrons/sec on a 20% Pb radiator and a 10% Be target, about 8% of the events had embedded $e^+e^-$ tracks. These embedded pairs were due either to more than one particle in the same RF bucket or particles from adjacent buckets. The vertex detector sees a pair mainly as a single track at 0 degrees not associated with the production vertex and having a pulse height consistent with 2 minimum ionizing particles.

The overall detection efficiency of every plane is $> 99\%$. The extrapolated transverse error to the mean interaction point in the target (placed 7 cm upstream of the first microstrip plane) is about 9 microns. The efficiency of the reconstruction code is 96%, on the average, for the tracks of $D\bar{D}$ events, including multiple scattering effects; contamination of spurious tracks is about 2.7%.

In order to face the increased photon flux we are considering two upgrades for the Microstrip vertex detector. One upgrade involves speeding up the analog electronics in preparation for higher incident photon flux and the second concerns reducing by 1/3 the detector thickness to minimize the effects of multiple Coulomb scattering.

### 3.2.1 Electronics upgrade

The present rate capability of the microvertex detector is limited by the duration of the analog signal at the input of the ADC's, which is about 130 nsec. When operating the Microvertex system at a $e^+e^-$ rate higher than 5 MHz, as foreseen for the upgraded experiment, the probability for an out-of-time signal to be partly intercepted by the ADC gate would be very high(80%). To avoid contamination of out-of-time events the shaping time of the analog signal has to be reduced. This process could be accomplished by replacing the analog electronics with a faster electronics, but, at the same time, it would require a complete substitution of the cables connecting the preamplifiers, in the experimental hall, to the amplifiers, in the counting room. The new cables should propagate signals with very short rise times, in the range of 20-25 nsec. As a consequence this solution would be very expensive and time consuming and will be considered

as a the last resort. We think that the best solution is to utilize the fact that, while the instantaneous rate over the whole detector is very high, the rate on an individual strip is low and does not cause any significant pile-up of signals even with the present electronics. Thus we could simply reduce the time width of the signals from the amplifiers without reducing the intrinsic filtering time of the amplifiers. The analog information could be compressed into the charge and the time position of a delta function. Another possibility would preserve all the present electronics and split the outputs of the amplifiers to the ADC's and to a parallel array of constant fraction discriminators; their outputs would be latched only by the right trigger and the out-of-time signals could be eliminated by comparing the pattern of the ADC outputs with that of the constant-fraction discriminators. These solutions are currently under investigation.

### 3.2.2 Thickness reduction

The thickness of the microstrip detectors could be reduced from the present value of 300 microns to 200 microns with a corresponding reduction of the multiple Coulomb scattering error. (such thinner detectors are already commercially available). This reduction in thickness would improve the track reconstruction, reduce the vertex position uncertainty, and lower the $e^+e^-$ pair rate in the spectrometer.

## 3.3 Enhanced Vertex tracking

Short-lived secondary decays could be more easily separated from the primary interaction if additional tracking information close to primary interaction was available. Two different ideas have been discussed. One idea is to install a pixel device upstream of the microstrip system and immediately downstream of the Beryllium target. Such a device would help in tracking a charged charmed parent or would help in identifying the parent as neutral. An alternate scheme would be to install 10 micron pitch silicon detectors at the end of the target.

## 3.4 Proportional Wire System

The proportional wire system has three planes in each station that are perpendicular (Y) or nearly perpendicular (U,V) to the bend plane. If no changes are made, the PWC's will have to operate at 5 times the current draw they ran at in E687. Experience with the chambers suggests that this would not be possible. We will exploit the fact that nearly all (greater than 90%) of the current draw occurs within a narrow region around the beam and is due to $e^+e^-$ pair production in the target and in the material of the spectrometer. The beam size is about $\pm 2$ cm at the tails. The $e^+e^-$ pairs are spread out in a vertical swath by the action of the first analysis magnet. The second magnet recombines the pairs so that they form a fairly small spot at the last PWC,

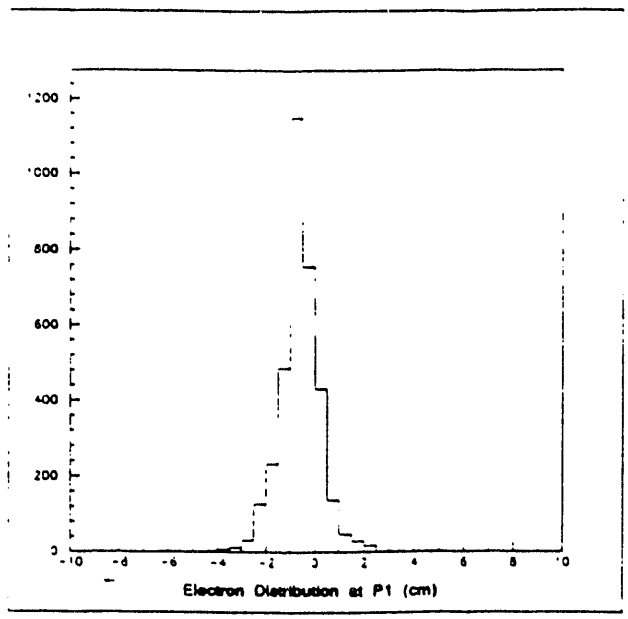


Figure 14: Pair distribution at chamber plane P1

P4. The recombination is not perfect because of bremsstrahlung energy loss by electrons and positrons in the material of the spectrometer. Pairs generated by photons interacting after the beginning of M1 are also not properly recombined and populate a much larger vertical swath at P4. The parts of the chambers outside the pair region will be able to handle the increased rate but we plan to deaden this central region. Figure 14 shows the distribution of hits from our 'pair' trigger at the chamber P1. The rates after the second magnet are such that deadening is unnecessary for P3 and P4.

There are several ways to deaden the pair region in P0, P1, and P2. The one that seems most promising to us was invented at Saclay and has been used extensively by E771 at Fermilab. Extra thickness of copper or silver is electroplated onto the sense wires in the region that is to be deadened. The extra thickness lowers the gain of the wire. This has been used on wires as thin as 0.6 mil. Our planes are 0.8 mil (P0) and 1.0 mil (P1,P2). Deadened regions can be produced with complicated shapes using this technique.

If we were to simply deaden the middle 4 cm of the spectrometer in X over the full height of the chamber, ±115 cm, we would loose some charm events. By simply taking a sample of reconstructed $D^{\pm}$ mesons and asking how many had tracks that crossed the pair (deadened) region in P0,P1, OR P2, we find that we lose about 10% of our events. We therefore wish to recover the deadened region by instrumenting it with systems that can more easily withstand the high rate of pairs. In the horizontal coordinate this is simple. We plan to cover the deadened region with a small array of straw tubes. There will be two layers of overlapped 4mm diameter tubes. The vertical coordinates in this region will be measured by two new views of straw tubes. They will be angled at ±45°. Each view will be a double layer of 4mm straws and will cover the deadened area. The total number of straws is about 4500. These tubes will be instrumented with preamps and good amplifier/discriminators so they will be able to withstand the

high rates. One advantage of this system is that if a wire breaks or a whisker grows in a tube, the tube can be disconnected easily from the system. The straw tubes add 1.4% multiple scattering to the detector. They will need only latches for readout.

In addition to covering the deadened region, these planes will give us two whole new projections in the front of the system and will strengthen all aspects of our tracking, including the region outside of the deadened zone. The steep angle with respect to the other planes will improve the matching of all views significantly.

The alternative, a small system of 45° tubes to cover just the pair region, looks less desirable. The electronics and cable requirements are the same and the support is more of a problem. They provide no help outside the pair region.

We are studying the question of whether 6mm straws would be adequate for the planes stationed near the chambers P1 and P2. This would lower the channel count by about 1000. It may also make sense to drop coverage of the extreme corners of the aperture. This would also lower the channel count another 1000.

Finally, we can improve the rate performance, as well as the overall reliability and performance of the whole system by making certain improvements that will lower the gain at which we must operate the existing E687 chambers. These improvements were employed on the PWC P4 which was rebuilt between the 1987/88 and 1990 run. These improvements used all experience gained from operating the system during the first run. They included:

- Employing 3.3 mm pitch for the anode wires instead of the original 3 mm pitch for P1 and P2 . The rebuilt P4 used 3.3 mm pitch. This permitted us to lower the voltage by 200 volts for the same gas gain. The integrated mass resolution of the system was hardly affected by this change and the chamber achieved higher efficiency than any other chamber in the experiment.

- Modifying the gas box for P0, P1, P2, and P3 so that signals are fed to the outside through header pins as they are in the modified P4. In the original design, cables run through slits from the inside to the outside of the gas box. The cables are sealed with RTV. The modified P4 had the lowest gas leak rate of any of the chambers. The noise was also lowest for this chamber although we cannot really claim that this was related to the modified gas box. Whatever the cause, P4 ran at the lowest threshold of any plane which permits reduced gas gain.

- We would like to redo the sense and high voltage planes using the 'machine planing' method that was used to get a tolerance of $\pm 1.5$ mils for P4's gap. When the gap is uniform, all parts of the chamber plateau at the same voltage and this obviously produces the best running condition.

- We would like to redo the artwork of the high voltage planes for at least P1 and P2 using the 'longer' high voltage pads that were employed for

P4. The major reliability problem we encountered with the PWC's was that occasionally a spark, trip, or other upset would cause a high voltage wire to come lose. Almost all such wires were at the edge of a cathode pad (16 wires ran to each pad). It was hard to get enough solder on the edge wires to make a secure contact. By making the pads much longer in the direction of the wire, this problem was completely eliminated in P4.

- We want to replace the 'ancient' amplifier discriminators on the chambers P0 and P3 with the more modern ones used on the other chambers. These planes suffered from oscillation problems. The method for doing this was used in the 1987/88 run and is well understood.

These improvements should allow us to lower the threshold and the voltage and help sustain higher fluxes. they should also reduce the downtime from chamber problems in the experiment which, while small, was not negligible.

This is a somewhat 'belt-and-suspenders' approach to a problem which can make or break the experiment. The chambers have to work. If we can improve them enough so deadening is not an issue, that would be excellent but we have no way of being certain of that so we wish to embark on the straw tube construction as well.

Finally, we will explore the use of preamps and the use of gas mixtures other than 65-35 argon-ethane. Rate capability will be a major concern here.

## 3.5 Muon detectors

### 3.5.1 Inner Muon Detector

The inner muon system used in E687 consists of several coarser granularity scintillator hodoscope and 4 arrays of 5 cm diameter proportional tubes. The muon proportional tube system provided the high granularity position information required to match the muon hits to the proper track measured in the upstream spectrometer. The scintillation counter array was used for muon triggering and confirming the muon identification by providing additional coincidences. We intend to augment the existing E687 inner muon system with a relatively fine granularity x & y scintillator hodoscope placed just downstream of the hadrometer. There are two motivations for this proposed upgrade.

- The use of scintillator allows for a very tight (1 RF bucket) latch which should perform better than the muon proportional tube system (which required a roughly 1 $\mu$s readout time) given the higher rates envisioned in P831. Because of the superior time resolution of scintillator, the proposed new hodoscope should should significantly reduce potential muon backgrounds due to halo muons.

- The upstream placement of this hodoscope should significantly (by factors of 5) improve our ability to match hits in the muon system to tracks

measured in the upstream spectrometer by significantly reducing the lever arm for multiple coulomb scattering by the hadrometer.

Given our multiple scattering environment, calculations indicate that 4 cm wide scintillation counters provide good position resolution over the muon momentum range(10 GeV $< P_\mu <$ 50 GeV) relevant for semileptonic charm decay. In order to achieve single RF bucket timing resolution, we are restricted to using a maximum optical path of less than 3 meters. Since we must span a transverse area of 2 meters by 3 meters, the natural solution is to use two spans (of 1.5 meters or 1 meter) to cover the full horizontal and vertical aperture. Hence a total of 250 scintillation counters will be required to construct this hodoscope.

The virtue of a fine granularity system is likely to be a simplicity in the light collection system since the counters are by necessity fairly narrow. For example, we have considered reading out each of the 250 hodoscope elements consisting of 1 cm thick scintillator by an individual 25 mm diameter photomultiplier tubes optically coupled directly to one end (without adiabatic light guides). Under these conditions, a large enough number of photoelectrons (several hundred) should be collected per minimum ionizing particle thus allowing the use of commercial fast discriminators and modest gain photomultiplier tubes.

We are presently studying the possibility of backing up the 4 cm wide hodoscope with a much coarser grain (16 cm wide) hodoscope placed downstream of the second slab of muon steel. The better filtered coarse array, would serve to both confirm the identification provided by the upstream array (with even more hadronic absorption), and serve as a backup to match upstream tracks for those events where the upstream array is confused by hadronic shower leakage or $\delta$- rays.

### 3.5.2 Outer Muon Detectors

The outer muon system is located directly behind the yoke of M2 and consists of two scintillator arrays and two proportional tube arrays. The scintillators are used for triggering while the proportional tubes are used to associate the muon "hit" with the wire chamber tracks. As in the inner muon system, the outer muon proportional tubes will be too slow to handle the anticipated rates and must be replaced. We are presently considering two options to replace the proportional tubes.

The first option involves building an outer scintillator array with 5cm wide strips that has adequate granularity for matching the muon tracks. This design would be similar to the proposed inner muon array. The second option involves reconfiguring the existing outer muon scintillators. The reconfiguring would involve additional light guides and phototubes to achieve an acceptable muon hit efficiency. The advantage of the second option is that the detector would require less space. In both designs an additional 300 new photomultiplier tubes and bases would be required.

## 3.6 Hadron Calorimeter

The hadron calorimeter for E831 has to perform the following functions, ordered by priority:

1. Provide a fast trigger decision based on total hadronic energy. This trigger decision must be available in time for the Level I trigger to avoid substantial Level II deadtime. The trigger must be formed in about 100-150 ns.

2. Provide a possible second level trigger based on total $E_{perp}$. This kind of trigger has been used by E691 and others to achieve a factor of 2-3 reduction in trigger rate while being about 80% efficient for charm. Our own simulation demonstrates similar results.

3. Provide measurement of the position and energy of neutral showers.

The first item is crucial to the success of the experiment. The second item would be a very useful option for reducing the total amount of data recorded. The third item, neutral shower reconstruction, would be a nice addition to the experiment and would allow access to some interesting states containing neutrons, $K^0$'s, and $\Sigma$'s, if it worked well, but is not critical to achieving the main goals of the experiment.

The present gas/proportional tube hadrometer produces pulses that are 800 ns long. This makes it unusable in the Level I trigger. (In the lower rates of E687, it was possible to use the hadrometer information in the second level trigger so this was not a problem).

A calorimeter based on scintillator meets these requirements. We have investigated two designs: scintillator strips and scintillating tiles. Figure 15 shows a possible tile arrangement. The best arrangement will be determined from a detailed simulation of the $E_{perp}$ trigger.

At present, we favor the tile design over the (long) strips for the following reasons:

- The mounting scheme is much easier. In particular, the need for both X and Y readout for the $E_{perp}$ trigger will be difficult (although not impossible) to do in a strip geometry.

- Light attenuation corrections are practically negligible for the tile geometry as compared to the long strips. This is especially important for the use of the device in the Level I trigger, where there is no time to correct for attenuation. Even in the Level II trigger, it simplifies the electronics if it is unnecessary to make large corrections.

- It is possible to achieve much better segmentation with the tiles, which is useful for both the Level II trigger and for the reconstruction of neutral showers. The offline shower reconstruction is much simpler with a pad/tower geometry.

The biggest drawback to our use of the tile design is that we haven't built anything like it before. We have discussed the tile calorimeter with many people at Fermilab who are actively involved in developing this technology and are convinced that enough is known so that we can be confident that we can construct such a device and that it will meet all our requirements.

The device that we have simulated uses the steel plates from the existing E687 hadron calorimeter, which has 28 1.75" thick plates. We would place planes of 2 cm thick scintillating tiles between these plates. The expected energy resolution for this system is $\frac{75\%}{\sqrt{E}}$. With the segmentation shown in the figure each plane will have 88 tiles. The tiles would be ganged into 3 or 4 towers longitudinally. In the scheme we have modelled, the signals from plates 1-5, 6-9, 10-14, and 15-28 were ganged together. Each longitudinal sample then has about the same energy deposition for the 125 GeV tracks striking the calorimeter. The total number of readout channels (PMTs going to ADC's) is 352. This is to be compared with 570 channels in the existing E687 calorimeter.

The light from the tiles will be collected by fibers inserted into machined grooves in the tiles. The design is copied from the CDF/SDC tests. The main difference is that we are using thicker scintillator and larger size tiles than that group used. We will have to perform a test to see how the signals scale with tile thickness and area. The result might influence the number or arrangement of fibers within the tiles.

The Level I trigger is formed by adding the the pulses in groups, whose duration is about 20 ns, integrating them, digitizing them, and converting them to a level. The levels from various sectors are then added and sent to a flash adc. The digital output is compared to one (or more) thresholds. This can easily been done in 100-150 ns available.

Only preliminary studies of the use of this device in the Level II trigger have been carried out. The final pad geometry and and the longitudinal segmentation are not yet worked out. The biggest problem, as we see it, is to include the information on the $E_{perp}$ from the nearly 2000 channels of electromagnetic calorimetry into the summation.

We have also done a comparative cost analysis of the tile and strip geometries. The costs for materials, photomultipliers, electronics, cables, triggers, etc are about the same. The labor costs for the tile system are harder for us to estimate and we have drawn heavily on experience from CDF/SDC prototype development. The costs of the two systems are not significantly different.

## 3.7 Beam Instrumentation and Flux Monitors

After radiating photons in the lead radiator (27% $X_o$ for E-687), the recoiling electrons and positrons are detected in a series of electromagnetic shower hodoscope detectors.[39] See Figure 16. In order to account for the coincident multiple bremsstrahlung photons emitted by a single electron, a Beam Gamma Monitor (BGM) electromagnetic shower detector is placed in the zero degree

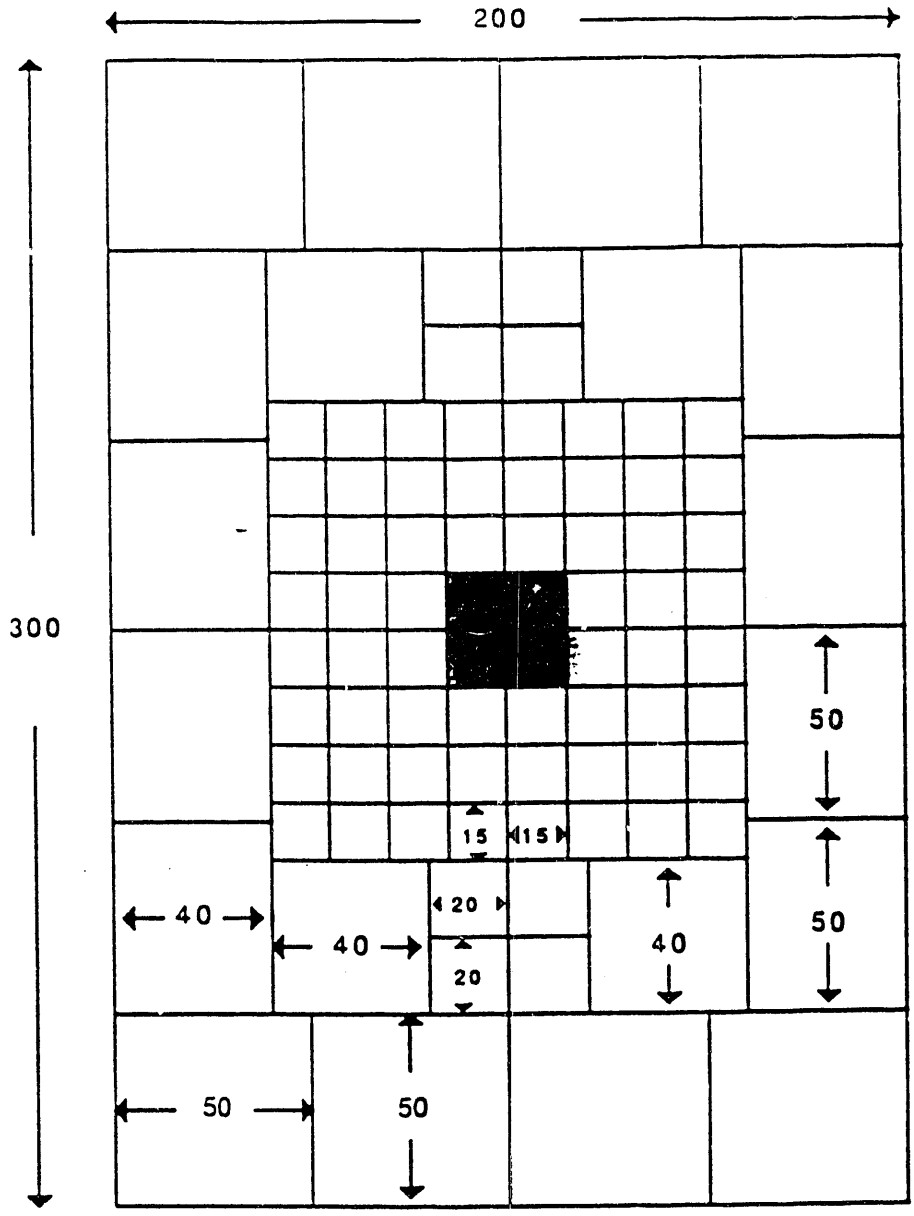


Figure 15: Transverse segmentation of proposed tile calorimeter

photon beam at the downstream end of the spectrometer. In order to get the energy of the photon initiating the hadronic event, the additional multi-bremsstrahlung energy in BGM was subtracted from the tagged electron (or positron) energy loss on an event by event basis. BGM was also used to measure the incident photon flux. The silicon microstrip-based incident beam momentum tagging system[40] measured the momentum of each incident electron or positron.

Experience during the previous E-687 runs has indicated that care must be taken in preparing for the increased beam intensity and luminosity proposed for P-831. In addition, there are some obvious upgrades that will also improve the performance, triggering, and data analysis for P-831.

The ability to accurately measure and to monitor the incident photon kinematics benefits the study of most of the physics topics of P-831. However. many physics topics such as charm particle spectroscopy, relative branching fractions. and Dalitz plot analysis can be accomplished without explicit knowledge of an individual photon energy. The measurement of the photon energy on an event by event basis, the overall photon energy distributions, and flux normalization are vital to studies involving cross sections and production dynamics.

### 3.7.1 Higher Luminosity Issues

During the 1990 and 1991 Fixed Target Physics running periods, E-687 ran successfully at sustained average incident rates of $10^7$ electrons per second. Dividing by the 53 MHz RF structure and multiplying by a factor of 3 to account for both the gross and fine time structures in the beam, this corresponded to an average electron occupancy of 0.6 per RF bucket. Pile-up from random coincidences was starting to become bothersome. For P-831, we propose to run at a factor of 5 higher instantaneous rate, giving average electron occupancies up to 3.0 per RF bucket!

There are three distinct classes of pileup: (1) DC or slowly varying baseline shifts due to the overall rate or very long tails of distributions, (2) adjacent RF bucket interferences, due to instrumental resolving times or signal tails of the scale of a few RF bucket spacings in time, and (3) multiple incident electrons coincident within the same RF bucket, within 1 nsec of each other. It is assumed class (1) can be cured by just very hard analog work and class (2) can be cured by improving the signal crispness and timing characteristics and reducing the coincidence resolving times. Pileup class (3), however, represents an irreducible challenge, requiring new types of hardware, rather than simply speeding up that already existing in E-687.

We assume that we will be able to procure ADCs and Coincidence Registers that can be made to work efficiently at 53 MHz single bucket resolution (18 nsec gating) and adjacent bucket double pulse rejection for the existing BGM, RESH, and POSH systems, as well as for possible electron and positron trajectory tracking systems.

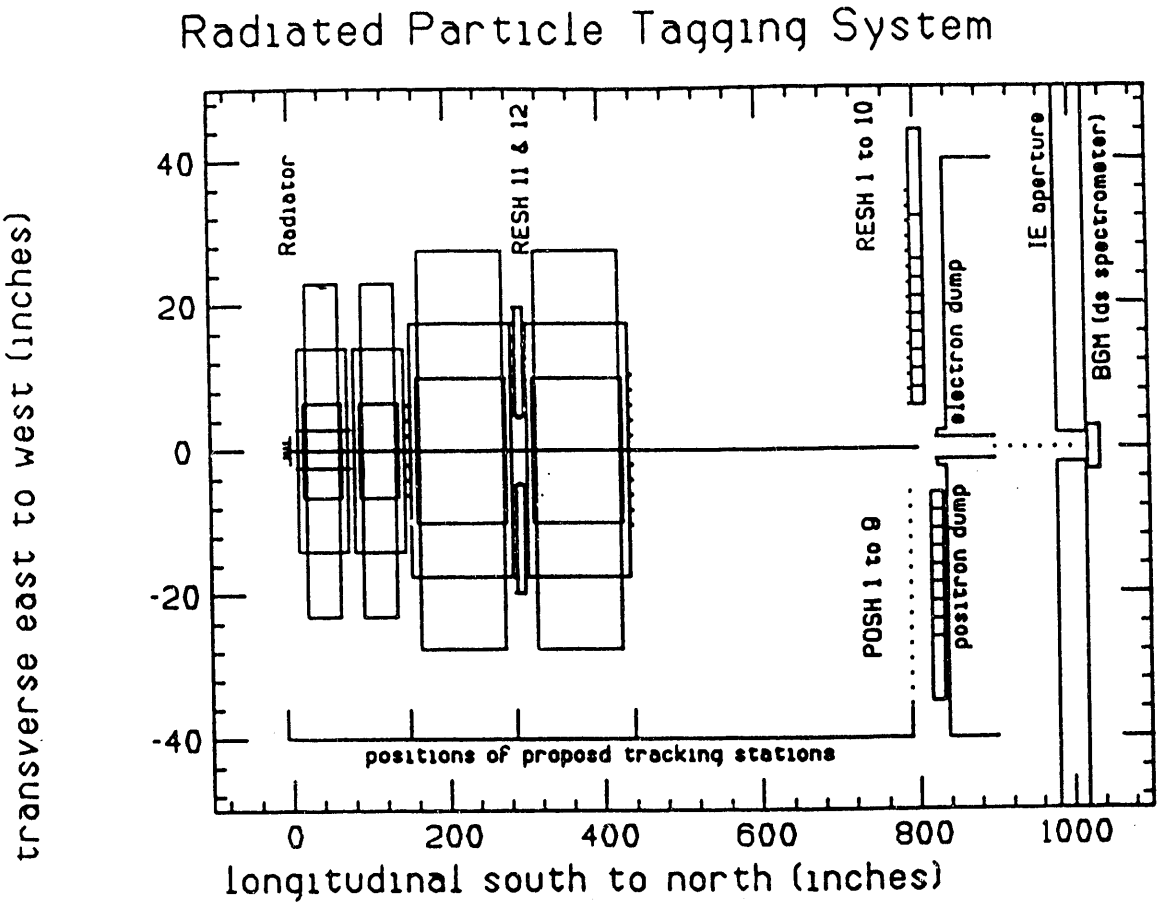


Figure 16: Existing Radiated Particle Spectrometer (including BGM). The positions of proposed additional tracking planes are indicated.

BGM

The BGM counter was a conventional lead + polyvinyltoluene scintillator (Pilot B) electromagnetic shower calorimeter. In effect, it was the photon beam dump. In order to minimize radiation damage, it was operated in a nitrogen atmosphere. Over the course of the 1990 FT run, it did suffer 15% signal degradation about the central beam position. Scaling by the increased luminosity expected, or even by logarithm of luminosity, would indicate that we are headed for trouble. The most troublesome aspect of the radiation damage proved not to be the magnitude, but its spatial distribution. The radiation damage followed the spatial distribution of the photons. Without position resolution, it was impossible to tell where the shower occurred and therefore to correctly estimate the detector gain response. This was the limiting factor for the photon energy resolution.

Possible solutions for investigation include an easily replaceable liquid scintillator (if a sufficiently fast one can be found), incorporating the BGM in a pressure vessel to allow clearing with high pressure $O_2$ (a slow process, at best), more radiation resistant scintillators, possibly scintillating fibers, or shower position readout to monitor the radiation damage and correct for the reduced detector response on an event-by-event basis.

Pileup due to occupancies of nearby buckets could be monitored and corrected with BGM analog fanout capability and dedicating additional ADC channels to measure the energy deposition for nearby RF buckets. The BGM gain monitor (a QVT-based stand-alone data acquisition system) will be triggered by an individual RESH logic bit(s) giving monochromatic tagged energy spectrum line(s). This will be much easier to monitor rather than the photon continuum end-point energy, especially in an environment with substantial pileup in the same RF bucket.

The BGM also served as an important Luminosity Monitor for the experiment.[41] Previously, this application was based on simply counting the number of photons above some discriminator threshold, typically above 100 GeV. This digital counting method breaks down when the instantaneous intensity gets too high or incident electron occupancies approach 1 per RF bucket. Since this is very definitely expected to occur for P-831, another approach such as a Wilson quantameter [42] could be employed. A simple hybrid of interspersing a few (thin) integrating ionization chambers, every 3 $X_o$ or so, within the scintillation calorimeter seems promising.

RESH and POSH

The existing recoil spectrometer for the radiated electrons and positrons (Figure 16) is based on lead-lucite and lead-scintillator EM shower calorimeter detectors used to identify electrons and positron by correlating deposited energy with the momentum dispersion of the tagging dipoles. The position at the RESH and POSH arrays can be quickly decoded by discriminator bit patterns and can be further refined by analyzing the energy sharing between adjacent RESH or POSH counters. The on-line Level II event trigger required a RESH

or POSH hit pattern consistant with only one electron or positron. Events with extra discriminator hits were vetoed. However patterns consistant with TWO electrons hitting the same RESH or POSH elements were accepted for later rejection by pulse height analysis.

A serious question for the operation of RESH and POSH concerns how greedy one wishes to be in striving to pick up LOWER energy tagged photons. These are closer to the beam giving higher rates in the innermost counters, gain changes due to radiation damage, and poorer photon energy resolution due to the reduced spatial dispersion.

These systems, both logical and analog, need to work at the 53 MHz RF rate. This will require some work in improving the optimization of the analog signals through photomultiplier bases, amplifiers, cables, delays, noise suppression, etc. Even the digital pulses, discriminated locally near RESH and POSH, suffered from drive capability and cable dispersions to be a problem in setting and maintaining the efficiency of the logic and trigger system. This could be greatly alleviated by the introduction of higher performance CAMAC coincidence registers whose timing performance will depend mainly on the gating signal and not strongly depend on the characteristics of the signal shapes for each individual channel. Additional dedicated RESH-POSH trigger logic calibration (frequent automated delay curves) and monitoring fanouts and scalers would be appreciated.

The RESH and POSH triggers for E-687 required simply more than about 20% of the nominal energy deposition in a given single counter. This provided adequate trigger selection since those counters with E/P = 20% were, in fact, almost always adjacent to another counter with E/P = 80%. Especially with the non-negligble hadronic background in the positron beam, we may desire to tighten up the E/P trigger logic requirements, both on the low end to reject hadrons and on the high end to reject two electrons or positrons hitting the same counter. Since the size of highest rate RESH and POSH detectors is approximately 2/3 the transverse size of the EM shower, forming analog sum pairs such as 1+2, 2+3, 3+4, ...(i-1)+i will insure total energy containment (E/P close to 1) for triggering with tight thresholds.

Although it would be desirable to have functioning veto shower counters within the electron and positron dumps, in E-687 it has proven difficult to keep them from dying from radiation damage within a few days. Such beam vetoes would be especially helpful to reject events in which an electron experiences a small energy loss in the radiator, not enough to be swept into RESH, but the photon converts in the radiator and hits either RESH or POSH (cross-vetoes will not allow both RESH and POSH hits) and gives a false tag with minimal energy hitting the experiment target.

### 3.7.2 Additional Features for Improved Performance

By improved performance, we mean not only improved resolution and physics capability, but also ease of operation, monitoring, calibrating, and analysing. Some of these proposed improvements, such as easier timing curves, gain monitoring, vetoes, etc., have already been mentioned in the Luminosity Upgrade Section. The possibilty of actually tracking the radiated electron and positron trajectories will not only enhance photon energy resolutions, but also improve primary vertex localization analysis methods, and help facilitate the full use of the silicon incident beam tagging spectrometer for events with more than one incident electron or positron per RF bucket.

**Recoil Electron and Positron Tracking**

Currently, the horizontal electron (and positron) trajectories are measured about the last horizontal bend in the incident electron beamline.[40] This gives the incident electron momentum before radiating. In order to get optimal resolution of the radiated electron and positron tagging spectrometer, it is desirable to know the trajectory of the projected electron from the radiator, past the RESH and POSH detectors, to the experiment target. The interacting photon position at the target is measured by spectrometer vertex silicon microstrip detector system, to an accuracy of a few microns in three dimensions. The horizontal position of the electron at the radiator could be projected using the beam tag track traced though the last stage triplet focussing quadrupole magnets. Continuing to the target has shown that a resolution in matching the projected electron trajectory to the reconstructed vertex position of $\sigma_x = 3$ mm is attainable. Another horizontal tracking plane at the radiator capable of withstanding high rates, would better pin down the projected electron (and photon) trajectory even better. This would greatly improve the resolution of the radiated electron spectrometer. In addition, the projected horizontal trajectory could then serve as a road for searching for primary event verticies, much as incident beam silicon hodoscopes for hadron experiments.

If we also add a vertical position detector at the radiator, we can then correlate the event vertex position with the position of the incident electron at radiator and get both horizontal and vertical photon directions and event production angles. This may be interesting for some exclusive physics such as the study of photoproduction of vector mesons.

So far, we have only discussed single electrons or positrons per RF bucket. The beam tagging silicon spectrometer is capable of reconstructing more than one track per RF bucket (up to five!). The problem is in determining which of these tracks actually radiated the photon in question. Since we are using a thick (27% Xo) radiator, the flip answer is that all of the electrons radiated! If we have, for example two electrons reconstructed in the beam and one in the RESH, we would have to do some TRACKING in the radiated particle spectrometer to disentangle. This could be either horizontal (large aperture requiring many detector elements) or vertical (smaller aperture, scaled to the vertical beam size,

Table 9: Multiple Scattering in Radiator Projected to Target

| $k_{photon}$ GeV | e' GeV | $\sigma_y$ mm |
|---|---|---|
| 100 | 150 | 0.67 |
| 150 | 100 | 0.92 |
| 200 | 50 | 1.75 |

rather than the horizontally dispersed radiated beam size). So far, we have only considered the vertical tracking option.

A simple calculation has shown that a useful projected vertical (or horizontal) trajectory attainable from such a radiated particle spectrometer would require a resolution with $\sigma_y$ less than about 1 mm. This would allow disentangling the pair conversions in the target from photons from multiple incident electrons with a high degree of reliability. This would also form a useful road-width seed for primary vertex reconstruction algorithms. Finally, this resolution is about what is expected for multiple scattering of the incident and radiated electron in the thick radiator. Therefore, there is no justification for attempting any finer resolution.

The multiple scattering in the radiator can be simply modelled by considering, on the average, two radiators, each of 1/2 thickness. The incident 250 GeV electron scatters in the first. The radiated electron, whose energy depends on the photon radiated, scatters in the second section. This gives the vertical resolution projected to the target due to multiple scattering in the radiator as a function of the photon energy. This simple model will have to be further refined before designs for this tracking system are finalized.

In order to obtain this spectrometer resolution of $\sigma_y = 1$ mm, we would require vertical detector elements of 1.5 mm size at the radiator, at the exit from the last tagging dipole, and at the RESH and POSH detector planes. In addition, if we desired to vertically tag for particles that only hit RESH12 and POSH12, we would require 0.75 mm detector elements between the second and third tagging elements and at the RESH12 and POSH12 detector planes. In addition, the vertical detector elements at the radiator would have to be reduced to 0.75 mm size also. This is due to the reduced lever arm and the more upstream position of RESH12/POSH12 relative to the main RESH and POSH arrays. Adding the two additional upstream stations in the tracking reconstruction algorithm for particles that reach the main RESH/POSH arrays adds little gain to the overall resolution.

Finally, there would be one or two slanted planes (1.5 mm element size) at the radiator, coupling the horizontal and vertical views and allowing the correlation of the multiple horizontally momentum measured tracks with the vertical trajectory of the electron or positron giving the RESH or POSH trigger.

This system would require the addition of the following stations, element sizes, and channel counts:

| Station-view | Element Size | Number of Elements | V x H Size |
|---|---|---|---|
| Radiator-x | 0.75 mm | 64 | 5 cm x 5 cm |
| Radiator-y | 0.75 mm | 64 | 5 cm x 5 cm |
| Radiator-u | 1.5 mm | 64 | 5 cm x 5 cm |
| Radiator-v | 1.5 mm | 64 | 5 cm x 5 cm |
| M2-M3 - y | 0.75 mm | 2 x 64 | 5 cm x 12.5 cm |
| RESH12-y | 0.75 mm | 2 x 64 | 5 cm x 37.5 cm |
| M4 ds - y | 1.5 mm | 2 x 32 | 5 cm x 25 cm |
| RESH-y | 1.5 mm | 2 x 32 | 5 cm x 75 cm |
| Totals | 0.75 mm | 384 | |
| Totals | 1.5 mm | 186 | |
| Grand Total | | 576 | |

These detectors could be silicon microstrips at the radiator (but watch the additional multiple scattering), overlapping layers of scintillating fibers (can be fairly thick for adequate number of photoelectrons) with multi-anode photomultiplier readout, or any other detector giving adequate resolution and single RF bucket timimg. The resolutions and geometric area coverage for those detectors downstream of the radiator look about ideal for straw tubes. However, taking 4 mm (minimum?) diameter straw tubes, the maximum charge collection time would be on the order of 70 nsec or 4 RF buckets (drift velocity of about 3 cm/$\mu$-sec in $Ar - C0_2$). These straws would cover only the aperture of the RESH and POSH arrays, so would not have to respond to every incident beam particle. Multiple layers of straw tubes per station and multi-hit TDCs appear to be able to provide adequate time resolution to perform the multi-RF bucket pattern recognition.

Once we do have the trajectories to determine the momentum of each of the two or more incident electrons and determined which electron actually struck the RESH, we know the energy loss and photon spectrum for that identified electron. However, there still remains the additional radiation from the other electron(s) that will be producing confusion due to additional photons striking BGM but not correlated with our identified tagged electron. In fact, the average electron or positron incident upon the radiator would deposit approximately 1/4 of its energy in BGM, yet still not be detected in either RESH or POSH. We still must understand how to deal with such BGM pileup.

Finally, we may desire to have better position resolution in front of our large momentum bite detectors such as RESH1, RESH2, POSH1, POSH2, RESH12, and POSH12. Either finer granulariy shower counters or position hodoscopes could be considered.

### 3.7.3 Event Cleanliness

Additional hardware will be investigated to improve event tagging cleanliness. The analog sum E/P = 1 trigger described above will reduce hadronic and multiple radiated electrons or positrons per event. The beam dump counters RESH0 and POSH0 to veto the false tag trigg-rs due to second order processes involving minimally-radiated electrons or positrons will be difficult to keep alive at the proposed electron beam intensities. Similarly, there has been preliminary studies performed by E-774 in this beamline of electron identification by synchrotron radiation tagging. In principle, this could detect the presence of protons, the main hadronic background in the positron beam. However, the phase space of the electron and positron beams make problematic the optimal placement of synchrotron radiation detectors close enough to the beams. It is also difficult to imagine how a veto can operate efficiently on a "NO" or lack of signal in coincidence with one or two positive "YES" signals in the same RF bucket. Still much more thinking, research, and development are needed.

## 3.8 Triggering

The triggering strategy will have to be changed in this experiment. Previously our group has always tried to write out all hadronic events on-line and then sort out the good events in software where more information is available (such as the number of charged tracks in the silicon microstrip). Rates will now be high enough to require that fast decisions need to be made during data-taking.

The $e^+e^-$ pair rate is expected to be 5M$Hz$ with a hadronic rate of 5k$Hz$. As explained in the trigger counters section the hadron calorimeter is being incorporated into the Level I trigger. It is assumed that essentially all pairs are removed by the Level I trigger and that the surviving events are more than 80% hadronic. However the hadronic rate is such that we will need to reduce it by a factor of 4 before events can be written to tape.

We plan to implement a combination of photon energy and track multiplicity to get rid of events initiated by low energy photons (which have very low charm cross section) or events which come from primarily soft scattering processes. This will result in a reduction of at least a factor of two.

A final factor of at least 2 will be achieved by using an $E_{perp}$ trigger formed of information from the Inner Electromagnetic Calorimeter, the Outer Electromagnetic Calorimeter and the Hadron Calorimeter. This trigger is very similar to the trigger used by E691. In that experiment a factor of 2.5 was gained in the charm to hadron ratio. This $E_{perp}$ trigger is presently being studied. Studies performed at Breckenridge and at Snowmass indicated that much larger improvement factors could, in fact, be made.

## 3.9 Data Acquisition

The problems of triggering and data-acquisition (DAQ) are closely related: the better the trigger, the lower the requirements on the DAQ. We assume that the combination of the first and second level triggers will produce a total of 25,000 events per spill which need to be read in. The average event size is 3 kilobytes so the total amount of data is 75 megabytes per spill.

The following is the organization of the present E687 DAQ:

- Front-end digitizing electronics. This consists of five data streams: Microstrip detector ADC's designed by Milan, Lecroy 4290 TDC's with Fermilab readouts, Smart Crate Controller readout of Fermilab and Lecroy PCOS latches, and two Fastbus crates of Lecroy 1885 ADC's.

- Real-time data buffering. The data streams are read into separate 4 megabyte Lecroy 1892 Fastbus memories. The trigger must remain disabled while this transfer occurs, introducing dead time. The average readout time for each stream is summarized in table 10. Data rate requirements here are the stream data block sizes divided by the acceptable readout time.

- Spill buffering. A GPM Fastbus Master processor merges the data streams from the Fastbus memories into event records. Blocks of event records are transmitted by Branch Bus to a 60 megabyte spill memory buffer located in the PANDA VME crate. Data rate requirements here are the average total data per spill divided by the active 20 second spill time.

- Data recording. The data is recorded on up to four Exabyte 8200 8mm tape drives in parallel. Data rate requirements here are the average total data per spill divided by full 60 second spill cycle.

Some changes to the existing Data Acquisition system are required to meet the required five fold increase in data rate.

With about 1 millisecond between events, an acceptable 10% deadtime requires 100 $\mu sec$ real time data buffering. Table 10 shows that the microstrip stream and the SCC latch stream need no revision. The ADC and TDC systems must read the data out at higher speeds.

There are several options for speeding up the TDC readout.

- Presently, the TDC readout time is limited by the speed and number of the readout controllers. Some speedup can be achieved by increasing the number of 'readout' controllers. However, for events with a very large number of hits (perhaps of electronic noise/oscillations), this does not necessarily solve the problem. The next option is to speed up the data transport within individual crates. This option is being investigated. It would require the design and construction of about 30 modified crate

Table 10: Average readout times for E687 data streams

| Data Stream | readout time ($\mu sec$) |
|---|---|
| Microstrips | 20 |
| latches | 50 |
| TDC's | 300-600 |
| ADC (1) | 1000 |
| ADC (2) | 1000 |

controllers and possibly some modifications to the TDC's themselves. We would have to do a systems test to confirm that the system really achieved the desired speed fairly soon in order to have confidence in this approach.

- The TDC system could be replaced by a new system such as the one designed by the Fermilab Physics Department. This system is now being tested and seems to work well. The readout speed meets our requirements. The cost is about $35/channel and we need 13,500 channels of TDC.

- The TDC system could be replaced by latches. For the most part, we do not make much use of the timing information and the mass resolution is dominated in many cases by multiple scattering. The latches would be about 1/3 the price of the TDC's. Latch systems of the appropriate type might be available from existing electronics inventory.

The problem of speeding up the TDC readout is largely one of cost optimization. Several technical solutions are available.

P831 will have about 2800 channels of pulse height information, slightly less than E687. E687 used LeCroy 1885 Fastbus ADC's. The 1885 Fastbus ADC digitization time alone is nearly half a millisecond. It will therefore be necessary to use a different ADC system. There are commercial options available, such as the Lecroy FERA system, which would achieve the required speed. This system is quite expensive. There is a design for a Fastbus ADC by the Fermilab Physics department which has very fast readout speed and is suitable in all other ways for the experiment and which is estimated to cost less than $75/channel. LeCroy is planning a new ADC, the 188X, which has much shorter digitization time and on-board pedestal suppression. It has suitable sensitivity and range for our needs. The cost per channel is projected at $60-70/channel. Readout will take between 50 and 100 $\mu$sec. The device is now in the prototype stage and will be tested shortly at Fermilab. Assuming it lives up to its specifications, this would probably be the best choice.

The old E687 data buffering and logging system would be pushed to or beyond its limits in logging the nominal 1 Megabyte per second of data. The maximum event rate ever achieved in the event building stage was about 20,000 small events per spill, with a very large dead time.

We plan to simplify the system, using existing, proven modules in supported configurations. Front ends should be read out through standard RS-485 data cables. We would like to use a supported generic commercial workstation to perform event building, filtering, data logging, monitoring and run control. Realtime programs and special device drivers should not be required. We will continue the very successful practice of depending on Fermilab Computing Division software support for major elements of this system.

We will use VDAS memory buffers, originally developed by Fermilab for E687, to provide both real time and spill buffering. EBI modules provide a simple, inexpensive, and fast connection from VDAS to the VME bus of the data logging workstation. This technology also gives us the option of using the primary data paths for interspill calibrations. A memory module planned as part of the DART system will combine the VDAS and EBI functionality on a single VME card, and when available could replace the VDAS/EBI combination.

Data will be logged on 8mm tape using Exabyte 8500 double density tape drives. At half a megabyte per second per drive, we will log to two drives in parallel. Data logging rates can be increased by adding more drives to the output SCSI bus, or adding additional SCSI adaptors to the workstation. For short calibration runs, higher rate data logging to disk will be possible.

In conclusion, the DAQ can be upgraded with existing technology to operate at the required rate. If the trigger rate exceeds the target of 25,000/spill by a factor of two, the "downstream" portion of the system can handle the situation with no trouble. The "front-end" will produce a factor of two more deadtime, which will result in an increase from 10% to 20%, an acceptable situation.

# 4 Upgrades to Spectrometer to Improve Efficiency

Some part of the improvement in the charm and beauty yield are obtained by improving the efficiency of the spectrometer for reconstructing these events. These improvements are described in this section.

## 4.1 Cerenkov Counters

This section reviews the layout and performance of the present E687 Cerenkov system, and discusses a possible improvement for a new run. Our basic conclusion is that the existing system performs well for the charm physics of a new photoproduction run but we are studying a modification which might extend the capabilities of the experiment. The present E687 Cerenkov system consists of three multicell Cerenkov counters with different Cerenkov thresholds. Table 11 summarizes the cell count and thresholds for the existing Cerenkov system.

Low momentum (or wide angle) tracks which fail to traverse the M2 aperture are analysed by both C1 and C2; tracks which traverse the M2 aperture are

Table 11: Characteristics of the Čerenkov Counters

| Counter | Gas | Threshold (GeV/c) | | | No. of Cells |
|---|---|---|---|---|---|
| | | Pion | Kaon | Proton | |
| C1 | $HeN_2$ | 8.4 | 29.6 | 56.4 | 90 |
| C2 | $N_2O$ | 4.5 | 16.2 | 30.9 | 110 |
| C3 | He | 17.0 | 61.0 | 116.2 | 100 |

analyzed by all three counters. The existing Cerenkov system allows protons and kaons to be separated from pions over a momentum range of 4.5 GeV to to 61 GeV and provides unambiguous electron identification for momenta up to 17 GeV for tracks traversing the M2 aperture. We used pure helium in C3 in order to achieve the highest possible Cerenkov threshold available using an atmospheric pressure counter. The Cerenkov thresholds of C1 and C2 were matched to the C3 threshold to provide a continuous momentum range for particle identification (e.g. the kaon threshold of C1 matches the proton threshold of C2 and the proton threshold of C1 matches the kaon threshold of C3).

The present E687 Cerenkov counter system performed well in both the 1988 and 1990 run period. Figure 17 shows an inclusive, combined $D \rightarrow K\pi, K2\pi$,and $K3\pi$ signal obtained in our 1988 run with and without Cerenkov identification requirements on the kaon. About 60% of the total charm signal survives the Cerenkov cut. If one considers cases where the kaon traverses the M2 aperture and thus has a chance of being identified by C3, the kaon is Cerenkov identified as definite kaon or kaon/proton ambiguous about 70 % of the time. These identification fractions include the effects of Cerenkov confusion due to overlapping tracks as well as the effects of the finite Cerenkov identification momentum range. The good performance of the present Cerenkov system can also be confirmed through the decays $\phi \rightarrow K^+K^-$, $K_s \rightarrow \pi^+\pi^-$ and $\Lambda \rightarrow P\pi^-$. Roughly 80% of protons from $\Lambda$ decays are identified as proton or kaon/proton ambiguous in our 1988 data.

The kaon identification range of the Cerenkov system performs well for most of the charm physics goals of E687. At present, both C2 and C3 have close to optimal performance with asymptotic photoelectron yields in excess of 8 photoelectrons. The photoelectron yield of C1 is about 3 photoelectrons primarily owing to its small physical length (only about 1.4 meters) and relatively high pion threshold (8.4 GeV). It might be possible to extend the C1 radiator length. A 2 foot extension would raise the photoelectron yield to about 4.3 photoelectrons. Extra photoelectrons would significantly solidify particle identification for the case of well isolated tracks. The penalty of a 2 foot extension would be a 40 % increase in the radius of Cerenkov light for each track which would

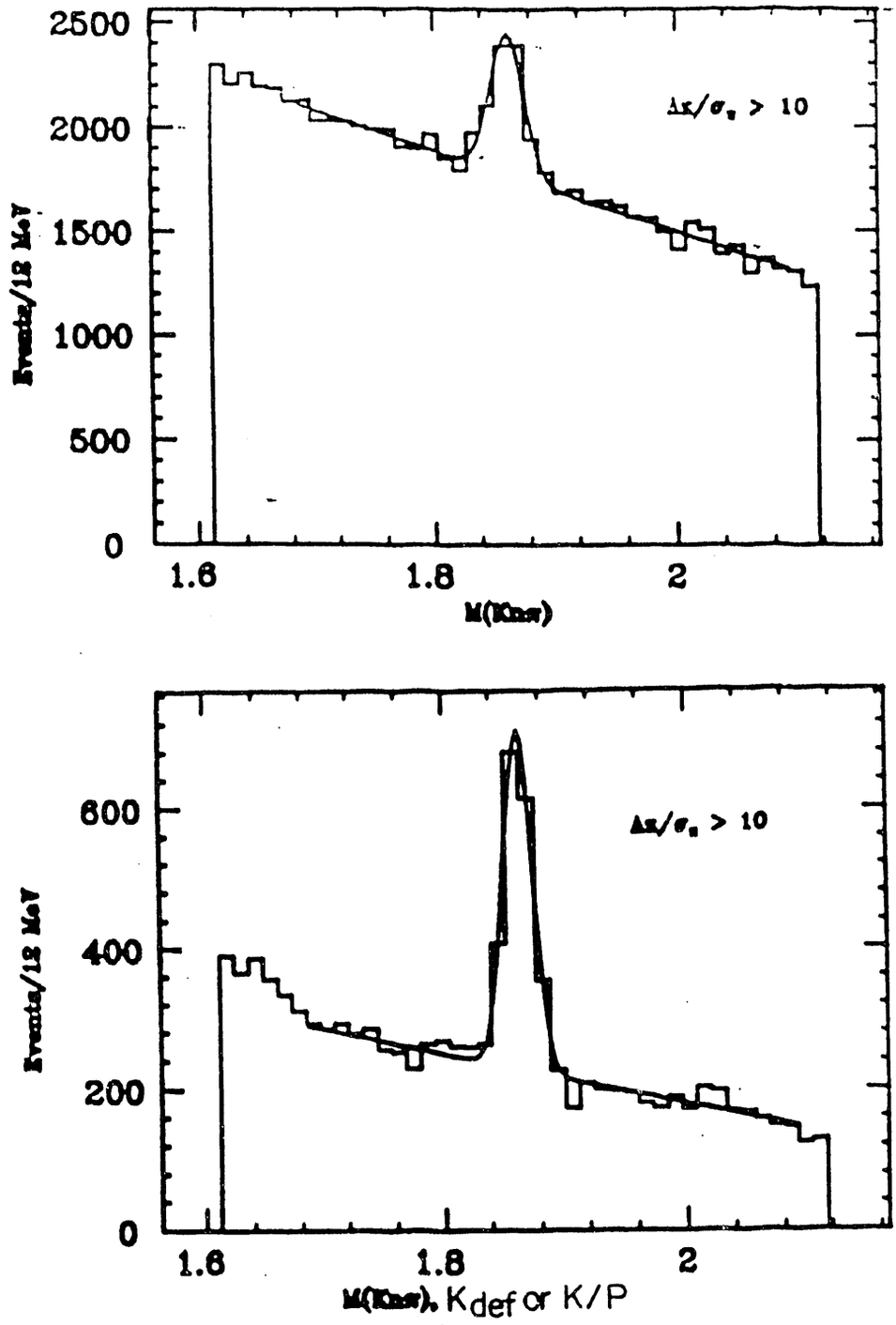


Figure 17: Performance of Cerenkov counters

tend to increase confusion in tightly clustered events. In addition, adding more radiator will increase the P0 $\rightarrow$ P2 lever arm by 12 % which will cause a small decrease in our total acceptance.

## 4.2 Electromagnetic calorimeters

### 4.2.1 Inner electromagnetic calorimeter

The Inner Electromagnetic Calorimeter or IE is a 25 radiation length lead-scintillator sandwich calorimeter which is used to identify electrons and photons. The device is divided into 3 longitudinal modules and is readout by X and Y strips. In order to-match X and Y fiber strips that are "hit", there are two additional 45 degree scintillator arrays called tiebreakers.

Thus far we have used the device to reconstruct semileptonic decays to electrons and have identified many charm channels containing $\pi^0$'s. The efficiency for identifying electrons hitting the inner electromagnetic calorimeter is approximately 90% with a $e/\pi$ rejection ratio of 1/50. This efficiency can be improved, but then we have more pion contamination. However, the efficiency is quite acceptable. Our photon reconstruction efficiency for photons striking the IE calorimeter is between 50% and 60%. This low efficiency is partly due hadronic showers overlapping photonic showers and partly due to the tiebreaker matching. We are presently investigating replacing the tiebreakers with a single layer of tiles 7.5cm $\times$ 7.5cm $\times$ 2cm thick. A total of 480 tiles would be required. By removing the tiebreakers we would save 156 channels such that an additional 324 new channels would need to be obtained. While this design needs to be further studied in Monte Carlo, it appears that we may be able to double the number of $\pi^0$'s reconstructed in the IE with such an addition.

Finally, we need to create an $E_{perp}$ trigger from energy which is deposited in the IE. We presently plan to implement such a trigger by weighting the pulse heights from the X and Y strips in the middle longitudinally segmented module by the distance the strips are away from the beam direction. The phototubes have dynode outputs which were designed for such a plan.

### 4.2.2 Outer electromagnetic calorimeter

The E687 OE is a lead-scintillator sandwich calorimeter, with active media readout done with fine-grained (3.3 cm) strips, covering the wide-angle region (from $\sim 40\,mrad$ up to $\sim 120\,mrad$). The two halves of the detector are separated by an adjustable gap with respect to the magnet bend plane (in E687 set to 9 cm), therefore the pile-up due to pairs will be easily kept under control.

Two upgrades are considered for this detector. The inner part of the detector will be modified in order to improve the shower reconstruction efficiency in the highest occupancy region, i.e. in the region close to the hole where X-Y strips matching is most problematic. The second upgrade will consist in inserting the OE information in the second level triggering logic.

The inner region will be replaced by a monolithic detector made of plastic scintillating fibers embedded in a lead matrix with a 50:35 scintillator-to-lead volumic ratio, fibers parallel to the beam axis and tower-like readout. This *head-on* technique has been used in the $(20\,MeV - 5\,GeV)$ energy range attaining $6\%/\sqrt{E[GeV]}$ energy resolution [37, 38]. Prototyping and testing have been performed in Frascati. The upgraded region will consist of two monolithic Pb-scintillating fibers structures, each one symmetric to the magnet bending plane, running along the vertical gap and the central hole with a 25 cm width in the (X,Y) plane and 32 cm ($20X_o$) thickness. Each structure is made of grooved lead foils (1.3 mm thickness) and 1mm-diameter scintillating fibers. During the assembly, fibers are pre-cut to measure and positioned in a transport frame which allows to stack and glue lead foils together. Once assembled, fibers are uniformly positioned throughout the lead volume forming a periodical hexagonal lattice. The interaxial distance from each fiber to its closest neighbours is 1.35 mm. Such an inner region in addition will improve both energy and spatial resolution for photons. More than 90% of the photon pairs from $\pi^o$ in charm decays in the OE angular acceptance are wider than 10cm. The present design sees a $(5 \times 5)\,cm^2$ readout granularity leading to 240 counters in total.

The strip-like structure of the readout elements permits to design an $E_{perp}$ fast trigger based on thresholds varying with the distance from the beam axis. Before being converted, a small fraction of the counters' signal is picked-up and sent to a low-threshold discriminator. Such front-end electronics has been prototyped and tested, about 500 channels are available.

# 5 Computing Requirements

The event reconstruction of the data for the present run of E687 is now complete. It required about 600 VAX/780-years. This was accomplished in 10 months using UNIX farms. Since the data-set anticipated for the 1993-1994 run is 5 times larger, it is reasonable to estimate a requirement of 4500 VAX/780-years. We use a factor of 7.5 rather than 5 because the trigger will preferentially eliminate the lowest multiplicity, simplest events. This amount of computing should be readily available at affordable prices by 1994/5, when it would be needed. However, we anticipate reducing computer use by approximately a factor of two by not performing the whole analysis on every event. One possible strategy would be to perform all the track reconstruction and fast particle identification algorithms (< 40% of the present offline analysis package) and only further analyze those events with evidence for a secondary vertex, or unusual final state particles (e.g. multiple kaons and protons and/or leptons). From our present analysis, we estimate that less than 20% of the events will survive these selection criteria. (We have previously skimmed with an algorithm that selected 10% of the events while still being 80% efficient for reconstructable charm decays.) Extensive hadron and electromagnetic calorimetry analysis would only be performed for the skimmed events. This should result in a requirement of less than 1500 Vax years. If one takes the point of view that 900 additional VAX/780-years will need to be acquired for this experiment, then, assuming $50/VUP by 1994/5 (as compared to $118/VUP in FNAL's last acquisition), the incremental cost of the computing is $45,000. It should be noted that the proposed gains come from doing less analysis on events which are already believed to be uninteresting, not by doing a less-than-complete microstrip or spectrometer tracking. We will, of course, investigate whether partial tracking can further reduce the CPU requirement.

During E687, it was possible to analyze about 25% of the events during data taking. We hope to have the analysis ready at the start of E831 so we would like to have the full reconstruction capacity available from the beginning of the run to keep up with data-taking.

# 6 Beam Request and Running Conditions

## 6.1 Beam Request

We can most realistically formulate our beam request by scaling from the 1990/92 runs. This will fold in the effects of real-life problems that occur during data-taking.

In 1990/91, we accumulated about 15 million events per week and got an effective 35 weeks of data. If we had sustained the optimum running conditions for the experiment, we would have accumulated about 28 milliion events/week. There was very little down time from malfunctioning of experimental equipment. The difference between the optimum and the reality was due to accelerator and beam downtime, 'edge effects' such as tuning and beam instabilities, low machine intensity, and, to some extent, time needed for calibration. In the 1991 run, calibration time was especially long because of the presence of E683 which needed separate beam calibration time. In addition, in 1991, E683's running condition limited the beam intensity to 3E12 when E687 could easily have taken 4 or 5E12. In the two runs, we were charged for about 5000 beam hours.

We therefore request a running period of 1000 beam hours for setup and 4000 beam hours for data-taking. The 1000 hours represents more than was required for either the 1990 or 1991 startup. However, we will have many new components that will have to be calibrated and we will have to learn their idiosyncracies. We will also have to learn how to run at the higher rates. When we brought the experiment up for the first time, in 1987/88, it took us about 1000 hours to get everything working and the trigger understood.

Our desired running conditions are 900 GeV/c proton beam with 5E12 protons on target. The rep rate should be about 1 spill/minute. The flat top should be at least 20 seconds. Intensities during tuneup can be lower, beginning at 2E12.

We expect to operate the secondary beam in double band mode. We need to use the liquid deuterium production target to achieve the required photon yield. Other modifications to the beam have been described above.

We strongly prefer a single Fixed Target running period to complete the above goals.

## 6.2 Special Considerations

This experiment will be much more sensitive to spill structure than our previous efforts. We would strongly urge the lab to fold standard spill quality monitoring, feedback, and spill improvement into its plans for the upcoming fixed target run. We believe the average 'coarse spill duty factor' of around 40-50% should be improved to at least 80%, a number that has been achieved under some circumstances. We believe that additional attention should be devoted to studying and improving the spill 'micro-structure'– bucket to bucket correlations,etc.

## References


[1] I. Bigi,$D^0\bar{D}^0$ Mixing and CP Violation in D Decays- Can There Be High Impact Physics in Charm Decays?, Tau-Charm Factory Workshop,SLAC,Stanford,May,1989

[2] A. Datta and D. Kumbhakar,Z.Phys.C,27(1985),515

[3] Lincoln Wolfenstein,Phys. Lett.,164B,(1985)170

[4] P. Colangelo,G. Nardulli, and N. Paver, Phys. Lett. B, 242(1990)71

[5] N. Isgur and M. B. Wise, Weak Decays of Heavy Mesons in the Static Quark Approximation,Phys. Lett,232B,113,1989

[6] Sheldon Stone, HEPSY preprint 1-92, April 1992

[7] H. Abramowicz *et al.*, *Z.Phys. C* **15**, 19(1982)

[8] Joseph M. Izen, "Semileptonic Charm Decay at a Tau Charm Factory", contributed to SLAC-Report-343, June 1989, pp. 605-615.

[9] R.M. Baltrusaitis *et al.*, *Phys. Rev. Lett.* **54**, 1976(1985)

[10] R.M. Baltrusaitis *et al.*, *Phys. Rev. Lett.* **66** 142(1991)

[11] K. Kodama *et al.*, *Phys. Rev. Lett.* **66** 1819(1991)

[12] G. Crawford *et al.*, *Phys. Rev.* **D44** 3394(1991)

[13] J.C. Anjos *et al.*, *Phys. Rev. Lett.* **62**, 1587(1989)

[14] J. Adler *et al.*, *Phys. Rev. Lett.* **62**, 1821(1989)

[15] J. Adler *et al.*, *Phys. Rev. Lett.* **60**, 89(1988)

[16] J.R. Raab *et al.*, *Phys. Rev.* **D37**, 2391(1988)

[17] J.C. Anjos *et al. Phys. Rev. Lett.* **62**, 1717(1989)

[18] P. Avery *et al. Phys. Rev.* **D41**, 774(1990)

[19] H. Albrecht *et al. Phys. Lett.* **B232**, 398(1989)

[20] H. Albrecht *et al. Phys. Lett.* **B231**, 422(1989)

[21] H. Albrecht *et al. Phys. Lett.* **B231**, 208(1989)

[22] H. Albrecht *et al. Phys. Lett.* **B230**, 162(1989)

[23] M.B. Voloshin and M.A. Shifman, ZH. Eksp. Teor.Fiz. **91**,1180 (1986) and B. Guberina *et.al.*, Z.Phys **C33**,297 (1983).

[24] This is actually the ratio of the $\tilde{\pi}$ energy in the $D^{*+}$ rest frame to the $D^{*+}$ mass. Fluctuations in this energy ratio due to the finite energy release, Q, implies a roughly $\pm$ 16% measurement of the parent $D^{*+}$ momentum can be obtained by rescaling the $\tilde{\pi}$ momentum by a factor of 13.8.

[25] See Figure13 for the charm-anticharm $P_t$ balance observed in a sample of $\approx$ 200 fully reconstructed $D$ and $\overline{D}$ obtained during the 1990 run of E687.

[26] M. Mangano, P. Nason and G. Ridolfi, Nucl. Phys. B 373 (1992) 295.

[27] *Studies of Fully Reconstructed $D\overline{D}$ Events in High Energy Photoproduction.* Contributed paper to the *XXVI International Conference on High Energy Physics*, Dallas TX (USA), August 6-12, 1992; by Rob Gardner for the Fermilab E687 Collaboration.

[28] NA14 Collab., M.P. Alvarez *et al.*, Phys. Lett. B 278 (1992) 385.

[29] For the case of $D^o$ recoil candidates, we first remove any primary vertex tracks consistent with forming a $D^{*+}$ with the *recoil* $D^o$ by eliminating tracks within $\pm 3$ MeV of the known $D^* - D$ mass difference. Such tracks create a significant wrong sign background to the $\tilde{\pi}$ sample.

[30] G. Jaross, PhD thesis, *Photoproduction of $D^{*\pm}$ and $D^o$ Mesons* , University of Illinois at Champaign-Urbana (1991), page 118

[31] *Measurement of the Branching Ratio* $\Gamma(D^0 \to K^-\mu^+\nu)/\Gamma(D^0 \to K^-\pi^+)$, Contributed paper to the *XXVI International Conference on High Energy Physics*, Dallas TX (USA), August 6-12, 1992; by Gianpaolo Bellini for the Fermilab E687 Collaboration.

[32] I.I. Bigi "CP Violation in D Decays", p169-195, Tau-charm Factory Workshop,SLAC,Stanford, May 23-27,1989
and Ling-Lie Chau "CP Noninvariance: A Charm Possibility" p695-705. Tau-charm Factory Workshop,SLAC,Stanford, May 23-27,1989

[33] M. Golden and G. Grinstein, Phys. Lett. **B222**, 501 (198 9);
K.Kleinknecht and B. Renk,*Z.Phys. C* **34**, 209(1987).

[34] A. Datta *Phys. Lett.* **B154** 170(1985)

[35] E.D. Commins and P.H. Bucksbaum, "Weak Interactions of Leptons and Quarks", Cambridge University Press (1983)

[36] I.I. Bigi and A.F. Sanda, *Phys. Lett.* **B171** 320(1985)

[37] D.W. Hertzog *et al.*, *Nucl. Instr. and Meth.* **A294**, (1990) 446-459.

[38] S. Bianco *et al*, *Nucl. Instr. and Meth.* **A315**, (1992) 322-326.

[39] The E687 Collaboration, Description and Performance of the Fermilab E687 Spectrometer, FERMILAB-Pub-90/258-E (1990). Section 2.2 describes the Beam Tagging System and Beam Gamma Monitor for the 1987-88 running period and due to space considerations was not included in the article accepted for publication in NIM.

[40] G. Alimonti, et al., Nucl. Instr. and Meth. **A314**(1992)411.

[41] Karen Lingel, Ph.D. thesis, U. of Illinois, 1990;
Hector Mendez, Ph.D. thesis, U. of Mexico, 1990;
R. Yoshida, Nucl. Instr. and Meth. **A302**(1991)63.

[42] J. Knauer, et al., Some Photon and Neutron Calorimeters for FNAL Experiment 87, Proc. Calorimeter Workshop, Fermilab, 1975, page 215.

# APPENDIX B

## SLD Collaboration Presentations

# A TEST OF THE FLAVOR INDEPENDENCE OF $\alpha_s$ AT THE $Z^0$ RESONANCE*

The SLD Collaboration

Represented by

THOMAS R. JUNK
*Department of Physics, Stanford University*
*Stanford, CA 94305*

ABSTRACT

We compare the ratio of the strong coupling $\alpha_s$ measured in $Z^0 \to b\bar{b}$ events to that measured in $Z^0 \to q\bar{q}$ ($q$=$u$,$d$,$s$,$c$) in the SLD experiment at SLAC. $Z^0 \to b\bar{b}$ events are identified with the aid of a precision silicon vertex detector by requiring that at least three charged tracks pass more than $3.0\sigma$ from the $Z^0$ decay vertex. This method has an estimated efficiency of 54% with a purity of 71%. Jets are identified and counted by clustering charged tracks according to the JADE algorithm. By comparing the 3-jet fraction in tagged events to that in all hadronic events, we extract a preliminary result of $\alpha_s(b)/\alpha_s(udsc) = 1.18 \pm 0.11(stat) \pm 0.05(sys)$.

## 1. Detector and Data Sample

The SLAC Large Detector[1] (SLD) analyzes the decays of $Z^0$ bosons produced in $e^+e^-$ collisions at the SLC. The analysis presented here takes advantage of two tracking components, the Central Drift Chamber (CDC) and the Silicon Vertex Detector (VXD)[2]. The CDC consists of 80 layers of sense wires, 48 of which are stereo layers, in an axial magnetic field of 0.6 T. Tracks with polar angle $|cos(\theta)| < 0.71$ traverse all 80 layers, with good reconstruction extending to $|cos(\theta)| < 0.80$. The VXD consists of 480 silicon CCD chips with a total of 120 million 22x22 $\mu$m pixels. Charge division between neighboring pixels affords an intrinsic position resolution of 6 $\mu$m. The CCD chips are arranged in four layers, ranging from 29.5 mm to 41.5 mm in radius. Track acceptance for the VXD extends to $|cos(\theta)| < 0.75$. The VXD is described in more detail in these proceedings.[3,4]

Well-measured tracks are required to pass within a cylinder of radius 5 cm and half-length 10 cm along the beam axis, centered on the interaction point. In addition, they must be contained within $|cos(\theta)| < 0.8$ and have a momentum transverse to the beam axis of at least 150 MeV/c.

For a $Z^0$ decay to be selected for use in this analysis, it must have at least 5 well-measured tracks, at least 20% of the total center-of-mass energy must be visible in well-measured tracks, and $|cos(\theta_{thrust})| < 0.71$. These requirements ensure good containment in the barrel of the detector. Of 11659 $Z^0$ candidates, 5602 satisfy these criteria and are used in this analysis.

## 2. Tagging $Z^0 \to b\bar{b}$ Events

Events with B hadron decays are tagged using the x-y distance of closest approach (DOCA) of charged tracks to the interaction point (IP). In addition to the normal track selection cuts, further restrictions on tracks contributing to the tag are imposed to ensure good measurements of their DOCAs. Tracks must have at least 2 clusters of hits in different CCDs of the VXD, they must have at least 40 out of a possible 80 hits in the CDC, and they must have $\chi^2/DOF < 5.0$ in a track fit to the CDC hits. They must not pair with other charged tracks to form $K^0$, $\Lambda^0$, or photon conversion candidates. The error on the DOCA measurement arises from the intrinsic resolution of the VXD and multiple scattering terms which become dominant at low momentum. The average error on the DOCA of a track is given by $< \sigma_{DOCA} >= 13\mu\text{m} \oplus 70\mu\text{m}/(P\sqrt{sin^3(\theta)})$, where $P$ is the track momentum in GeV. Tracks with $\sigma_{DOCA} > 250\mu\text{m}$ are not used in the tag.

The interaction point (IP) is found by combining tracks from several events and fitting for a common origin. The SLC IP measures 2 $\mu$m in x and y, and 650 $\mu$m in z. The location of the IP is stable within 20 $\mu$m over periods of more than 200 hours. As only the x-y position of the IP is necessary for this analysis, the errors in its measured location may be neglected.

For each event, tracks passing the above selection criteria are extrapolated past the IP and their DOCA to the IP is measured. A sign is applied to the DOCA by comparing the track to the nearest jet axis. Jets used for the purpose of signing the DOCA are found using the JADE algorithm[5] with $y_{cut} = 0.02$. If the x-y projection of a track intersects the projection of the jet axis on the opposite side of the IP in which the track travels, the DOCA is negative.

The normalized DOCA is formed by dividing the DOCA by its measurement error. To identify an event as a $Z^0 \to b\bar{b}$ event, at least $N_{trk}$ charged tracks must have normalized DOCAs exceeding $N_{sig}$. Fig. 1 illustrates the estimated efficiency and purity of the b tag for various values of $N_{trk}$ and $N_{sig}$, using JETSET 6.3 with the SLD heavy quark decay package,[7] along with full GEANT detector simulation and SLD event reconstruction. The values of $N_{trk} = 3$ and $N_{sig} = 3.0$ are used in this analysis. Using this identification procedure, we estimate an efficiency of $54.0\% \pm 1.6\%$ with a purity of $71.0\% \pm 2.5\%$.[3] Of the 5602 hadronic events used in this analysis, 919 are tagged as $Z^0 \to b\bar{b}$ decays.

## 3. Measuring $\alpha_s(b)/\alpha_s(udsc)$

A jet rates analysis[6] was performed on the b tagged sample and on the hadronic dataset using the JADE algorithm. The ratio of the 3-jet rates in these samples, $R_{meas} = f_3(b\text{-}tag)/f_3(hadr)$, is shown as a function of $y_{cut}$ in fig. 2. Because each event in the sample contributes to each point, the values of $R_{meas}$ at different $y_{cut}$ are correlated. To quote a result with proper errors, one point on fig. 2 is selected. We adopt the convention[8] of the L3 collaboration and quote our results at $y_{cut} = 0.05$, at which the measured ratio is $R_{meas} = 1.11 \pm 0.07(stat)$.

If the purity of the $Z^0 \to b\bar{b}$ tag is $\mathcal{P}$ and the $b\bar{b}$ fraction of the hadronic sample is $R_b$, then the ratio of the three-jet rate of b decays to that in udsc decays, $f_3(b)/f_3(udsc) = (R_{meas}(1-R_b)+\mathcal{P}-1)/(\mathcal{P}-R_bR_{meas})$. The weak decay of the B hadrons produces many tracks with large $p_t$ and increases the expected 3-jet rate. A correction to the observed 3-jet rate ratio is estimated from Monte Carlo to be $0.99 \pm 0.02$. The correction to the 3-jet rates owing to detector acceptance cancels in the ratio $R_{meas}$. Another correction arises from the nonuniformity of the tag efficiency as a function of $y_{cut}$ and amounts to $0.99 \pm 0.04$ at $y_{cut} = 0.05$. Bhabha and tau contamination contribute $< 1\%$ to the systematic error. The corrected 3-jet ratio, using the Standard Model value of $R_b = 22.1\%$, is $f_3(b)/f_3(udsc) = 1.16 \pm 0.11(stat) \pm .05(syst)$.

The QCD prediction for $f_3(y_{cut})$ has been calculated[9] up to second order in perturbation theory. For $y_{cut} = 0.05$ the second order corrections amount to 0.5% and are neglected here. With this approximation we write $\alpha_s(b)/\alpha_s(udsc) = f_3(b)/f_3(udsc)$. The high mass of the b quark reduces the available phase space for high momentum gluon emission, which amounts to a 2% decrease[10,11] in the expected 3-jet rate. After all corrections, the SLD preliminary measurement for the ratio of the strong couplings is

$$\alpha_s(b)/\alpha_s(udsc) = 1.18 \pm .11(stat) \pm .05(sys).$$

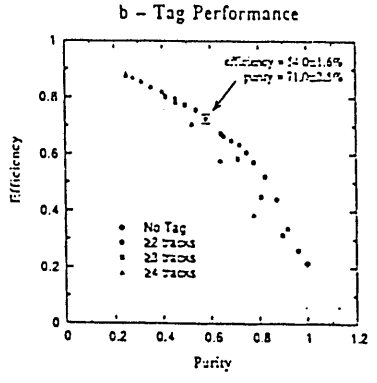

Fig. 1

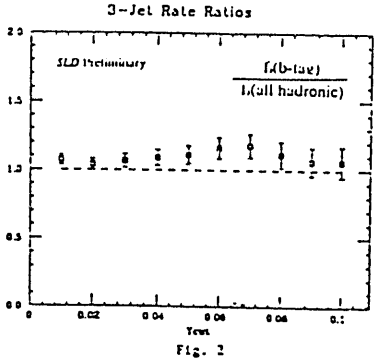

Fig. 2


1. *SLD Design Report*, SLAC Pub. 273 (1984)
2. G.D. Agnew et. al, *Proceedings of the XXVI International Conference on High Energy Physics, Dallas* (1992)
3. SLD Collab, represented by D. Su, these proceedings.
4. SLD Collab, represented by M. Strauss, these proceedings.
5. JADE Collaboration, *Z. Phys.* **C33** (1986) p. 23.
6. SLD Collab, represented by J. Lauber, these proceedings.
7. *Proceedings of the SLD Physics Week*, SLAC Pub. 354 (1989) p. 175-185
8. L3 Collaboration, *Phys. Lett.* **B271** (1991) 461-467.
9. Kunszt and Nason, *Z Physics at LEP I*, Vol. 1, CERN-89-08 (1989) p. 373.
10. B.L. Ioffe, *Phys. Lett.* **B78** (1978) p. 277-280.
11. A. Ballestrero, E. Maina, and S. Moretti, DFTT 32/92 (1992)

# A STUDY OF JET RATES AND MEASUREMENT OF $\alpha_s$ AT THE $Z^0$ RESONANCE

The SLD Collaboration

represented by

JAN A LAUBER
*University of Colorado*
*Boulder, CO 80309, USA*

ABSTRACT

We present jet rates in hadronic decays of $Z^0$ bosons measured by the SLD experiment at SLAC. The data are analyzed in terms of the JADE and recently proposed Durham algorithms, and are found to be in agreement with the predictions of perturbative QCD plus fragmentation Monte Carlo models of hadron production. Corrected 2, 3 and 4-jet rates are well described by $\mathcal{O}(\alpha_s^2)$ perturbative QCD calculations. From fits to the differential 2-jet distribution the strong coupling $\alpha_s(M_Z)$ is measured to be $\alpha_s(M_Z) = 0.119 \pm 0.002(\text{stat.}) \pm 0.003(\text{exp.syst.}) \pm 0.014(\text{theory})$ (preliminary). The largest contribution to the error arises from the theoretical uncertainty in choosing the QCD renormalisation scale.

## Event Selection and Measurement

The SLAC Linear Collider (SLC) produces electron-positron annihilation events at the $Z^0$ resonance which are recorded by the SLC Large Detector (SLD). In the first physics run from February to September 1992, a sample of about 12000 $Z^0$ decays had been accumulated by the SLD.

The analysis presented here used charged tracks measured in the central drift chamber (CDC). A set of cuts was applied to select well-measured tracks and events well-contained within the detector acceptance.[1] 5500 events survived these cuts. The total background was estimated to be at the level of 0.3%. We reconstructed jets using the Durham (D)[2] jet-finding algorithm as well as with the E, E0 and p schemes which are variations of the JADE algorithm.[3] The $n$-jet rates $R_n(y_{cut})$ reconstructed from the SLD data with the D algorithm are shown in Fig. 1 for the cases $n = 2,3,4,\geq 5$. The data were corrected by standard procedures[1] for the effects of initial state radiation, detector acceptance and resolution, analysis cuts, unmeasured neutral particles, decays of unstable particles and hadronization. Also shown in Fig. 1 are the predictions of the JETSET 6.3 and HERWIG 5.3 perturbative QCD plus fragmentation Monte Carlo programs, which are seen to be in agreement with the data.

$R_3(y_{cut})$ and $R_4(y_{cut})$ have been calculated to next-to-leading and leading order, respectively, in QCD perturbation theory.[4,5] $R_2(y_{cut})$ is derived by applying the unitarity constraint $R_2 = 1 - R_3 - R_4$. The free parameters in the calculations are the QCD interaction scale $\Lambda_{\overline{MS}}$ and the renormalization scale factor $f = \mu^2/E_{cm}^2$.

To avoid the correlations between adjacent points in Fig. 1 it is customary to fit the QCD calculations to the differential 2-jet rate $D_2(y_{cut})$ defined as: $D_2(y_{cut}) \equiv [R_2(y_{cut}) - R_2(y_{cut} - \Delta y_{cut})]/\Delta y_{cut}$, shown in Fig. 2, where each event enters the plot only once. Also shown are two fits of the $\mathcal{O}(\alpha_s^2)$ calculation by Kunszt

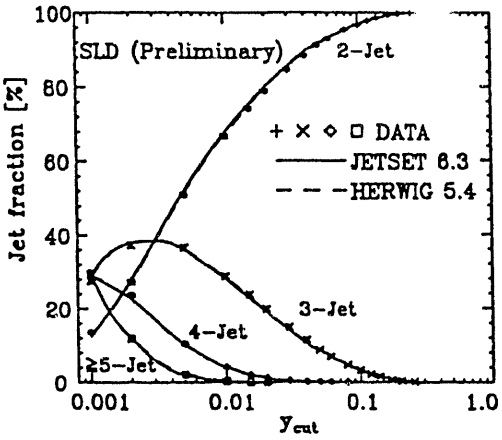


Fig. 1 Jet rates measured by SLD with the Durham algorithm

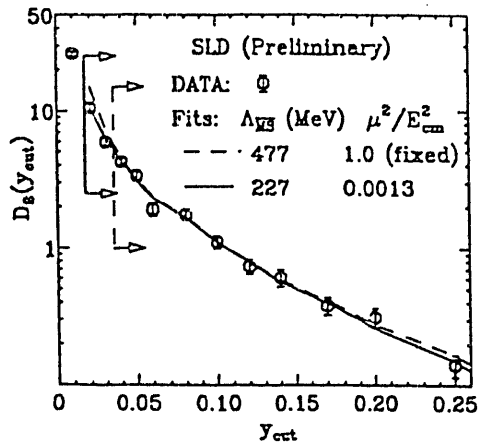


Fig. 2 Differential 2-Jet Rate and QCD fits to the data

and Nason.[5] In the first fit (dashed line) the renormalization scale factor $f$ was fixed to unity and the single parameter $\Lambda_{\overline{MS}}$ was fitted. In the second case (solid line) a two-parameter fit to $\Lambda_{\overline{MS}}$ and $f$ was performed. To $\mathcal{O}(\alpha_s^2)$ $R_4$ is only calculated to leading order and $R_5$ does not contribute at all. The fits were therefore restricted to regions of $y_{cut}$ where $R_4 < 1\%$ for $f = 1$ and $R_5 < 1\%$ for free $f$. The resulting values for $\Lambda_{\overline{MS}}$ can be translated into $\alpha_s(M_Z)$ measurements using the renormalization group equation, giving $\alpha_s(M_Z) = 0.125 \pm 0.002$ and $0.120 \pm 0.002$ respectively. A similar analysis was performed for the E0, E and p schemes. The results are shown in Table 1.

| | ($f$ = 1) | | ($f$ fitted) | | |
|---|---|---|---|---|---|
| scheme | $\Lambda_{\overline{MS}}$ (MeV) | $\chi^2/d.o.f$ | $\Lambda_{\overline{MS}}$ (MeV) | $f = \mu^2/E^2_{cm}$ | $\chi^2/d.o.f$ |
| D | $477 \pm 41$ | 7/8 | $227 \pm 18$ | $0.0013 \pm 0.0002$ | 7/10 |
| E0 | $258 \pm 35$ | 14/8 | $109 \pm 12$ | $0.0045 \pm 0.0005$ | 15/10 |
| E | $528 \pm 50$ | 9/4 | $89 \pm 8$ | $0.0001 \pm 0.0001$ | 7/6 |
| P | $326 \pm 48$ | 5/8 | $209 \pm 13$ | $0.023 \pm 0.0012$ | 8/10 |

**Table 1** Results of fitting $\mathcal{O}(\alpha_s^2)$ QCD calculations to SLD data, for fixed and variable renormalization scales. The errors are statistical only.

For each jet-finding scheme the results from the two fits were averaged and listed in Table 2. Also listed in Table 2 are the errors contributing to this measurement: the statistical error $\leq 2\%$ and the experimental systematic error $\leq 3\%$ for all algorithms; $\Delta\alpha_s(had.)$ is the error introduced by the modelling of the hadronization process, estimated by comparing results from two different fragmentation models in JETSET 6.3 and HERWIG 5.3; $\Delta\alpha_s(Q_0)$ is the uncertaintiy introduced by the choice of the lower cutoff for parton branching $Q_0$. $Q_0$ was varied between 0.5 and 5 GeV and the largest difference in the final result is quoted in the error. The largest error is introduced by the scale uncertainty, $\Delta\alpha_s(scale)$, estimated from the difference between the measured values of $\Lambda_{\overline{MS}}$ with $f = 1$ and with $f$ as a free parameter. In Fig. 3 the behavior of $\alpha_s$ as a function of the renormalization scale $f$ is shown. The fitted values of $f$ lie very close to the minimum for each jet-finding algorithm. The scale uncertainty is taken to be the difference between the minimum of each curve

and the value at $f = 1$. Uncertainties introduced by varying the fit range of $y_{cut}$ were found to be negligible. These results agree within experimental errors with previous measurements from SLC and LEP[6] as well as with our own measurement of $\alpha_s$ from energy-energy correlations.[6]

| Scheme | $\alpha_s(M_{Z^0})$ | $\Delta\alpha_s(stat.)$ | $\Delta\alpha_s(exp.)$ | $\Delta\alpha_s(had.)$ | $\Delta\alpha_s(Q_0)$ | $\Delta\alpha_s(scale)$ |
|---|---|---|---|---|---|---|
| D | 0.125 | ±0.002 | ±0.003 | ±0.003 | ±0.004 | ±0.007 |
| E0 | 0.112 | ±0.002 | ±0.003 | ±0.003 | ±0.002 | ±0.007 |
| E | 0.119 | ±0.002 | ±0.003 | ±0.003 | ±0.005 | ±0.013 |
| P | 0.120 | ±0.002 | ±0.003 | ±0.003 | ±0.005 | ±0.009 |

Table 2 Summary of results for $\alpha_s$ and the errors contributing to the measurement uncertainty. The values for $\alpha_s$ are the average of the results from the two fits.

## Summary and Discussion

We have presented an analysis of jet rates from a data sample of about 12000 hadronic $Z^0$s recorded by the SLD. We have determined the value of the strong coupling, $\alpha_s(M_{Z^0})$, using four different jet finding algorithms (E0,p,E and D). These measurements were compared with analytic calculations in complete second order perturbative QCD. The QCD parameter $\Lambda_{\overline{MS}}$ , and thus $\alpha_s(M_{Z^0})$, was then determined in fits of the QCD calculations to the corrected data distributions.

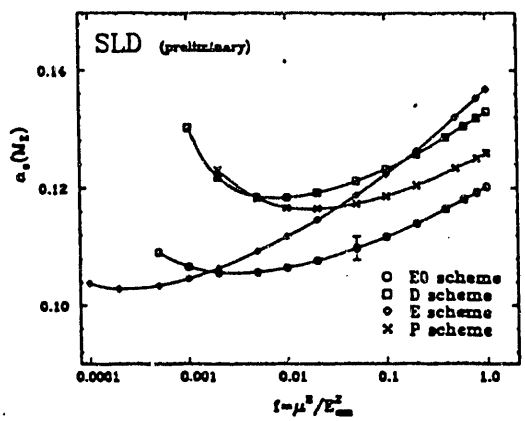


Fig.3 $\alpha_s$ as a function of the scale $f$

The average of the four results is

$$\alpha_s(M_Z) = 0.119 \pm 0.002 \text{ (stat.)} \pm 0.003 \text{ (exp.syst.)} \pm 0.014 \text{ (theory)}.$$

Experimental uncertainties are at the level of < 4%(stat.+syst.). The theoretical error quoted above is the sum of $\Delta\alpha_s(had.)$, $\Delta\alpha_s(Q_0)$ and $\Delta\alpha_s(scale)$ added in quadrature, for the E scheme, which yields the largest uncertainties. We find that the largest error in this measurement is the theoretical error from varying the renormalization scale $f$. Our result is in good agreement with results from the LEP experiments.

## References


1. SLD Collab., P.N. Burrows *et al.*, SLAC-PUB 5802 (1992).
2. N. Brown, W.J. Sterling, RAL-91-049 (1991).
3. JADE Collaboration: S.Bethke *et al.*, Phys. Lett. **B213** (1988) 235.
4. G. Kramer, B. Lampe, Fort. Physik, **37** (1989), 161.
5. Z. Kunszt *et al.*, Z Physics at LEP I, Vol. I, CERN–89–08 p.373, (1989).
6. S. Bethke, Proc. of the *XXVI* Int. Conf. on HEP, Dallas (1992).

DRAFT

# A PRELIMINARY MEASUREMENT OF $R_b = \frac{\Gamma(Z^0 \to b\bar{b})}{\Gamma(Z^0 \to \text{hadrons})}$ AT SLD*

THE SLD COLLABORATION
*Represented By*

D. SU
*Rutherford Appleton Laboratory*
*Chilton, Didcot, Oxon England*

## ABSTRACT

We present a preliminary measurement of $R_b$, the ratio of $\Gamma(Z^0 \to b\bar{b})$ relative to $\Gamma(Z^0 \to \text{Hadrons})$ using the silicon CCD-pixel vertex detector of the SLD at SLAC Linear Collider (SLC). An impact parameter method and a displaced vertex method are applied to all charged tracks, to efficiently tag $Z^0 \to b\bar{b}$ events. From the impact (displaced vertex) approach we find $R_b$=0.218±0.013±0.026 ($R_b$=0.199±0.012±0.034), consistent with the standard model value.

## 1. Introduction

The branching fraction ratio $R_b$ measures the sum of the squares of the vector and axial vector couplings of the b-quark to the $Z^0$. As the CKM parameter $V_{tb} \approx 1$ one anticipates large vertex and external radiative corrections ($\Delta V \propto (M_t/M_Z)^2$) for $M_t \gg M_Z$. $R_b$ isolates the vertex corrections, as oblique corrections largely cancel in the ratio, being common to all fermions.[1] This is reflected in the weak dependence of $R_b$ on $\sin^2\theta_W$, and on QCD corrections.[i] These insensitivity's to conventional rad. corrections make $R_b$ an excellent variable in the search for New Physics once $M_t$ is known, and $\delta R_b \sim 1\%$ is obtained. We present herein preliminary results on the measurement of $R_b$ from a sample of 11.6K polarized $Z^0$ events collected at $\sqrt{s}$=91.55 GeV in the SLD detector at the SLC, using a CCD vertex detector. $Z^0$ events containing b-decays are tagged by two techniques; one similar to MARKII,[2] namely the counting of *all* tracks with large impact parameters (b) to the interaction point (IP), and one that counts displaced vertices from b and c-quark decays directly. High efficiencies and purities are achieved as *both* hadrons and leptons are included in the tagging procedures.

## 2. Detector Description and Tracking Performance

For this analysis, only a subset of the elements of SLD are utilized; the drift chamber (CDC) [3] covering 85% $4\pi$ sr, the CCD vertex detector (VXD)[4] covering 75% $4\pi$ sr, and the liquid argon calorimeter (LAC), covering 95% $4\pi$ sr.[5] The LAC is used in the SLD trigger. Charged tracks are reconstructed in the CDC and linked with pixel-

* Work supported in part by the U.S. Department of Energy Under Contract DE-AC03-76SF00515

[i] Oblique corrections renormalize the value of $\sin^2\theta_W$ (as characterized by $\Delta\rho$). The fractional change in Rb is less than 5% of any fractional change induced in $\sin^2\theta_W$. Similarly, a 10% change in $\alpha_s$ results in a 0.05% change in $R_b$.

DRAFT

clusters in the VXD. A combined fit using the Billior method[6] is performed, to properly account for multiple scattering as the track is extrapolated through the VXD material and the 25mm radius Be-beam pipe, into the IP. The angular errors of the CDC combined with local $<\delta\phi>$ and $<\delta z>$ of VXD clusters of 5μm and 8μm, respectively, lead to XY (⊥ to the $e^+e^-$ beams) and Rz (the plane containing the beam axis) impact resolutions of $(\alpha,\beta)_\phi = (13\mu m, 70\mu m)$ and $(\alpha,\beta)_{Rz} = (52\mu m, 70\mu m)$, respectively.[ii]

**3. Beam Position**

The beams of the SLC have RMS profiles averaged over our sample of $2 \otimes 2$ $\mu m^2$ in X and Y; while the luminous region in Z is ~ 650μm. Frequent beam-beam scans coupled with a feedback utilizing the pulse to pulse beamstrahlung monitor information is used to maintain the beams in collision and stabilize the IP position. The IP is *tracked* in SLD utilizing $Z^0$ events. A fit is performed for the X,Y IP position and error ($\sigma_x$, $\sigma_y$) using ~ 50 time ordered tracks of small b, from ~10 $Z^0$. Each sample spans ~0.5 hr but ≤3 hrs. of operation, for stability. The 447 measurements for the 1992 data run have $\sigma_x$, $\sigma_y$ ≅10–15μm. The impact parameter of $\mu^+\mu^-$ & $e^+e^-$ to the IP (Fig. 1) gives $<\sigma_{IP}> \approx 11\mu m$.

**4. Detector and Event Selection**

The SLD trigger is based on loose calorimetric criteria to eliminate primary beam related backgrounds; conventional $e^\pm$and γ scattered from the beam pipe and masks, and upstream electroproduced muons, unique to SLC. The former are reduced by total energy and asymmetry cuts, while the latter utilizes the fine grained tower structure of LAC and the pattern of energy deposition of the muons.

Hadronic $Z^0$ events are selected off-line for analysis from the sample of triggers. We require visible energy in tracks $E_V$>18 GeV and that the thrust axis lie within $|\cos(\theta_T)|<0.71$ where tracking is optimal. We require the number of charged tracks $N_{chrg} \geq 7$, eliminating 2γ and τ–pair events. Bad running periods and events with number of CDC/VXD linked tracks<3 are rejected. We typically retain 4684$Z^0$ events with an estimated background contamination of <1%. The flavor dependence of the selection for b-quarks relative to all hadronic $Z^0$ events is estimated to be 1.000±0.007.

**5. The Determination Of $R_b$**

*5.1 The Impact Technique*

After event selection the set of CDC tracks having a VXD fit is further refined. We require CDC tracks start at a radius r<0.4m, to have $N_{hit}$ >40 and to have good fit quality ($\chi^2$/df <5). Tracks originating from identified long lived vees and γ–conversions are eliminated. Tracks are extrapolated to the XY point of closest approach to the IP, and the 2-D impact parameter(b) and error ($\sigma_b$) are calculated. We require |b|<0.3cm and $\sigma_b$ < 250 μm corresponding to a momentum cut $p \gtrsim 0.5$ GeV/c . All tracks are required to extrapolate to within 1cm of the average beam position in Z.

---

[ii] Here we parametrize the impact resolution function as : $\alpha \oplus \beta/P\sqrt{\sin^3\theta}$, where the sum is taken in quadrature.

DRAFT

The JADE algorithm[iii] using charged tracks isolates jets. Each track is assigned to the spatially nearest jet and a sign is attached to |b|. The +(-) convention is chosen for tracks crossing the jet axis in front (in back) of the IP. A non-zero lifetime preferentially populates +|b|, while -|b| tracks reflects uncertainty in the jet direction and the tracking resolution. The normalized impact parameter ($b_{norm}$) is formed from the signed b divided by $\sigma_b$ in quadrature with $\sigma_{IP}$ along the $\hat{b}$ direction.

The Monte Carlo (MC) simulation contains knowledge of resolution, geometry, efficiency and backgrounds, but unmodeled effects remain. These are associated with detailed CDC waveforms, models of drift velocity variation and residual misalignments and distortions. The MC is adjusted (as a function of p) to match tracking efficiency and resolution by removing 6% of the tracks and increasing $\sigma_b$ to put $b_{norm}$ in the data and the MC into agreement for $b_{norm} \leq 0$. Since -|b| tracks reflect resolution effects and not the lifetime effects of b and c-quarks, this is an unbiased procedure for correcting the simulation of $b_{norm} \geq 0$ tracks.

The first tagging technique for $b\bar{b}$ events utilizes the property that b-quarks have a large decay length (~0.2cm) resulting in many large $P_t$ tracks having large +|b|. We cut on the number of tracks ($\geq N_{sign}$) in an event having $b_{norm} > 3$. Fig. 2 shows $b_{norm}$ for uds, c and b decays from MC and data, while Fig. 3 shows the tagging efficiency ($\varepsilon_b$) and purity ($\Pi_b$) vs. $N_{sign}$. The standard model cross-sections for $Z^0 \rightarrow q\bar{q}$ are used to estimate the $\Pi_b$. Choosing $N_{sign} = 3$, we tag 786 of 4684 events (Fig.5 ), resulting in $\varepsilon_b = 0.54$, $\varepsilon_c = 0.14$, $\varepsilon_{uds} = 0.04$ and $\Pi_b = 0.71$. We obtain $R_b = 0.218 \pm 0.013$ (statistical error only).

*5.2 I The Displaced Vertex Technique*

The second technique is based on the observation that b-quark hadronization results in more 2-prong vertices displaced from the IP, than uds or c decays. Pairs of tracks, each with p>0.3 GeV, |b| < 0.3cm, and $|Z_0|$< 1cm are combined to find candidate 2-prong vertices. The cut on |b| already is effective in vee and $\gamma \rightarrow e^+e^-$ rejection. To reduce combinatorics of tracks from opposing jets, the opening angle of a pair must be less than $90^0$ in the lab. A 3-D fit on each vertex must satisfy $\chi^2 < 5$. The decay length L ($= \mathbf{l} \cdot \mathbf{P_V} / |\mathbf{P_V}|$) from the IP to the fitted vertex must be $> 4\sigma_L$ ($\sigma_L = \sigma_V \oplus \sigma_{IP}$, where $\sigma_V$ is the flight distance fit error). The tag requires a minimum of vertices $N_V$ to satisfy this cut. Fig. 4 shows $\varepsilon_b$, $\Pi_b$ and $\varepsilon_{udsc}$ vs. $N_V$. For $N_V \geq 6$, (Fig. 6) we retain 756 of 4824 events with $\varepsilon_b = 0.56$, $\Pi_b = 0.73$, $\varepsilon_c = 0.12$, and $\varepsilon_{uds} = 0.04$. An overlap with the impact technique of 427 events is observed. The vertex analysis yields $R_b = 0.199 \pm 0.012$ (stat. error only).

## 6. Systematic Errors

Our preliminary estimates of systematic errors for the impact parameter and vertex techniques are shown in Table I. Detector errors are conservative estimates. The b-lifetime is varied from 1.2-1.5ps. The fragmentation has been studied with LUND, using Pederson functions with ($\langle x_e \rangle$, $\varepsilon$)=(0.494±0.025,0.06) and (0.700±0.020,0.006) for c and b-quarks respectively. Exclusive models of the decays of b and c hadrons have been adjusted to reflect present knowledge of their decays. [iv] The $\Gamma(B \rightarrow D^0)/\Gamma(B \rightarrow D^+)$ ratio

---

[iii] The parameter YCUT=0.02 is used for the jet discrimination.

[iv] Models have been adjusted to reflect recent data presented from LEP, on fragmentation. CLEO, Argus

DRAFT

error was found to have a negligible effect. The value[7] of $\Gamma(Z^0 \rightarrow c\bar{c})/\Gamma(Z^0 \rightarrow \text{hadrons}) = 0.17 \pm 0.03$ is varied about its error. The charged track multiplicity of b decays = 5.35±0.25 was varied about its error. The measured values for $R_b$ without radiative corrections are $R_b = 0.218 \pm 0.013 \pm 0.026$ (Impact Method) and $R_b = 0.199 \pm 0.012 \pm 0.034$ (Vertex Method), where the first error is statistical and the second systematic. These results are consistent with the prediction of $R_b \approx 0.22$ in the standard model.[8]

**Table I. Systematic Errors (%)**

| SOURCE | IMPACT | VERTEX |
|---|---|---|
| Tracking Resolution | 0.07 | 0.10 |
| Tracking Efficiency | 0.09 | 0.11 |
| Beam Position | 0.01 | 0.01 |
| **Subtotal** | **0.11** | **0.15** |
| b-Lifetime | 0.02 | 0.02 |
| b-Fragmentation | 0.02 | 0.02 |
| b-Decay Properties | 0.02 | 0.07 |
| c-Fragmentation | 0.02 | 0.02 |
| **Subtotal** | **0.04** | **0.08** |
| **TOTAL** | **0.12** | **0.17** |

## 7. Conclusions

Tagging methods that exploit the small and stable SLC IP and the 3D information of the CCD-pixel vertex detector are found to be highly efficient for b-decays and to provide excellent background rejection against lighter quarks. These approaches systematically differ from conventional lepton tagging both in physics bias and the level required for detector modelling. The large systematic errors at present reflect our preliminary detector simulation and do not represent fundamental limits to the methods.

## 8. References


1. Boulware and Finnell, *Phys. Rev.* **D44** (1991) 2054, and references therein.
2. R.G.Jacobsen et. al., **PRL** 67 (1991) 3347.
3. SLD Design Report, *SLAC-REPORT* **273** (1984)
   W.B.Atwood et. al., *NIM* **A252**, (1986) 295.
4. See, M. Strauss, The SLD Collaboration, these Proceedings, for details of the performance of the silicon CCD vertex detector in the SLD.
5. D. Axen et. al., *SLAC-PUB* **5354**, (1992). To be published in *NIM*.
6. P. Billior, *NIM* **225**, (1984) 352.
7. P. Kluit, "Heavy Flavor Physics at LEP", Lecture presented at the SLAC Summer Institute, (1992).
8. W.Hollik, *Fortschrift Phys* . **38** (1990) 165, and references therein.


on exclusive beauty decays and multiplicity, MARKIII and the Particle Data Group on charm decays and multiplicities. See J.Snyder, D. Su, R. Schindler, G. Punkar SLD B-Physics Internal Memo (10-15-92).

DRAFT

## 9. Figure Captions

1. The XY impact parameter to the IP for tracks from muon-pair and WAB events.
2. The signed and normalized impact parameter $b_{norm}$ for all $Z^0$ candidate events.
3. The impact tagging efficiency (a) and purity (b) as a function of $N_{sign}$ from MC.
4. The vertex tagging efficiency (a) and purity (b) vs. $N_V$ for $L/\sigma_L>4$ .
5. The distribution of $N_{sign}$ over the $Z^0$ sample for $b_{norm}>3$. The MC is superimposed.
6. The distribution of $N_V$ for $L/\sigma_L>4$ over the $Z^0$ sample.

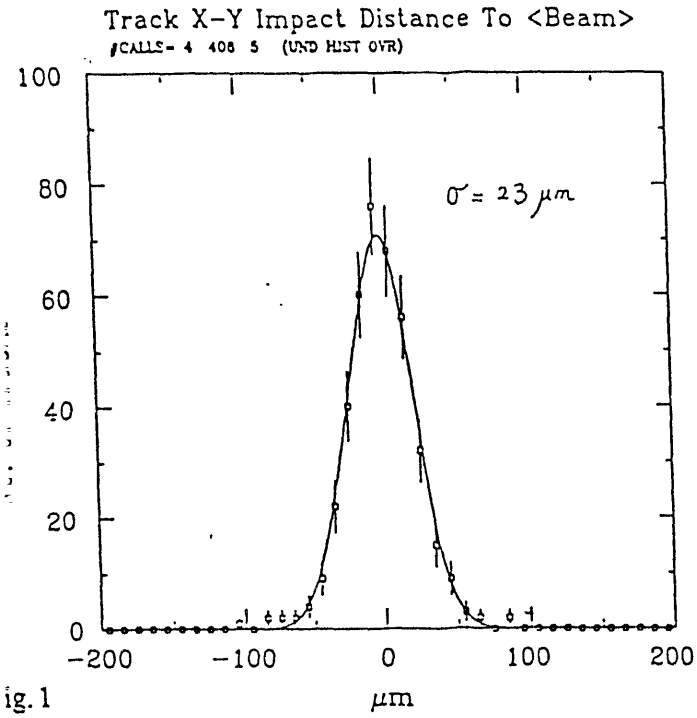


ig. 1

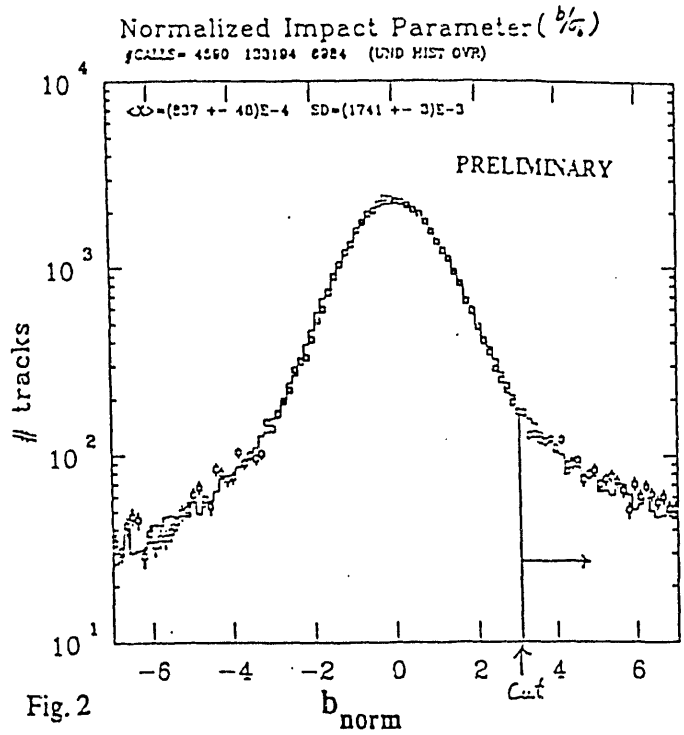


Fig. 2

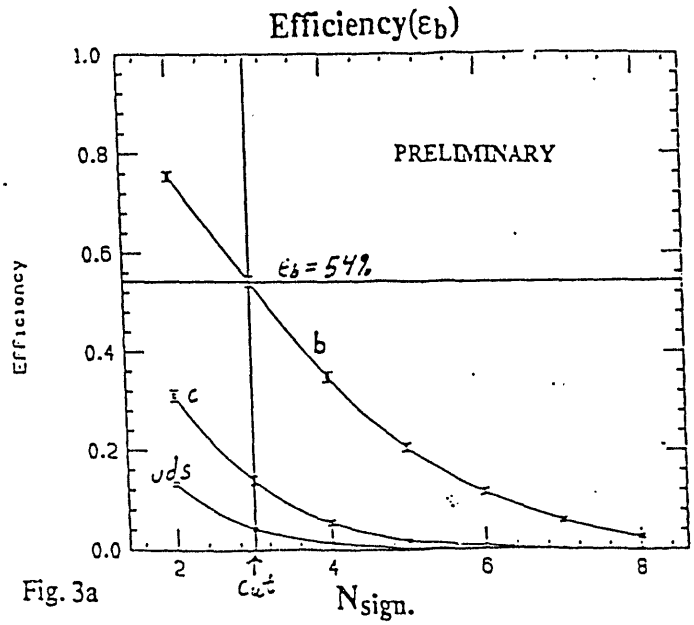


Fig. 3a

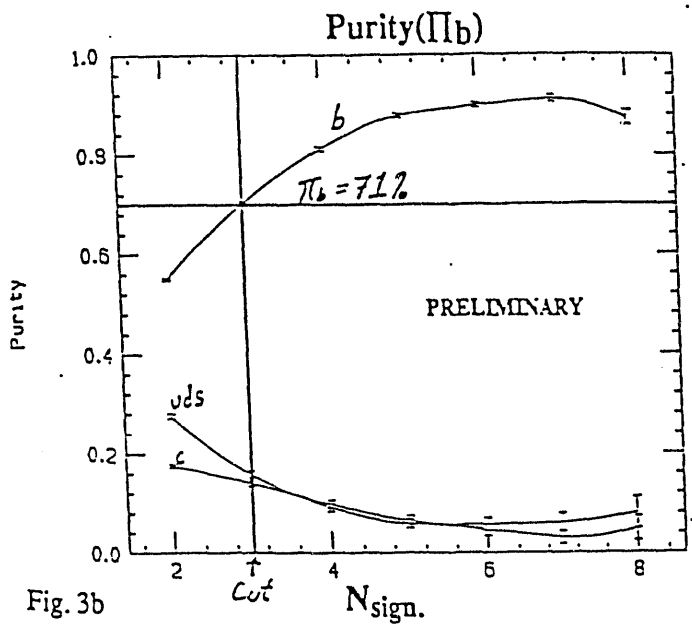


Fig. 3b

DRAFT

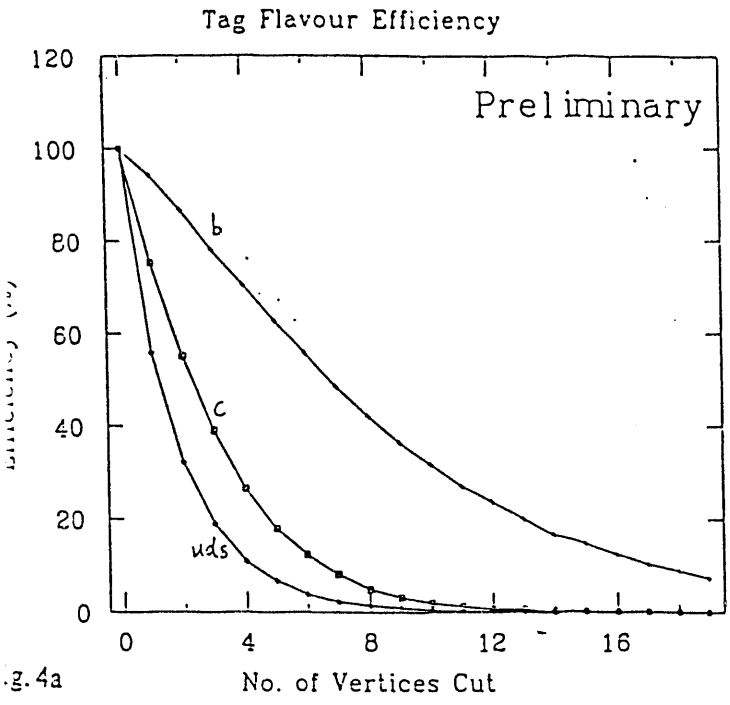


Fig. 4a

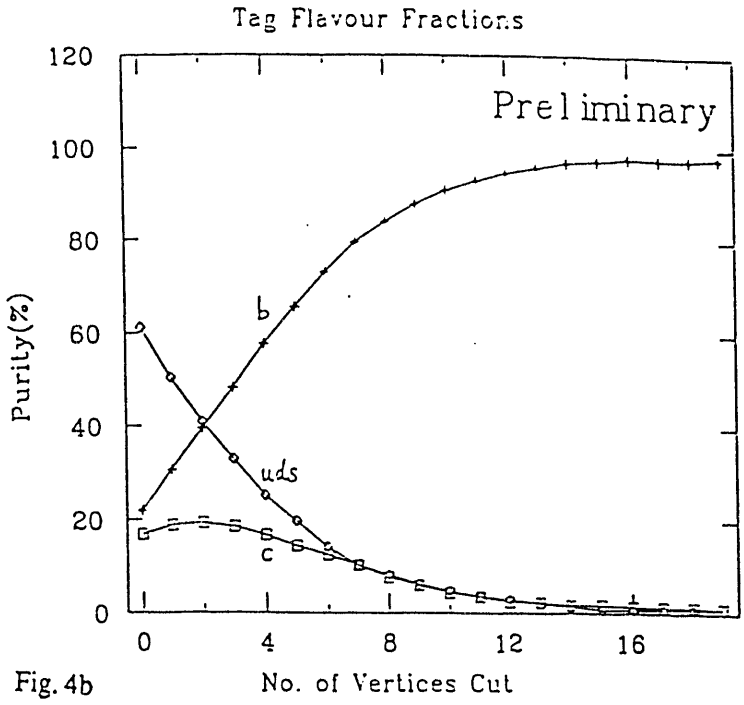


Fig. 4b

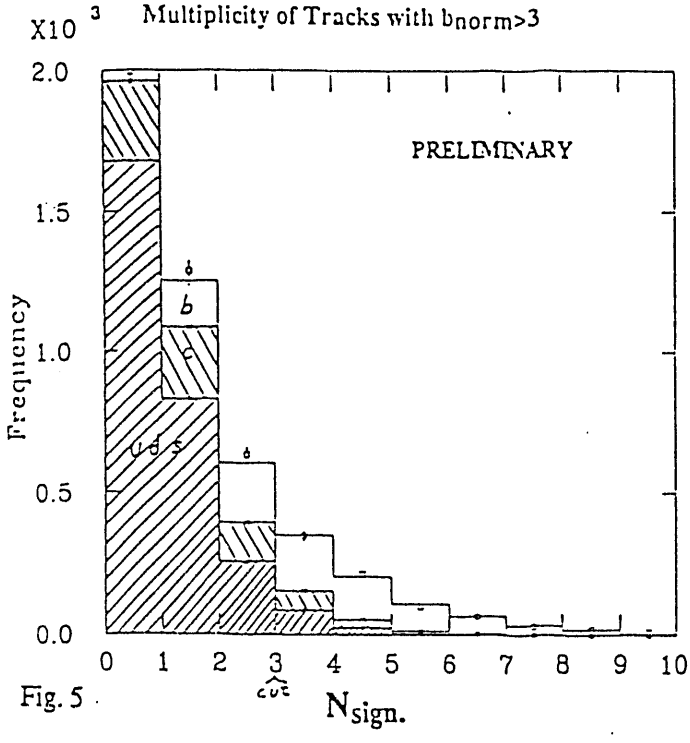


Fig. 5

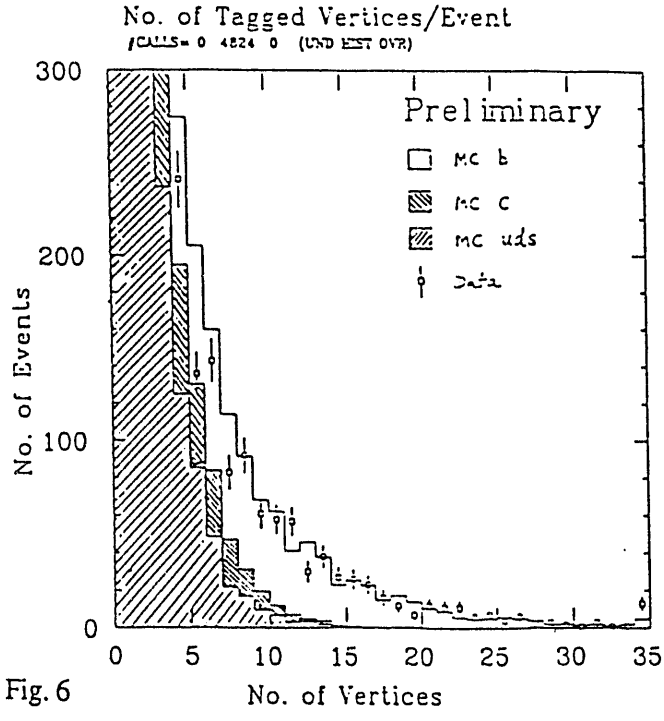


Fig. 6

DRAFT

MEASUREMENTS OF GLUON SPIN-SENSITIVE QUANTITIES AT THE $Z^0$ RESONANCE

The SLD Collaboration

*Presented by* Cheng-Gang Fan

**Abstract**

We present preliminary measurements of scaled jet energies and the Ellis-Karliner angle in 3-jet hadronic events from the $Z^0$ decay. Good agreement is found between the data and the QCD prediction. A scalar gluon model is clearly excluded.

## 1. Introduction

Distributions of the scaled jet energies and the Ellis-Karliner angle[1], $\theta_{EK}$, in $Z^0 \longrightarrow q\bar{q}g$ events are sensitive to the spin of the gluon. Several groups[2,3] have used these distributions to determine the gluon spin and to test a scalar gluon model at energies around 30 GeV. We present these distributions at the $Z^0$ resonance, where the differences between the vector gluon (QCD) predictions and the scalar gluon predictions are larger. Similar analyses were done at OPAL[4] and L3[5].

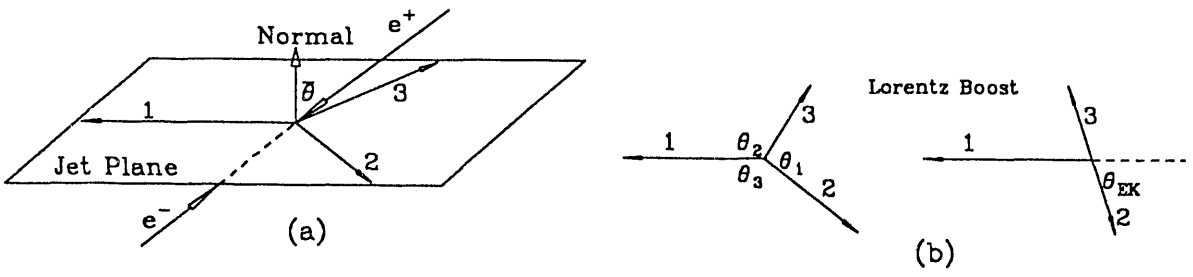


**Fig 1.** the 3-jet event plane (a), and the Ellis-Karliner Angle (b).

The $\mathcal{O}(\alpha_s)$ cross-section for $q\bar{q}g$ events in $e^+e^-$ annihilation at the $Z^0$ resonance can be written, assuming massless partons, as[6,7]:

$$\frac{d^2\sigma^V(x_1,x_2)}{dx_1dx_2} \sim \frac{x_1^2+x_2^2+(2-x_1-x_2)^2}{(1-x_1)(1-x_2)(x_1+x_2-1)} \tag{1}$$

$$or \quad \frac{d^2\sigma^S(x_1,x_2)}{dx_1dx_2} \sim \frac{x_1^2(1-x_1)+x_2^2(1-x_2)+(2-x_1-x_2)^2(x_1+x_2-1)}{(1-x_1)(1-x_2)(x_1+x_2-1)} - \frac{10C_a^2}{C_v^2+C_a^2} \tag{2}$$

where $x_i = 2E_i/E_{cm}$, $x_1 > x_2 > x_3$, are the scaled parton energies (Fig. 1a), and $C_v$ and $C_a$ are the vector and axial-vector coupling constants. Eq. (1) is from the vector gluon (the standard QCD) theory, and Eq. (2) is from a scalar gluon model. For massless partons, one has:

$$x_i = \frac{sin\theta_i}{sin\theta_1 + sin\theta_2 + sin\theta_3} \quad (i = 1,2,3) \tag{3}$$

$$cos\theta_{EK} = \frac{(x_2 - x_3)}{x_1} \tag{4}$$

where the $\theta_i$ are the angles between the two jets opposite to jet $i$; and $\theta_{EK}$, the Ellis-Karliner angle, is the angle between jets 1 and 2 in the rest frame of jets 2 and 3 (see Fig. 1b). The cross-section can also be written in terms of any single $x_i$ and $cos\theta_{EK}$. Distributions of each individual variable, obtained by integration of the above cross-sections, are clearly different for the two gluon spins.

## 2. Data Selection

A total of 9,000 hadronic $Z^0$s measured by the SLD[8] experiment are used in this analysis. We use only the charged tracks measured in the central drift chamber[8]. Details of the track and event selection cuts are described elsewhere[9]. 3-jet events are selected at $y_{cut} = 0.02$ using the JADE jet-finding algorithm[10]. We require $|cos\bar{\theta}| > 0.704$ where $\bar{\theta}$ is the angle between the electron beam direction and the normal to the event plane (Fig. 1a). 1418 events survived these cuts. The background in the three-jet sample from non-hadronic $Z^0$ decays is negligible.

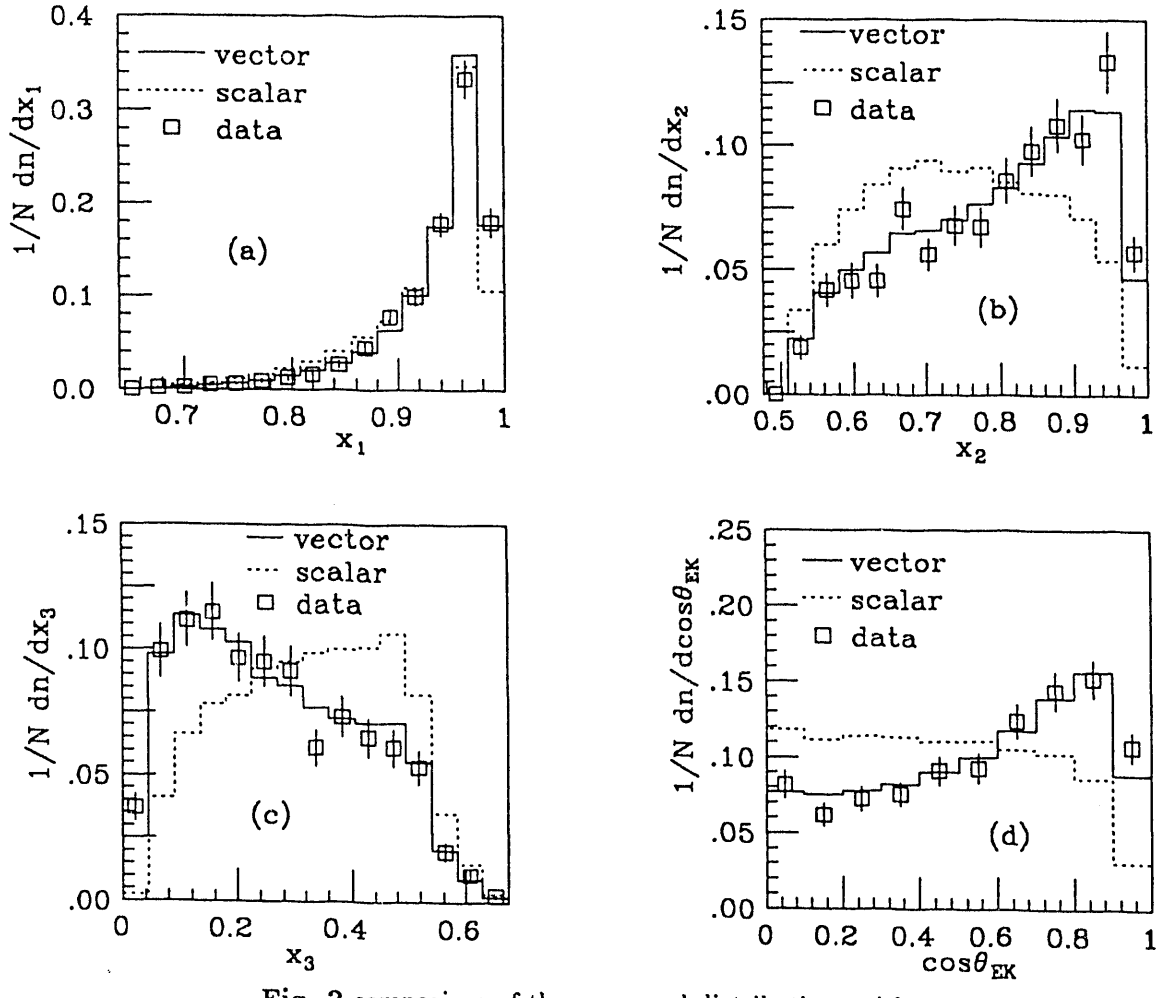


Fig. 2 comparison of the measured distributions with vector(QCD) and scalar gluon predictions at the parton level.

## 3. Results and Conclusion

The variables $x_i$ and $cos\theta_{EK}$ are calculated using Eqs. (3) and (4) and the jet axes from the JADE jet-finding algorithm. Using only the angles reduces the effects of not detecting all the energy in each jet. Monte Carlo events are generated using the JETSET 6.3[11] and HERWIG 5.3[12] programs and passed through a detailed SLD detector simulation and the same selection criterion as applied to the real data. The Monte Carlo results and the data agree well within statistical errors. A bin-by-bin correction is applied using the JETSET 6.3 simulation to correct the data to the parton level. Fig. 2 shows the corrected distributions of $x_1$, $x_2$, $x_3$ and $cos\theta_{EK}$, compared with leading order scalar and vector (QCD) gluon calculations. Both equations 1 and 2 are implemented in JETSET 7.3[11] program, by which all the theoretical distributions are generated. The vector gluon calculation agrees with the data. The scalar gluon model does not agree with the data. The following table shows the $\chi^2$ per degree of freedom between the data and calculations.

**$\chi^2/df$ between data and vector/scalar gluon predictions.**

| | $x_1$ | $x_2$ | $x_3$ | $cos\theta_{EK}$ |
|---|---|---|---|---|
| Vector Gluon | 0.69 | 1.17 | 1.01 | 0.99 |
| Scalar Gluon | 7.33 | 17.1 | 16.5 | 22.9 |

In conclusion, a scalar gluon model is convincingly excluded by the data, which is in good agreement with the predictions of QCD. Similar results were obtained at OPAL[4] and L3[5].

## References


1. J. Ellis, I. Karliner, *Nucl. Phys.* **B148** (1979) 141
2. S.L. Wu, *Physics Reports* **107** (1984) p.162-163
3. Mark J Collab., J.D. Burger *et al. Journal de Physique* **43**, C3-C6
4. The OPAL collab., G. Alexander, *et al., Z. Phys.* **C52** (1991) 543
5. L3 Collab., B. Adeva, *et al., Phys. Lett.* **B263** (1991) 551
6. G. Kramer, *Springer Tracts in Modern Physics*, **vol. 102** (1984) p.39
7. E. Laermann, K.H. Streng and P.M. Zerwas, *Z. Physik* **C3** (1980)289
8. SLD Design Report, SLAC Report **273** (1984).
9. SLD Collab., P.N. Burrows *et al.*, SLAC-Pub-5802 (1992).
10. JADE Collab., S. Bethke *et al.*, *Phys. Lett.* **213B** (1988) 235
11. T. Sjöstrand, *Comput. Phys. Commun.* **39** (1986) 347; **43** (1987) 367.
12. G. Marchesini, B.R. Webber, *Nucl. Phys.* **B310** (1988) 461

# FIRST MEASUREMENT OF THE LEFT-RIGHT CROSS SECTION ASYMMETRY IN Z BOSON PRODUCTION AT $E_{CM}$ = 91.55 GEV

THE SLD COLLABORATION
*represented by*
BRUCE A. SCHUMM
*Physics Division*
*Lawrence Berkeley Laboratory, Berkeley, California 94720*

ABSTRACT

The left-right cross section asymmetry for $Z^0$ boson production in $e^+e^-$ annihilation ($A_{LR}$) has been measured at $E_{cm}$ = 91.55 GeV with the SLD detector at the SLAC Linear Collider (SLC) using a longitudinally polarized electron beam. The electron polarization was continuously monitored with a Compton scattering polarimeter, and was typically 22%. We have accumulated a sample of $\sim 10,000$ $Z^0$ events. We find that $A_{LR} = 0.100 \pm 0.044 \pm 0.003$ where the first error is statistical and the second is systematic. From this measurement, we determine the weak mixing angle defined at the $Z^0$ boson pole to be $\sin^2\theta_W^{\rm lept} = 0.2378 \pm 0.0056$.

The left-right asymmetry is defined as

$$A_{LR} \equiv \frac{\sigma(e^+e_L^- \to Z^0) - \sigma(e^+e_R^- \to Z^0)}{\sigma(e^+e_L^- \to Z^0) + \sigma(e^+e_R^- \to Z^0)}, \tag{1}$$

where $\sigma(e^+e_L^- \to Z^0)$ and $\sigma(e^+e_R^- \to Z^0)$ are the production cross sections for $Z^0$ bosons with left-handed and right-handed electrons, respectively. Within the context of the Standard Model, this quantity is a sensitive function of the electroweak mixing parameter $\sin^2\theta_W^{\rm lept}$ :

$$A_{LR} = \frac{2v_e a_e}{v_e^2 + a_e^2} = \frac{2\left[1 - 4\sin^2\theta_W^{\rm lept}\right]}{1 + \left[1 - 4\sin^2\theta_W^{\rm lept}\right]^2}, \tag{2}$$

where $v_e$ and $a_e$ are the vector and axial vector coupling constants of the $Z^0$ boson to the electron current. The left-right asymmetry has the following properties: it is sensitive to the initial state couplings and is insensitive to the final state couplings; it is sensitive to virtual electroweak corrections; it is insensitive to real radiative corrections; it is a weak function of center-of-mass energy, $E_{cm}$, near the $Z^0$ pole; and it is expected to be relatively large, in the range 0.10-0.15.

The SLC was designed to allow the production, acceleration, and collision of a spin-polarized electron beam with an unpolarized positron beam. Polarized $e^-$ beams are produced by injecting the LINAC with electrons of $\sim$ 28% polarization, produced by the illumination of a GaAs photocathode with circularly polarized laser light.[1] The electron helicity is randomized by changing the laser helicity on a cycle-by-cycle (120 Hz) basis. During the process of acceleration and transport, the

beam suffers partial depolarization in the damping rings and arcs, arriving at the IP with a polarization of $\sim 22\%$. The electron and positron beams are then transported to beam dumps, where the beam energies are continuously monitored by a pair of precision energy spectrometers.[2] The mean electron and positron energies were measured to be 45.71 GeV and 45.84 GeV, respectively, yielding a mean cms energy of $\langle E_{cm} \rangle = 91.55 \pm 0.04$ GeV.

Polarimetry is accomplished by passing the electron beam through a circularly polarized ($P = 93 \pm 2\%$) Nd:YAG laser beam of wavelength $\lambda = 532\ nm$. In order to avoid systematic effects, the sign of the circular polarization is changed randomly on sequential laser pulses. Compton scattered electrons are then dispersed horizontally by a beamline dipole magnet ($p_\perp$ kick = 828 MeV) and exit the vacuum system through a thin window. Electrons in the energy interval 15-30 GeV are detected and momentum analyzed by a pair of redundant multichannel detectors (a Cherenkov detector and a proportional tube detector), which measure the asymmetry in the Compton scattering process for anti-parallel and parallel photon/electron beam helicities, as a function of transverse distance from the unscattered beam. The electron beam polarization is extracted from the overall normalization of the measured asymmetry function, which is given by the product of the laser and electron beam polarizations. Polarimeter data are logged continuously for intervals of 20,000 SLC cycles (~3 min) and written in summary form onto SLD data tapes.

To check for depolarization due to spin precession during the transport of the beam between the SLD and Compton IP's, we have run beams through the IP region with the SLD solenoid and intervening quadrupoles turned off. The stability of the beam trajectory under this change limits the change in polarization between the two IP's to be less than 0.1%.

Figure 1 shows the measurement of the asymmetry function in the Cherenkov detector, averaged over polarimeter data from the entire 1992 run. Also shown is the theoretical asymmetry curve; agreement between the measured and theoretical asymmetry function is quite good. We estimate the relative systematic error on the Compton Polarimeter measurement to be $\pm 3\%$, dominated by the $\pm 2\%$ uncertainty in the laser circular polarization.

The absolute sign of the electron beam helicity is inferred from the sign of the Compton asymmetry, which is larger for parallel than anti-parallel spins. The absolute helicity of the laser polarization was determined with a quarter-wave plate for which the fast axis had been identified by several independent optical techniques.

The polarized $e^+e^-$ collisions are measured by the SLD detector.[3] The $Z^0$ decay selection criteria used were based primarily on information from the projectively segmented Liquid Argon Calorimeter (LAC).[4] $Z^0$ candidates were required to have at least 20 GeV of visible energy deposited in the LAC, in each hemisphere a LAC tower (i.e., single electronics channel) of at least 500 MeV, and a normalized energy imbalance of less than 0.8. Wide-angle Bhabha's, which exhibit a different left-right asymmetry than other final states due to interference with the purely QED t-channel process, are removed by requiring that the sum of the two largest LAC towers in each hemisphere (4 towers total) contain less than 30 GeV (12 GeV) of

deposited energy for $\theta$ greater than (less than) 15°. We estimate that the resulting sample contains $\sim 0.5\%$ wide-angle Bhabha's, and less than 1% single-beam and two-photon backgrounds. Neither of these contaminations has an appreciable effect on our determination of $A_{LR}$. After an additional requirement that there be a measurement of the beam polarization within 1 hour of each $Z^0$ event, the resulting sample contains 10224 $Z^0$ candidates, consisting of 5226 events produced with left-handed beam, and 4998 events produced with right-handed beam.

We have performed several checks to ensure that the beam conditions are left-right symmetric. We have binned beamstrahlung and beam deflection data according to left- and right-handed electron beam, and determined that the left-right luminosity asymmetry is less than $10^{-3}$. A more direct, but statistically weaker, measurement of the luminosity asymmetry is given by the left-right asymmetry of 25615 small-angle Bhabha's identified by the silicon-tungsten luminosity monitoring system:[5] $A_{LR}^{Bhabha} = .002 \pm .006$. The left-right polarization asymmetry, measured with the entire sample of Polarimeter data, is $< 5 \cdot 10^{-3}$. We have also checked that the numbers of left-handed and right-handed pulses logged by the SLD data acquisition system are equal to within statistical errors.

With the luminosity and electron polarization left-right symmetric, and negligible event backgrounds, we calculate $A_{LR}$ via the following simple expression:

$$A_{LR} = \frac{A_{meas}}{\mathcal{P}} = \frac{1}{\mathcal{P}} \cdot \left( \frac{N_L - N_R}{N_L + N_R} \right), \tag{3}$$

where $\mathcal{P}$ is the luminosity-weighted average polarization, and $N_L$ and $N_R$ are the total event counts produced by left- and right-handed electron beam, respectively. The luminosity weighted average polarization is given by

$$\mathcal{P} \equiv \frac{1}{N_Z} \sum_{i=1}^{N_Z} \mathcal{P}_i = 22.4 \pm 0.7\%, \tag{4}$$

where $N_Z$ is the total number of $Z^0$ events, and $\mathcal{P}_i$ is the polarization that was measured when the $i^{th}$ event was logged. The uncertainty is dominated by the 3% relative systematic uncertainty on the polarimeter measurements. Combining this with the left- and right-handed event samples quoted above, we find that

$$A_{LR} = 0.100 \pm 0.044(\text{stat.}) \pm 0.003(\text{syst.}). \tag{5}$$

The small systematic error is dominated by the systematic error on the mean polarization. Based on formula (2), this yields a value of the electroweak mixing parameter

$$\sin^2 \theta_W^{\text{lept}} = 0.2378 \pm 0.0056(\text{stat.} + \text{sys.}). \tag{6}$$

This value includes a small (+.0003) correction to account for the effects of initial state radiation, and for the fact that the mean cms energy $\langle E_{cm} \rangle = 91.55\ GeV$ was slightly above the $Z^0$ peak. Both the value of $A_{LR}$ and $\sin^2 \theta_W^{\text{lept}}$ quoted here are consistent with recent results from LEP experiments.

In the upcoming 1993 run, we anticipate an accumulated data sample of at least 50,000 events, with a mean electron polarization of 40%. With such a sample, we would measure $A_{LR}$ to $\pm.011$, and $\sin^2\theta_W^{lept}$ to $\pm.0014$. In addition, it may be possible to make use of the recent development of strained lattice cathodes to achieve source polarizations in excess of 80%,[6] further increasing the statistical power of the $A_{LR}$ measurement.

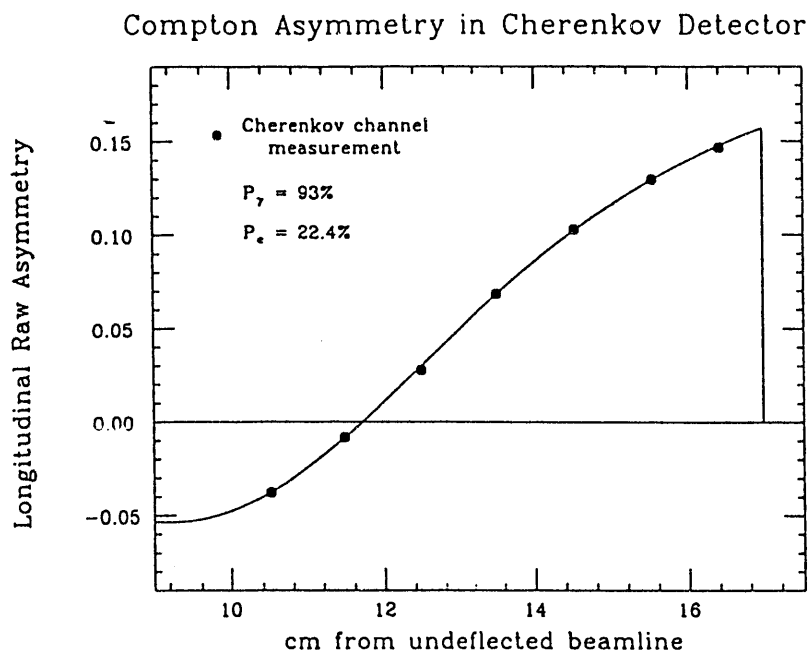


Figure 1: Comparison between theoretical asymmetry function and individual Cerenkov channel measurements (dots), averaged over the entire Polarimeter data set.

## References


1. D. Schultz *et al.*, SLAC-PUB-5768, 1992.
2. J. Kent *et al.*, SLAC-PUB-4922, 1989.
3. The SLD Design Report, SLAC Report 273, 1984.
4. D. Axen *et al.*, SLAC-PUB-5354, 1992 (to be published in Nucl. Instr. and Meth.).
5. S. C. Berridge *et al.*, SLAC-PUB-5694, 1991 (to be published in IEEE Trans. Nucl. Sci.).
6. T. Maruyama *et al.*, *Phys. Rev.* **B46**, 4261 (1992).

# PERFORMANCE OF A SILICON CCD PIXEL VERTEX DETECTOR IN THE SLD

The SLD Collaboration

Presented By

M.G. Strauss

*University of Massachusetts*
*Amherst, Massachusetts USA*

DPF Meeting, November, 1992

## OUTLINE

- Overview and Construction
- Backgrounds and Reliability
- Tracking
- Impact Parameter Resolution

CDC alone and CDC+VXD Track Errors

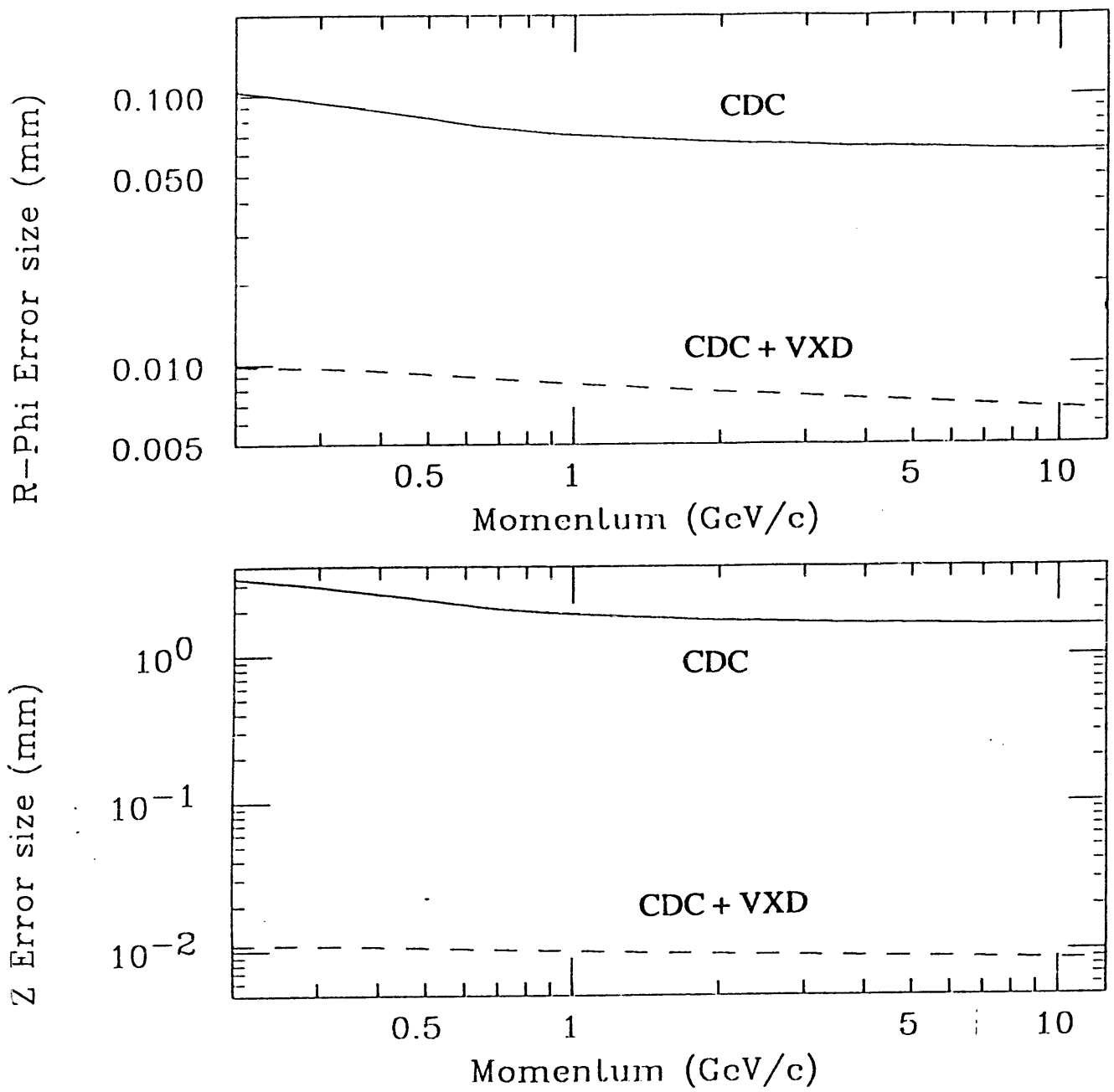

- SLC is an excellent environment to study short lived heavy quark decays
  - Small beam size
    - $2 \times 2$ μm in the transverse direction
    - $\approx 650$ μm along beam pipe
  - 25 mm radius beam pipe

To fully exploit this, we have installed a CCD pixel vertex detector which is ideally suited to the SLC operating at 120 Hz.

# VXD Overview

- 480 CCDs ($\approx .8 \times 1.2$ cm)
- 250K pixels/CCD ($22 \times 22$ μm)
- Data suppressed by 0.01%
- Operated at -80° C
- 12W power dissipated
- 160 ms readout time (19 beam crossings)
- Average amount of material is $L/L_R = 4\%$
- Material in front of VXD is $L/L_R = 0.4\%$
- Covers 75% of $4\pi$

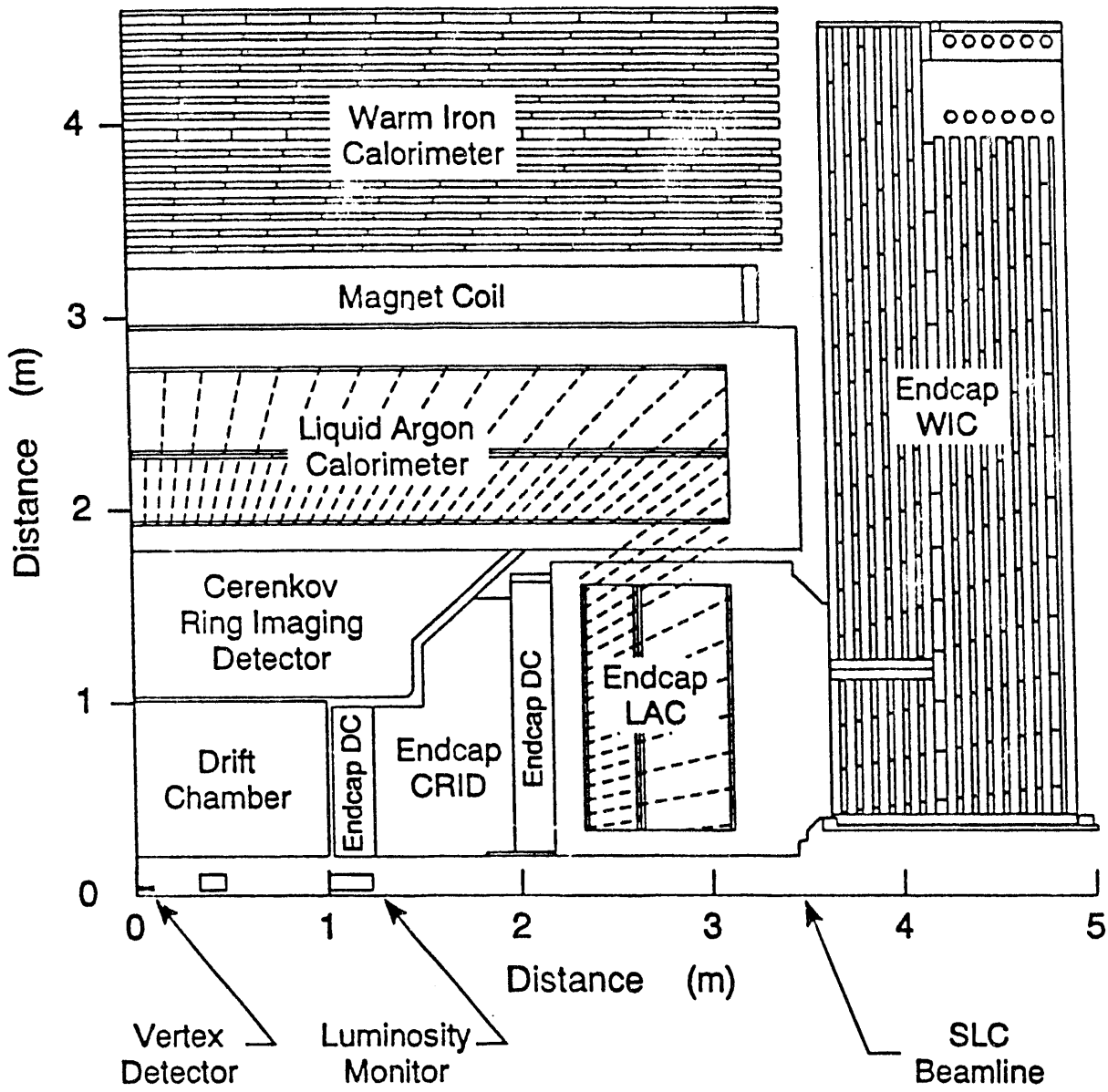
Warm Iron
Calorimeter
Magnet Coil
Liquid Argon
Calorimeter
Cerenkov
Ring Imaging
Detector
Drift
Chamber
Endcap DC
Endcap
CRID
Endcap DC
Endcap
LAC
Endcap
WIC
Distance (m)
0
1
2
3
4
5
Vertex
Detector
Luminosity
Monitor
SLC
Beamline

10-92
7282A2

# VXD Milestones

- 1986: R&D Begun
- Feb 1990: First Ladder Produced
- Dec 1990: VXD1 3 ladder prototype installed in SLD
- Jul 1991: Ladder production complete
- 12 Oct 1991: Optical survey complete
- 21 Oct 1991: Testing at RAL complete
- 24 Oct 1991: Detector moved to SLAC and installed on SLC beam pipe (R20 module).
- 12 Dec 1991: Installation of R20 into SLD
- Mar 1992: Run began
- 17 Mar 1992: 18 Ladder wedge operational in SLD data aquistition. First tracks linked three days later.
- 4 Apr 1992: Full detector in data aquisition

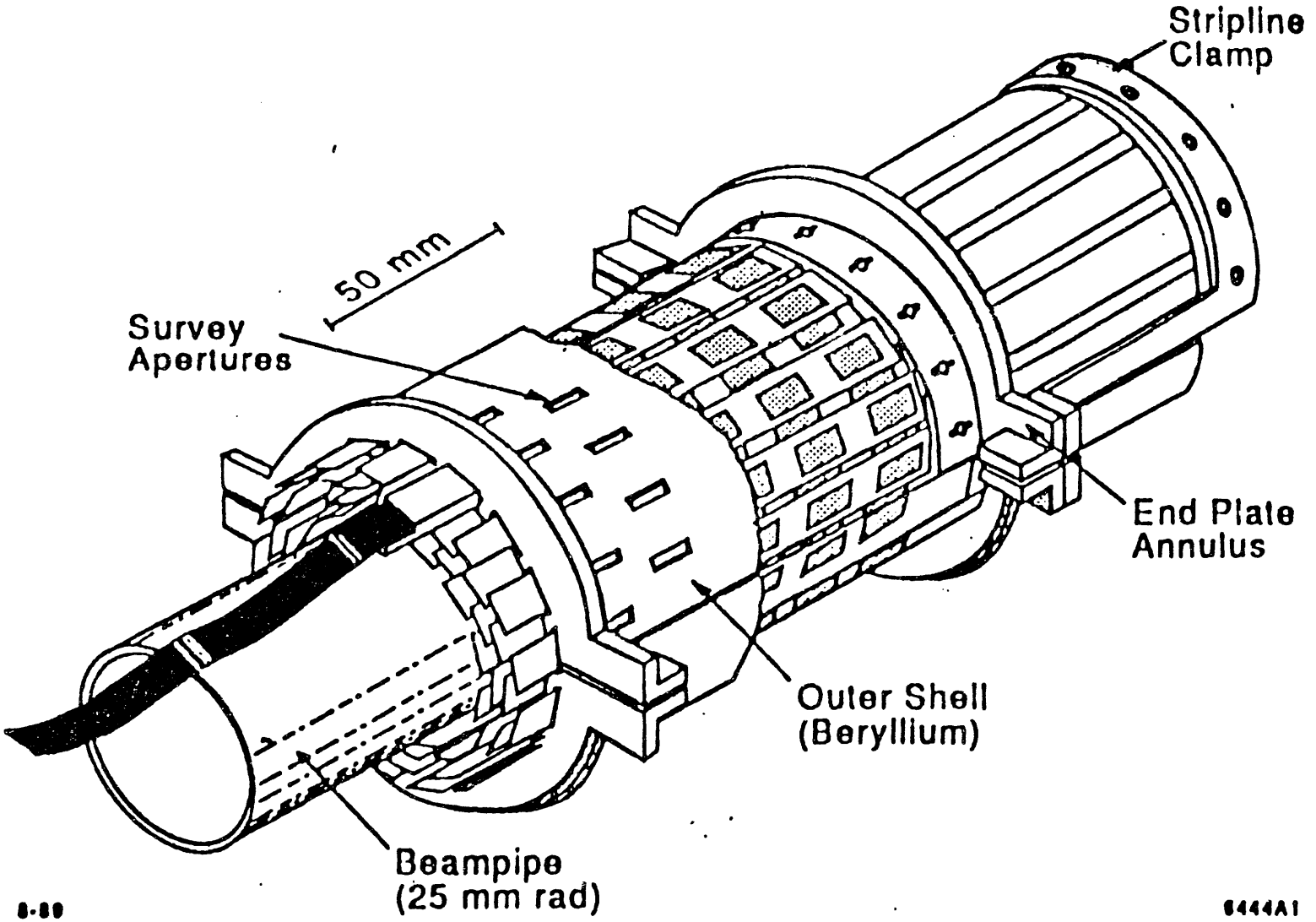
Stripline
Clamp
50 mm
Survey
Apertures
End Plate
Annulus
Outer Shell
(Beryllium)
Beampipe
(25 mm rad)

8-89

6444A1

ID=SCT1

# VXD-2 GEOMETRY

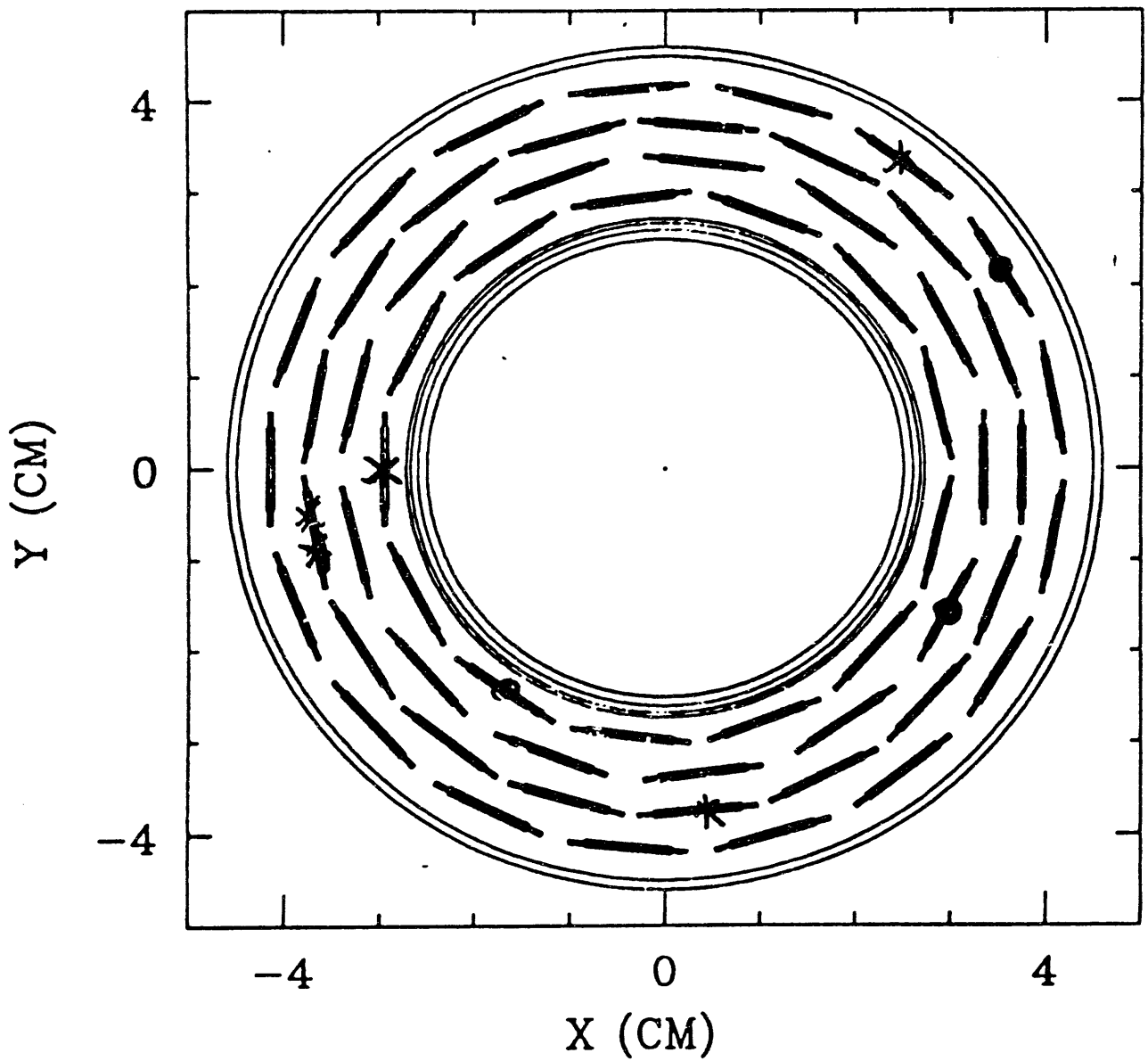


● 2 DEAD LADDERS
-electronics & connectors

* 2 DEAD CCDS
B3-9-4
B4-2-4

- 94% OF DETECTOR IS FULLY FUNCTIONAL AND RELIABLE

o INEFFICIENT LADDER
* INEFFICIENT CCD

HANDYPAK 15:40:18 16SEP92

# VXD ELECTRONICS

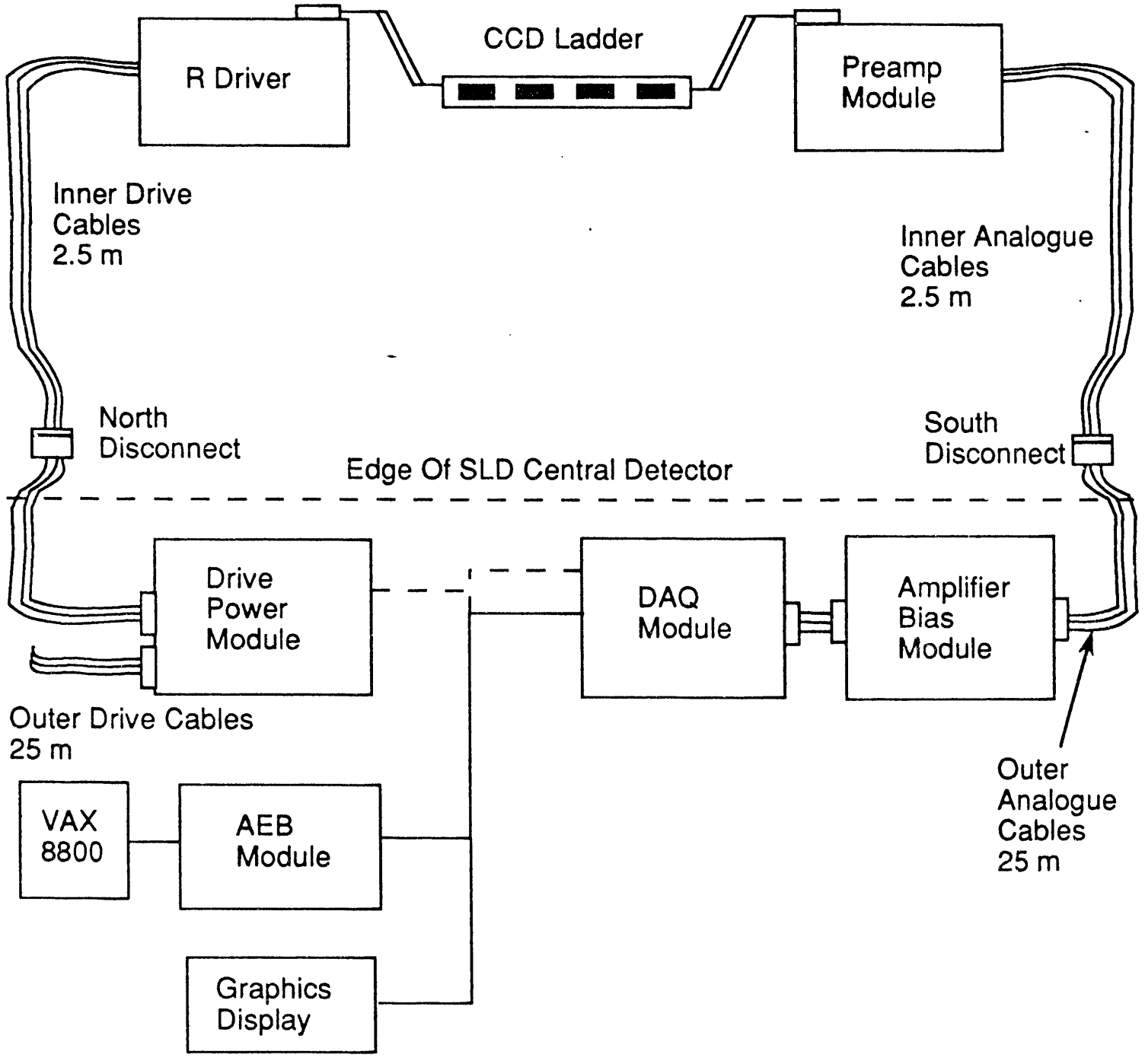

Clusters Linked to Tracks with p>1 GeV

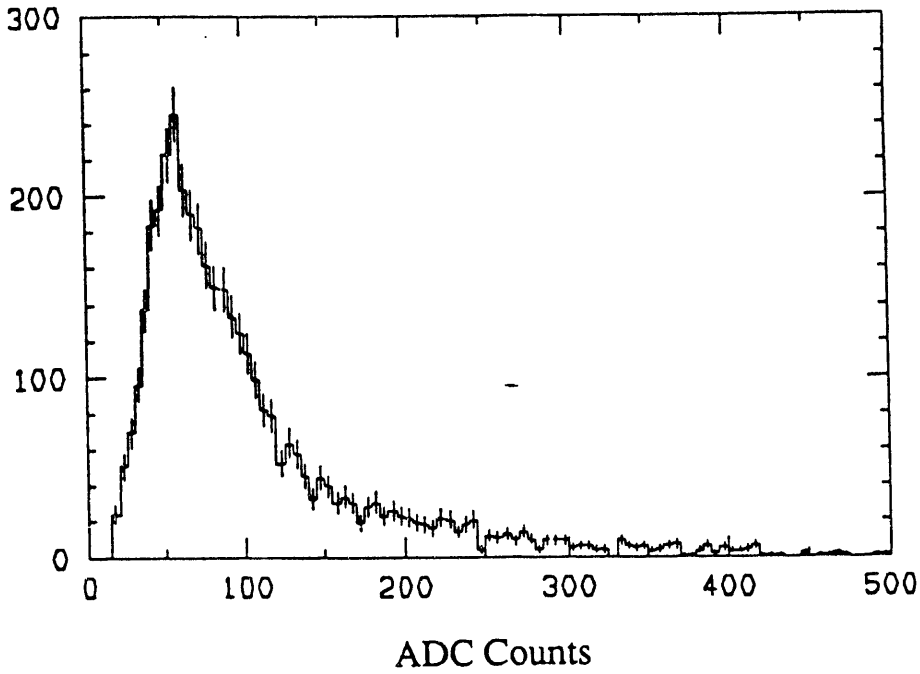

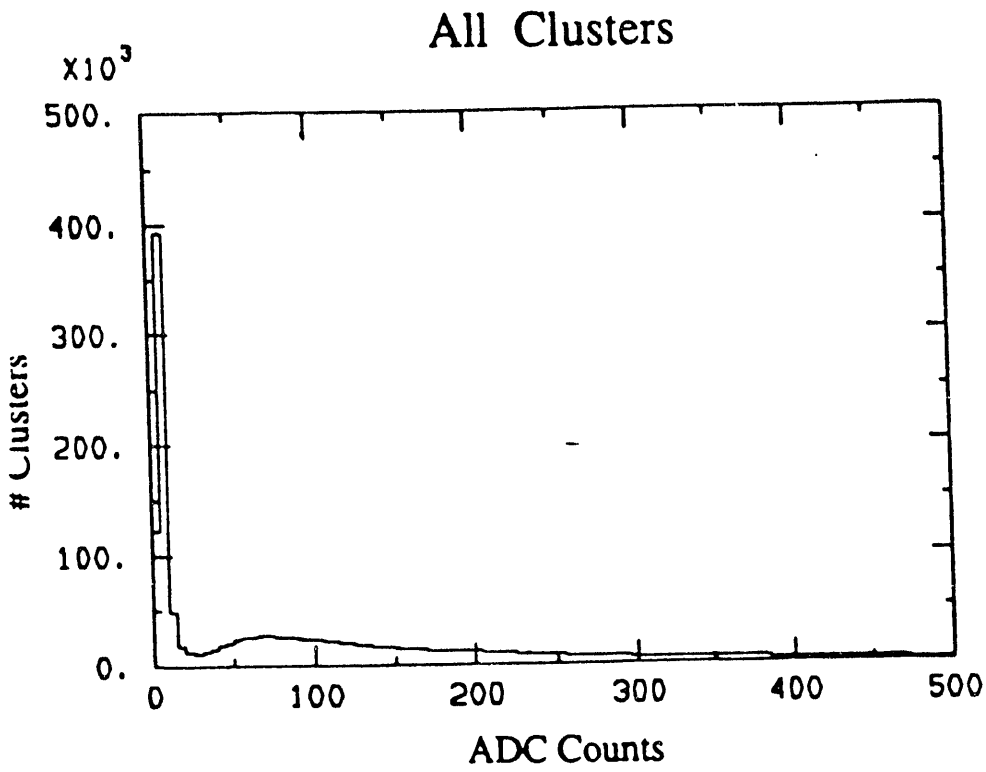
All Clusters
X10^3
500.
400.
300.
200.
100.
0.
# Clusters
0
100
200
300
400
500
ADC Counts

14e⁻/ADC

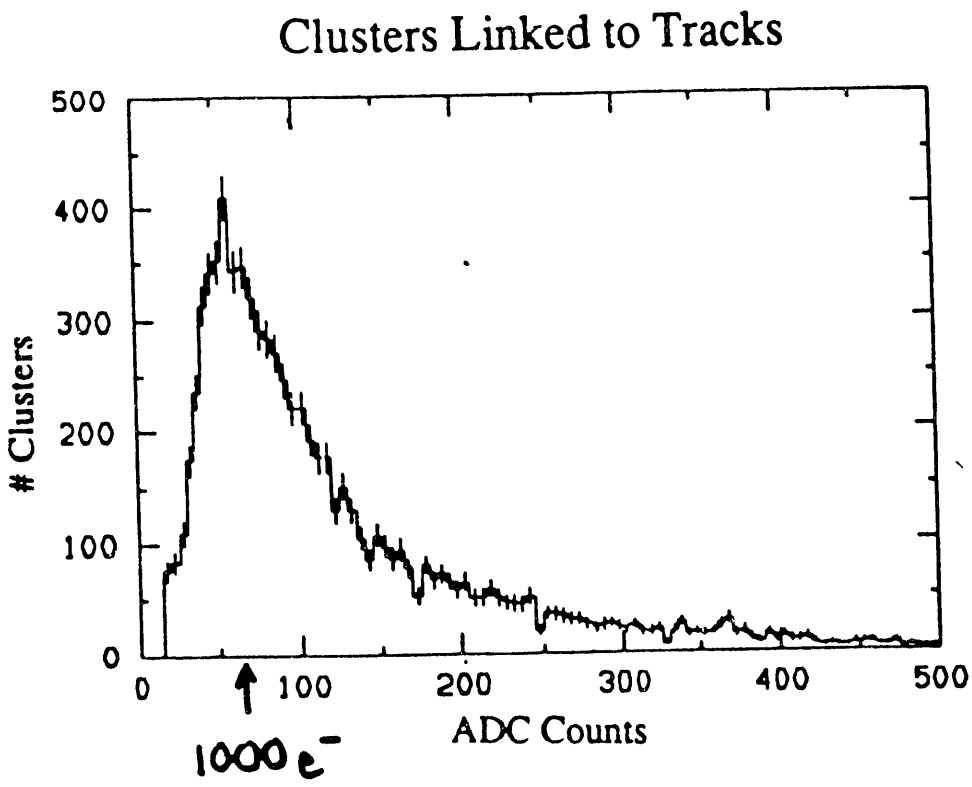
Clusters Linked to Tracks
500
400
300
200
100
0
# Clusters
0
100
200
300
400
500
ADC Counts
1000 e⁻

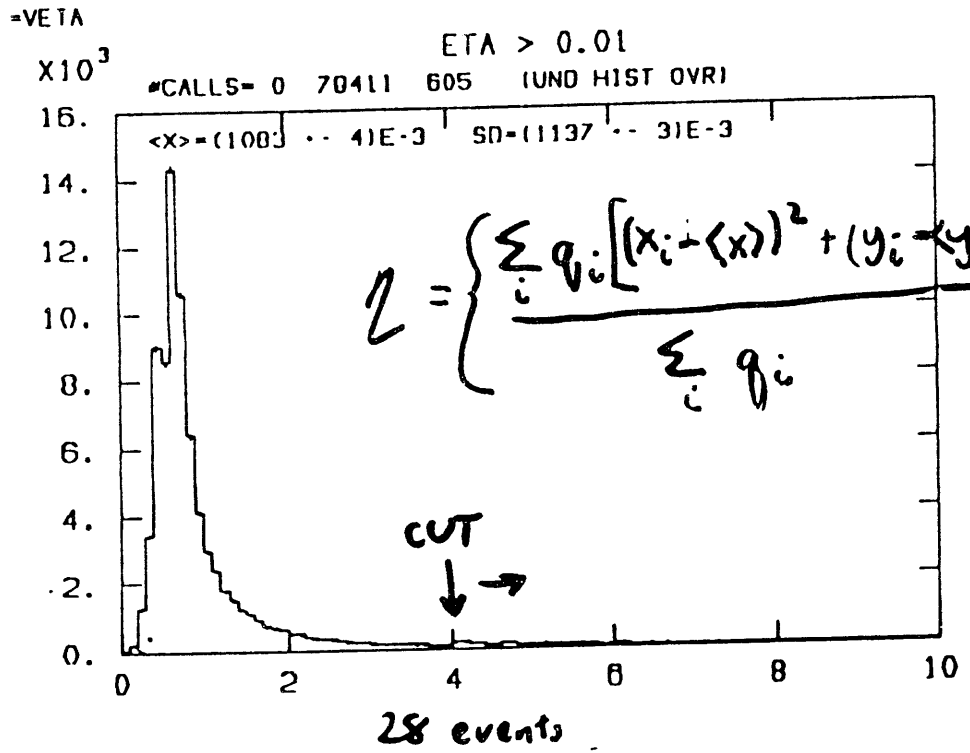


$$\ell = \left\{ \frac{\sum_i q_i \left[ (x_i - \langle x \rangle)^2 + (y_i - \langle y \rangle)^2 \right]}{\sum_i q_i} \right\}^{1/2}$$

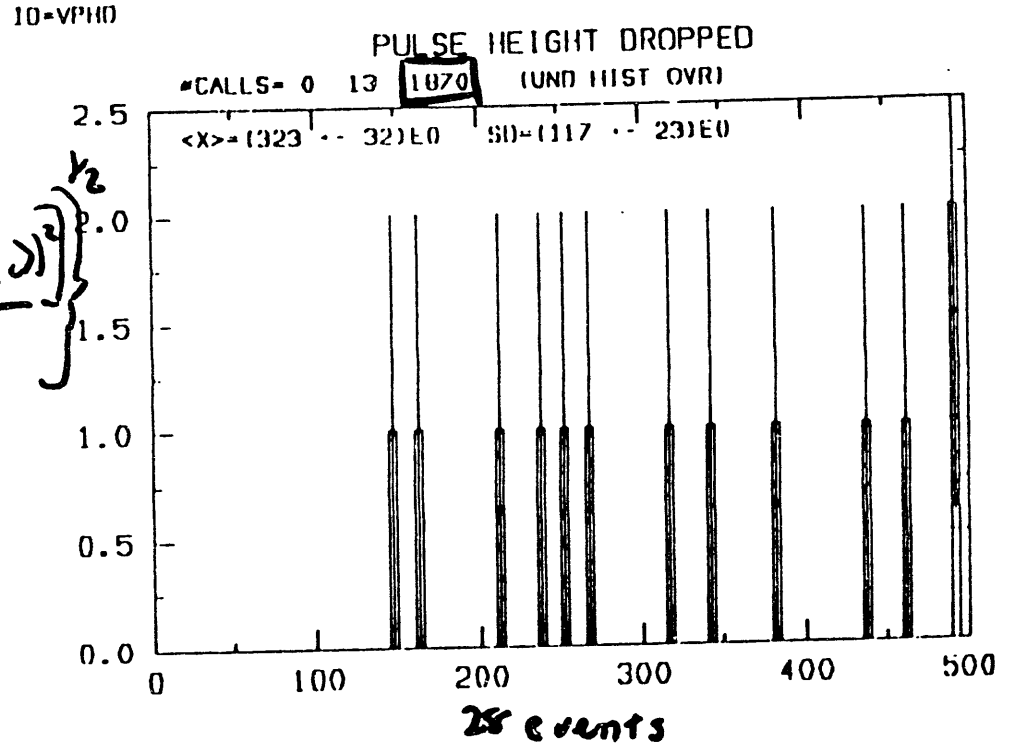


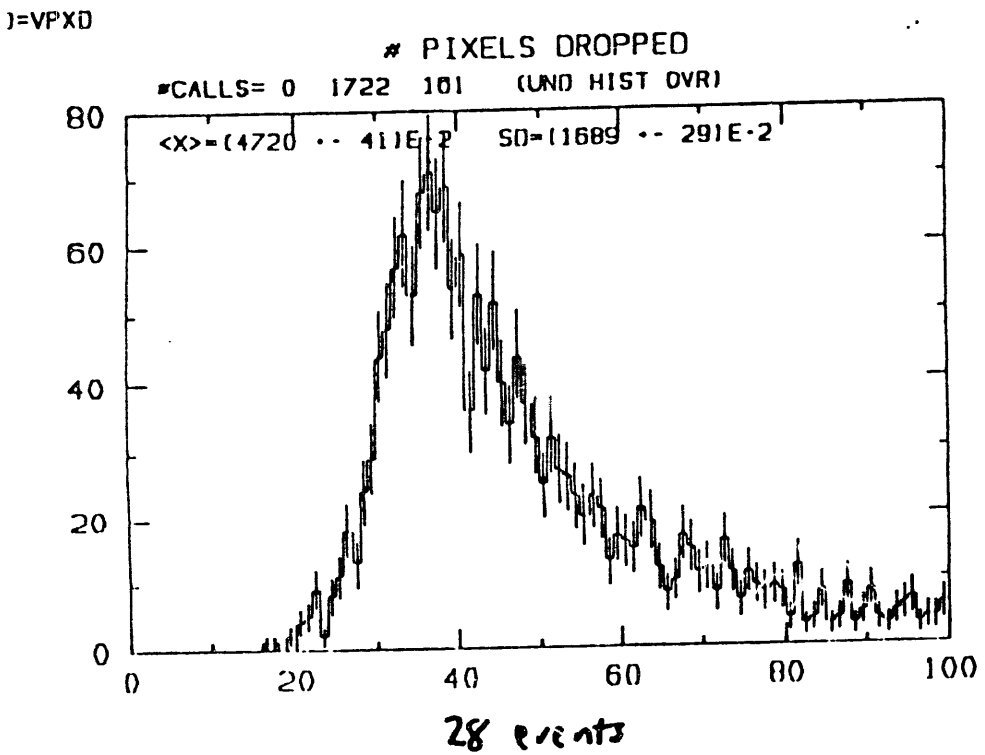


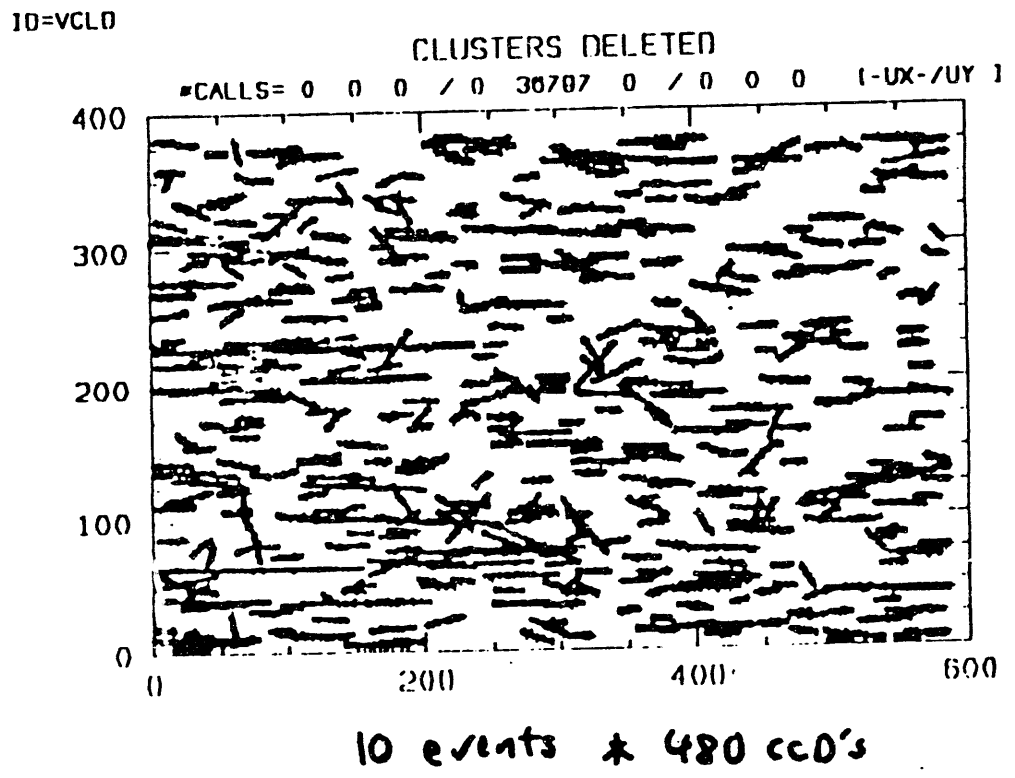

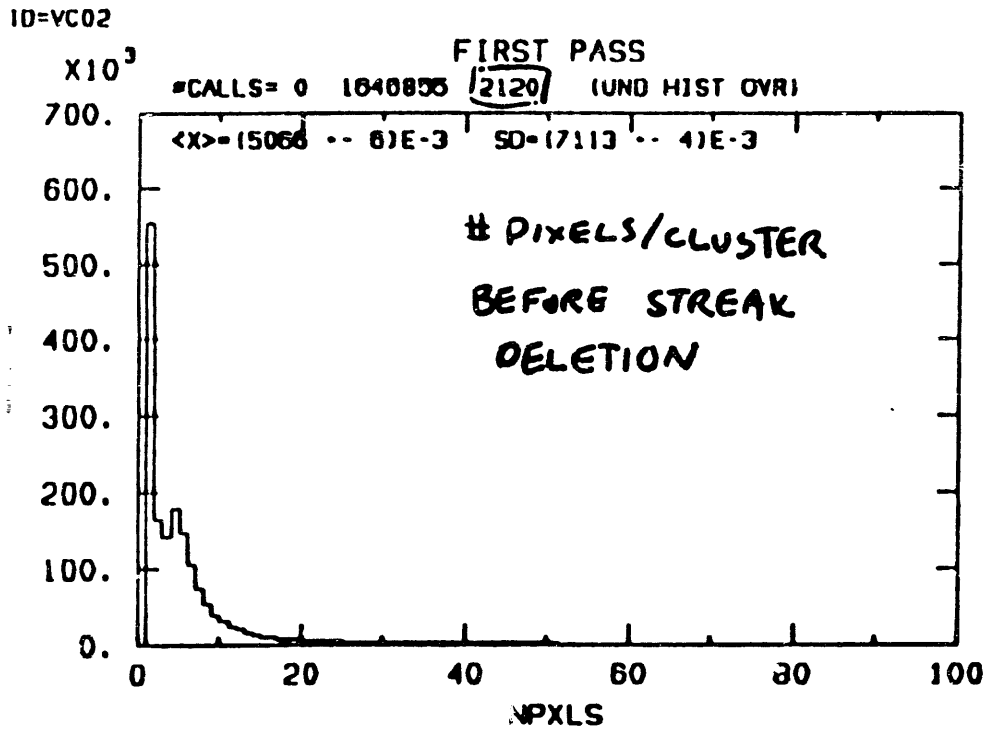
ID=VC02
FIRST PASS
X10^3
#CALLS= 0 1640855 2120 (UND HIST OVR)
<X>=(5066 -- 6)E-3 SD=(7113 -- 4)E-3
# PIXELS/CLUSTER
BEFORE STREAK
DELETION
NPXLS

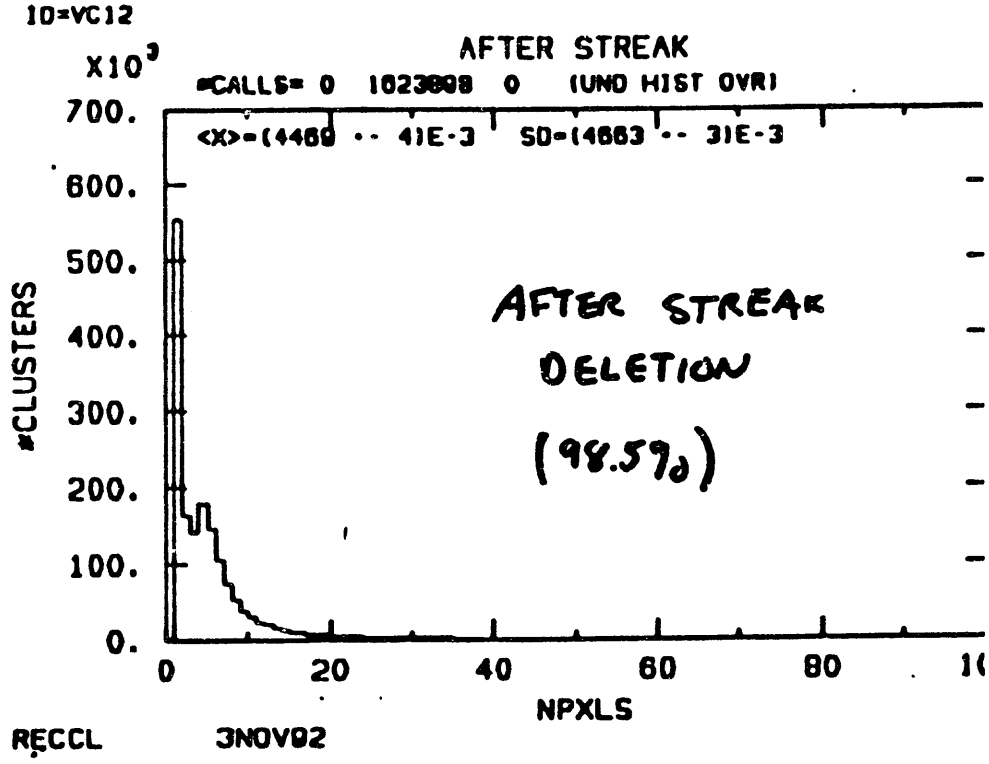
ID=VC12
AFTER STREAK
X10^3
#CALLS= 0 1623898 0 (UND HIST OVR)
<X>=(4469 -- 4)E-3 SD=(4663 -- 3)E-3
AFTER STREAK
DELETION
(98.5%)
#CLUSTERS
NPXLS
RECCL 3NOV92

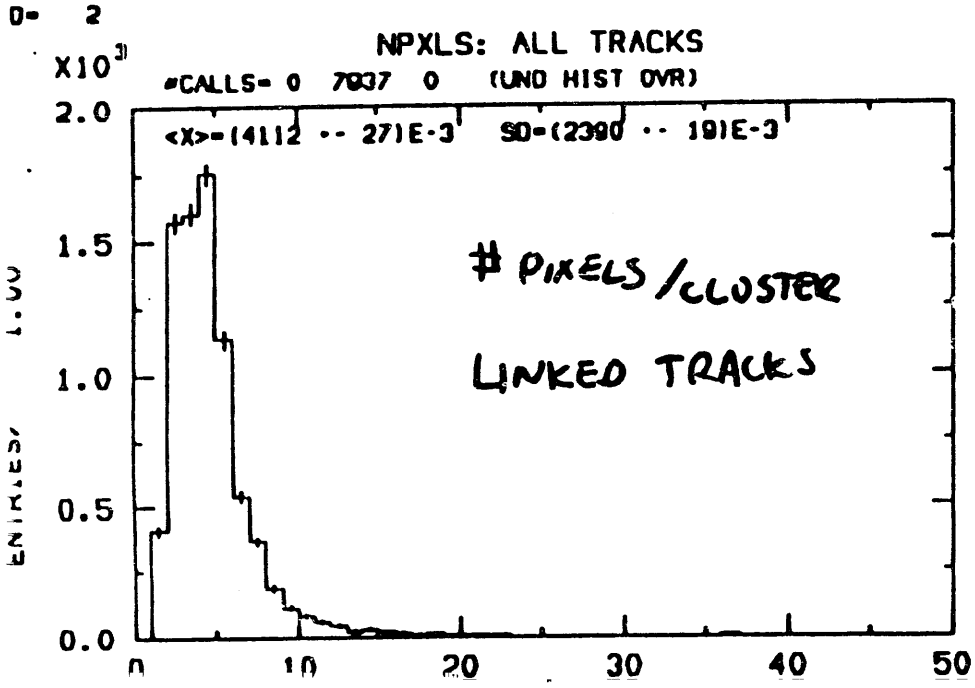
ID= 2
NPXLS: ALL TRACKS
X10^3
#CALLS= 0 7937 0 (UND HIST OVR)
<X>=(4112 -- 27)E-3 SD=(2390 -- 19)E-3
# PIXELS/CLUSTER
LINKED TRACKS

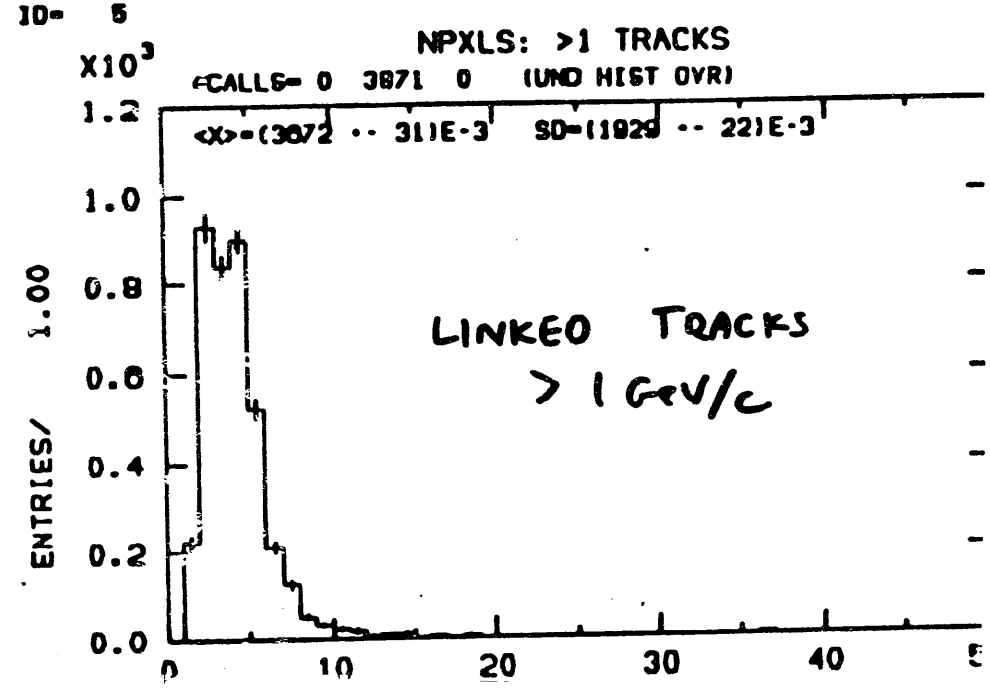
ID= 5
NPXLS: >1 TRACKS
X10^3
#CALLS= 0 3871 0 (UND HIST OVR)
<X>=(3872 -- 31)E-3 SD=(1929 -- 22)E-3
LINKED TRACKS
> 1 GeV/c
ENTRIES/ 1.00

# Movements of VXD relative to Support Cones

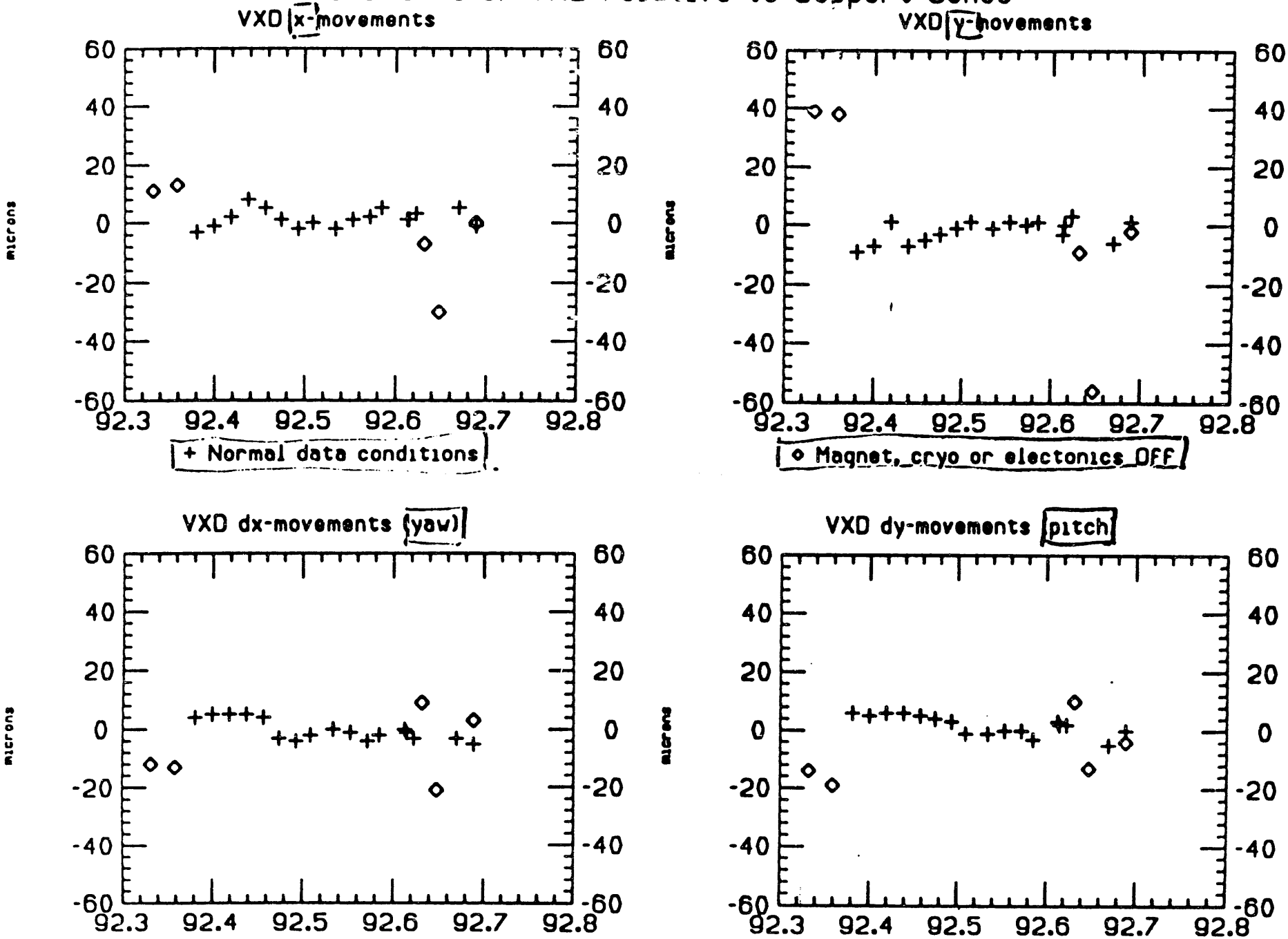


10 micron dx or dy => 30 microRadians rotation

# Monitoring VXD position relative to CDC

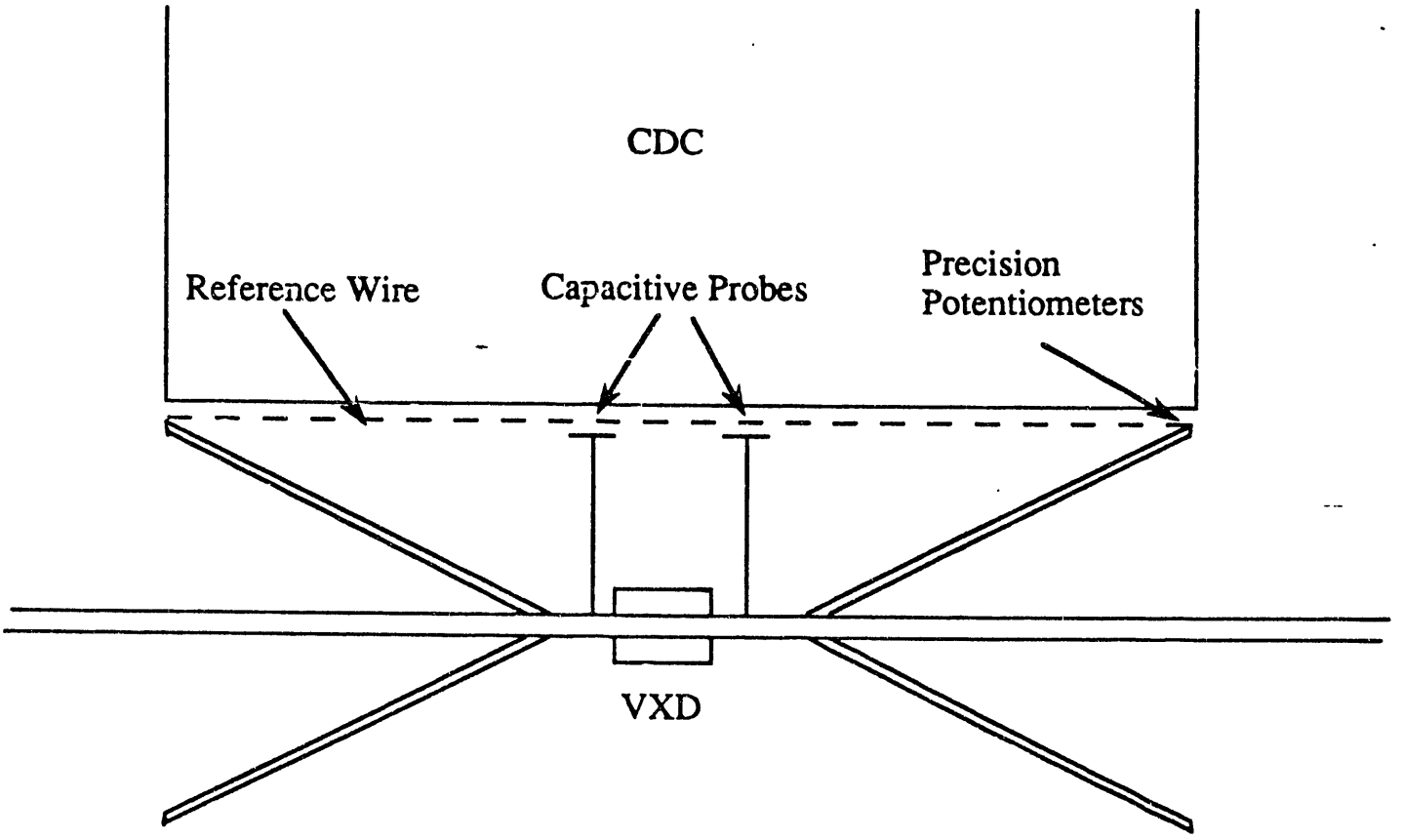

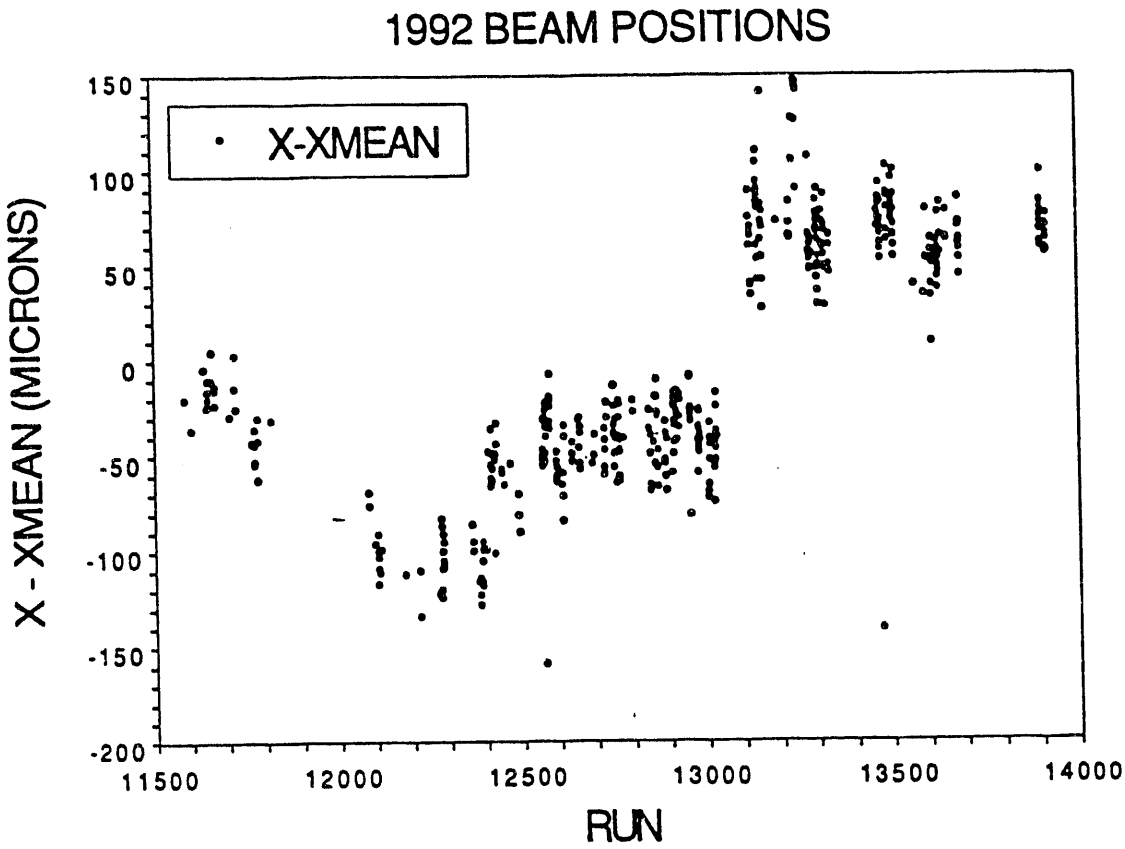
1992 BEAM POSITIONS
X-XMEAN
X - XMEAN (MICRONS)
150
100
50
0
-50
-100
-150
-200
11500
12000
12500
13000
13500
14000
RUN

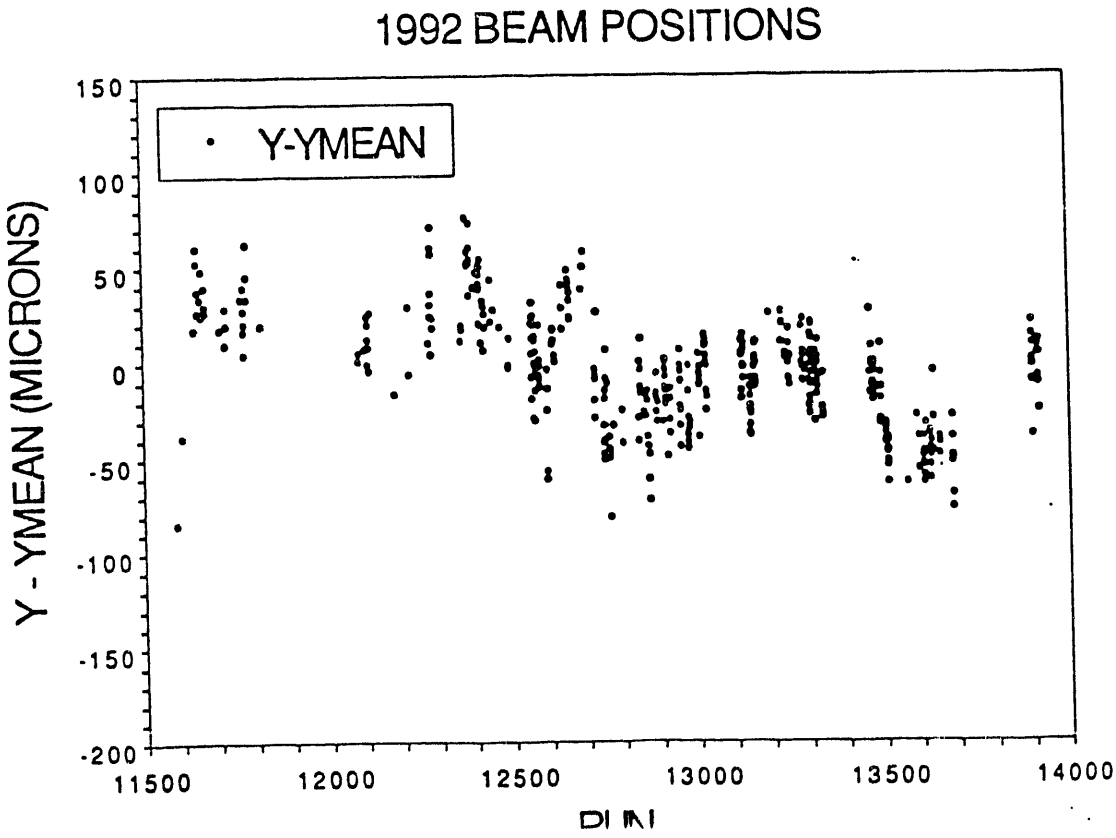
1992 BEAM POSITIONS
Y-YMEAN
Y - YMEAN (MICRONS)
150
100
50
0
-50
-100
-150
-200
11500
12000
12500
13000
13500
14000

# SLD Beam Stability Analysis

- Establish Course Periods of Beam Stability
  - Map out detector access, cooling, and solenoid changes
  - There were ≈ 4 major epochs during the 1992 run

- Group Data in Short Periods (50 Track or < 3 Hours) & Fit for X,Y Beam Posaition Using Tracks with $b_{ip}$ < 250 μm
  - Fit errors per grouping are ≈ 15 microns
  - Stability over short identifiable periods is typically

$$\sigma_{X,Y} = 18 \pm 2 \mu m$$

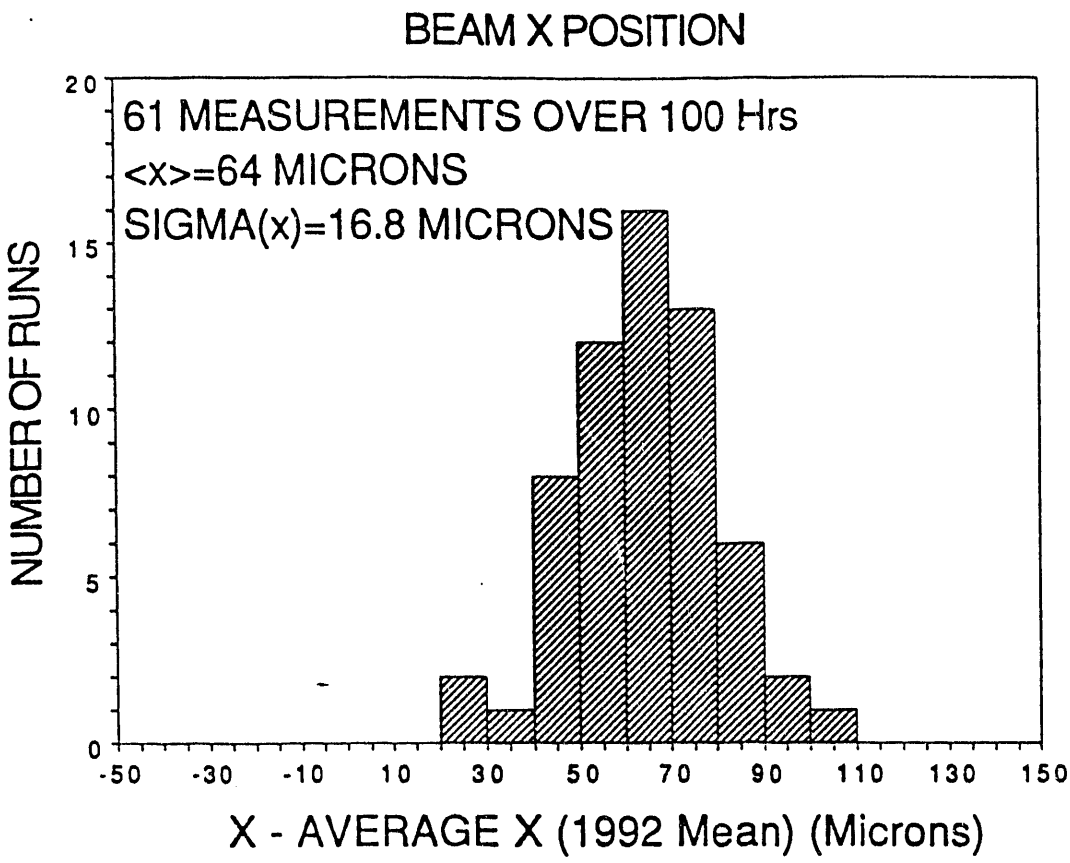
BEAM X POSITION
61 MEASUREMENTS OVER 100 Hrs
<x>=64 MICRONS
SIGMA(x)=16.8 MICRONS
NUMBER OF RUNS
0
5
10
15
20
-50
-30
-10
10
30
50
70
90
110
130
150
X - AVERAGE X (1992 Mean) (Microns)

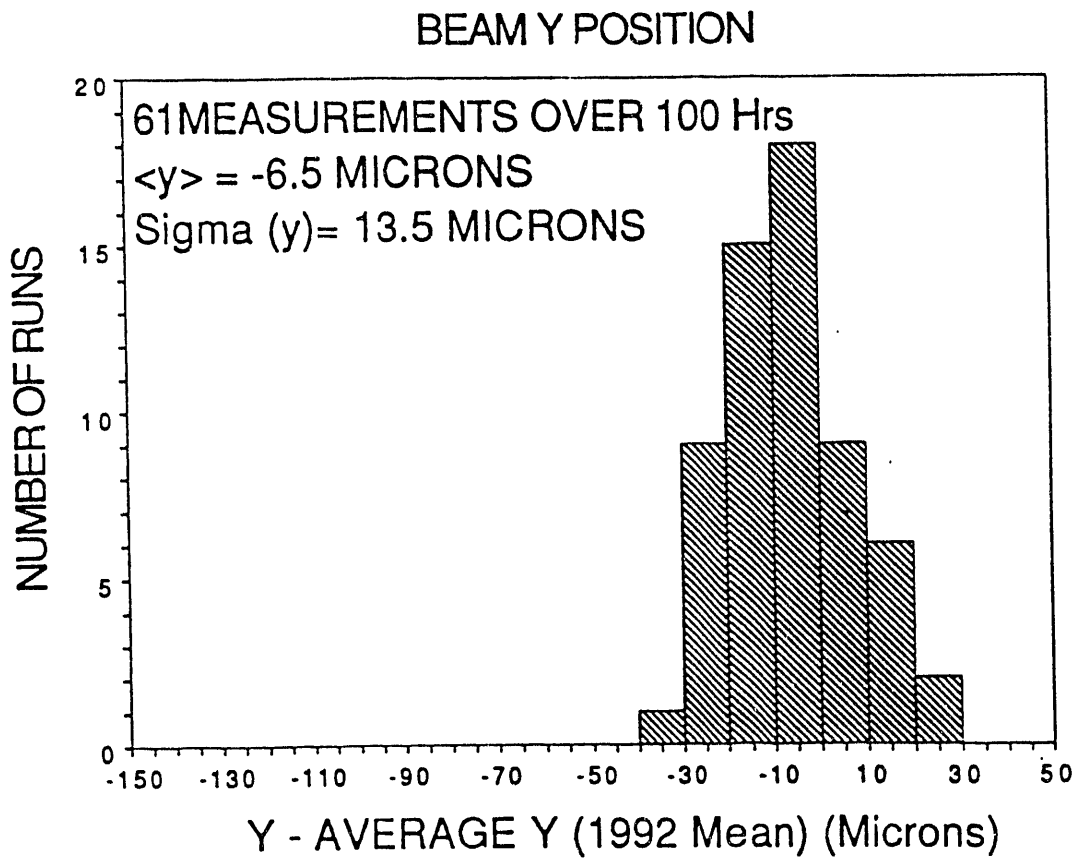
BEAM Y POSITION
61MEASUREMENTS OVER 100 Hrs
<y> = -6.5 MICRONS
Sigma (y)= 13.5 MICRONS
NUMBER OF RUNS
0
5
10
15
20
-150
-130
-110
-90
-70
-50
-30
-10
10
30
50
Y - AVERAGE Y (1992 Mean) (Microns)

# Cluster Finding Efficiency

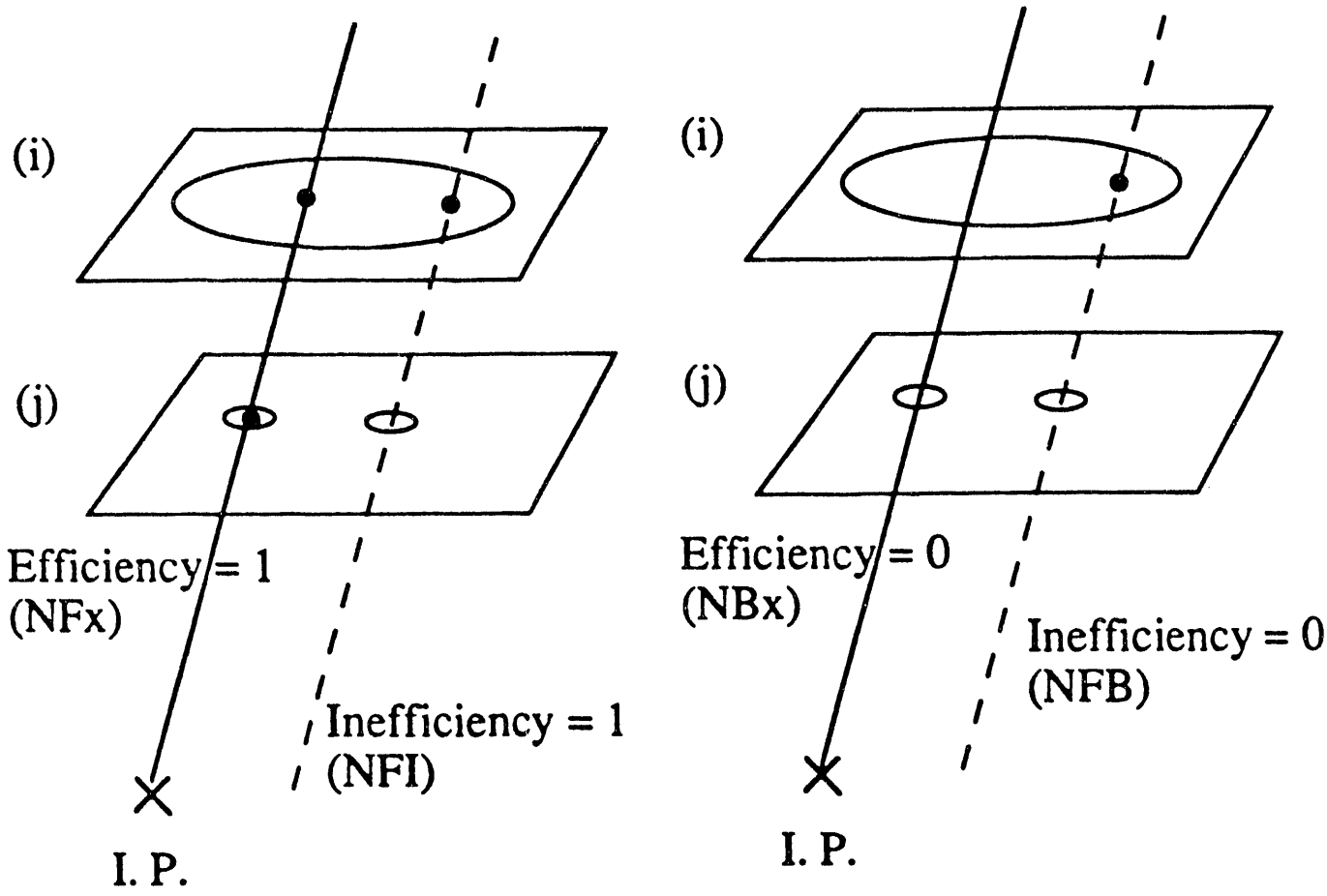


**REAL**
**(EVENT N)**

**BACKGROUND**
**(EVENT N+1)**

$$\text{Efficiency}(j) = \Sigma(NFx-NBx)/\,[\Sigma(NFx-NBx) + \Sigma(NFI-NBI)]$$

**CLUSTER EFFICIENCY = 99 ± 1 %**

# Linking CDC Tracks to VXD Hits

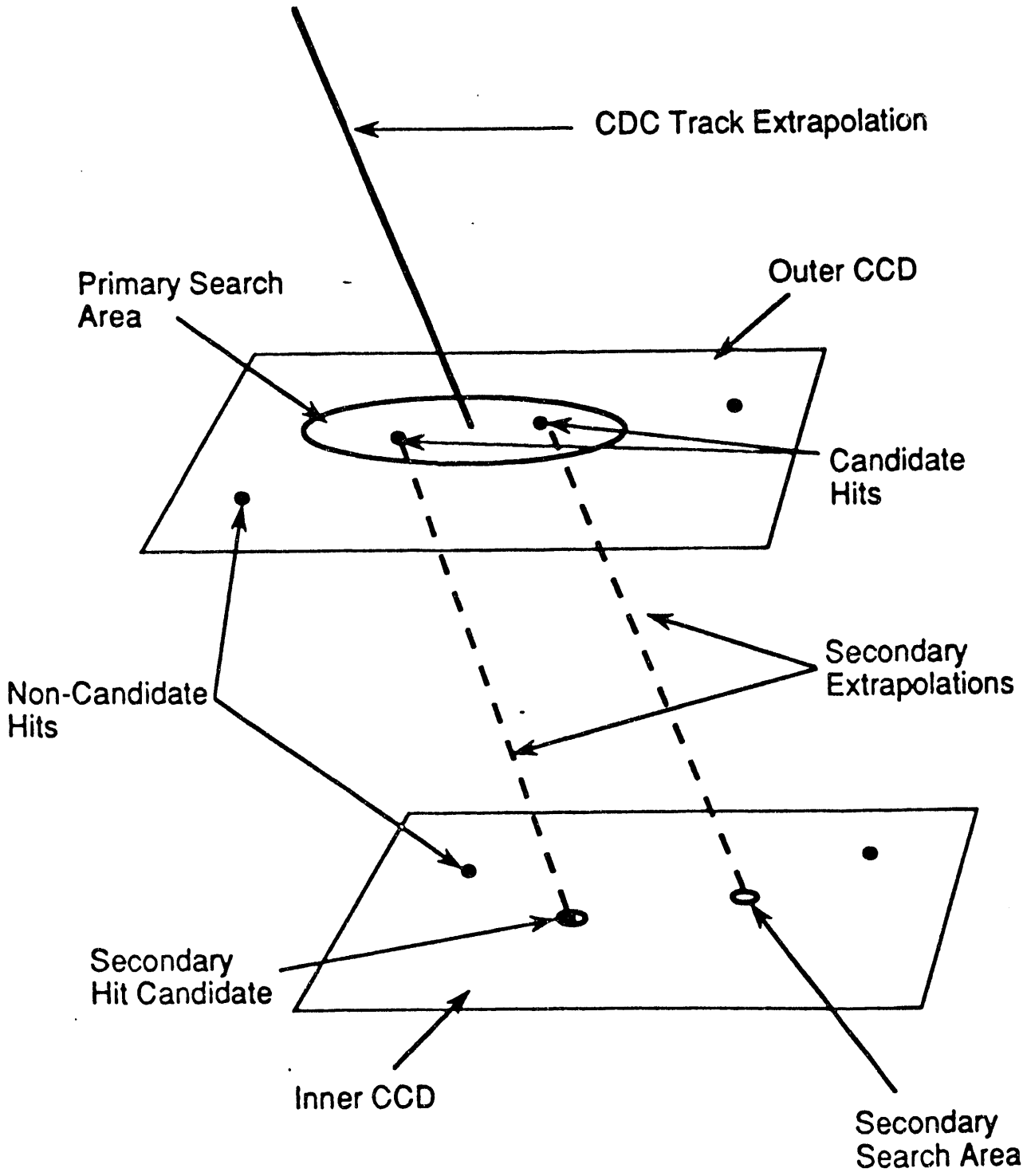

Data Efficiency for Linking Tracks in VXD

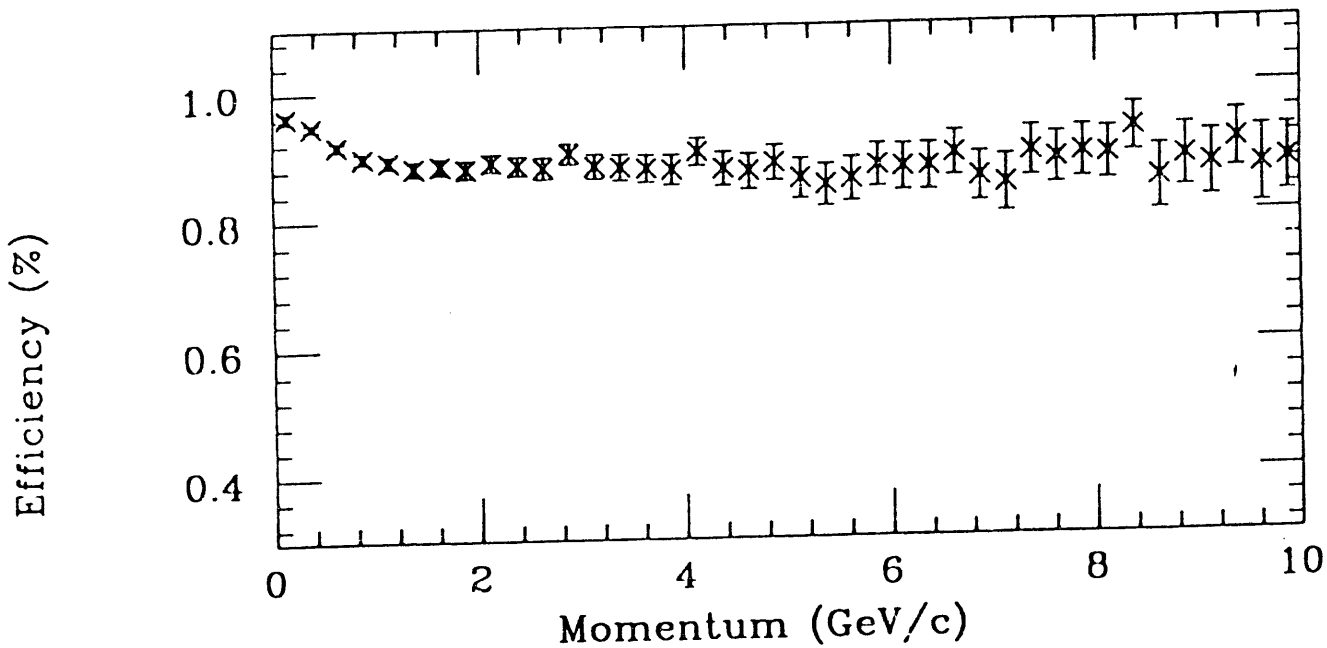


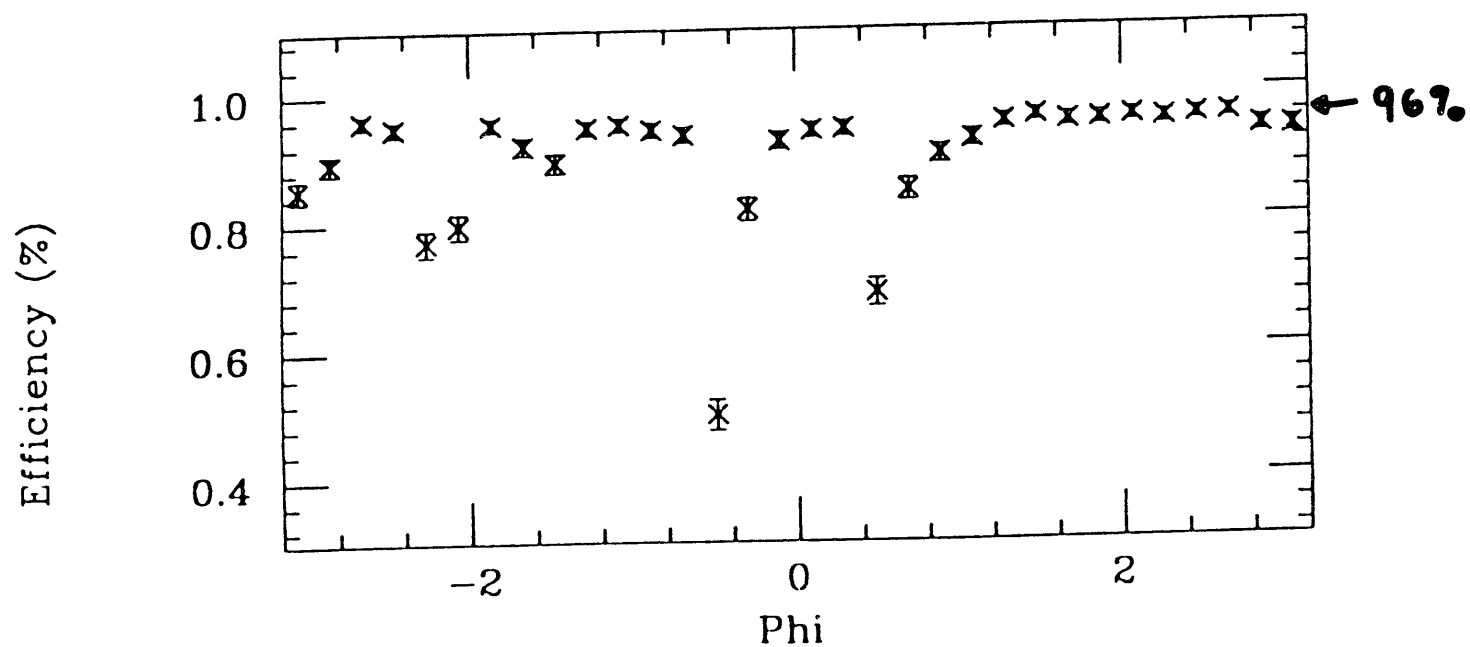


CDC TRACK CUTS

1) $\Delta XY < 2$ mm @ I.P.
2) $\Delta Z < 1$ cm @ I.P.
3) $\geq 40$ HITS ON TRACK (80 WIRES)
4) $R_{MIN} < 35$ cm

Monte Carlo Efficiency for Linking Tracks in VXD

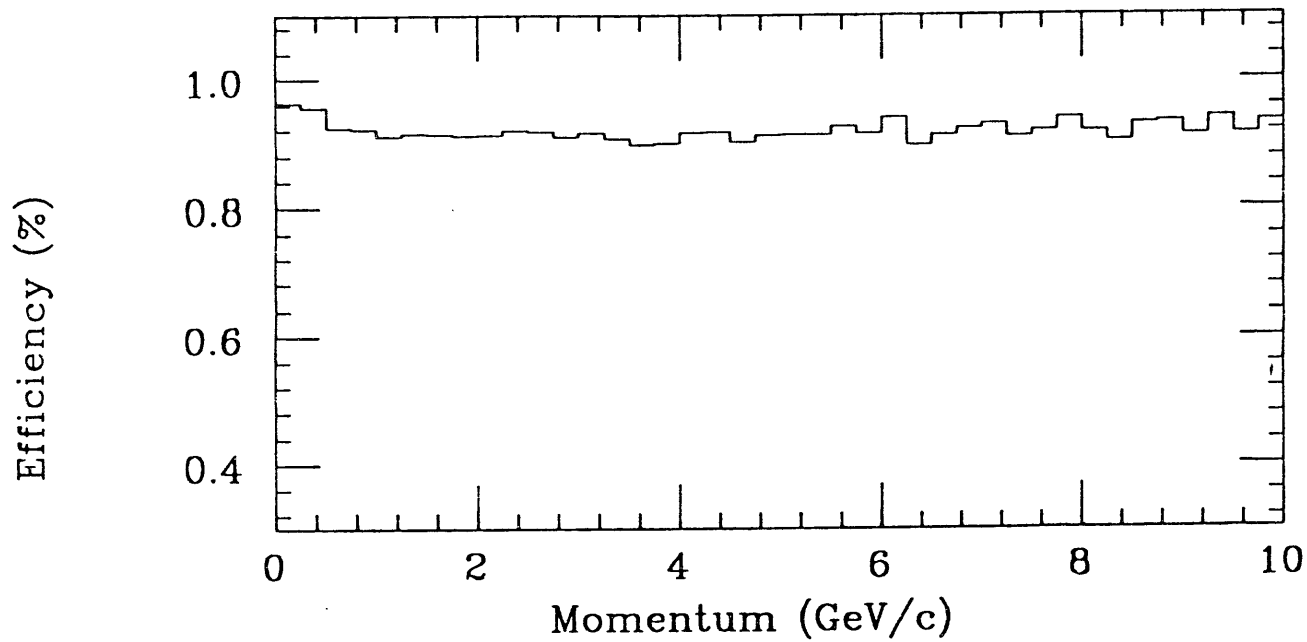


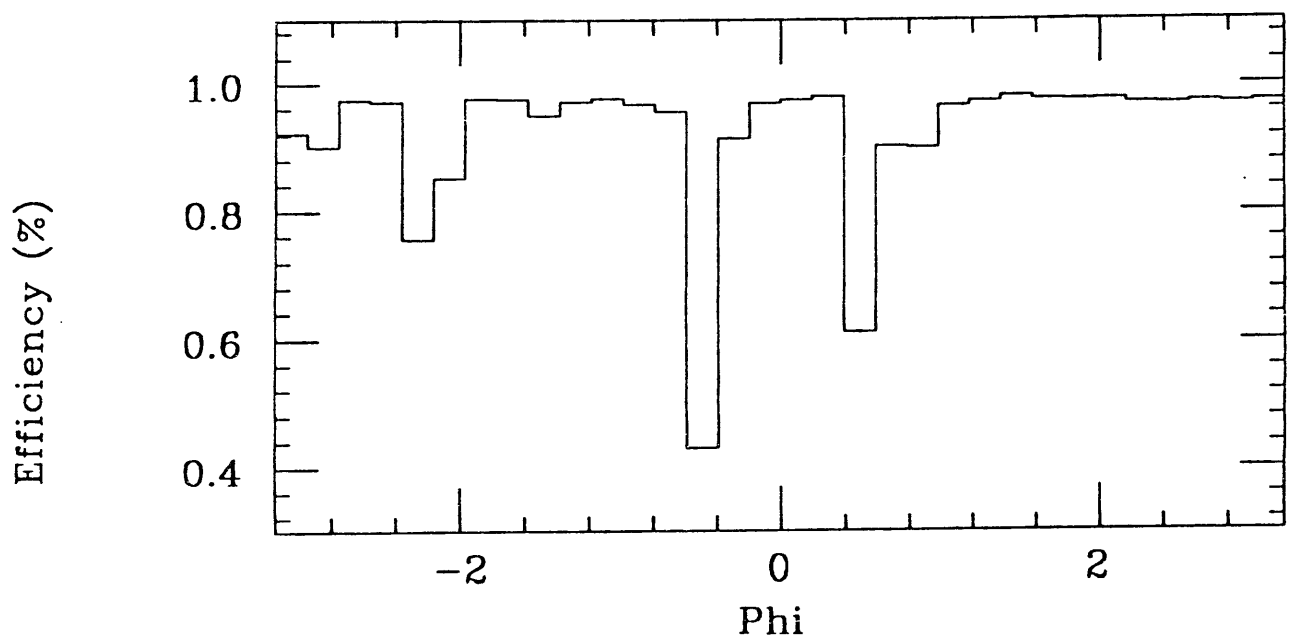

# DATA

ALL CDC TRACKS WHICH EXTRAPOLATE BACK TO THE VXD

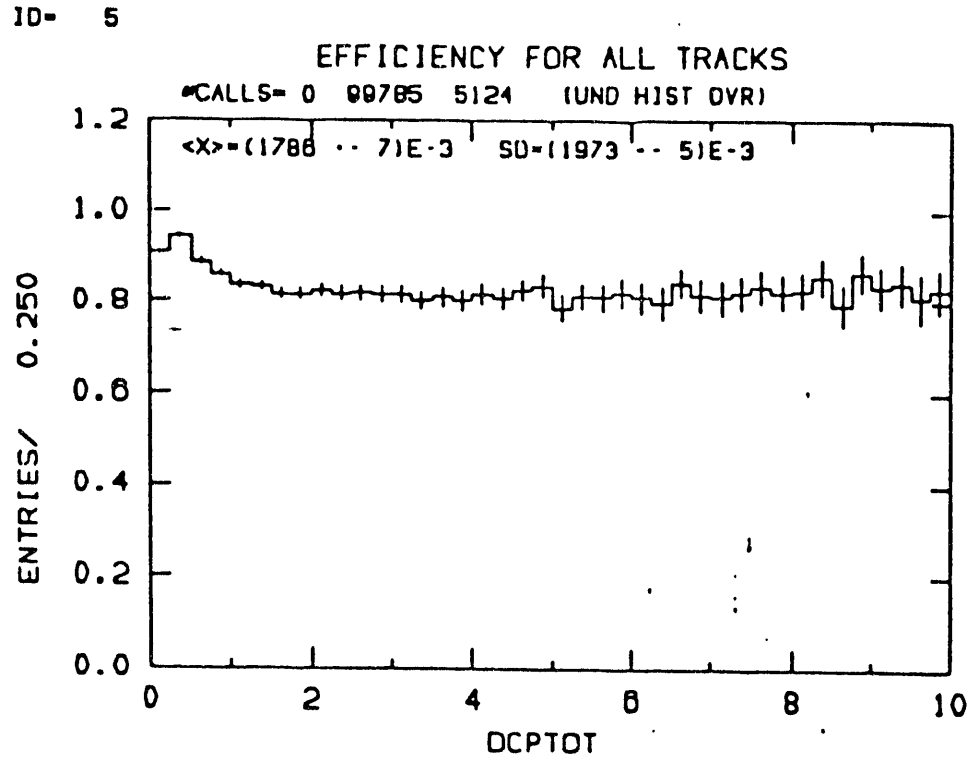


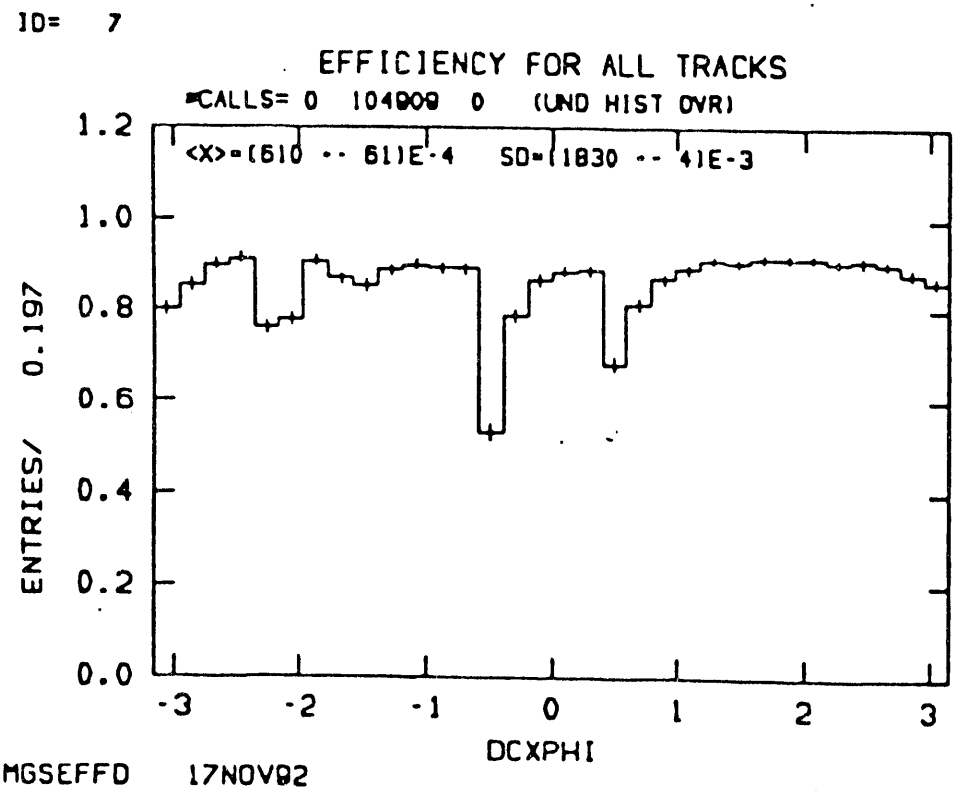


MGSEFFD 17NOV92

# MONTE CARLO

ID= 5

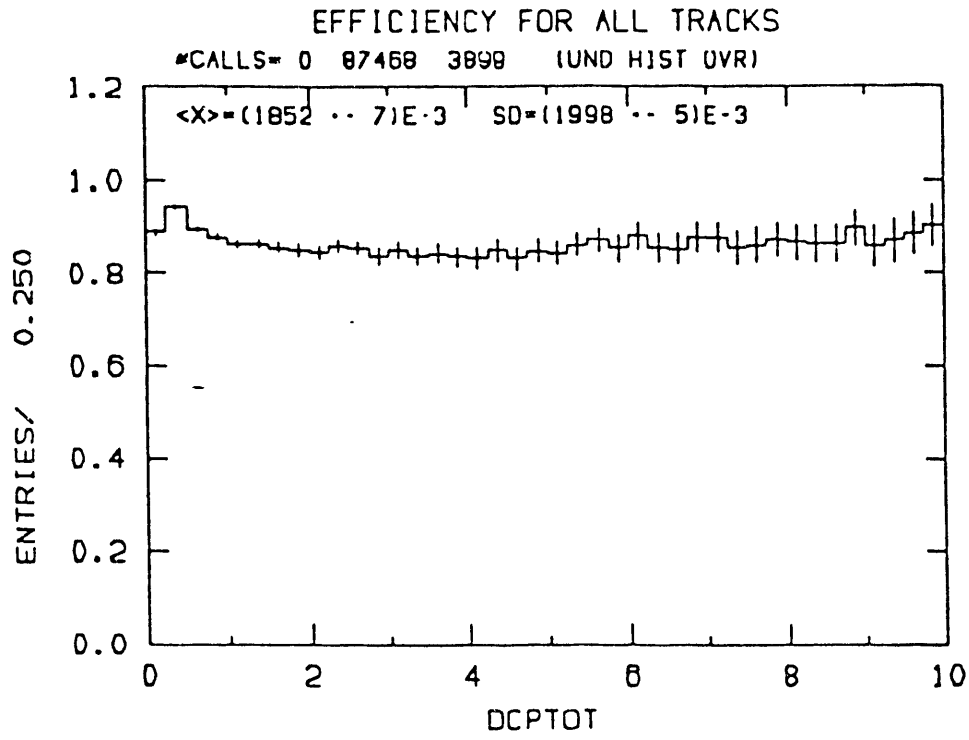


ID= 7

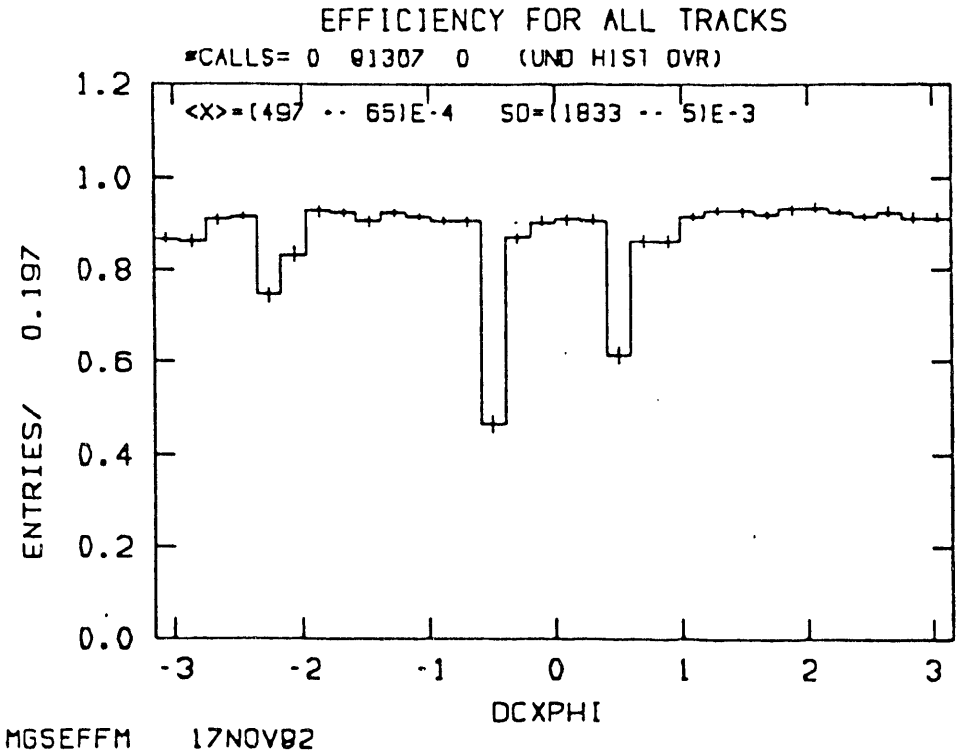


MGSEFFM 17NOV82

DATA

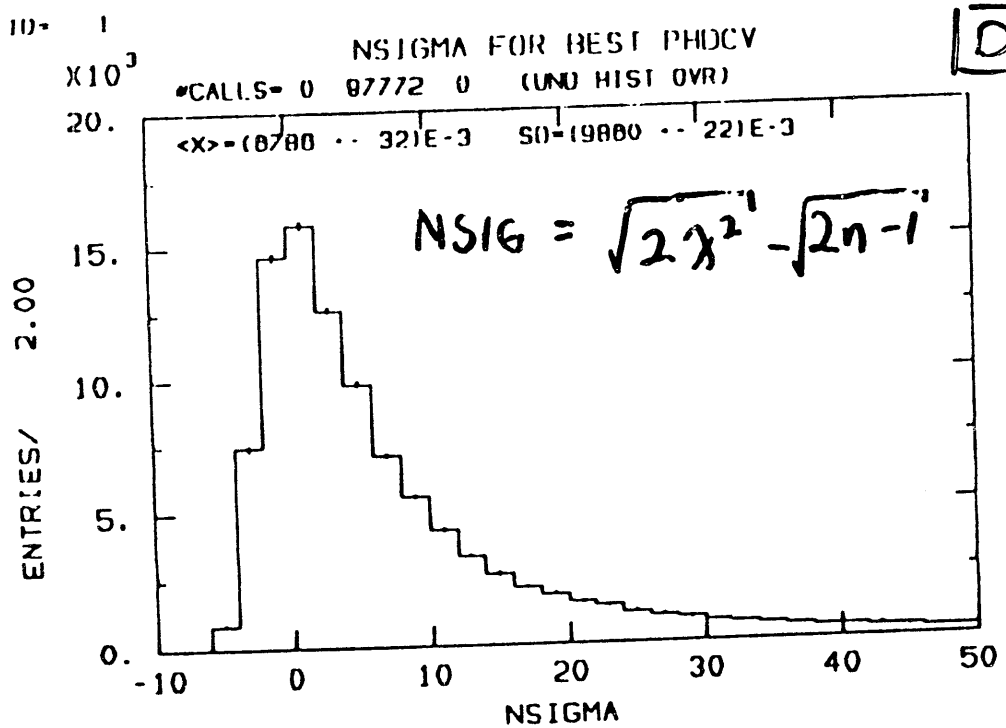
ID= 1
NSIGMA FOR BEST PHDCV
#CALLS= 0 97772 0 (UND HIST OVR)
<X>=(8780 -- 321E-3 SD=(9880 -- 221E-3
NSIG = √(2χ²) − √(2n−1)
ENTRIES/ 2.00
NSIGMA

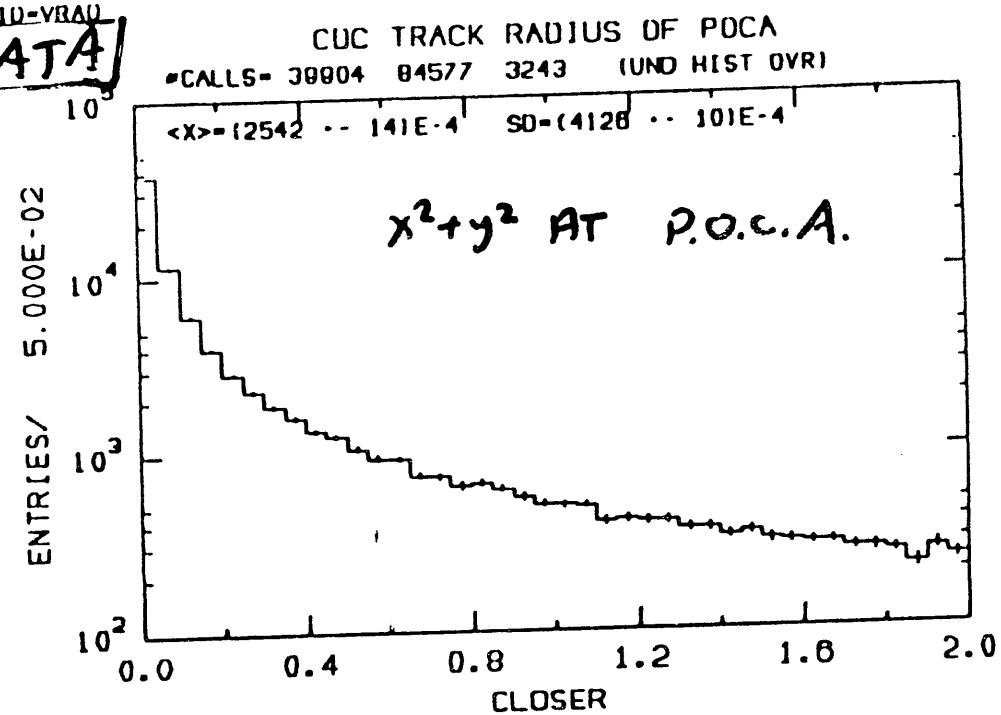
ID=VRAD
CDC TRACK RADIUS OF POCA
#CALLS= 39904 84577 3243 (UND HIST OVR)
<X>=(2542 -- 141E-4 SD=(4128 -- 101E-4
x²+y² AT P.O.C.A.
ENTRIES/ 5.000E-02
CLOSER

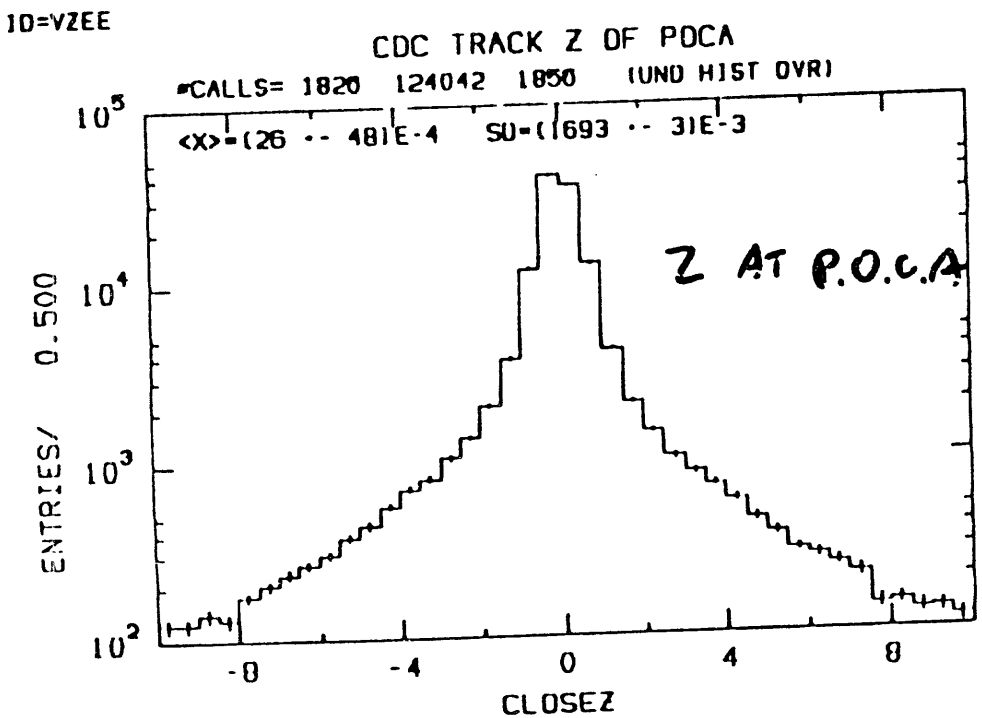
ID=VZEE
CDC TRACK Z OF POCA
#CALLS= 1820 124042 1850 (UND HIST OVR)
<X>=(26 -- 481E-4 SD=(1693 -- 31E-3
Z AT P.O.C.A.
ENTRIES/ 0.500
CLOSEZ

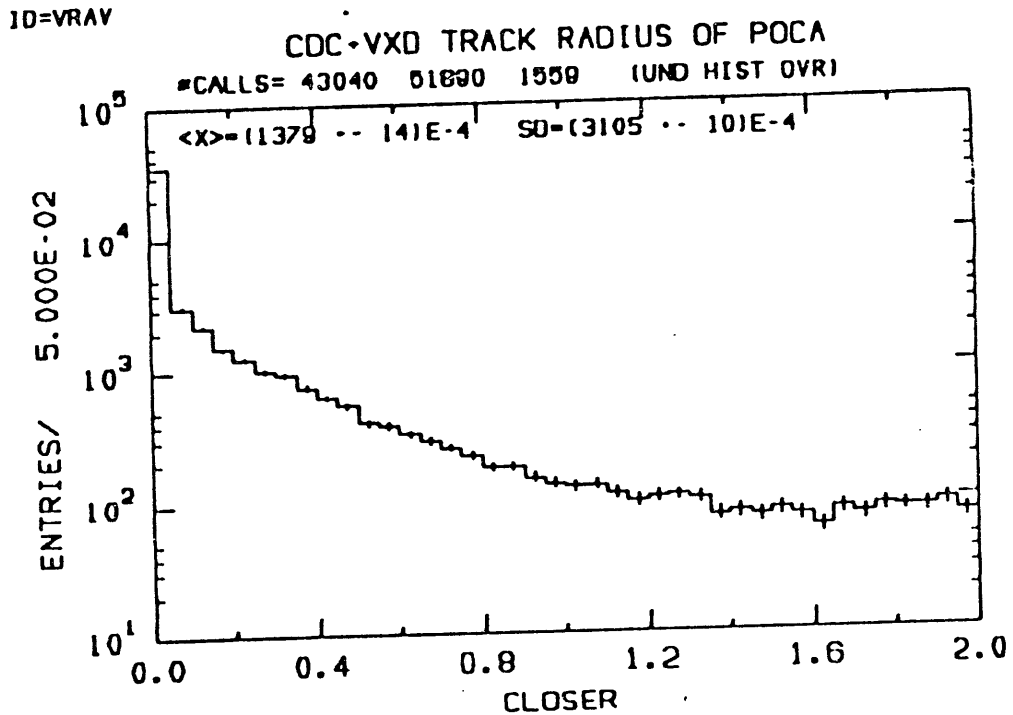
ID=VRAV
CDC+VXD TRACK RADIUS OF POCA
#CALLS= 43040 61890 1559 (UND HIST OVR)
<X>=(1379 -- 141E-4 SD=(3105 -- 101E-4
ENTRIES/ 5.000E-02
CLOSER

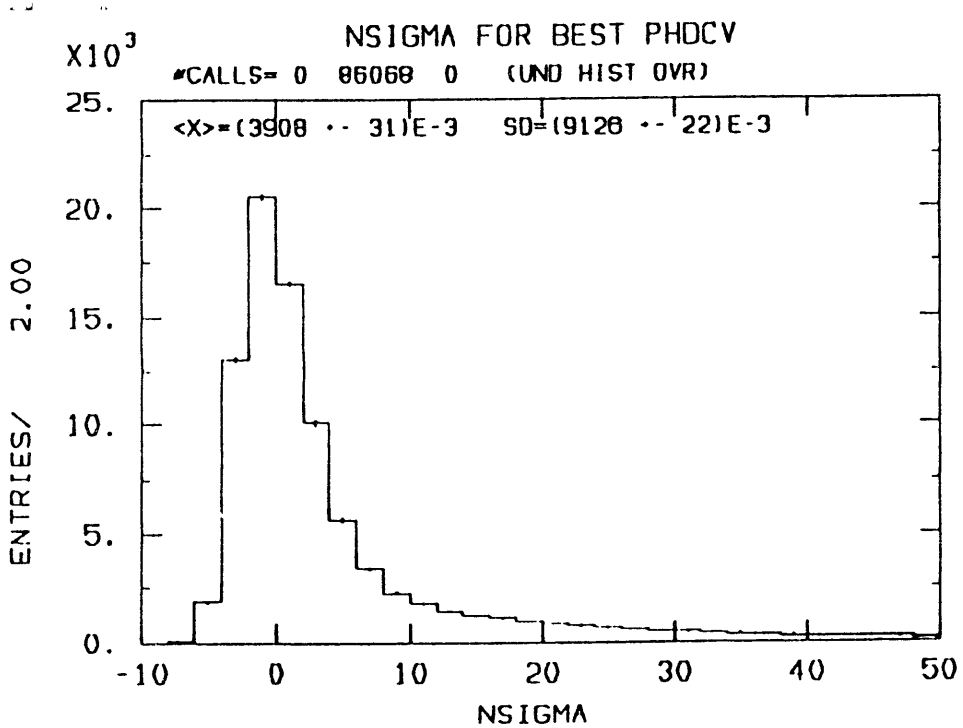


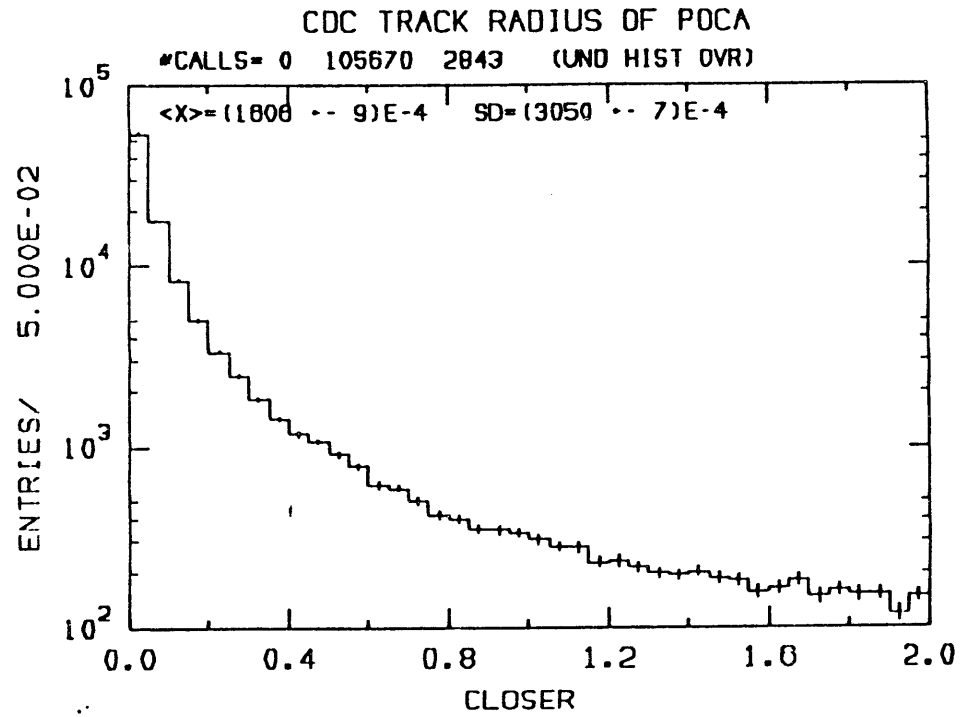


ID=VZEE

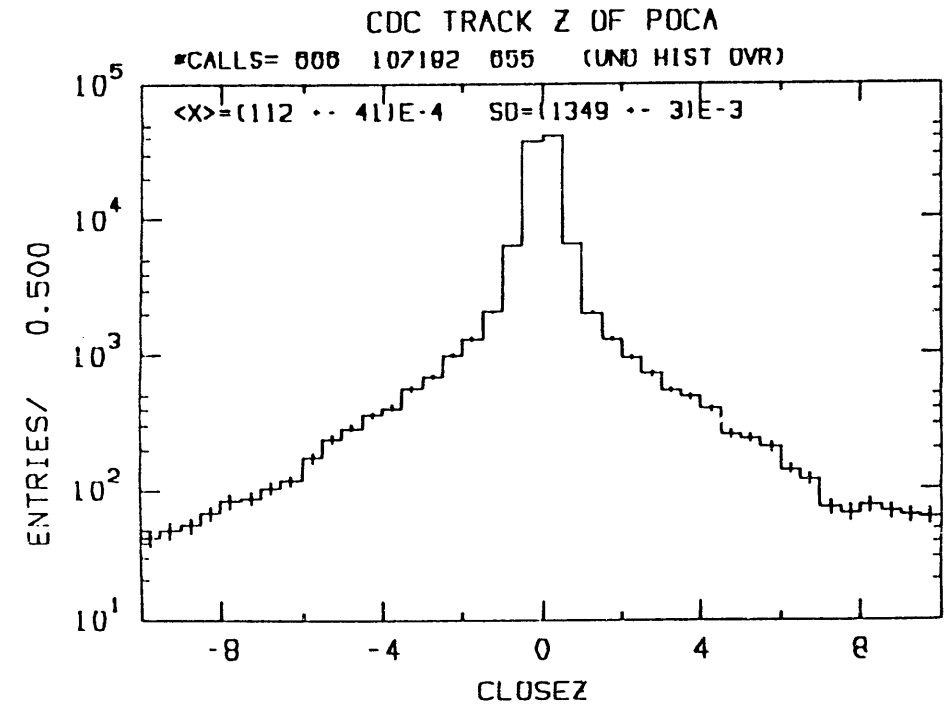


ID=VRAV

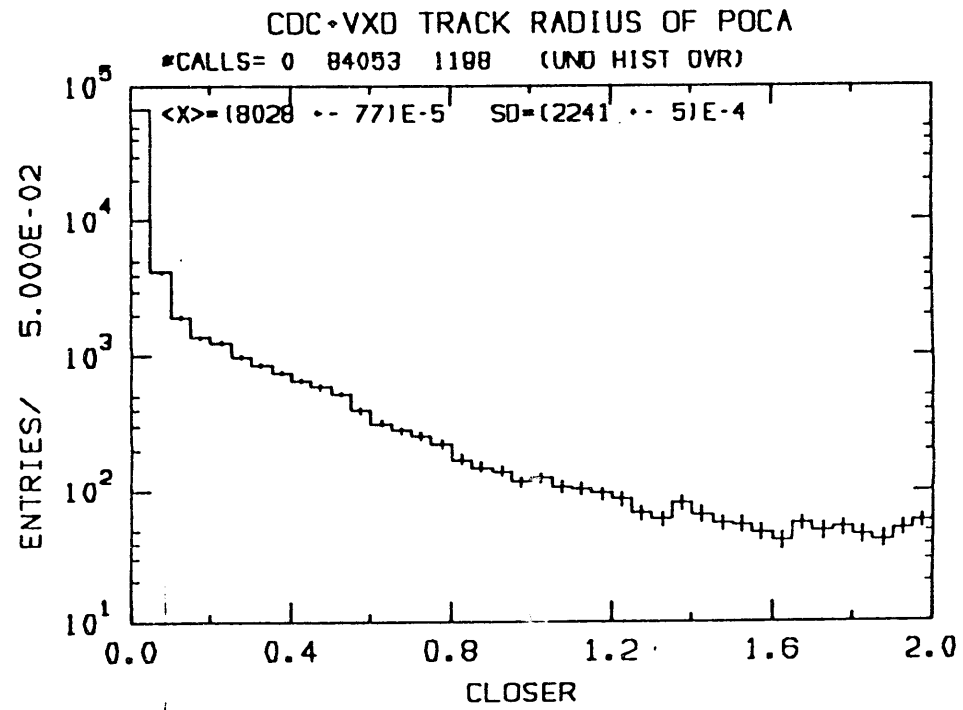


MGSEFFM 17NOV92

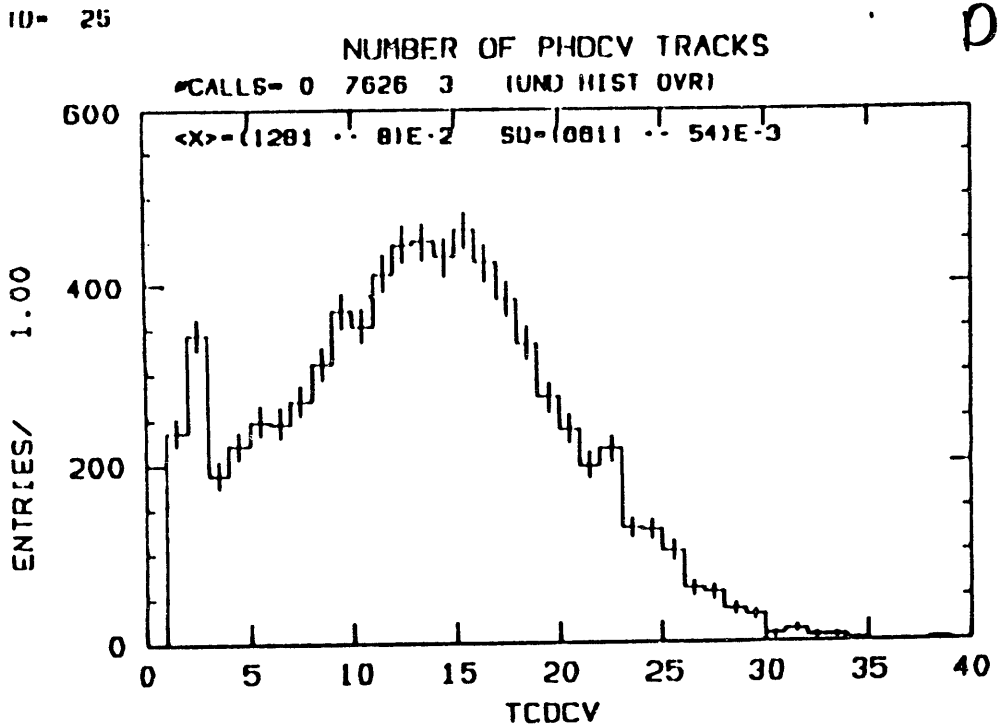


DATA

$\langle N \rangle = 12.8$

# LINKED TRACKS

M.C

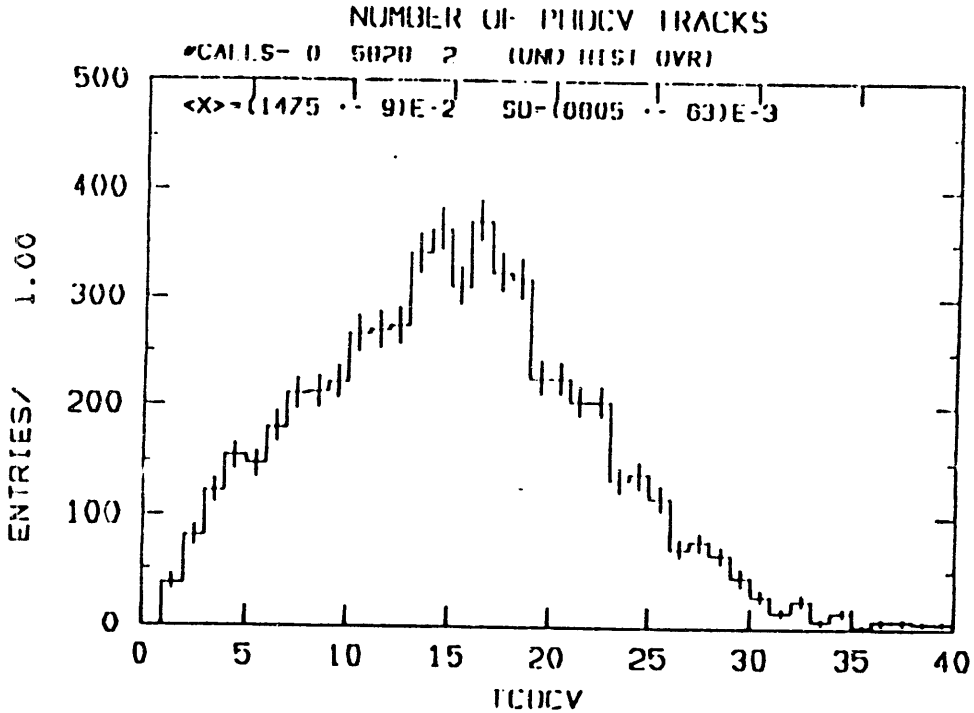


$\langle N \rangle = 14.8$

# EFFICIENCY SUMMARY

| DATA SET (DENOMINATOR) | GOOD $\phi$ REGION | TRACKS $p > 1$ GeV/c | TOTAL |
|---|---|---|---|
| DATA (LOOSE) | .89 | .83 | .87 |
| MC (LOOSE) | .93 | .86 | .89 |
| DATA (TIGHT) | .96 | .88 | .90 |
| MC (TIGHT) | .98 | .91 | .92 |
| MC (TRUE) | .96 | .90 | .87 |

LOOSE: CDC TRACK EXTRAPOLATES TO VXD

TIGHT: CDC $\Delta XY < 2$ mm, CDC $\Delta Z < 1$ cm, $> 40$ HITS, $R_{MIN} > 35$ cm

TRUE: TRUE 2 HIT TRACKS IN VXD WITH FOUND CDC TRACKS

# Alignment and Spatial Resolution

- Original alignment done optically before installation
  - *Precision of 5 μm for CCDs on individual ladder*
  - *Precision of 10 μm from ladder to ladder*

- Alignment with tracks was done using tracks with 3 VXD hits

*1. Two hits on a single ladder (third hit on different ladder)*

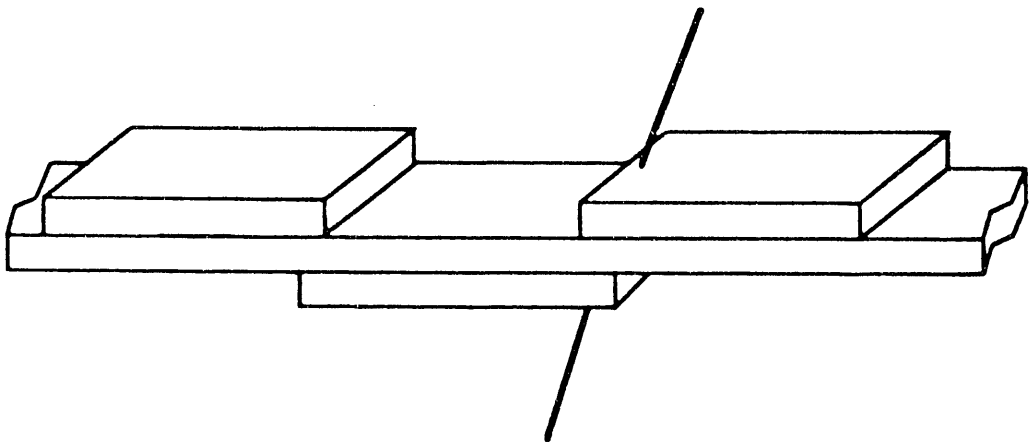

*2. Three hits on different ladders*

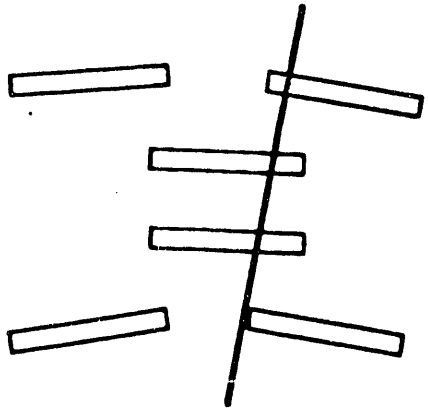

# Single Ladder Triplet Residuals

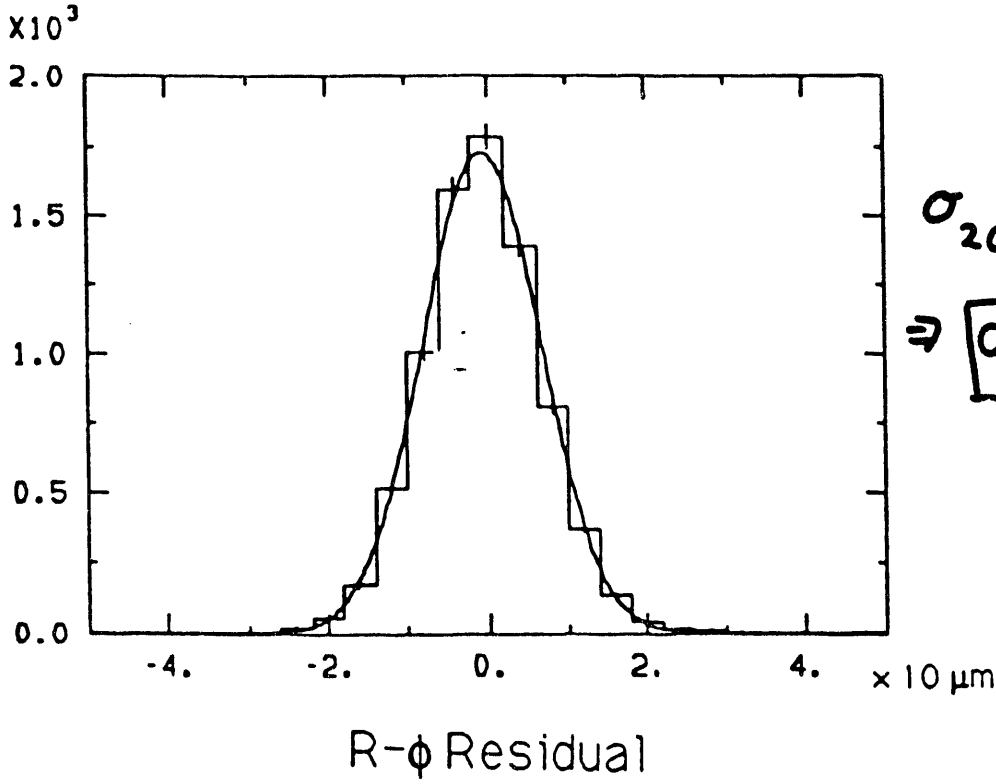


$\sigma_{2CLUS} = 7\,\mu m$

$\Rightarrow \boxed{\sigma_{1CLUS} = 5\,\mu m}$

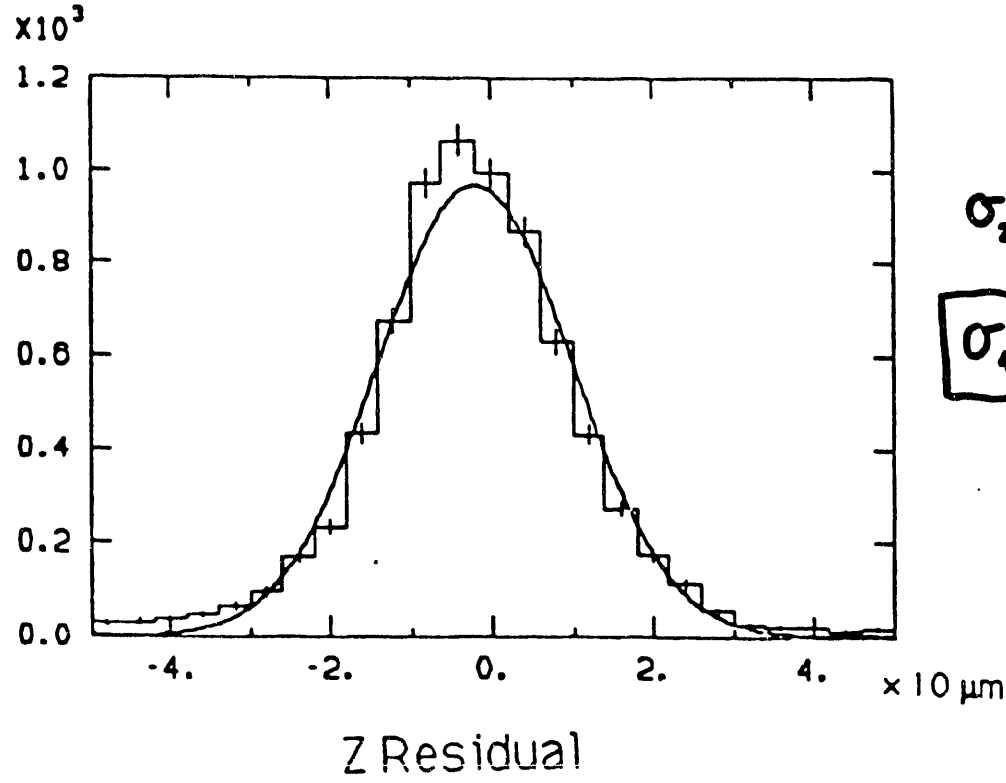


$\sigma_{2CLUS} = 12\,\mu m$

$\boxed{\sigma_{1CLUS} = 8\,\mu m}$

# Multiple Ladder Triplet Residuals

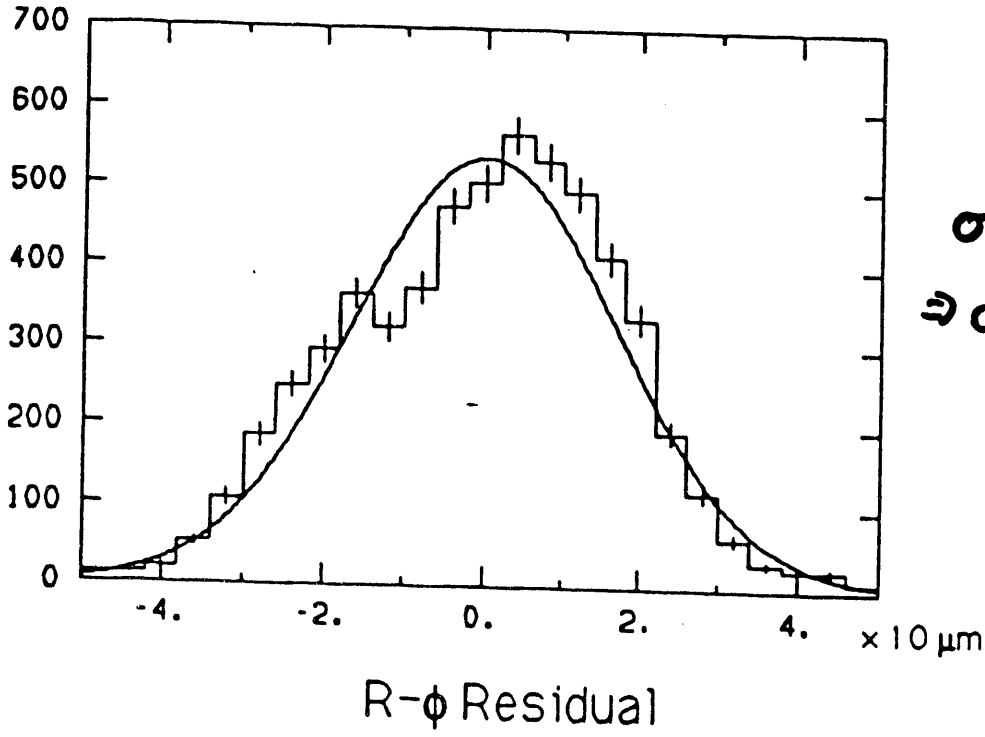


$\sigma_{1CLUS} = 16\,\mu m$

$\Rightarrow \sigma_{2CLUS} = 13\,\mu m$

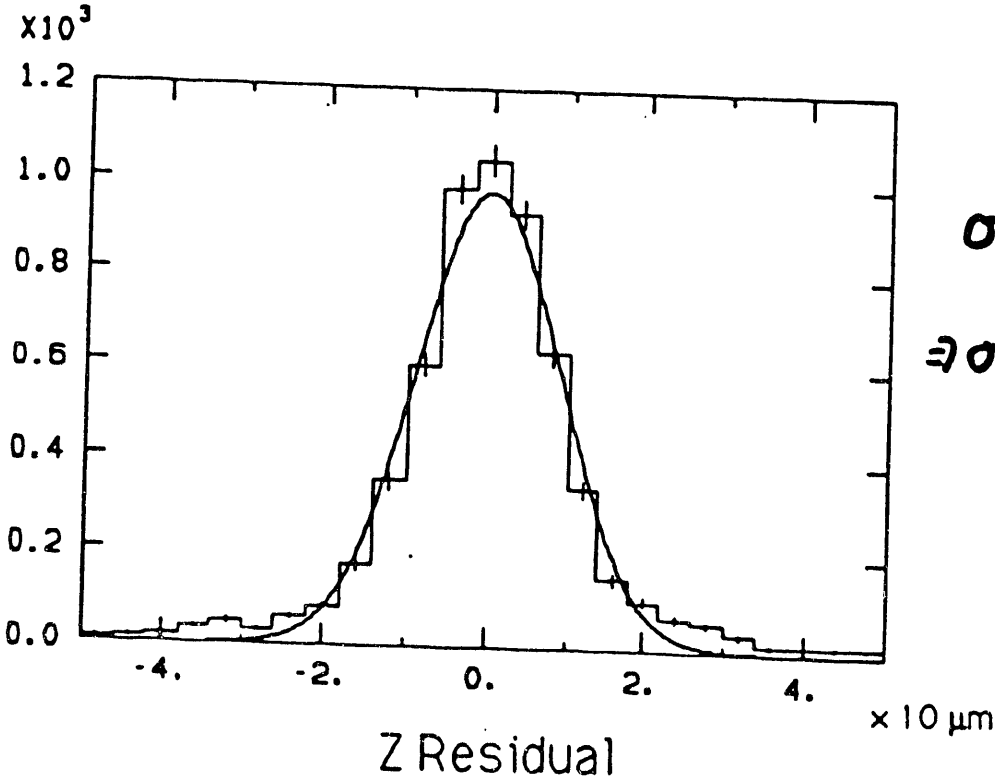


$\sigma_{1CLUS} = 10\,\mu m$

$\Rightarrow \sigma_{2CLUS} = 8\,\mu m$

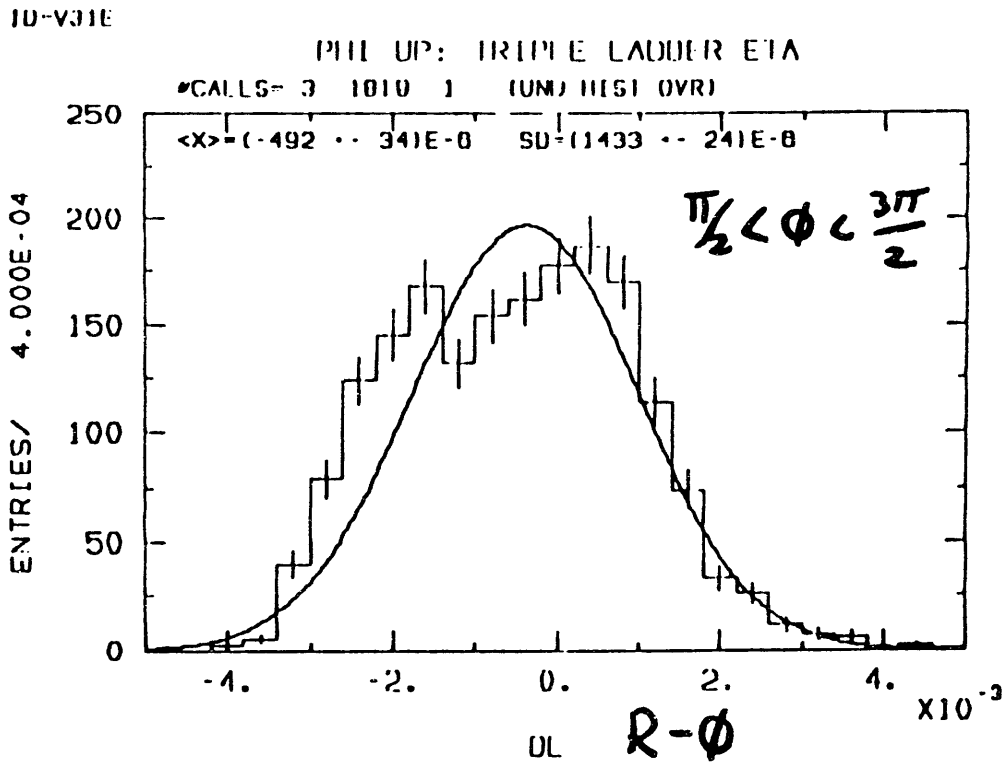
ID=V31E
PHI UP: TRIPLE LADDER ETA
#CALLS= 3 1010 1 (UND HIST OVR)
<X>=(-492 -- 34)E-6 SD=(1433 -- 24)E-6
ENTRIES/ 4.000E-04
250
200
150
100
50
0
-4.
-2.
0.
2.
4.
X10^-3
DL
R-Φ
π/2 < Φ < 3π/2

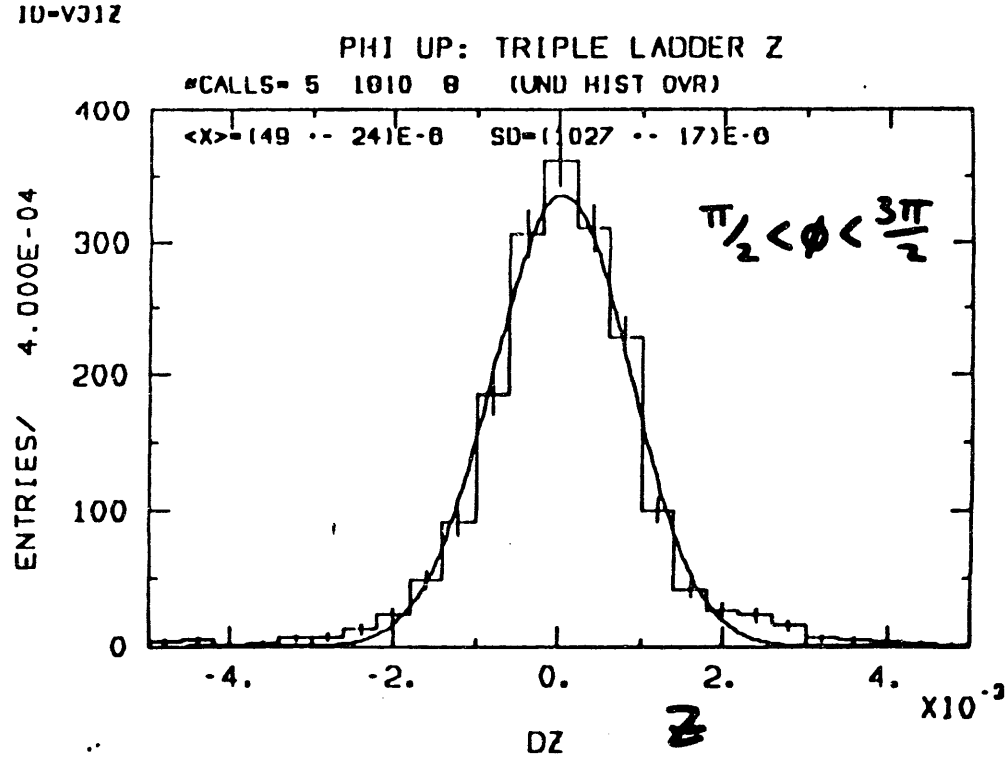
ID=V31Z
PHI UP: TRIPLE LADDER Z
#CALLS= 5 1010 8 (UND HIST OVR)
<X>=(49 -- 24)E-6 SD=(1027 -- 17)E-6
ENTRIES/ 4.000E-04
400
300
200
100
0
-4.
-2.
0.
2.
4.
X10^-3
DZ
Z
π/2 < Φ < 3π/2

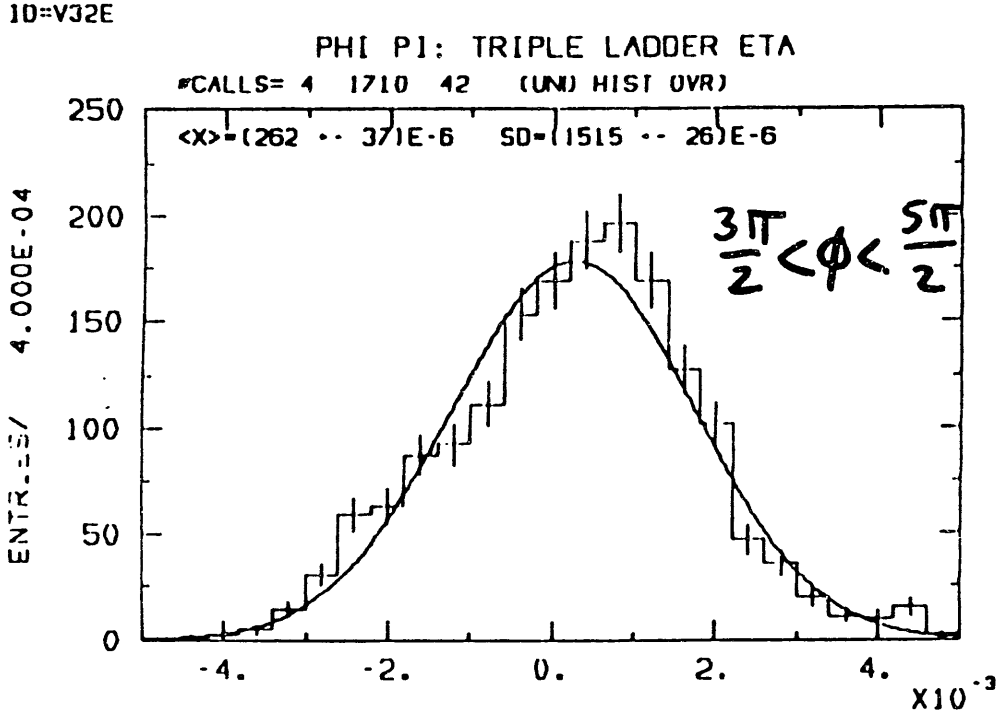
ID=V32E
PHI PI: TRIPLE LADDER ETA
#CALLS= 4 1710 42 (UND HIST OVR)
<X>=(262 -- 37)E-6 SD=(1515 -- 26)E-6
ENTRIES/ 4.000E-04
250
200
150
100
50
0
-4.
-2.
0.
2.
4.
X10^-3
DE
3π/2 < Φ < 5π/2

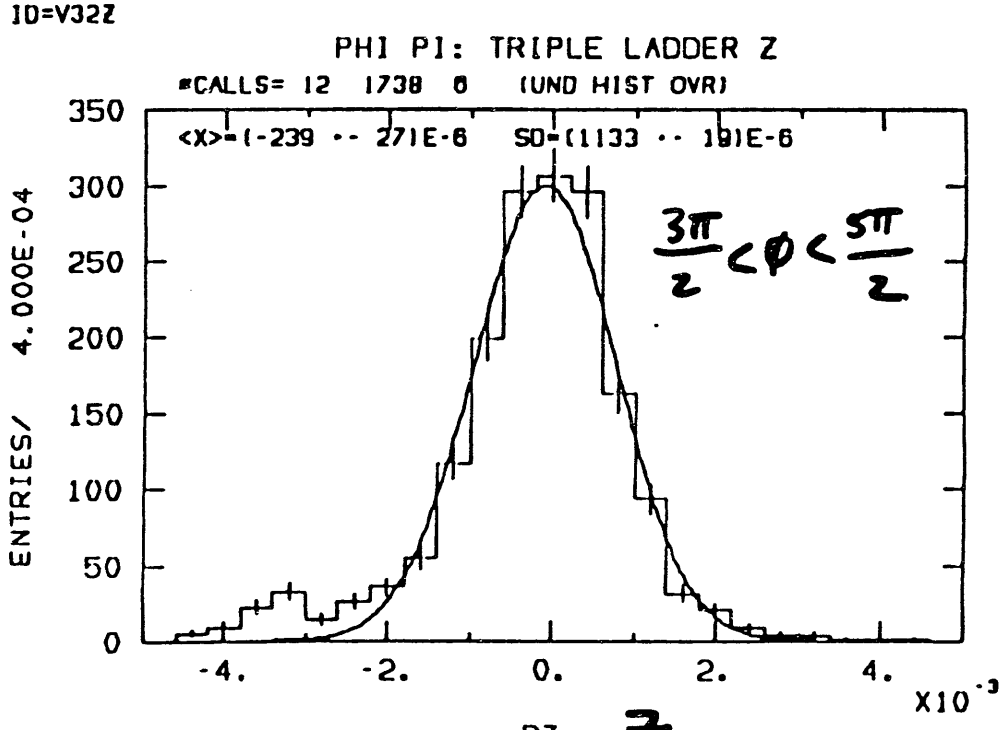
ID=V32Z
PHI PI: TRIPLE LADDER Z
#CALLS= 12 1738 8 (UND HIST OVR)
<X>=(-239 -- 27)E-6 SD=(1133 -- 19)E-6
ENTRIES/ 4.000E-04
350
300
250
200
150
100
50
0
-4.
-2.
0.
2.
4.
X10^-3
DZ
Z
3π/2 < Φ < 5π/2

ID=V33E

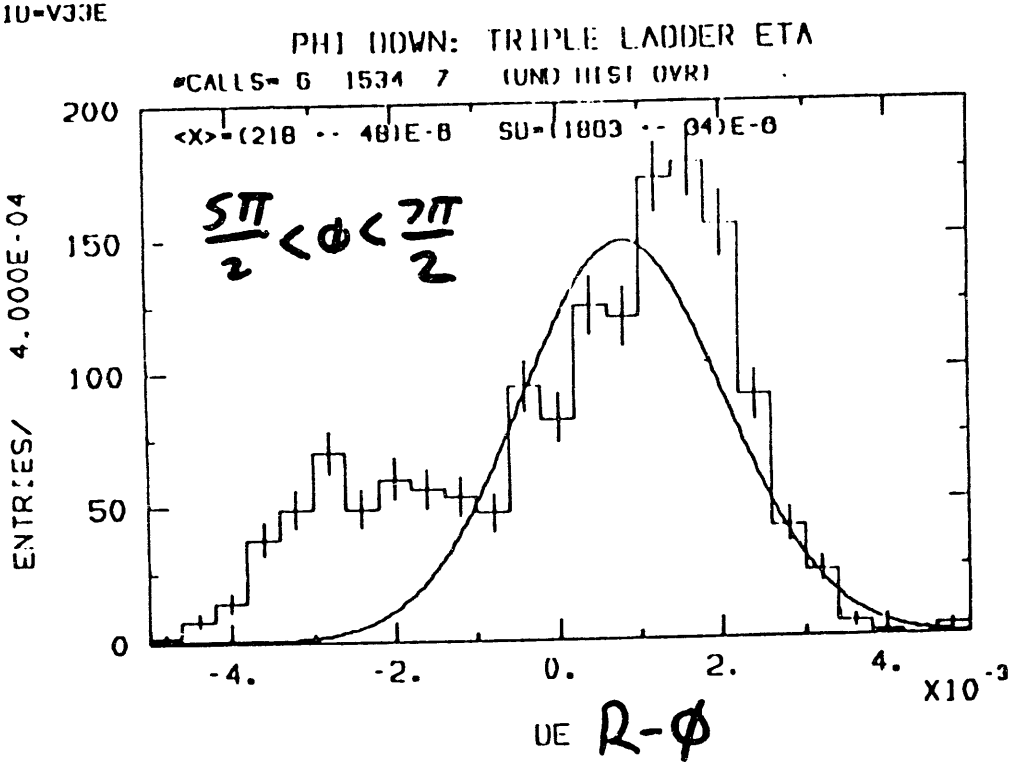


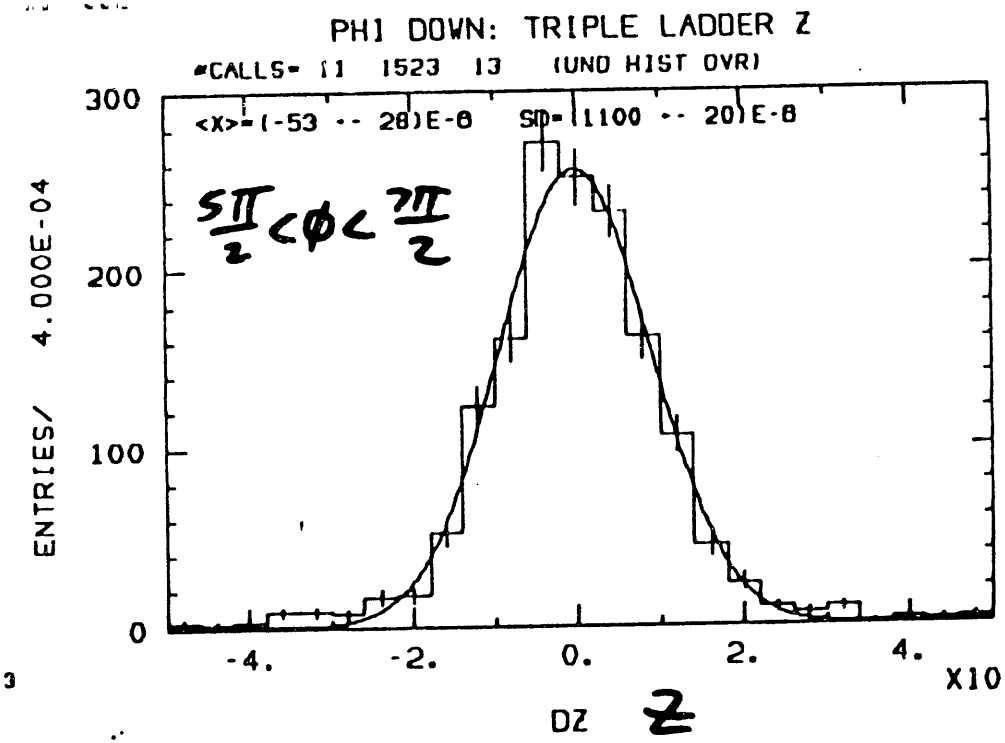


ID=V34E

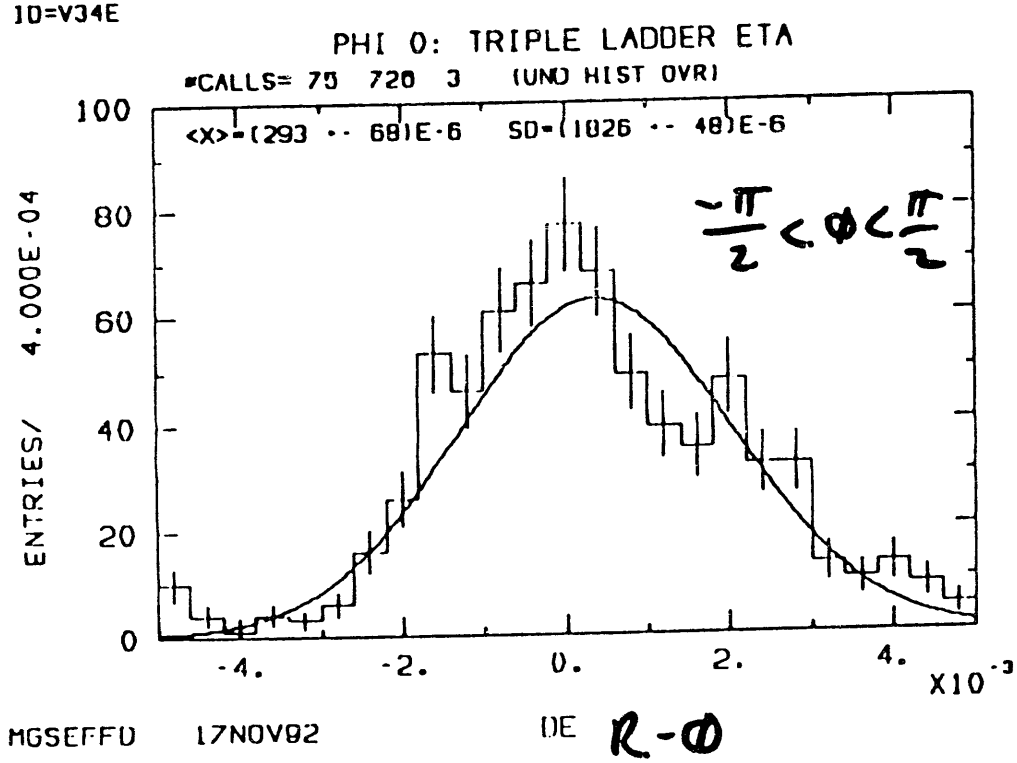


ID=V34Z

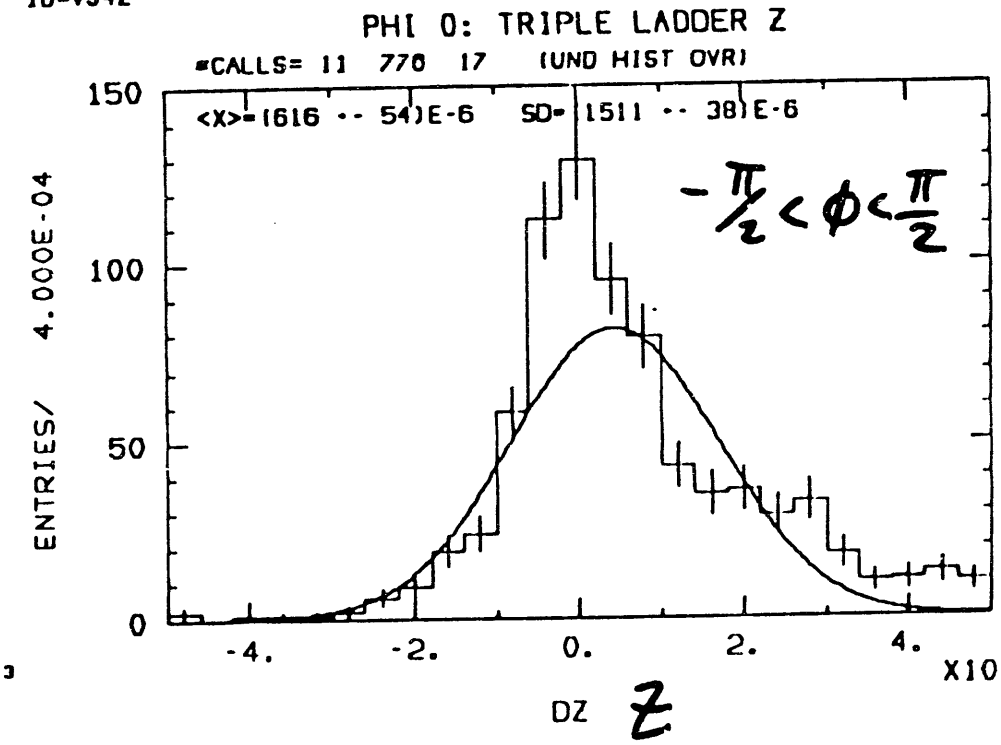


MGSEFFD 17NOV92

$\mu^+\mu^-$ MISSED DISTANCE

RUN 10745, EVENT 4170
6-APR-1992 03:13
SOURCE: RUN DATA POL: 0

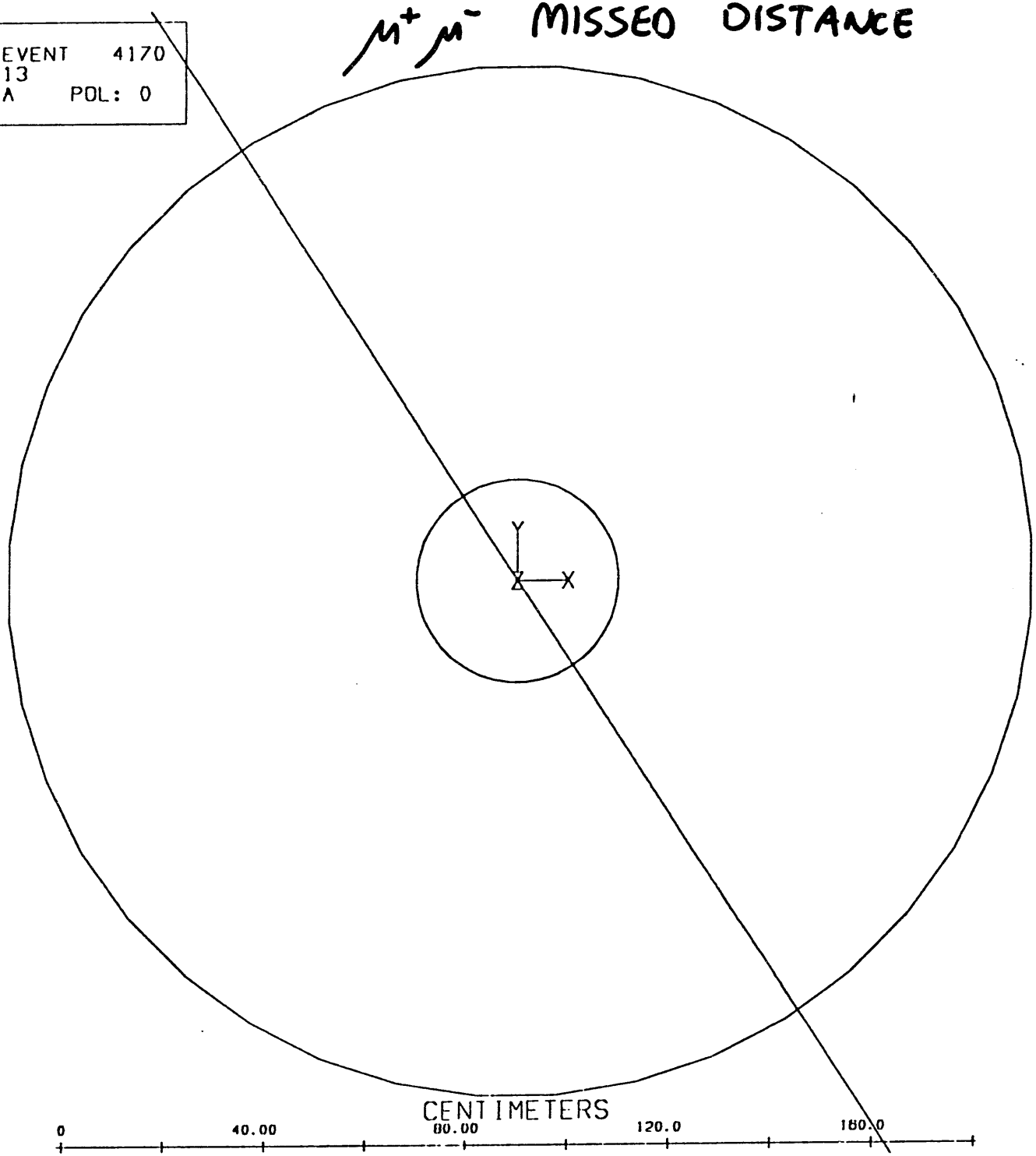

# $\mu^+\mu^-$ Missed Distance

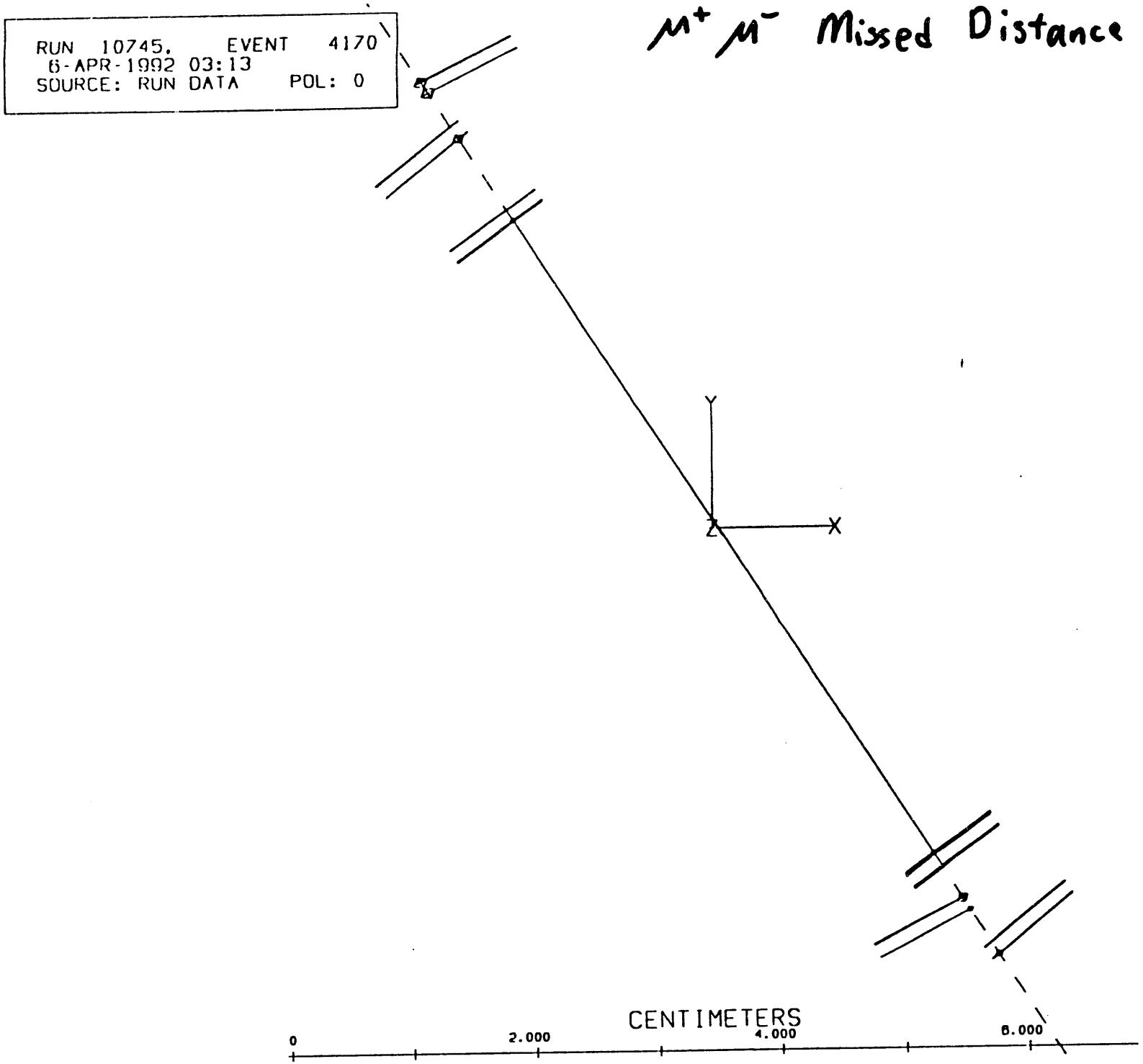

RUN 10745, EVENT 4170
6-APR-1992 03:13
SOURCE: RUN DATA POL: 0

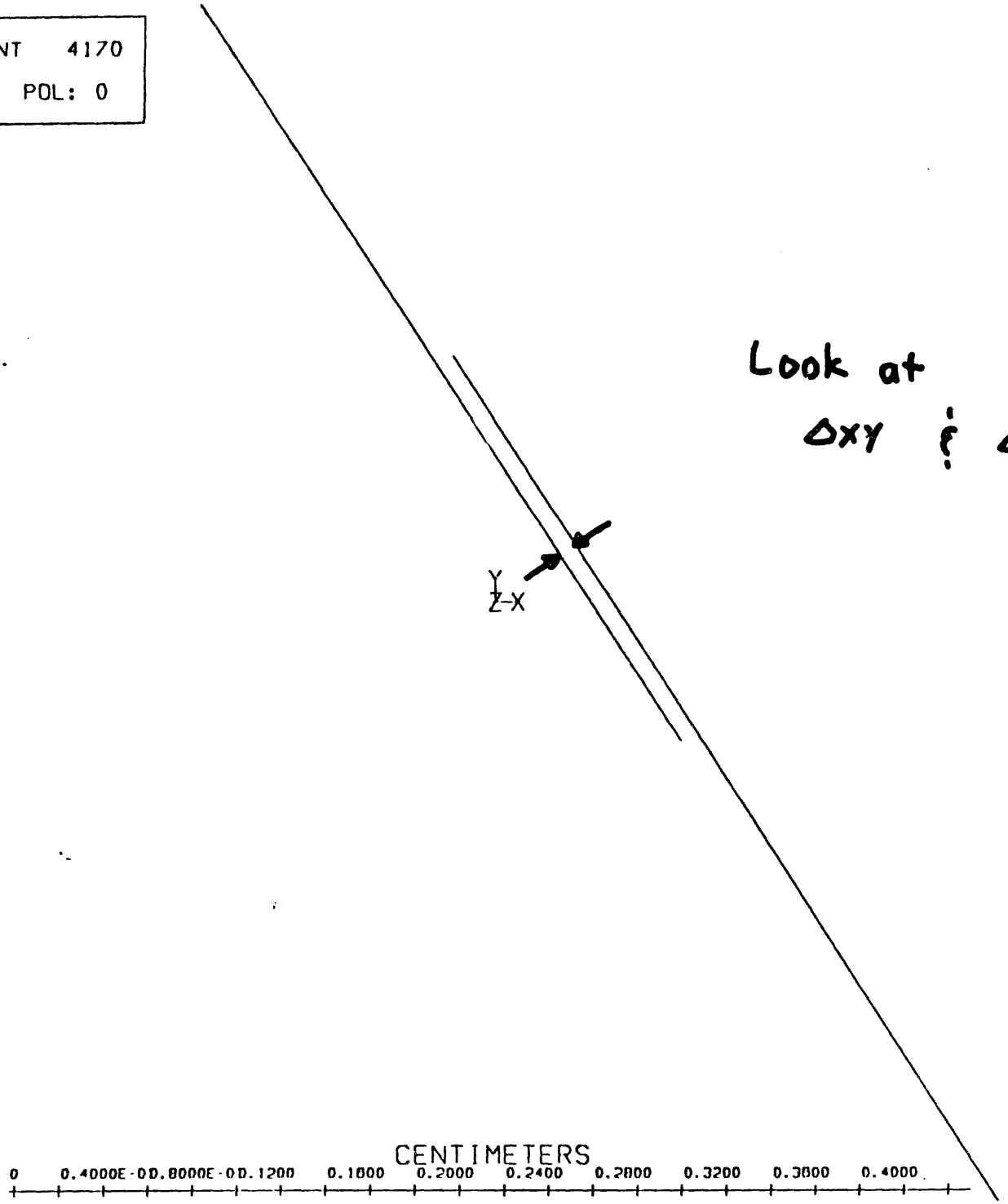


Look at
ΔXY & ΔRZ

# Muon Missed Distance

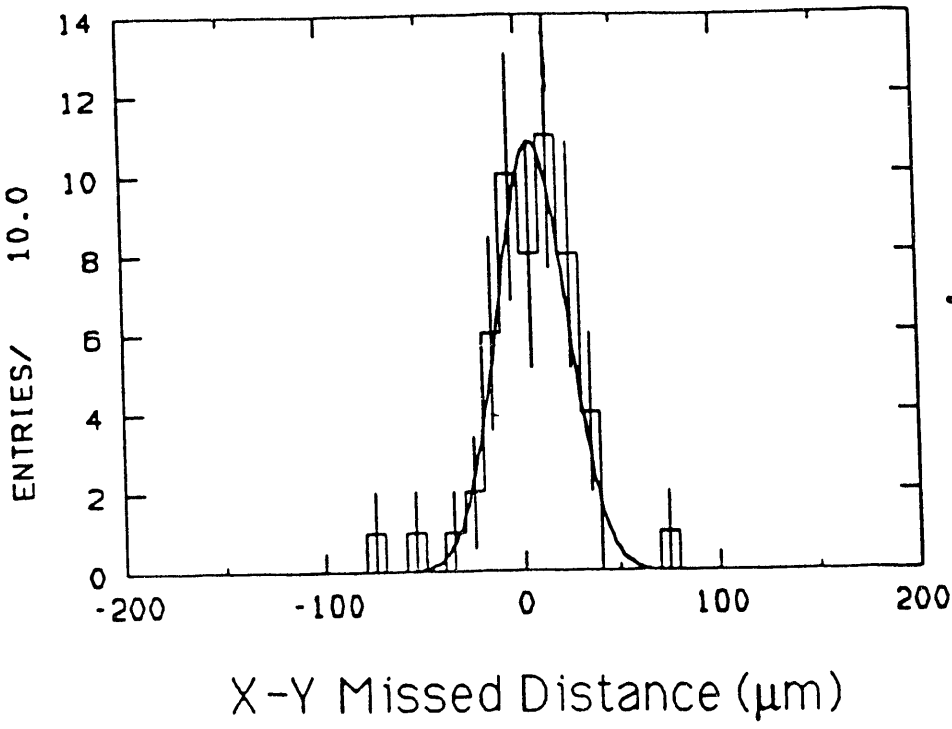


$\sigma_{XY}(2\,TRK) = 18\,\mu m$

$\Rightarrow \boxed{\sigma_{XY}(1\,TRK) = 13\,\mu m}$

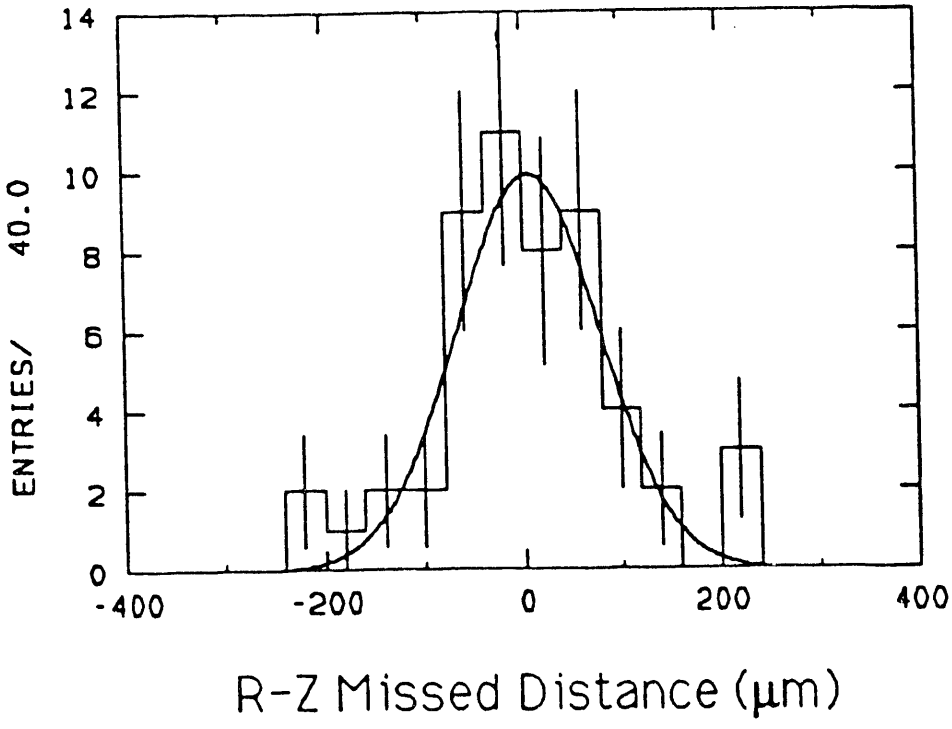


$\sigma_{RZ}(2\,TRK) = 79\,\mu m$

$\Rightarrow \boxed{\sigma_{RZ}(1\,TRK) = 52\,\mu m}$

DATA: UDS events with $N_T(\frac{\sigma_b}{\sigma_b} > 3) = 0$

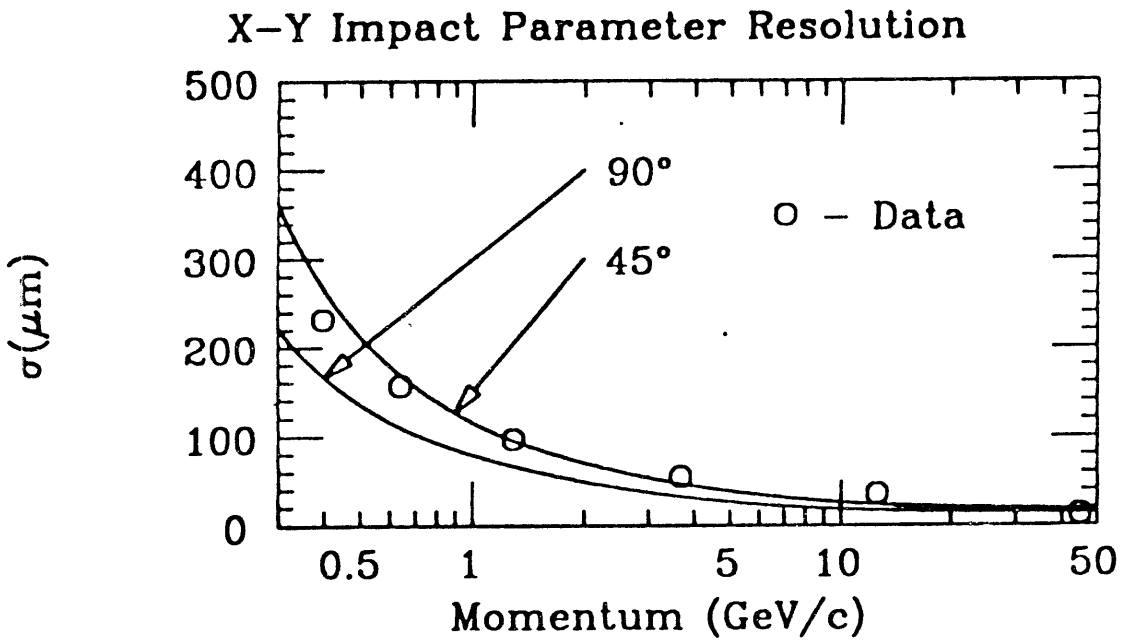


$$\sigma_b(XY) \approx \sqrt{13^2 + \left(\frac{70}{p}\right)^2}$$

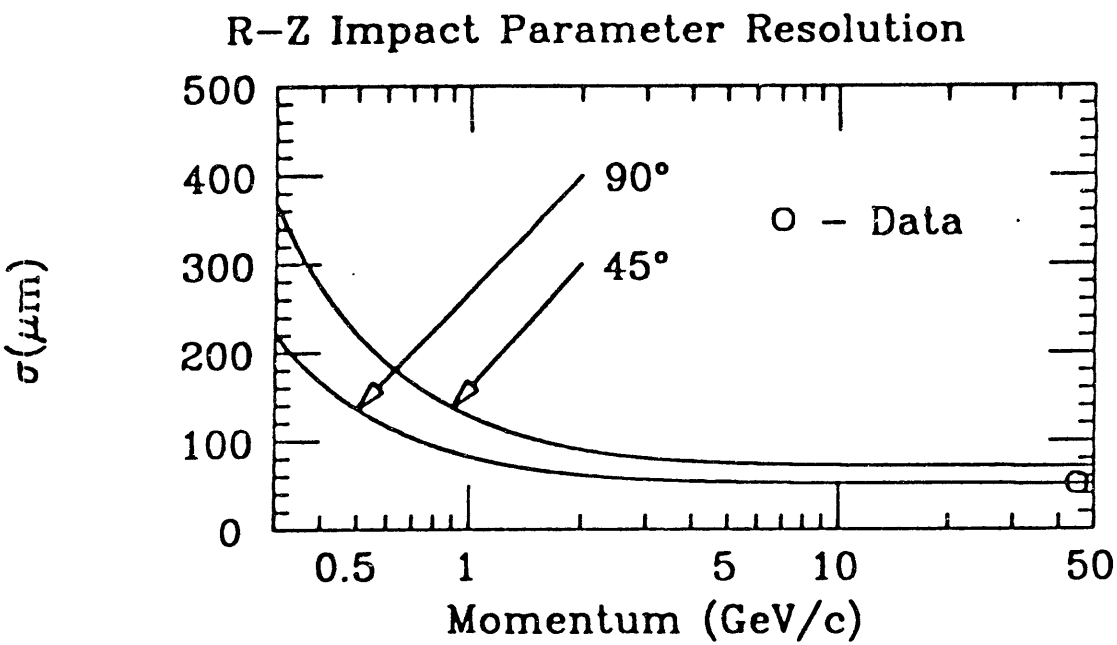


$$\sigma_b(RZ) = \sqrt{52^2 + \left(\frac{70}{p}\right)^2}$$

# $\mu^+\mu^- + e^+e^-$

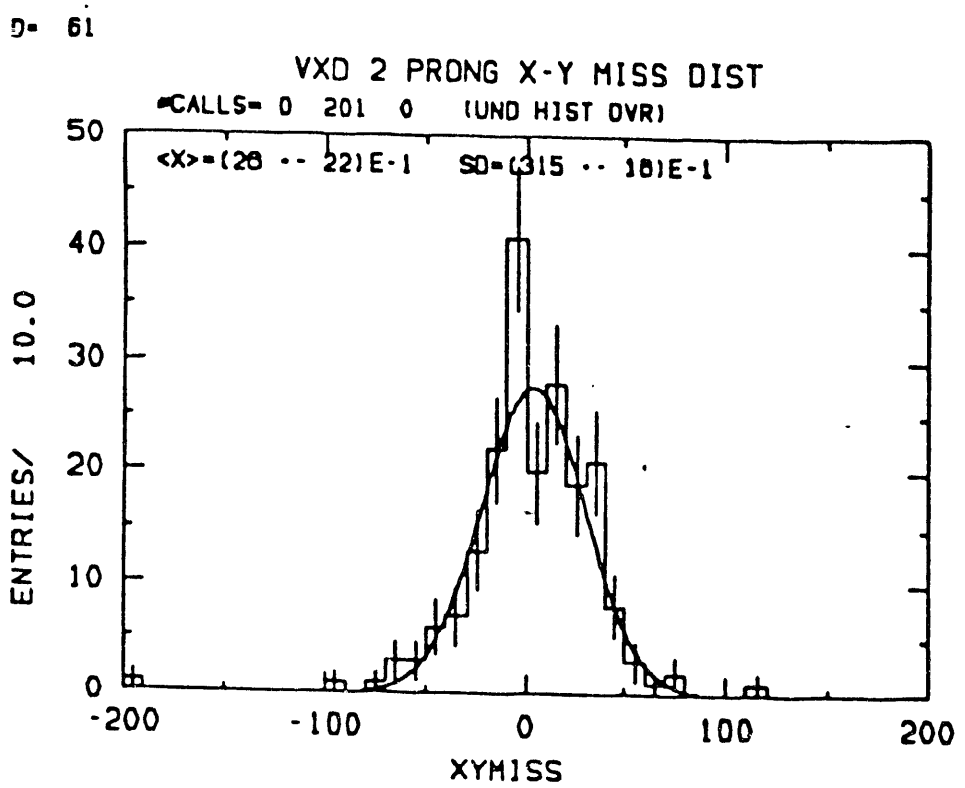


$\sigma_{xy}(2) = 26\,\mu m$

$\boxed{\sigma_{xy}(1\ \text{TRACK}) = 19\,\mu m}$

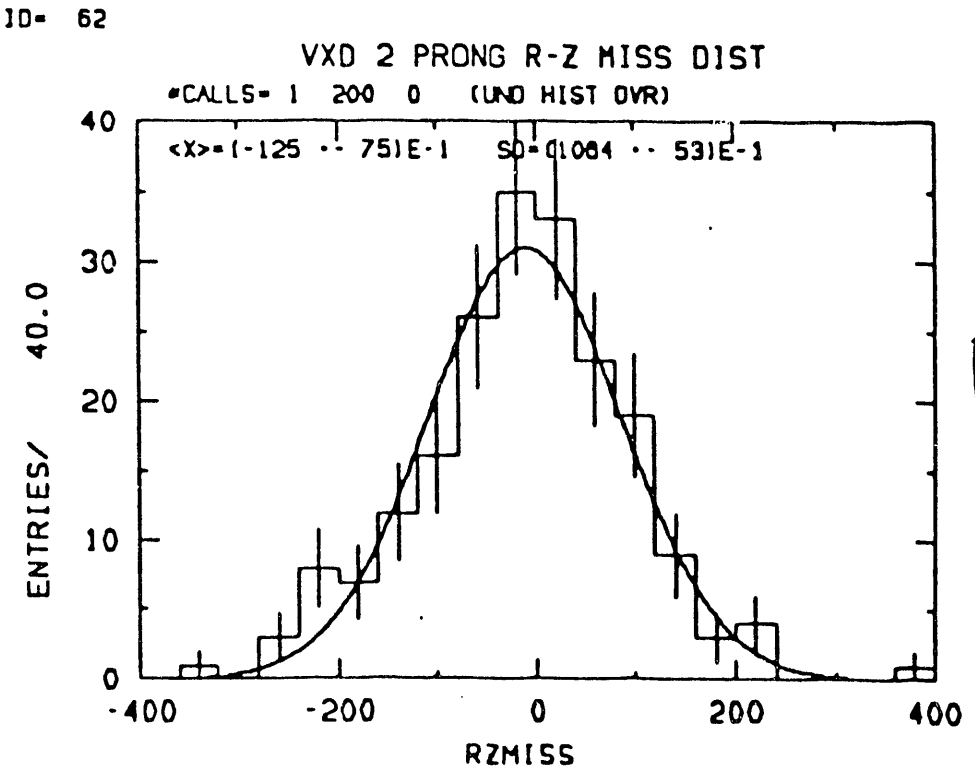


$\sigma_z(2) = 98\,\mu m$

$\boxed{\sigma_z(1\ \text{Track}) = 69\,\mu m}$

$\mu^+\mu^- + e^+e^-$

Distance from nominal I.P.

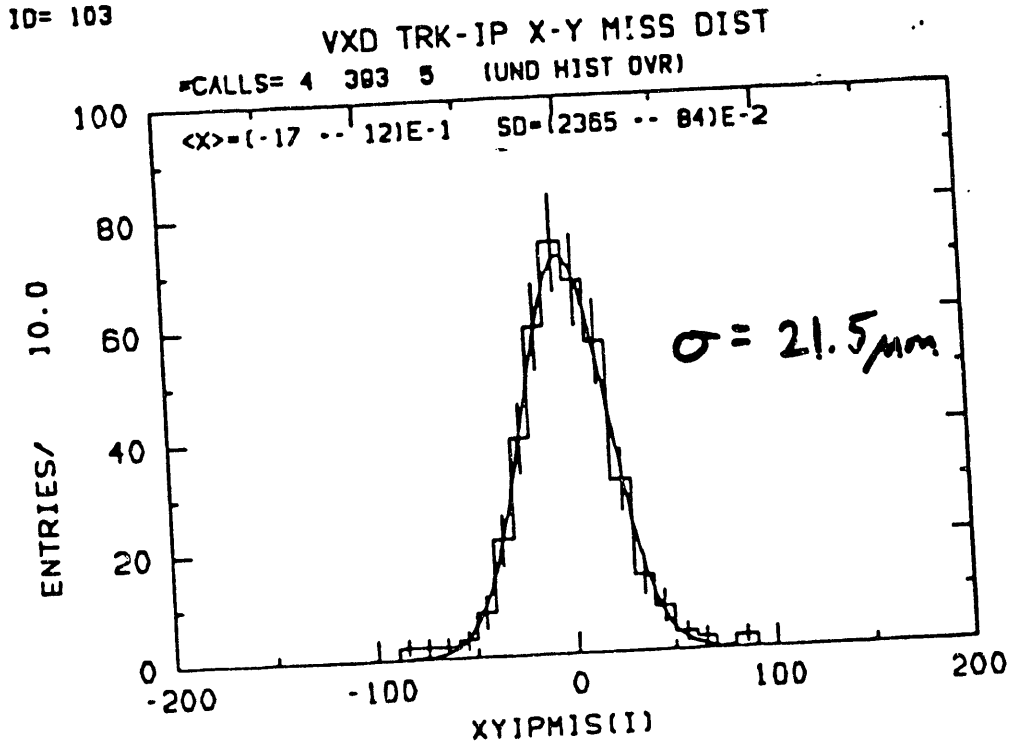


$$\sigma^2 = \sigma_{IP}^2 + \sigma_{TRACK}^2$$

$\sigma \uparrow 21.5$ $\qquad$ $\sigma_{TRACK} \uparrow 18.5$

$$\Rightarrow \boxed{\sigma_{IP} = 11\,\mu m}$$

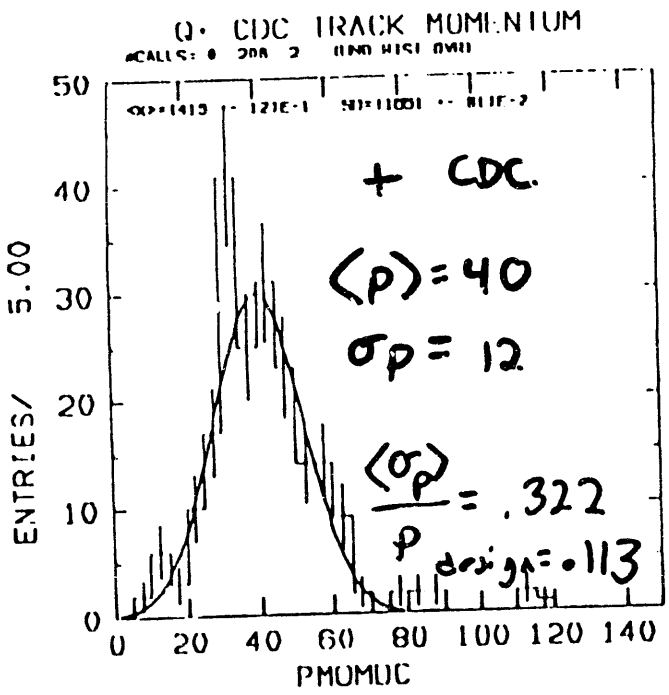


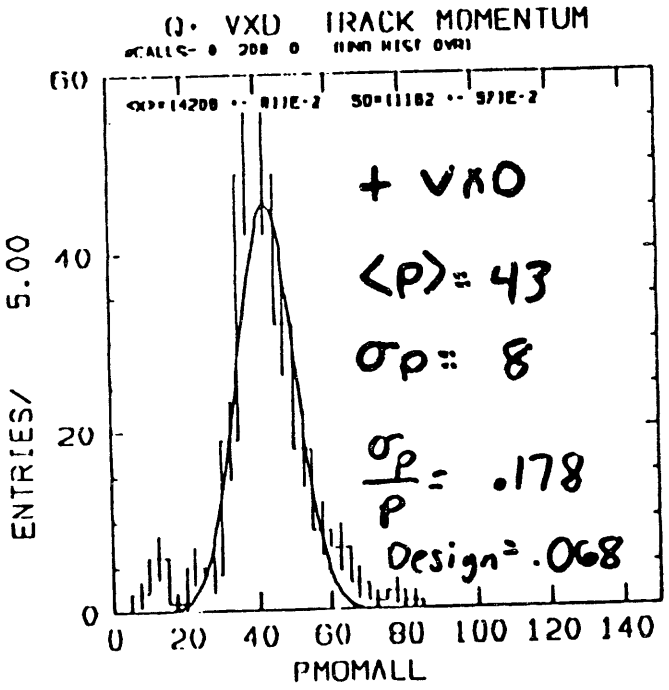


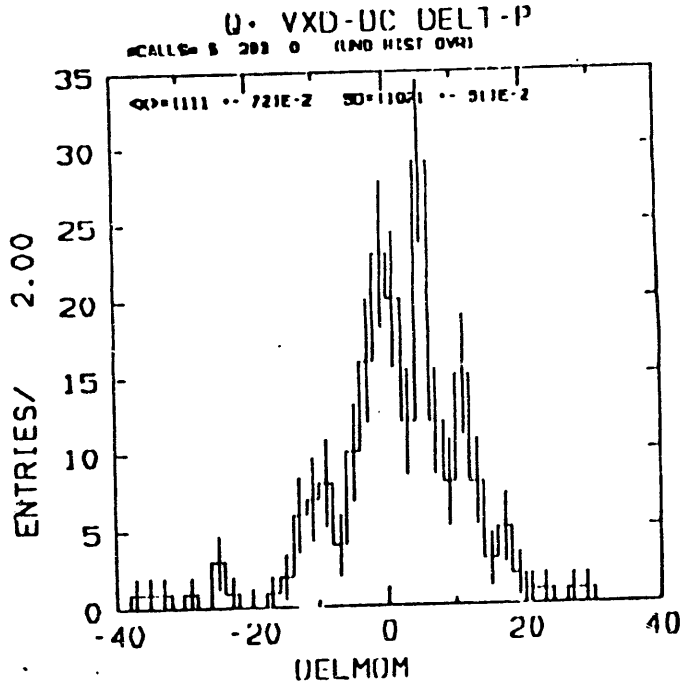


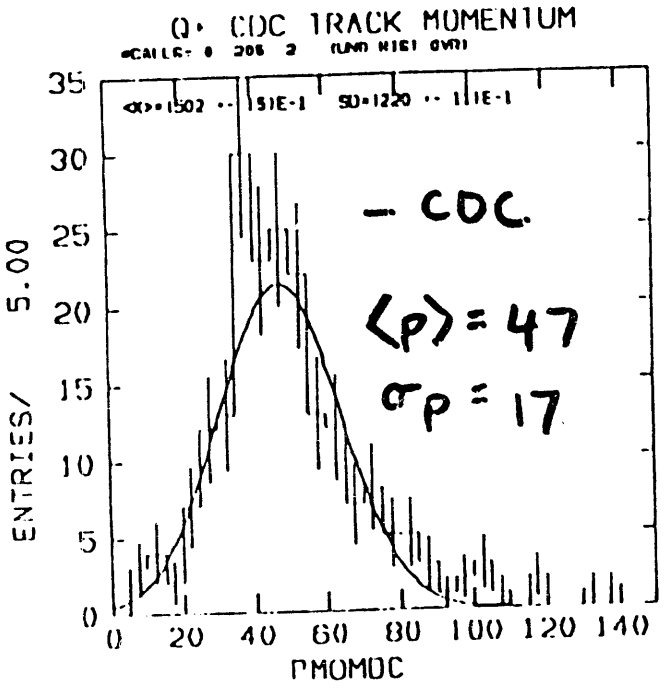


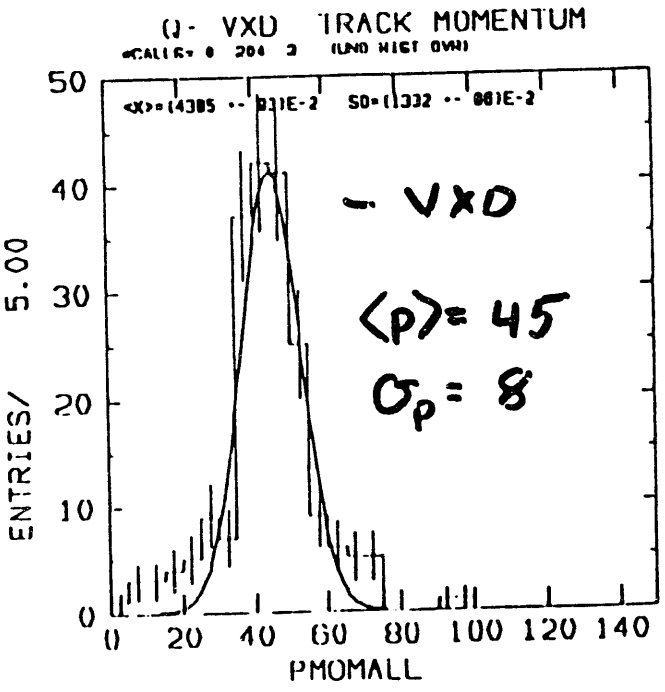


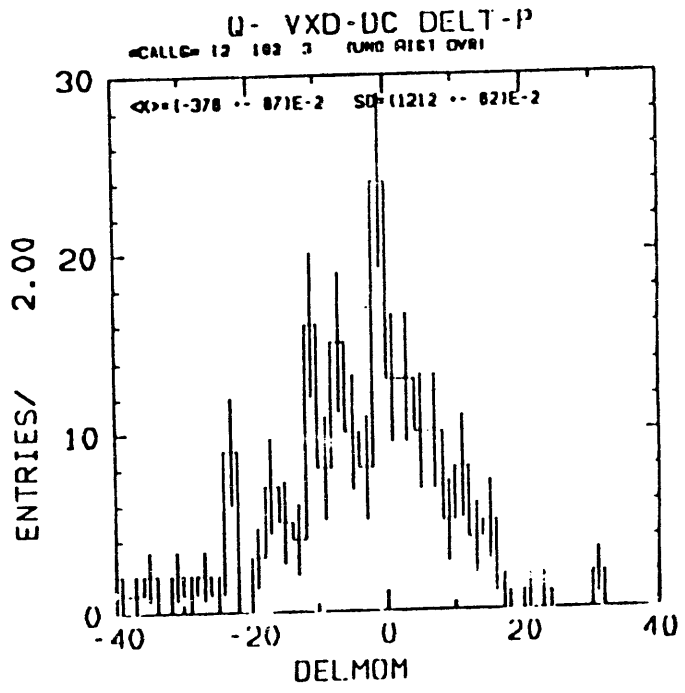


16:51:19 17NOV92

3+1 $\tau^+\tau^-$

X-Y VIEW

Run 11649, EVENT 864
24-MAY-1992 18:38
Source: Run Data Pol: L
Trigger: Energy CDC Hadron NAB
Beam Crossing 9267460

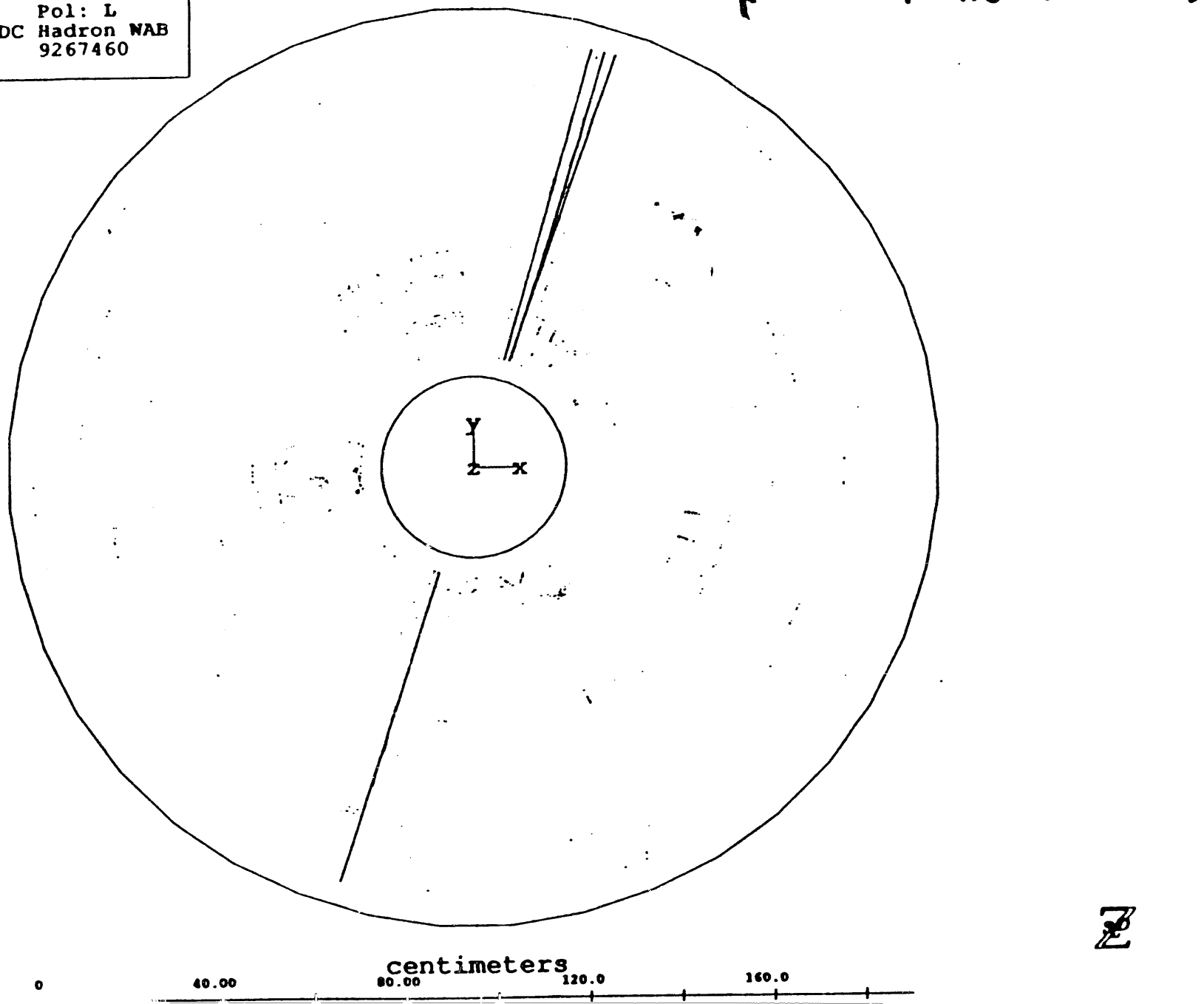

Run 11649, EVENT 864
24-MAY-1992 18:38
Source: Run Data Pol: L
Trigger: Energy CDC Hadron WAB
Beam Crossing 9267460

XY VIEW

|-1cm-|

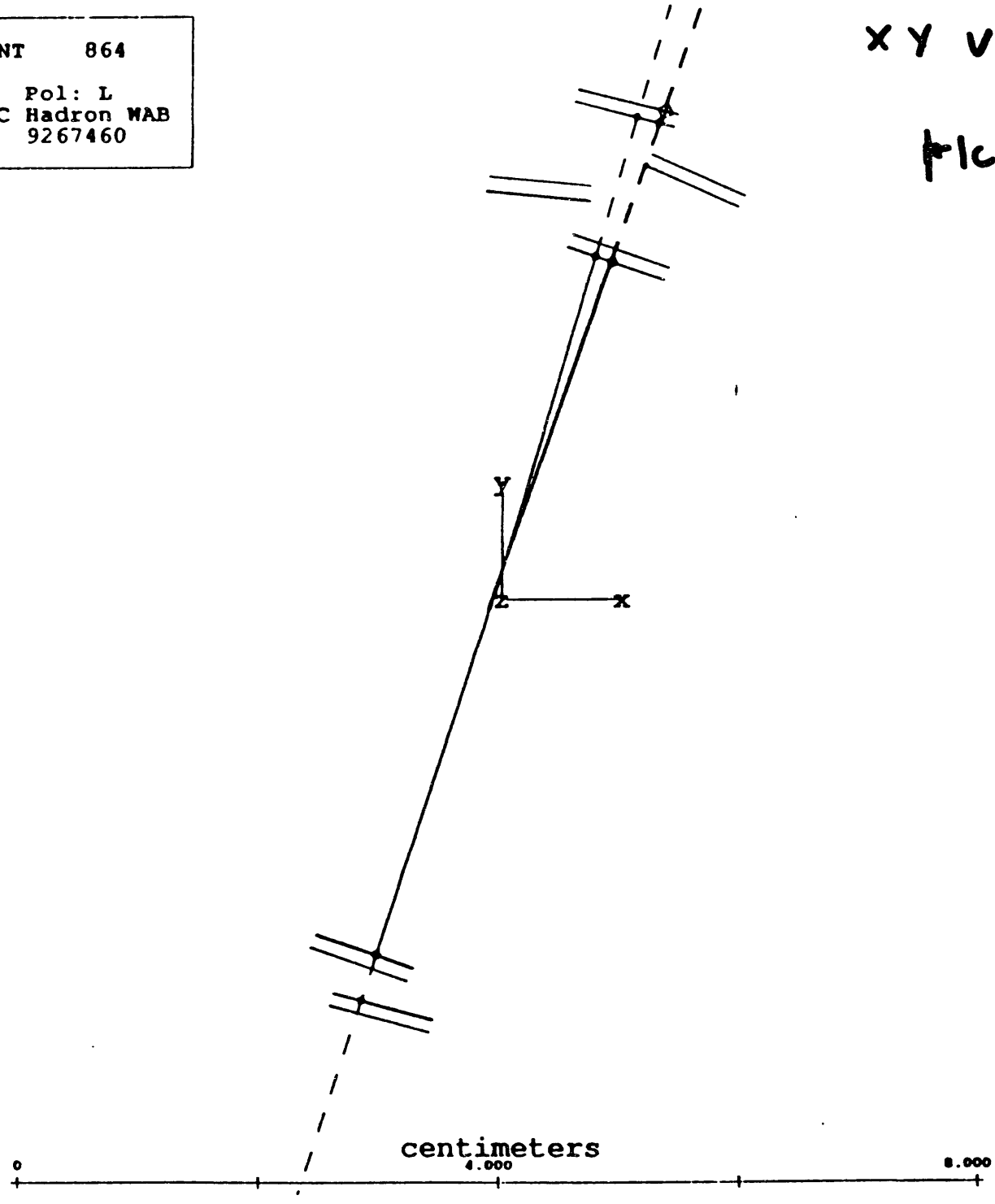


Z

R-Z VIEW

← 1 meter →

Hard Copy Done

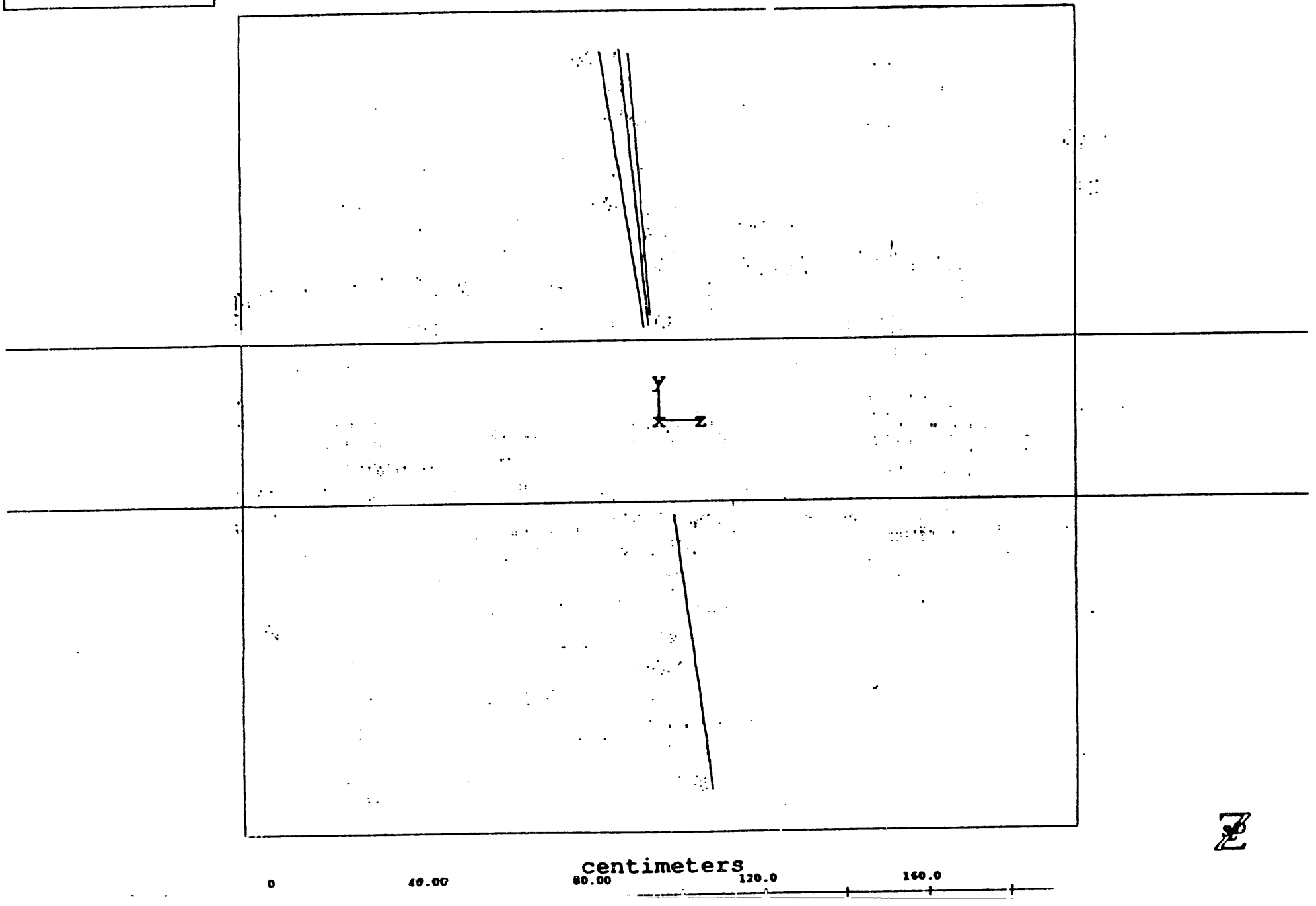

R-Z VIEW

Run 11649, EVENT 864
24-MAY-1992 18:38
Source: Run Data Pol: L
Trigger: Energy CDC Hadron WAB
Beam Crossing 9267460

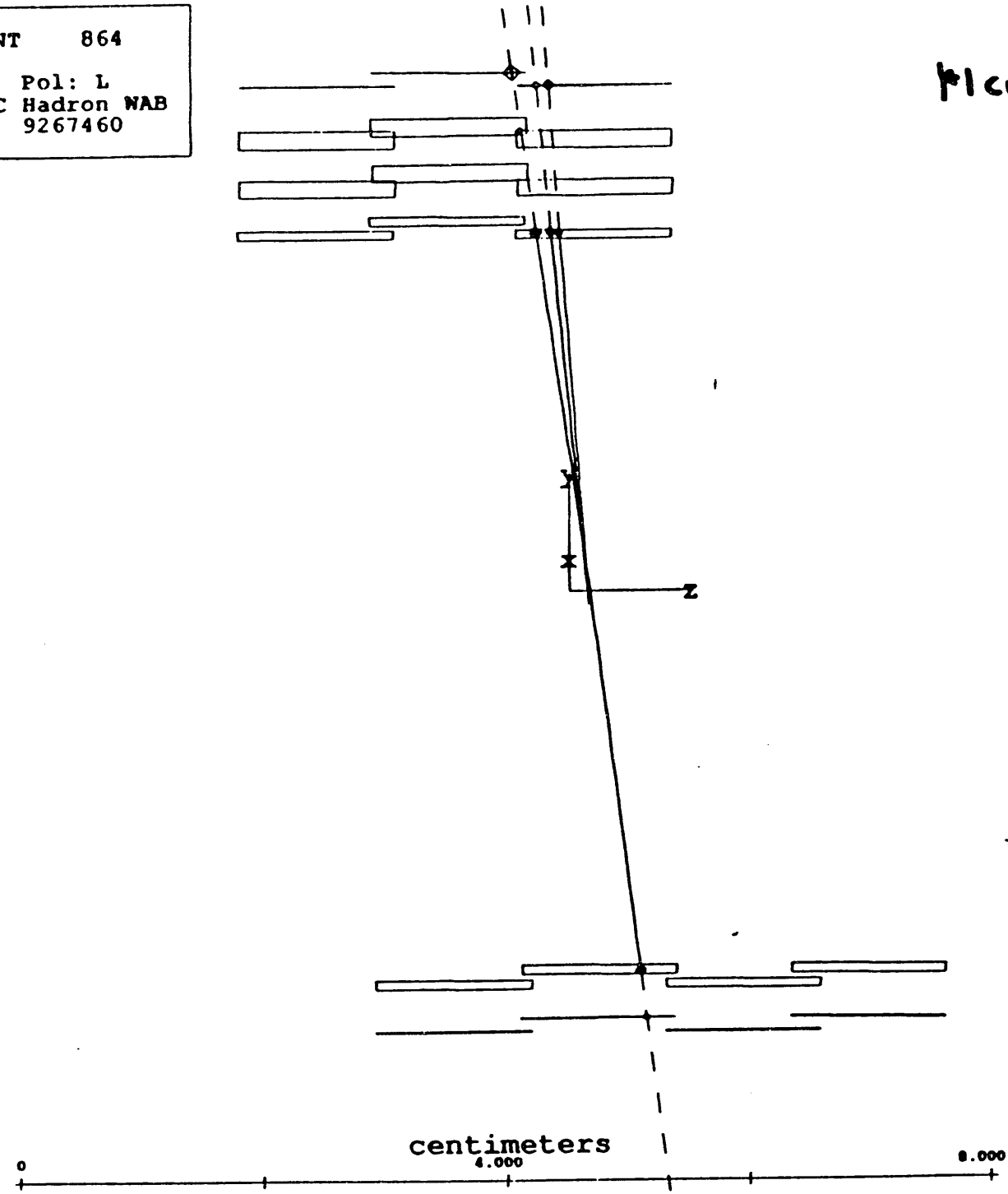


Z

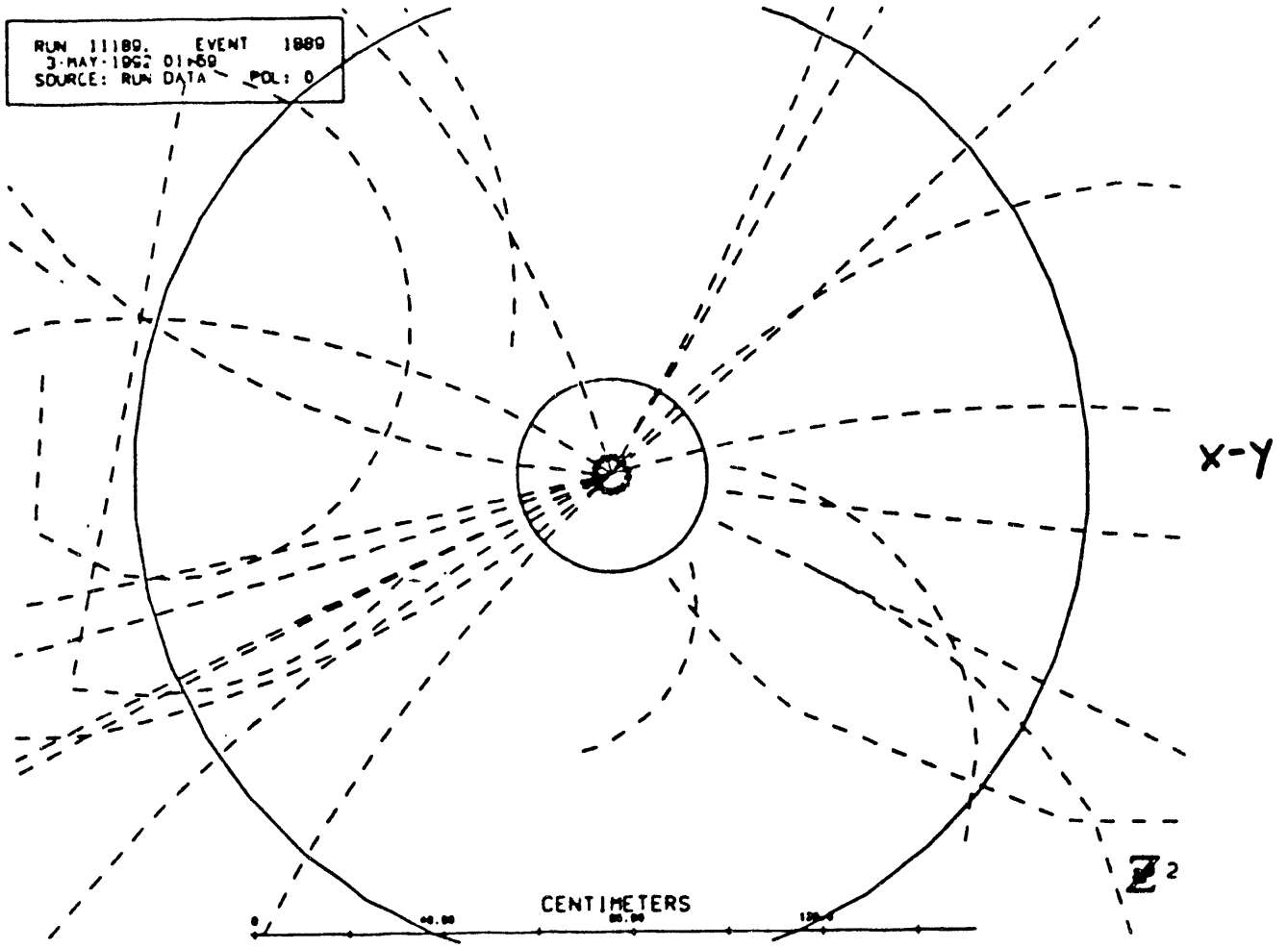
RUN 11189. EVENT 1889
3-MAY-1992 01:59
SOURCE: RUN DATA POL: 0
CENTIMETERS
0
40.00
80.00
120.0
X-Y
Z2

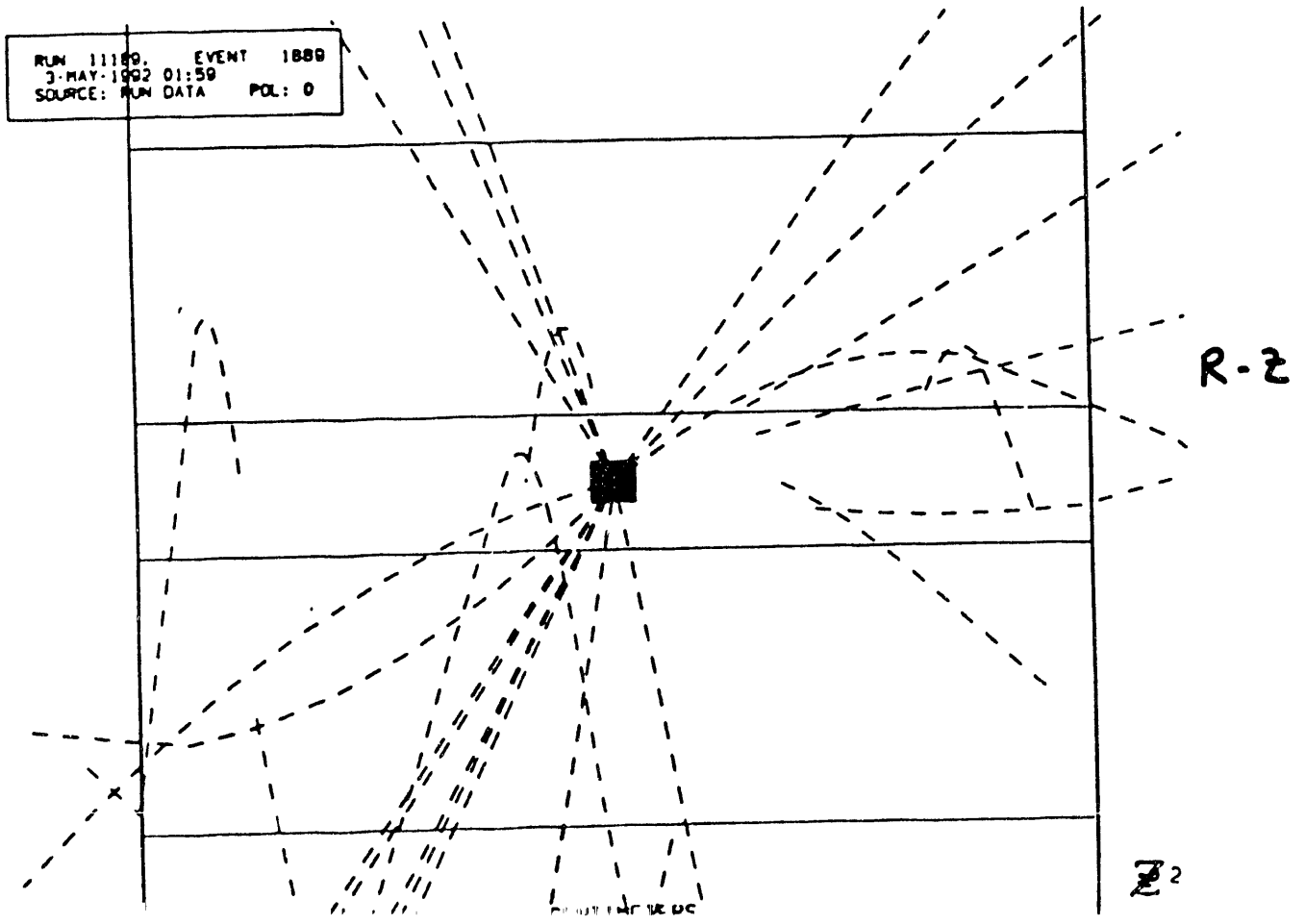
RUN 11189. EVENT 1889
3-MAY-1992 01:59
SOURCE: RUN DATA POL: 0
R-Z
Z2

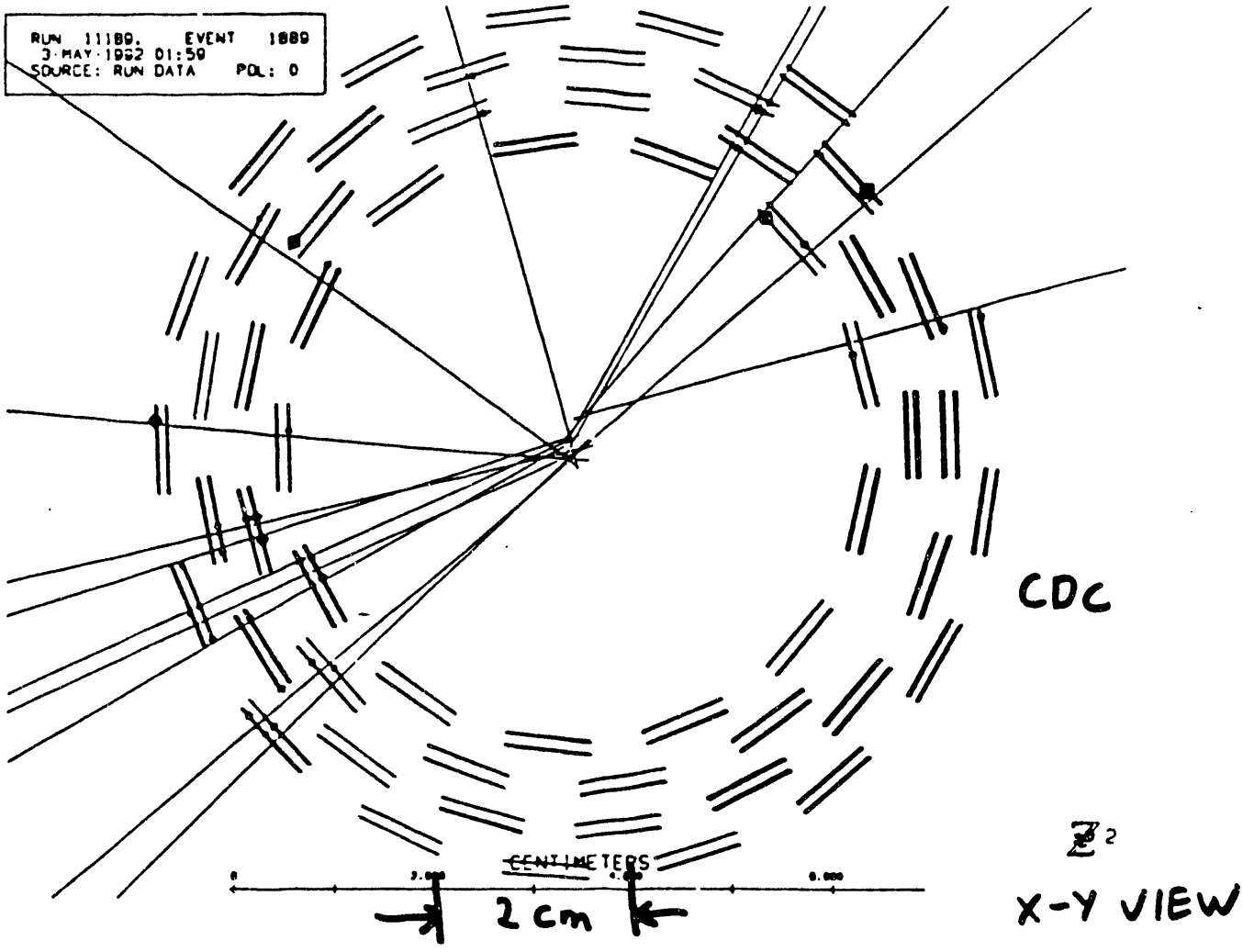
RUN 11189. EVENT 1889
3-MAY-1992 01:59
SOURCE: RUN DATA POL: 0
CDC
CENTIMETERS
2 cm
X-Y VIEW

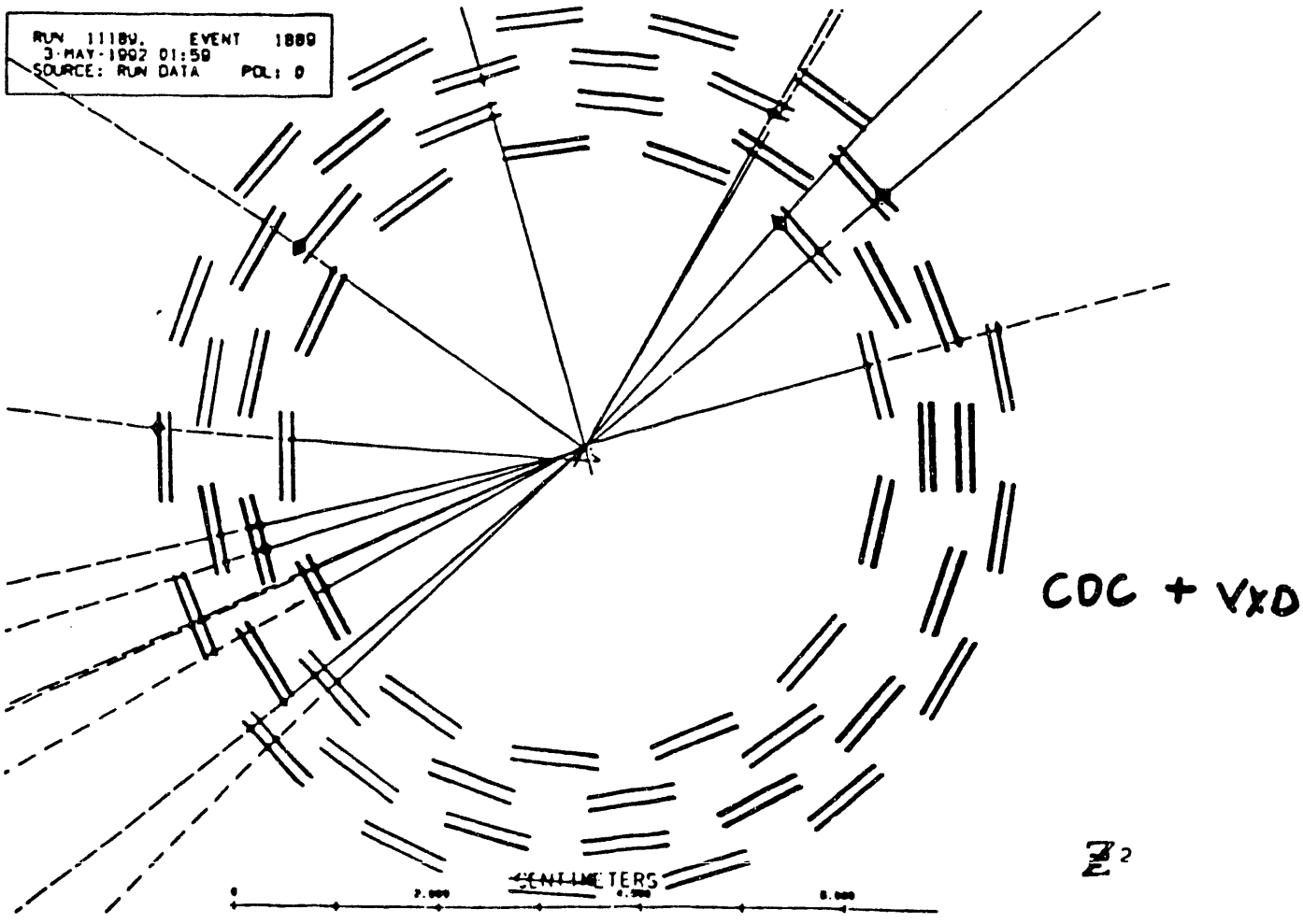
RUN 11189. EVENT 1889
3-MAY-1992 01:59
SOURCE: RUN DATA POL: 0
CDC + VXD
CENTIMETERS

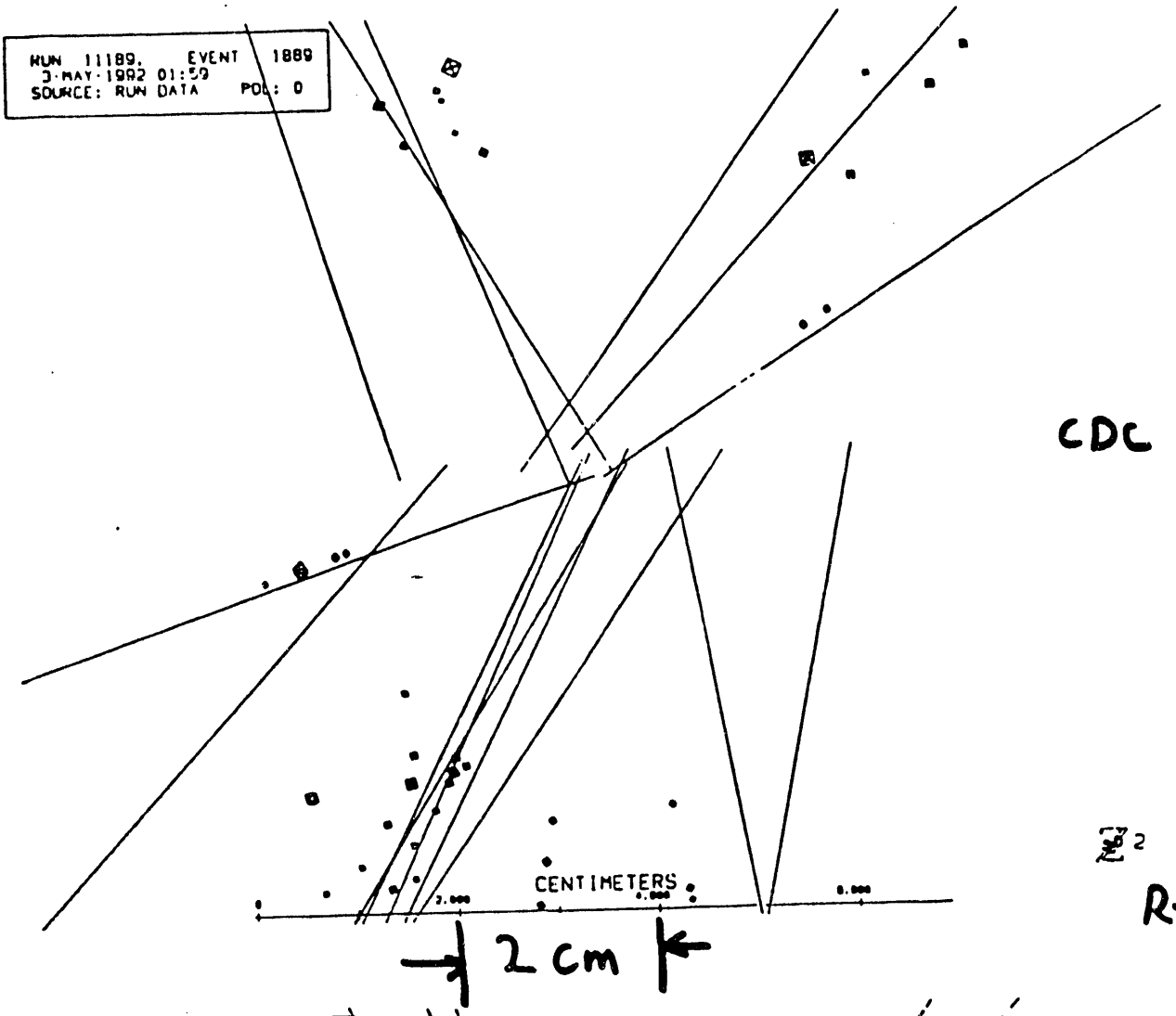
RUN 11189. EVENT 1889
3-MAY-1992 01:59
SOURCE: RUN DATA POL: 0
CDC
CENTIMETERS
2 cm
R-Z VIEW

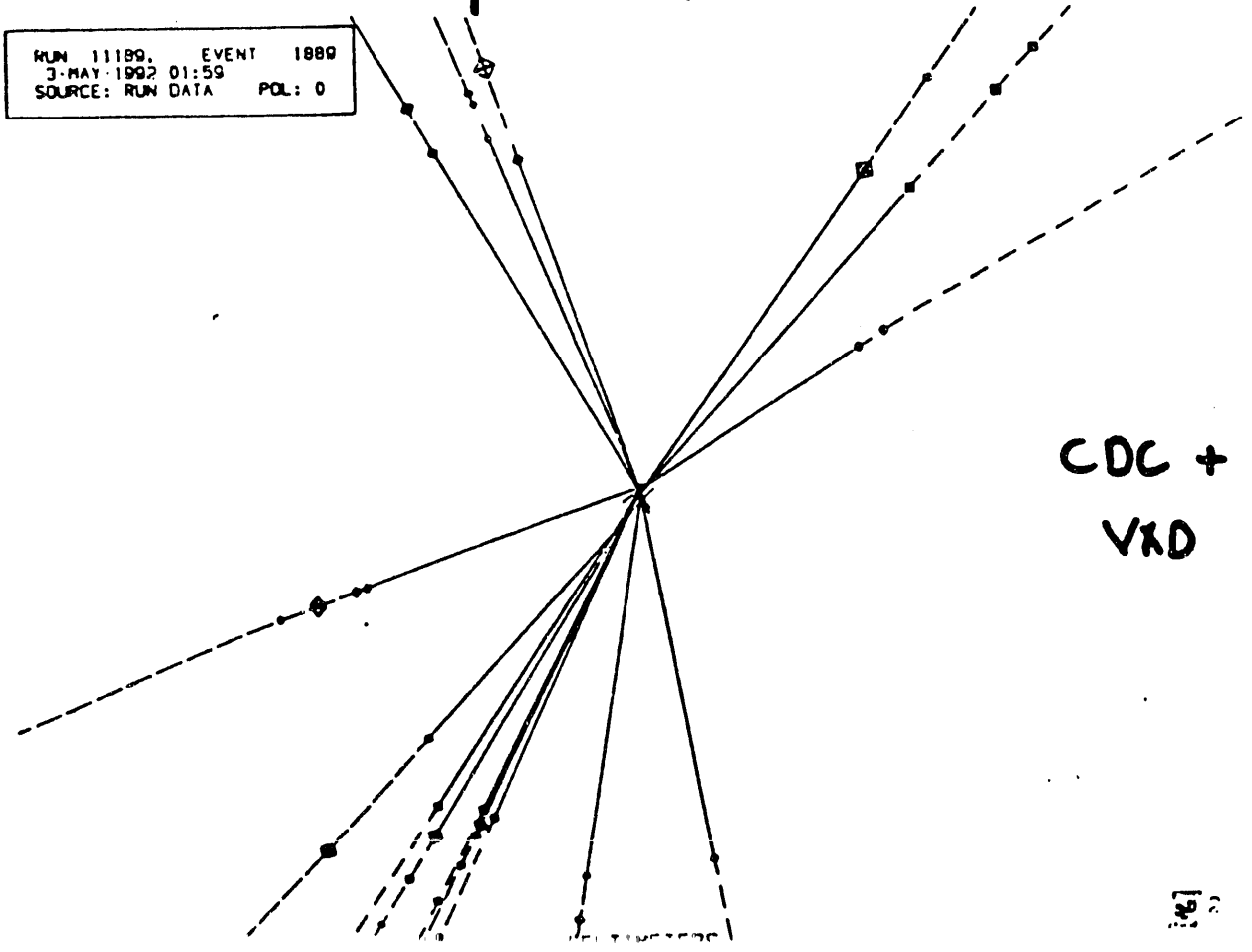
RUN 11189. EVENT 1889
3-MAY-1992 01:59
SOURCE: RUN DATA POL: 0
CDC +
VXD

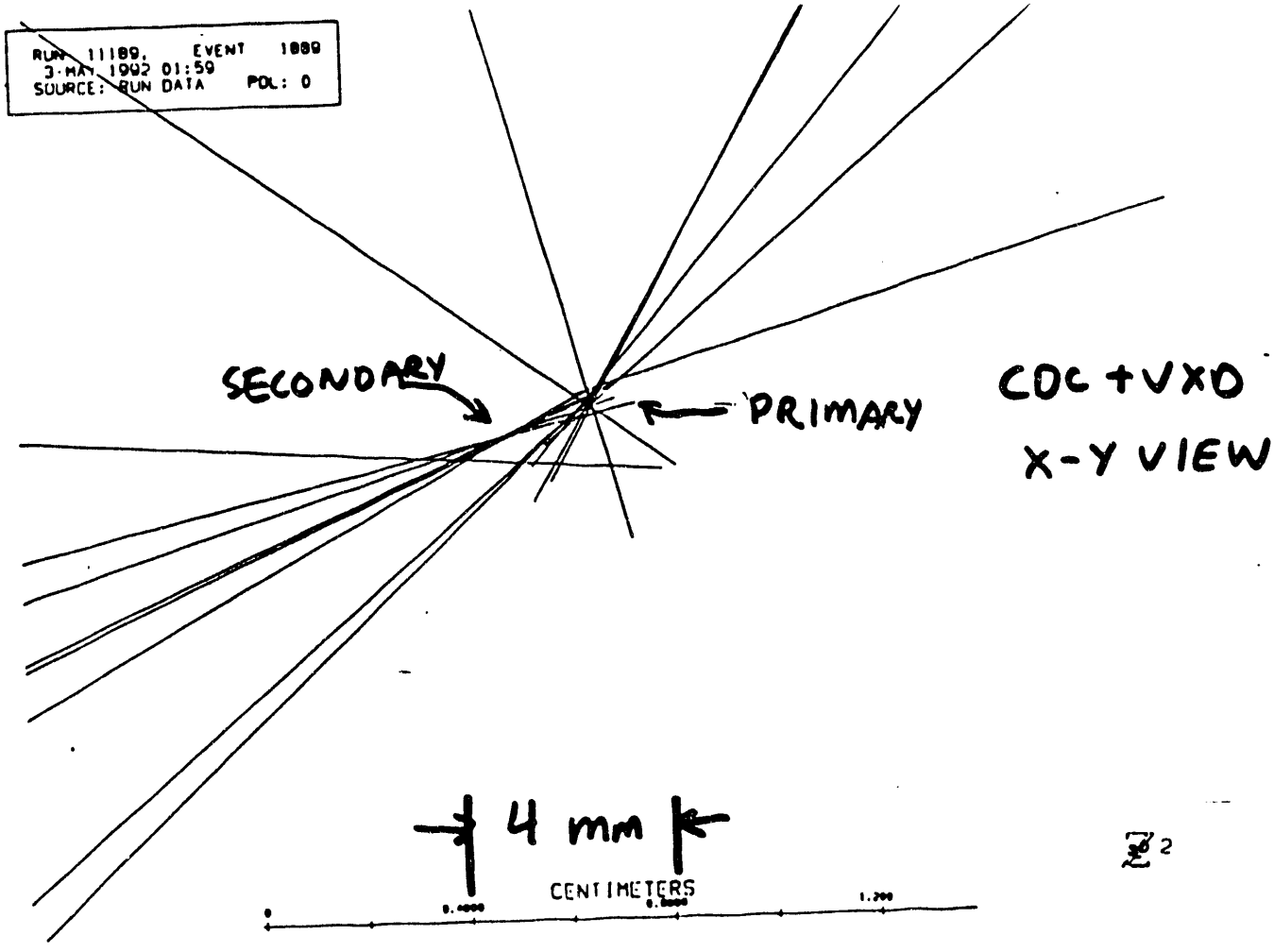
RUN 11189. EVENT 1889
3-MAY-1992 01:59
SOURCE: RUN DATA POL: 0
SECONDARY
PRIMARY
CDC + VXD
X-Y VIEW
4 mm
CENTIMETERS
0.4000
1.200

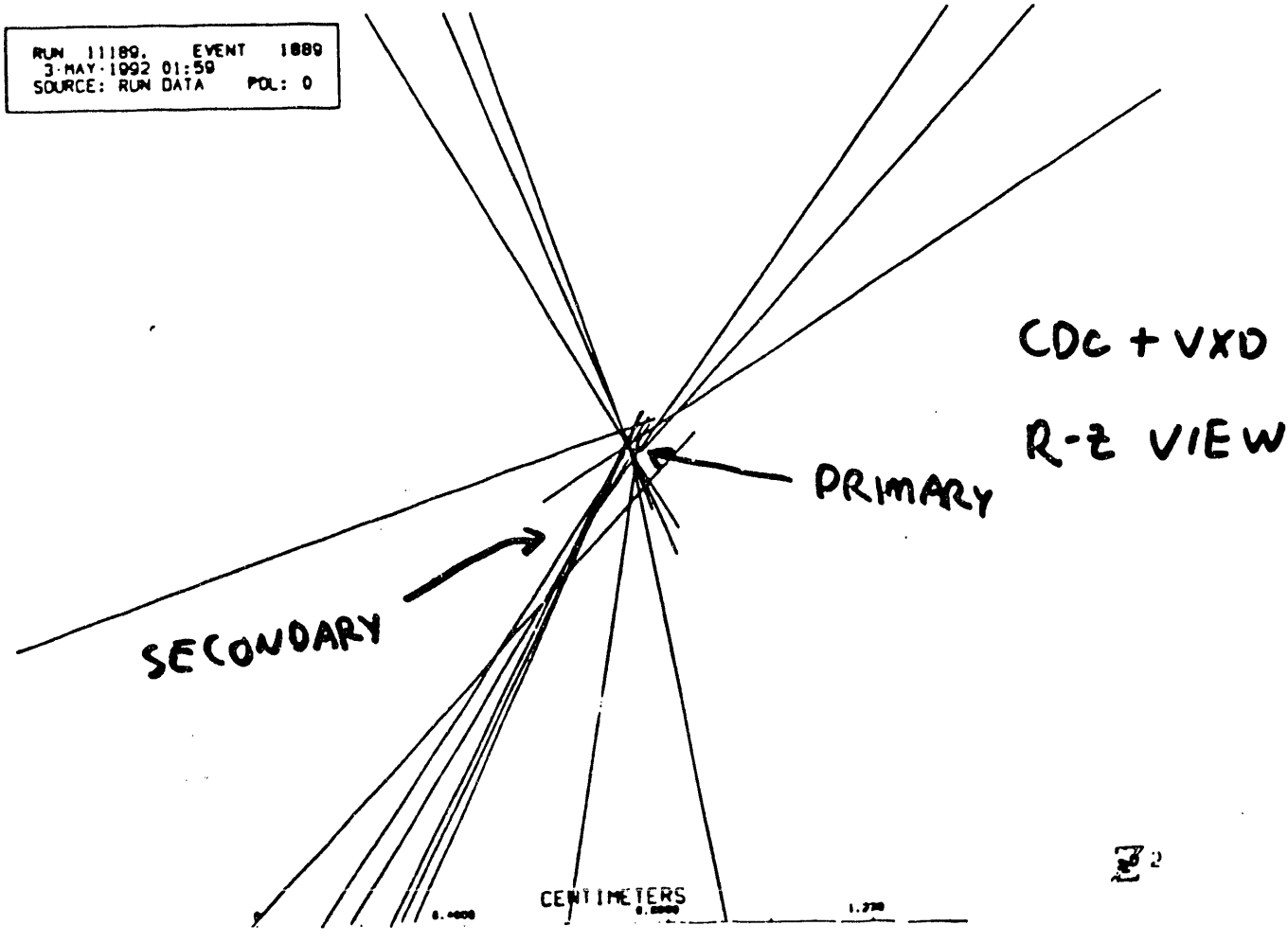
RUN 11189. EVENT 1889
3-MAY-1992 01:59
SOURCE: RUN DATA POL: 0
CDC + VXD
R-Z VIEW
PRIMARY
SECONDARY
CENTIMETERS
0.4000
1.270

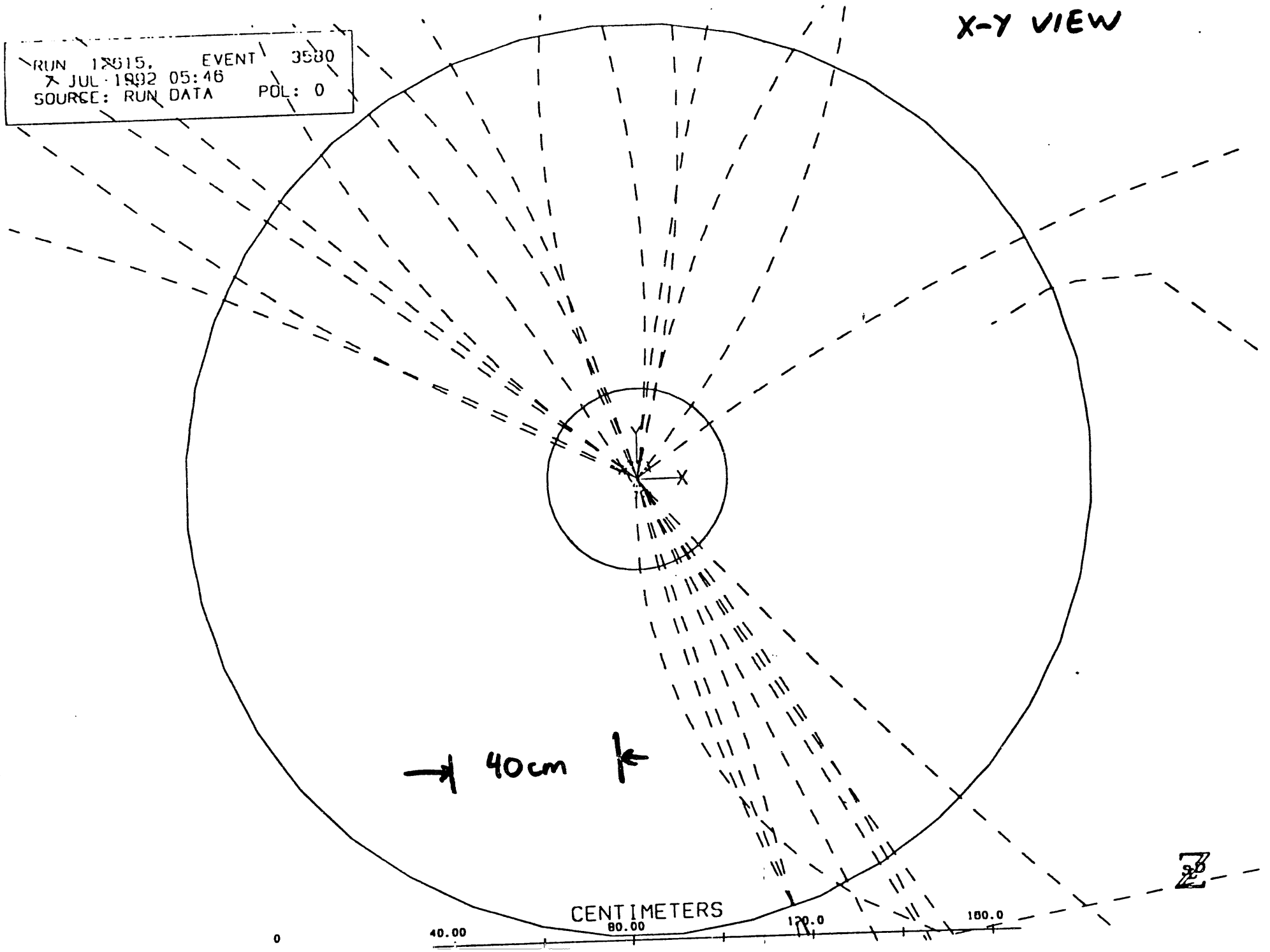
X-Y VIEW
RUN 12615, EVENT 3580
7 JUL 1992 05:46
SOURCE: RUN DATA POL: 0
40cm
X
Z
CENTIMETERS
0
40.00
80.00
120.0
160.0

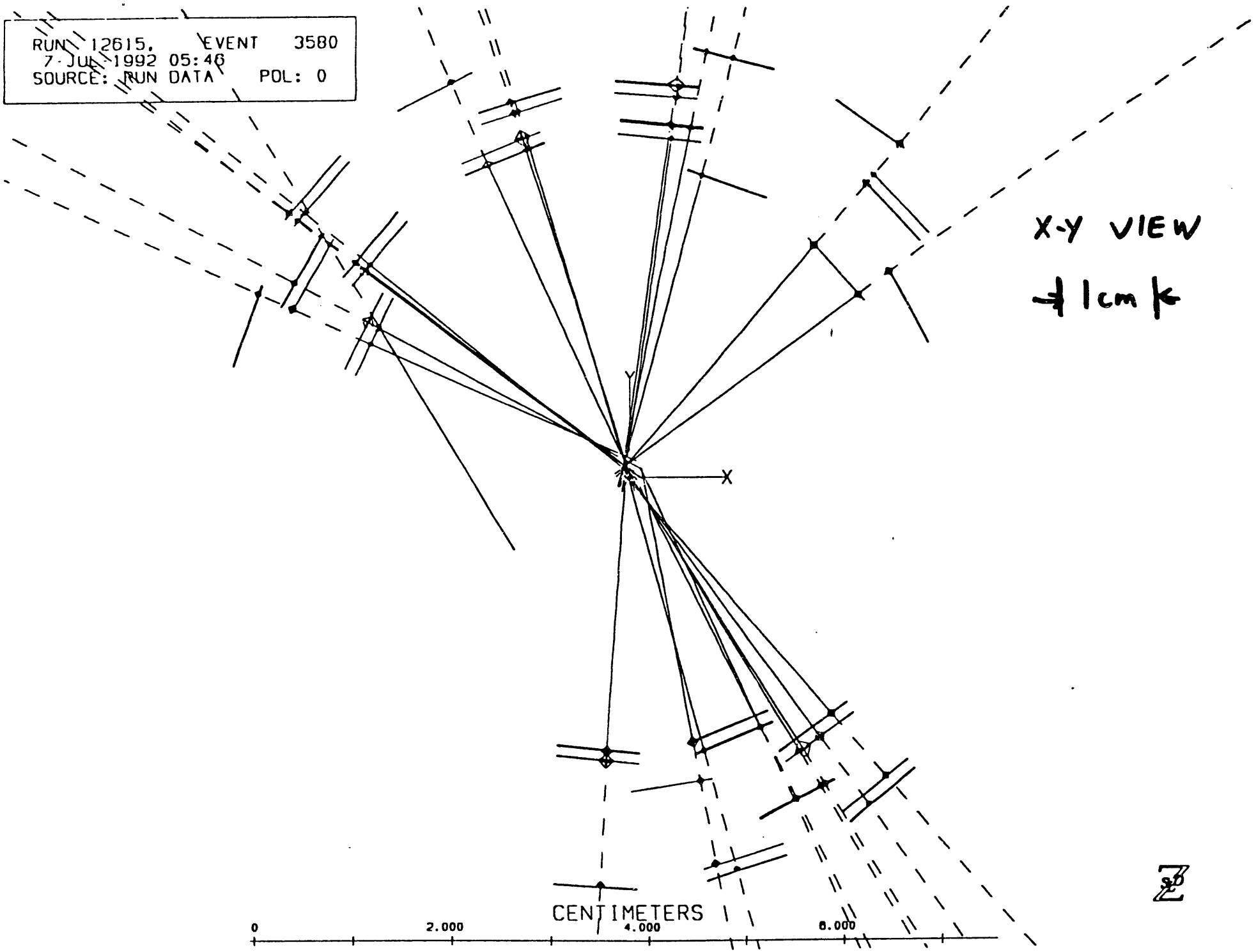
RUN 12615, EVENT 3580
7-JUL-1992 05:46
SOURCE: RUN DATA POL: 0
X-Y VIEW
1cm
Y
X
CENTIMETERS
0
2.000
4.000
6.000

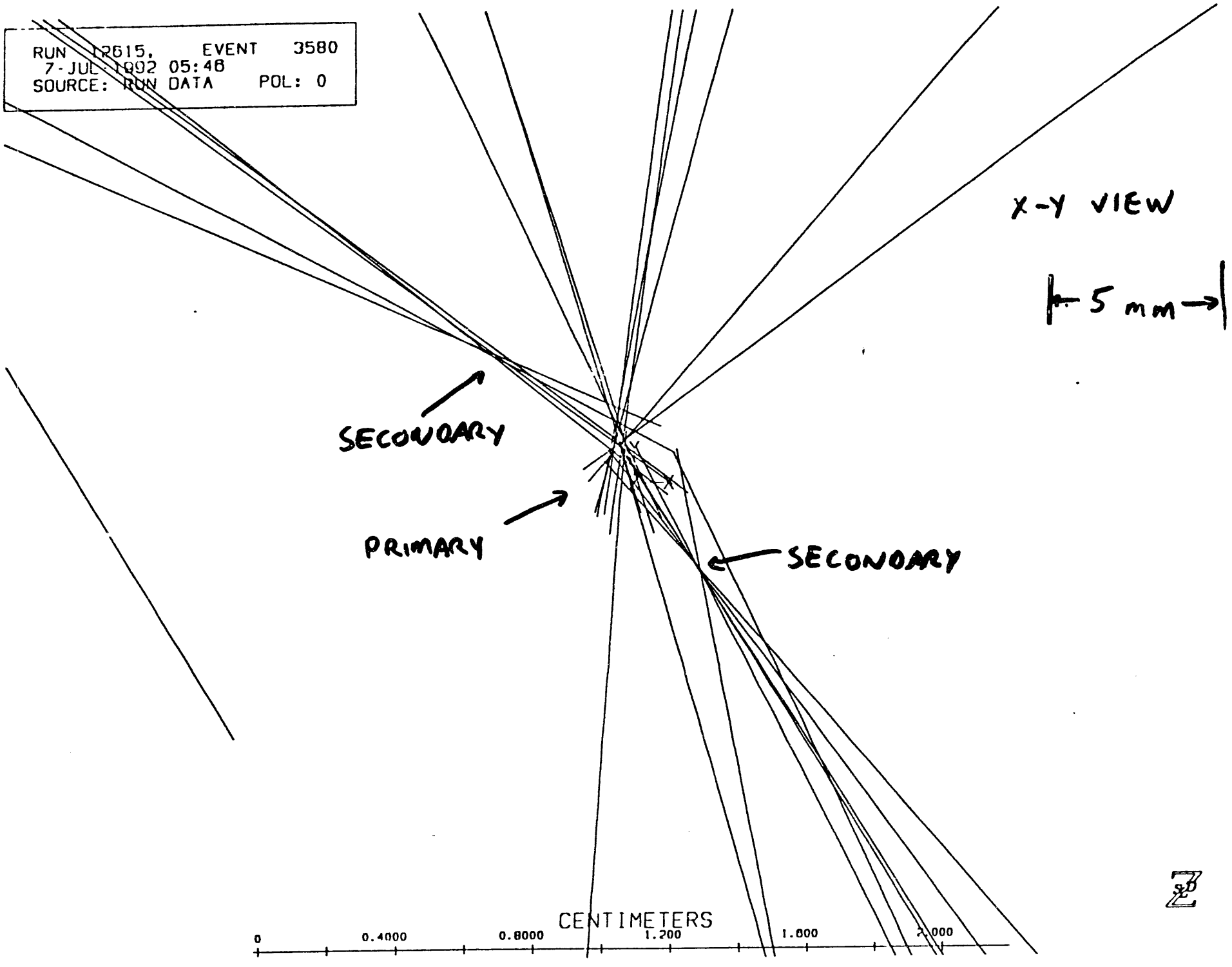
RUN 12615, EVENT 3580
7-JUL-1992 05:46
SOURCE: RUN DATA POL: 0
X-Y VIEW
5 mm
SECONDARY
PRIMARY
SECONDARY
CENTIMETERS
0
0.4000
0.8000
1.200
1.600
2.000

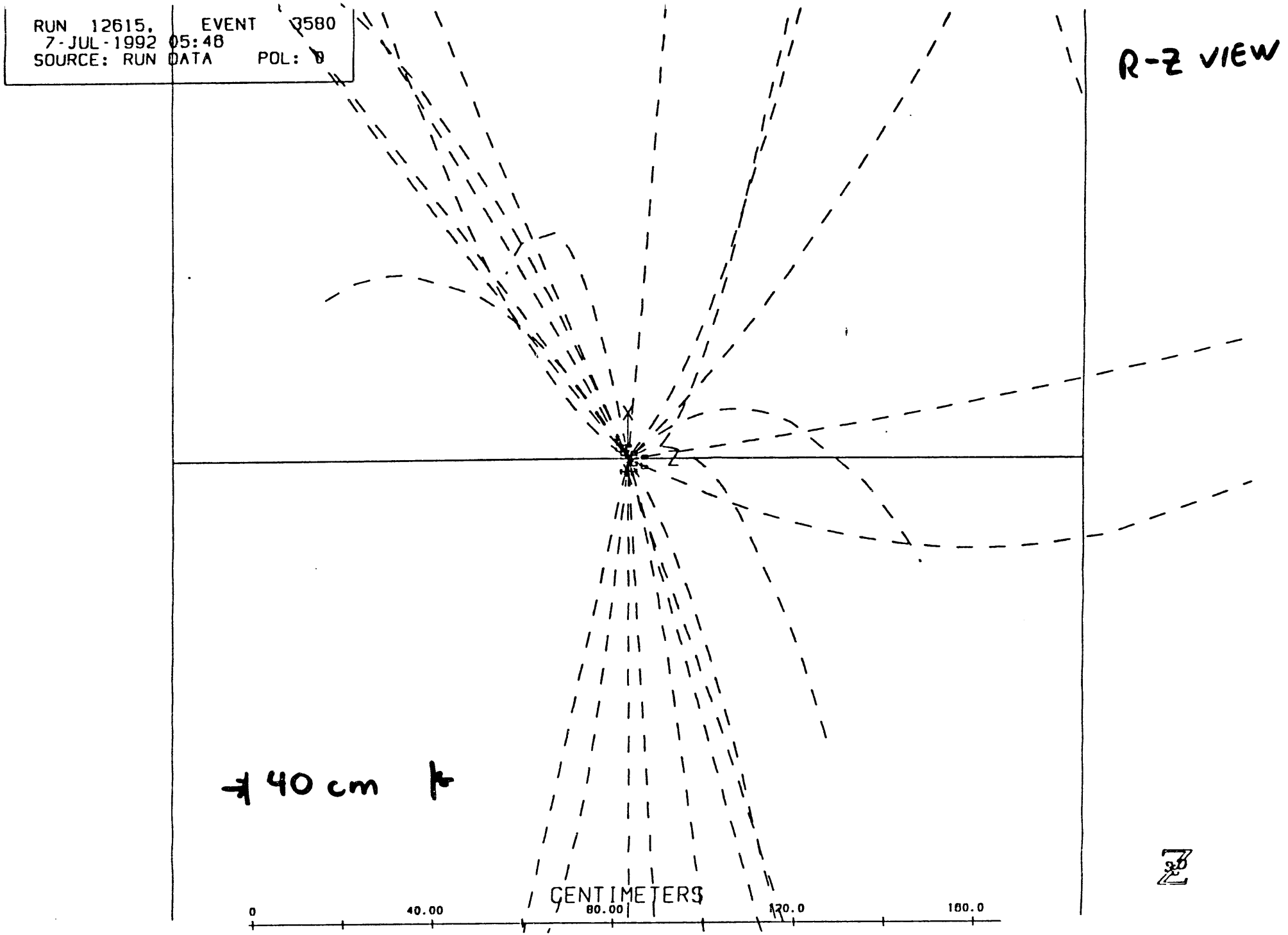
RUN 12615, EVENT 3580
7-JUL-1992 05:48
SOURCE: RUN DATA POL: B
R-Z VIEW
40 cm
Z
CENTIMETERS
0
40.00
80.00
120.0
160.0

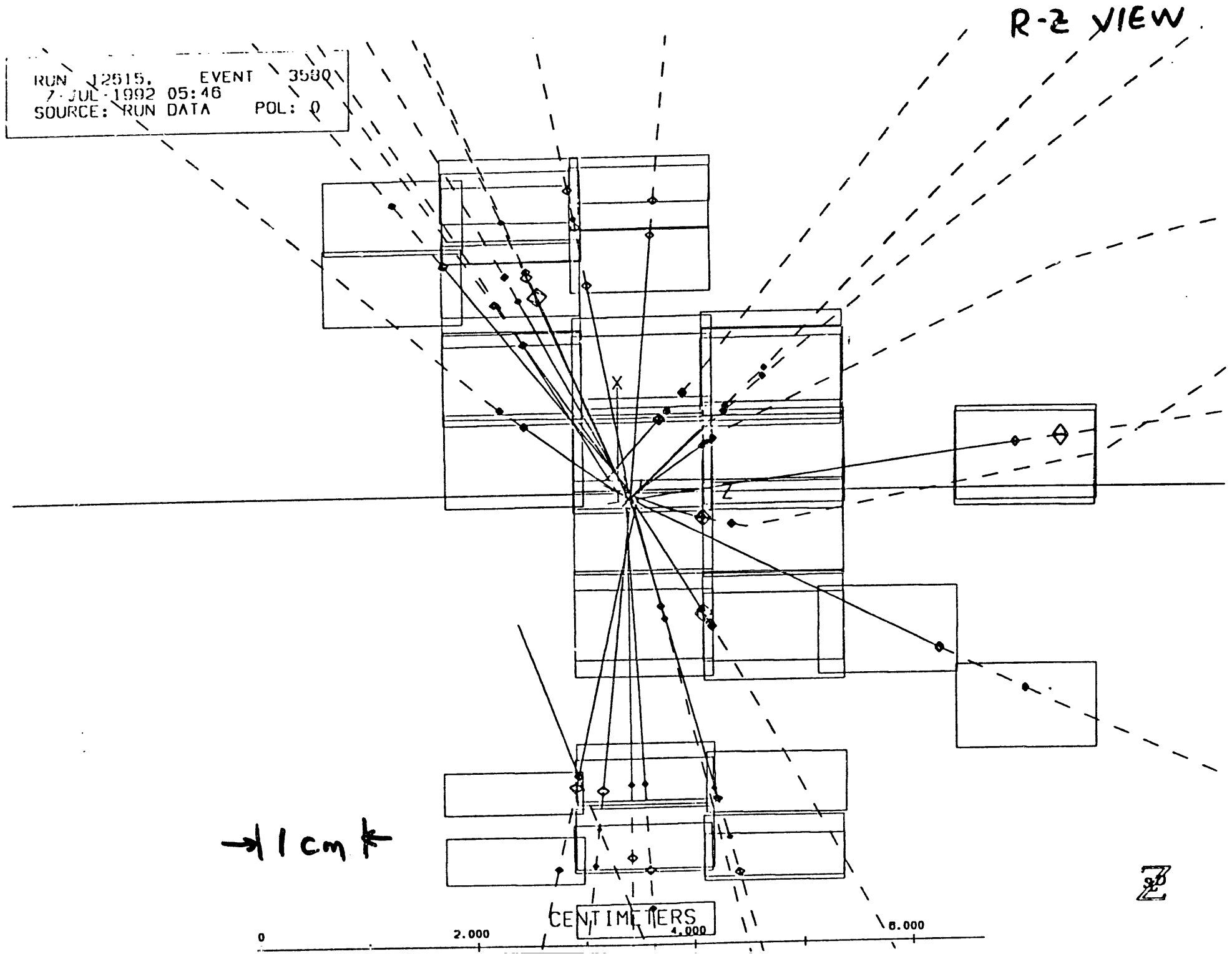
R-Z VIEW
RUN 12515. EVENT 3580
7-JUL-1992 05:46
SOURCE: RUN DATA POL: 0
X
Z
1 cm
CENTIMETERS
0
2.000
4.000
6.000
Z

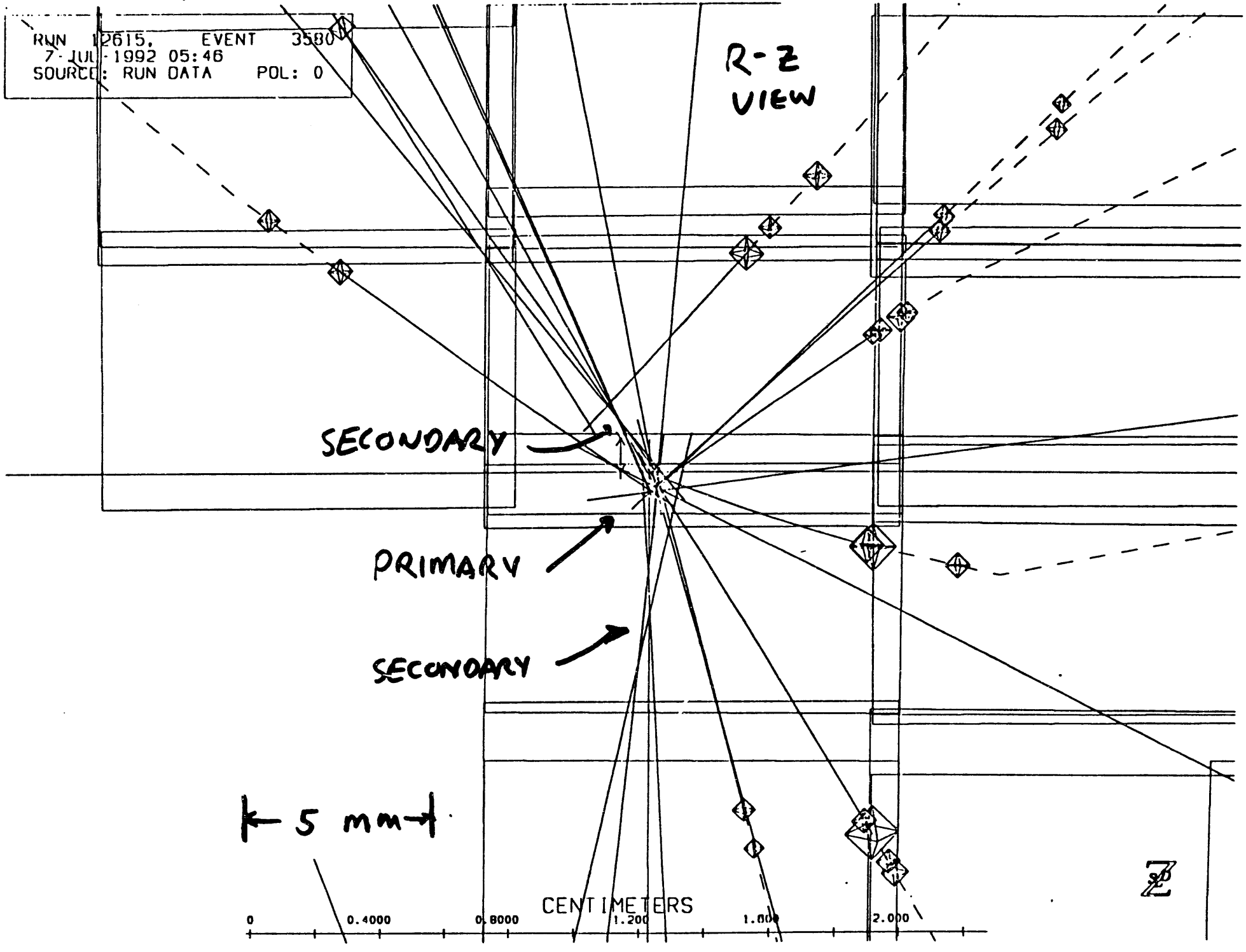
RUN 12615. EVENT 3580
7-JUL-1992 05:46
SOURCE: RUN DATA POL: 0
R-Z
VIEW
SECONDARY
PRIMARY
SECONDARY
5 mm
CENTIMETERS
0
0.4000
0.8000
1.200
1.600
2.000
Z

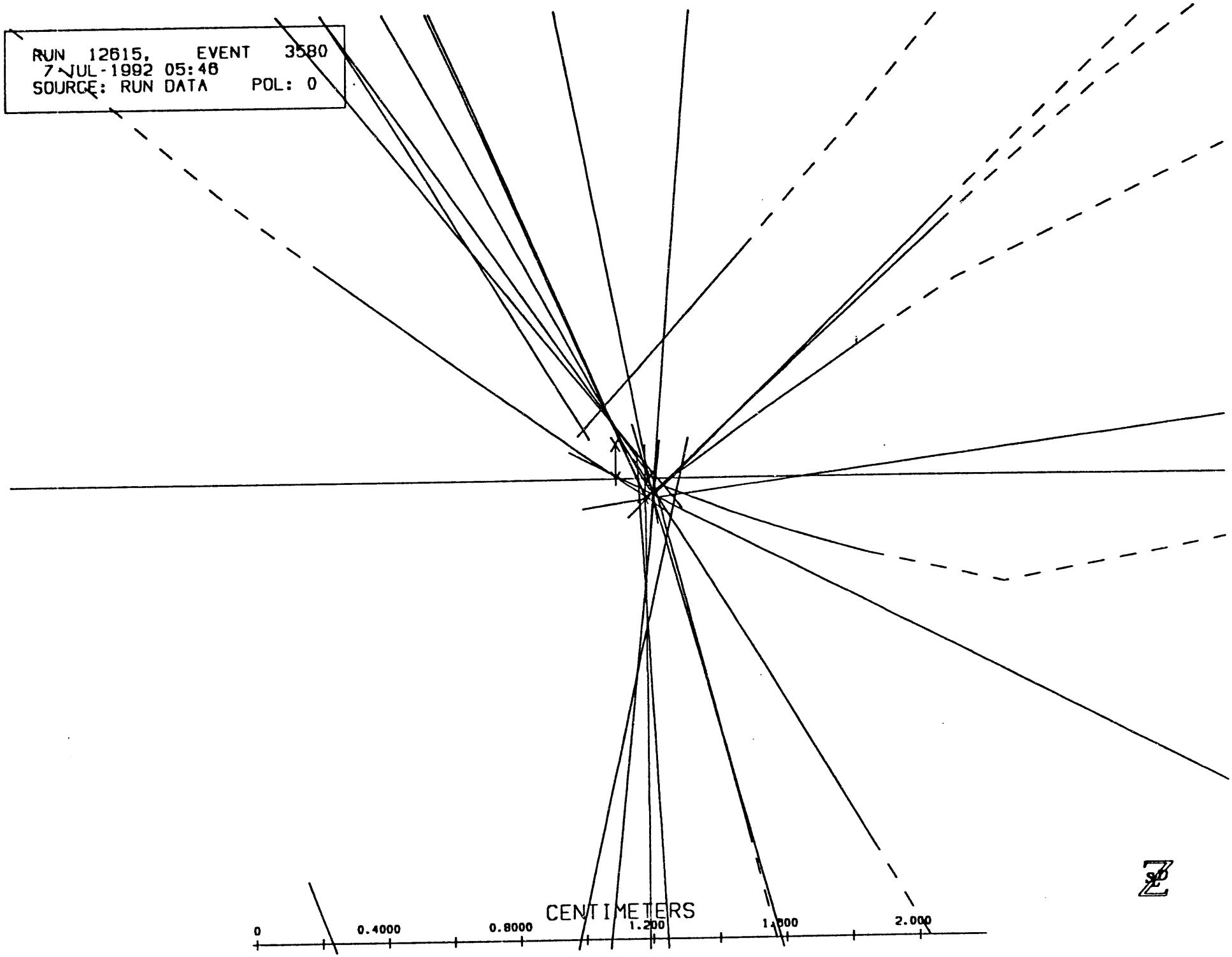
RUN 12615, EVENT 3580
7-JUL-1992 05:46
SOURCE: RUN DATA POL: 0
CENTIMETERS
0
0.4000
0.8000
1.200
1.600
2.000
Z

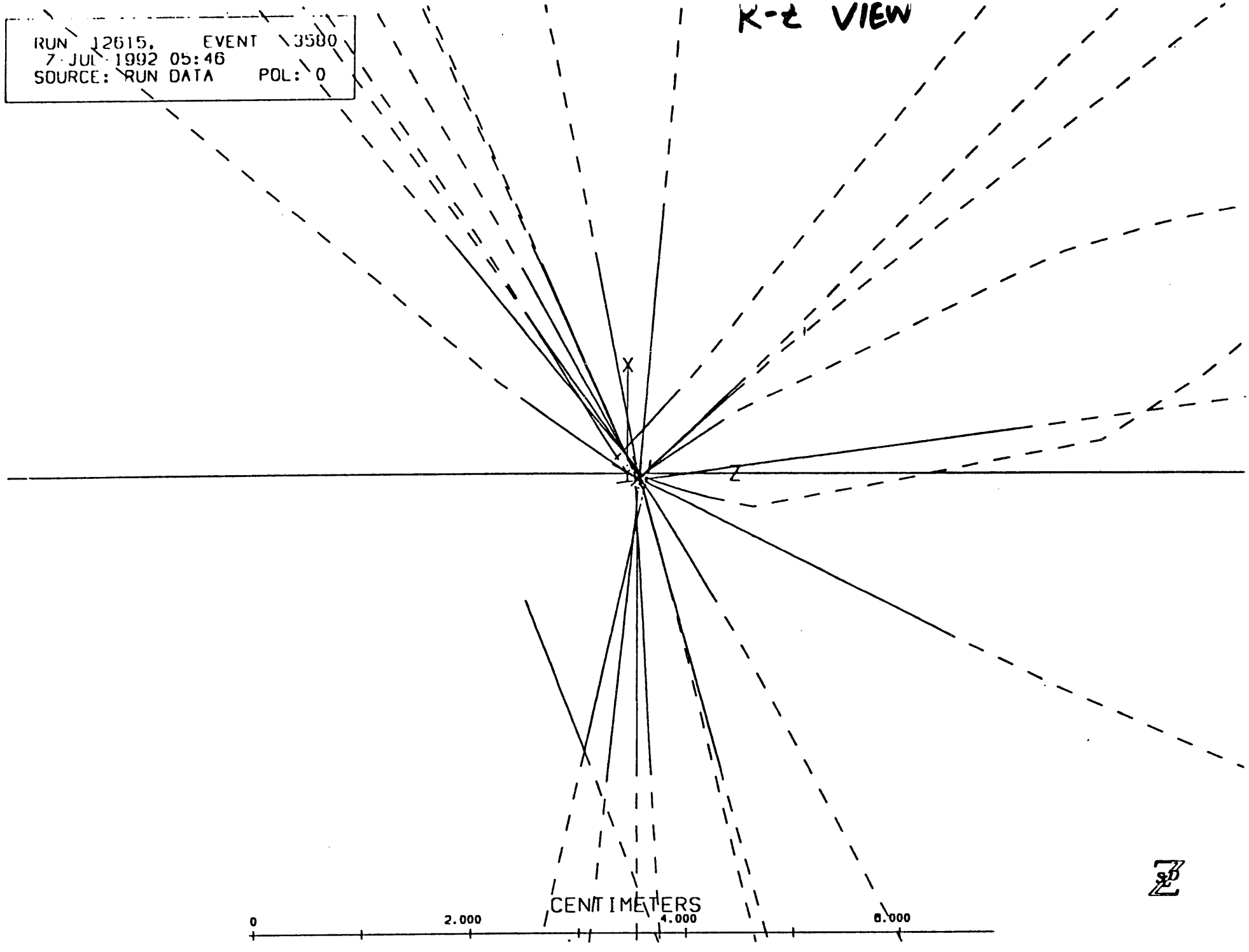
K-Z VIEW
RUN 12615, EVENT 3580
7 JUL 1992 05:46
SOURCE: RUN DATA POL: 0
X
Z
CENTIMETERS
0
2.000
4.000
6.000

# CONCLUSIONS

- SLD Vertex Detector is operating well in the SLC environment
- >94% of VXD is fully operational and reliable
- Track linking efficiency is ≈ 96% in good regions of the VXD
- Spatial resolution is 10 μm in XY, 8 μm in RZ
- $\sigma_b(XY) \approx \sqrt{13^2 + \left(\frac{70}{p}\right)^2}$ , $\sigma_b(RZ) = \sqrt{52^2 + \left(\frac{70}{p}\right)^2}$

  with σ in μm and p in GeV/c

- Physics is being done with the VXD. Talks at this conference given by D. Su and T. Junk.

# APPENDIX C

## ITEP Group
## Activites for GEM

*April - October 1992*

# Monte Carlo simulation study for GEM colaboration calorimeter system.

by A.Savin

During the 1992 following MC studies have been performed for GEM calorimeter :

1. Higgs mass reconstruction from gamma+gamma for different options.
2. Influence of cráks/dead matherial in different EM calorimeter options.
3. Effect of dead material before and after EM calorimeter for electrons and gammas.
4. Calibration of BaF2 EM calorimeter by non-interacted hadrons and RFQ system.
5. Simulation of ScintCal Beam test prototype.
6. Simulation of jets in Hybrid Option.
7. Simulation of Hadron calorimeter Massless Gap for response correction in Hybrid option.
8. Simulation of Cherenkov Quartz fibers calorimeter - Electrons,Pions, Jets and Muons.

Simulations were mainly performed at PDSF SSCLab.
These results were presented at the meetings of GEM collaboration and printed in GEM technical notes GEM TN-92-143 and TN-92-213.

## 1.Higgs mass reconstruction from gamma+gamma for different options

Events Higgs -> gamma+gamma were generated by PYTHIA5.6 .
No pile-up, isolation cuts were applied - clean EM calorimeter effects were studied. In case of interaction with tracker matherial (energy deposit in tracker > 1MeV) photons assumed to be lost. Dead zones in calorimeter and energy resolution were taken fron Baseline. Next options were studied ;

1. BaF2 (Barell + EndCAp) (Fig 1.1, 1.2, 1.3)
2. LAr (Barell + EndCAp) accordeon (Fig. 1.1, 1.2, 1.3)
3. LKr (Barell + EndCAp) accordeon (Fig. 1.2, 1.3, 1.4)
4. LAr accordeon in Endcap, LKr accordeon in Barell (Fig. 1.2)
5. Parallel Plate LKr (Barell + EndCAp) (Fig. 1.1)

Conclusion : From these studies BaF2 should have better resolution for H0 reconstruction in the mass range 80 - 150 GeV (Fig. 1.1, 1.2, 1.3, 1.5). Stochactic resolution in End Caps is less critical for H0 mass reconsrtuction since the energy of gammas are larger at larger pseudorapidity.

# HIGGS MASS RECONSTRUCTION

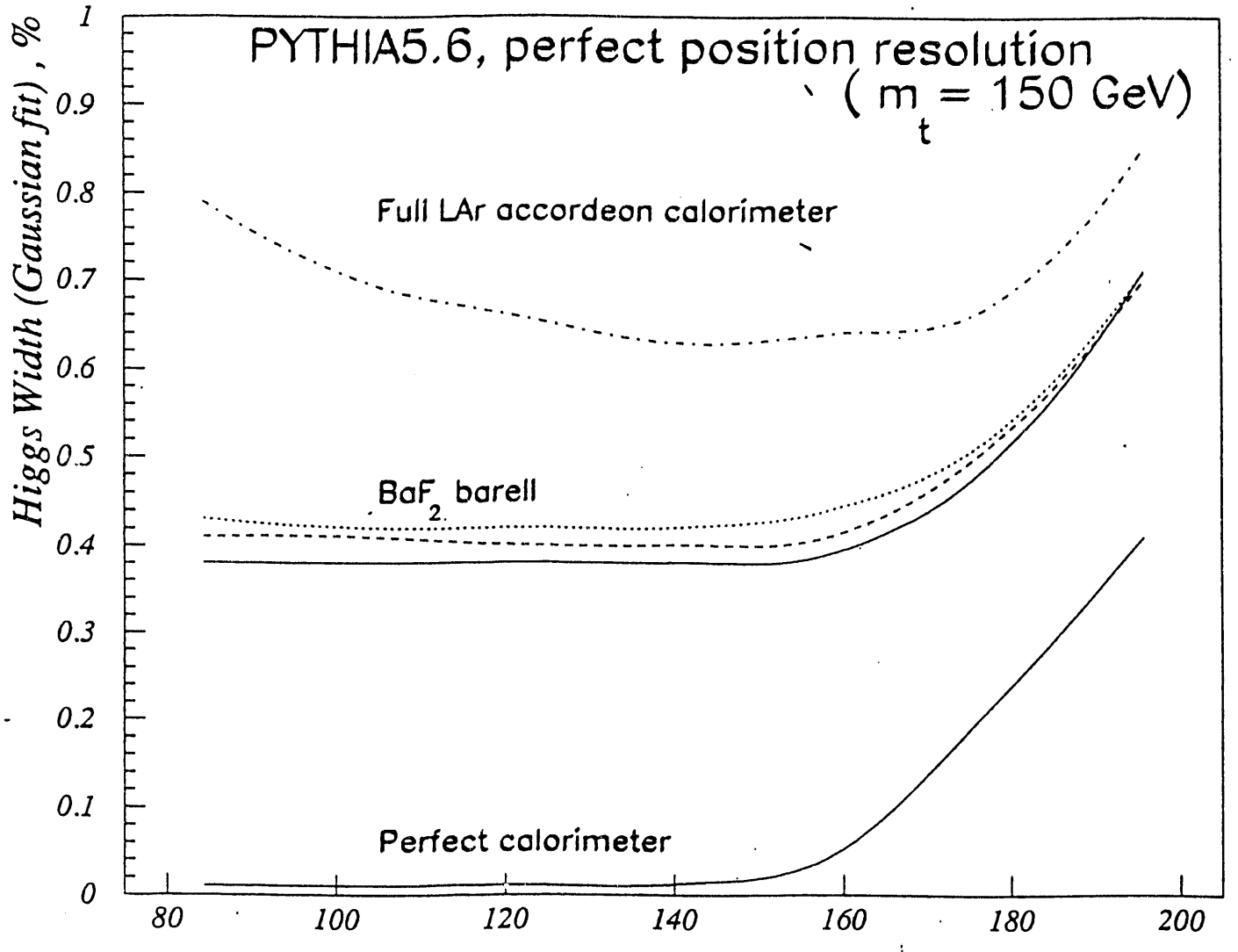


HIGGS MASS (GeV)

$BaF_2$+LAr accordeon endcap

$BaF_2$+LAr plates endcap

$BaF_2$ full calorimeter

Fig 1.1

# HIGGS MASS RECONSTRUCTION

PYTHIA5.6, $m_t$ = 150 GeV, perfect position resolution

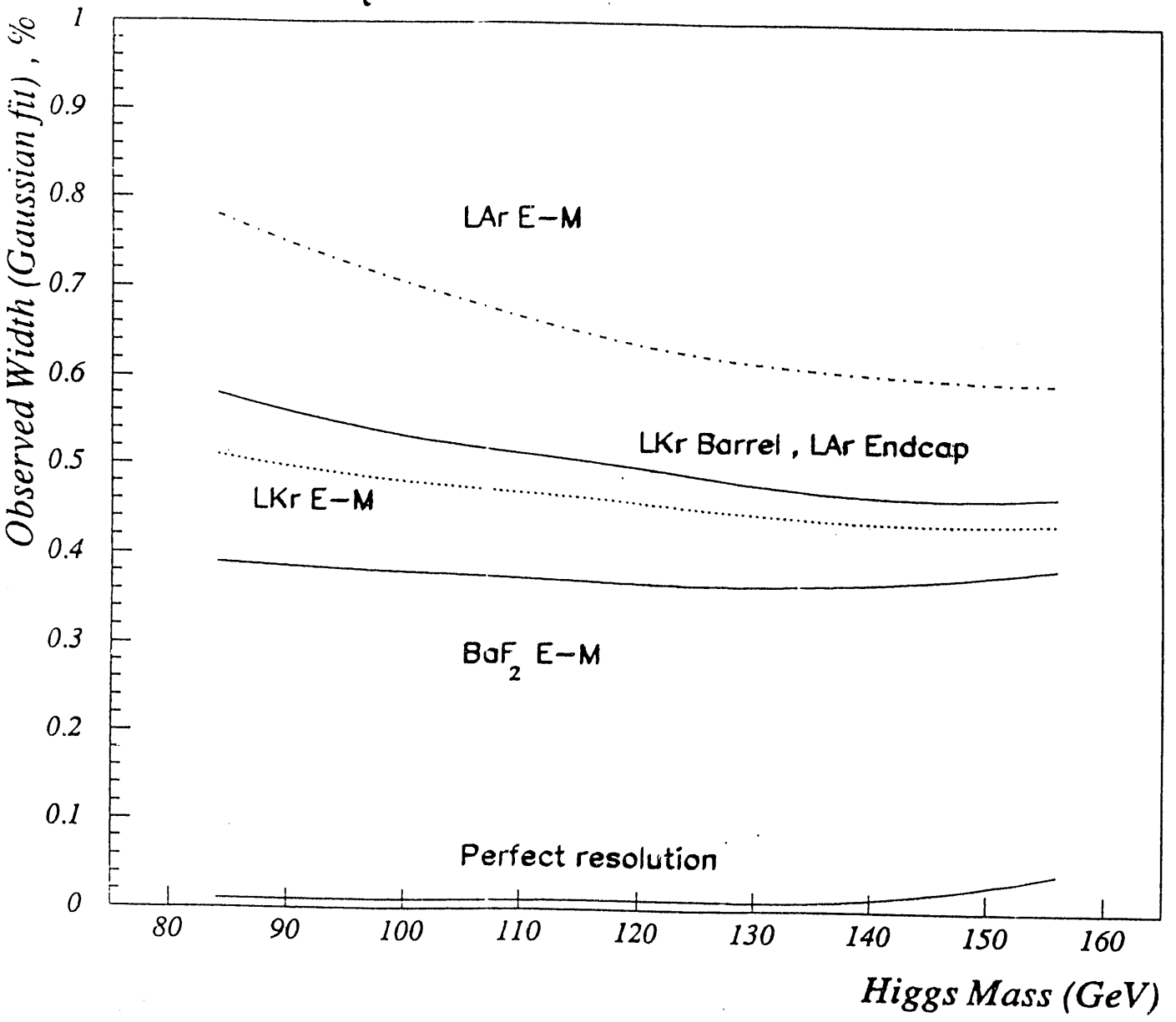


LAr resolution 7.5%/sqrt(E) + 0.4%

LKr resolution 5.0%/sqrt(E) + 0.4%

BaF2 resolution 2.5%/sqrt(E) + 0.5%

Fig 1.2

92/08/30 21.46

# HIGGS MASS RECONSTRUCTION

PYTHIA5.6 $m_t$ = 150 GeV ,perfect position resolution

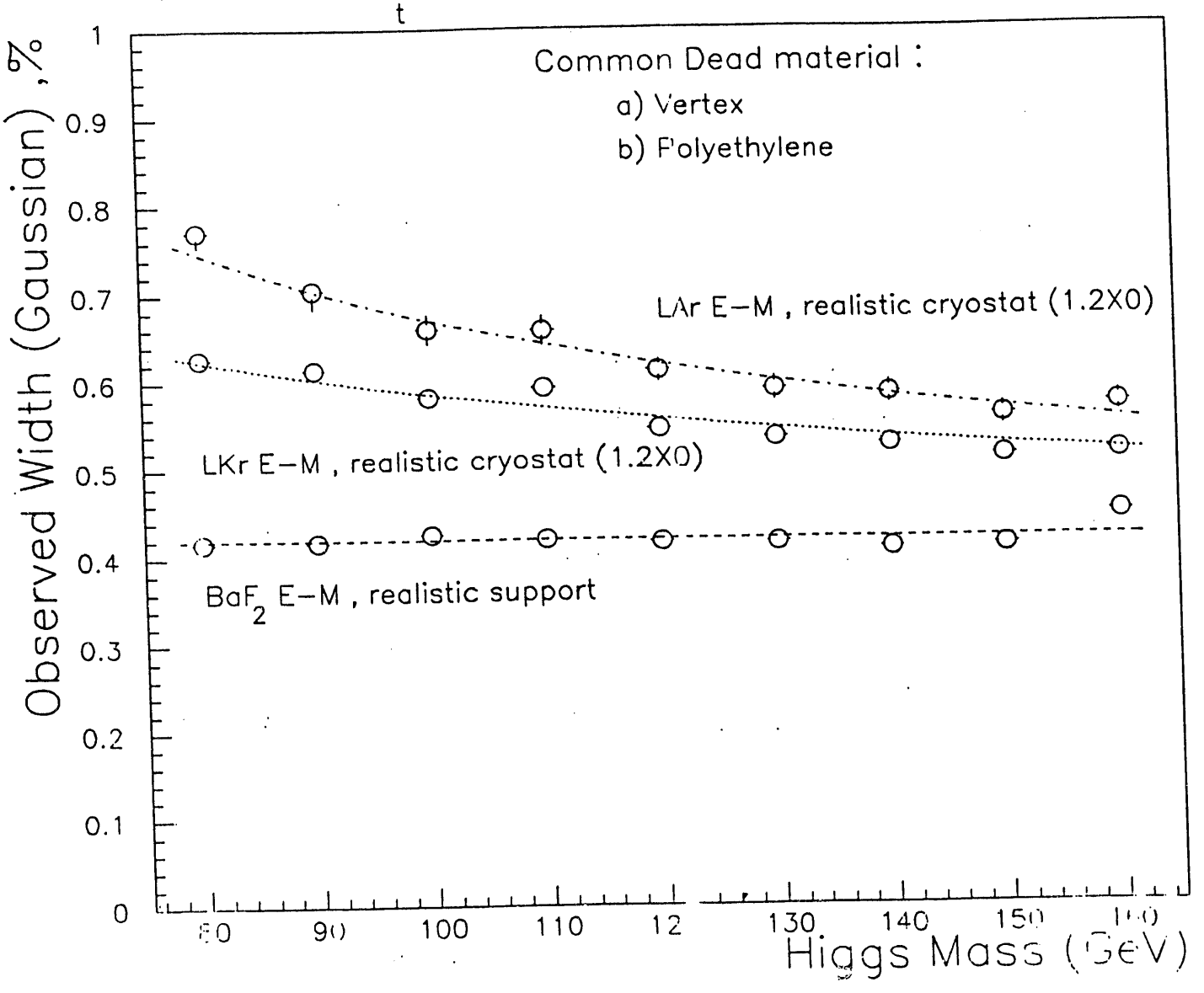


A.Savin

Fig. 1.3

92/08/30 21.46

# HIGGS MASS RECONSTRUCTION

PYTHIA5.6 $m_t$ = 150 GeV ,perfect position resolution

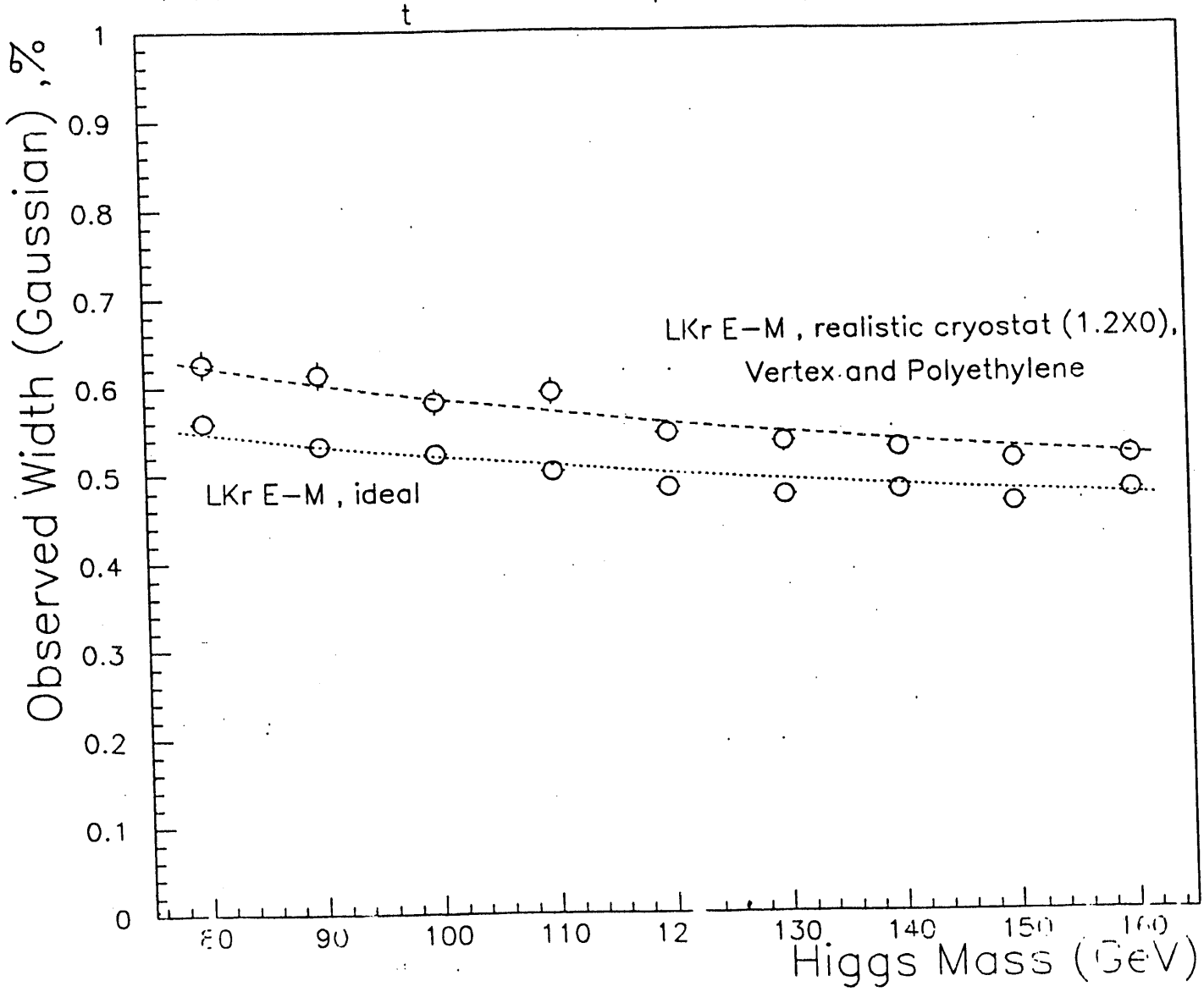


A.Savin

Fig 1.4

92/08/30 21.46

# Significance

Significance = Acceptance * Fraction ± 1.4σ(%) / Witdh(%)

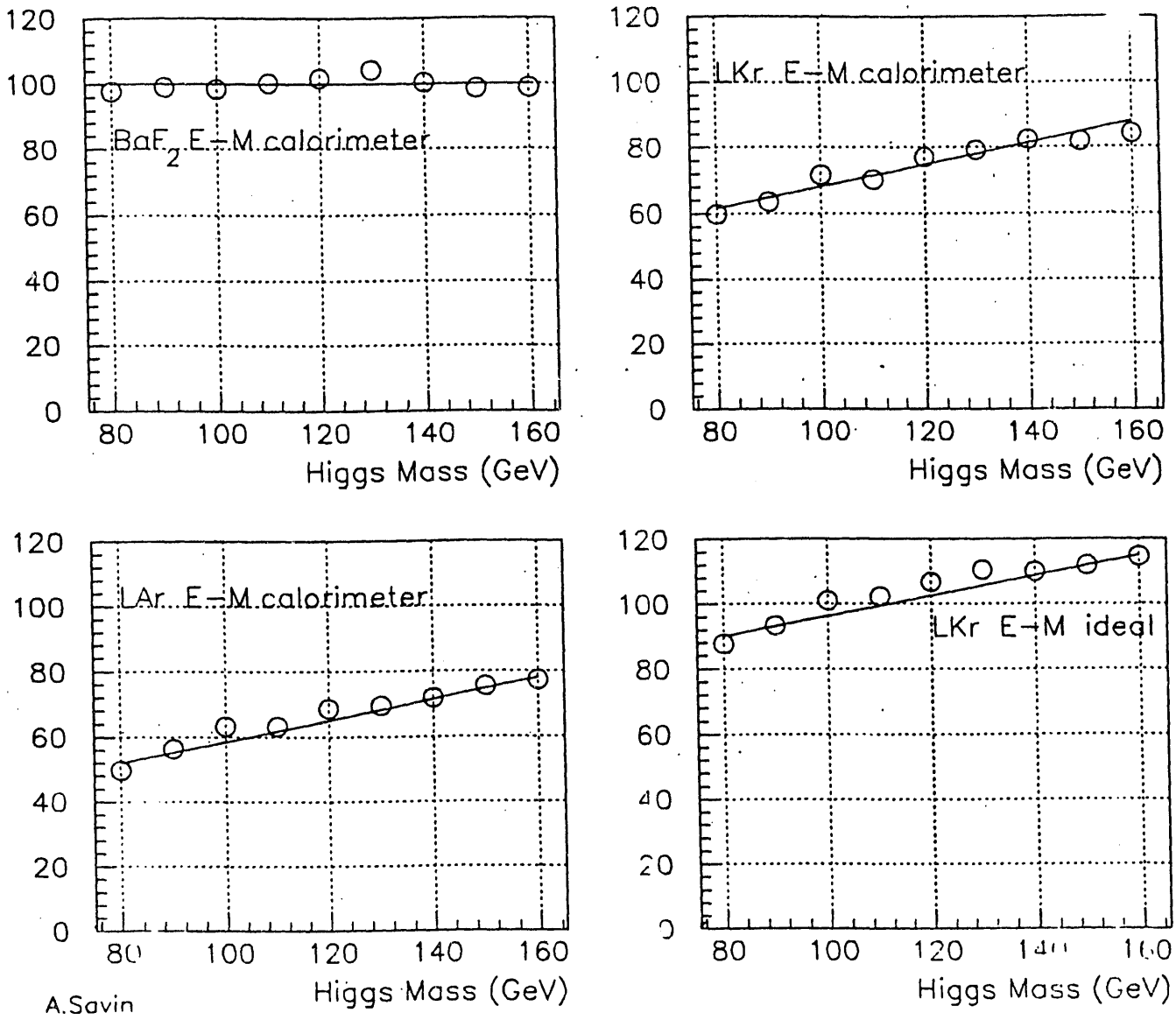


Fig 1.5

## 2.Influence of craks/dead matherial in different EM calorimeter options.

Higgs -> gamma+gamma process was generated by PYTHIA5.6. Efficiensy of two gammas registration was studied for all proposed options of GEM EM calorimeter:

1. LKr accordeon (Fig.2.1, 2.4)
2. Two Cap accordeon design (Fig.2.2, 2.5)
3. LKr parellel plates (Fig.2.3, 2.6)

Interaction of photons in tracker assumed to 'kill' photon by misidentification.
All options have Etha-limit = 3.

Conclusion : All options have similar efficiencies for Higgs --> gamma+gamma.
about 65% without losses in tracker and 50% with losses in tracker.

# LIQUID ARGON CALORIMETER - 12 X 14 LAMBDA, FLAT ENDCAP HEAD

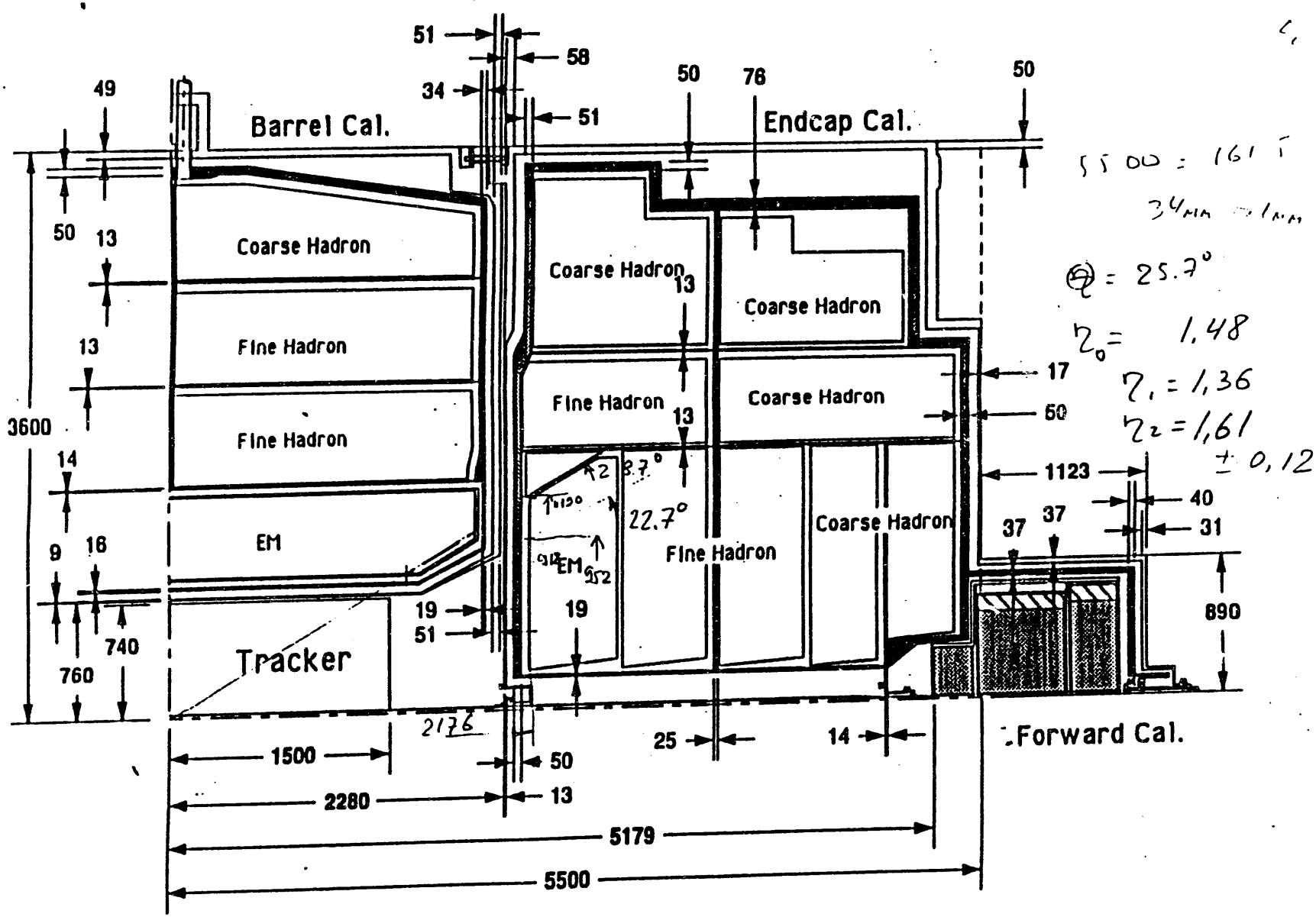


Fig. 2.1

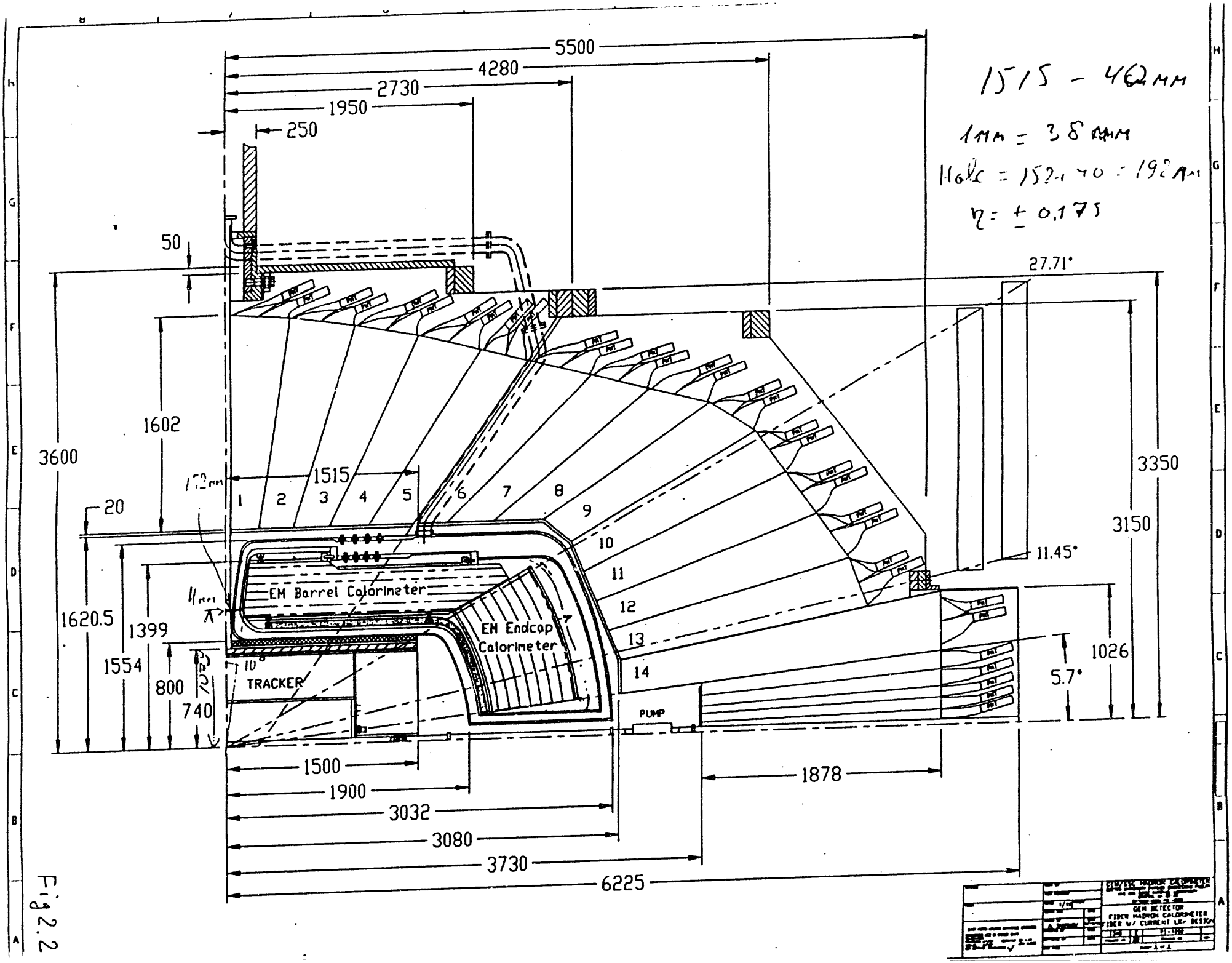
5500
4280
2730
1950
250
50
1602
3600
1515
1
2
3
4
5
6
7
8
9
10
11
12
13
14
20
EM Barrel Calorimeter
EM Endcap Calorimeter
TRACKER
PUMP
1620.5
1399
1554
800
740
1026
5.7°
11.45°
27.71°
3350
3150
1500
1900
3032
3080
3730
6225
1878
1515 - 462 MM
1MM = 38 MM
Hole = 152.40 = 198 MM
η = ± 0.175

Fig 2.2

Pressure Rating
44 psi Internal
15 " Vac
5 " overpressure

# END PLUG DESIGN
# GEM LKr

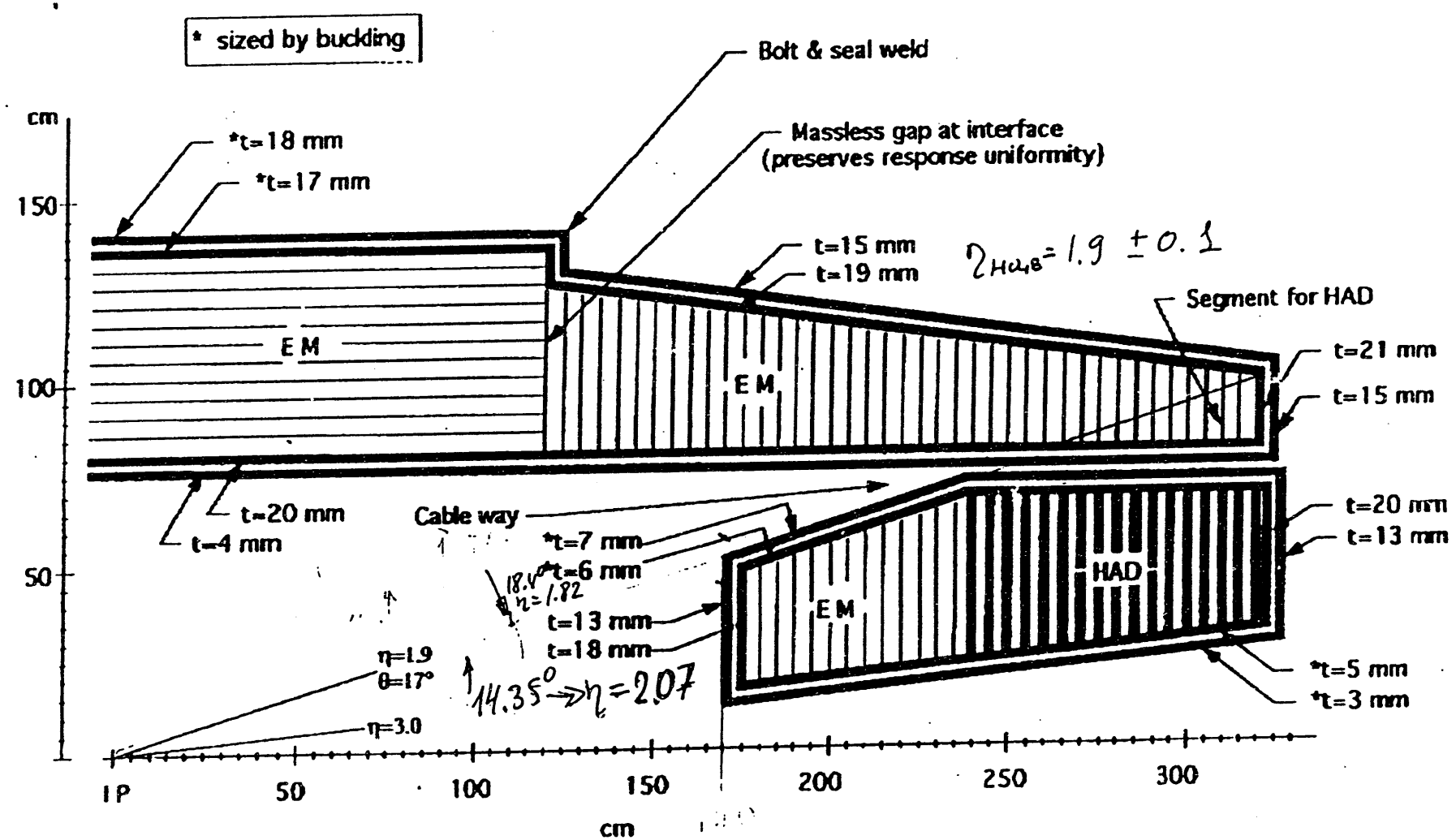


Fig 2.3

9/18/92
P. M. Mockett

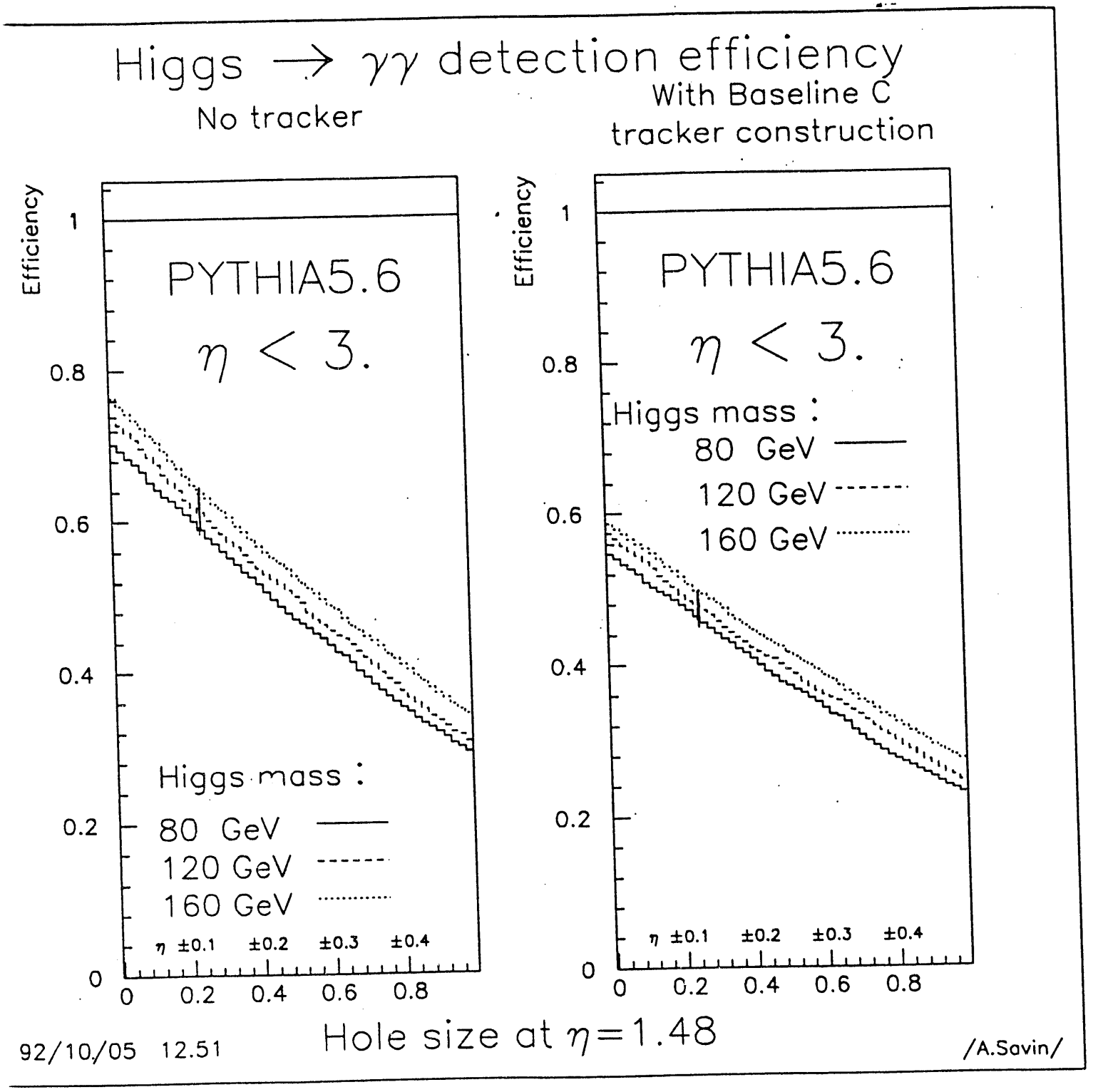
Higgs → γγ detection efficiency
No tracker
With Baseline C
tracker construction
Efficiency
PYTHIA5.6
η < 3.
Higgs mass :
80 GeV
120 GeV
160 GeV
η ±0.1 ±0.2 ±0.3 ±0.4
0 0.2 0.4 0.6 0.8 1
Hole size at η=1.48
92/10/05 12.51
/A.Savin/

Fig. 2.4.

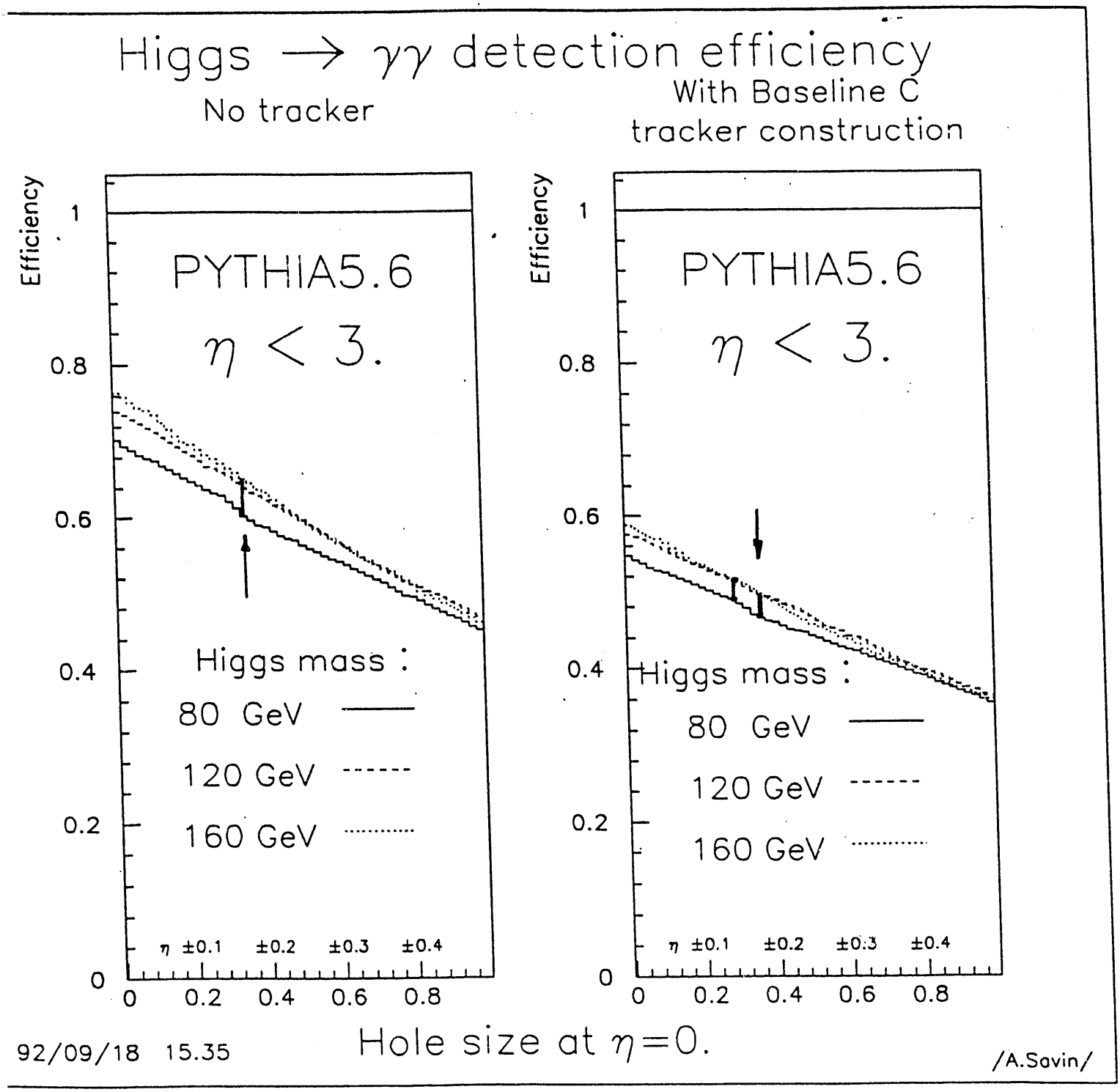
Higgs → γγ detection efficiency
No tracker
With Baseline C
tracker construction
Efficiency
PYTHIA5.6
η < 3.
Higgs mass :
80 GeV
120 GeV
160 GeV
η ±0.1 ±0.2 ±0.3 ±0.4
0 0.2 0.4 0.6 0.8 1
Hole size at η=0.
92/09/18 15.35
/A.Savin/

Fig. 2.5.

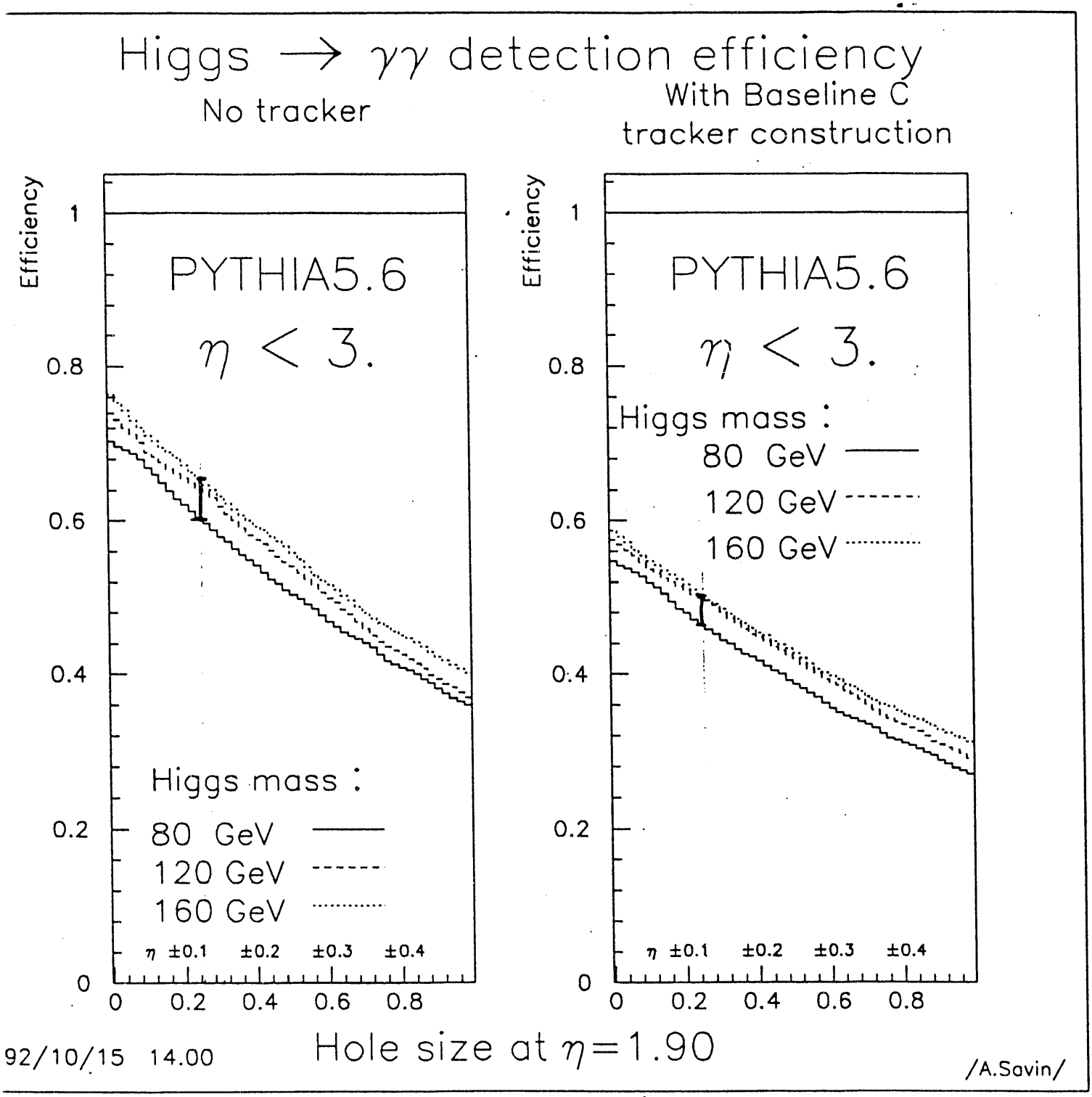
Higgs → γγ detection efficiency
No tracker
With Baseline C
tracker construction
Efficiency
PYTHIA5.6
η < 3.
Higgs mass :
80 GeV
120 GeV
160 GeV
η ±0.1 ±0.2 ±0.3 ±0.4
0 0.2 0.4 0.6 0.8 1
Hole size at η=1.90
92/10/15 14.00
/A.Savin/

Fig.2.6

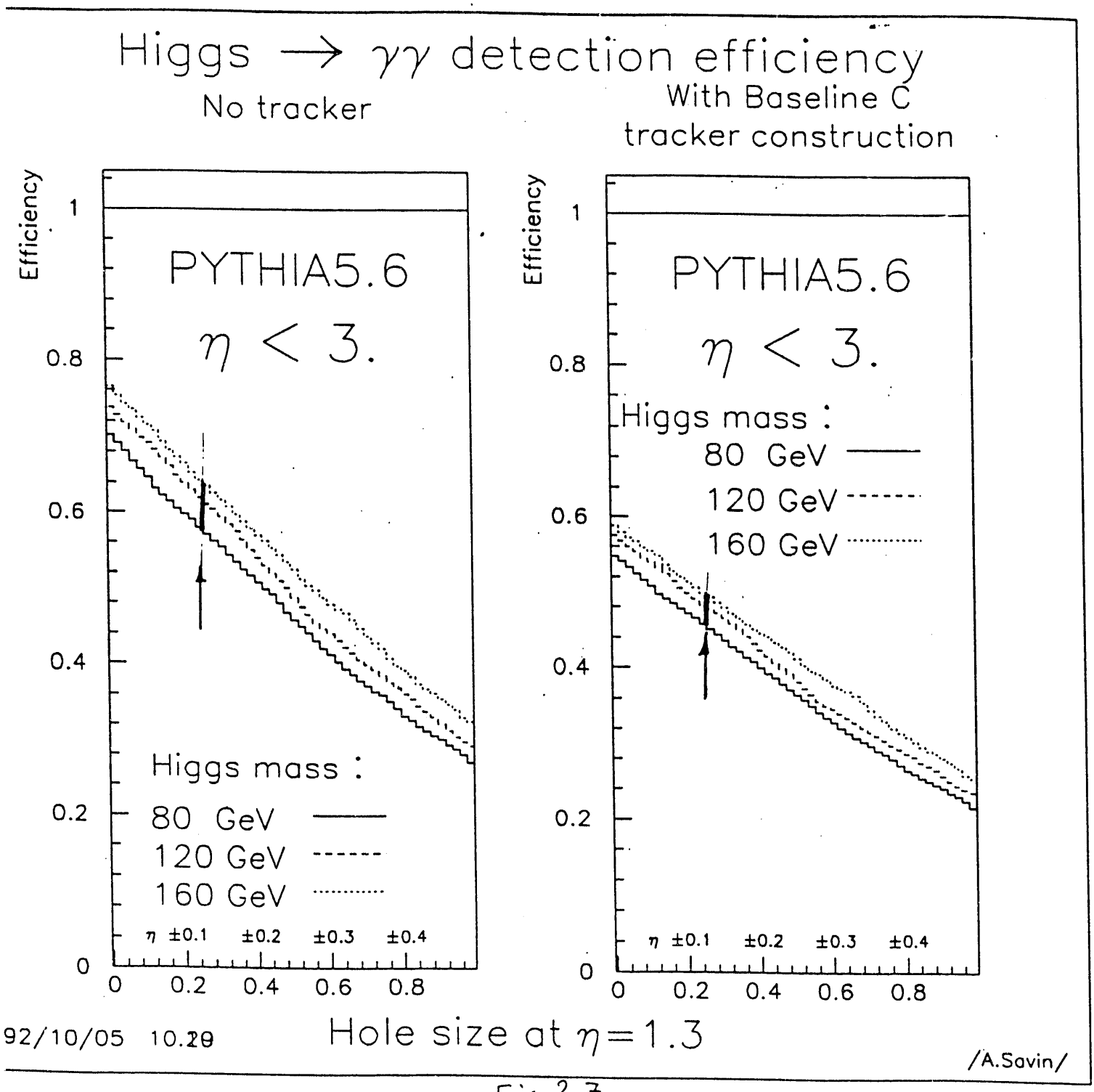
Higgs → γγ detection efficiency
No tracker
With Baseline C
tracker construction
Efficiency
PYTHIA5.6
η < 3.
Higgs mass :
80 GeV
120 GeV
160 GeV
η ±0.1 ±0.2 ±0.3 ±0.4
0 0.2 0.4 0.6 0.8 1
92/10/05 10.28
Hole size at η=1.3
/A.Savin/

Fig. 2.7.

## 3.Effect of dead material before and after EM calorimeter for electrons and gammas

GEANT3.15 was applied to study dead material effects for electrons and photons in LKr calorimeter. Calorimeter was simulated as a bulk of Pb/LKr mixture with longitudinal segmentation. Different anount of dead material was added before EM calorimeter (Fig.3.9 - 3.12) or between EM calorimeter and Hadrom calorimeter (Fig.3.2 - 3.8). Loses in front walls (1X0-4X0) were studied for electrons and photons in energy range 10GeV - 1TeV , and leakages to HC (Fig.3.1) were studied for 1TeV electrons and photons and dead material 1.7X0 and 2.8X0. Different ways of leakage correction were tested -

1. Correction for HC response. (40%-80%)/sqrt(E) resolution was studied
2. Correction for last 1X0 section of EM calorimeter response
3. Correction for Baseline segmentation of EM = 8X0+17X0
4. Correction by massless gap before HC

Main conclusions :

I. Leakage from EM to HC may be effectively corrected by methods 1. and 2. (Fig.3.2, 3.3, 3.4, 3.6, 3.7); Method 3. doesn't provide essential correlations (Fig.3.5, 3.8); Method 4. is good, but for massless gap with thickness 0.3X0

II. Energy losses in dead matherial are different for photons and electrons and are energy dependent (Fig.3.9 - 3.12).

III. Losses in dead matherial before EM seriously damage performance of EM calorimeter in case of Noble Liquid option, and active massless gap or preshower is required to preserve situation.

# *Energy fluctuations*

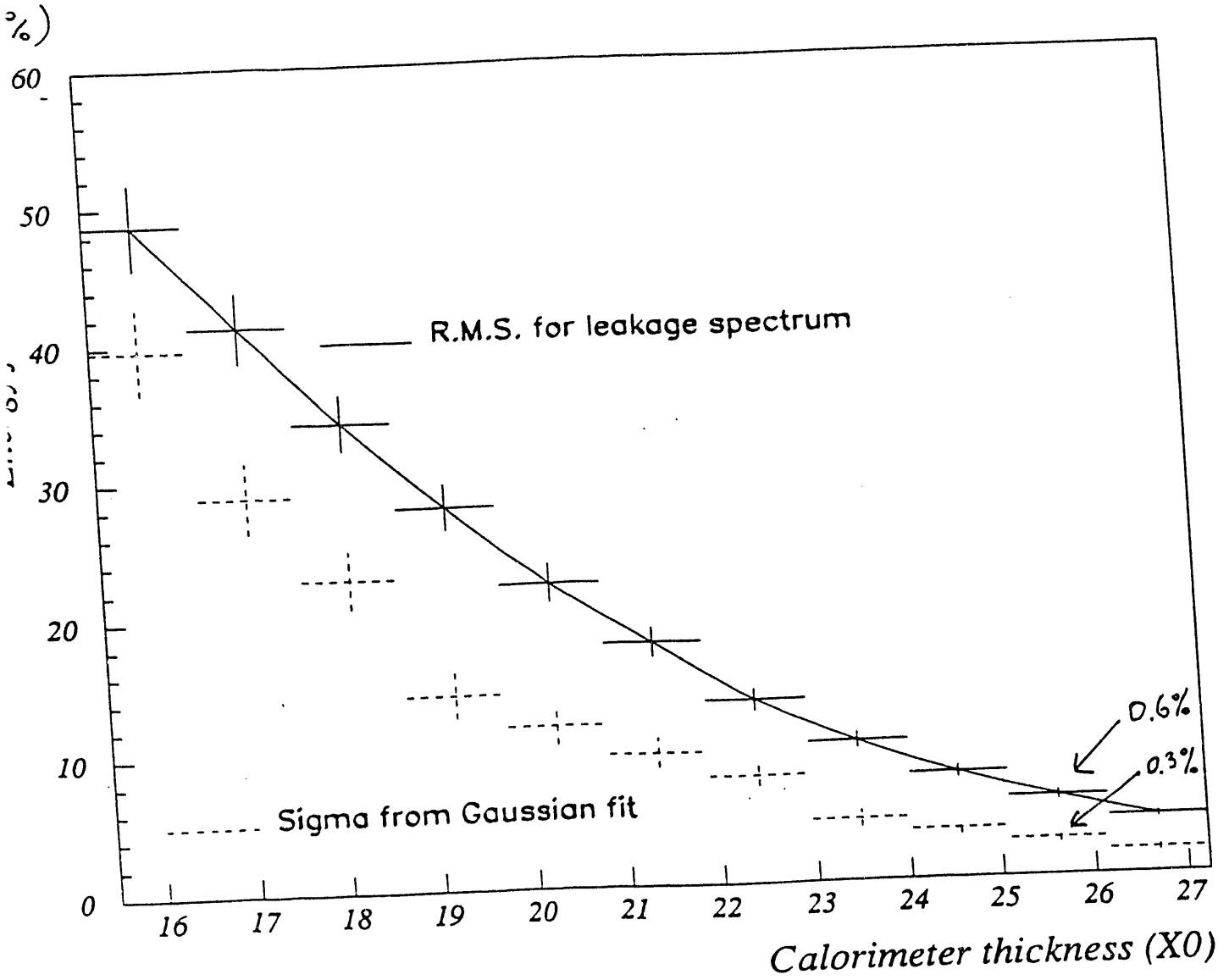


Fig. 3.1

/A. Savin/

F

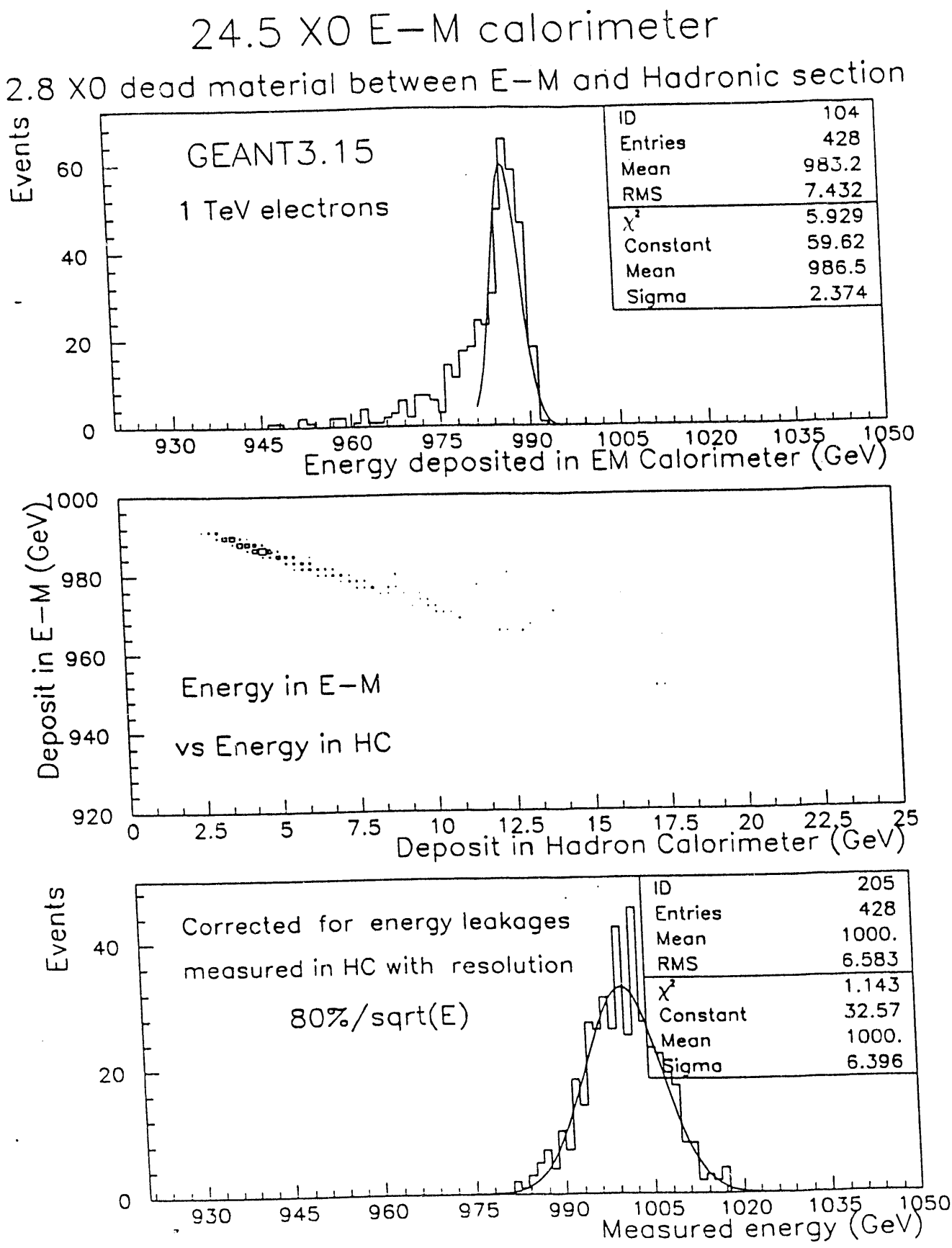


'A.Savin/

Fig. 3.2

Fig

2.8 X0 dead material between E–M and Hadronic section

24.5 X0 E–M calorimeter

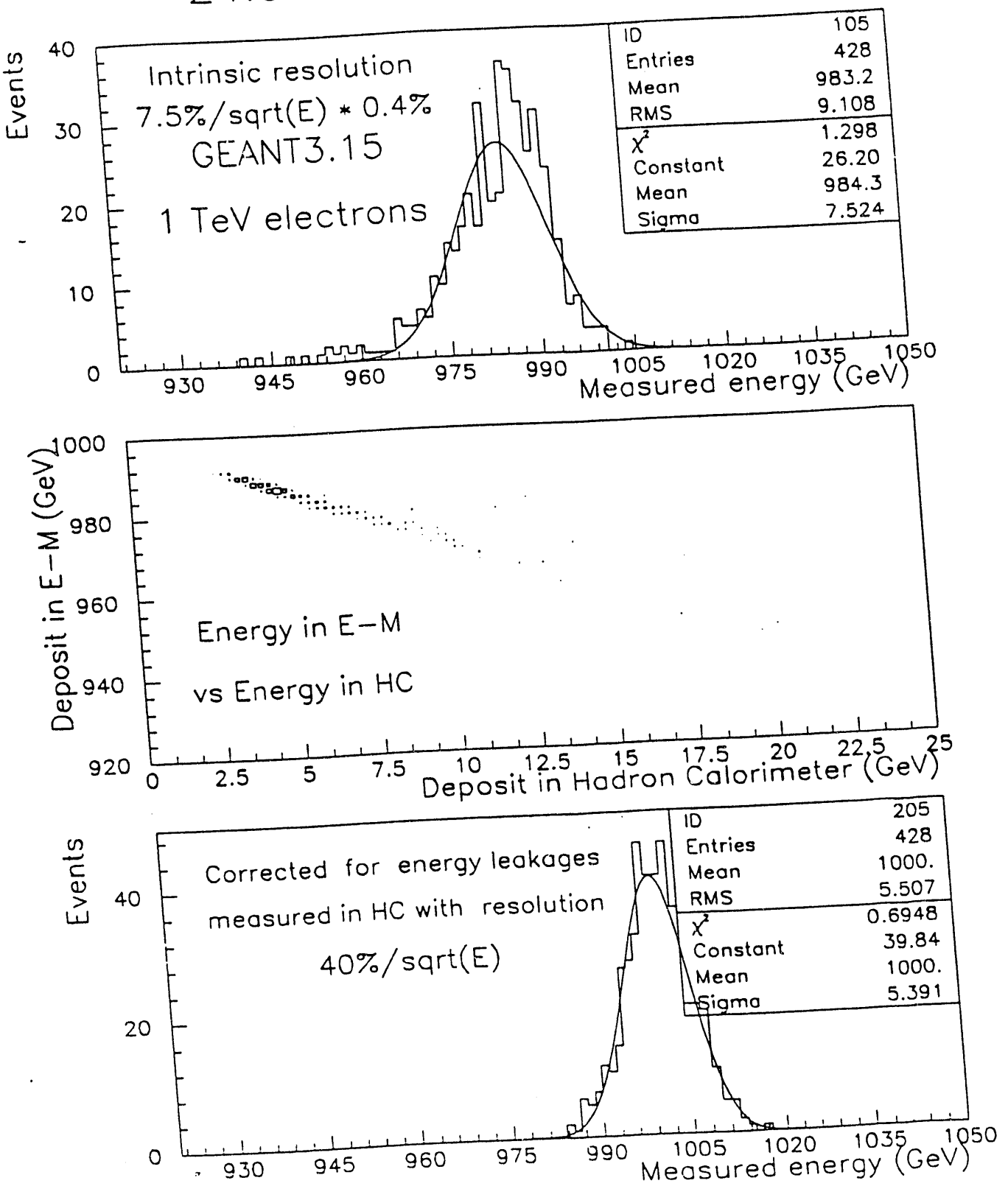


'A.Savin/

Fig. 3.3

# 24.5 X0 E−M calorimeter

2.8 X0 dead material between E−M and Hadronic section

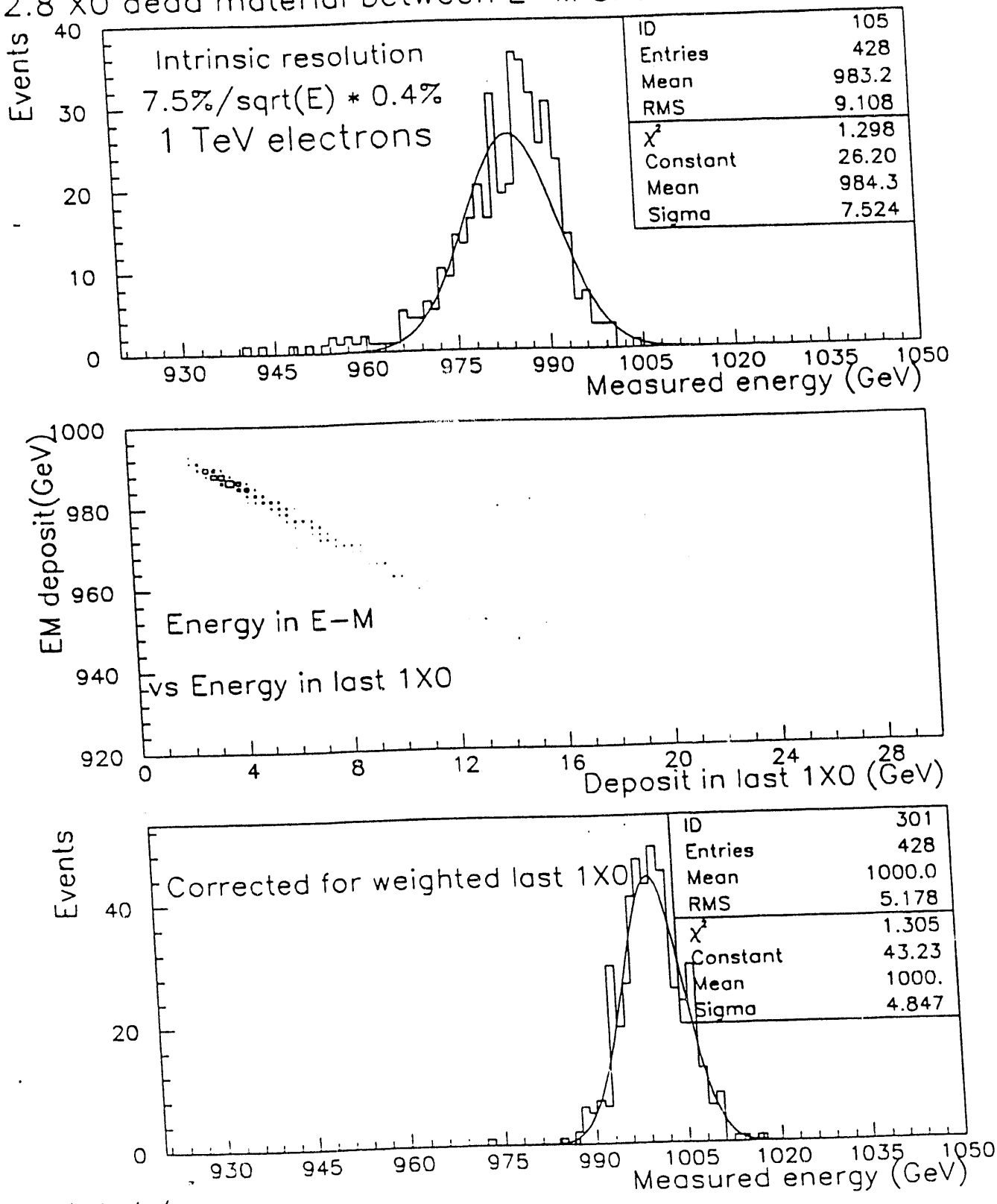


'A.Savin/

Fig. 3.4

Fig

# Front section 8X0

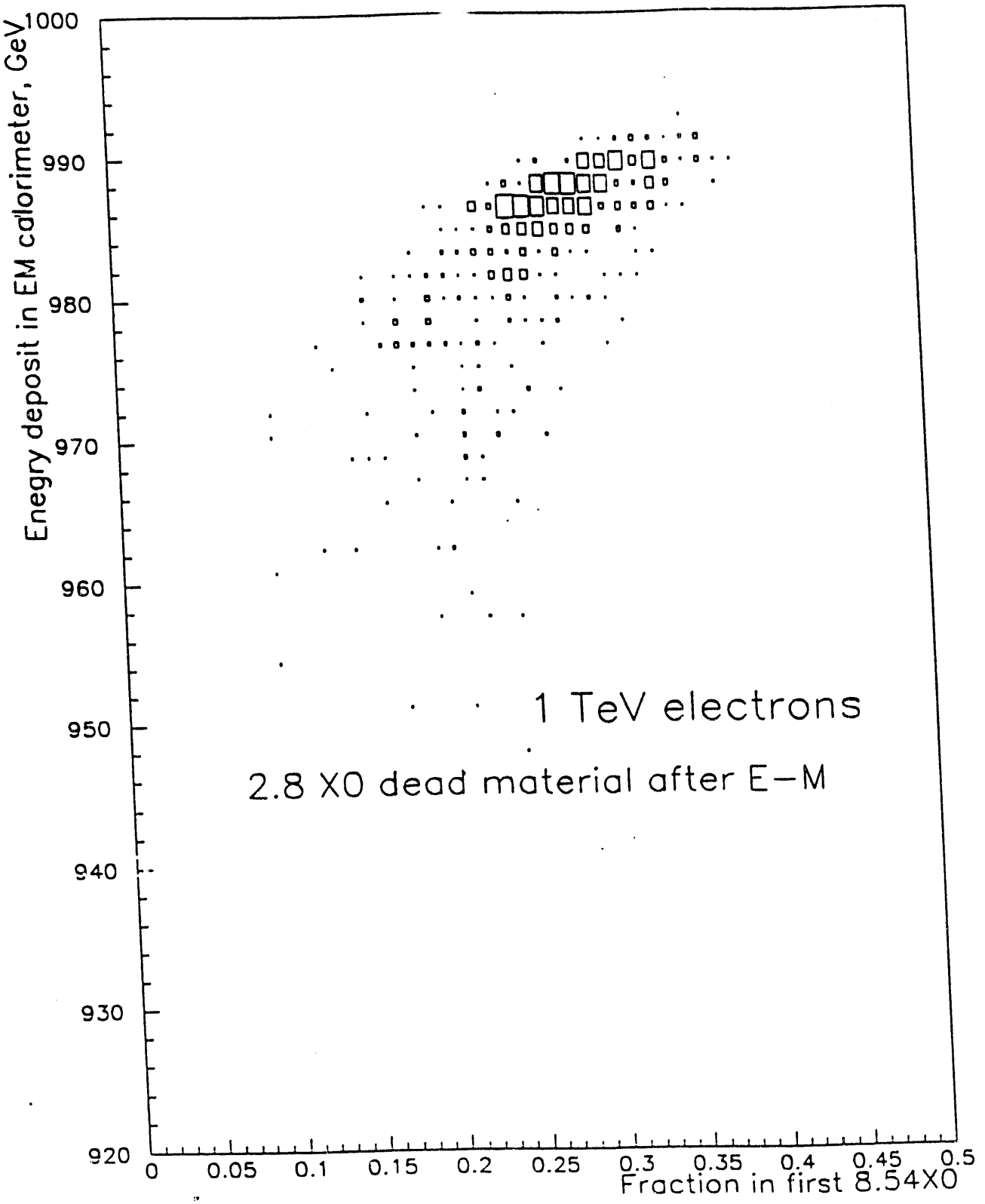


Fig. 3.5.

'A.Savin/

Fig II

2.8 X0 dead material between E−M and Hadronic section

24.5 X0 E−M calorimeter

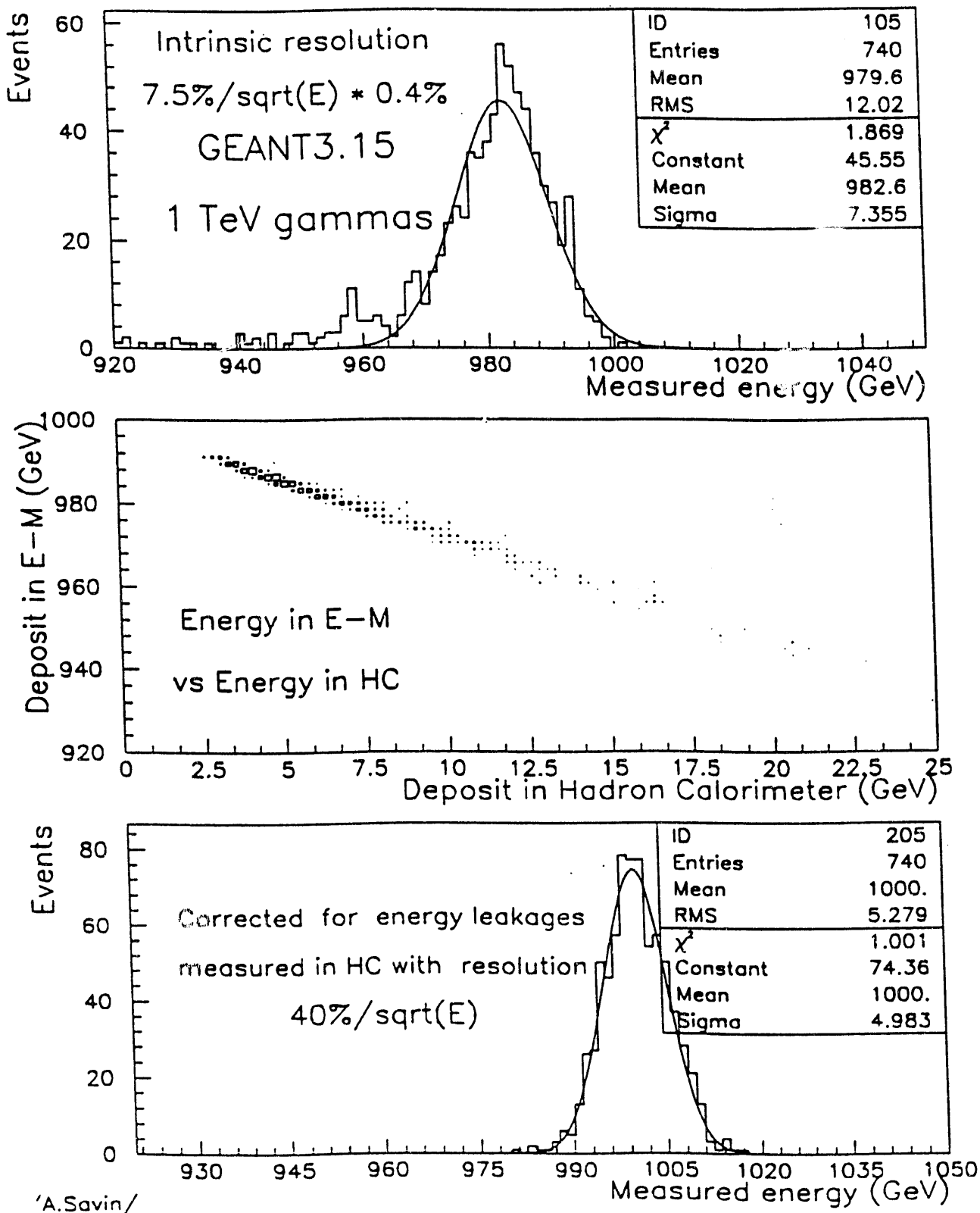


'A.Savin/

Fig. 3.6

Fig

# 24.5 X0 E−M calorimeter

## 2.8 X0 dead material between E−M and Hadronic section

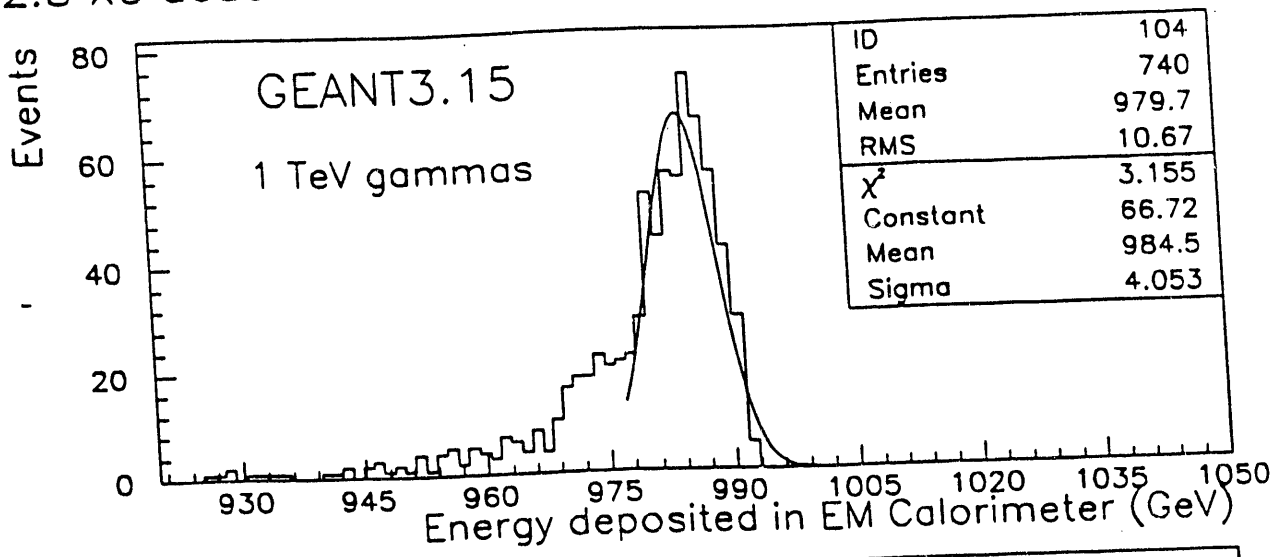


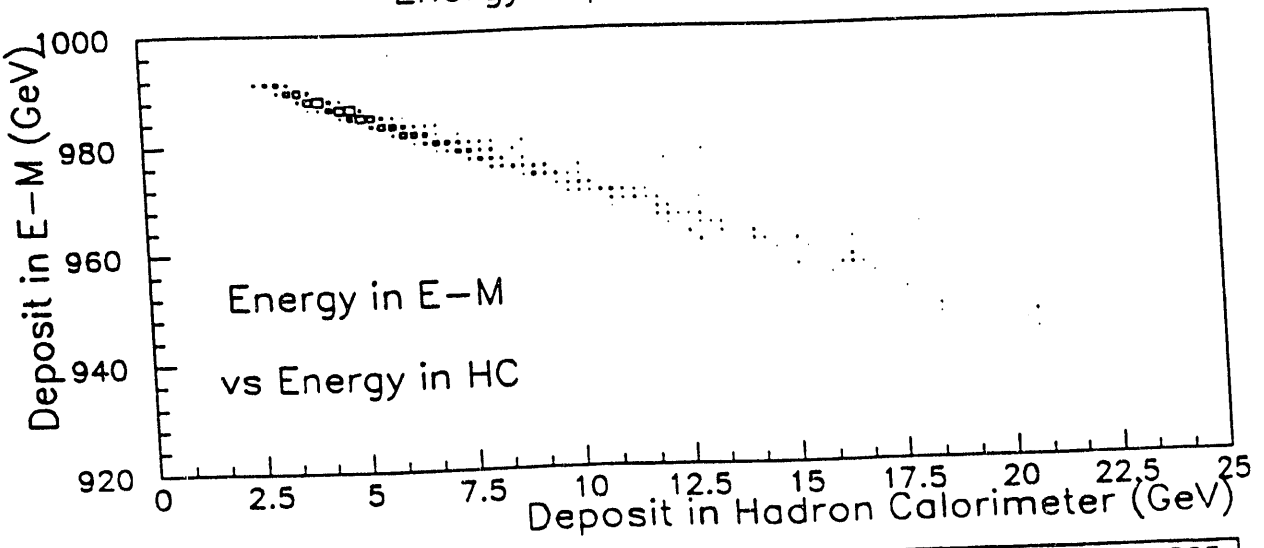


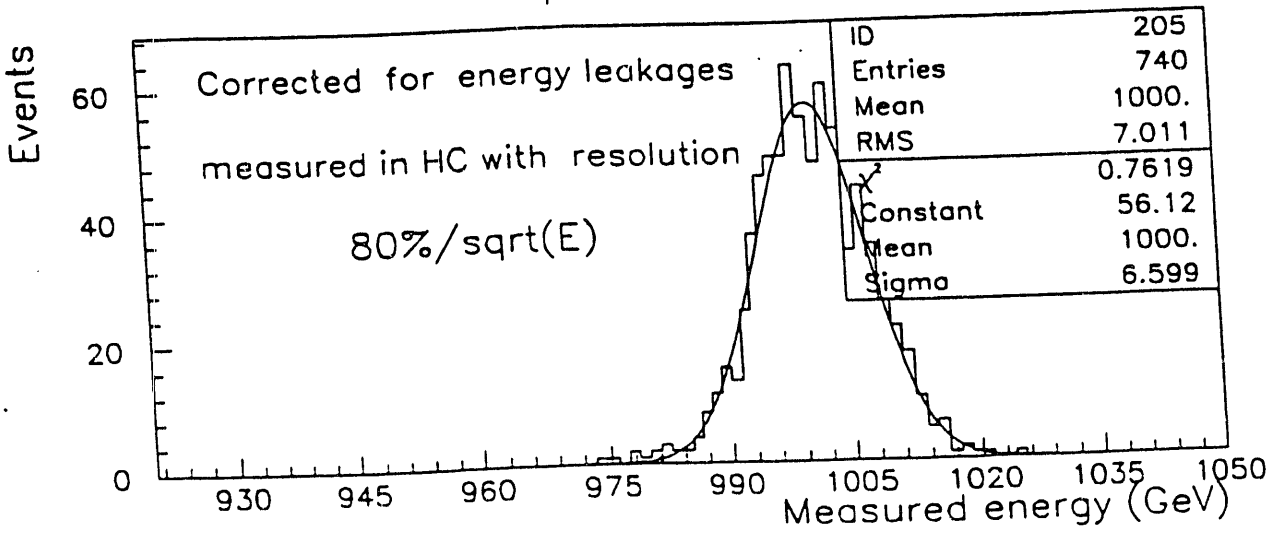


'A.Savin/

Fig. 3.7

Fig. 1

# Front section 8X0

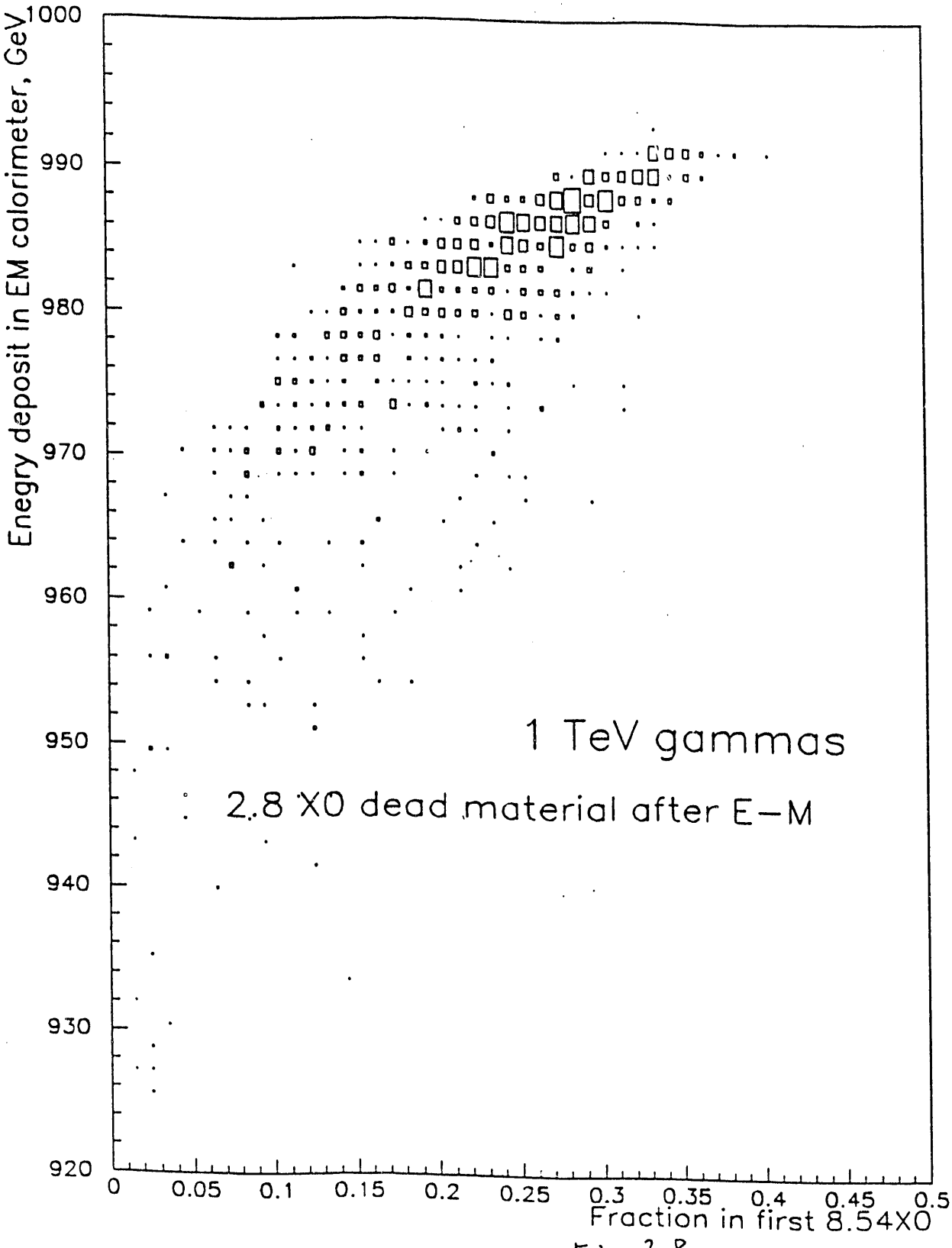


'A.Savin/

Fig. 3.8

**Dead material in front of EM calorimeter**

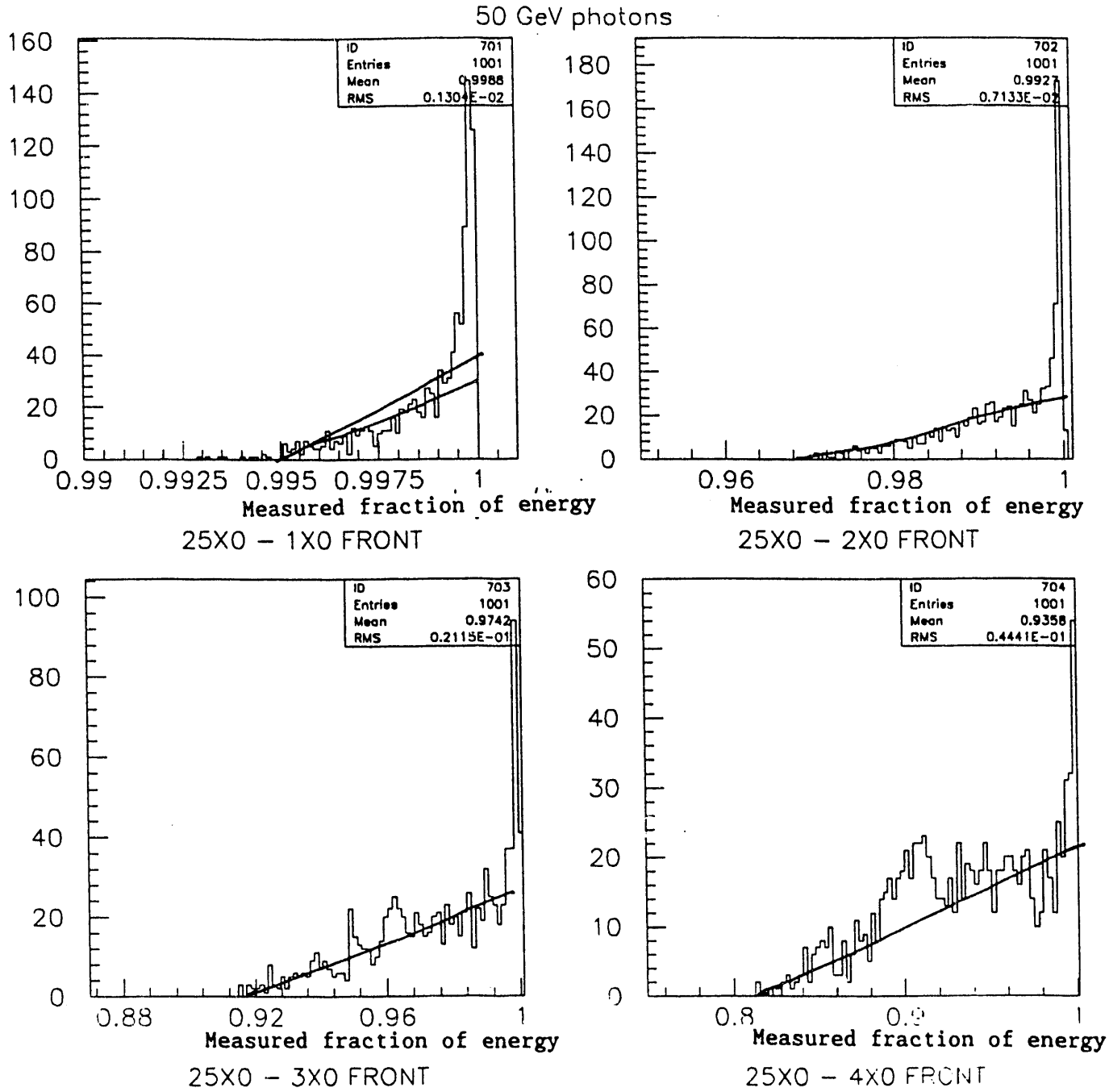


Fig. 3.9

Dead material in front of EM calorimeter

1000 GeV electrons

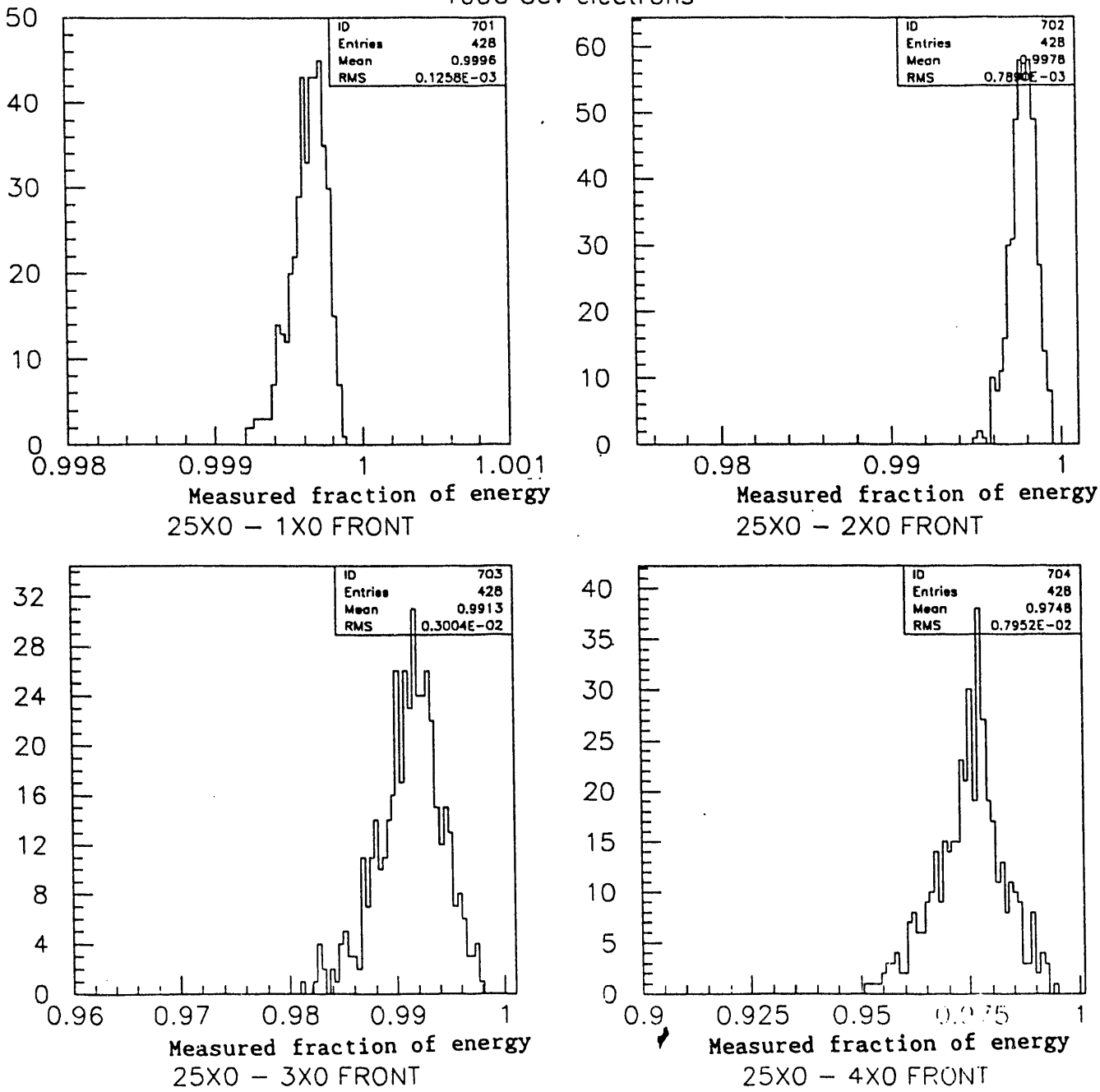


Fig. 3.10

Dead material in front of EM calorimeter

50 GeV electrons

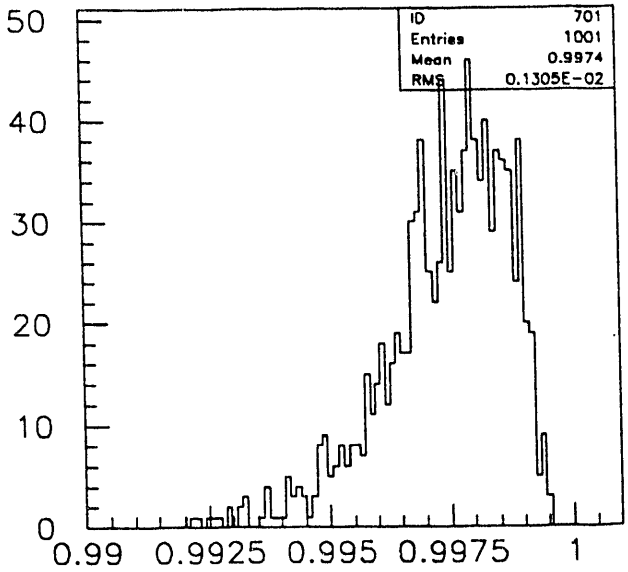


25X0 – 1X0 FRONT

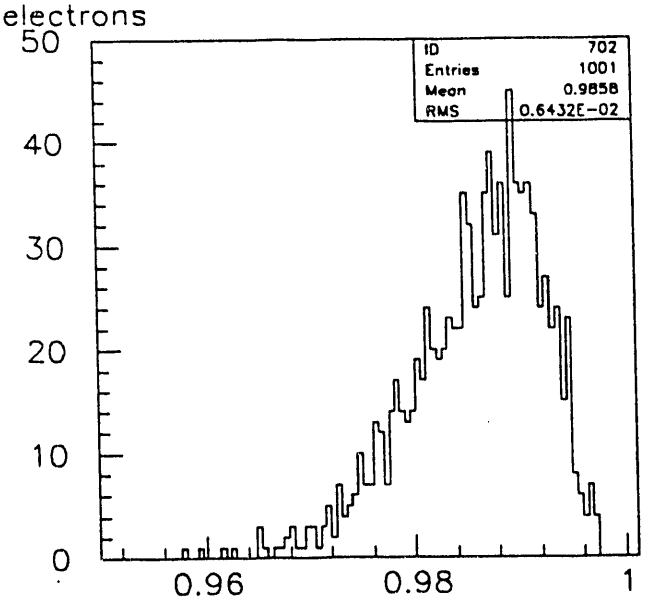


25X0 – 2X0 FRONT

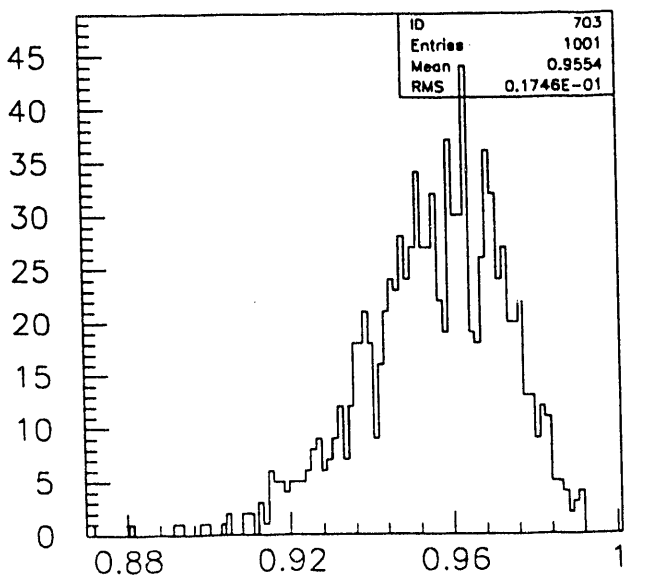


25X0 – 3X0 FRONT

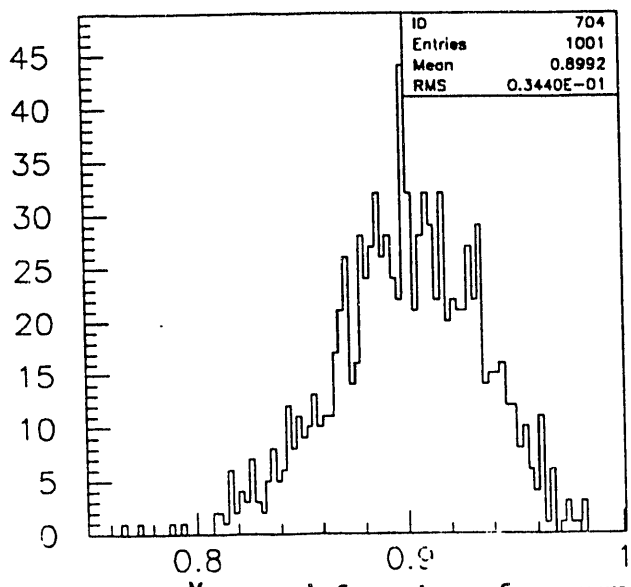


25X0 – 4X0 FRONT

Fig. 3.11

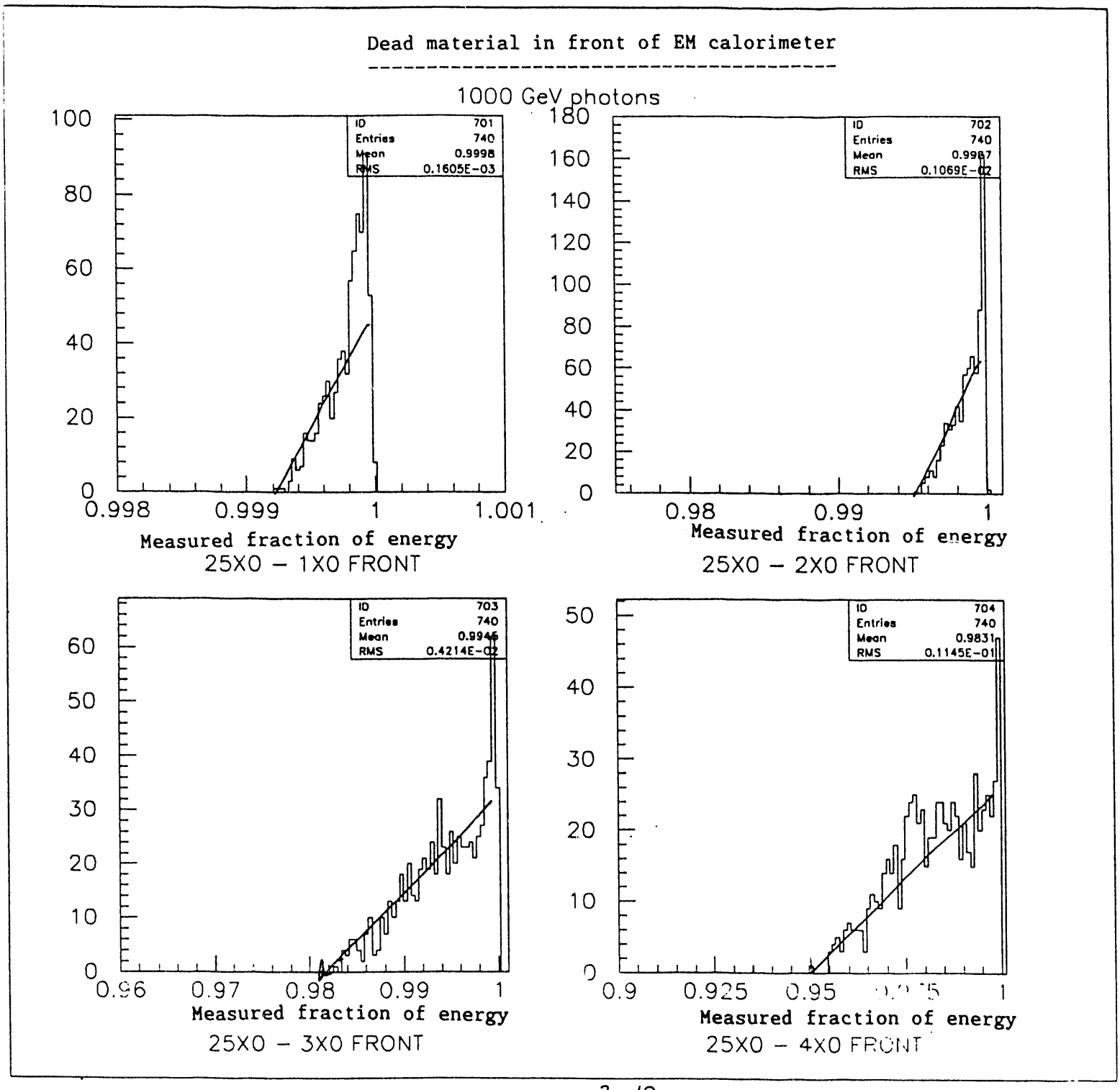
Dead material in front of EM calorimeter
1000 GeV photons
ID 701
Entries 740
Mean 0.9998
RMS 0.1605E-03
Measured fraction of energy
25X0 – 1X0 FRONT
ID 702
Entries 740
Mean 0.9987
RMS 0.1069E-02
Measured fraction of energy
25X0 – 2X0 FRONT
ID 703
Entries 740
Mean 0.9946
RMS 0.4214E-02
Measured fraction of energy
25X0 – 3X0 FRONT
ID 704
Entries 740
Mean 0.9831
RMS 0.1145E-01
Measured fraction of energy
25X0 – 4X0 FRONT

Fig. 3.12

## 4.BaF2 MIP and RFQ calibration

PYTHIA5.6 was used to generate MiniBias events with requared 1.6 interaction/crossing mean rate. Generated particles were transported by GEANT3.15 in detailed geometry of BaF2 calorimeter with magnetic filed. By simple isolation criteria non-interacting hadrons were selected (Fig.4.1), and clear 'MIP'-looking peak was observed (Fig.4.2, 4.3). Good photons suppression may be achieved by requarement of energy deposit in HC behind selected crystal.'MIP' rate appear to be about 1'MIP'/crossing , high enough to calibrate each crystal of BaF2 calorimeter in few hours with precision 0.3%. Luminosity dependance was studied for range 10**33 - 10**34 (Fig.4.4, 4.5).

6 MeV photons from RFQ source were transported through RFQ elements, tracker and detailed BaF2 crystals geometry to study energy deposit distribution, time requarements and machanical stability of RFQ source.

Main conclusion : MiniBias events are good source for BaF2 'MIP' calibration for SSC luminocity from 10**33 to 10**34, providing precision relative calibration with 0.3% precision during acceptable time interval (less than 1.5 sec in case of 100% trigger efficiensy) as well as RFQ calibration system.

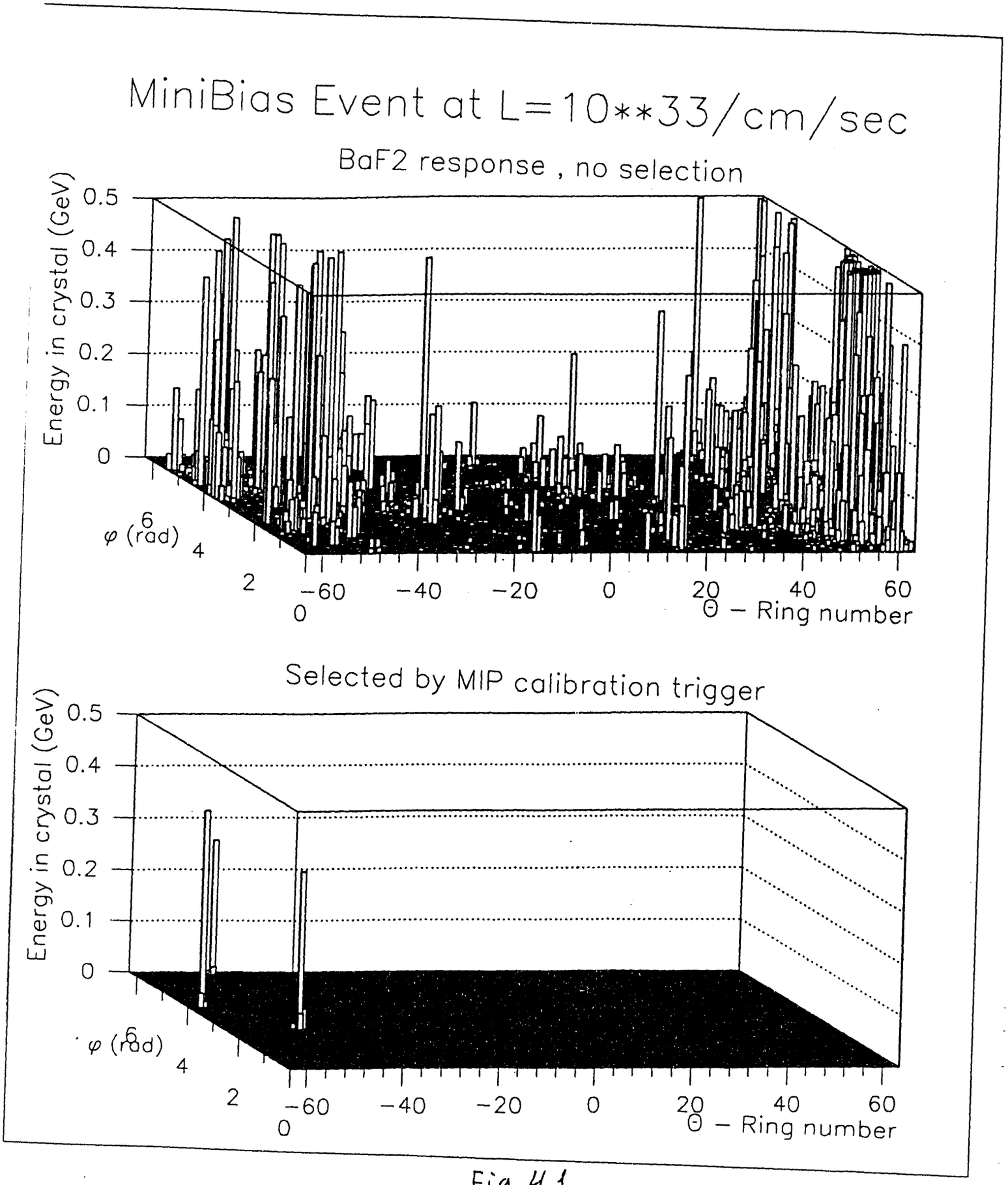
MiniBias Event at L=10**33/cm/sec
BaF2 response , no selection
Energy in crystal (GeV)
0.5
0.4
0.3
0.2
0.1
0
φ (rad)
6
4
2
0
−60
−40
−20
0
20
40
60
Θ – Ring number
Selected by MIP calibration trigger
Energy in crystal (GeV)
0.5
0.4
0.3
0.2
0.1
0
φ (rad)
6
4
2
0
−60
−40
−20
0
20
40
60
Θ – Ring number

Fig. 4.1

# Punch Through Calibration

## 620 Bunch Crossings

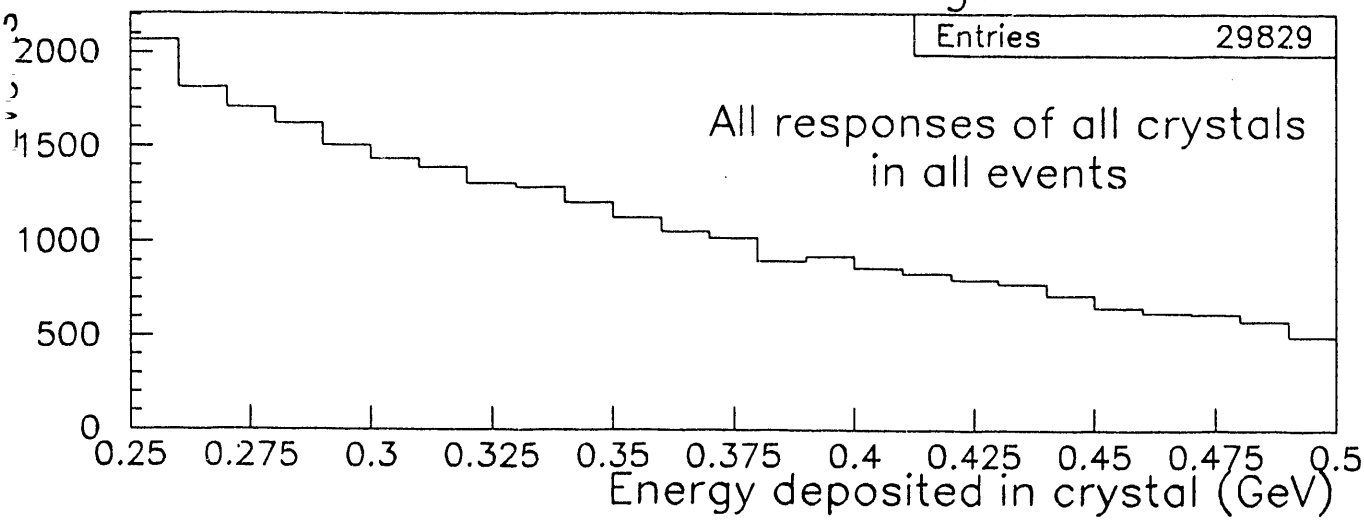


## Isolation threshold (3x3) = 95 MeV

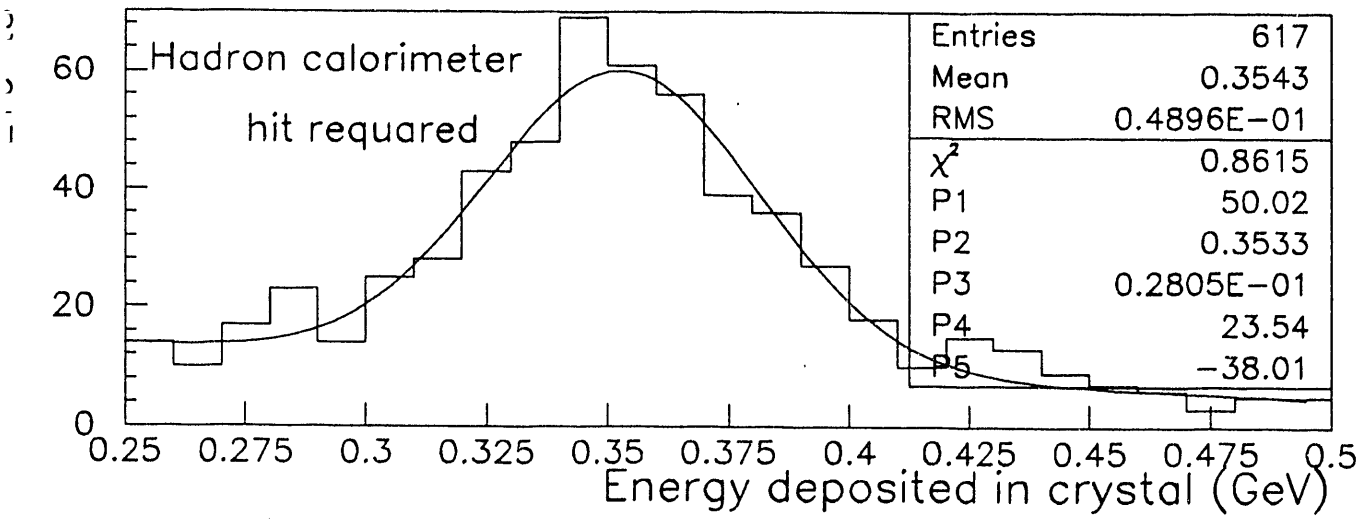


## Rate vs Θ − Ring Number

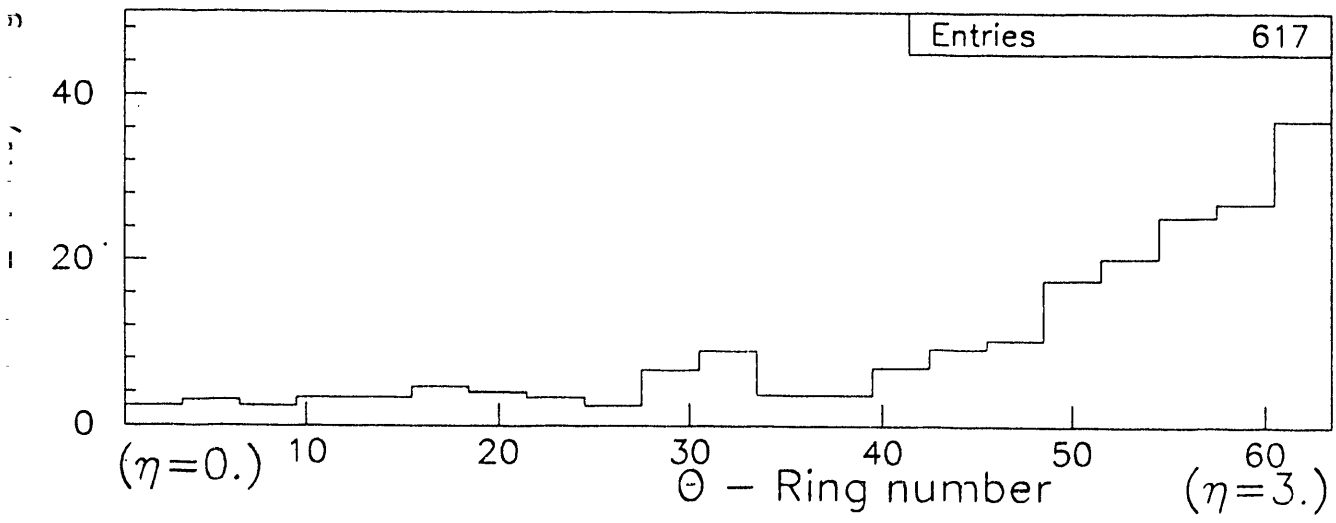


Fig. 4.2

# Punch Through Calibration

## 620 Bunch Crossings

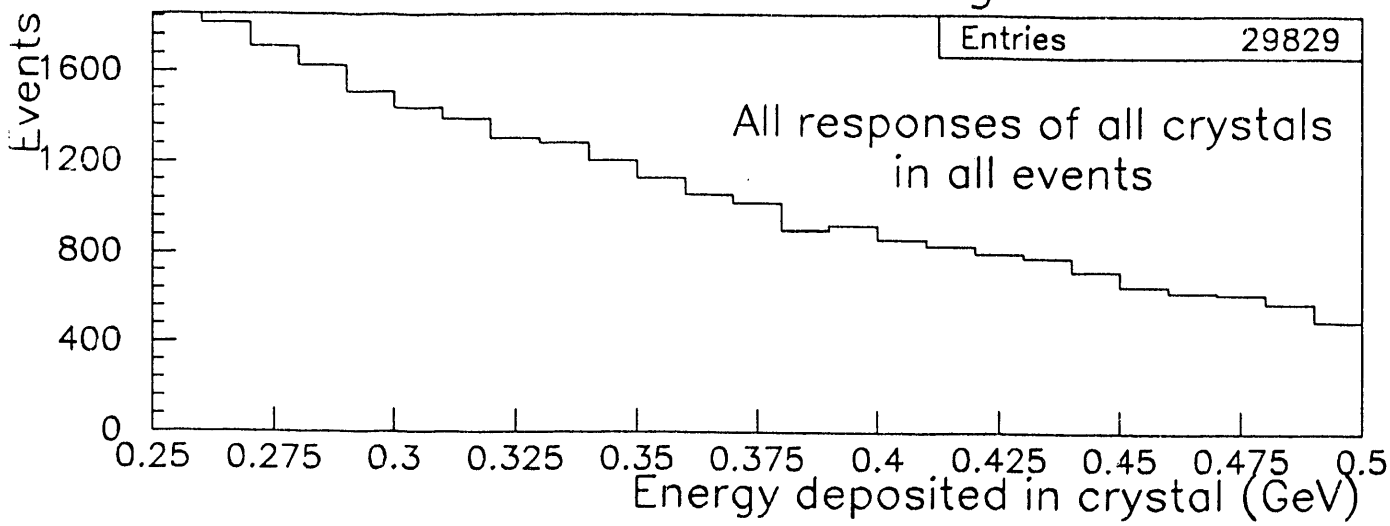


## Isolation threshold (5x5) = 200 MeV

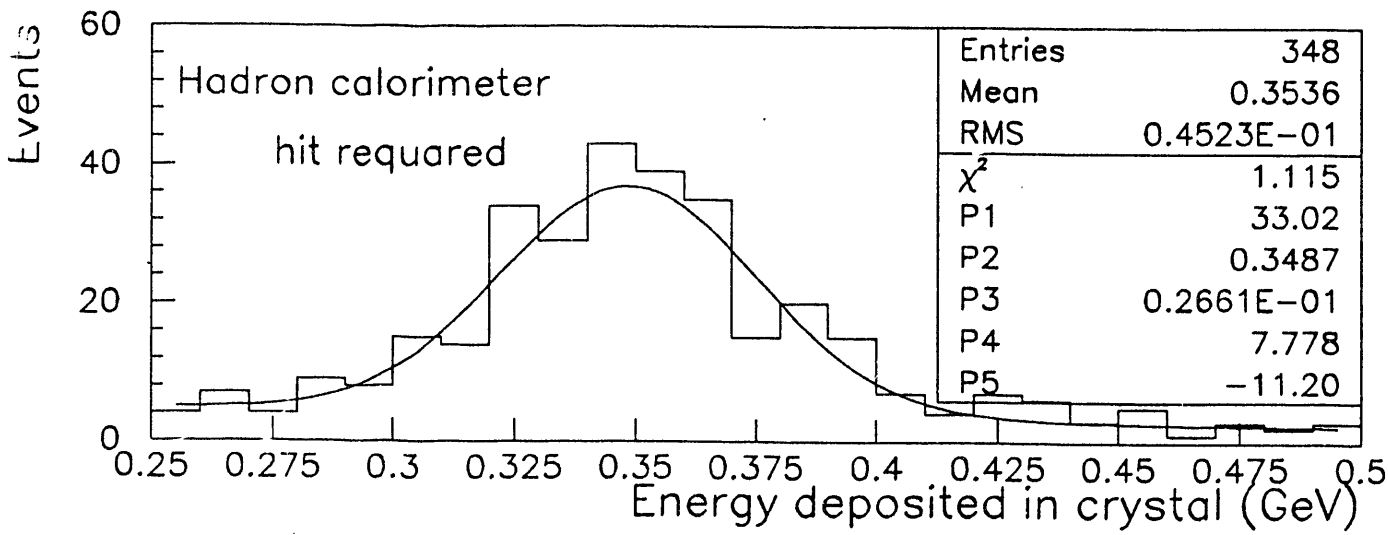


## Rate vs Θ − Ring Number

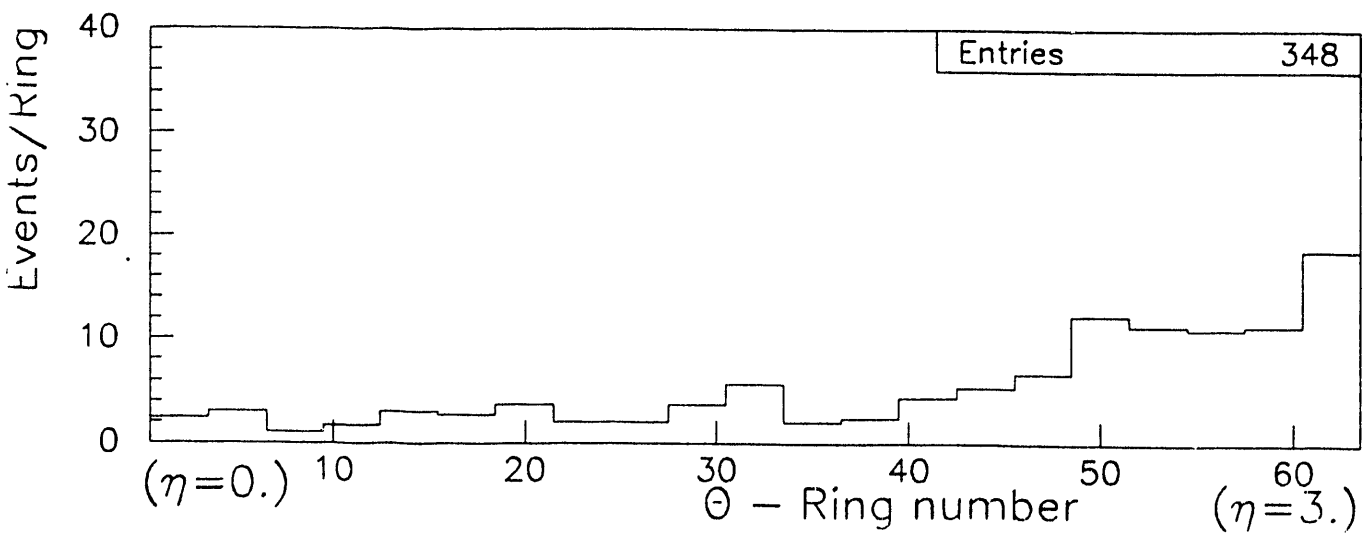


Fig.4.3

# Punch Through Calibration

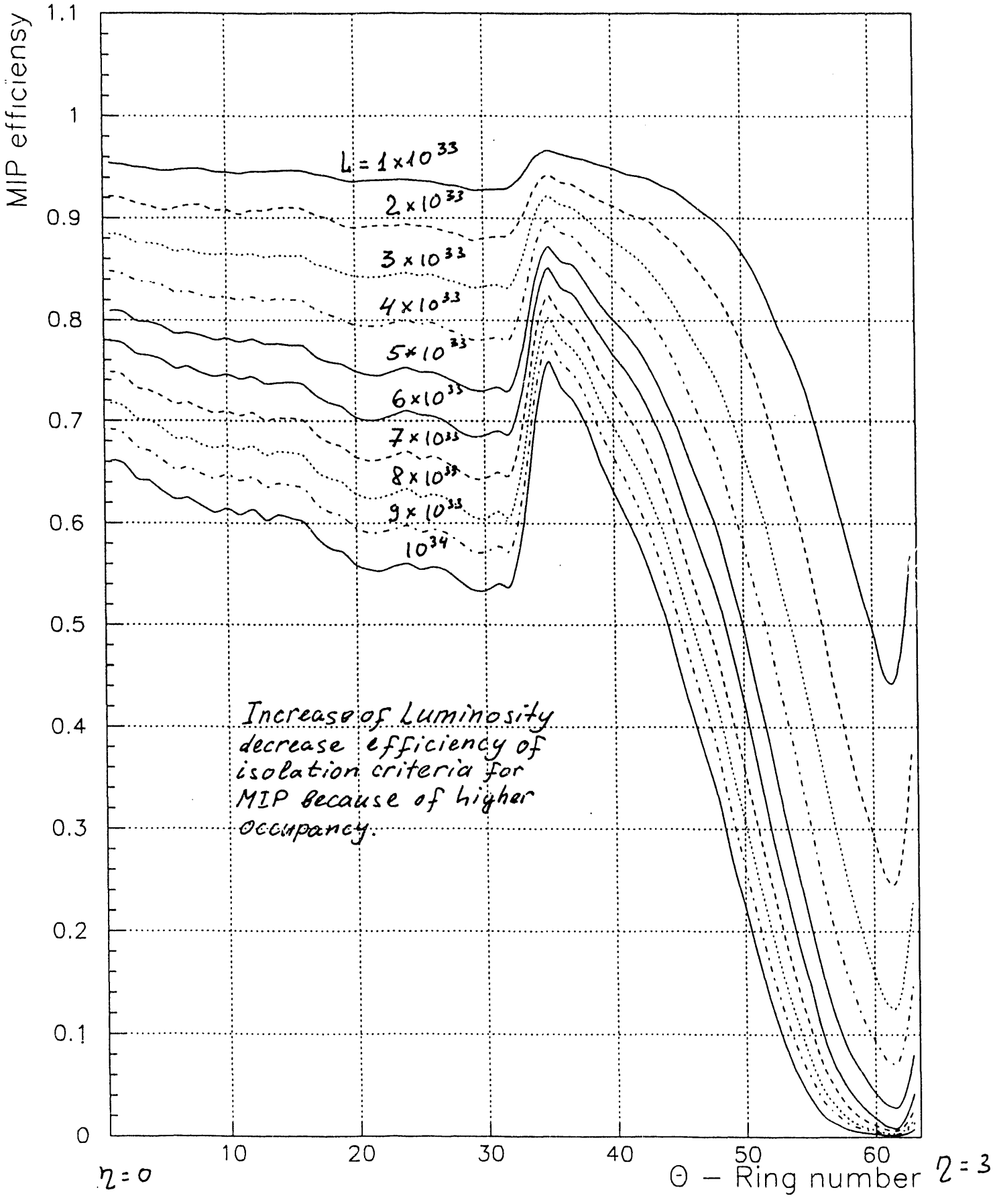


Fig. 4.4

# Punch Through Calibration

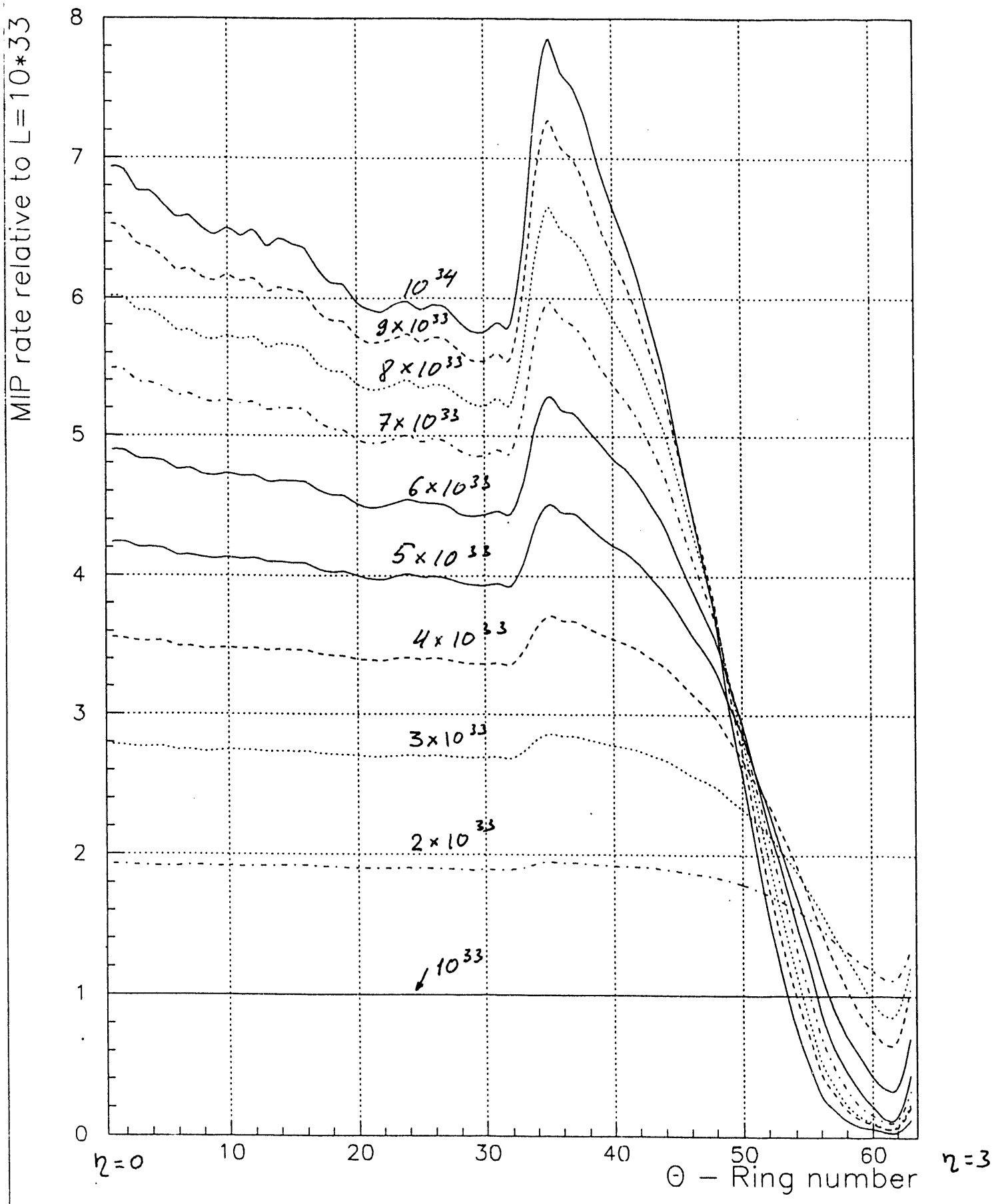


Fig. 4.5

## 5. Simulation of ScintCal Beam test prototype.

Cu/ScintFibers geomatry was simulated by GEANT3.15 (GHEISHA). Low energy cuts 100keV were used to provide detailed responce analysis. Pions with energy 5,10,15, 20GeV were used to fit experimental data (BNL92 test, Fig.5.1). Incident angle was 1.5 degrees like in beam test. Fibers 1.3mm diameter assumed to have Birks coeficient 0.015cm/MeV. Different attenuation lenghts were studied to check influence of attenuation to response spectrum shape. Simulated spectra appear to be very close to experimental. Differense in Gaussian Fit Sigma is less than 6%, and in RMS less than 10% (Fig.5.6, 5.7). It looks like lower RMS for simulated data comes from lack of statistics in tail of spectrum, so data are generated for higher statistics.

To check 'channeling' effect coming from particles running along fiber two 'testing' geometries were simulated : transwersal fibers with the same parameters and 1mm plastic tiles were simulated with the same sampling fraction. Results are under study, but preliminary conclusion is that for energyes 20 GeV and below attenuation in fibers doesn't play role in spactrum tail production (Fig.5.2 - 5.5).

Possible interpretations are :

1. 'Parallel channeling', producing tails in ordinary scintillating fibers because of 'forward' angle distribution of particles in shower;
2. 'Transwersal channeling', produsing tails in tiles and not produsing in transwersal fibers because of small solid angle for such effect;
3. Recoil protons produsing rare but large signal in plastic - this mechanism works for all geometryes but only for lowest energyes.
4. Influence of attenuation in fibers is negligible for resolution in energy range 5-20 GeV.

Main conclusion : Used program produce quite adequate simulation of Cu/ScintFibers system and may be used for Jet simulation for GEM calorimeter.

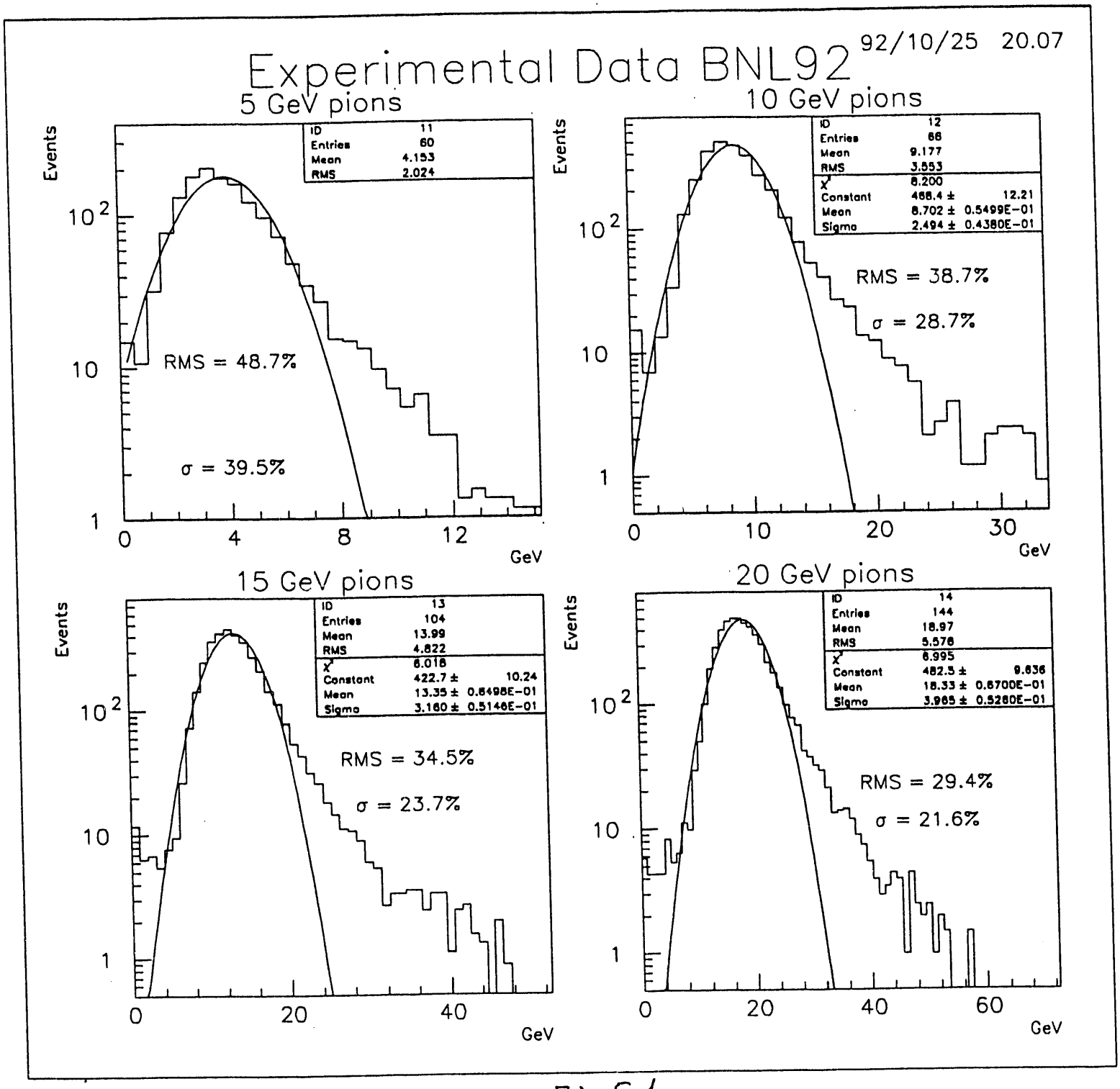
Experimental Data BNL92
92/10/25 20.07
5 GeV pions
ID 11
Entries 60
Mean 4.153
RMS 2.024
RMS = 48.7%
σ = 39.5%
10 GeV pions
ID 12
Entries 66
Mean 9.177
RMS 3.553
χ² 8.200
Constant 468.4 ± 12.21
Mean 8.702 ± 0.5499E-01
Sigma 2.494 ± 0.4380E-01
RMS = 38.7%
σ = 28.7%
15 GeV pions
ID 13
Entries 104
Mean 13.99
RMS 4.822
χ² 6.018
Constant 422.7 ± 10.24
Mean 13.35 ± 0.8498E-01
Sigma 3.160 ± 0.5146E-01
RMS = 34.5%
σ = 23.7%
20 GeV pions
ID 14
Entries 144
Mean 18.97
RMS 5.576
χ² 6.995
Constant 482.5 ± 9.636
Mean 18.33 ± 0.6700E-01
Sigma 3.965 ± 0.5280E-01
RMS = 29.4%
σ = 21.6%
Events
GeV

Fig.5.1.

Sampling 2.25% volume
∴ = > T

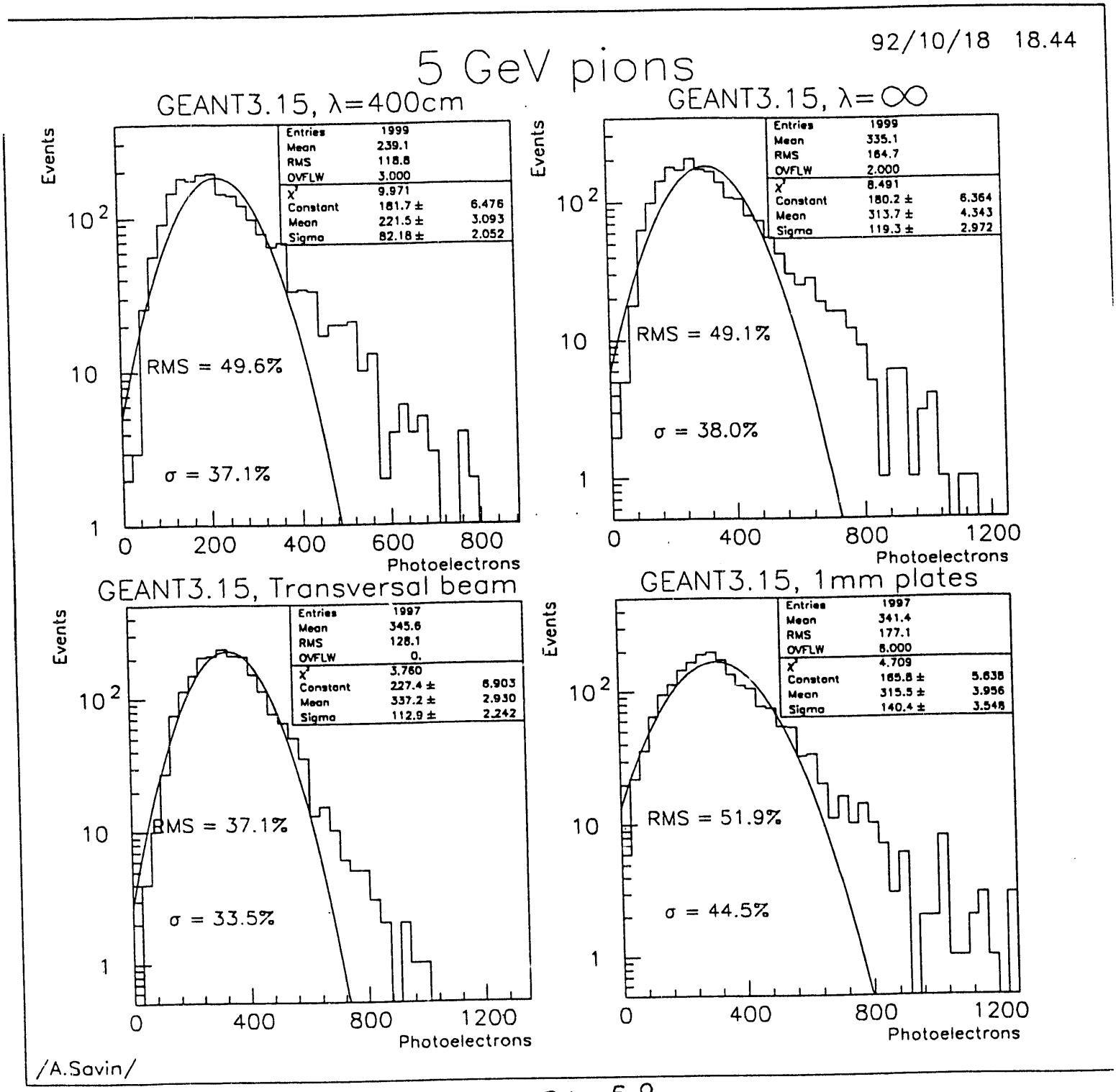


Fig. 5.2.

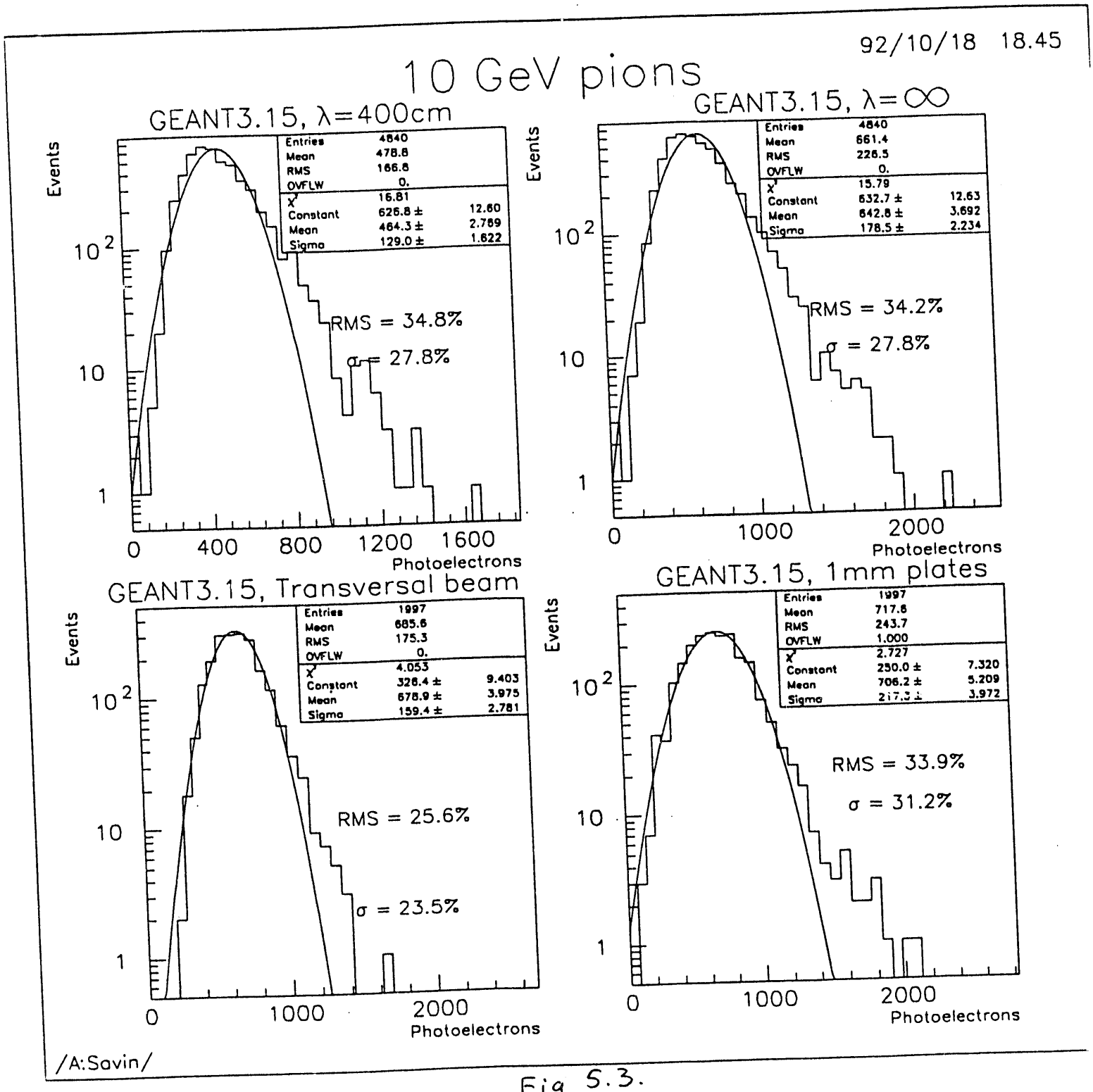
92/10/18 18.45
10 GeV pions
GEANT3.15, λ=400cm
Entries 4840
Mean 478.8
RMS 166.8
OVFLW 0.
χ² 16.81
Constant 626.8 ± 12.60
Mean 464.3 ± 2.769
Sigma 129.0 ± 1.622
RMS = 34.8%
σ = 27.8%
Events
Photoelectrons
GEANT3.15, λ=∞
Entries 4840
Mean 661.4
RMS 226.5
OVFLW 0.
χ² 15.79
Constant 632.7 ± 12.63
Mean 642.8 ± 3.692
Sigma 178.5 ± 2.234
RMS = 34.2%
σ = 27.8%
GEANT3.15, Transversal beam
Entries 1997
Mean 685.6
RMS 175.3
OVFLW 0.
χ² 4.053
Constant 326.4 ± 9.403
Mean 678.9 ± 3.975
Sigma 159.4 ± 2.781
RMS = 25.6%
σ = 23.5%
GEANT3.15, 1mm plates
Entries 1997
Mean 717.6
RMS 243.7
OVFLW 1.000
χ² 2.727
Constant 250.0 ± 7.320
Mean 706.2 ± 5.209
Sigma 217.3 ± 3.972
RMS = 33.9%
σ = 31.2%
/A:Savin/

Fig. 5.3.

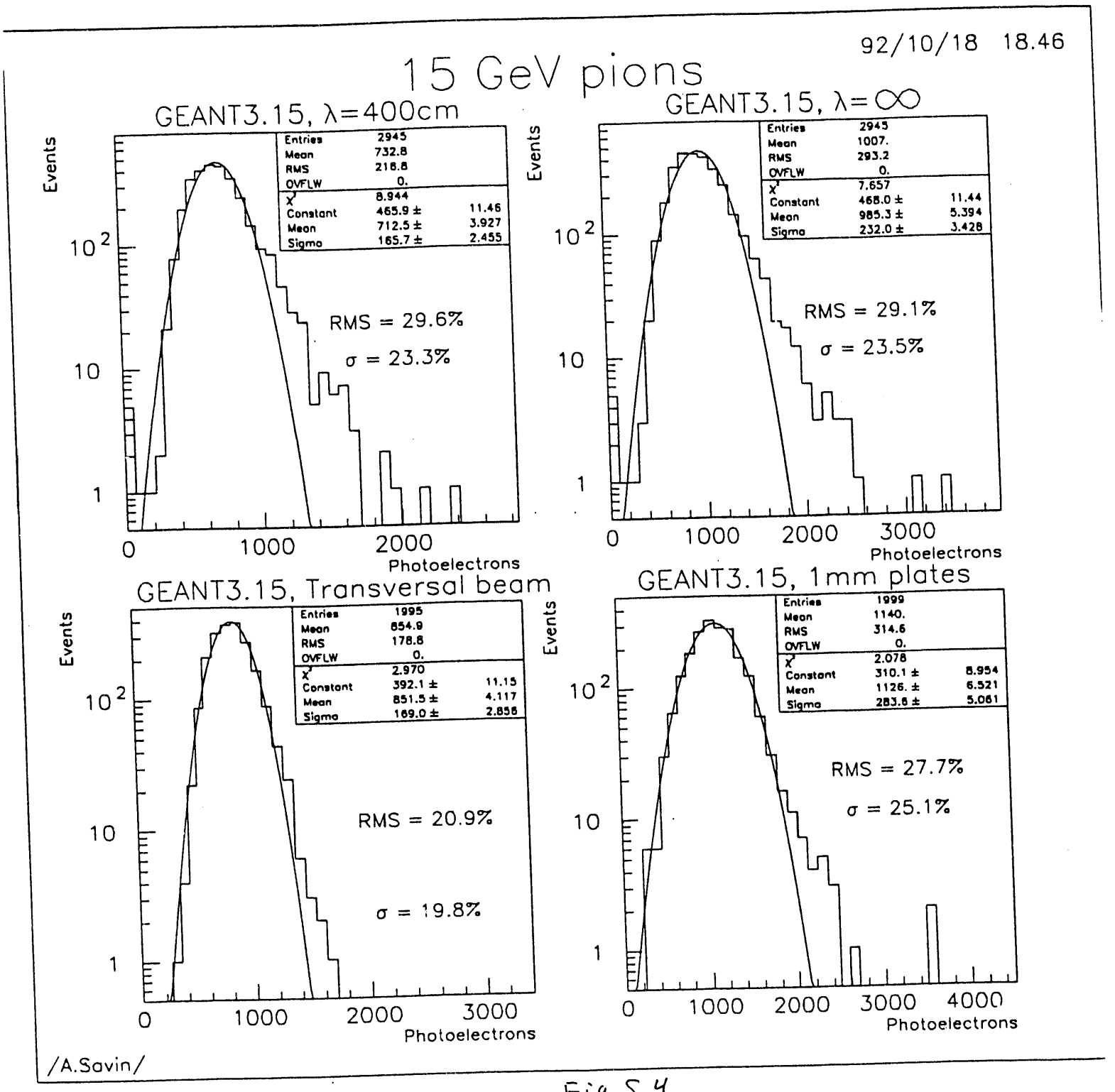
92/10/18 18.46
15 GeV pions
GEANT3.15, λ=400cm
Entries 2945
Mean 732.8
RMS 216.8
OVFLW 0.
χ² 8.944
Constant 465.9 ± 11.46
Mean 712.5 ± 3.927
Sigma 165.7 ± 2.455
RMS = 29.6%
σ = 23.3%
Events
Photoelectrons
GEANT3.15, λ=∞
Entries 2945
Mean 1007.
RMS 293.2
OVFLW 0.
χ² 7.657
Constant 468.0 ± 11.44
Mean 985.3 ± 5.394
Sigma 232.0 ± 3.428
RMS = 29.1%
σ = 23.5%
Events
Photoelectrons
GEANT3.15, Transversal beam
Entries 1995
Mean 854.9
RMS 178.8
OVFLW 0.
χ² 2.970
Constant 392.1 ± 11.15
Mean 851.5 ± 4.117
Sigma 169.0 ± 2.856
RMS = 20.9%
σ = 19.8%
Events
Photoelectrons
GEANT3.15, 1mm plates
Entries 1999
Mean 1140.
RMS 314.6
OVFLW 0.
χ² 2.078
Constant 310.1 ± 8.954
Mean 1126. ± 6.521
Sigma 283.6 ± 5.061
RMS = 27.7%
σ = 25.1%
Events
Photoelectrons
/A.Savin/

Fig. 5.4

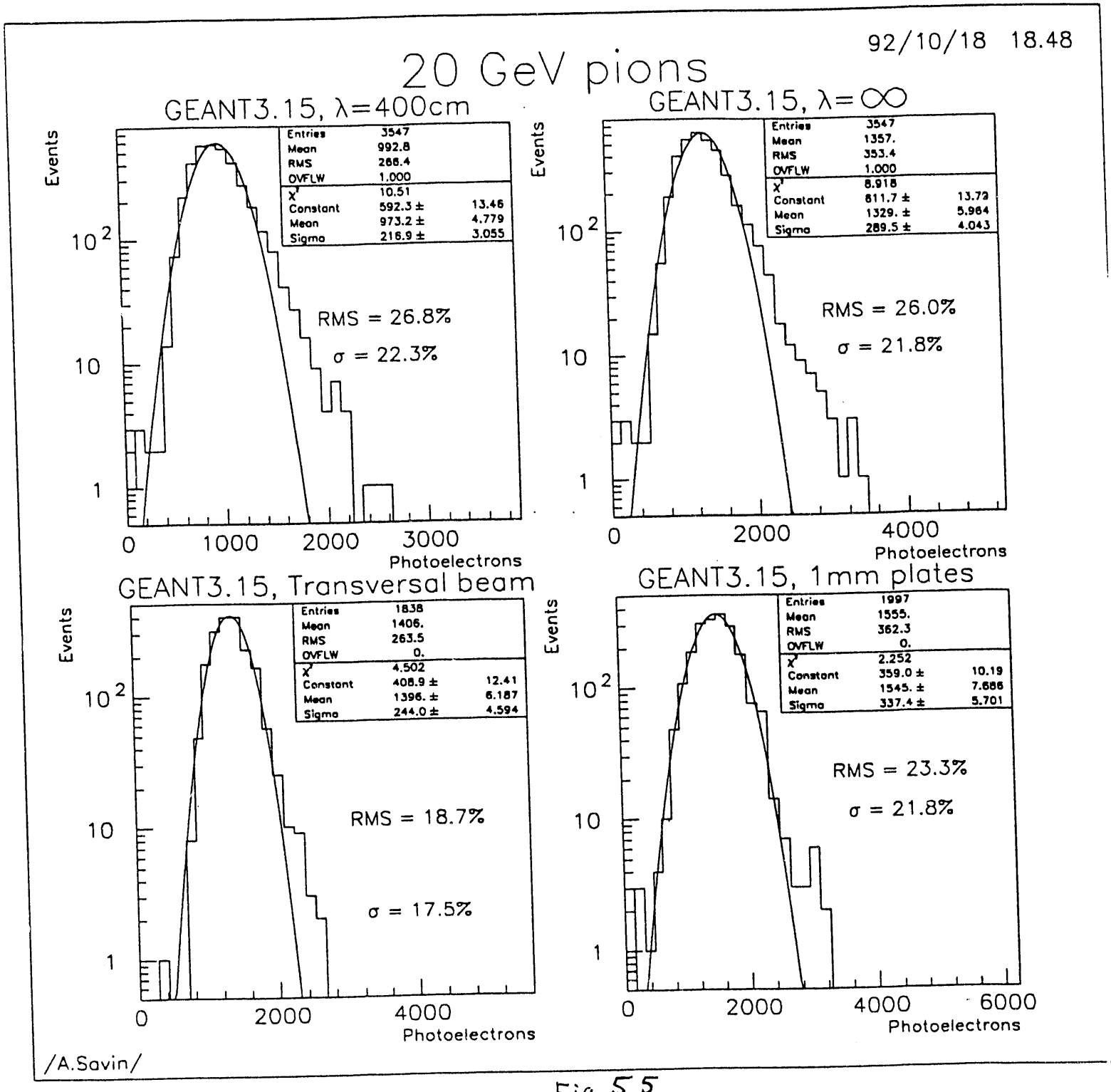
92/10/18 18.48
20 GeV pions
GEANT3.15, λ=400cm
Entries 3547
Mean 992.8
RMS 266.4
OVFLW 1.000
χ² 10.51
Constant 592.3 ± 13.46
Mean 973.2 ± 4.779
Sigma 216.9 ± 3.055
RMS = 26.8%
σ = 22.3%
Events
Photoelectrons
GEANT3.15, λ=∞
Entries 3547
Mean 1357.
RMS 353.4
OVFLW 1.000
χ² 8.918
Constant 611.7 ± 13.72
Mean 1329. ± 5.964
Sigma 289.5 ± 4.043
RMS = 26.0%
σ = 21.8%
Events
Photoelectrons
GEANT3.15, Transversal beam
Entries 1838
Mean 1406.
RMS 263.5
OVFLW 0.
χ² 4.502
Constant 408.9 ± 12.41
Mean 1396. ± 6.187
Sigma 244.0 ± 4.594
RMS = 18.7%
σ = 17.5%
Events
Photoelectrons
GEANT3.15, 1mm plates
Entries 1997
Mean 1555.
RMS 362.3
OVFLW 0.
χ² 2.252
Constant 359.0 ± 10.19
Mean 1545. ± 7.686
Sigma 337.4 ± 5.701
RMS = 23.3%
σ = 21.8%
Events
Photoelectrons
/A.Savin/

Fig. 5.5

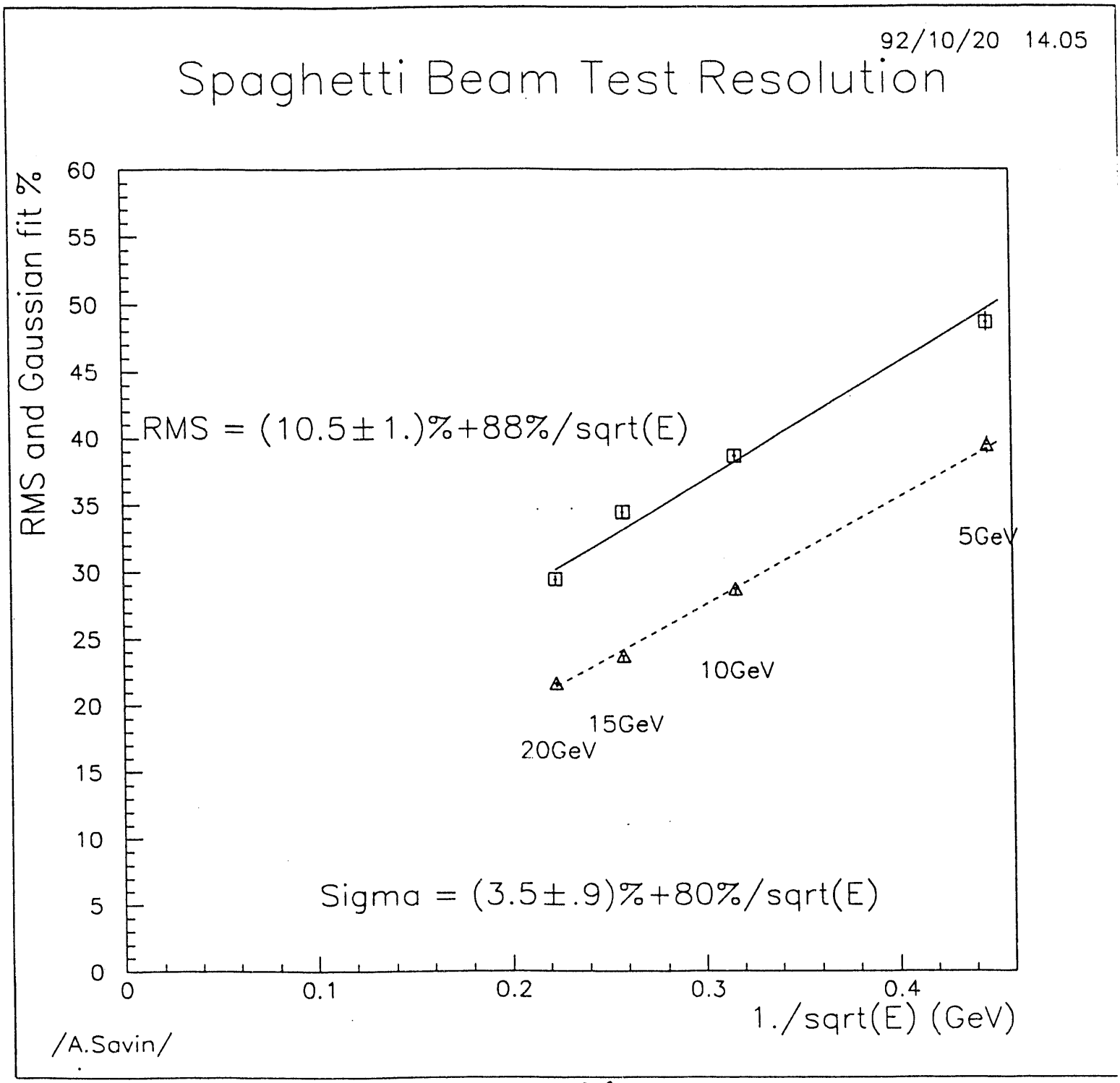
92/10/20 14.05
Spaghetti Beam Test Resolution
RMS and Gaussian fit %
60
55
50
45
40
35
30
25
20
15
10
5
0
RMS = (10.5±1.)%+88%/sqrt(E)
5GeV
10GeV
15GeV
20GeV
Sigma = (3.5±.9)%+80%/sqrt(E)
0
0.1
0.2
0.3
0.4
1./sqrt(E) (GeV)
/A.Savin/

Fig. 5.6.

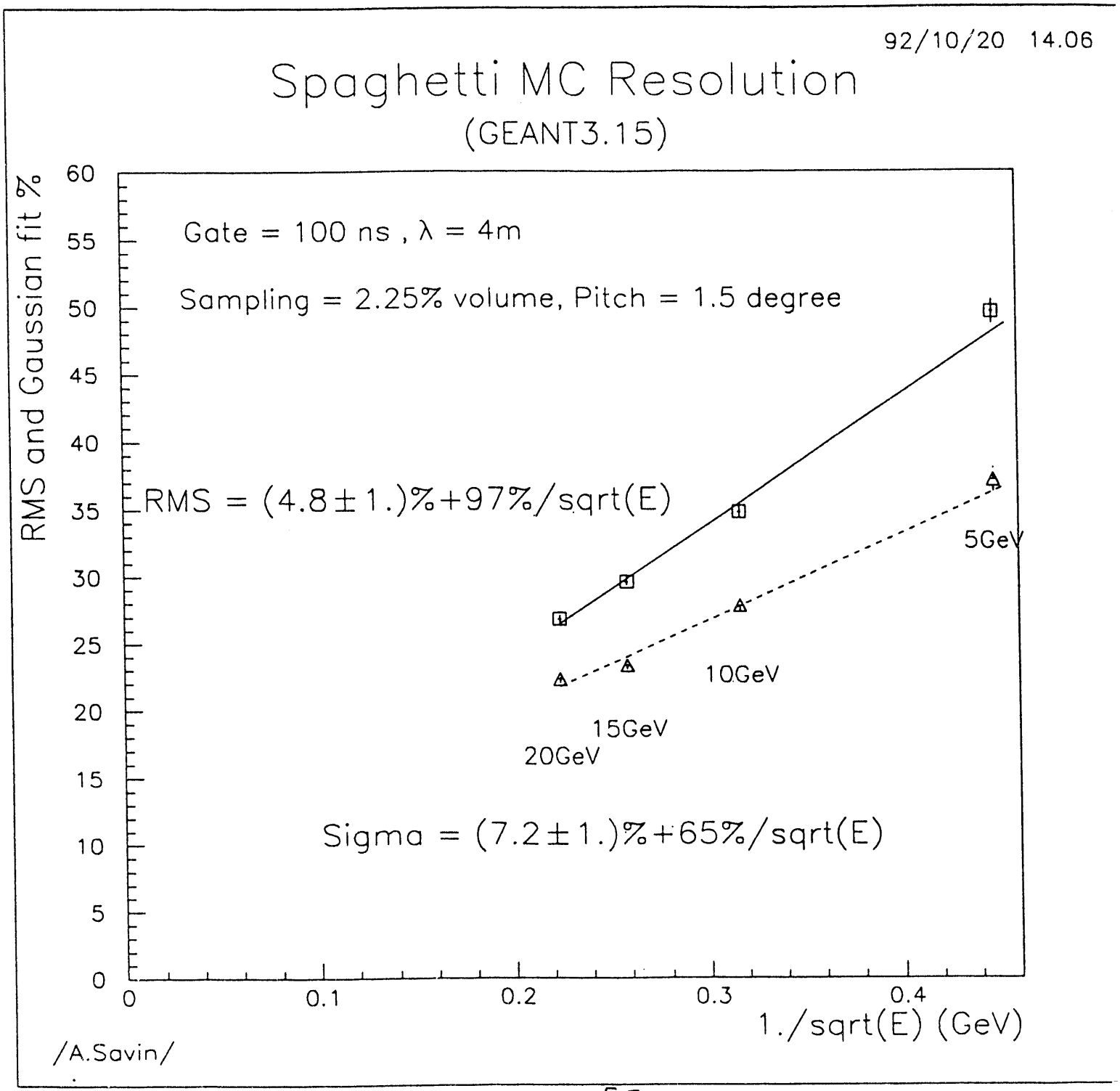
92/10/20 14.06
Spaghetti MC Resolution
(GEANT3.15)
Gate = 100 ns , λ = 4m
Sampling = 2.25% volume, Pitch = 1.5 degree
RMS = (4.8±1.)%+97%/sqrt(E)
Sigma = (7.2±1.)%+65%/sqrt(E)
5GeV
10GeV
15GeV
20GeV
RMS and Gaussian fit %
1./sqrt(E) (GeV)
0
5
10
15
20
25
30
35
40
45
50
55
60
0
0.1
0.2
0.3
0.4
/A.Savin/

Fig. 5.7.

## 6.Simulation of jets in Hybrid Option.

Electromagnetic LKr/Pb calorimeter wit realystic gaps and dead material was added to HC from previous section. Jets were generated by JETSET for energyes 10,20,100,200 GeV and 1TeV. Magnetic fielt 0.8 Tesla is applied. EM and HC responses were weighted (Fig.6.2, 6.3) to provide optimal energy resolution (Fig.6.1) for each energy. EM and HC weights appear to be energy dependent. Energy resolution is well described by 4.3(+/-0.3)%+64(+/-1.5)%/sqrt(E) (Fig.6.4).

Main conclusion: Correct matching of EM and HC give energy resolution 4.3%+64%/sqrt(E) for Jets. Jet energy resolution is better than single hadron resolution.
More analysis will be made for optimisation of matching procedure. Massless gap before HC will be tested as additional longitudinal segment to improve resolution.

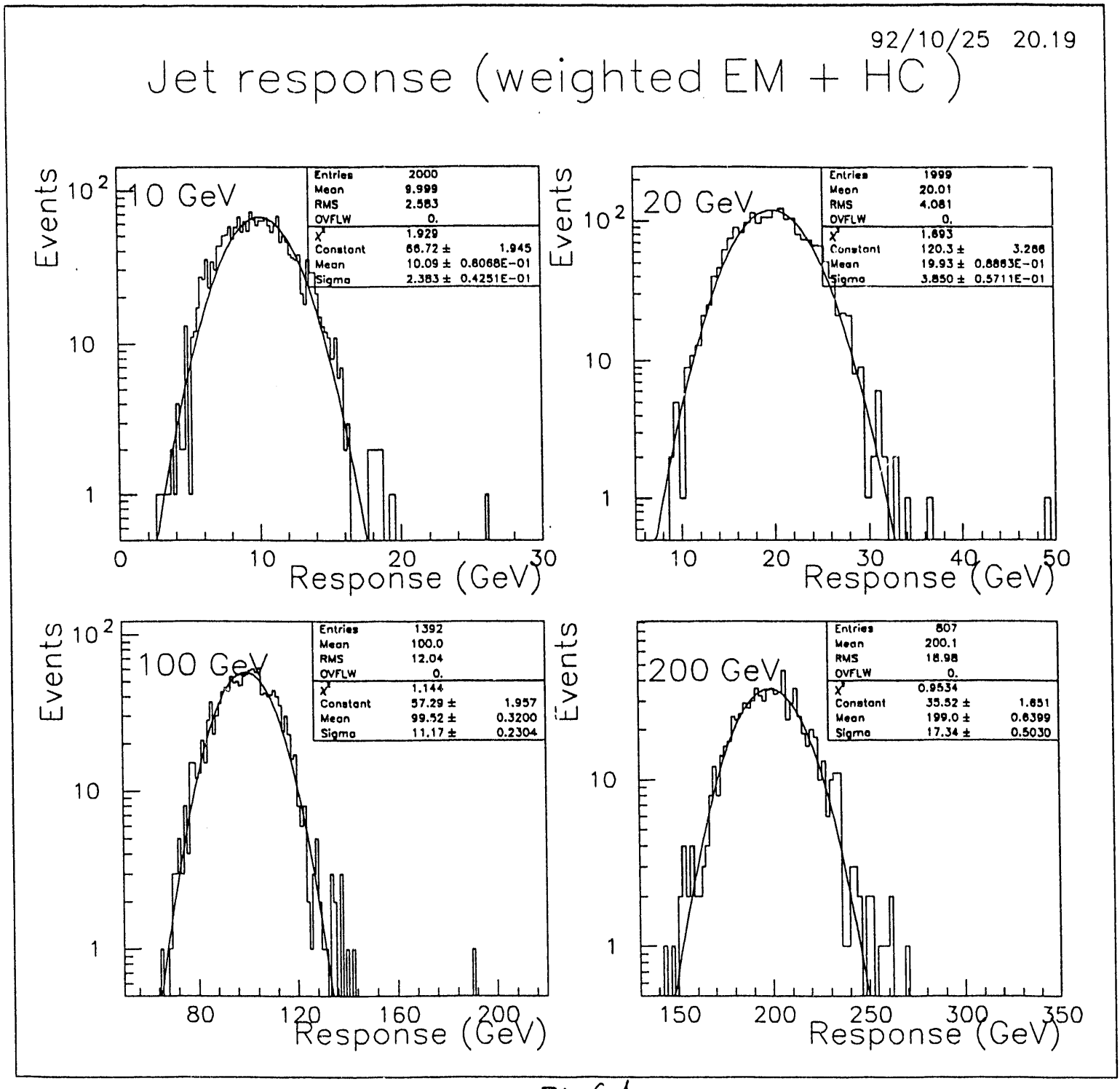
92/10/25 20.19
Jet response (weighted EM + HC )
10 GeV
Entries 2000
Mean 9.999
RMS 2.583
OVFLW 0.
χ² 1.929
Constant 66.72 ± 1.945
Mean 10.09 ± 0.6068E-01
Sigma 2.383 ± 0.4251E-01
20 GeV
Entries 1999
Mean 20.01
RMS 4.081
OVFLW 0.
χ² 1.693
Constant 120.3 ± 3.266
Mean 19.93 ± 0.8863E-01
Sigma 3.850 ± 0.5711E-01
100 GeV
Entries 1392
Mean 100.0
RMS 12.04
OVFLW 0.
χ² 1.144
Constant 57.29 ± 1.957
Mean 99.52 ± 0.3200
Sigma 11.17 ± 0.2304
200 GeV
Entries 807
Mean 200.1
RMS 18.98
OVFLW 0.
χ² 0.9534
Constant 35.52 ± 1.851
Mean 199.0 ± 0.6399
Sigma 17.34 ± 0.5030
Events
Response (GeV)

Fig 6.1

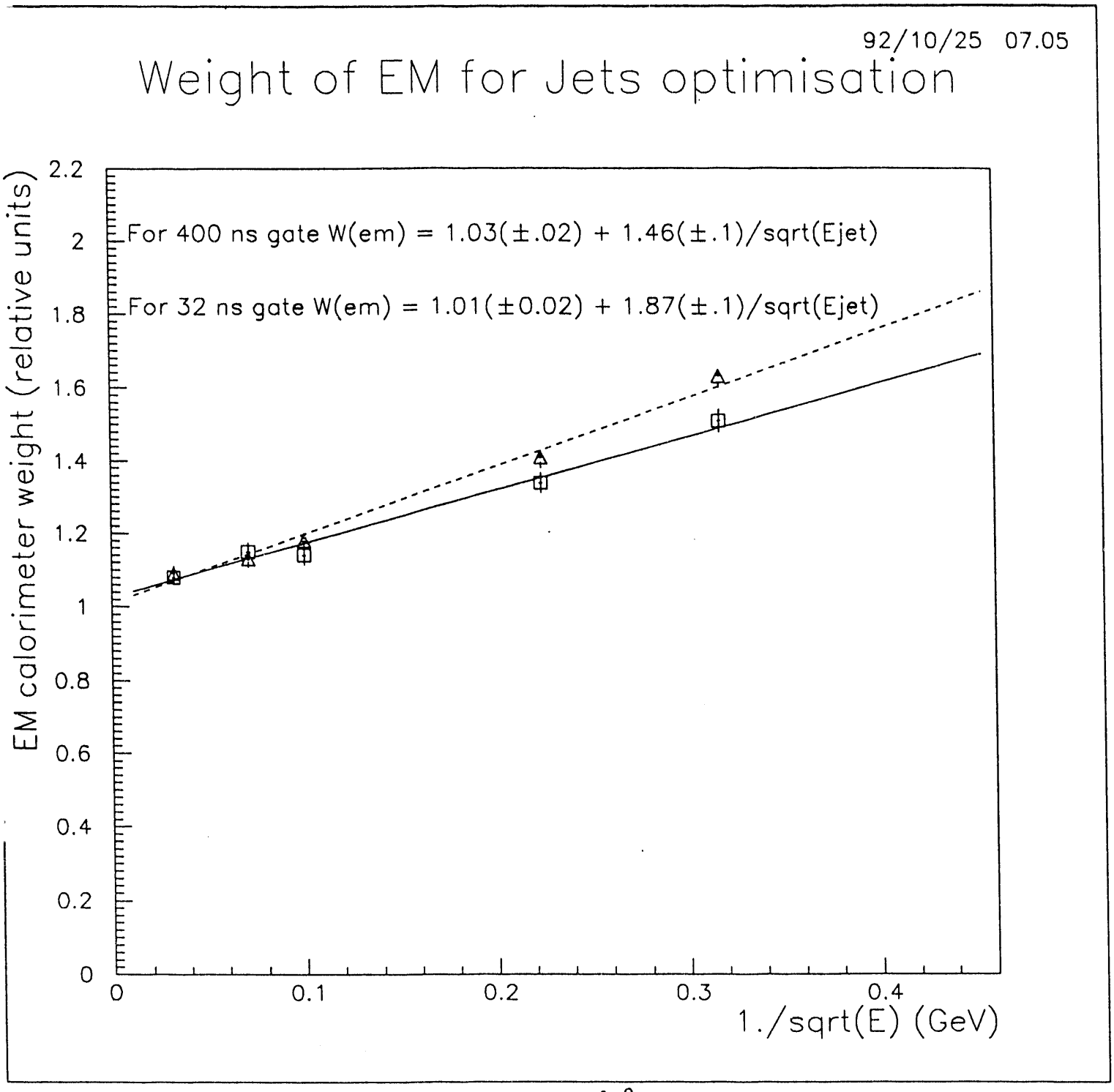
92/10/25 07.05
Weight of EM for Jets optimisation
For 400 ns gate W(em) = 1.03(±.02) + 1.46(±.1)/sqrt(Ejet)
For 32 ns gate W(em) = 1.01(±0.02) + 1.87(±.1)/sqrt(Ejet)
EM calorimeter weight (relative units)
2.2
2
1.8
1.6
1.4
1.2
1
0.8
0.6
0.4
0.2
0
0
0.1
0.2
0.3
0.4
1./sqrt(E) (GeV)

Fig. 6.2

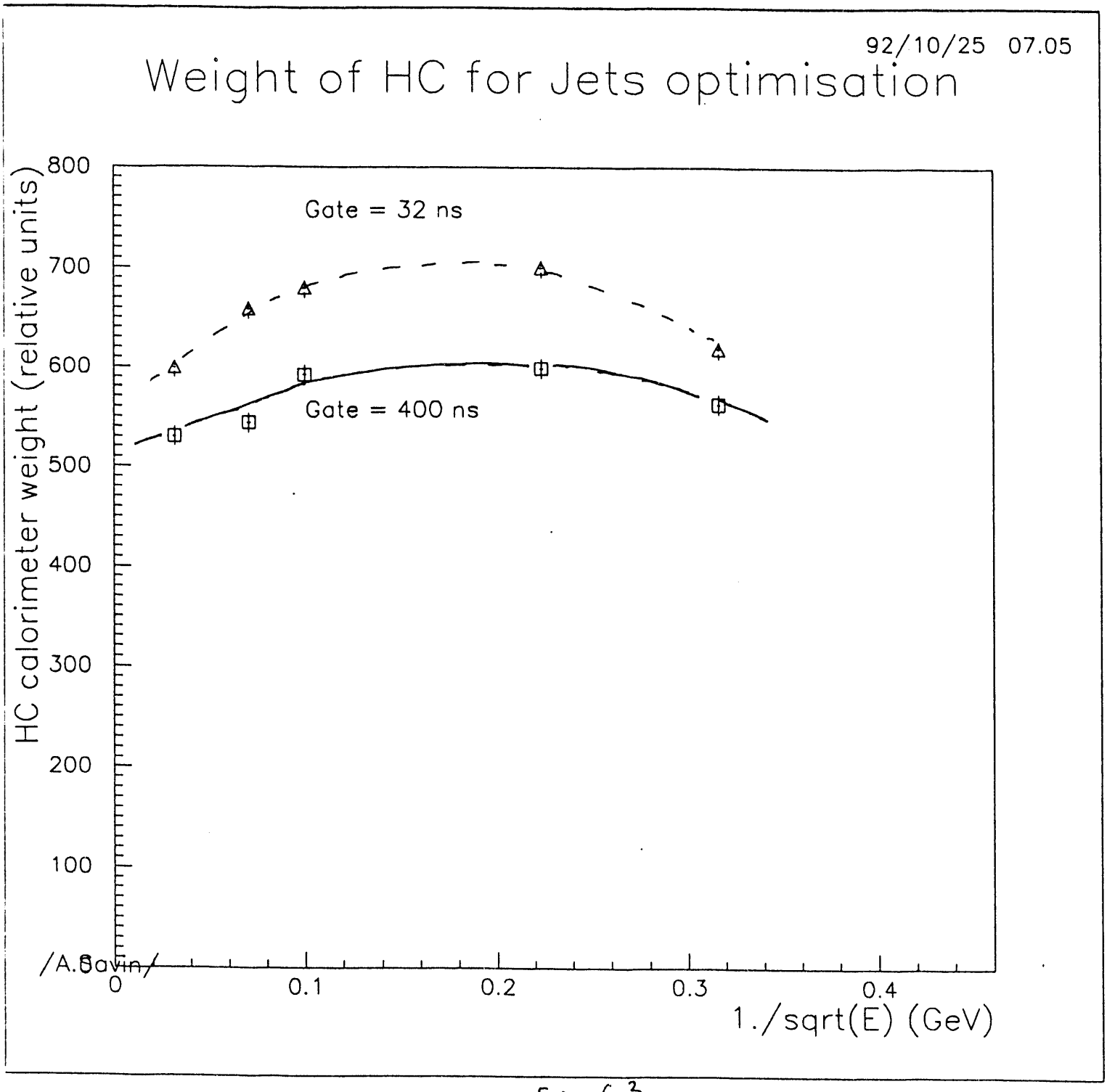
92/10/25 07.05
Weight of HC for Jets optimisation
HC calorimeter weight (relative units)
800
700
600
500
400
300
200
100
Gate = 32 ns
Gate = 400 ns
/A.Savin/
0
0.1
0.2
0.3
0.4
1./sqrt(E) (GeV)

Fig. 6.3

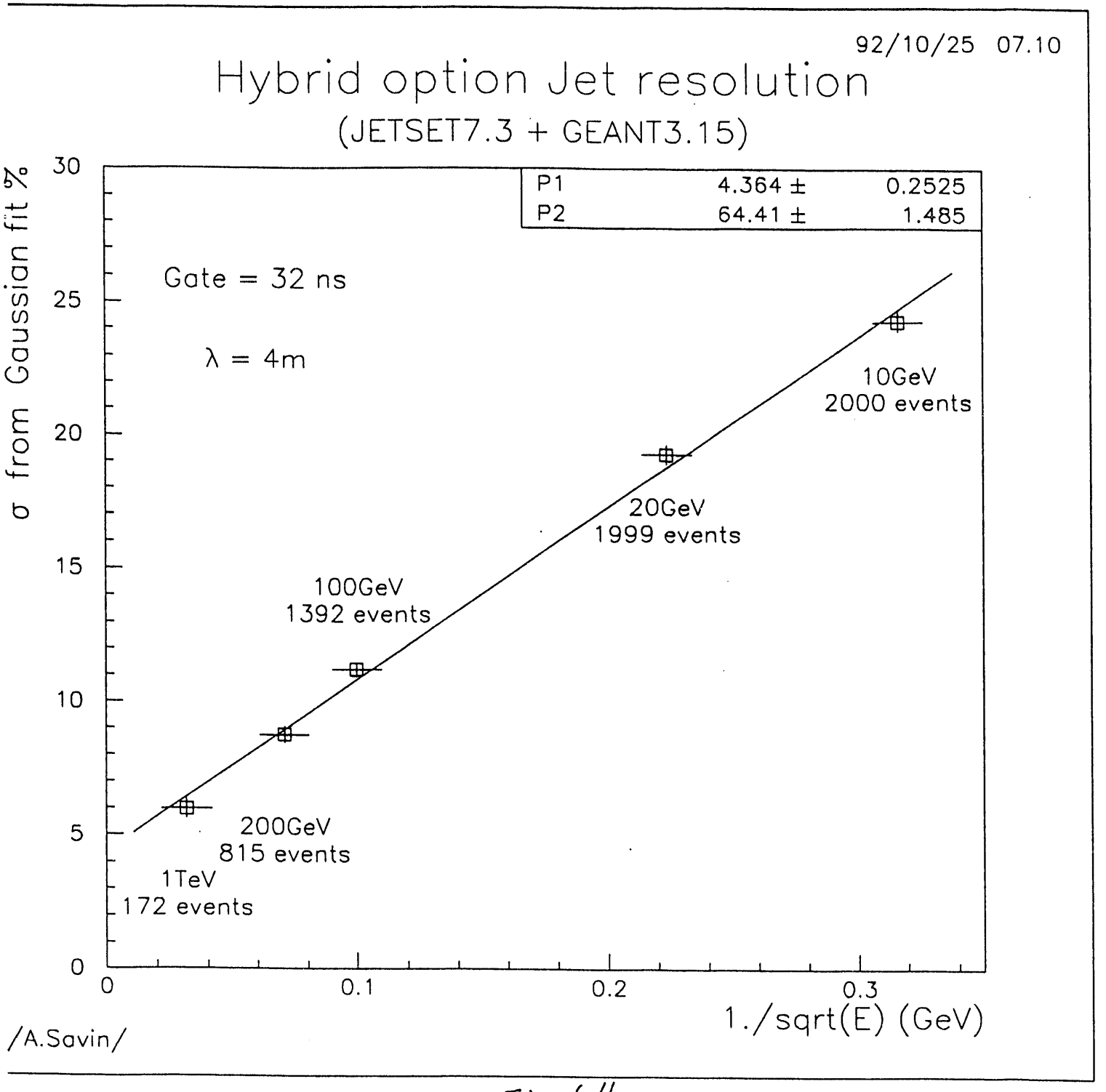
92/10/25 07.10
Hybrid option Jet resolution
(JETSET7.3 + GEANT3.15)
P1 4.364 ± 0.2525
P2 64.41 ± 1.485
Gate = 32 ns
λ = 4m
10GeV
2000 events
20GeV
1999 events
100GeV
1392 events
200GeV
815 events
1TeV
172 events
σ from Gaussian fit %
1./sqrt(E) (GeV)
/A.Savin/

Fig. 6.4.

## 7.Massless Gap for response correction in Hybrid option

Massless gap (1cm scintillator) was added before HC to correct losses in dead material and longitudinal nonuniformity of hadronic calorimeter. Single pions with energyes 5,10,20,100,200 GeV, 1, 2 TeV are generated and transported by GEANT3.15 in 0.8 Tesla magnetic field. Three weght coeficients are to be ajusted to optimize energy resolution of system (Fig.7.1 - 7.3).

Preliminary results : Massless gap gives improvement of constant term in resolution for individual hadrons in Hybrid HC option (Fig.7.4 - 7.9). Shape of spectra became 'more Gaussian' - differense between RMS and Sigma became smaller. Non-linear procedure for massless gap to be studied (may improve the resolution farther Fig.7.8,7.9).

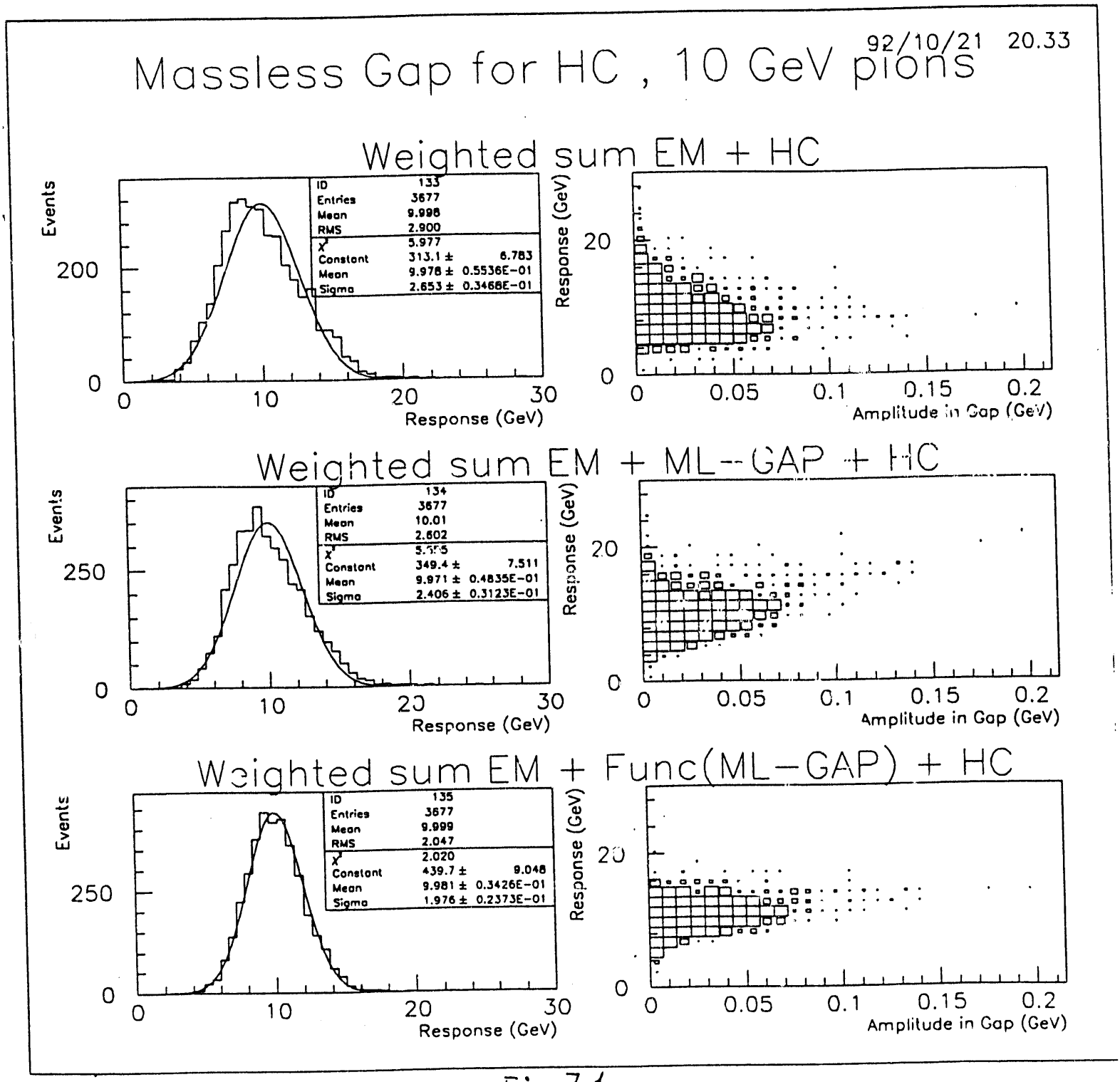
92/10/21 20.33
Massless Gap for HC , 10 GeV pions
Weighted sum EM + HC
ID 133
Entries 3677
Mean 9.998
RMS 2.900
χ² 5.977
Constant 313.1 ± 6.783
Mean 9.978 ± 0.5536E-01
Sigma 2.653 ± 0.3468E-01
Events
Response (GeV)
Amplitude in Gap (GeV)
Weighted sum EM + ML-GAP + HC
ID 134
Entries 3677
Mean 10.01
RMS 2.602
Constant 349.4 ± 7.511
Mean 9.971 ± 0.4835E-01
Sigma 2.406 ± 0.3123E-01
Weighted sum EM + Func(ML-GAP) + HC
ID 135
Entries 3677
Mean 9.999
RMS 2.047
χ² 2.020
Constant 439.7 ± 9.048
Mean 9.981 ± 0.3426E-01
Sigma 1.976 ± 0.2373E-01

Fig. 7.1

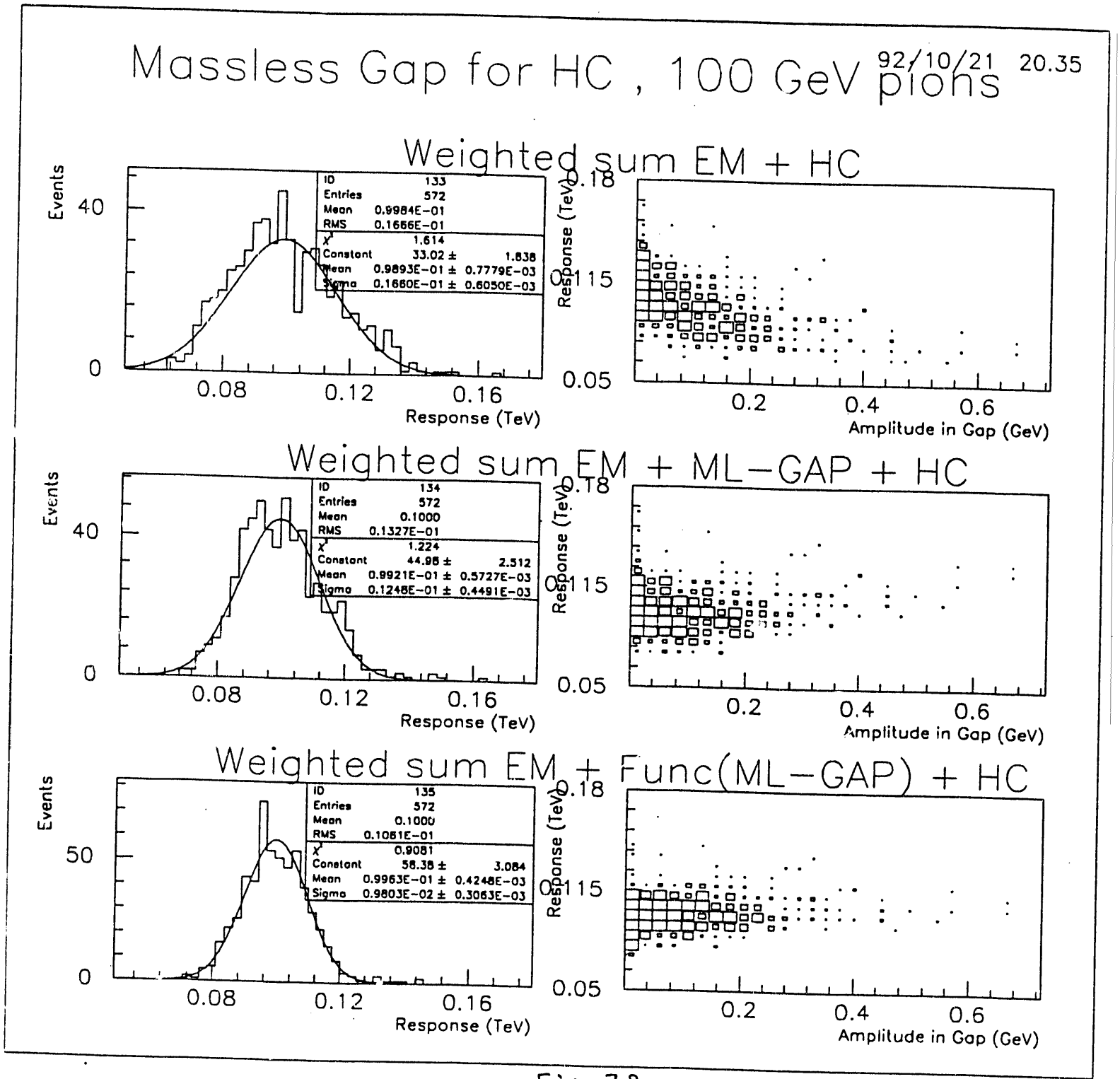
Massless Gap for HC , 100 GeV pions
92/10/21 20.35
Weighted sum EM + HC
ID 133
Entries 572
Mean 0.9984E-01
RMS 0.1666E-01
χ² 1.614
Constant 33.02 ± 1.838
Mean 0.9893E-01 ± 0.7779E-03
Sigma 0.1660E-01 ± 0.6050E-03
Events
Response (TeV)
Amplitude in Gap (GeV)
Weighted sum EM + ML-GAP + HC
ID 134
Entries 572
Mean 0.1000
RMS 0.1327E-01
χ² 1.224
Constant 44.98 ± 2.512
Mean 0.9921E-01 ± 0.5727E-03
Sigma 0.1248E-01 ± 0.4491E-03
Weighted sum EM + Func(ML-GAP) + HC
ID 135
Entries 572
Mean 0.1000
RMS 0.1061E-01
χ² 0.9081
Constant 58.38 ± 3.084
Mean 0.9963E-01 ± 0.4248E-03
Sigma 0.9803E-02 ± 0.3063E-03

Fig. 7.2

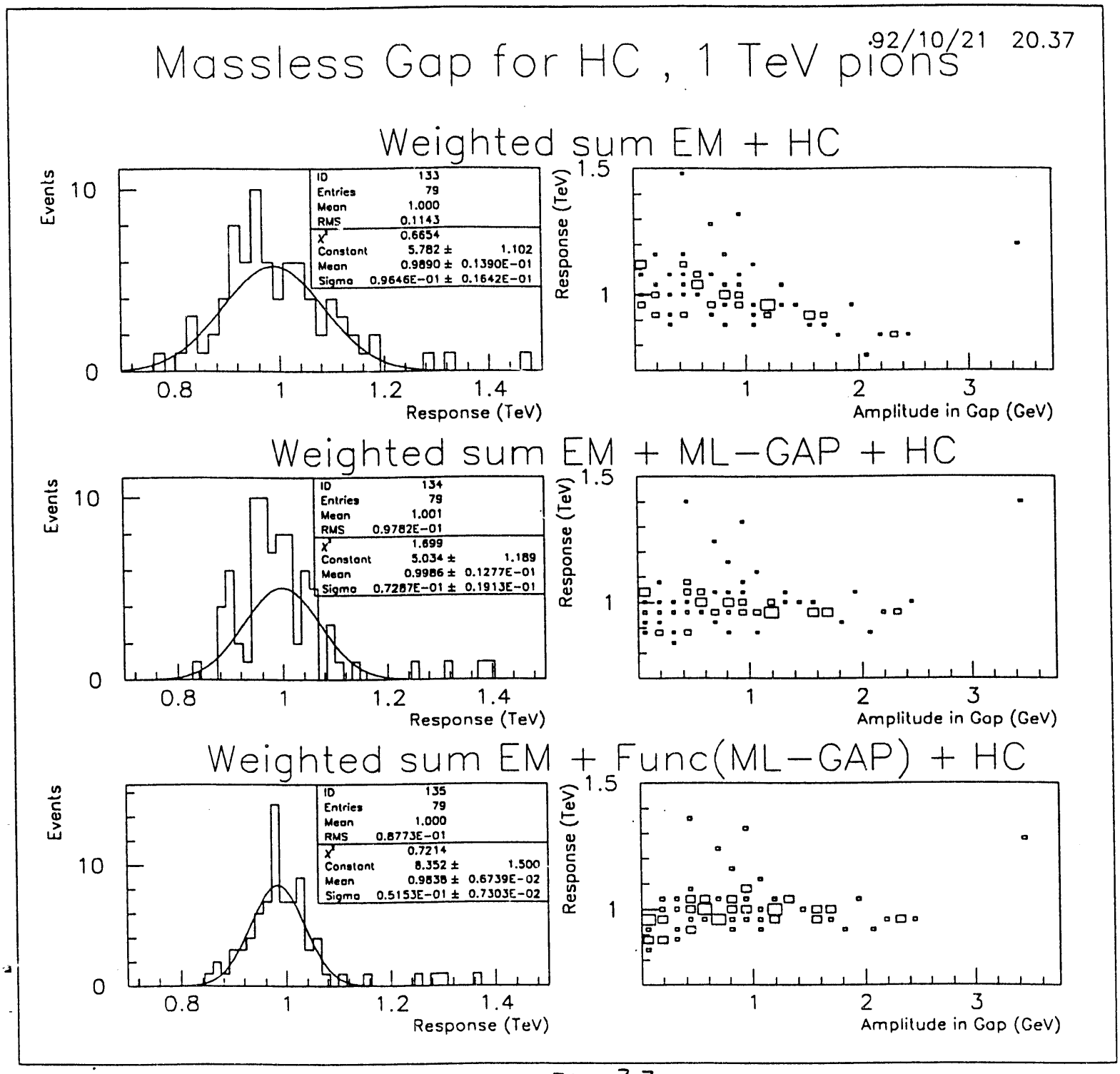
92/10/21 20.37
Massless Gap for HC , 1 TeV pions
Weighted sum EM + HC
ID 133
Entries 79
Mean 1.000
RMS 0.1143
χ² 0.6654
Constant 5.782 ± 1.102
Mean 0.9890 ± 0.1390E-01
Sigma 0.9646E-01 ± 0.1642E-01
Events
Response (TeV)
Amplitude in Gap (GeV)
Weighted sum EM + ML-GAP + HC
ID 134
Entries 79
Mean 1.001
RMS 0.9782E-01
χ² 1.699
Constant 5.034 ± 1.189
Mean 0.9986 ± 0.1277E-01
Sigma 0.7287E-01 ± 0.1913E-01
Weighted sum EM + Func(ML-GAP) + HC
ID 135
Entries 79
Mean 1.000
RMS 0.8773E-01
χ² 0.7214
Constant 8.352 ± 1.500
Mean 0.9838 ± 0.6739E-02
Sigma 0.5153E-01 ± 0.7303E-02

Fig. 7.3

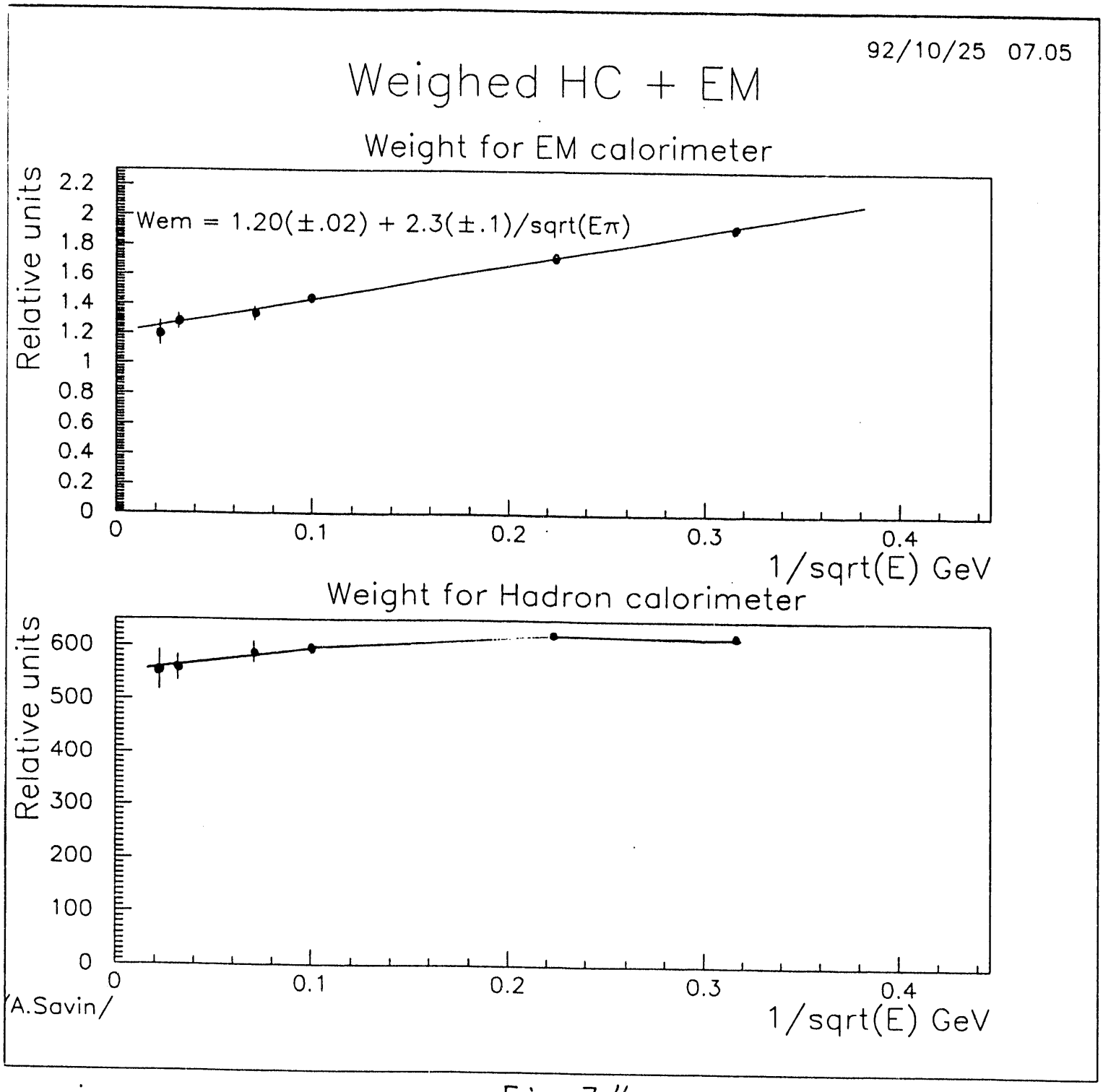
92/10/25 07.05
Weighed HC + EM
Weight for EM calorimeter
Relative units
Wem = 1.20(±.02) + 2.3(±.1)/sqrt(Eπ)
2.2
2
1.8
1.6
1.4
1.2
1
0.8
0.6
0.4
0.2
0
0
0.1
0.2
0.3
0.4
1/sqrt(E) GeV
Weight for Hadron calorimeter
Relative units
600
500
400
300
200
100
0
0
0.1
0.2
0.3
0.4
1/sqrt(E) GeV
/A.Savin/

Fig. 7.4.

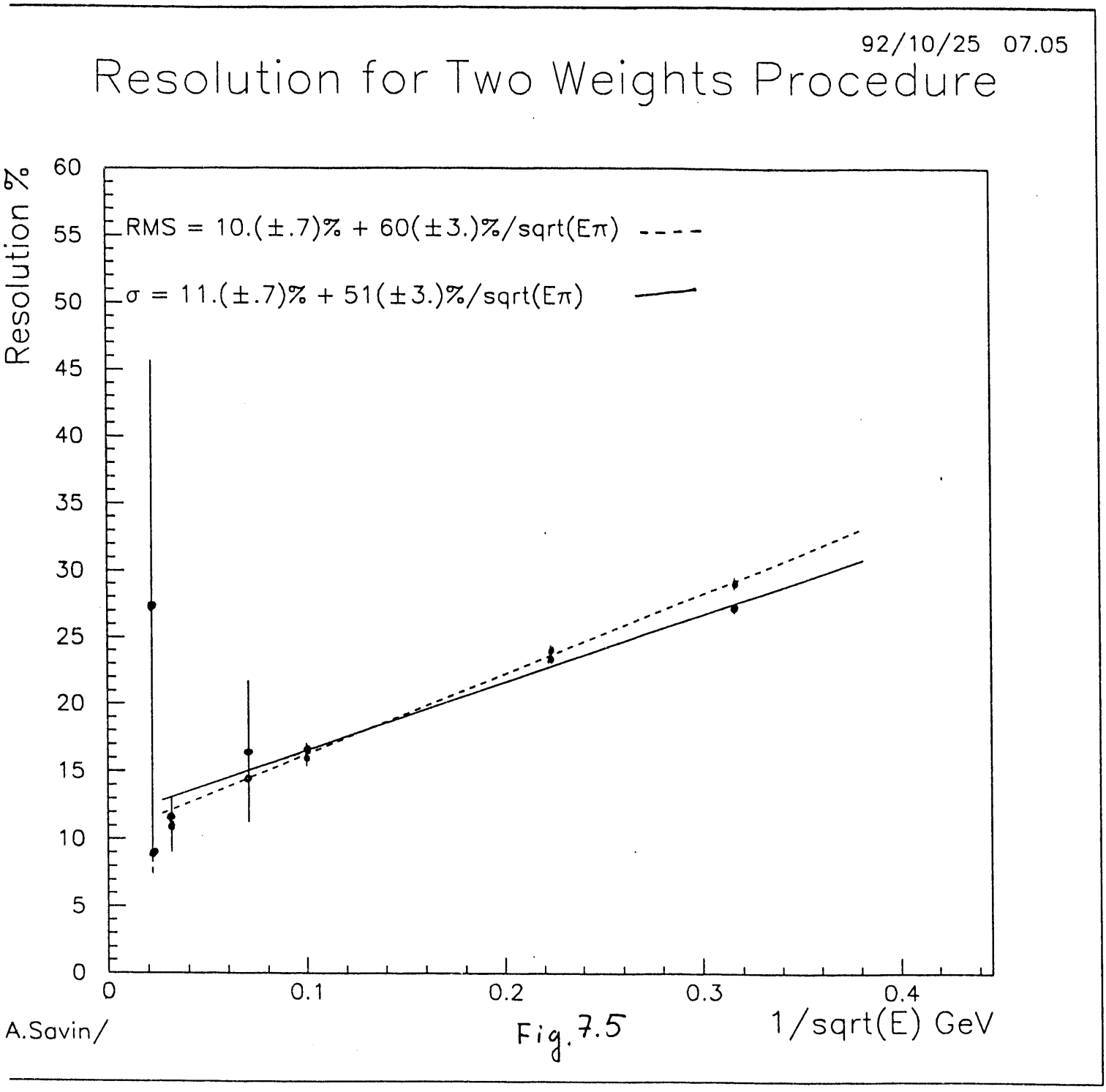
92/10/25 07.05
Resolution for Two Weights Procedure
Resolution %
RMS = 10.(±.7)% + 60(±3.)%/sqrt(Eπ)
σ = 11.(±.7)% + 51(±3.)%/sqrt(Eπ)
0
5
10
15
20
25
30
35
40
45
50
55
60
0
0.1
0.2
0.3
0.4
1/sqrt(E) GeV
A.Savin/

Fig. 7.5

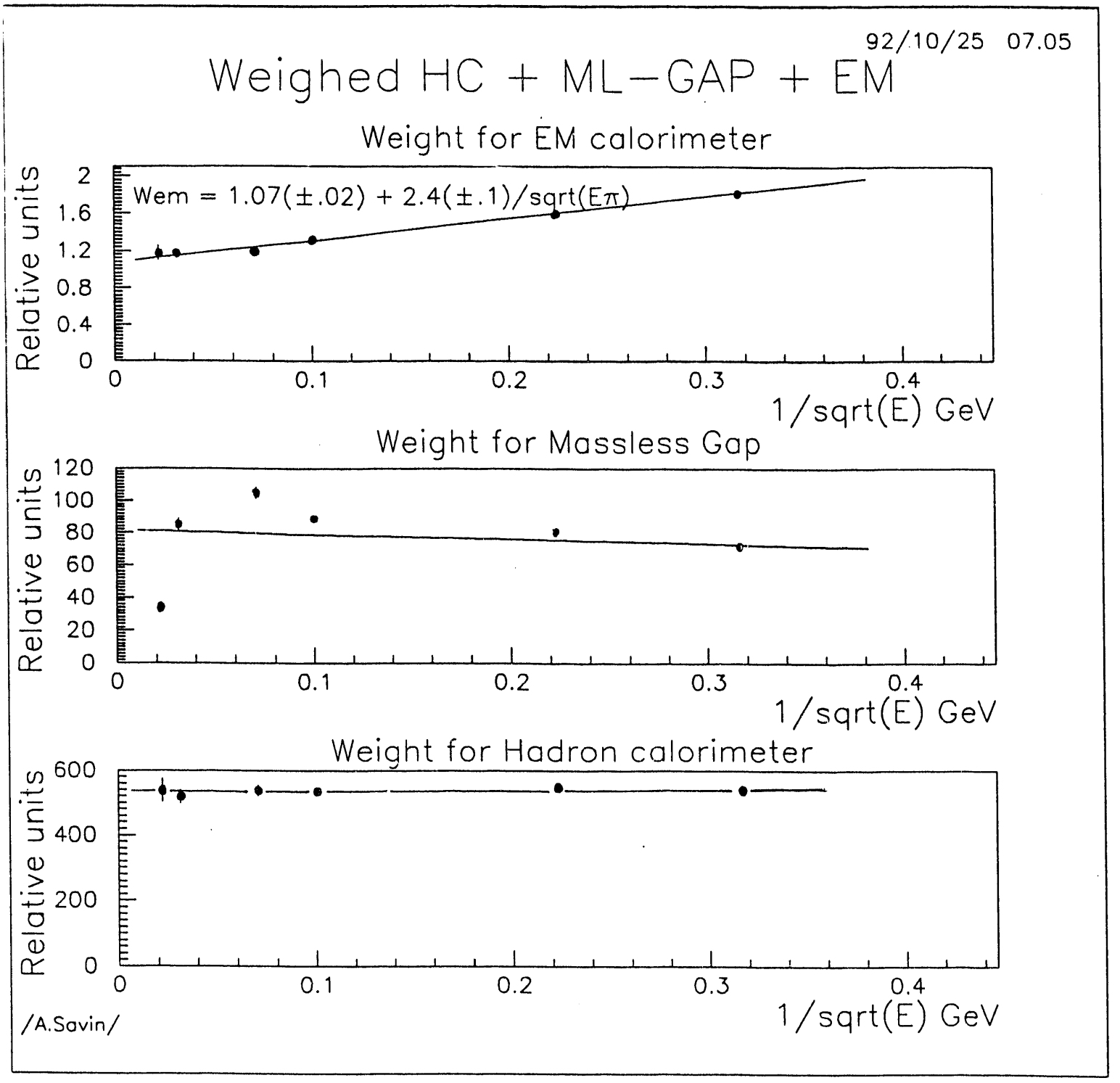
92/10/25 07.05
Weighed HC + ML−GAP + EM
Weight for EM calorimeter
Wem = 1.07(±.02) + 2.4(±.1)/sqrt(Eπ)
Relative units
2
1.6
1.2
0.8
0.4
0
0
0.1
0.2
0.3
0.4
1/sqrt(E) GeV
Weight for Massless Gap
Relative units
120
100
80
60
40
20
0
0
0.1
0.2
0.3
0.4
1/sqrt(E) GeV
Weight for Hadron calorimeter
Relative units
600
400
200
0
0
0.1
0.2
0.3
0.4
1/sqrt(E) GeV
/A.Savin/

Fig. 7.6

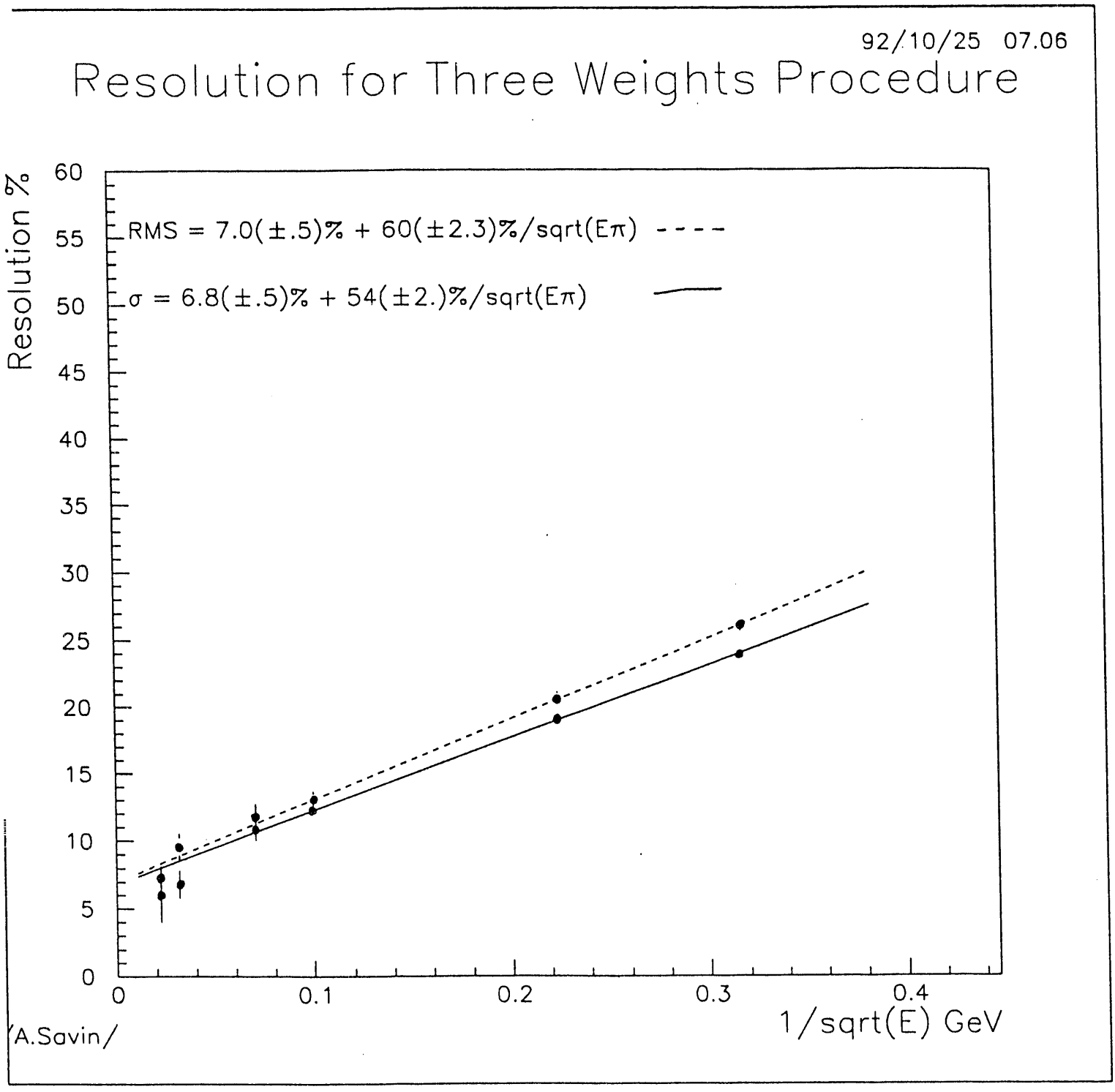
92/10/25 07.06
Resolution for Three Weights Procedure
Resolution %
RMS = 7.0(±.5)% + 60(±2.3)%/sqrt(Eπ)
σ = 6.8(±.5)% + 54(±2.)%/sqrt(Eπ)
60
55
50
45
40
35
30
25
20
15
10
5
0
0
0.1
0.2
0.3
0.4
1/sqrt(E) GeV
'A.Savin/

Fig. 7.7

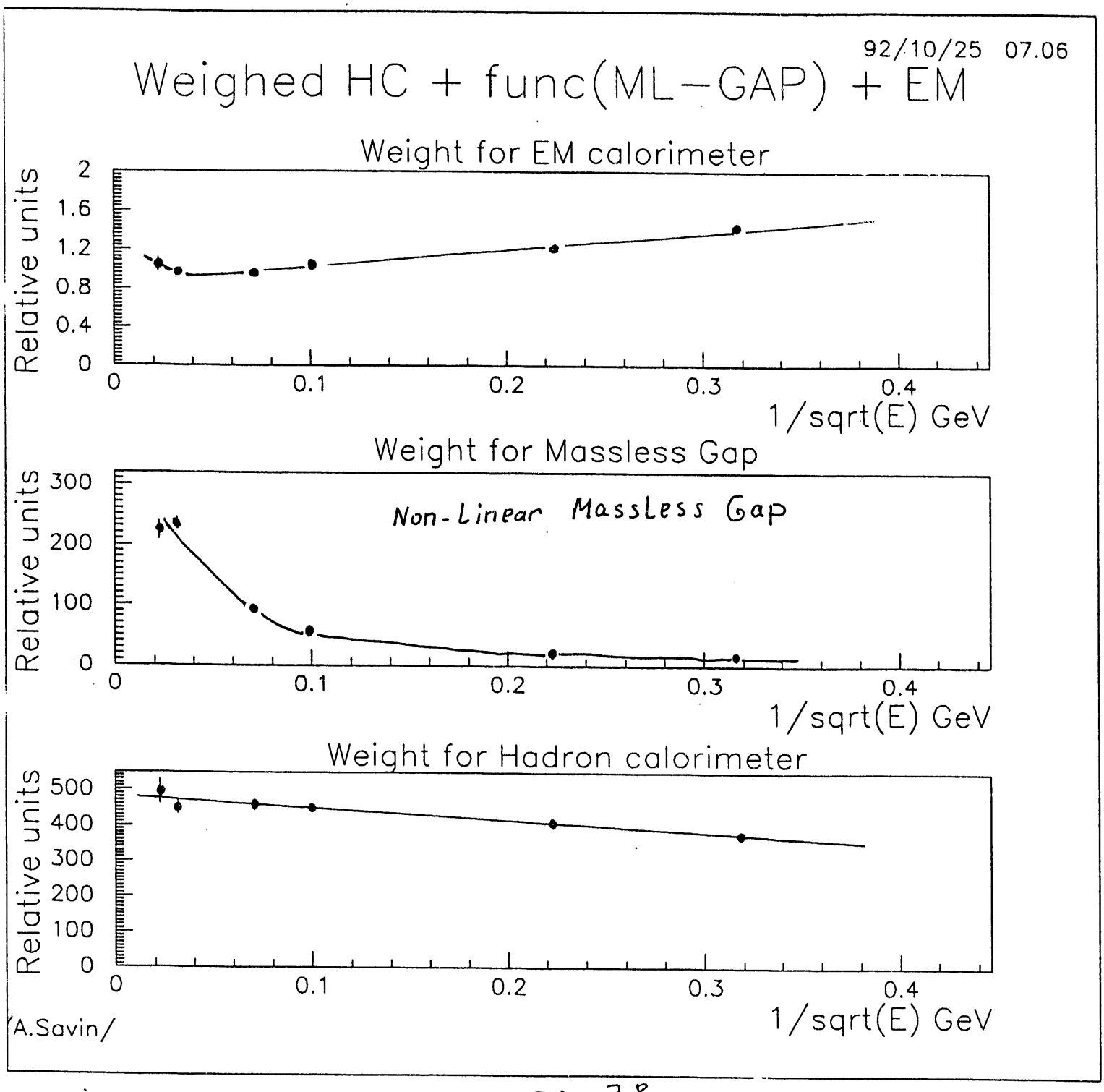
92/10/25 07.06
Weighed HC + func(ML−GAP) + EM
Weight for EM calorimeter
Relative units
2
1.6
1.2
0.8
0.4
0
0
0.1
0.2
0.3
0.4
1/sqrt(E) GeV
Weight for Massless Gap
Non-Linear Massless Gap
Relative units
300
200
100
0
0
0.1
0.2
0.3
0.4
1/sqrt(E) GeV
Weight for Hadron calorimeter
Relative units
500
400
300
200
100
0
0
0.1
0.2
0.3
0.4
1/sqrt(E) GeV
/A.Savin/

Fig. 7.8

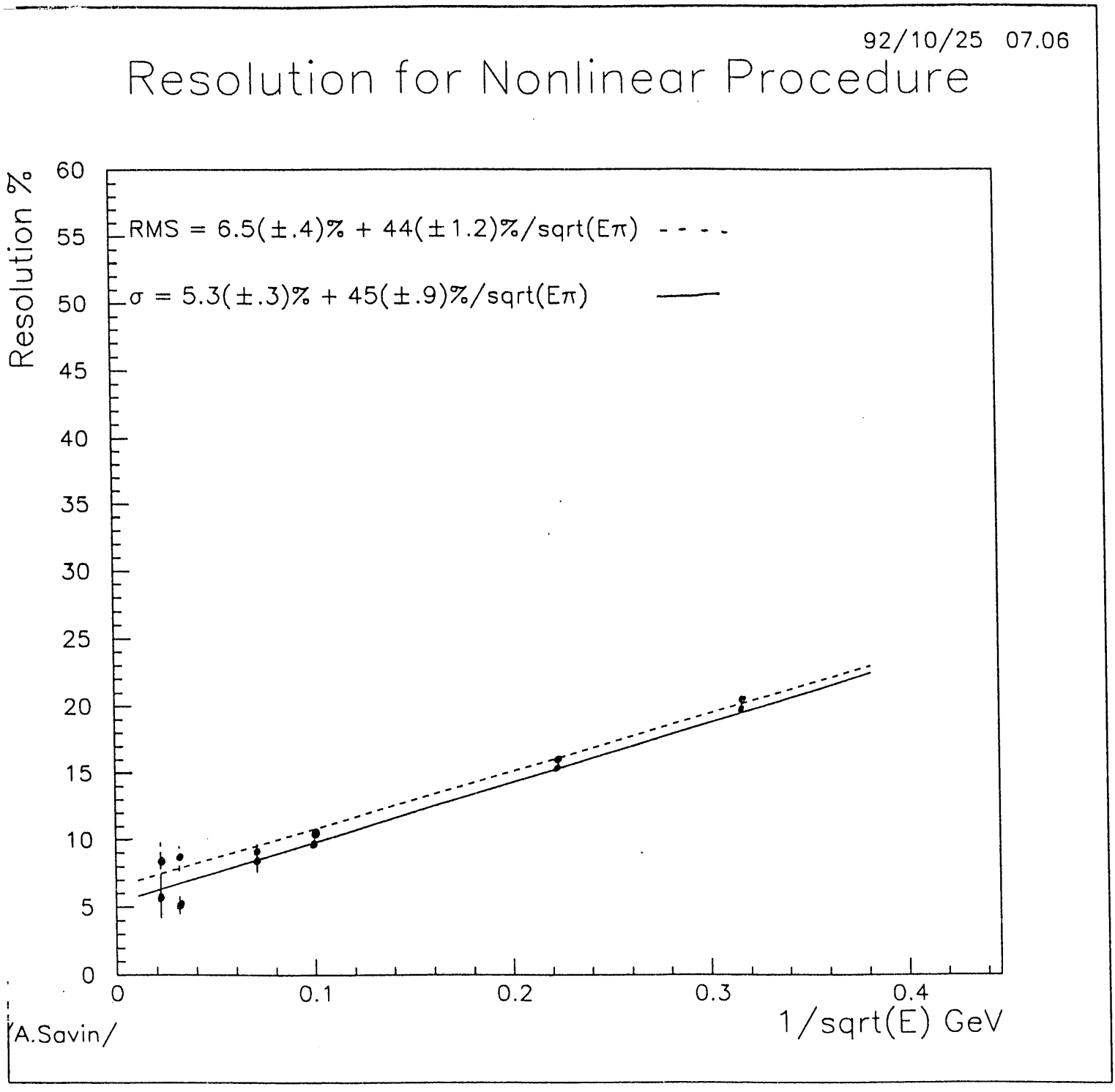
92/10/25 07.06
Resolution for Nonlinear Procedure
Resolution %
RMS = 6.5(±.4)% + 44(±1.2)%/sqrt(Eπ)
σ = 5.3(±.3)% + 45(±.9)%/sqrt(Eπ)
60
55
50
45
40
35
30
25
20
15
10
5
0
0
0.1
0.2
0.3
0.4
1/sqrt(E) GeV
A.Savin/

Fig. 7.9.

## 8.Cherenkov Quartz fibers calorimeter - Electrons,Pions,Jets and Muons.

Response of Cherenkov fibers as function of particle speed, inrinsic angle and impact parameter was calculated by E.Tarkovsky.

Electrons, Pions, Muons and Jets 10 and 100 GeV are under generation for Cu/Quartz Fibers calorimeter. Diameter 1mm was choosen for fibers. Concentration of fibers was 20%, 10% and 3% of volume . For 20% and 3% fibers were parallel to incident particle, for 10% fibers were pitched to 1 degree.

Preliminary results :

Responce for electrons (Fig.8.1) about 2.*R(%)p.e/GeV,
where R - volume % of fibers in calorimeter
Resolution for electrons varies from 2.4%+56%/sqrt(E) for 3% volume fibers
to 0.8%+18%/sqrt(E) for 20% volume fibers.

Responce for pions (Fig.8.2) about 1.2*R(%)p.e/GeV,
Resolution for pions is weekly dependent on finer density and
is about 18%+(34-37)%/sqrt(E)

Responce for jets (Fig.8.3) about 1.4*R(%)p.e/GeV,
Resolution for jets is weekly dependent on finer density and
is about 18%+(34-37)%/sqrt(E)

Some non-linearity is seen between 10 and 100 GeV .

To be studied : More energy points to be generated to understand non-linearity and energy resolution dependance vs energy. Angle variations and other absorbers are to be tested.

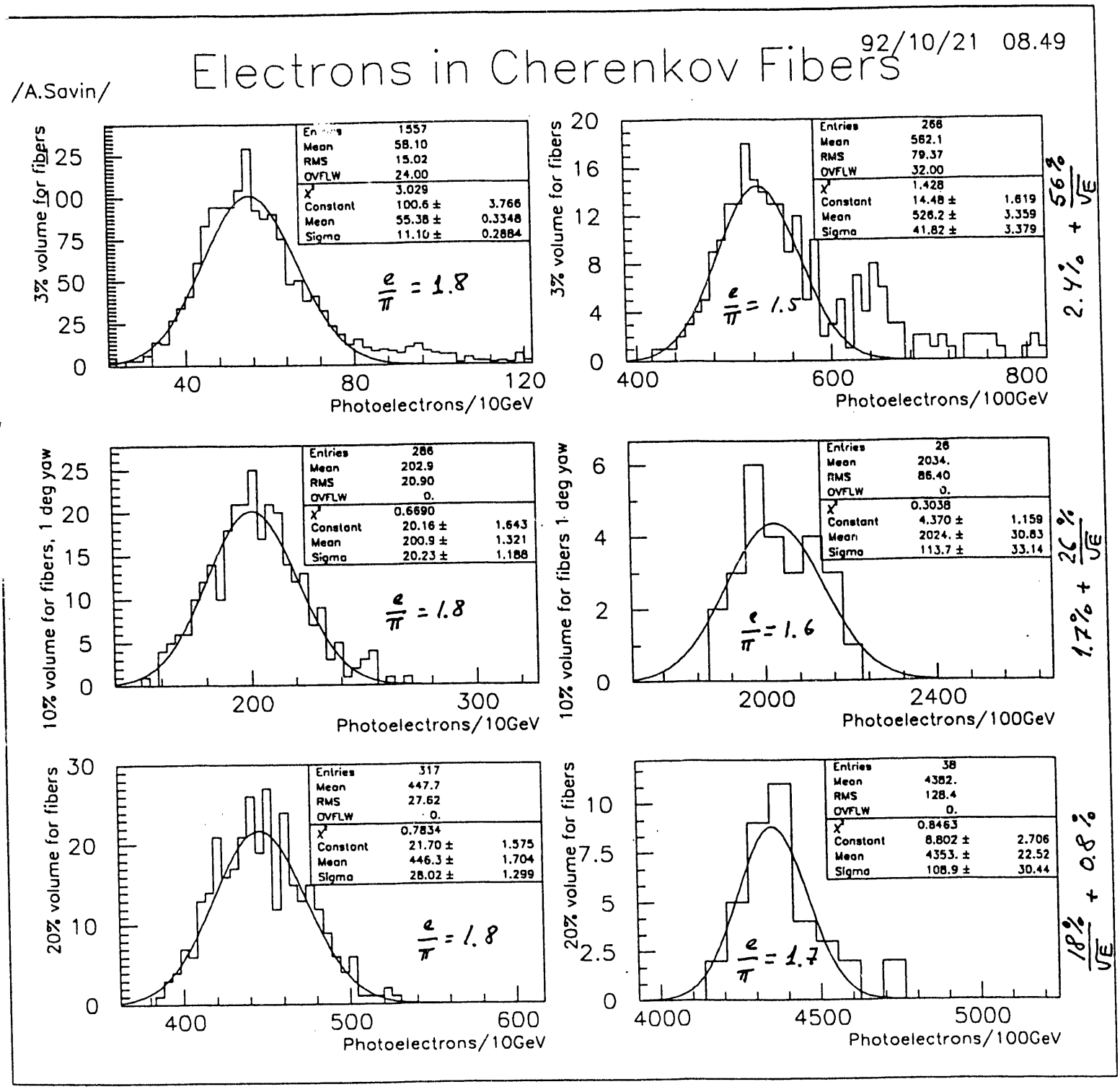
92/10/21 08.49
Electrons in Cherenkov Fibers
/A.Savin/
3% volume for fibers
Entries 1557
Mean 58.10
RMS 15.02
OVFLW 24.00
χ² 3.029
Constant 100.6 ± 3.766
Mean 55.38 ± 0.3348
Sigma 11.10 ± 0.2884
e/π = 1.8
Photoelectrons/10GeV
3% volume for fibers
Entries 268
Mean 562.1
RMS 79.37
OVFLW 32.00
χ² 1.428
Constant 14.48 ± 1.619
Mean 526.2 ± 3.359
Sigma 41.82 ± 3.379
e/π = 1.5
Photoelectrons/100GeV
2.4% + 56%/√E
10% volume for fibers, 1 deg yaw
Entries 286
Mean 202.9
RMS 20.90
OVFLW 0.
χ² 0.6690
Constant 20.16 ± 1.643
Mean 200.9 ± 1.321
Sigma 20.23 ± 1.188
e/π = 1.8
Photoelectrons/10GeV
10% volume for fibers 1 deg yaw
Entries 26
Mean 2034.
RMS 86.40
OVFLW 0.
χ² 0.3038
Constant 4.370 ± 1.159
Mean 2024. ± 30.83
Sigma 113.7 ± 33.14
e/π = 1.6
Photoelectrons/100GeV
1.7% + 26%/√E
20% volume for fibers
Entries 317
Mean 447.7
RMS 27.62
OVFLW 0.
χ² 0.7834
Constant 21.70 ± 1.575
Mean 446.3 ± 1.704
Sigma 28.02 ± 1.299
e/π = 1.8
Photoelectrons/10GeV
20% volume for fibers
Entries 38
Mean 4382.
RMS 128.4
OVFLW 0.
χ² 0.8463
Constant 8.802 ± 2.706
Mean 4353. ± 22.52
Sigma 108.9 ± 30.44
e/π = 1.7
Photoelectrons/100GeV
18%/√E + 0.8%

Fig. 8.1

/A.Savin/

# Pions in Cherenkov Fibers

92/10/21 08.50

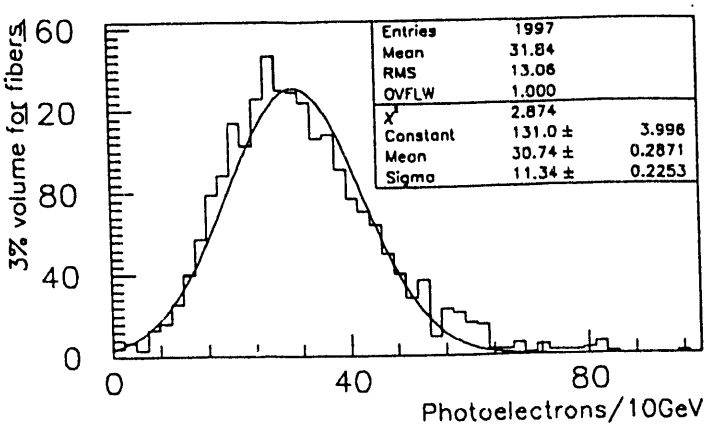


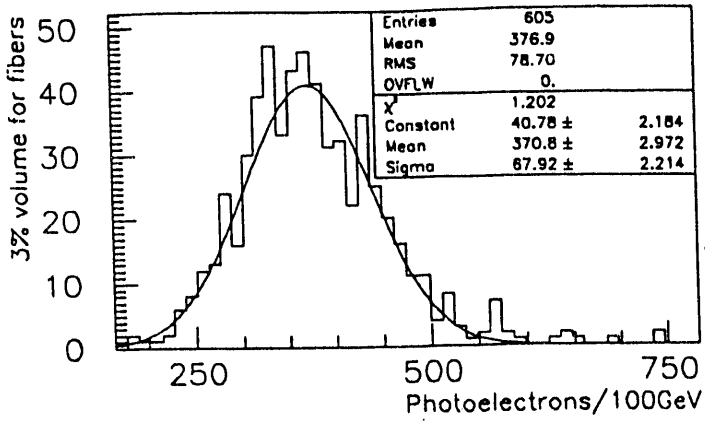


$\frac{88\%}{\sqrt{E}} + 10\%$

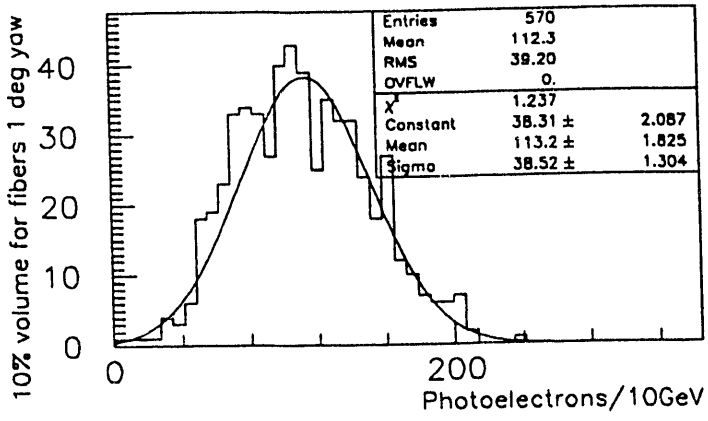


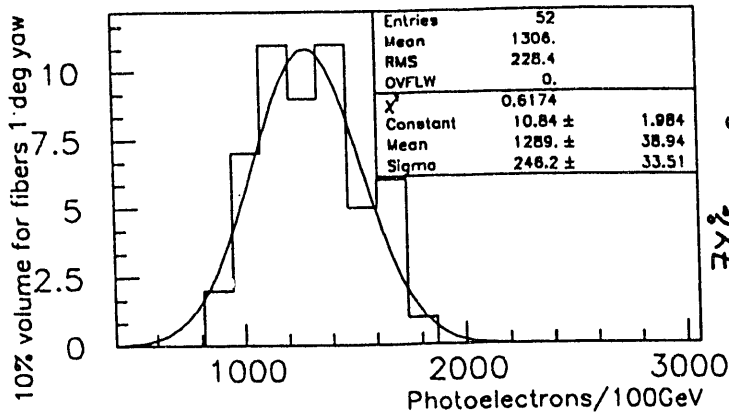


$\frac{74\%}{\sqrt{E}} + 10\%$

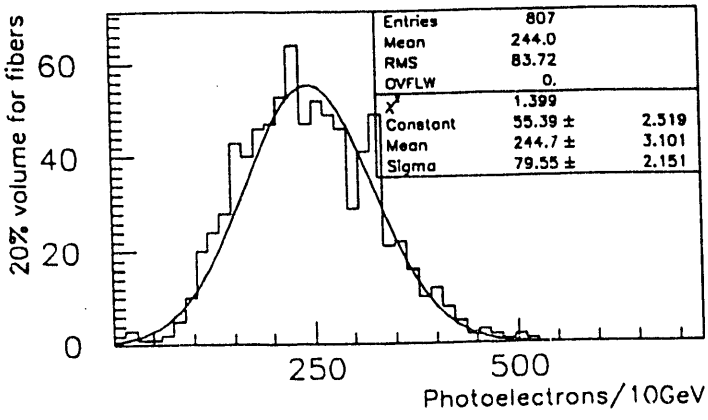


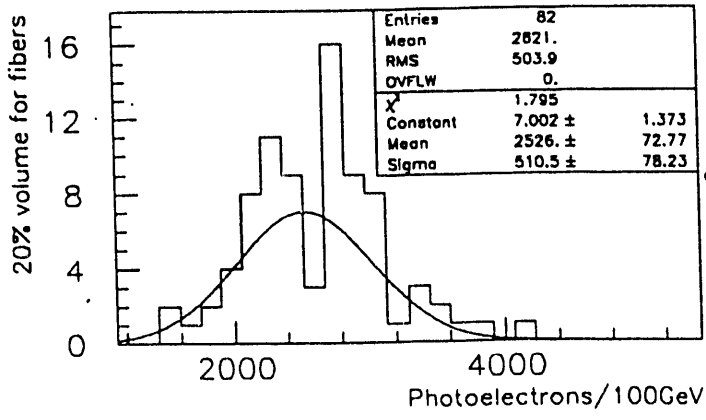


$\frac{70\%}{\sqrt{E}} + 10\%$

Fig. 8.2

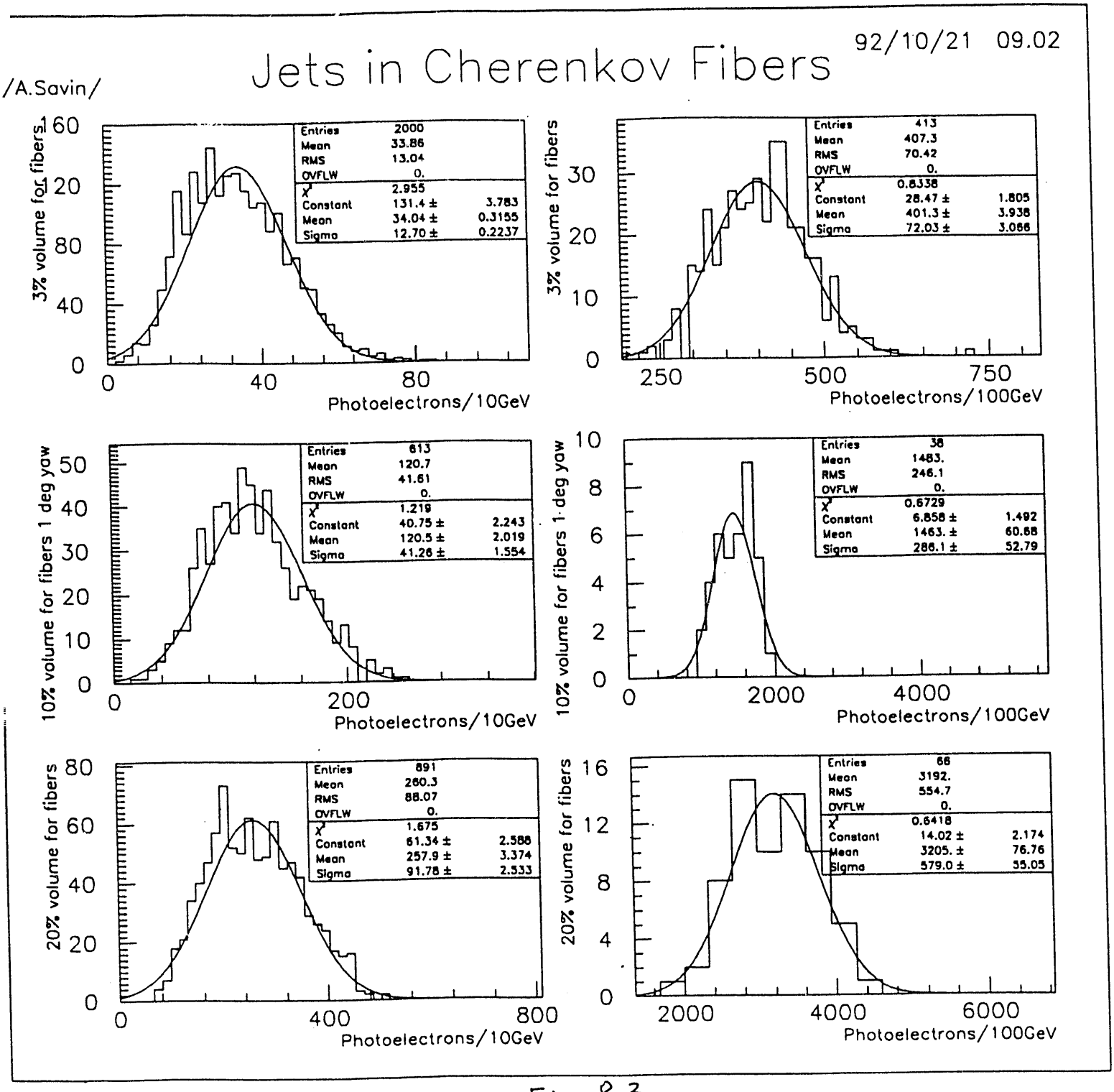
Jets in Cherenkov Fibers
92/10/21 09.02
/A.Savin/
3% volume for fibers
Entries 2000
Mean 33.86
RMS 13.04
OVFLW 0.
χ² 2.955
Constant 131.4 ± 3.783
Mean 34.04 ± 0.3155
Sigma 12.70 ± 0.2237
Photoelectrons/10GeV
3% volume for fibers
Entries 413
Mean 407.3
RMS 70.42
OVFLW 0.
χ² 0.8338
Constant 28.47 ± 1.805
Mean 401.3 ± 3.938
Sigma 72.03 ± 3.066
Photoelectrons/100GeV
10% volume for fibers 1 deg yaw
Entries 613
Mean 120.7
RMS 41.61
OVFLW 0.
χ² 1.219
Constant 40.75 ± 2.243
Mean 120.5 ± 2.019
Sigma 41.26 ± 1.554
Photoelectrons/10GeV
10% volume for fibers 1 deg yaw
Entries 38
Mean 1483.
RMS 246.1
OVFLW 0.
χ² 0.6729
Constant 6.858 ± 1.492
Mean 1463. ± 60.68
Sigma 286.1 ± 52.79
Photoelectrons/100GeV
20% volume for fibers
Entries 891
Mean 260.3
RMS 88.07
OVFLW 0.
χ² 1.675
Constant 61.34 ± 2.588
Mean 257.9 ± 3.374
Sigma 91.78 ± 2.533
Photoelectrons/10GeV
20% volume for fibers
Entries 66
Mean 3192.
RMS 554.7
OVFLW 0.
χ² 0.6418
Constant 14.02 ± 2.174
Mean 3205. ± 76.76
Sigma 579.0 ± 55.05
Photoelectrons/100GeV

Fig. 8.3

## Plans for further simulations .

1. Fine tuning of GEANT3.15 for simulation of hadronic cascades in GEM calorimeter.

2. Study of electromagnetic leakages and losses in dead material for various geometries of calorimeter.

3. Application of massless gap detector (between EM and hadronic section) for jet energy correction.

4. Optimization of weighting procedure for EM calorimeter, massless gap and Hadron Calorimeter for individual hadrons, jets and electromagnetic leakages.

5. Simulation of theta-angular dependance of response in hadron calorimeter. Resolution and weighting procedure vs theta.

6. Continue study of Cherenkov quartz fibers calorimeter - study fiber angular dependances, optimisation of absorber and fibers structure (core/cladding refractive indexes, diameter).

7. Parametrization of jets/hadrons response and resolution in GEM calorimetry system. Parametrization of theta-dependance of calorimeter response and realistic simulation of cracks and dead regions.

8. Application of this parametrization to fast simulation . Study of calorimeter potential for various physical processes: decays with WW pairs, Z′ and heavy HO.

# APPENDIX D

## SSC R&D
## Paper on Basic Mechanisms

# Fast Neutron-Induced Changes in Net Impurity Concentration of High-Resistivity Silicon

I. Tsveybak and W. Bugg
University of Tennessee*, Knoxville, TN

J. A. Harvey
Oak Ridge National Laboratory**, Oak Ridge, TN

J. Walter
IntraSpec Inc., Oak Ridge, TN

*Abstract*

Resistivity changes produced by 1 Mev neutron irradiation at room temperature have been measured in float-zone grown n and p-type silicon with initial resistivities ranging from 1.8 to 100 kΩcm. Observed changes are discussed in terms of net electrically active impurity concentration. A model is presented which postulates escape of Si self-interstitials and vacancies from damage clusters and their subsequent interaction with impurities and other pre-existing defects in the lattice. These interactions lead to transfer of B and P from electrically active substitutional configurations into electrically inactive positions ($B_i$, $P_i$, and E-center), resulting in changes of net electrically active impurity concentration. The changes in spatial distribution of resistivity are discussed, and the experimental data are fit by theoretical curves. Differences in the behavior of n-type and p-type material are explained on the basis of a faster removal of substitutional P and a more nonuniform spatial distribution of the original P concentration.

## I. Introduction

Fast neutron damage in silicon radiation detectors shows up as compensation level changes, increases in leakage current and its associated noise, and decreases in charge collection efficiency. Recent studies demonstrate that in spite of a progressive increase in leakage current and deterioration of charge collection efficiency with radiation dose, silicon detectors can survive in some applications at fast neutron fluences up to $10^{15}$ cm$^{-2}$ [1] as long as they retain their ability to be totally depleted.
The depletion depth in a Si diode detector is given by:

$$W=3.63\cdot 10^{7}\left[\frac{U}{|N|}\right]^{\frac{1}{2}} \qquad (1)$$

$$N=N_d-N_a \qquad (2)$$

where W is the depletion depth in μm, U the reverse bias in volts, N the net impurity concentration in cm$^{-3}$, $N_d$ the donor concentration, and $N_a$ the acceptor concentration. To achieve optimum characteristics, detectors are usually operated in a totally depleted mode. According to Eq.(1), the voltage required for total depletion depends on the detector's thickness and the net impurity concentration. For the example of a 400 μm thick totally depleted detector, N should not exceed $10^{12}$cm$^{-3}$ if the bias voltage is to remain under 200 volts. Also, major spatial variations in N can cause a non-uniform distribution of field strength in the depletion region of a radiation detector. Consequently, radiation damage induced changes in N can constitute a major problem for radiation detectors.

High resistivity float-zone (FZ) Si used for radiation detector production is usually highly compensated, i.e. it contains both shallow donors (P) and acceptors (B) in quantities much larger than the net impurity concentration. It also contains oxygen and other background defects which are electrically inactive in non-irradiated crystals. Fast neutron radiation damage of Si at room temperature leads to: i) a decrease in the net impurity concentration [2, 3, 4], ii) changes in the spatial distribution of resistivity [5], iii) lowering of carrier mobility [3, 6], iv) formation of oxygen-vacancy complexes [7, 8, 9], and v) introduction of deep levels, such as divacancies and E-centers [3, 9, 10], which show up as generation-recombination centers [11]. In the general case, experimentally observed changes in the electrical properties of Si may represent the result of superposition of all of these processes.

Radiation damage in high purity Si occurs when scattering interactions result in the displacement of Si atoms from their normal sites in the lattice, resulting in the creation of Frenkel pairs. In the case of high energy neutrons, the energy transfer can be large enough to result in a cascade of displacements which form a primary damage cluster [12, 13]. If the average energy of incident neutrons is about 1 MeV, the average energy transmitted to a Si atom per neutron collision is about 50 to 70 keV [14, p.337]. This energetic Si atom is able to produce about 1000 displacements [12] in a region with a size of about

1000 A° [14, p.382]. The primary displacement defects in the damage cluster are Si self-interstitials ($Si_i$) and vacancies (V), produced originally in equal numbers. These primary defects are essentially unstable and quickly disappear via secondary interactions; mainly by self-annihilation, but in some cases by interactions with other defects. Finally, after a short period of thermal stabilization, the damage cluster represents a disordered crystalline region with a high concentration of lattice defects.

Several models have been previously proposed to explain radiation damage induced changes in the resistivity of Si. These models are discussed below, and in Section II we posit a simpler quantitative model based on direct interactions between the primary damage induced defects and the doping impurities in the Si.

### *A. The Model of Terminal Clusters*

This model [15, 16] was created to explain "carrier removal" and mobility drop in neutron damaged low resistivity Ge and Si. The model postulates that a typical concentration of lattice defects within the disordered region is about $5 \cdot 10^{18}$ $cm^{-3}$, with their energy levels close to the middle of the band-gap. The difference in the position of the Fermi level inside and outside the cluster produces a spherical space charge region which insulates the disordered region from the matrix. The presence of insulated regions will decrease the measured values of the conductivity ($\sigma$) and mobility ($\mu$). The effect of "insulating voids" leads to the following expressions for conductivity and mobility from Ref.[17]:

$$\mu^M = \mu \frac{1 - \frac{f}{4}}{1 + \frac{f}{4}} \qquad (3)$$

$$\sigma^M = \sigma \frac{1 - f}{1 + \frac{f}{2}} \qquad (4)$$

where $\sigma^M$ and $\mu^M$ are measured values, and f is the fraction of the total volume occupied by "voids".

Lately this model became a subject of criticism [22]. Considering the subcluster pattern of the damaged region and size of the subclusters, the ability of this region to trap free carriers seems significantly overestimated. In fact, a simple calculation shows that each subcluster is able to capture only 1 or 2 carriers at most [22]. Therefore one can reasonably conclude that at the relatively small fast neutron fluences in these experiments, formation of the damage clusters would not affect carrier concentration [2, 3, 18, 19].

### *B. The Model of Deep Level Introduction*

Deep levels introduced into the silicon band-gap by fast neutrons have been the subject of much attention [9, 12, 20, 21, 22]. The existence of deep levels has been used for a qualitative [9, 20] and quantitative [22] explanation of observed "carrier removal". According to the model, the deep levels created by fast neutron irradiation serve as traps for majority carriers, driving the Fermi level closer to the middle of the band-gap. Trapped carriers convert the trapping centers into fixed charge scattering centers which reduce the mobility of the remaining carriers. For n-type silicon, these effects are described by the formula [22]:

$$\sigma = \sigma_0 \left(1 - K_1 \Phi - \frac{2 K_{dv} \Phi}{1 + K_{dv} \Phi}\right) \qquad (5)$$

where $\sigma$ is conductivity, $K_1$ and $K_{dv}$ are introduction rates of divacancy and "donor-vacancy" trapping centers.

Deep levels behave as generation-recombination centers and represent the major source of G-R noise and leakage current in Si diode detectors. As to the net impurity concentration, the deep levels may not represent the major reason for its change. Carrier trapping should depend strongly on the mutual positioning of the Fermi level and the trap level. In high-resistivity Si the Fermi level before irradiation is already positioned close to the level of introduced traps, and N may not be affected by them. On the other hand, formation the deep level E-center ($P_s$-V complex) always requires removal of one shallow donor. Based on this we come to the conclusion that interactions between defects and impurities rather than trapping may be involved in changes in the compensation level.

The model of "carrier removal" due to the introduction of deep levels is based on assumptions which are confirmed neither by a rigorous calculation of the Fermi level position nor by investigation of the electron structure of the proposed defects. This model is especially misleading in the case of high-resistivity silicon, where the Fermi level is already located close to the middle of the band-gap.

Both of the preceding models also fail to explain a spatially non-uniform distribution of resistivity changes in damaged Si.

## II. Model of Compensation Level Changes: Direct Interaction of Radiation Induced Lattice Defects with Impurities

Although both of the preceding models may have significance for low-resistivity Si at high damage levels, they do not fit the data for high-resistivity Si at low damage levels. In addition, they are unnecessarily vague and complex. We propose an alternative model based on the well established facts that the primary displacement defects ($Si_i$ and V) are mobile at room temperature and some of them (referred to herein as "free") are able to migrate out

of damage clusters and participate in direct reactions with impurities and other defects already present in the lattice [5, 23].

*A. Free Si Self-Interstitials*

The enthalpy of formation of a $Si_i$ is about 4-4.5 eV [24], and it is essentially non-equilibrium and reactive. $Si_i$'s are highly mobile at room temperature and are able to eject both B and P from substitutional into interstitial positions [23, 25, 26, 27] according to following reactions:

$$Si_i + B_s \rightarrow Si_s + B_i \qquad (6)$$

$$Si_i + P_s \rightarrow Si_s + P_i \qquad (7)$$

In fact, $Si_i$ migrates athermally and is so-unstable that it has never been detected, even at liquid He temperatures [23, 24]. Our model postulates that both B and P ejected into the interstitial position are electrically inactive. Consequently, the reactions (6) and (7) change the net impurity concentration. The model also postulates that there are other sinks for $Si_i$ and V. These sinks may be other substitutional impurities, free vacancies, radiation damage clusters, pre-existing defect clusters, dislocations, and crystal surfaces. We assume that reactions between free self-interstitials and these other sinks have no direct effect on the net impurity concentration. Thus, after escaping from the primary damage cluster, a $Si_i$ has a two-fold choice: to affect the net impurity concentration by interaction with $B_s$ and $P_s$, or to vanish into the other sinks without changing the net impurity concentration. The equations which express the rate of conversion of $B_s$ and $P_s$ to electrically inactive $B_i$ and $P_i$ are:

$$dN_B = -\frac{N_B\sigma_B}{N_B\sigma_B + N_P\sigma_P + A_i}\gamma_i d\Phi \qquad (8)$$

$$dN_P = -\frac{N_P\sigma_P}{N_B\sigma_B + N_P\sigma_P + A_i}\gamma_i d\Phi \qquad (9)$$

where $N_B$ and $N_P$ [$cm^{-3}$] are the concentrations of B and P in substitutional positions (electrically active B and P), $\sigma_B$ and $\sigma_P$ [$cm^2$] the cross-sections for $Si_i$ to be captured by $B_s$ and $P_s$, $\gamma_i$ [$cm^{-1}$] the yield of free $Si_i$ (number of free self-interstitials produced per one incident neutron), $\Phi$ [$cm^{-2}$] the neutron fluence and $A_i$ [$cm^{-1}$] the probability (in events per cm) for a free $Si_i$ to be captured by other sinks. $A_i$ may vary with the neutron dose and depend on pre-existing defects in the Si crystal. However, we will restrict our present analysis with assumption that $A_i$ is a constant.

The multi-term denominators in equations (8) and (9) reflect the fact that only a limited number of free $Si_i$ are produced during irradiation, and crystal defects (both impurities and other lattice defects) compete to capture them.

The main simplifying assumption for the case of high-resistivity Si is that the concentrations of B, P, and O are low, and therefore the probability of free $Si_i$ or vacancies interacting with B, P, and O is much less than the probability of their vanishing into the other sinks. Thus, the equations (8) and (9) can be simplified to:

$$dN_B = -\frac{N_B\sigma_B\gamma_i}{A_i} d\Phi \qquad (10)$$

$$dN_P = -\frac{N_P\sigma_P\gamma_i}{A_i} d\Phi \qquad (11)$$

*B. Free Vacancies*

The enthalpy of formation of V is about 2.5 to 3 eV [24]. V is mobile at room temperature and able to interact with impurities, form divacancies and vacancy clusters by interaction with other vacancies, annihilate with $Si_i$, and disappear on the crystal surface. An interaction between a V and a $B_i$ leads to the formation of an unstable complex which self anneals below room temperature [23] by the reaction:

$$B_i + V \rightarrow [B_i - V] \rightarrow B_s \qquad (12)$$

This reaction restores $B_s$ and therefore affects the net impurity concentration. Interaction between a V and a $P_s$ leads to the formation of an E-center, which is stable at room temperature:

$$P_s + V \rightarrow [P_s - V] \qquad (13)$$

This reaction removes one shallow donor from the Si forbidden gap and therefore affects N. In high-resistivity Si, the Fermi level is positioned close to the level of the E-center. Therefore, we shall ignore the effect of the E-center on the Fermi level.

Interactions between interstitial oxygen and free vacancies may comprise reactions of first, second, and third order:

$$O_i + V \rightarrow O_s \qquad (14)$$

$$O_s + V \rightarrow [O_s^+ V^-] \qquad (15)$$

$$[O_s^+ V^-] + V \rightarrow [O_s^{2+} V^-] + V^- \qquad (16)$$

Reaction (14) describes formation of an A-center. In the forbidden gap of high-resistivity Si the electron trap level of the A-center is above the Fermi level, therefore, we postulate that its formation can not directly affect N. The second order reaction (15) and the third order reaction (16) describe formation of oxygen-related shallow donors. For the sake of simplicity, we treat formation of oxygen-vacancy complex donors as a reaction of the second order. Thus, a free vacancy has a two-fold choice: to affect the net impurity concentration by reactions with $P_s$, $B_i$, and $O_i$, or to disappear by reactions with other species without changing N. The equation describing formation of E-center is:

$$dN_P = -\frac{N_P \alpha_P \gamma_V}{A_V} d\Phi \qquad (17)$$

The equation describing recovery of $B_s$ is:

$$dN_B = \frac{(N_B^0 - N_B)\, \alpha_B \gamma_V}{A_V} d\Phi \qquad (18)$$

The equations for oxygen-related donor formation are:

$$dN_{O_i} = -\frac{N_{O_i} \alpha_{O_i} \gamma_V}{A_V} d\Phi \qquad (19)$$

$$dN_{O_s} = -\frac{N_{O_s} \alpha_{O_s} \gamma_V}{A_V} d\Phi - dN_{O_i} \qquad (20)$$

where $N_{Oi}$ and $N_{Os}$ are the concentrations of O in interstitial and substitutional positions, $\alpha$'s are the free vacancy capture cross-sections, $\gamma_v$ the yield of free vacancies, and $A_v$ the probability (in events per cm) for a free vacancy to be captured by other species without changing the net impurity concentration. Similarly to $A_i$, we shall treat $A_v$ as a constant.

Equations (10), (11), and (17) - (20) form a closed system which describes the change of net electrically active impurity concentration during irradiation as a result of the direct interaction between impurities and free displacement defects. Solving of these equations yields the following functions for $P_s$, $B_s$, and oxygen-related donors.

For phosphorus:

$$N_P = N_P^0 e^{-\beta_P \Phi} \qquad (21)$$

$$\beta_P = \frac{\sigma_P \gamma_i}{A_i} + \frac{\alpha_P \gamma_V}{A_V} \qquad (22)$$

For boron:

$$N_B = N_B^0 \frac{\beta_{B,V} + \beta_{B,i} e^{-\beta_B \Phi}}{\beta_B} \qquad (23)$$

$$\beta_{B,V} = \frac{\alpha_B \gamma_V}{A_V}; \; \beta_{B,i} = \frac{\sigma_B \gamma_i}{A_i}; \qquad (24)$$

$$\beta_B = \beta_{B,V} + \beta_{B,i} \qquad (25)$$

where $\sigma_B$ [cm$^2$] represent the cross-section for $Si_i$ to be captured by $B_s$ and $\alpha_B$ is the free vacancy capture cross-section by $B_i$. For oxygen-related donors:

$$N_{O_d} = N_O^0 \left(1 - \frac{\beta_{O_i} e^{-\beta_{O_s}\Phi} - \beta_{O_s} e^{-\beta_{O_i}\Phi}}{\beta_{O_i} - \beta_{O_s}}\right) \qquad (26)$$

$$\beta_{O_i} = \frac{\alpha_{O_i} \gamma_V}{A_V}; \; \beta_{O_s} = \frac{\alpha_{O_s} \gamma_V}{A_V} \qquad (27)$$

where $\alpha$'s represent cross-sections for a free vacancy to be captured by interstitial and substitutional oxygen.

Equations (21) and (23) predict an exponential decrease in concentrations of electrically active substitutional P and B removed during reactions of the first order.

Creation of oxygen-related donors is a second order reaction which requires accumulation of substitutional oxygen. Equation (26) predicts slow introduction of oxygen-related donors at low neutron fluences and acceleration of this process at the higher fluences. The conductivity of the silicon with higher oxygen content may eventually be driven to n-type by oxygen related donor formation. It is believed that the oxygen content in FZ Si is relatively low. However, detectors which are oxide passivated may have high concentrations of oxygen diffused to significant distances from the surface during the oxidation step. We have previously suggested that oxygen donors generated in these regions by radiation damage may be responsible for the n-type layers observed in neutron damaged Si detectors [5, 32].

Information about the concentration and behavior of oxygen in FZ silicon crystals is insufficient to forecast its effect on carrier concentration. Therefore, we will limit our consideration to phosphorus and boron.

The dramatic effect of initial compensation level on the behavior of Si during irradiation is shown in Fig. 3 and 4. The heavier the compensation, the more pronounced is the initial net impurity concentration increase due to the fact that $P_s$ is lost more rapidly than $B_s$. Curves 2 and 3 in Fig. 3 and curves 3 and 4 in Fig. 4 demonstrate that improperly chosen compensation level may cause the carrier concentration to exceed useful limits. The result will be under-depletion and operational failure of the detector.

## III. Experimental Methods

The materials investigated in this study were high-resistivity silicon wafers, both n- and p-type, cut from float-zone (FZ) commercially grown crystals supplied by Topsil (n-type) and Wacker Siltronic (p-type and n-type). We also studied extra-high purity p-type crystals grown by multi-pass FZ refining (mpFZ) at the Westinghouse R&D center. The mpFZ crystals were expected to be higher purity, particularly in P content, and less compensated. The wafers were 50 to 76 mm in diameter, and 2 to 4 mm thick with both surfaces lapped. The resistivity of the samples prior to irradiation covered the range from 1.8 to 100 kΩcm. The properties of the starting crystals are listed in Table 1.

**Table I**

| Crystal code | Growth method | Vendor | Type, Dop. | ρ(KΩcm) 300 K | Diam. mm |
|---|---|---|---|---|---|
| 24802 | FZ | TOPSIL | n, P | 1.8 - 3.3 | 51 |
| 34383-1048 | FZ | WACKER | n, P | 5 - 10 | 77 |
| 34383-1090 | FZ | WACKER | p, B | 3.8 - 4.5 | 51 |
| FZT-4A-3 | FZ | WEST. | p | 20 - 100 | 76 |
| FZH-Q1-3 | FZ | WEST. | p | 12 - 43 | 71 |

Net impurity concentration changes produced by neutron irradiation were studied using d.c. four-point probe resistivity measurements at room temperature. A cryogenic thermoelectric probe was used to determine the conductivity type and distinguish between localized regions of high resistivity n- and p-type material. This probe uses a cold tip (200K) applied to room temperature Si sample in a dry atmosphere. The polarity of the voltage deflection in a high impedance electrometer is used to determine the conductivity type. Hall effect measurements with a magnetic-flux density of 2 kG were performed on some wafers at room temperature to verify the resistivity measurements.

The ORNL pulsed electron accelerator (ORELA) with a tantalum target was used as a fast neutron source with an average neutron energy close to 1 MeV. The source to sample distance was about 4 m, providing uniform illumination across the entire sample. The neutron fluence varied from $2\cdot10^{12}$ to $1.4\cdot10^{13}$n/cm$^2$ and the total time of radiation exposure varied from 48 to 72 hours. Up to 9 samples were irradiated at the same time to produce identical doses. A 2 cm thick lead shield was placed in front of the holder to maximize the neutron to γ ratio. The resulting n/γ ratio was not measured, but is believed to be high enough to justify neglecting the γ-related effects. All of the resistivity measurements were carried out within 3 to 48 hours after irradiation.

The total fluence (Φ) received by the wafers was calculated on the basis of the monitored heat power (Q) dissipated in the target during the irradiation. The fluence was calculated by the formula:

$$\Phi = \frac{\Psi Q}{4\pi r^2} e^{-\sigma_{Pb} N_{Pb} t} \qquad (28)$$

where Ψ is the flux to heat ratio ($1.0\cdot10^{12}$n s$^{-1}$·kWhr$^{-1}$, calculated by ORELA computer simulation), r is the distance between target and sample (4 m), $\sigma_{Pb}$ is the 1 Mev neutron scattering cross section of lead (6 b), $N_{PB}$ is the atomic density of lead and t the thickness of lead shield (2 cm). We used a silicon diode detector as a cross check on the neutron source calibration. The diode was irradiated together with the samples and its leakage current was measured and compared to the results from the luminosity calculations. The 300 μm thick, 5 x 5 mm detector was supplied by Brookhaven National Laboratory. The leakage current was measured at 20°C at a reverse bias of 100 V. The neutron fluence was calculated by the formula:

$$\Phi = \frac{I_L}{\alpha} \qquad (29)$$

where $I_L$ [Amp/cm$^3$] is the leakage current per unit of active (depleted) volume of detector, and α is the damage coefficient ($8\cdot10^{-17}$ A/cm for 1 Mev neutrons [28, 29]). The value of Ψ calculated on the basis of the detector's leakage current was $1.1\cdot10^{12}$n s$^{-1}$·kWhr$^{-1}$. This latter value, which agreed with the luminosity calculation within 10%, was used in the fluence calculations.

## IV. Results of Neutron Irradiation Experiments

### *A. p-Type Silicon*

The fast neutron damage induced changes in the resistivity of a p-type crystal grown by Westinghouse are shown in Fig. 5. For this crystal (with initial resistivity of 10 to 20 kΩcm) the resistivity increased to about 200 kΩcm after a fluence of $1.4\cdot10^{13}$ n/cm$^2$. For Wacker p-type crystals with an initial resistivity of 3 to 5 kΩcm, irradiation with a fluence of $1.4\cdot10^{13}$n/cm$^2$ produced an increase in resistivity to about 30 kΩcm. Hall effect measurements carried out on p-type Si crystals indicated only a slight drop in the hole mobility, so most of the increases in resistivity

of damage clusters and participate in direct reactions with impurities and other defects already present in the lattice [5, 23].

*A. Free Si Self-Interstitials*

The enthalpy of formation of a $Si_i$ is about 4-4.5 eV [24], and it is essentially non-equilibrium and reactive. $Si_i$'s are highly mobile at room temperature and are able to eject both B and P from substitutional into interstitial positions [23, 25, 26, 27] according to following reactions:

$$Si_i + B_s \rightarrow Si_s + B_i \qquad (6)$$

$$Si_i + P_s \rightarrow Si_s + P_i \qquad (7)$$

In fact, $Si_i$ migrates athermally and is so unstable that it has never been detected, even at liquid He temperatures [23, 24]. Our model postulates that both B and P ejected into the interstitial position are electrically inactive. Consequently, the reactions (6) and (7) change the net impurity concentration. The model also postulates that there are other sinks for $Si_i$ and V. These sinks may be other substitutional impurities, free vacancies, radiation damage clusters, pre-existing defect clusters, dislocations, and crystal surfaces. We assume that reactions between free self-interstitials and these other sinks have no direct effect on the net impurity concentration. Thus, after escaping from the primary damage cluster, a $Si_i$ has a two-fold choice: to affect the net impurity concentration by interaction with $B_s$ and $P_s$, or to vanish into the other sinks without changing the net impurity concentration. The equations which express the rate of conversion of $B_s$ and $P_s$ to electrically inactive $B_i$ and $P_i$ are:

$$dN_B = -\frac{N_B\sigma_B}{N_B\sigma_B + N_P\sigma_P + A_i}\gamma_i d\Phi \qquad (8)$$

$$dN_P = -\frac{N_P\sigma_P}{N_B\sigma_B + N_P\sigma_P + A_i}\gamma_i d\Phi \qquad (9)$$

where $N_B$ and $N_P$ [$cm^{-3}$] are the concentrations of B and P in substitutional positions (electrically active B and P), $\sigma_B$ and $\sigma_P$ [$cm^2$] the cross-sections for $Si_i$ to be captured by $B_s$ and $P_s$, $\gamma_i$ [$cm^{-1}$] the yield of free $Si_i$ (number of free self-interstitials produced per one incident neutron), $\Phi$ [$cm^{-2}$] the neutron fluence and $A_i$ [$cm^{-1}$] the probability (in events per cm) for a free $Si_i$ to be captured by other sinks. $A_i$ may vary with the neutron dose and depend on pre-existing defects in the Si crystal. However, we will restrict our present analysis with assumption that $A_i$ is a constant.

The multi-term denominators in equations (8) and (9) reflect the fact that only a limited number of free $Si_i$ are produced during irradiation, and crystal defects (both impurities and other lattice defects) compete to capture them.

The main simplifying assumption for the case of high-resistivity Si is that the concentrations of B, P, and O are low, and therefore the probability of free $Si_i$ or vacancies interacting with B, P, and O is much less than the probability of their vanishing into the other sinks. Thus, the equations (8) and (9) can be simplified to:

$$dN_B = -\frac{N_B\sigma_B\gamma_i}{A_i} d\Phi \qquad (10)$$

$$dN_P = -\frac{N_P\sigma_P\gamma_i}{A_i} d\Phi \qquad (11)$$

*B. Free Vacancies*

The enthalpy of formation of V is about 2.5 to 3 eV [24]. V is mobile at room temperature and able to interact with impurities, form divacancies and vacancy clusters by interaction with other vacancies, annihilate with $Si_i$, and disappear on the crystal surface. An interaction between a V and a $B_i$ leads to the formation of an unstable complex which self anneals below room temperature [23] by the reaction:

$$B_i + V \rightarrow [B_i - V] \rightarrow B_s \qquad (12)$$

This reaction restores $B_s$ and therefore affects the net impurity concentration. Interaction between a V and a $P_s$ leads to the formation of an E-center, which is stable at room temperature:

$$P_s + V \rightarrow [P_s - V] \qquad (13)$$

This reaction removes one shallow donor from the Si forbidden gap and therefore affects N. In high-resistivity Si, the Fermi level is positioned close to the level of the E-center. Therefore, we shall ignore the effect of the E-center on the Fermi level.

Interactions between interstitial oxygen and free vacancies may comprise reactions of first, second, and third order:

$$O_i + V \rightarrow O_s \qquad (14)$$

$$O_s + V \rightarrow [O_s^+ V^-] \qquad (15)$$

$$[O_s^+ V^-] + V \rightarrow [O_s^{2+} V^-] + V^- \qquad (16)$$

Calculations on the basis of equations (21) and (23) require the use of number of unknown parameters: $\gamma_i$, $\gamma_v$, $\sigma$'s, $\alpha$'s, $A_i$, and $A_v$. It is impossible to estimate them experimentally on the basis of radiation induced changes in N, because they never appear separately in the equations, but always as a ratios. The yields $\gamma_i$, $\gamma_v$ and cross-sections $\sigma$'s and $\alpha$'s are fundamental parameters which should be fixed for all calculations. The other parameters including $A_i$ and $A_v$ may vary from crystal to crystal. Therefore, $\beta$'s which combine $\gamma$'s, $\alpha$'s, $\sigma$'s and A's can be treated as adjustment parameters of the model as well as initial impurity concentrations $N_B^0$ and $N_P^0$.

The ratio $\beta_P/\beta_B$ estimated from our experimental data on high-resistivity silicon is in the range of 2 to 3. This means that P is removed from its substitutional position faster than B. The results of calculations based on equations (21), (23) with $\beta_P/\beta_B=2$, $\beta_{B,i}=4.4\cdot10^{-13}cm^2$, and $\beta_{B,v}=1.7\cdot10^{-14}cm^2$ are presented in Figs. 1 and 2.

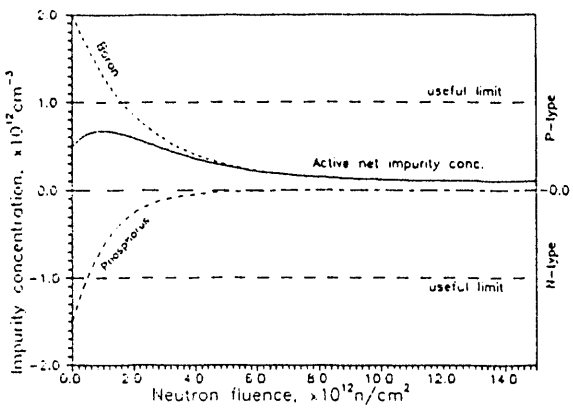


Fig. 1 P-type silicon: calculated electrically active impurity concentration vs neutron fluence; $N_P^0=1.5\cdot10^{12}$ $cm^{-3}$, $N_B^0=2\cdot10^{12}$ $cm^{-3}$

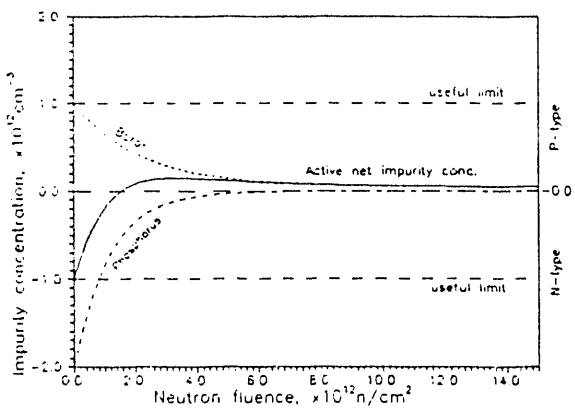


Fig. 2 N-type silicon: calculated electrically active impurity concentration vs neutron fluence; $N_P^0=2\cdot10^{12}$ $cm^{-3}$, $N_B^0=1\cdot10^{12}$ $cm^{-3}$

The model predicts that the difference in $Si_i$ and V capture cross-sections for $B_s$ and $P_s$ may dominate changes in resistivity at low fluences. For p-type silicon at low doses, the net electrically active impurity concentration decreases slowly (or may even increase as shown in Fig. 1) due to faster $P_s$ removal. For n-type Si (Fig. 2), the model predicts type conversion at fluences of 1 to $3\cdot10^{12}n/cm^2$. For crystals free of oxygen the model predicts that, independent of starting conductivity type, increasing neutron damage ultimately yields very high-resistivity p-type Si because of the annealing of $B_i$ into $B_s$ by reaction with V's.

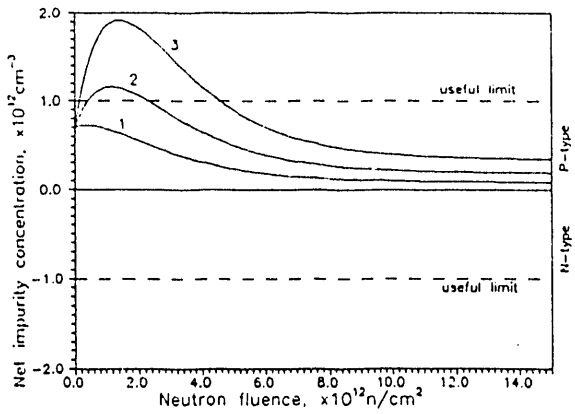


Fig. 3 P-type silicon with different compensation levels: calculated electrically active net impurity concentration vs neutron fluence;
1 - $N_B^0 = 1.7\cdot10^{12}cm^{-3}$, $N_P^0 = 1\cdot10^{12}cm^{-3}$
2 - $N_B^0 = 3.7\cdot10^{12}cm^{-3}$, $N_P^0 = 3\cdot10^{12}cm^{-3}$
3 - $N_B^0 = 6.7\cdot10^{12}cm^{-3}$, $N_P^0 = 6\cdot10^{12}cm^{-3}$

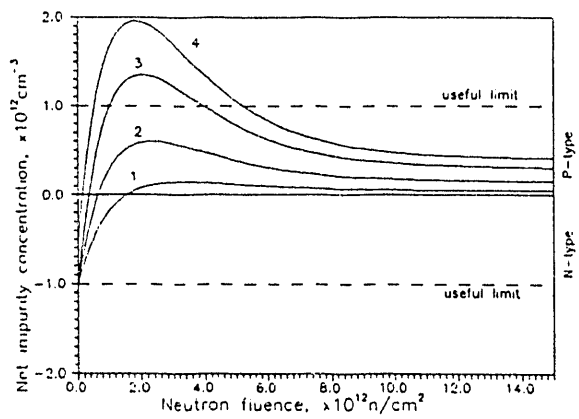


Fig.4 N-type silicon with different compensation levels: calculated electrically active net impurity concentration vs neutron fluence;
1 - $N_B^0 = 1\cdot10^{12}cm^{-3}$, $N_P^0 = 2\cdot10^{12}cm^{-3}$,
2 - $N_B^0 = 3\cdot10^{12}cm^{-3}$, $N_P^0 = 4\cdot10^{12}cm^{-3}$,
3 - $N_B^0 = 6\cdot10^{12}cm^{-3}$, $N_P^0 = 7\cdot10^{12}cm^{-3}$
4 - $N_B^0 = 8\cdot10^{12}cm^{-3}$, $N_P^0 = 8.5\cdot10^{12}cm^{-3}$

are associated with the decreases in the net impurity concentration.

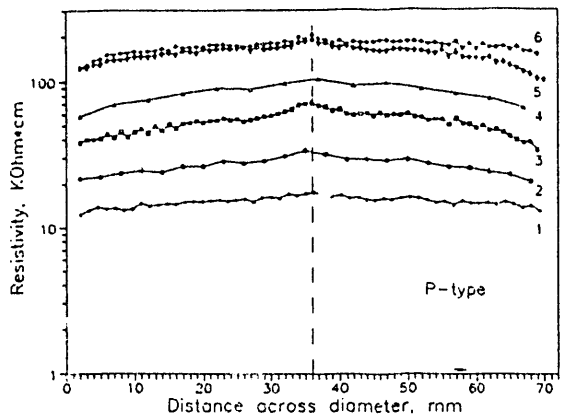


Fig.5 Resistivity of Westinghouse p-type multi-pass FZ purified wafer FZH-Q1-3:
1 - prior to irradiation, 2 - $2\cdot10^{12}$n/cm$^2$,
3 - $4.1\cdot10^{12}$n/cm$^2$, 4 - $6\cdot10^{12}$n/cm$^2$,
5 - $9.6\cdot10^{12}$n/cm$^2$, 6 - $1.36\cdot10^{13}$n/cm$^2$

The net impurity concentrations vs neutron fluence for two p-type samples grown by Westinghouse and one p-type sample grown by Wacker are presented in Fig. 6, 7, 8. The open circles are experimental data points and the curves are the results of fitting by our model. When plotted in semilogarithmic coordinates, all of the p-type samples show either a small net impurity concentration decrease, or even a slight increase (see Fig. 7), at fluences below $4\cdot10^{12}$n/cm$^2$.

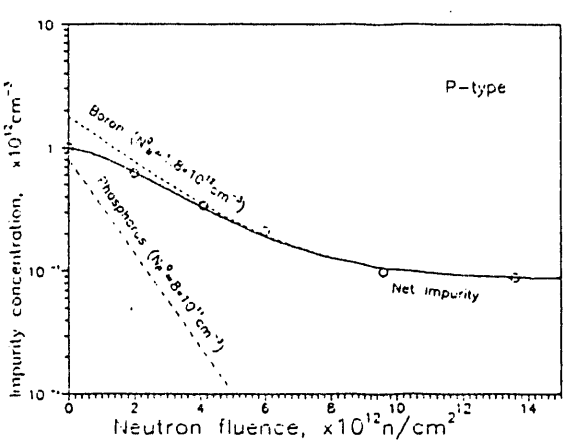


Fig.6 P-type wafer FZH-Q1-3: electrically active impurity concentration vs neutron fluence; dashed and solid lines represent theoretical curves

The theoretical curves fit the experimental points best for the ratio $\beta_P/\beta_B$ equal to 2. Extrapolation of the fitted curves to the point of zero fluence gives the initial concentrations of B and P.

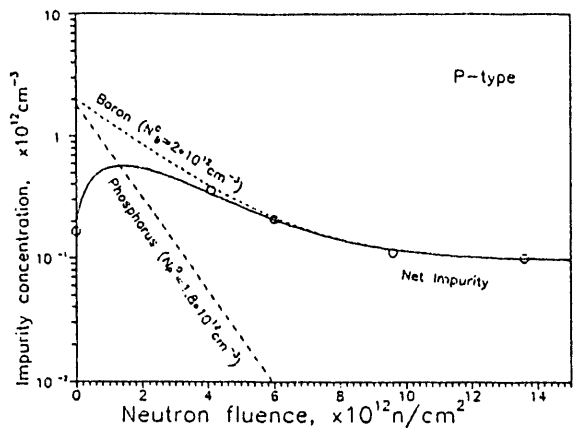


Fig.7 P-type wafer FZT-4A-3: electrically active impurity concentration vs neutron fluence; dashed and solid lines represent theoretical curves

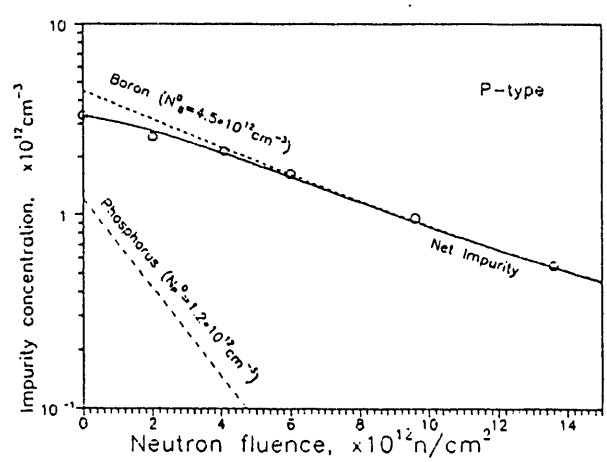


Fig.8 P-type wafer 34383-1090: electrically active impurity concentration vs neutron fluence; dashed and solid lines represent theoretical curves

Based on this, we suggest that neutron irradiation at low fluences may be a useful tool for estimating the original compensation levels in high-resistivity silicon.

*B. n-Type Silicon*

The resistivity change in an n-type wafer grown by Wacker is shown in Fig. 9. After a fluence of $1.4\cdot10^{13}$ n/cm$^2$ the resistivity increased from 8 kΩcm to about 500 kΩcm.

Partial conversion of the conductivity type from n to p was observed after a dose of $4 \cdot 10^{12}$n/cm$^2$. The presence of regions of n and p-type conductivity in this sample was identified with the cryogenic probe.

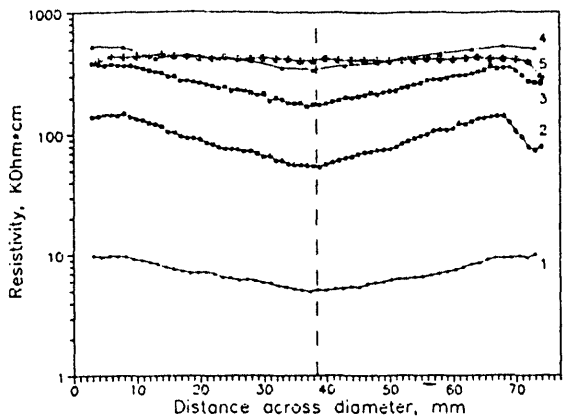


Fig.9 Resistivity of Wacker n-type wafer 34383-1048: 1 - prior to irradiation (n-type), 2 - $2 \cdot 10^{12}$n/cm$^2$ (n-type), 3 - $4.1 \cdot 10^{12}$n/cm$^2$ (mixed type), 4 - $6 \cdot 10^{12}$n/cm$^2$(mixed type), 5 - $1.4 \cdot 10^{13}$n/cm$^2$(p-type)

Hall effect measurements performed on this sample revealed that after a fluence of $1.4 \cdot 10^{13}$n/cm$^2$ the low field Hall mobility for holes was reduced to about 50% of its initial value. In the past, this sort of mobility drop was explained in terms of carrier scattering by damage clusters [3], or in terms of scattering on charged deep traps [22]. We believe, however, that a fluence of $1.4 \cdot 10^{13}$n/cm$^2$ is too small to produce damage clusters or deep levels in concentrations sufficient to cause this effect. A simple explanation of this phenomena may be found in the natural non-uniformity of the distribution of electrically active impurities. When the conductivity of silicon is close to intrinsic, a spatially nonuniform distribution of donors and acceptors may cause formation of built-in electric fields and local p-n junctions which act as scattering borders that reduce the mobility at low field strengths [30]. This type of low Hall mobility at low fields (on the order of a few volts/cm) has been observed in very high purity Ge which has not been radiation damaged [31]. These low field mobility problems have no obvious relevance to the high field mobilities that are important for good charge collection in radiation detectors.

C. Spatial Distribution of Resistivity

In our experience, non-irradiated n-type Si crystals have much more non-uniform spatial resistivity distribution than p-type crystals. The explanation of this phenomena lies in the behavior of B and P during crystal growth. The segregation coefficient of P is considerably less than unity, while the segregation coefficient of B is close to unity. Therefore, P has a tendency to be more non-uniformly distributed in a growing crystal. Fast neutron damage at fluences of 2 to $6 \cdot 10^{12}$n/cm$^2$ enhances the non-uniform spatial resistivity distribution in n-type crystals (see Fig. 10). On the contrary, the irradiation of p-type crystals with the same fluence may not result in an increased non-uniformity in the spatial resistivity distribution (see Fig. 11).

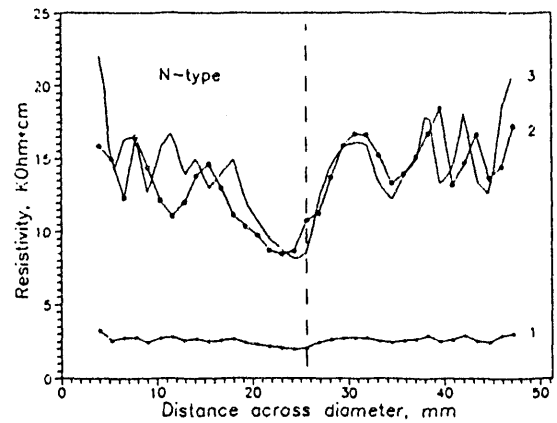


Fig.10 Spatial resistivity distribution in n-type Topsil wafer 24802: 1 - prior to irradiation, 2 - $3 \cdot 10^{12}$n/cm$^2$, 3 - theoretical curve

The observed difference is consistent with the predictions of our model. Let us assume that the original B distribution across the n-type wafer is uniform, and all the non-uniformity in the resistivity distribution is due to P. Faster $P_s$ removal decreases the net impurity concentration while the resistivity is still dominated by P. This leads to "magnification" of the original non-uniformities since net active impurity concentration is the difference between the concentrations of $B_s$ and $P_s$. The theoretical result shown as curve 3 in Fig. 10, calculated with $\beta_P/\beta_B=2$, is a reasonable fit to the experimental data shown as curve 2.

The resistivity profiles obtained on a high-purity p-type wafer FZT-4A-3 grown by Westinghouse serves as a good illustration of this point. This crystal showed significant

Fig.11 Spatial resistivity distribution in p-type Wacker wafer 34383-1090: 1 - prior to irradiation, 2 - $4.1 \cdot 10^{12}$n/cm$^2$

non-uniformity in spatial resistivity distribution prior to irradiation (Fig. 12). We believe that the high resistivity region close to the outside surface of the crystal is a result of P accumulation in an annular region during multi-pass FZ crystal growth (see curve 1 in Fig. 12). Neutron irradiation leads to a faster removal of $P_s$ than $B_s$. As a result, in curve 2 the net impurity concentration decreases and the resistivity increases in the core region where the crystal is less compensated; while the net impurity concentration increases and the resistivity decreases in the annular region close to the rim where the crystal is more heavily compensated. After most of the $P_s$ is removed (curve 3),

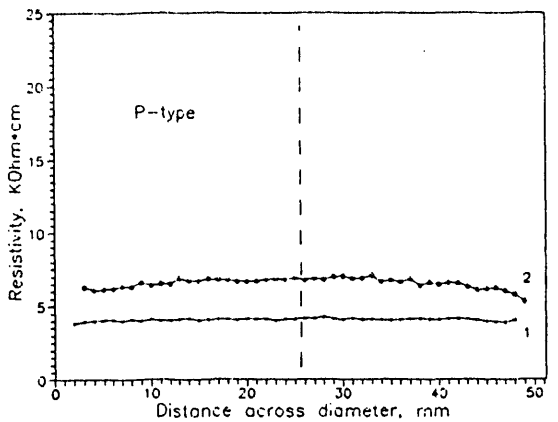


the resistivity uniformly increases with neutron fluence, reflecting removal of residual $B_s$.

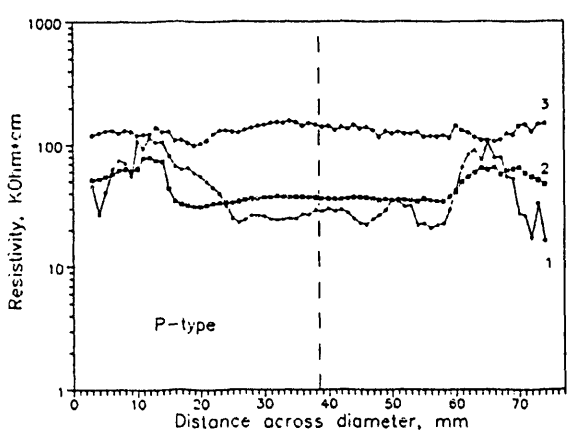


Fig.12 Spatial resistivity distribution in p-type Westinghouse wafer FZT-4A-3: 1 - prior to irradiation, 2 - $4.1 \cdot 10^{12}$n/cm$^2$, 3 - $1.36 \cdot 10^{13}$n/cm$^2$

## V. Summary

1. Changes in resistivity produced in FZ Si by 1 MeV neutron irradiation at room temperature have been measured. The resistivity of p-type samples progressively increased and saturated at the level of about 200 kΩcm. Essentially all changes in resistivity of p-type samples are believed to result from changes in net impurity concentration. Fast neutron irradiation did not increase spatial non-uniformity of resistivity in p-type silicon.

2. The resistivity of n-type silicon increased, passed through type conversion at about $4 \cdot 10^{12}$n/cm$^2$ and saturated at about 500 kΩcm. This type conversion was confirmed by the sign of the Hall coefficient and by cryogenic probe. A significant drop in low field Hall mobility for holes was found in very high resistivity crystals which were converted to p-type from n-type by radiation damage. A comparable change in hole mobility was not observed for samples which were originally p-type and received the same neutron dose. This supports the perception that the drop in low field mobility was caused by nonuniform distribution of donors and acceptors. Fast neutron irradiation significantly amplifies non-uniformities in the spatial distribution of the resistivity of n-type Si.

3. The observed changes in silicon resistivity are discussed from the point of view of changes in the net electrically active impurity concentration. A model is proposed which postulates escape of Si self-interstitials and vacancies from damage clusters and their subsequent interaction with impurities and other pre-existing defects in the Si lattice. These interactions lead to transfer of B and P from substitutional sites where they are electrically active into interstitial sites where they are electrically inactive, resulting in changes in the net uncompensated impurity density. Observed changes in resistivity, including its spatial distribution are explained in terms of faster phosphorus removal.

## Acknowledgements

This work benefitted from several discussions with H. Kraner and Z. Li at Brookhaven National Laboratory (who also furnished the Si dosimeters) and with G. Lindström and R. Wunstorf at the University of Hamburg. In particular, we wish to thank Nat Hill and other members of the ORELA staff without whose enthusiastic support and assistance this work would not have been possible.

* Work supported in part by U.S. DOE Grant DE-FG-O591ER-40627 to the University of Tennessee.

** The Oak Ridge National Laboratory is operated by Martin Marietta Energy Systems, Inc. for U. S. DOE under contract DEAC05-84OR21400.

## References

[1] E. Fretwurst et al. "Radiation Hardness of Silicon Detectors for Future Colliders", 6th European Symp. on Semicond. Detectors, Milano, Feb. 1992.

[2] R.F. Bass, *Bull. Amer. Phys. Soc.*, vol. 11, p. 193 (1966)

[3] H.J. Stein, *Phys. Rev.*, vol. 163, p. 801 (1967)

[4] H.J. Stein and R. Gereth, *J. Appl. Phys.*, vol. 39, p. 2890 (1968)

[5] J. Walter and I. Tsveybak, "Radiation Damage: Its Impact on the Cost and Feasibility of Large Scale Use of Silicon Detectors for Particle Physics", Workshop on Radiation Damage of Si, Minsk, USSR, October, 1991.

[6] S. Padgaonkar et al., *J.Phys. D*, vol. 24, p. 702 (1991)

[7] T. Tanaka and Y. Inuishi, *J. Phys. Soc. Jap.*, vol. 19, p. 167 (1964)

[8] R.E. Whan, *J. Appl. Phys.*, vol. 37, p. 3378 (1967)

[9] L.J. Cheng and J. Lori, *Phys. Rev.*, vol. 171, p. 856 (1968)

[10] P.F. Lugakov et al., *Phys. Stat. Sol. (a)*, vol. 74, p. 445 (1982)

[11] V.A.J. van Lint et al., *Mechanisms of Radiation Effects in Electronic Materials,* vol.1, J. Wiley & Sons, NY, 1980, pp. 142-153

[12] H.J. Stein, "Atomic Displacement Effects in Neutron Transmutation Doping" in *Neutron Transmutation Doping in Semiconductors*, ed. J.M. Meese, 1978, p. 229

[13] V.A.J. van Lint et al., *IEEE Trans. Nucl. Sci.*, vol. NS-19, p. 181 (1972)

[14] *Solid State Physics*, vol.2, edited by F. Seitz and D. Turnbull, (Academic Press, NY, 1956)

[15] B.R. Gossik, *J. Appl. Phys.*, vol. 30, p. 1214 (1959)

[16] J.H. Crawford and J.W. Cleland, *J. Appl. Phys.*, vol. 30, p. 1204 (1959)

[17] H.J. Jurechke et al., *J. Appl. Phys.*, vol. 27, p. 838 (1956)

[18] L.C. Kimerling and P.J. Drevinsky, *IEEE Trans. Nucl. Sci.*, vol. NS-18, p. 60 (1971)

[19] M.G. Bueler, *Proc. IEEE*, vol. 56, p. 1741 (1968)

[20] P.V. Kuchinski and V.M. Lomako, "Radiation Damage in Neutron-Irradiated High-Resistance Silicon", Oak Ridge Meeting on Radiation Detectors, Oak Ridge, 1991.

[21] H.W. Kraner, *Nuc. Instr. Meth.*, vol. 225, p. 615 (1984)

[22] G.C. Messenger, *IEEE Trans. Nuc. Sci.*, vol. NS-39, p. 468 (1992)

[23] G.D. Watkins, "The Lattice Vacancy in Silicon", in *Deep Centers in Semiconductors*, ed. S. Pantelides, NY, 1986

[24] S.S. Gorelik and M.Ya. Dashevski, *Material Science of Semiconductors and Dielectrics*, (Metallurgia, Moscow, 1988, in Russian), p. 297

[25] G.D. Watkins, *Phys. Rev. B*, vol. 12, p. 5824 (1975)

[26] J.W. Corbett and J.C. Bourgoin, *Point Defects in Solids, Semiconductors and Molecular Crystals*, vol. 2, ed. by J.H. Crawford and L.M. Slifkin (plenum Press, NY, 1975), Chapt.1.

[27] G.D. Watkins, in *Radiation Damage in Semiconductors*, ed.by P. Baruch (Dunod, Paris, 1965), p. 97

[28] H.W. Kraner, et al., *Nucl. Instr. Meth.*, vol. A 279, p. 266 (1989)

[29] E. Fretwurst, et al., *Nucl. Instr. Meth.*, vol. A 288, p. 1 (1990)

[30] J.I. Pankove, *Optical Processes in Semiconductors*, Doker Publ., NY 1971, pp. 10 -12.

[31] IEEE Standard for Characterizing High-Purity Germanium, ANSI IEEE Std. P1160D3 - 1992, Draft, March, 1992

[32] J. Walter, W. Bugg, and I. Tsveybak, in "Radiation Damage and Large Scale Application of Silicon Detectors", Conf., Firenze, Italy, Jul. 23 - 24, 1991

*"Research in Theoretical High Energy Physics"*

# PROGRESS REPORT TO DEPARTMENT OF ENERGY

# DOE DE-FG05-91ER40627

## TASK B

**Bennie F. L. Ward**

## Progress Report

## TASK B

**B. F. L. Ward**

The research in Task B during 1991-1992 focussed on the further development and application of our new YFS (Yennie-Frautschi-Suura) Monte Carlo approach[1] to $SU_2 \times U_1$ radiative corrections in the $Z^\circ$ physics scenarios at the SLC and LEP. In addition, progress was made on the application of perturbative QCD methods to heavy quark decay physics in the context of B–Factory high energy $e^+e^-$ collider physics and on manifestly gauge invariant covariant (closed) string field theory.

Specifically, during 1990-1991, we completed the implementation of our YFS[1] Monte Carlo procedure to the processes $e^+e^- \to f\bar{f} + n\gamma$, $f = \mu, \tau$, neutrino, quark, to the level of .1% accuracy. Thus, the LEP and SLC collaborations all have implemented the respective YFS2 Fortran program which allows them to simulate ,in the presence of detector cuts, the effects of multiple photon radiation on an event–by–event basis; the respective multiple photon 4-vectors are included in the list of final particle 4-vectors with no restriction on their number for the first time ever in $SU_2 \times U_1$ radiative correction simulations. Additionally, we succeeded in integrating this YFS2 calculation into the pure electroweak corrections program KORALZ in

version KORALZ3 [2], so that for the first time one may study the interplay of pure electroweak effects on the one hand with multiple photon effects on the other hand,on an event-by-event basis. This program KORALZ3 is now in use by all LEP and SLC collaborations (for SLC, this is the SLD Collaboration) and has been useful in the respective $f\bar{f} + n(\gamma)$ final states physics analyses, $f \neq e$. It has been demonstrated that the various pure weak libraries in KORALZ3 (one by W. Hollik, one by D. Bardine et al. and one unsupported library by R. Stuart) agree within .3% on the absolute normalization of the cross section near the Z° resonance in $e^+e^-$ annihilation so that, for the present at SLC and LEP, we have an adequate knowledge of the respective pure weak effects. We must improve on this agreement in the not-too-distant future, in view of the current Z° production rate at LEP and the expected long term rate at the SLC.

Indeed, we are in the process of making an independent check of the pure weak libraries by Hollik, Stuart and Bardine et al. as they are implemented in KORALZ3. This we are doing in collaboration with Prof. Jadach in Krakow, Poland, with possible further collaboration from Prof. Zralek in Silesia, Poland. We have made substantial progress in our check and we hope to report more on this progress soon. Here, we may note that recently, using our results on the interplay of pure weak corrections and QED, we resolved the issue operationally of the gauge invariance of the renormalized Z° rest mass [3]. This shows that the mass measured at LEP/SLC for the Z° is in fact gauge invariant.

In addition, we have made progress in resolving the question left by the LEP100 Line Shape Group in CERN–89–08, Vol. 1: "What is the best way of exponentiating QED corrections?." For, in their final report, the authors of the Line Shape section of the LEP100 Workshop Report were only able to show that five different methods agreed to .2–.3%. In Ref. 4, we show that the YFS–based method is the best one by looking into an exact model calculation and comparing the various ansatz's in the Line Shape Report with the exact result. Thus, our work substantiates the preference of the method based on our YFS procedure over the other naive exponentiation procedures considered in that report. Our work has been recently corroborated by F. Chen et al. (Beijing preprint, 1991).

In view of the need to study in detail the cross section asymmetries in $e^+e^- \to f\bar{f} + n(\gamma)$ in order to complete the high precision $Z^\circ$ physics programs at the SLC and LEP, using YFS2 [1], we have analyzed [5], in the presence of detector cuts, the multiple photon effects in asymmetries for the cases $f = \mu$, b. We find that the multiple photon effects are significant and that $A_{FB}(b)$ at LEP is competitive with $A_{LR}$ at SLC for its assessibility in the presence of multiple photon radiation and its sensitivity to $\sin^2\theta_W$ when the high luminosity at LEP is taken into account. Thus, it affords another path to $\sin^2\theta_W$ in the high precision $Z^\circ$ physics tests of the Standard Model.

We have recently[6] used our KORALZ3 Monte Carlo to look into the pure weak effects in our $A_{FB}$ ($\mu$) analysis. We find that the pure weak corrections do not alter the general conclusions in Ref. 5 but that their dependence on $m_t$ and $m_H$ will

mean that, using KORALZ3, the allowed parameter space for $m_t$ and $m_H$ can be extracted from the LEP data with all multiphoton–detector cut effects properly taken into account.

Indeed, we have recently introduced [7] the new YFS Monte Carlo event generator YFS3, which treats for the first time $n(\gamma)$ final state multiphoton radiation in $e^+e^- \to f\bar{f} + n(\gamma)$, with $\underline{f \neq e}$. We are currently implementing it into the SLC/LEP experimental activities and refining its precision tag as dictated by the LEP(/SLC) data. Such final state radiation data afford new roads for Standard Model tests.

Concerning the basic luminosity process $e^+e^- \to e^+e^- + n\gamma$ at low angles, we recall that we had implemented, during 1989–1990, our BHLUMI Monte Carlo YFS program[8] at SLC and at LEP, so that indeed the higher order corrections to the luminosity were known to 1%. This result already played a significant role in controlling the systematic error on the measurement of the luminosity at SLC and LEP and, hence, it made a significant contribution to the 1989 MkII discovery that the number of massless neutrino generations is 3 (this MkII finding was immediately corroborated by ALEPH on using our BHLUMI program to calculate the higher order corrections to their luminosity). Thus, we feel that our YFS methods were brought to the level of implementation which was sufficient for the 1989–early 1990 scenario in bhabha scattering at low angles. However, for the current and long term SLC-LEP objectives, we needed to carry this level of accuracy on the bhabha luminosity process to the .2% and below .1% regimes, respectively.

Accordingly, Prof. Jadach and the PI, working with Drs. Z. and E. Was, have

established [9] an $0(\alpha)$ baseline description of the luminosity cross section so that it is understood in absolute normalization from both an analytic and Monte Carlo standpoint at the .1% level. This, we expected, would then allow us to check our Monte Carlo methods for BHLUMI for their absolute normalization to the .2% level by 11/1/90 and to below .1% ultimately with the corresponding improvement in the baseline description to the below .1% regime; we explained this in detail in our 1991–1992 renewal proposal.

And, indeed, during 1990–1991, we developed[10] two independent $0(\alpha^2)$ LL YFS exponentiated Monte Carlo's for the higher order corrections to the SLC/LEP luminosity so that, in a CERN Theory Division Seminar by Jadach in 12/90, we already presented a procedure[10] for correcting $O(\alpha)$ Monte Carlo luminosity simulations for higher order effects which was accurate to .2% on the pure bremmstrahlung and to .3% for the total luminosity. In addition, we developed, for the first time, analytic improved naive exponentiated formulae[10] for the luminosity process accurate to a technical precision of .02% so that we could check the normalization of BHLUMI 1.13 to .15%. Finally, to obviate the need of using two different MC simulations in the complicated software management environment of a LEP/SLC collaboration, we developed[10] BHLUMI 2.00 as a single, YFS MC solution to the luminosity problem at SLC/LEP with a total precision of .25%, including an allowance for pairs, vacuum polarization uncertainty, etc. For reference, the current best experimental error from LEP on the luminosity measurement is ALEPH's .5%. Thus, we are currently providing a sufficiently accurate simulation;

we must improve this in the near future, when ALEPH installs its new luminosity monitor.

In fact, BHLUMI 2.01, recently published in Ref. 11, is now in use at LEP [12] for the analyses of the 1991 LEP data (BHLUMI has always been used at MkII and SLD for data analysis). This means that during 1991-1992, we have succeeded with the implementation and acceptance of BHLUMI 2.01 as the basic luminosity data analysis radiative corrections simulator at LEP as a replacement of the Berends-Kleiss-Hollik generator BABAMC [13], which had been the standard data analysis luminosity generator at LEP since 1989-(BHLUMI was previously only used for the higher-order corrections to BABAMC at LEP, as we have explained; now, it is the program which generates the events which are passed through the long LEP detector simulations. This has greatly improved the understanding of these detectors' responses so that it has facilitated the precision tag of ~.5% which ALEPH has reached with its current luminosity monitor. Thus, this represents a major achievement for the DOE's investment in Task B.)

What we should emphasize as one our most important successes is our work between SLAC and CERN during the period April, 1989 - September, 1989, as we described in detail in our renewal proposal for 1990–1991. During this period, we and our collaborators resolved discrepancies in KORALZ3 libraries and in the luminosity calculations so that these calculations were in a usable state for the SLC and LEP turn–on's (our higher order bhabha work made the $N_\nu = 3$ discovery possible). We continued this commuting approach between SLAC and CERN during

1990 and 1991 – in the former case, working directly with physicists in both places, we were able to formulate and develope the benchmark $O(\alpha)$ process simulation[9] for the crucial luminosity problem and in the latter case, we were able to arrive at the desired .25% accuracy for our BHLUMI (YFS) calculation using this benchmark. In addition, our interactions with Drs. Locci (ALEPH) and Komamiya (OPAL) allowed us to start the implementation of our wide–angle YFS bhabha MC event generator BHLUMI 3.0, which we had made available to the SLD Collaboration at SLAC (it has already been used in analyzing the initial SLD engineering data (1991) and is now being used, in a new polarization version, on the new $10^4$ 20% beam polarization Z° data sample (1992)). During 1991-1992, we continued our commuting approach between SLAC and CERN and thereby made the important acceptance and implementation of BHLUMI 2.01 at LEP possible. Further, we made BHLUMI 3.0 available to OPAL and continued to interact with that Collaboration in its implementation and use at LEP. These achievements were only possible because I was able to work directly with the members of the CERN EWMC Working Groups, and my collaborators Drs. Jadach, Ricter–Was, and Was, as we explain in our proposal for 1990-1991 and as we review in our 1991–1992, 1992–1993 and 1993-1994 proposals.

We have recently[14] made progress in understanding the possible meaning of the value $N_\nu = 3$, where $N_\nu$ is the number of massless neutrino generations. We interpret this as evidence for an $SU(3)^f$ family symmetry which breaks at a scale ~ 100 TeV. The attendant association of the C–K–M matrix with $SU(3)^f$ mixing

interactions then gives the prediction for $m_t$ in terms of $\alpha \equiv V_{cb}/V_{ub}$ and the light quark masses $m_q$, q = u,d,s,c,b (the respective formula is given in Ref. [14] and in our 1992–1993 renewal proposal). The recent CLEO–ARGUS results for $\alpha$ then allow us to conclude with 95% confidence that

$$67.8 \text{ GeV} \lesssim m_t \lesssim 127.9 \text{ GeV}.$$

This result is extremely interesting from the standpoint of the CDF Standard Model limit $m_t > 91$ GeV. Perhaps, top will be discovered soon!

We should note that with Dr. Zhang, our former post-doc, and with our collaborators in Cracow, Poland, Prof. Jadach's Group, we have succeeded[15] in obtaining an analytic result for the total differential distribution in $e^+e^- \to \mu\bar{\mu} + 2\gamma$. This result and its generalizations have been used to carry our YFS2 FORTRAN simulations beyond the .1% precision regime in $Z^\circ$ physics. We began a similar analysis for the process $e^+e^- \to e^+e^- + 2\gamma$ with our former post–doc, Dr. S. Lomatch. We had a preliminary[16] formula for the real bremsstrahlung process $e^+e^- \to e^+e^- + 2\gamma$ at SLC/LEP energies and, with Dr. S. Yost, we our replacement for Dr. Lomatch, we have recently completed[17] the calculation of $2\gamma$ emission part of $\mathbb{B}_2$ for the bhabha process and moved the theoretical uncertainty on the bremsstrahlung process in BHLUMI to the below .1% regime as desired.

Continuing with our effort to reach the below .1% regime of precision for BHLUMI 2.01, we recently finished with our post-doc M. Skrzypek the calculation[18] of new formulae for the pairs production effect in the Bhabha

scattering luminosity process at SLC/LEP. We are currently in the process of implementing this calculation in BHLUMI so that the soft pairs four-vectors will be available to the experimentalists in the final particle list. This soft pairs effect represents an important step on the way to below .1% precision luminosity simulations.

In the area of QCD methods in heavy quark decay physics, we most recently[19] analyzed the decay $B \to \psi/JK^*_+$ from the standpoint of the luminosity requirement for CP violation studies at a SLAC–LBL–LNL–type B–Factory. We find that, in three relativistically invariant models, the CP even decay final state is dominant so that, indeed, this decay can be used for CP violation studies at a SLAC-LBL–LNL–type B–Factory. The attendant reduction in luminosity required is ~ 2.5. In fact, our result for the Lepage–Brodsky theory prediction for this decay is in agreement in detail with recent measurements by ARGUS[20].

And, recently, following further preliminary work by ARGUS[21], we analyzed[22] the decays $B \to \chi_c K_s$ as possible further new modes for CP violation exploration at the SLAC-LBL-LLNL Asymmetric B-Factory device. We find agreement with the ARGUS results $B(B \to \chi_c \chi) = (1.05 \pm .35 \pm .25)\%$ and $B(B \to \chi_c K^+) = (.19 \pm .13 \pm .06)\%$ and that the ratio of CP odd to CP even final states is ~.38, so that, indeed, such modes as $B \to \chi_c K_s$ can be used to further reduce the required luminosity in the SLAC B-Factory project. (Just how much it is reduced requires more analysis.)

Continuing our study of new modes for exploration of CP violation in a B–Factory of the SLAC–LBL–LNL asymmetric variety, we have recently developed[23] a benchmark analysis of the decays $D \to \pi\pi$, KK for testing how well one might hope to predict a mode like $B \to \pi\pi$, where isospin considerations have recently been advanced for removing the unwanted penguin–type contributions in the measurement of the unitarity triangle angle $\alpha$. What we find is that our methods, based on Lepage–Brodsky theory, allow us to predict $\Gamma(D \to K^+K^-)/\Gamma(D \to \pi^+\pi^-) \approx 2.00$, $\Gamma(D \to K^+K^-) \approx .561\%$, $\Gamma(D \to \pi^+\pi^-) \approx .280\%$, to be compared with the ARGUS–CLEO results $2.42 \pm .42$, $.46 \pm .06\%$, $.210 \pm .031\%$ respectively. Hence, it seems that 25% knowledge of $B \to \pi\pi$ rates and ratios of rates might be possible with our methods and we are currently attempting to realize this.

Finally, we had a small amount of time to devote to our quantum gravitation research. The recent result[24] is a solution for the ground state of string theory in the open string case. We used the methods of the operator field to show that the tachyon is really absent in the true spectrum of the theory. After discussion with Prof. M. E. Peskin of SLAC, we have extended[25] the first paper in Refs. 24 to address several questions which are not discussed therein. We may now hope to incorporate this result into our earlier results[24] for the manifestly gauge invariant closed string field theory to arrive at a sound physical framework from which to study the true spectrum of the heterotic string theory of Gross et. al. eventually. We must emphasize that our pre–occupation with SLC–LEP physics research will not allow us to devote very much time to string theory, however. And, this is as it should be.

Finally, it is appropriate to report that, on March 20, 1991, we were awarded Texas National Research Laboratory Commission grant number RCFY9101 for applying our YFS methods developed in TASK B to higher order radiative corrections to SSC physics processes. On January 15, 1992, this award was renewed for a second year. These awards were major achievements for the research in TASK B and we feel that this successful application of the work developed in Task B shows that the DOE's investment therein was and is well-placed. (For reference, we list a recent preprint from our SSC physics activity [26].) We hope it encourages the DOE to continue to expand its support for Task B so that even larger applications will be possible.

## References


1. S. Jadach and B. F. L. Ward, Phys. Rev. D38, 2897 (1988); ibid. 39, 1472 (1989); Phys. Lett. B220, 611 (1989); Comp. Phys. Commun. 56, 351 (1990).
2. See D. Bardine et al., report of the LEP100 Monte Carlo Working Group, in LEP100 Yellow Book, ed. G. Altarelli (CERN, Geneva, 1989); CERN-TH-5994/91, Computer Phys. Commun., 1991, in press.
3. B. F. L. Ward, IC/91/161; Nucl. Phys. B (Proc. Suppl.), 1992, in press.
4. S. Jadach, M. Skrzypek and B. F. L. Ward, UTHEP-90-0601, 1990; Phys. Lett. B257, 173 (1991).
5. S. Jadach and B. F. L. Ward, Phys. Rev. D42, 1404 (1990).
6. S. Jadach et al., Phys. Lett. B257, 213 (1991).
7. S. Jadach and B. F. L. Ward, Phys. Lett. B274, 470 (1992).

8. S. Jadach and B. F. L. Ward, Phys. Rev. D40, 3582 (1989).

9. B. F. L. Ward, talk to CERN Th. Division, 8/17/90; S. Jadach et al., Phys. Lett. B253, 469 (1991).

10. S. Jadach et al., Phys. Lett. B260, 438 (1991); Phys. Lett. B268, 253 (1991); Phys. Rev. D44, 2669 (1991).

11. S. Jadach et al., Comp. Phys. Commun. 70, 305 (1992).

12. See H. Meinhard, Proc. 1992 Rochester Conf., in press.

13. F. A. Berends, R. Kleiss, and W. Hollik, Nucl. Phys. B304, 712 (1988).

14. B. F. L. Ward, UTHEP–89–1202; IL Nuovo Cimento A, 1992, in press.

15. S. Jadach et al., Phys. Rev. D42, 2977 (1990).

16. S. Lomatch et al., unpublished.

17. S. Jadach, B. F. L. Ward and S. Yost, UTHEP-92-0601, 1992, to appear.

18. S. Jadach, M. Skrzypek and B. F. L. Ward, UTHEP-92-0701, 1992, to appear.

19. B. F. L. Ward, invited talk at the SLAC B–Factory Workshop, June, 1990; ICTP preprint 1990 IC/90/271, Proc. SLAC B–Factory Workshop, ed. D. Hitlin (SLAC, Stanford, CA, 1991), p. 123; Phys. Rev. D45, 1544 (1992); UTHEP–91–0102.

20. H. Schroder, 1990 Rochester Conf., Proceedings, (S. E. Asia Th. Phys. Assoc. et al., Singapore, 1991).

21. H. Albrecht et al., DESY-91-077, July, 1991.

22. B. F. L. Ward, in Proc. 1992 SLAC B-Fact. Workshop, in press; UTHEP-92-0502.

23. B. F. L. Ward, talk presented at the 1991 SLAC B–Factory Workshop, June, 1991; UTHEP-91-0901; UTHEP-92-0702.

24. B. F. L.Ward, UTHEP-90-0101; UTHEP–89–0101; IL Nuovo Cimento 105A, 603 (1992).

25. B. F. L. Ward, UTHEP–91–0601.

26. D. DeLaney, S. Jadach, Ch. Shio, G. Siopsis and B. F. L. Ward, "Multiple Photon Effects in p p Scattering at SSC Energies," UTHEP-92-0501, in press at Phys. Lett. B, 1992.

## List of Preprints and Publications

## Task B

1. Ward, B. F. L., "Theoretical Uncertainties in Semileptonic ß Decay," in CP Violation and Beauty Factories and Related Issues in Physics, Vol. 619 of the *Annals of the New York Academy of Sciences*, February 14, 1991, pp. 104-107.

2. Jadach, S. and Ward, B. F. L., "Multiple Photon Emission and b-Quark Asymmetries," in CP Violation and Beauty Factories and Related Issues in Physics, Vol. 619 of the *Annals of the New York Academy of Sciences*, February 14, 1991, pp. 99-102.

3. Ward, B. F. L., "Number of B Mesons Needed to See CP Violation," UTHEP-90-1101, Phys. Rev. D44, 2050 (1991).

4. Jadach, S., Ward, B. F. L. and Was, Z., "The Monte Carlo Program KORALZ, Version 3.8, for the Lepton or Quark Pair Production at LEP/SLC Energies," CERN-TH.5994/91, Comp. Phys. Commun. 66, 276 (1991).

5. Jadach, S., Richter-Was, E., Ward, B. F. L. and Was, Z., "QED Multiphoton Corrections to Bhabha Scattering at Low Angles-Monte Carlo Solution," CERN-TH.6118/91, Phys. Lett. B268, 253 (1991).

6. Jadach, S., Richter-Was, E., Ward, B. F. L. and Was, Z., "High Precision Improved Analytic Exponentiation Results for Multiple Photon Effects in Low Angle Bhabha Scattering at SLC and LEP," UTHEP-91-0101, Phys. Rev. D44, 2669 (1991).

7. Ward, B. F. L., "Investigations of Dynamical Models of $B \to \psi/JK^*_+$," Phys. Rev. D45, 1544 (1992) and UTHEP-91-0102,; abbreviated version in Proc. 4th Int. Symp. on Heavy Flavors, 1991.

8. Ward, B. F. L., Jadach, S., Richter-Was, E. and Was, Z., "Small Angle Bhabha Scattering," UTHEP-91-0902; in Proc. LPHEP91, 1991.

9. Ward, B. F. L., "On the Ground State of String Theory," IL Nuovo Cimento Vol. 105A, 603 (1992).

10. Jadach, S. and Ward, B. F. L., "Final State Multiple Photon Effects in Fermion Pair Production at SLC/LEP" UTHEP-91-0903, Phys. Lett. B274, 470 (1992).

11. Jadach, S., R.-Was, E., Ward, B. F. L. and Was, Z, "Monte Carlo Program BHLUMI2.01 for Bhabha Scattering at Low Angles with Yennie-Frautschi-Suura Exponentiation," CERN-TH-6230/91, Comp. Phys. Commun. 70, 305 (1992).

12. Ward, B. F. L., "Non-Tachyonic Ground State for String Theory," UTHEP-91-0601, 1991.

13. Ward, B. F. L., "How Big Are Penguins?," UTHEP-91-0901, submitted to Phys. Rev. D.

14. DeLaney, D., Jadach, S., Shio, Ch., Siopsis, G. and Ward, B. F. L., "Multiple Photon Effects in Fermion-(Anti)-Fermion Scattering at SSC Energies," UTHEP-92-0101, submitted to Phys. Rev. D.

15. DeLaney, D., Jadach, S., Shio, Ch., Siopsis, G. and Ward, B. F. L., "Multiple Photon Effects in p p Scattering at SSC Energies," UTHEP-92-0501, in press at Phys. Lett. B, 1992.

16. Ward, B. F. L., "Theoretical Estimates of $B \to \chi_c K_s$," UTHEP-92-0502, to appear in Proc. SLAC B-Factory Workshop, April, 1992.

17. Ward, B. F. L., "Size of Penguins in D Decay," UTHEP-92-0701, submitted to Phys. Rev. D.

18. Ward, B. F. L., "On Gauge Invariance of the Renormalized Z° Rest Mass," IC/91/161, in press at Nucl. Phys. B (Suppl.), 1992.

19. Ward, B. F. L., Jadach, S., Richter-Was, E., and Was, Z., "Monte Carlo Program BHLUMI2.01 for Bhabha Scattering at Low Angles with Yennie-Frautschi-Suura Exponentiation," invited talk in 1992 Rochester Conference, UTHEP-92-0902, to appear in Proc. 1992 Rochester Conf., in press.

20. Jadach, S., Placzek, W., Richter-Was, E., Ward, B. F. L. and Was, Z., "QED Corrections to Small Angle Bhabha and Quark-Electron Scattering," Nucl. Phys. B (Proc. Suppl.), 1992, in press.

## List of Preprints and Publications

### Task B

1. Ward, B. F. L., "Theoretical Uncertainties in Semileptonic ß Decay," in CP Violation and Beauty Factories and Related Issues in Physics, Vol. 619 of the *Annals of the New York Academy of Sciences*, February 14, 1991, pp. 104-107.

2. Jadach, S. and Ward, B. F. L., "Multiple Photon Emission and b-Quark Asymmetries," in CP Violation and Beauty Factories and Related Issues in Physics, Vol. 619 of the *Annals of the New York Academy of Sciences*, February 14, 1991, pp. 99-102.

3. Ward, B. F. L., "Number of B Mesons Needed to See CP Violation," UTHEP-90-1101, Phys. Rev. D44, 2050 (1991).

4. Jadach, S., Ward, B. F. L. and Was, Z., "The Monte Carlo Program KORALZ, Version 3.8, for the Lepton or Quark Pair Production at LEP/SLC Energies," CERN-TH.5994/91, Comp. Phys. Commun. 66, 276 (1991).

5. Jadach, S., Richter-Was, E., Ward, B. F. L. and Was, Z., "QED Multiphoton Corrections to Bhabha Scattering at Low Angles-Monte Carlo Solution," CERN-TH.6118/91, Phys. Lett. B268, 253 (1991).

6. Jadach, S., Richter-Was, E., Ward, B. F. L. and Was, Z., "High Precision Improved Analytic Exponentiation Results for Multiple Photon Effects in Low Angle Bhabha Scattering at SLC and LEP," UTHEP-91-0101, Phys. Rev. D44, 2669 (1991).

7. Ward, B. F. L., "Investigations of Dynamical Models of $B \to \psi/JK^*_+$," Phys. Rev. D45, 1544 (1992) and UTHEP-91-0102,; abbreviated version in Proc. 4th Int. Symp. on Heavy Flavors, 1991.

8. Ward, B. F. L., Jadach, S., Richter-Was, E. and Was, Z., "Small Angle Bhabha Scattering," UTHEP-91-0902; in Proc. LPHEP91, 1991.

9. Ward, B. F. L., "On the Ground State of String Theory," IL Nuovo Cimento Vol. 105A, 603 (1992).

10. Jadach, S. and Ward, B. F. L., "Final State Multiple Photon Effects in Fermion Pair Production at SLC/LEP" UTHEP-91-0903, Phys. Lett. B274, 470 (1992).

11. Jadach, S., R.-Was, E., Ward, B. F. L. and Was, Z, "Monte Carlo Program BHLUMI2.01 for Bhabha Scattering at Low Angles with Yennie-Frautschi-Suura Exponentiation," CERN-TH-6230/91, Comp. Phys. Commun. 70, 305 (1992).

12. Ward, B. F. L., "Non-Tachyonic Ground State for String Theory," UTHEP-91-0601, 1991.

13. Ward, B. F. L., "How Big Are Penguins?," UTHEP-91-0901, submitted to Phys. Rev. D.

14. DeLaney, D., Jadach, S., Shio, Ch., Siopsis, G. and Ward, B. F. L., "Multiple Photon Effects in Fermion-(Anti)-Fermion Scattering at SSC Energies," UTHEP-92-0101, submitted to Phys. Rev. D.

15. DeLaney, D., Jadach, S., Shio, Ch., Siopsis, G. and Ward, B. F. L., "Multiple Photon Effects in p p Scattering at SSC Energies," UTHEP-92-0501, in press at Phys. Lett. B, 1992.

16. Ward, B. F. L., "Theoretical Estimates of $B \to \chi_c K_s$," UTHEP-92-0502, to appear in Proc. SLAC B-Factory Workshop, April, 1992

17. Ward, B. F. L., "Size of Penguins in D Decay," UTHEP-92-0701, submitted to Phys. Rev. D.

18. Ward, B. F. L., "On Gauge Invariance of the Renormalized Z° Rest Mass," IC/91/161, in press at Nucl. Phys. B (Suppl.), 1992.

19. Ward, B. F. L., Jadach, S., Richter-Was, E., and Was, Z., "Monte Carlo Program BHLUMI2.01 for Bhabha Scattering at Low Angles with Yennie-Frautschi-Suura Exponentiation," invited talk in 1992 Rochester Conference, UTHEP-92-0902, to appear in Proc. 1992 Rochester Conf., in press.

20. Jadach, S., Placzek, W., Richter-Was, E., Ward, B. F. L. and Was, Z., "QED Corrections to Small Angle Bhabha and Quark-Electron Scattering," Nucl. Phys. B (Proc. Suppl.), 1992, in press.

# END

# DATE FILMED

4 / 30 / 93